Manufacturing Technology Research

Electrical Discharge Machining (EDM)

Types, Technologies and Applications

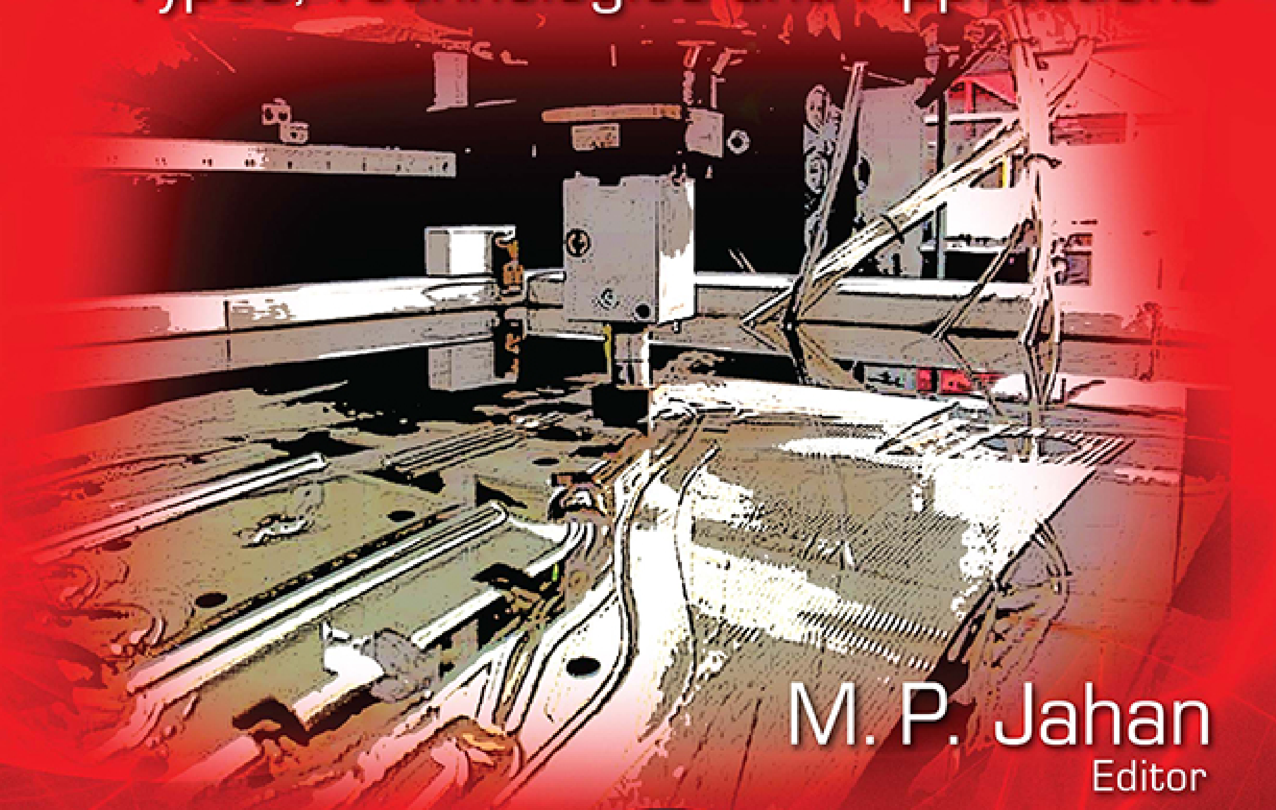

M. P. Jahan
Editor

NOVA

Complimentary Contributor Copy

MANUFACTURING TECHNOLOGY RESEARCH

ELECTRICAL DISCHARGE MACHINING (EDM)

TYPES, TECHNOLOGIES AND APPLICATIONS

MANUFACTURING TECHNOLOGY RESEARCH

Additional books in this series can be found on Nova's website
under the Series tab.

Additional e-books in this series can be found on Nova's website
under the e-book tab.

MANUFACTURING TECHNOLOGY RESEARCH

ELECTRICAL DISCHARGE MACHINING (EDM)

TYPES, TECHNOLOGIES AND APPLICATIONS

M. P. JAHAN
EDITOR

nova publishers
New York

Library of Congress Cataloging-in-Publication Data

Electrical discharge machining (EDM) : types, technologies and applications / editor, M. P. Jahan (Department of Architectural and Manufacturing Sciences, Western Kentucky).
pages cm -- (Electrical engineering developments.)
Includes index.
ISBN:978-1-63483-598-5 (eBook)
1. Electric metal-cutting. I. Jahan, M. P., editor.
TJ1191.E298 2014
671.3'5--dc23
2015029239

Published by Nova Science Publishers, Inc. † New York

CONTENTS

PREFACE

Electrical Discharge Machining (EDM) is one of the earliest and most widely used non-conventional machining processes. The major advantage of EDM is that it is capable of machining electrically conductive materials irrespective of the material's hardness, strength and other mechanical properties. The EDM is capable of machining parts and components with complex geometries maintaining high level of dimensional accuracy and acceptable surface finish. Nowadays, EDM is used extensively for many important applications in die and mold, aerospace, automotive, micro-electronic and biomedical industries. Die-sinking EDM and wire-EDM are the two major types of EDM, where milling EDM is gaining popularity due to its capability of machining three dimensional (3D) shapes similar to conventional milling process. Due to the growing trend of miniaturization, micro scale EDM is becoming more popular among the industries. All three varieties of EDM: die-sinking, wire-cut and milling EDM have demonstrated the capability of fabricating micro scale intricate features for various industrial applications. Another recent advancement in the area of EDM is the EDM-based hybrid processes. The objective of the hybrid machining processes is to minimize shortcomings of EDM or to solve a specific issue of EDM, by integrating other machining processes with EDM and/or applying assistance from external sources into the EDM process.

In this book, various aspects of EDM have been discussed including the major types, technologies and applications of EDM. The main goal was to accumulate all the possible topics on various aspects of EDM in a comprehensive collection, that could help the educators, researchers, engineers, technologists, and students working on EDM. The present book can be used as a research book for final year undergraduate engineering and technology course as well as a topic on manufacturing for Masters and Doctoral level course. In addition, this book can serve as a reference book for students, researchers, engineers, teachers and working professionals in non-traditional manufacturing processes related industries. This book would be very useful for the students and researchers who are planning to start their investigations studies on the area of EDM and related processes. Therefore, the scientific interest in this book is evident for universities, research centers, as well as industries.

The first chapter of the book discusses the history, principle, system component, parameters, variations, applications and recent advances of die-sinking EDM. In the second chapter, a detail overview of the wire EDM process covering the system component, wire materials, parameters, process responses and applications is presented. The third chapter describes various aspects of EDM modeling and simulations including EDM gap phenomena, single and multiple discharges, temperature distributions and material removal mechanism. Chapter 4 is dedicated to the surfaces generated during the EDM process that discusses the surface topography, sub-surface microstructures, residual stress, hardness, micro-cracks and other surface characteristics produced from the EDM process. The chapter 5 deals with one of the EDM-based hybrid machining processes, ultrasonically aided electrical discharge machining process, providing an insight of the process and rationale of improvement in machining performance. Chapter 6 describes the hybrid micro-EDM/ECM process and its applications for the fabrication of complex 3D microstructures. In chapter 7, various aspects orbital electro discharge machining have been discussed including strategies for orbital tool movement and effect of orbital movement on the machining performance. Chapter 8 focuses on another EDM-based hybrid machining process named powder mixed EDM. Chapter 9 discusses an interesting application of Micro-EDM process in patterning conducting polymer Polypyrrole. Chapter 10 describes application of block-EDM for the fabrication of microgrinding tool and use of the fabricated tool for glass microgrinding. Chapter 11 discusses the electrical discharge machining characterization and optimization of metal metrix composites (MMCs) and metal matrix nano composites (MMNCs). Chapter 12 describes the application of EDM for the non-metal based fabrication processes, covering the EDM of silicon and conducting polymer based materials. Chapter 13 discusses the application of micro-EDM for machining another novel material reaction-bonded silicon carbide. The chapter 14 presents the recent research works and development on the EDM of shape memory alloys.

The Editor acknowledges Nova Science for this opportunity and their professional support. Finally, the Editor would like to thank all the authors who contributed to this book.

M. P. Jahan
June, 2015

CONTRIBUTORS

M. P. Jahan, PhD
Department of Architectural and Manufacturing Sciences,
Western Kentucky University,
Bowling Green, KY 42101, USA

D. Ghodsiyeh, PhD
Department of Mechanics and Aerospace,
Politecnico di Torino,
10129 Torino, Italy

M. Moradi, MSc
Department of Mechanics and Aerospace,
Politecnico di Torino,
10129 Torino, Italy

Dr. sc. Umang Maradia
Institute of Machine Tools and Manufacturing,
ETH Zurich,
Switzerland

Prof. Dr. Konrad Wegener
Institute of Machine Tools and Manufacturing,
ETH Zurich,
Switzerland

Bülent EKMEKCİ, PhD
Department of Mechanical Engineering,
Bülent Ecevit University,
Zonguldak, Turkey

Nihal EKMEKCİ, PhD
Department of Mechanical Engineering,
Bülent Ecevit University,
Zonguldak, Turkey

Hamidullah YAŞAR, MEng
Department of Mechanical Engineering,
Bülent Ecevit University,
Zonguldak, Turkey

Daniel Ghiculescu, PhD
Department of Machine Building Technology,
Polytehnic University of Bucharest,
Romania

Minh Dang Nguyen, PhD
Department of Mechanical Engineering,
National University of Singapore,
Singapore

Mustafizur Rahman, PhD
Department of Mechanical Engineering,
National University of Singapore,
Singapore

Yoke San Wong, PhD
Department of Mechanical Engineering,
National University of Singapore,
Singapore

Harshit K. Dave, PhD
Department of Mechanical Engineering,
Sardar Vallabhbhai National Institute of Technology,
Surat, India

Harit K. Raval, PhD
Department of Mechanical Engineering,
Sardar Vallabhbhai National Institute of Technology,
Surat, India

Keyur P. Desai, PhD
Department of Mechanical Engineering,
Sardar Vallabhbhai National Institute of Technology,
Surat, India

Golam Kibria, PhD
Department of Mechanical Engineering,
Aliah University,
Kolkata, India

Assistant Prof. Ishwer Shivakoti
Department of Mechanical Engineering,
Sikkim Manipal Institute of Technology (SMIT),
Sikkim, India

B. Bhattacharyya, PhD
Production Engineering Department,
Jadavpur University,
Kolkata, India

Mohammed Muntakim Anwar, MSc
Electrical and Computer Engineering,
University of British Columbia,
Vancouver, Canada

Kenichi Takahata, PhD
Electrical and Computer Engineering,
University of British Columbia,
Vancouver, Canada

John D. Madden, PhD
Electrical and Computer Engineering,
University of British Columbia,
Vancouver, Canada

Asma Perveen, PhD
Mechanical Engineering Department,
Bursa Orhangazi University,
Bursa, Turkey

S. Gopalakannan, PhD
Department of Mechanical Engineering,
Adhiparasakthi Engineering College,
Melmaruvathur, Tamilnadu, India

Tanveer Saleh, PhD
Department of Mechatronics Engineering,
International Islamic University Malaysia,
Malaysia

Pay Jun Liew, PhD
Manufacturing Process Department, Faculty of Manufacturing Engineering,
Universiti Teknikal Malaysia Melaka,
Hang Tuah Jaya, 76100 Durian Tunggal, Melaka, Malaysia.

Jiwang Yan, PhD
Department of Mechanical Engineering, Faculty of Science and Technology,
Keio University,
Hiyoshi 3-14-1, Kohoku-ku, Yokohama 223-8522, Japan

Pegah Kakavand, MSc
Department of Architectural and Manufacturing Sciences,
Western Kentucky University,
Bowling Green, KY 42101, USA

In: Electrical Discharge Machining (EDM)
Editor: M. P. Jahan
ISBN: 978-1-63483-591-6

Chapter 1

DIE-SINKING ELECTRICAL DISCHARGE MACHINING

M. P. Jahan*

Department of Architectural and Manufacturing Sciences, Western Kentucky University, Bowling Green, KY, US

ABSTRACT

Electrical discharge machining (EDM) is the process of removing electrically conductive materials by means of rapid repetitive electrical discharges in the presence of dielectric liquid. Die-sinking EDM and wire-EDM are the two major types of EDM used widely in industries for various applications. This chapter will provide an overview of the die-sinking EDM. The chapter covers the history of EDM, working principle of the die-sinking EDM, brief overview of the basic components of the die-sinking EDM system, and brief description of the operating parameters and machining characteristics of sinking EDM. The chapter also covers some of the important applications of die-sinking EDM reported in both industries and academia. The chapter concludes with highlighting the recent advances and future scopes in the area of die-sinking EDM.

Keywords: Die-sinking EDM, EDM system components, operating parameters, machining characteristics, applications of die-sinking EDM

HISTORY OF EDM

Electrical Discharge Machining (EDM) is one of the earliest and most widely used non-conventional machining processes, having an inception 75 years ago in a simple die-sinking application. Nowadays, EDM is used extensively for many important applications in die and mold, aerospace, automotive, micro-electronic and biomedical industries. The origin of the EDM process can be considered as early as around the year 1700, when the scientist Benjamin Franklin reported the phenomenon of metal erosion by electrical sparks. Later in 1770, the scientist Joseph Priestly discovered the erosive effect of electrical discharges [1].

* Corresponding author: M.P. Jahan, E-mail: muhammad.jahan@wku.edu.

However, the process was not established until 1940's, when two Russian scientists, Dr. B.R. Lazarenko and Dr. N.I. Lazarenko first applied it to a machine for stock removal by controlled erosion through a series of sparks [2]. The Lazarenko scientist couple developed a controlled process of electrical discharge machining to investigate the destructive effects of electrical discharges and to identify how to remove materials to produce any desired shape by controlling the spark discharges. During their effort, they invented a simple servo controller to maintain the gap between the tool and the workpiece, which reduced the arcing and made the EDM process more profitable.

The die-sinking EDM process was invented as early as in the 1940's [3] with the advent of the pulse generators, planetary and orbital motion techniques, CNC and the adaptive control mechanism. The wire-EDM process was invented in the 1970's [4] that includes powerful generators, new wire electrodes, better mechanical concepts, improved machine intelligence, and better flushing. "Charmilles" was the first industry to manufacture first EDM machine for commercial use in 1952 [5]. The company presented the newly developed EDM machine for the first time at the European Machine Tool Exhibition in 1955 [5]. In 1969, another company "Agie" launched the world's first numerically controlled wire-cut EDM machine [5]. "Seibu" developed the first CNC wire EDM machine in 1972 and the first system was manufactured in Japan [5]. The micro scale EDM was first demonstrated by Kurafuji and Masuzawa [6] in 1968, when they drilled a minute hole in a 50 μm thick carbide plate. Since then significant amount of research efforts has been focused on the development of EDM and micro-EDM processes.

PRINCIPLE OF EDM AND DIE-SINKING EDM

The basic principle of EDM is necessarily same for both die-sinking EDM and wire-EDM with the difference in setup. Electrical Discharge Machining (EDM) process removes electrically conductive materials by means of rapid repeatitive spark discharges in the presence of dielectric liquid, while a voltage difference is applied between the electrode and workpiece. Figure 1 shows the schematic representation of basic principle of EDM [7]. In the EDM process a voltage difference is applied between the electrically conductive tool electrode and a workpiece material at a certain gap between the tool and electrode. As the tool electrode moves towards the workpiece in the presence of a dielectric fluid (usually deionised water or hydrocarbon oil, which acts as an insulator and coolant), a column of intense electromagnetic flux is formed upon nearing the metal work piece. The electrical field is the strongest (energy density of 10^{11} - 10^{14} W/m^2) at the point where the distance between the electrode and workpiece is minimum [8]. As the insulating effect of the dielectric fluid breaks down under high electric field, it causes a single spark to be discharged between the tool electrode and the workpiece. This single spark (which is 6000-12000°C depending on the machining conditions [9]), which occurs within a small gap between the electrode and the workpiece known as the spark gap, vaporizes and melts the material within this spark gap, forming a crater in the process. Due to the heat of the spark, the electromagnetic flux is broken down and therefore the spark breaks down, going back to the initial conditions again. At the same time, the dielectric fluid cools down the spark gap area and the electrode retracts away from the workpiece. This cycle is repeated many times during the machining process.

The magnitude of the current, which can be found by the open gap voltage and the resistance, determines the energy of the spark and therefore the spark gap area. The time period at which the current is turn on and off is known as the pulse duration (T_{on}) and pulse interval (T_{off}) time, and contributes to allowing the spark gap area to regenerate the conditions necessary for sparking again. Finally, the crater is formed by the implosion of the vapor bubble. The expelled metal solidifies into tiny spheres dispersed in the dielectric, which is flushed away by the dielectric during the pulse interval. The volume of material removed per discharge is typically in the range of 10^{-6}–10^{-4} mm^3 [8] depending on specific application. Since the shaped electrode defines the area in which the spark erosion will occur, the accuracy of the part produced after EDM is fairly high.

Die-sinking EDM, also called sinker EDM, cavity type EDM or volume EDM is one of the two most common types of EDM. In die-sinking EDM, the electrode is shaped and produces its negative form into the workpiece. The die-sinking EDM is a reproductive shaping process in which the form of the electrode is mirrored in the workpiece. The die-sinking EDM is more commonly used for machining parts with complex 3D shapes, often with small or odd shaped angles. The wear has to be very low, in order to keep the electrode's original shape unmodified during the whole machining process. In addition, it is important to monitor the gap conditions (voltage and current) and synchronously controls the different axes to machine the mirror image of the tool into the workpiece. Figure 2 shows the basic schematic representation of the die-sinking EDM [10].

DIE-SINKING EDM SYSTEM COMPONENTS

Figure 3 shows the schematic diagram representing the die-sinking EDM system. The basic components of a die-sinking systems are workpiece, electrode and dielectric, X-Y positioning or machine bed, servo controller, pulse generator, work tank or dielectric resorvoir, dielectric pump and filter [11]. The following section will provide a brief overview of different components of the die-sinking EDM system.

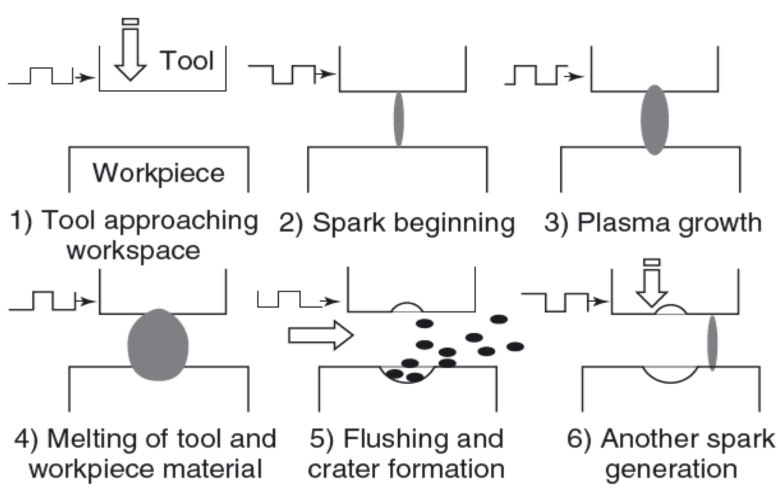

Figure 1. Schematic representation of the basic principles of EDM [9].

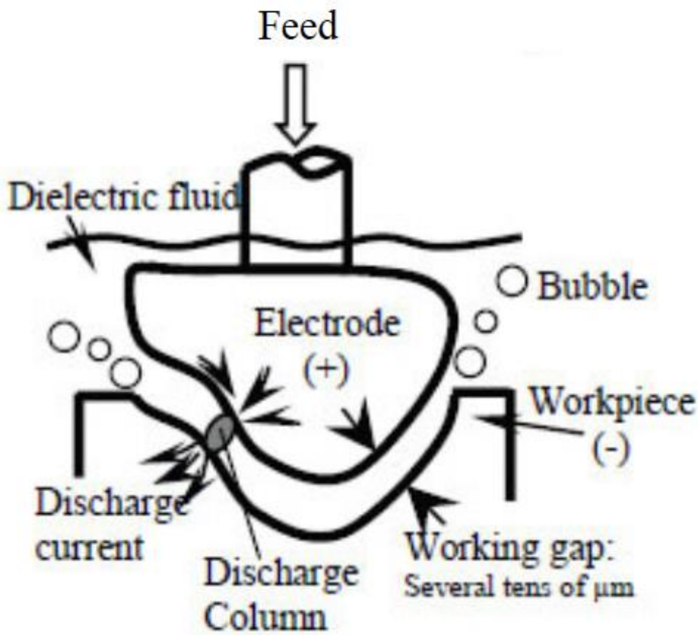

Figure 2. Schematic showing the principle of die-sinking EDM [10].

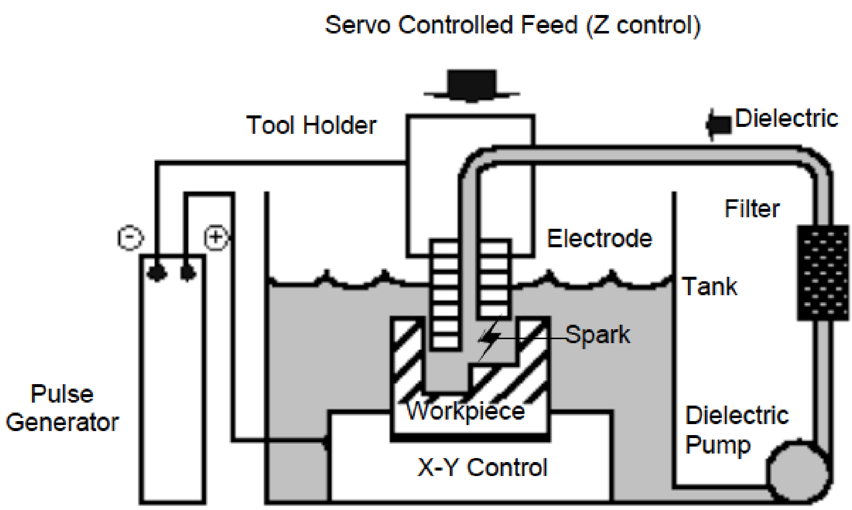

Figure 3. Schematic representation of the die-sinking EDM system.

Workpiece, Electrode and Dielectric

Workpiece Selection

The EDM process is capable of machining any electrically conductive materials irrespective of the hardness, strength and other mechanical properties. Therefore, the major requirement for any workpiece material in EDM is the electrical conductivity. However, as

EDM is an electro-thermal process of removing materials, both the electrical and thermal properties of the workpiece materials play role in determining the machining performance of that material. As a result, during the selection of workpiece material one has to consider following points as well as the purpose for which material is being selected [12]:

- Material
- Composition
- Dimension
- Material properties:
  - Density (kgm^{-3})
  - Melting point (^0C)
  - Boiling temperature (^0C)
  - Specific heat ($Jkg^{-1}K^{-1}$)
  - Hardness
  - Heat of formation ($kJmol^{-1}$)
  - Young's modulus (GPa)
  - Tensile strength (kg/mm^2)
  - Compressive strength (kg/mm^2)
  - Toughness (kg/mm^2)
  - Transverse rupture strength (MPa)
  - Coefficient of thermal expansion (K^{-1})
  - Thermal conductivity ($Wm^{-1}K^{-1}$)
  - Electrical resistivity (Ωm)

Tool Electrode Selection

Electrode selection is one of the very important factors to consider in die-sinking EDM. As during the EDM process, the material is removed from both workpiece and electrode simultaneously, it is important to select materials with higher wear resistance as electrode. One of the major disadvantages of EDM compared to the conventional machining processes is the higher electrode wear that sometimes makes the production process expensive. There have been many research on investigating the effect of electrode materials properties on the EDM performance and selection of optimum EDM electode material for any particular application [13]. Therefore, the electrode should be selected depending on type of workpiece to be machined and the following factors:

- Type of workpiece
- Metal removal rate
- Resistance to wear
- Surface finish desired
- Fabrication costs
- Raw materials costs
- Electrical properties: electrical conductivity or resistivity
- Thermal properties: melting temperature, specific heat, boiling point

There are mainly two major group of materials used as electrode material for the die-sinking EDM: metallic and graphite electrodes. The graphite electrodes have comparatively lower wear rate, therefore, are being used extensively for roughing operations. On the other hand, most of the metallic electrodes suffer from higher electrode wear. However, the electro-thermal properties of metallic electrodes made them suitable candidate for finishing operations in die-sinking EDM. Table 1 presents a comparative evaluation of the metallic and graphite electrodes based on their costs and performance [14]. A summary of the recommendation of electrode materials for some widely used workpiece materials is provided in table 2 [14]. The performance comparison of three most widely used electrode materials: graphite, copper and copper tungsten is provided in table 3 [15].

Table 1. Comparison of metallics and graphites electrode [14]

Metallic electrodes	Graphite electrodes
1. Low cost 2. High strength 3. Higher degree of machining safety 4. Good for inexperienced operators 5. Relatively clean, mirror finishes 6. Low grindability index 7. Slower machining speed and MRR 8. Higher wear	1. High cost 2. High strength 3. Lower degree of machining safety 4. Need experienced operators 5. Dust remains after machining 6. Good machinability 7. High machining speed and MRR 8. Excellent wear resistance

Table 2. Recommendation of electrodes for different types of workpiece [14]

Workpiece	Electrode	Electrode polarity	Recommended frequencies for rouging	Recommended frequencies for finishing
Steel	Graphite	Positive	Low	Med/High
Aluminium	Cu/CuW	Positive	Low	Med/High
Copper	Cu/CuW	Negative	High	High
Titanium	Cu/CuW	Negative	High	High
Carbides (WC)	Cu/CuW	Negative	High	High
Copper tungsten	Cu/CuW	Negative	High	High

Table 3. Comparison of the performances of graphite, copper and copper tungsten electrode in die-sinking EDM [15]

EDM characteristics parameters	Performance of graphite electrode	Performance of copper (Cu) electrode	Performance of copper tungsten (CuW) electrode
Material removal rate (MRR)	Highest among three electrode	Medium	Lowest
Relative wear Ratio (RWR)	Medium	Highest	Lowest
Surface roughness Parameter (R_a)	Highest value of R_a Poorest performance	Lower value, Best performance	Performance between the two

Selection of Dielectric Fluid

As both the electrode and workpiece are electrically conductive in EDM, upon applying the voltage there would be generation of uncontrolled sparking without the presence of dielectric. The dielectric material serves as insulator, which only breaks down during the application of voltage allowing controlled sparking to remove the materials from workpiece. In the die-sinking EDM, the machined zone is completely immersed inside the dielectric liquid. The dielectric liquid not only serves a purpose of controlled sparking, but also act as coolant and helps to flush the debris out of the machined zone. Therefore, the selection of dielectric fluid is an important task in the die-sinking EDM operation. The important properties of dielectric that should be considered during selection are chemical compositions, viscosity, dielectric strengths, and cooling rates. For better EDM performance, the following points should be considered during the selection of dielectric fluid [14]:

- Flash point: The higher flash point temperature is desirable for safety purposes.
- Dielectric strength: High dielectric strength can help in finer degree of control.
- Viscosity: The lower the viscosity of the dielectric fluid, the better the accuracy and finishing as it is much easier to flush small spark gaps with a lighter and thinner oil.
- Specific gravity: Lower specific gravity is desirable for better performance.
- Color: Dielectric fluid color should be as clear as possible.

The most frequently used dielectric fluids in the die-sinking EDM are mineral, hydrocarbon or EDM oil, kerosene and di-ionized water. Both water and oil has some advantages and disadvantages, which need to be considered for the selection of appropriate dielectric for EDM operation. A comparative study on the performance of water and oil as dielectric fluid is provided in table 4 as a guideline of selection procedure:

Table 4. Comparison of the performances of oil and water as dielectric for die-sinking EDM

Oil as a dielectric fluid	Water as a dielectric fluid
1. Do not cause any electrolytic damage	1. Electrolysis occur which may cause electrolytic damage
2. Become more susceptible to thermal damage and micro-cracking	2. May cause corrosion and rust due to electrolysis
3. Can make the EDMed surface more harder and hence more brittle	3. After machining the surface is not so hard and brittle
4. Limited cutting speed	4. Cutting speed may be high using water as a dielectric fluid
5. Better surface finish can be obtained	5. Surface becomes rougher after EDM
6. More frequently electrodes are used as positive polarity if oil is used as dielectric	6. In water as dielectric fluid, normally electrodes are used as negative polarity
7. Less electrode wear	7. Electrode wear is severe
8. Lower operating and maintenance costs	8. High operating and maintenance costs

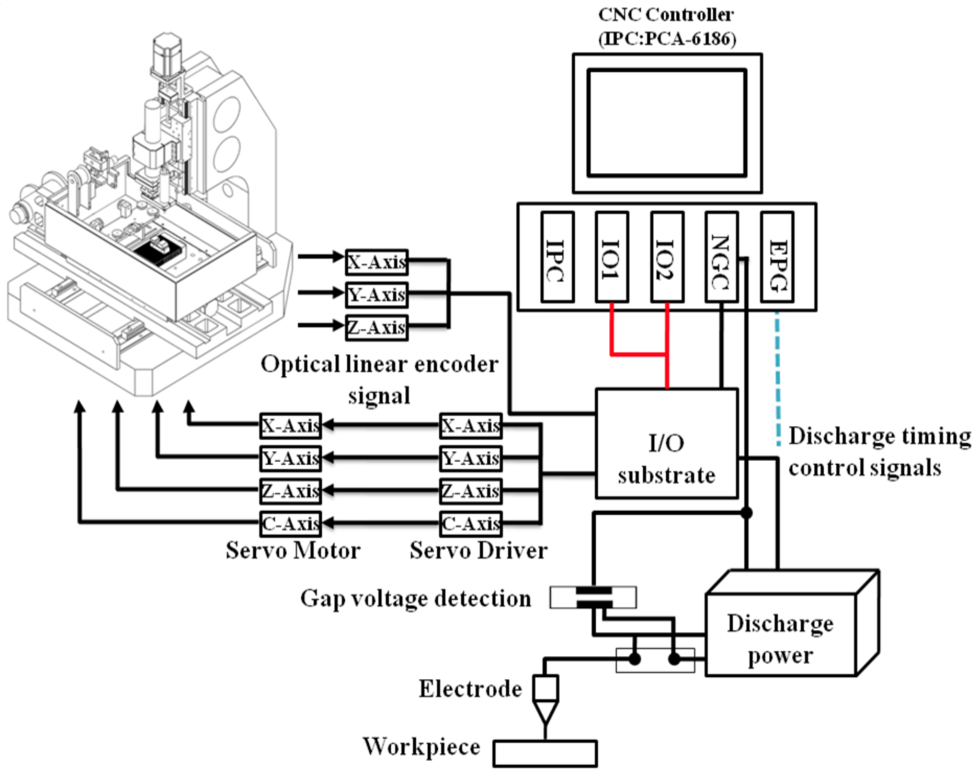

Figure 4. Schematic of the die-sinking EDM control system [16].

X-Y Positioning or Machine Bed

In modern die-sinking EDM, the X-Y positioning of the electrode and workpiece is necessary for machining complex shapes. The X-Y positioning is used to locate the position where the reverse image of the tool shape will be machined. The X-Y positioning can be done by installing machine bed or table for mounting the workpiece. In some of the modern computer numeric controlled (CNC) machine the X-Y positioning is placed with a system that moves the entire servo head. The X-Y positioning table has the facility (i.e., T-slots or tapped holes) of fixing the workpiece tightly with the table surface. Also it provides sub micron accuracy on the positioning of the workpiece. Usually, in die-sinking EDM the work tank is attached to the X-Y positioning table, and moves with the movement of the table.

Servo Control System

The servo control system is an important component of the die-sinking EDM system. The servo control system is an automatic system that maintains the proper spacing between the electrode and the workpiece during machining to ensure effective sparking. The servo control system is designed for working effectively with a wide range of electrodes ranging from several inches to micron sizes. During the EDM operation, the servo control system ensures that the electrode moves towards the workpiece, perform the efficient sparking and retract the electrode when inefficient sparking or arcing is noticed. The servo system is responsible for maintaining stable machining, as unstable machining can damage the machined surface, as well as affect the dimensional accuracy of the machined product adversely. The servo control system also maintains the gap voltage between the electrode and the workpice.

Figure 4 shows the schematic of the total control system of a die-sinking EDM machine [16]. The control system explains how the servo control system works in coordination with CNC controller and pulse generator system. The servo head is the main visible component of the servo control system. The servo head is the part of the machine assembly with electrode holder and electrode that automotically maintain the vertical position of electrode during machining. The die-sinking EDM machines use either electric motor or hydraulic unit to drive the servo-head assembly [11]. The design of the servo control system mainly depends on the type of applications and the size and weight of the electrodes to be maintained by the servo system. Generally, the larger machines with heavy electrodes use hydraulic servo, whereas the machines with smaller electrodes use electric motor driven servo control system [11]. The servo drive is mainly controlled by a micro-controller system, which sends digital signal, translate analog to digital signal by A/D module, and drive the motor by PWM module [17]. The servo control can be operated based on different algorithms or principles, such as: predicting the gap distance and offsetting tool position, ignition delay time, average gap voltage, the average delay time and so on [18].

Power Supply System or Pulse Generator

The power supply is the major component of any EDM system. The power supply of the EDM system is also named as pulse generator or simply generator. The major components of the power supply assembly are DC power source, servo control, AC-electric-power distribution and DC-arc protection unit [11]. There are mainly two major types of pulse generator: resistor-capacitor (RC) type pulse generator and transitor type or electronic switch ON/OFF pulse generator [11].

Figure 5 shows the schematic representation of the transistor type pulse generator [19]. The main components of a transistor pulse generator are the gate drive circuit consisting of several transistors (TR) and current limiting resistors (R) as well as a current transducer (CT). A series of resistances and transistors are connected in parallel between the direct current power supply and the discharge gap. The discharge current increases proportionally to the number of transistors which is switched on at the same time. The switching ON-OFF of gate control circuit is operated by the FET. In order to generate a single pulse, gap voltage is monitored to detect the occurrence of discharge and after preset discharge duration, the FET is switched off.

The transistor type pulse generator is the most widely used pulse generator in conventional die-sinking EDM. The major advantages of transitor type pulse generator is that the pulse duration and interval can be controlled precisely by the elctronic ON/OFF switching. In addition, transistor type pulse generator is able to produce higher discharge energy, thus provides higher material removal rate during the EDM.

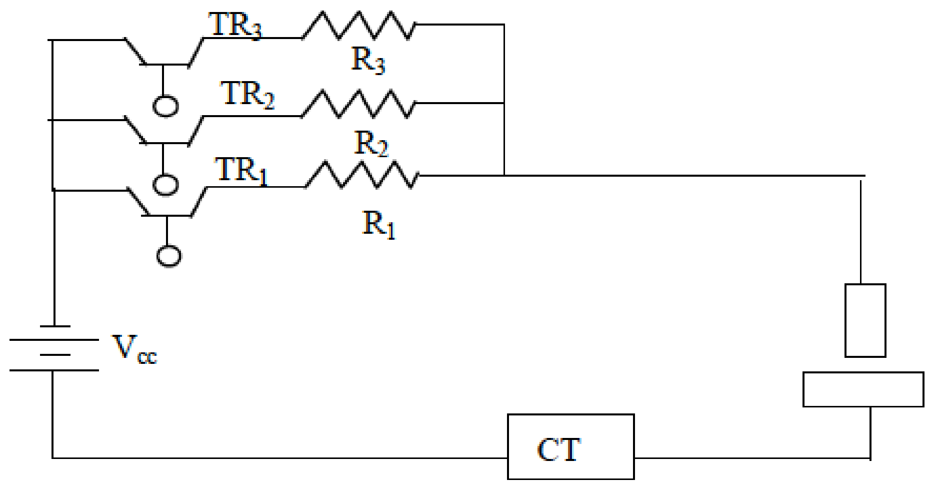

Figure 5. Schematic representation of the basic transistor type pulse generator [19].

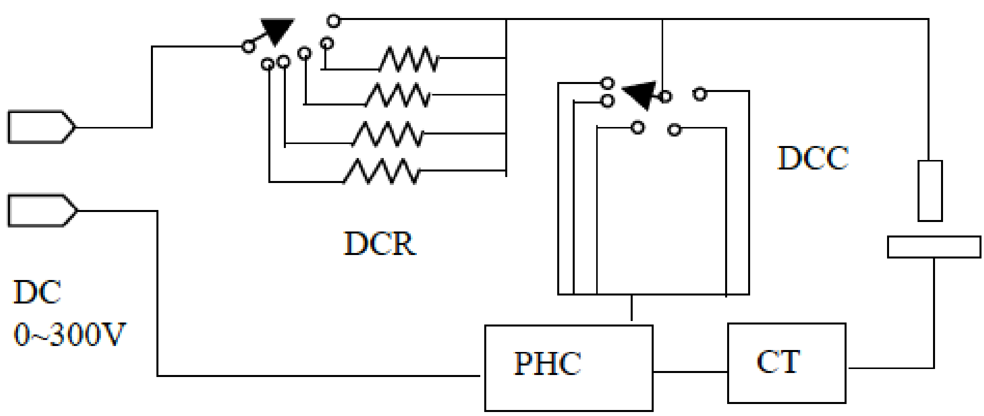

Figure 6. Schematic diagram of RC type pulse generator [19].

Figure 6 shows the schematic representation of the basic RC type pulse generator [19]. The main components of an RC generator are the discharge control resistors (DCR), the discharge control capacitors (DCC), the peak hold circuit (PHC), and the CT. In a RC or relaxation type circuit, discharge pulse duration is dominated by the capacitance of the capacitor and the inductance of the wire connecting the capacitor to the workpiece and the tool [7]. The frequency of discharge (discharge repetition rate) depends upon the charging time which is decided by the resistor (R) used in the circuit. Therefore, "R" should not be made very low because arcing phenomenon can occur instead of sparking and a critical resistance is desirable which will prevent arcing [20]. Discharge energy is determined by the used capacitance and by the stray capacitance that exists between the electric feeders, tool electrode holder and work table and between the tool electrode and workpiece [20].

Although RC type pulse generator was the first type of pulse generator used in the EDM, the discharge energy produced by the RC type is limited. Therefore, very high material removal rate is difficult to achieve by RC type pulse generator. However, the RC type pulse generator is most widely used in the recent micro-EDM machines because of its ability to produce very low level of discharge energy.

Dielectric Circulation and Flushing System

The dielectric circulation and flushing system is responsible for flushing out of removed materials and supplying fresh dielectric to the machining zone. The components of this system are tank or reservoir, dielectric pump, filter, pipe and nozzle. The pump is used to supply the dielectric fluid into the work tank and the filter is used to catch the debris particles from the dielectric and to ensure re-circulation of fresh dielectric to the machining zone. In EDM, the better the flushing condition, the less the off-time required for machining and finally the higher the efficiency the entire EDM operation. The main functions of the dielectric circulation and flushing unit are [14, 15]:

- To distribute the dielectric flow through the spark gap to remove gaseous and solid debris generated during EDM.
- To introduce fresh and clean dielectric fluid to the cut.
- To flush away the chips or metal particles generated in the spark gap.
- To maintain the dielectric temperature well below its flash point.
- To act as a cooler for cooling the electrode and workpiece.

In most of the die-sinking EDM operations, both the electrode and workpiece remain immersed into the dielectric and the flushing occurs due to the jump action of the electrode towards the workpiece. During the jump movement, turbulance is created in the liquid in between the electrode and workpiece to remove the debris particles from the spark gap. However, in modern die-sinking EDM there are mainly three types of flushing. The type of flushing should be selected based on the requirement of the job and applications. The types of flushing are:

- Pressure flushing or injection flushing
- Suction flushing
- Jet or side flushing

The flushing pressure is an important parameter to consider in die-sinking EDM. If the flushing pressure is too low, it is difficult to remove the gaseous and solid debris. On the other hand, excessive flushing pressure can accelerate electrode wear as well as create turbulence in the cavity. The effect of flushing pressure on the machining characteristics, as summerized from the literature, are listed in table 5.

Table 5. Effect of flushing pressure on the machining performance during EDM

Machining characteristics parameter	Effect of flushing pressure
Material removal rate (MRR)	The MRR slightly decreases with higher flushing pressure
Relative wear ratio (RWR)	RWR first decreases and then increases again on the increase of flushing pressure. An optimal flushing pressure can be found for each operation
Surface roughness (R_a)	Surface roughness tends to reduce first then again increase with the increase of flushing pressure.

MACHINING PARAMETERS OF DIE-SINKING EDM

During the EDM process, the machining performance is directly related to the discharge energy generated by the pulse generator. The discharge energy is a combined term that is determined by the operating parameters. As the working principles of transistor and RC type pulse generator are different, the operating parameters that influence the EDM performance are also different. In the following sections the operating parameters for transistor type and RC type pulse generator are discussed seperately.

Parameters for Transistor Type Pulse Generator

In transistor-type generator the discharge energy per pulse can be expressed as [21]:

$$E_p = V_p I_p T_{on} \frac{1}{T_{on} + T_{off}} \tag{1}$$

where, V_p = Voltage of a single pulse, I_p= Current of a single pulse, T_{on} = Pulse on-time, T_{off} = Pulse off-time. Again, $T_{on}/(T_{on}+T_{off})$ can be expressed as duty ratio which is denoted by η. Thus, the equation (1) can be modified as:

$$E_p = V_p I_p \eta \tag{2}$$

Therefore, the gap voltage, peak current, pulse duration, pulse interval and the duty ratio are the major operating parameters in transistor type pulse generator.

Gap Voltage

The gap voltage is defined as the voltage between the electrode and the workpiece during the EDM. Higher voltage settings increase the gap, which improves the flushing conditions and helps to stabilize the machining and increase MRR. But at the same time, higher voltage also contributes to poor surface roughness. Although higher voltage is required for faster machining, it can cause more electrode wear besides providing rougher surface finish. The gap voltage is measured by the unit Volt or [V].

Peak Current

The peak current is defined by the highest level of current that flows through the electrode and the workpiece during the machining. The peak current is responsible for breaking down the dielectric that generates the amount of heat necessary to remove the materials from workpiece. The higher the peak current, the larger is the discharge energy. During each on-time pulse, the current increases until it reaches a preset level, which is expressed as the peak current. Higher currents will improve MRR, but at the cost of surface finish and tool wear. The unit of the peak current is Ampere, which is also denoted as [A].

Pulse Duration

The pulse duration or pulse-on-time is defined as the time period when the pulse current is flowing in between the electrode and the workpiece, the dielectric breakdown occurs and finally removal of materials happen. This time period is the effective time period when machining is carried out in the EDM. The material removal rate is directly proportional to the value of pulse duration. The longer the pulse duration, the longer the curent passing through, and therefore the resulting craters will be broader and deeper. As a result, the surface finish will be rougher. On the other hand, shorter values of pulse duration create comparatively smaller craters which helps to obtain smoother surface finish. Although, higher pulse duration is better for faster machining, excessive pulse duration can be counter-productive by making the machining process unstable [22]. The pulse duration is generally in the unit of micro seconds [μs].

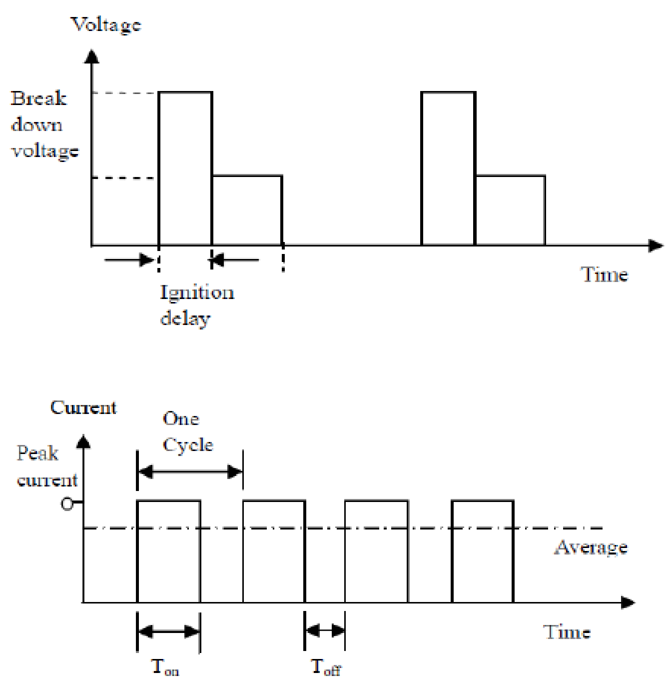

Figure 7. The ideal voltage and current waveforms of a transistor type pulse generator [19].

Pulse Interval

The pulse interval or pulse-off-time is defined as the time interval between two pulse duration. During the pulse interval, the current flowing through the electrode and workpiece is cut off, and hence there is no sparking during pulse interval. However, it is important to have suitable amount of pulse interval for effective flushing of debris from the machined zone. Typically, the higher the values of pulse-off-time, the slower the machining speed. However, too low or insufficient pulse interval makes the machining process instable. Thus, selection of pulse interval is very critical during die-sinking EDM. The unit of pulse interval is same as the unit for pulse duration. The unit is typically micro seconds [μs].

Duty Ratio

Duty ratio is defined by the ratio of pulse duration to the total cycle time (pulse duration + pulse interval). It defines how much percentage of time the current remains ON during a total cycle of sparking. It is the measure of pulse efficiency and usually with the increase of duty ratio the MRR increases.

The figure 7 shows the ideal discharge waveforms of a transistor type pulse generator indicating different operating parameters [19]

Parameters for RC Type Pulse Generator

In RC-type pulse generator the maximum discharge energy per pulse that can be obtained from RC circuit is [21]:

$$E_{ds} = \frac{1}{2} C V_s^{\,2} \qquad (3)$$

Where, C represents capacitance and V_s represents discharging voltage. So in RC-type the performance of the EDM process can be more precisely controlled by knowing the effect of only the discharging voltage and the capacitance.

Discharging and Breakdown Voltage

Discharge voltage is defined as the voltage at which the discharging occurs during EDM. The discharge voltage is dependent upon the spark gap and breakdown strength of the dielectric. Breakdown voltage is the threshold voltage at which the initiation of breakdown occurs. However, before current can flow, the open gap voltage increases until it has created an ionization path through the dielectric. Once the current starts to flow, voltage drops and stabilizes at the working gap level. The higher the value of discharging the voltage, the more the amount of material removal per pulse. The discharge voltage and breakdown voltage is denoted by Volt [V].

Capacitance

The capcitance is an integral component of the RC type pulse generator. The values of capacitance defines the amount of discharge energy per pulse at a given voltage. During EDM operation, the capcitor stores the energy while applying voltage potential and then delivers the discharge energy at the end of voltage pulse. In addition, the values of capacitance determines the discharge frequency. The pulse duration can be minimized to a great extent by using lower settings of capacitance during the EDM. That's why the RC type pulse generator is found to be more suitable for micro-EDM. Usually, the higher the values of capacitance, the higher the discharge energy, the faster the machining process. The unit of capacitance is denoted by pico Faraday (pF).

The figure 8 shows the ideal discharge waveforms of a RC type pulse generator indicating different operating parameters [19]

Gap Control Parameters

Although the gap control parameters are not considered as major operating parameters during the die-sinking EDM process, they play an important role in determining the machining stability and speed [23]. The main objective of all the gap control parameters is to monitor and control the gap distance and gap states. The gap distance is very important to consider for obtaining higher material removal rate (MRR) as well as high quality surface finish. In EDM if the gap distance is too small, the percentage of ineffective discharging pulses; short-circuiting and arcing increase which causes the machining process to become unstable. During these ineffective pulses, more materials are removed from tool electrode instead of removing materials from the workpiece. Therefore, the MRR decreases as machining time increases in addition to increase of tool wear ratio (TWR). On the contrary, if the gap distance is very high, numbers of open pulses increase that reduce the MRR significantly. To maintain continuous spark in between the electrode and workpiece, the speed of the Z-axis or tool electrode is controlled based on the following equation [20]:

$$F_Z = k\,\mathrm{sgn}[V_{gap} - V_{th}] \tag{4}$$

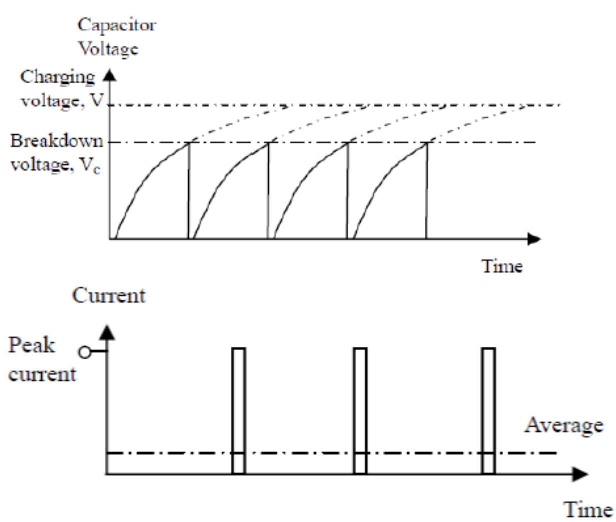

Figure 8. The ideal voltage and current waveforms of RC type pulse generator [19].

Where, F_Z is the Z-axis feed rate, V_{gap} is the gap voltage between the electrode and workpiece, V_{th} is the threshold value for the gap control and k is a control parameter that determines the speed of the micro-EDM gap control.

Gap Feed Rate

The gap feed rate basically defines the speed at which the tool advances towards the work piece. Having an excessive gap feed rate will increase the possibility of arcing, which then leads to poor machining conditions. The unit of gap feed rate is [mm/s] or [μm/s].

Gap Control Factor, k

The gap control factor also affects the speed at which the tool advances towards the work piece. However, the gap control factor is used with the proportion control program, whereby feed rate is defined as: Feed rate = k [Actual gap voltage – Threshold voltage]. Thus, k is essentially a magnification factor used in the above equation.

Gap Threshold Voltage

The user defines the gap threshold voltage to control the minimum allowable gap distance between the work piece and the electrode. When the gap voltage between the electrode and work piece is above the pre-set threshold voltage, the electrode will then move forward and vice versa. The threshold voltage is normally presented as a percentage of the supply voltage.

PERFORMANCE PARAMETERS OF DIE-SINKING EDM

Material Removal Rate

The material removal rate (MRR) is defined as the volume of material removed over a unit period of time. The MRR is more commonly expressed by the unit [mm^3/min]. The MRR can be calculated by calculating the volume of material from the machined feature geometry or from the weight difference of the workpiece before and after machining. The MRR is an indication of machining speed during EDM. The higher the MRR, the faster the machining speed. A higher value of discharging voltage, peak current, pulse duration, duty cycle and lower values of pulse interval can result in higher MRR. In addition to these electrical parameters, other non-electrical parameters and material properties have significant influence on MRR.

Tool Wear Ratio

The tool wear ratio (TWR) or electrode wear ratio (EWR) or relative electrode wear (REW) is defined as the ratio of volume of materials removed from the tool electrode to that of workpiece. This is a representation of the electrode wear in EDM, and is represented by percentage (%). Although sometimes frontal electrode wear or corner wear is measured (in mm or micron) to represent the electrode wear, the most accurate way of presenting electrode wear is the TWR. This is because during EDM, the electrode wears out from each side of the electrode rather than in a single direction. As it is expected that the electrode wear should be much lower than material removal from the workpiece, the TWR in fact represents the volumetric wear of electrode compared to that of workpiece. Lower value of TWR is always expected as it represents more stable and economic machining during EDM. The TWR is great dependent on the operating parameters. The higher values of gap voltage, capacitance, peak current and pulse duration increase the tool wear ratio. The tool wear ratio also depends on electrode polarity and the electrode materials properties. The volumetric wear ratio of the electrode becomes small for the electrode material with high boiling point, high melting point, and high thermal conductivity [24].

Surface Roughness

The surface roughness is a very important parameter to consider in die-sinking EDM. In most of the die-sinking operation, separate roughing and finishing operation are carried out to complete the final product. The surface roughness is represented by the 'average surface roughness (R_a)', which is measured in micron [μm]. The peak-to-valley surface roughness or maximum roughness (R_{max}) is another way of representing the roughness of the machined surface.

Sometimes, the surface quality is described by more comprehensive term 'surface integrity' which includes surface topography, crater characteristics, recast layer thickness, surface defects etc. along with surface roughness. The surface roughness increases with the increase of gap voltage, capacitance, peak current and pulse duration. In summary, the surface roughness increases with the increase of discharge energy. At higher settings of discharge energy, the crater sizes becomes coarser, which results in higher values of surface roughness [25]. The depth of recast layer is influenced by resistance and capacitance for RC type pulse generator, and by gap voltage, peak current and pulse duration for transistor type pulse generator, as these parameters impact on the discharge energy. Higher discharge energy leads to thicker recast layer [26]. The surface roughness also depends on non-electrical parameters. The surface roughness shows slightly decreasing trend with increasing dielectric flushing pressure. Finally, the surface roughness can vary based on the electrode materials also [25].

The performance of die-sinking EDM can be determined by the above mentioned performance parameters. Normally higher MRR can make the machining faster. On the other hand, for better finishing of the machined surface the value of surface roughness parameter should be lower. For saving the cost of electrodes, the electrode wear should be less. As a result, better performance can be denoted by higher MRR, lower RWR, and low value of R_a. One has to make a combination of the machining parameters to find the optimum performance for any job. The requirements of machining parameters for higher performance are listed in table 6 [15, 27, 28]:

Variations of Die-sinking EDM System

EDM Drilling

The most widely used variation of die-sinking EDM is the EDM drilling. The same die-sinking EDM machine can be used for deep hole drilling in difficult-to-cut materials [32]. This process of deep hole drilling are also termed as micro-EDM drilling. In EDM drilling, electrodes ranging from micro to meso sizes are used to ‘drill’ holes in the workpiece. Both tubular and solid electrodes are used for the drilling purpose. For tubular electrodes, jet flushing inside the tube is used, whereas for solid electrodes dielectric is fed to the machining zone by either suction or injection through pre-drilled holes. In some of the cases, the electrodes that are used for the drilling pupose are machined in the same setup using electrical discharge grinding process. This is done to improve the accuracy of drilling holes and to avoid the breakage of electrode material due to handling [33]. Moreover, in order to ensure the drilling accuracy to reduce the wobbling of the long thin electrode, guides are used with the electrode holder during the EDM drilling operation.

All kinds of micro-holes; e.g., irregular, tapered, curved, as well as inclined holes can be produced by EDM drilling process. Machining of high-aspect-ratio holes for fuel injection nozzle and cooling channels in turbine blades made of hard alloys are few typical applications of EDM drilling. Figure 9(a) shows the schematic of the EDM or micro-EDM drilling process [34].

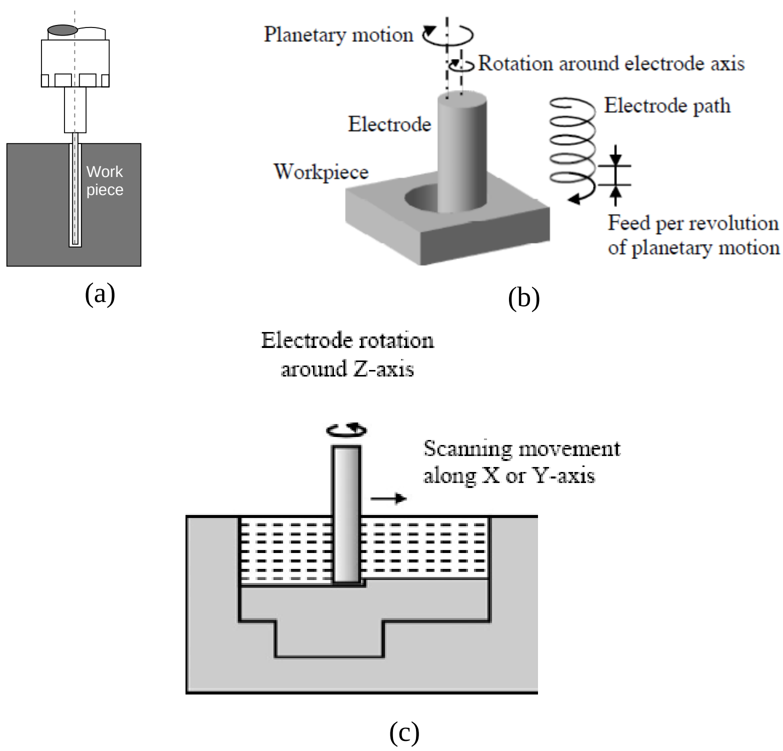

Figure 9. Schematic of (a) EDM drilling process [34], (b) planetary EDM process [36], and (c) EDM milling process [37].

Table 6. Summary of the effect of machining parameters on EDM performance

Machining parameters	To increase MRR (mm^3/min)	To lower the value of RWR (%)	To lower the value of R_a (μm)
Electrode polarity	Negative	Negative	Negative
Open circuit voltage	Low	Low	Low
Peak current	High	Moderate	Low
Pulse duration	High/moderate	Low	Low
Pulse interval	Low	Moderate	Moderate
Duty cycle	High	Low	Low
Pulse frequency	High	Low/moderate	Low
Flushing pressure	Low	Moderate	Moderate

Planetary EDM

One of the major challenges of die-sinking EDM is the flushing out of debris particle from the spark gap. As a result, the researchers have investigated various movement of the tool electrode to improve the flushing efficiency, thus to improve the machining stability and machined surface [35]. A significant enlargement of the field of application of die-sinking EDM or EDM drilling is the planetary EDM. The planetary EDM is also termed as orbital EDM [35, 36]. In the planetary EDM, a spatial translation movement of the tool electrode overlaps the conventional rectilinear sinking movement. The planetary EDM using the movement of the electrode was found to be very useful particularly in drilling of micro-holes as flushing is more difficult for a thin electrode [36]. Adding a relative motion between the electrode and workpiece, other than the electrode feeding motion, produces a wide clearance between them for fluid circulation and then reduces debris concentration, resulting a high material removal rate, low electrode wear ratio and higher machining accuracy. Figure 9(b) shows the schematic representation of the planetary or orbital EDM indicating the motion and path of the electrode [36]. The planetary EDM can be used for machining any circular, rectengular of hexagonal shaped features or holes by controlling the electrode movement during the EDM process.

Milling EDM

EDM milling is another recent variation of the die-sinking EDM process. The EDM milling process follows the algorithm of conventional 3 axis or 5 axis milling process. There are two major advantages of milling EDM over die-sinking EDM. Firstly, the flushing process is improved in the milling EDM due to the movement of the electrode and secondly, the shapes that are hard to replicate using die-sinking EDM can be machined using milling EDM process. Milling EDM is a comparatively newer process, which eliminates the need for complex-shape electrodes usually required in die-sinking. In this process, usually tubular or cylindrical electrodes are employed to produce the desired complex shape by scanning. A cylindrical electrode rotates around its axis (Z-axis) with the scanning movements in X and Y directions. The contour of a particular layer is specified in the part program of CNC. However, electrode compensation is an important factor to consider as electrode length is reduced after scanning every layer.

EDM milling is now replacing the die-sinking EDM in many applications of producing dies and 3D cavities, as die-sinking EDM requires fabrication of complex 3D electrode using other machining processes. Both blind 3D cavities and through structures can be machined using the EDM milling process. The application of EDM milling is more pronounced at micro-scale, as fabrication of microelectrodes with 3D features for die-sinking micro-EDM is a real challenge. Figure 9(c) shows schematic representaion of the EDM milling process [37].

(a)

(b)

Figure 10. Application of die-sinking EDM in mold making; (a) chromium copper electrode and fabricated mold for cell phone case [38], (b) electrode and the fabricated die [39].

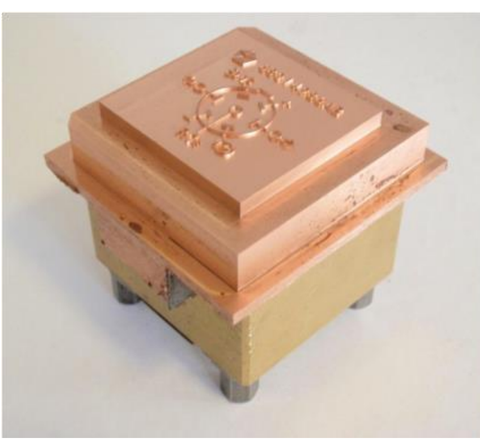

(a)

(b)

Figure 11. (a) A typical die-sinking EDM tool with the reversed features for engraving into the workpiece [40], (b) A complex engraved surface by die-sinking EDM [41].

INDUSTRIAL APPLICATIONS OF DIE-SINKING EDM

Mold Making and Injection Molding

The most common application of die-sinking EDM is the machining of complex shaped dies in difficult-to-cut materials. The mold is fabricated using the die-sinking EDM process and is used for mass fabrication of plastic or aluminium parts using the molds or dies. In injection molding the dies require many complex shapes with various depths which are difficult and time consuming to fabricate using conventional machining processes. Die-sinking EDM can fabricate those complex shapes with desired accuracy. Some of the common examples of mold making using die-sinking EDM are dies for cellular phone, injection molding dies etc. Figure 10 shows an example of mold making for cell phone and plastic injection molding. Figure 10(a) shows the electrode and the fabricated mold for mass fabrication of cell phone case machined by die-sinking EDM [38]. Figure 10(b) shows the electrode and fabricated mold for another complex shaped die [39].

Engraving

As die-sinking EDM can replicate or copy exactly the same features from the tool electrode to the workpiece, it is used for engraving of different letters, writing or logos on the difficult-to-cut materials. The engraving of difficult-to-cut materials by conventional machining process is a challenge. The die-sinking EDM can easily solve this problem because of its non-contact mechanism of material removal. Figure 11 shows examples of engraving using the die-sinking EDM process.

Fuel Injector or Automotive Nozzles

One of the major advantages of EDM over conventional manufacturing processes is that EDM is capable of machining high aspect ratio micro-holes in difficult-to-cut materials. Automotive fuel injector needs very small, yet high aspect ratio holes to supply the fuel inside the engine. The micro-EDM drilling, which is considered as one of the variation of the die-sinking EDM setup, can be used to machine holes as small as 50 micron with more than aspect ratio of 20 [29]. In addition to automotive fuel injector, those deep holes can be machined on other parts and components for various lubrication and cooling purposes [30]. Figure 12 shows application examples of deep hole EDM drilling. Figure 12(a) shows a diesel fuel injector with holes machined by the EDM process [42]. Figure 12(b) shows the machining of deep holes on top of a ball bearing using the EDM drilling process [43].

Mass Fabrication of Cooling Holes

Another important applications of EDM drilling is the fabrication of arrays of holes for various important applications, such as aerospace and automotive cooling holes in difficult-to-cut materials. The 5 axis computer numeric controlled (CNC) EDM is capable of machining both vertical and inclined holes at any surface, providing the flexibility of machining cooling holes. Figures 13(a) and (b) show the fabrication of vertical and inclined arrays of holes respectively, which are machined using the EDM drilling for different applications. Figure 13(a) shows the fabrication of arrays of holes for semiconductor injector [44]. Figure 13(b) shows an aerospace turbine blade made of high strength materials with cooling holes on it [45].

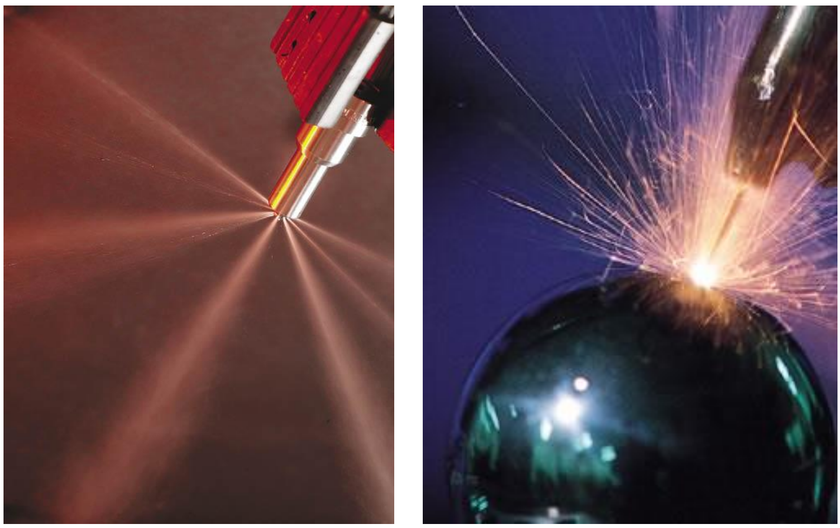

(a) (b)

Figure 12. (a) Diesel fuel injector with holes made via EDM equipment from AA EDM Corp. Photo courtesy AA EDM [42], (b) Difficult hard surfaces are easily drilled with small hole EDM, 0.040" diameter hole on center of .5000" diameter ball bearing [43].

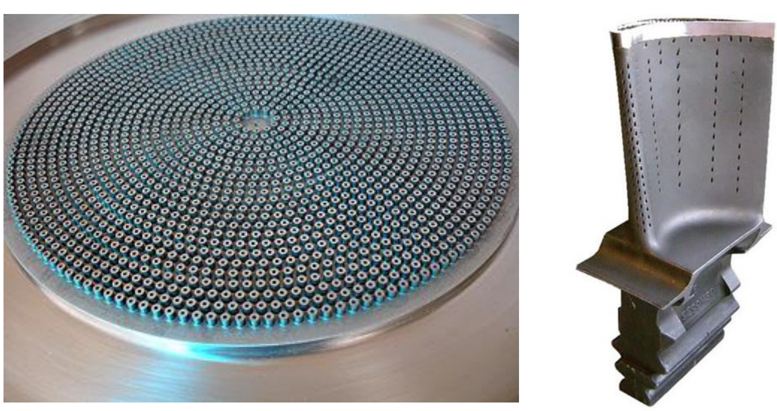

(a) (b)

Figure 13. (a) Arrays of vertical holes for semiconductor injector [44], and (b) arrays of inclined holes on turbine blade for aerospace cooling holes [45].

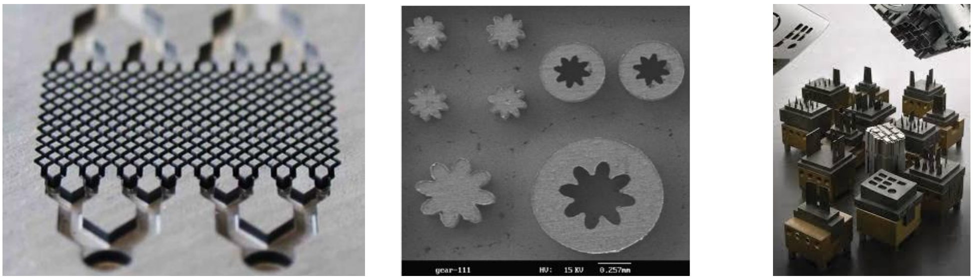

(a) (b) (c)

Figure 14. (a) Die-sinking electrode for micro-mixing device made of fine-grained graphite [46], (b) fabricated micro-gear-electrodes [46], and (c) various complex shaped electrodes for commercial die-sinking EDM [47].

Complex Micro and Meso Structures

The die-sinking EDM can be used to machine almost any complex shaped structures at micro and sub micron scale. The most important challenge is to create the complex shaped electrode that would be copied in the difficult-to-cut materials. However, the major advantage of die-sinking EDM is that the tool electrode can be softer materials than the workpiece, which allows to prepare the complex shaped electrode easily using softer material. Once the complex shaped electrode is fabricated, it would be machined on the workpiece material using the die-sinking EDM. Figure 14 shows the complex shaped electrodes in comparatively softer graphite materials for using in the die-sinking EDM of harder materials [46]. Figure 15 shows examples of complex shaped micro structures machined by die-sinking EDM [47].

Medical Instruments and Microelectronic Parts

The application of high strength alloy with excellent corrosion resistance (i.e., Titanium alloy, Stainless steel etc.) demands the use of non-conventional machining processes in the fabrication of medical instruments. EDM has the capability of machining any electrically conductive materials, particularly those used in the medical industries. Therefore, many medical instruments are fabricated by the EDM process. Most of the medical instrument needs machining operations from both die-sinking and wire EDM. Figure 16(a) shows some medical instruments fabricated by combined die-sinking and wire-EDM processes [50].

Another important application is the fabrication of complex shaped features in semiconductor materials using the EDM process. The wire-EDM process is used to cut the outside profile of the parts, whereas the inside profiles and holes are created by the die-sinking EDM process. Figure 16(b) shows the microelectronic parts and components machined by combined wire and die-sinking EDM processes [50].

(a)

(b)

Figure 15. (a) Complex shaped feature machined by die-sinking EDM [48], and (b) Complex shaped golf ball mold in copper machined by die-sinking EDM [49].

(a)

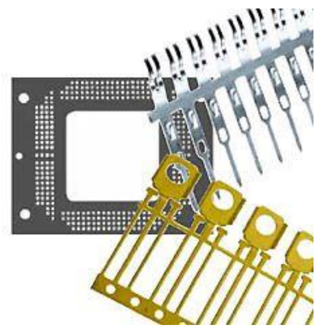

(b)

Figure 16. (a) Medical instruments and (b) microelectronic components fabricated by the EDM process [50].

RECENT ADVANCES IN DIE-SINKING EDM

There have been extensive research on the improvement of process and enhance application areas for the die-sinking EDM. The scaling down of the die-sinking EDM to the micro and nano level has been one of the major advances in die-sinking EDM. The micro and nano die-sinking EDM has been successfully demonstrated indicating the capability of fabricating complex micro and nano features in electrically conductive materials. Another recent advances in the area of die-sinking EDM are the development of compound and hybrid EDM processes. The main objective of the compound and hybrid machining processes is to minimize shortcomings of EDM or solving a specific issue in EDM, by integrating other machining processes with EDM or assistance from external sources. Compound machining is defined as the combination of two different machining processes in a single setup applied one after another. On the other hand, the hybrid machining process is defined as the integrated application or combination of different physical active principles in a single process.

In the following sections some recent advances in the area of die-sinking EDM will be presented. Each section will include the working principle of the process along with examples of important applications of the new process.

EDM-ECM Compound Process

One of the major shortcomings of the die-sinking EDM is the surface finish generated by the process. As EDM is an electro-thermal process of removing materials, the surface created by the process is composed of uniformly arranged craters along with sub-surface white layer and heat affected zone. Therefore, in recent years electro-chemical machining process (ECM) has been introduced with the EDM process to improve the surface finish as well to reduce the surface and sub-surface damage. The ECM process has been reported to be applied either concurrently or after the EDM process. The concurrent EDM-ECM is considered a hybrid process, where as sequencial EDM and ECM is considered as a compound machining process. Figure 17(a) shows the change of current due to discharge and dissolution in two stages of EDM and ECM [51]. Figure 17(b) presents the machined surface after die-sinking EDM, which clearly shows the craters generated from electrical discharges. Figure 17(c) shows the machined surface after EDM followed by the ECM finishing process. The improvement in the surface finish of the EDM-ECM compound process compared to that of EDM process along can clearly be seen from figures 17(b) and (c) [52].

Vibration-Assisted Die-sinking EDM

Another problem of the die-sinking EDM is the proper flushing out of debris from the small spark gap between the electrode and the workpiece. The flushing problems reduce the productivity by making the EDM process instable in addition to damaging the surface finish. In order to solve this problem, a new hybrid EDM process has been proposed. In this process either the workpiece or the electrode material is subjected to vibration, which helps in flushing out of debris from the small spark gap by creating turbulance in the dielectric [30]. The processs is termed as vibration-assisted EDM. Two major applications of vibration-assisted EDM are reported to be the machining of complex shaped micro-structures and machining of deep and high-aspect-ratio micro-holes, where the flushing out of debris become challenging. Figure 18(a) shows the working principle of vibration-assisted die-sinking EDM, where the workpiece is subjected to vibration during the EDM process with the help of peizoelectric actuator [53]. The machining of complex-shaped micro-structure and high-aspect-ratio holes are shown in figures 18(b) [53] and 18(c) [30] respectively.

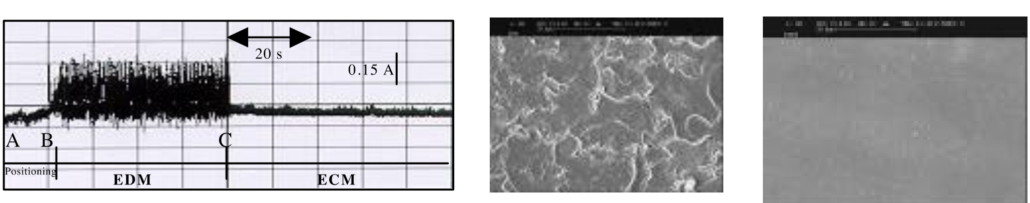

(a) (b) (c)

Figure 17. (a) Typical sparking in EDM and EDM processes [51], (b) surface generated by single EDM process, and (c) surface generated by the EDM-ECM compound process [52].

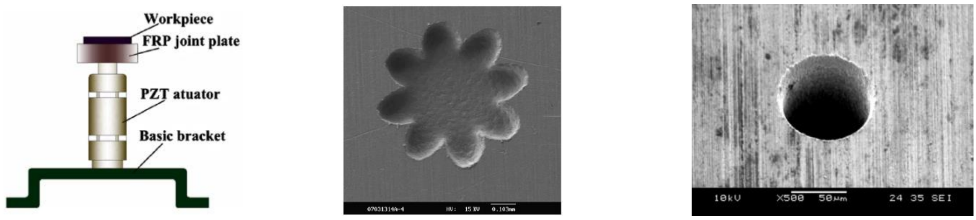

Figure 18. (a) Working principle of work-piece vibration-assisted die-sinking EDM [53], (b) fabrication of blind micro-structure/micro-mold using workpiece vibration-assisted EDM [53], (c) machining of high-aspect-ratio micro-holes [aspect ratio 16.7] in difficult-to-cut tungsten carbide using workpiece vibration-assisted micro-EDM [30].

Powder-Mixed Die-sinking EDM

Power-mixed die-sinking EDM is another recent advances to improve the surface finish in the EDM process. In this hybrid process, the electrically conductive or semi-conductive powder is mixed in the dielectric, which reduces the insulating strength of the dielectric fluid and increases the spark gap between the tool and workpiece. Enlarged spark gap makes the flushing of debris easier. As a result, the process becomes stable, improving the material removal rate (MRR) and surface finish [54]. The sparking is uniformly distributed among the powder particles in the spark gap thus reducing the intensity of a single spark, which results in uniform shallow craters instead of a single broader crater. Thus the surface finish improves. There may be some abrasive actions of the powder particles also during the finishing, which reduce the crater boundaries thus making the surface shiny. Figure 19(a) shows the working principle of powder-mixed micro-EDM [55]. The improvement in surface finish after applying powder-mixed dielectric is shown in figure 19(b) and (c) [56].

Micro and Nano Die-sinking EDM

Due to the growing trend of miniaturization, research has been carried out for applying the electro-discharge machining process at micro and nano scale. Micro-EDM has become a powerful bulk micromachining technique and hence a useful tool for fabricating microstructures for micro-electro-mechanical systems (MEMS). Some of the important applications of micro-EDM in MEMS are shown in figure 20 [57, 58].

The researchers have also been successful to apply electro-discharge machining at nano-scale [59, 60]. A novel nano-machining process termed as “nano-electro-machining (nano-EM) has been developed by modifying a scanning tunneling microscopy (STM) platform. The nano-EM setup can be compared to the conventional die-sinking EDM. In the nano-EM process, Platinum-Iridium [Pt-Ir (80:20)] or Tungsten [99.9%W] is used as a tool electrode, atomically flat gold surface as the workpiece and n-decane as the dielectric, similar to conventional electrical discharge machining (EDM). It has been demonstrated that the process is capable of fabricating sub 10 nm features with consistency and accuracy under both the liquid and air dielectric media [59, 60]. Figure 21 shows the machining examples of dry nano-

EM, where arrays of nano-holes have been fabricated with Pt-Ir tool in atomically flat gold surface using a single step machining [60].

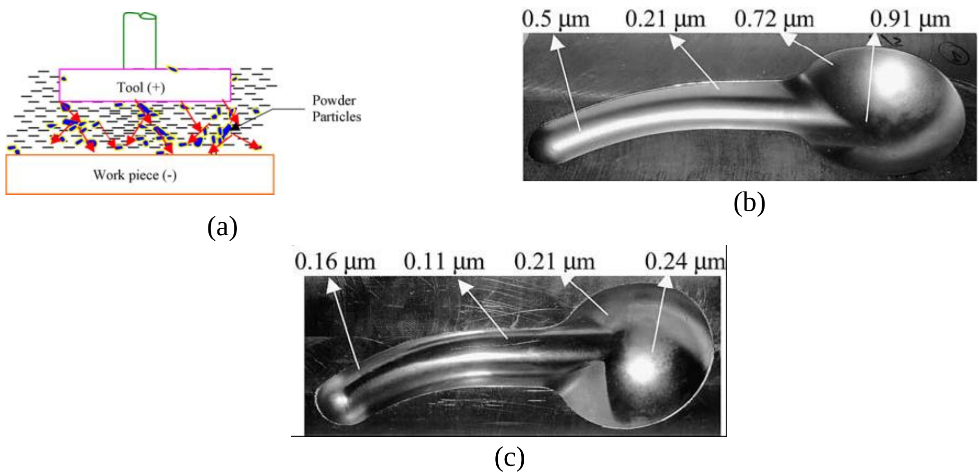

Figure 19. (a) Schematic of powder-mixed EDM [55], (c) mould cavity surface machined using regular EDM, (d) significant reduction of roughness after applying silicon powder-mixed EDM[56].

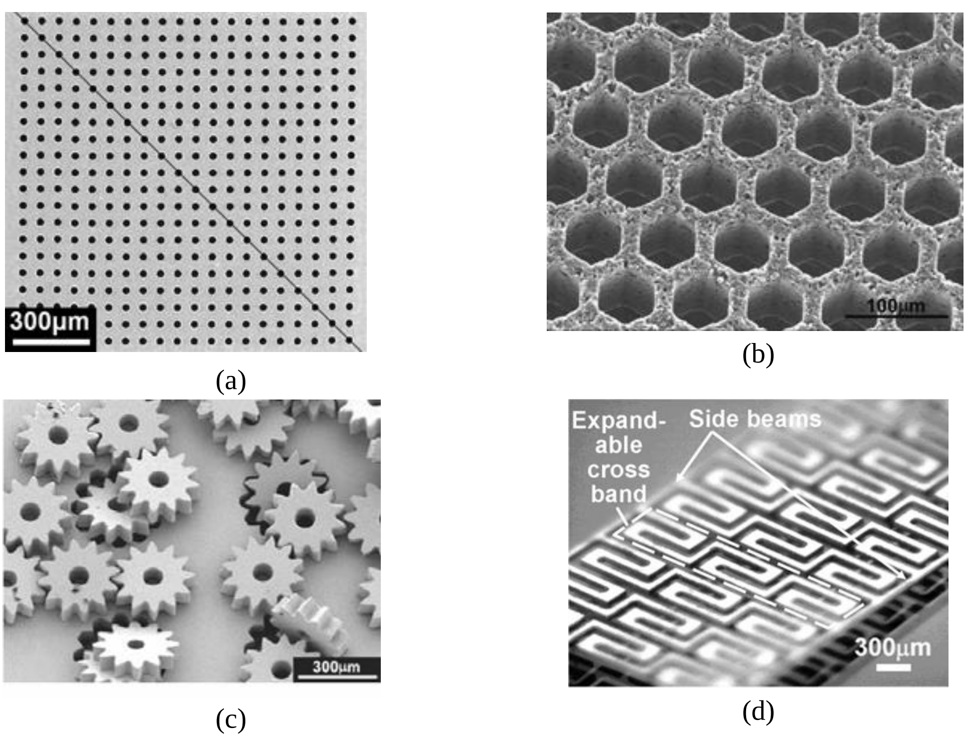

Figure 20. Application examples of micro-EDM in MEMS; (a) micro-hole array (20x20 array, 20-μm diameter, 60-μm pitch) [57], (b) Graphite honeycomb microstructures (hexagonal pitch of 70-μm and wall thickness of 16-μm) formed by batch-mode micro-EDM [57], (c) super-hard alloy gears batch produced by micro-EDM [58] and (d) 7-mm-long planar stent sample as cut by micro-EDM from 50-μm-thick stainless-steel foil [58].

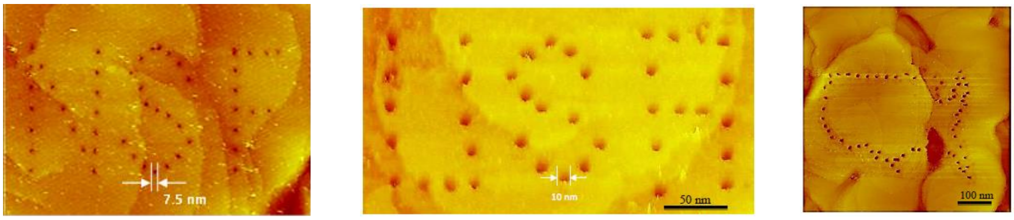

(a) (b) (c)

Figure 21. Machining examples of dry nano-EM; (a) Machining of “NSF” using 50 nano-features with average feature size of 7.5 nm by dry nano-EM, (b) Machining of letters “USA” using 10 nm diameter holes by dry nano-EM process, (c) image of machined “Map of USA” by dry nano-EM [60].

CONCLUSION

Die-sinking EDM is the oldest and the most widely used EDM process. Since its starting in 1943, the process is still being used extensively in industries. The current chapter provided an overview of the die-sinking EDM. The chapter started with the history of the EDM and die-sinking EDM process followed by the working principle and a brief overview of the system components of die-sinking EDM. A detail description of the machining and performance parameters of die-sinking EDM was provided. The variations of the die-sinking EDM were also discussed explaining the working principles and important applications. A section on the important industrial applications of die-sinking EDM were included. Finally, some recent advances in the field of die-sinking EDM has been discussed.

It was found that die-sinking EDM could be applied for a wide variety of applications ranging from microelectronics to the aerospace industries. Die-sinking EDM is an important manufacturing process for mold and die industries and plastic injection molding industries. The die-sinking EDM can be applied successfully at macro, micro and nano scale proving its versatility. The current research trend shows that, EDM process alone sometimes cannot fulfill all the product performance due to its limitation of lower machining speed and comparatively inferior surface finish. Therefore, compound and hybrid micro-machining processes based on EDM have been found to be very useful in solving the problems faced by the EDM process alone.

ACKNOWLEDGEMENT

The authors would also like to acknowledge the partial supports from WKU internal grant RCAP-1 Award #14-8054 and external grant KY-NSF EPSCoR subaward #3048111570-15-094.

REFERENCES

[1] Priestley, J. (1775). Experiments on the circular spots made on pieces of metal by large electrical explosions. *The history and present state of electricity with original experiments*, vol. II, 3rd ed. London.

[2] Lazarenko, B. R. (1943). About the inversion of metal erosion and methods to fight ravage of electric contacts. WEI-Institut, Moscow (in Russian).

[3] Ho, K. H. & Newman, S. T. (2003). State of the art electrical discharge machining (EDM). *International Journal of Machine Tools & Manufacture*, *43*, 1287–1300.

[4] Ho, K. H., Newman, S. T., Rahimifard, S. & Allen, R. D. (2004). State of the art wire electrical discharge machining. *International Journal of Machine Tools and Manufacture*, *44*, 1247-1259.

[5] Webzell, S. (2001). That first step into EDM, *Machinery*, *159*, (4040) Findlay Publications Ltd, Kent, UK, p. 41.

[6] Kurafuji. H. & Masuzawa, T. (1968). Micro-EDM of cemented carbide alloys. *Jpn Soc Electr Mach Eng*, *2*(3), 1–16.

[7] Rajurkar, K. P., Levy, G., Malshe, A., Sundaram, M. M., McGeough, J., Hu, X., Resnick, R. & DeSilva, A. (2006). Micro and Nano Machining by Electro-Physical and Chemical Processes, *Annals of the CIRP*, *55*(2), 643-666.

[8] Descoeudres, A. (2006). Characterization of electrical discharge machining plasmas, *PhD thesis*, *ÉCOLE POLYTECHNIQUE FÉDÉRALE DE LAUSANNE*, THÈSE NO, *3542*

[9] Schumacher, B. M. (2004). After 60 years of EDM the discharge process remains still disputed. *J Mater Process Technol*, *149*, 376–381.

[10] Amorim, F. L., Weingaertner, W. L. & Bassani, I. A. (2010). Aspects on the optimization of die-sinking EDM of tungsten carbide-cobalt, *J. Braz. Soc. Mech. Sci. & Eng.*, *32*(5), 496-502.

[11] Jameson, E. C. (2001). Description and development of electrical discharge machining (EDM), *Electrical Discharge Machining*, *Society of Manufacturing Engineers*, *Dearbern*, *Michigan*, 30-45.

[12] Jahan, M. P. (2009). Micro-EDM-based Multi-process Machining of Tungsten Carbide, *PhD thesis*, Department of Mechanical Engineering, National University of Singapore.

[13] Kunieda, M., Lauwers, B., Rajurkar, K. P. & Schumacher, B. M. (2005). Advancing EDM through fundamental insight into the process. *Annals of CIRP*, *54*(2), 599-622.

[14] Guitrau, E. B. (1997). *The EDM Handbook*, Hanser Gardner Publications, Cincinnati.

[15] Lee, S. H. & Li, X. P. (2001). Study of the effect of machining parameters of the machining characteristics in EDM of tungsten carbide. *Journal of Material processing technology*, *115*, 344-355.

[16] Chu, C-L., Tai, T-Y., Liu, Y-H., Lu, C-T., Chuang, C-H. & Liao, H-W. (2012). Development of High-precision Micro CNC Machine with Three-dimensional Measurement System. *International Journal of Automation and Smart Technology*, *2*(2), 95-101.

[17] Yang, G. H., Liu, F. & Lin, H. B. (2011). Research on an Embedded Servo Control System of Micro-EDM. *Applied Mechanics and Materials*, *120*, 573-577.

[18] Zhang, L., Jia, Z., Liu, W. & Li, A. (2012). A two-stage servo feed controller of micro-EDM based on interval type-2 fuzzy logic. *The International Journal of Advanced Manufacturing Technology*, *59*(5-8), 633-645.
[19] Jahan, M. P., Wong, Y. S. & Rahman, M. (2008). A Comparative Study of Transistor and RC Pulse Generators for Micro-EDM of Tungsten Carbide. *International Journal of Precision Engineering and Manufacturing*, *9*(4) 3-10.
[20] Wong, Y. S., Rahman, M., Lim, H. S., Han, H. & Ravi, N. (2003). Investigation of micro-EDM material removal characteristics using single RC-pulse discharges. *Journal of Materials Processing Technology*, *140*(1-3), 303-307.
[21] Jahan, M. P., Wong, Y. S. & Rahman, M. (2009). A study on the quality micro-hole machining of Tungsten Carbide by micro-EDM process using Transistor and RC-type pulse Generator. *J. Mater. Process. Technol.*, *209*(4), 1706-1716.
[22] Kumar, S., Singh, R., Singh, T. P. & Sethi, B. L. (2009). Surface modification by electrical discharge machining: A review. *Journal of Materials Processing Technology*, *209*, 3675–3687.
[23] Jahan, M. P., Wong, Y. S. & Rahman, M. (2009). Effect of non-electrical and gap control parameters in the micro-EDM of WC-Co. *Journal of Machining & Forming Technologies*, *1/2*, 51-78.
[24] Tsai, Y-Y. & Masuzawa, T. (2004). An index to evaluate the wear resistance of the electrode in micro-EDM. *J. Mater. Process. Technol.*, *149*, 304-309.
[25] Jahan, M. P., Wong, Y. S. & Rahman, M. (2009). A study on the fine-finish die-sinking micro-EDM of Tungsten Carbide using different electrode materials. *Journal of Materials Processing Technology*, *209*(8) 3956-3967.
[26] Klocke, F., Lung, D., Antonoglou, G. & Thomaidis, D. (2004). The Effects of Powder Suspended Dielectrics on the Thermal Influenced Zone by Electrodischarge Machining with Small Discharge Energies, *Journal of Materials Processing Technology*, 149 /1-3, 191-197.
[27] Yan, B. H., Huang, F. Y., Chow, H. M. & Tsai, J. Y. (1999). Micro-hole machining of carbide by electrical discharge machining. *J. Mater. Process. Technol.*, *87*, 139-145.
[28] Puertas, I., Luis, C. J. & Alvarez, L. (2004). Analysis of the influence of EDM parameters on surface quality, MRR and EW of WC-Co. *J. Mater. Process. Technol.*, 153-154, 1026-1032.
[29] Jahan, M. P., Wong, Y. S. & Rahman, M. (2012). Evaluation of the effectiveness of low frequency workpiece vibration in deep-hole micro-EDM drilling of tungsten carbide. *Journal of Manufacturing Processes*, *14*(3), 343-359.
[30] Jahan, M. P., Saleh, T., Rahman, M. & Wong, Y. S. (2010). Development, modeling and experimental investigation of low frequency workpiece vibration assisted micro-EDM of tungsten carbide, *Journal of Manufacturing Science and Engineering*, *132*(5), 054503, doi:10.1115/1.4002457.
[31] Masuzawa, T., Tsukamoto J. & Fujino, M. (1989). Drilling of Deep Microholes by EDM, *Annals of the CIRP*, *38*(1), 195-198.
[32] Liao, Y. S., Chang, T. Y. & Chuang, T. J. (2008). An on-line monitoring system for a micro electrical discharge machining (micro-EDM) process. *Journal of Micromechanics and Microengineering*, *18*, 035009 (8pp).
[33] Tsai, Y-Y. & Masuzawa, T. (2004). An index to evaluate the wear resistance of the electrode in micro-EDM. *Journal of Material Processing Technology*, *149*, 304–309.

[34] Lim, H. S., Wong, Y. S., Rahman, M. & Lee, E. M. K. (2003). A study on the machining of high-aspect ratio micro-structures using micro EDM. *Journal of Materials Processing Technology*, *140*, 318–325.
[35] Yu, Z. Y., Rajurkar, K. P. & Shen, H. (2002). High Aspect Ratio and Complex Shaped Blind Micro Holes by Micro EDM. *CIRP Annals - Manufacturing Technology*, *51*(1), 359-362.
[36] Egashira, K., Taniguchi, T. & Hanajima, S. (2006). Planetary EDM of Micro Holes, *International Journal of Electrical Machining*, *11*, 15-18.
[37] Bleys, P., Kruth, J. P. & Lauwers, B. (2004). Sensing and compensation of tool wear in milling EDM. *Journal of Materials Processing Technology*, *149*, 139–146.
[38] Moldmaster (XXXX), Processed Sample, Retrieved from http:// www.yawjet.com-/en/page/process_samples.html
[39] IS Machine, NOVICK EDM (XXXX), Industries/Applications, Retrieved from http://www.ismachine.com/customer-support/industries-application.html
[40] Revere Industries (XXXX), Electrical Discharge Machining Electrodes, Retrieved from http://www.revere-industries.com/engraving.htm
[41] Koehler (XXXX), Injection Mold Engraving, Retreived from http://www.koehlerinc.com/-engraving.htm
[42] Micromanufacturing (XXXX), Turbocharged Holemaking, Holemaking Methods, Retrieved from http:// www.micromanufacturing.com/ content/ turbocharged-holemaking
[43] XACT EDM (XXXX), EDM Gallery, Small Hole EDM, Retreived from http://www.xactedm.com/edm-gallery/
[44] Wire Cut Company (XXXX), EDM Hole Drilling, Retrieved from http://www.wirecutcompany.com/edm_hole_drilling.html
[45] TTL Solutions (XXXX), Adaptive Machining of Compressor and Turbine Aerofoils, Retrieved from http:// www.ttl-solutions.com/ aerofoils.html
[46] Uhlmann, E., Piltz, S. & Doll, U. Machining of micro/miniature dies and moulds by electrical discharge machining—Recent development. *Journal of Materials Processing Technology*, *167* (2005) 488–493.
[47] Micromanufacturing. (2013). Precision sinker EDMing: no margin for error, 6(6), Retrieved from http:// www.micromanufacturing.com/ content/precision-sinker-edming-no-margin-error
[48] Header Die and Tool (XXXX), Electrical Discharge Machining (EDM), Retrieved from http://www.header.com/capabilities/edm.html
[49] Modern Machine Shop Blog (2010). This Golf Ball Mold is Really Cool, Retrieved from http:// www.mmsonline.com/ blog/ post/ this-golf-ball-mold-is-really-cool
[50] Sarix Micro-EDM machine, Retrieved from http:// www.sarix.com/ index_e.html
[51] Campana, S. & Miyazawa, S. (1999). Micro-EDM and ECM in DI water, *Proceedings of Annual Meeting of American Society of Precision Engineering (ASPE)*.
[52] Zeng, Z., Wang, Y., Wang, Z., Shan, D. & He, X. (2012). A study of micro-EDM and micro-ECM combined milling for 3D metallic micro-structures. *Precision Engineering*, *36*(3), 500–509.
[53] Tong, H., Li, Y. & Wang, Y. (2008). Experimental research on vibration assisted EDM of micro-structures with non-circular cross-section, *Journal of Materials Processing Technology*, *208*(1-3), 289-298.

[54] Jahan, M. P., Anwar, M. M., Wong, Y. S. & Rahman, M. (2009). Nanofinishing of hard materials using micro-EDM, *Journal of Engineering Manufacture, 223*, 1127–1142.

[55] Kansal, H. K., Singh, S. & Kumar, P. (2007). Technology and research developments in powder mixed electric discharge machining (PMEDM), *Journal of Materials Processing Technology, 184,* 32–41.

[56] Pecas, P. & Henriques, E. A. (2003). Influence of silicon powder mixed dielectric on conventional electrical discharge machining. *International Journals of Machine Tools and Manufacture, 43,* 1465–1471.

[57] Takahata, K. & Gianchandani, Y. B. (2002). Batch mode micro-electro-discharge machining. *IEEE/ASME Journal of Microelectromechanical Systems, 11*(2), 102-110.

[58] Takahata, K. & Gianchandani, Y. B. (2004). A planar approach for manufacturing cardiac stents: Design, fabrication, and mechanical evaluation. *IEEE/ASME Journal of Microelectromechanical. Systems*, *13*(6), 933-939.

[59] Malshe, A. P., Virwani, K. R., Rajurkar, K. P. & Deshpande, D. (2005). Investigation of nanoscale electro machining (nano-EM) in dielectric oil. *Annals of the CIRP – Manufacturing Technology*, *54,* 175-178.

[60] Jahan, M. P., Malshe, A. P. Rajurkar, K. P. (2012). Experimental investigation and characterization of nano-scale dry electro-machining. *Journal of Manufacturing Processes, 14* (4) 443–451.

In: Electrical Discharge Machining (EDM)
Editor: M. P. Jahan
ISBN: 978-1-63483-591-6

Chapter 2

WIRE ELECTRICAL DISCHARGE MACHINING

D. Ghodsiyeh* and M. Moradi
Department of Mechanics and Aerospace, Politecnico di Torino, Torino, Italy

ABSTRACT

Nowadays, wire electrical discharge machining (WEDM) has become an important non-traditional machining process. The distinctive characteristics of this technique provides an effective solution for producing components made of advanced materials like metal matrix composites (MMCs), super alloys, titanium composites, advanced ceramics and polycrystalline diamond (PCD). Consequently, the market share of this technology is growing continuously from its invention in the late 1960s'.

WEDM process is widely used in aerospace, nuclear and automotive industries, in order to machine precise, complex and irregular shapes in various difficult-to-machine materials. WEDM process is divided into three main groups including dry, near dry and normal. The process parameters contain two main categories of electrical and non-electrical parameters. The main electrical parameters include pulse on time, pulse off time, peak current, gap voltage and the main non-electrical parameters include wire speed, wire tension and dielectric flow rate.

This chapter contains a brief history of WEDM followed by major aspects of technology, including different machining types, process variables and performance measurements. Furthermore, significant industrial and academic researches contributing to the performance measurements in WEDM, such as material removal rate, cutting speed, surface roughness, Kerf width (sparking gap) and wire wear ratio are discussed. Since WEDM is an expensive and widely used process, this chapter provides useful information to find optimal machine settings, which play a crucial role in order to increase economic efficiency. Because of the importance of wire selection in WEDM machining, manufacturing of the EDM wire, different types of wire characteristics and latest advances in the field of thin-wire are furthered described.

Keywords: Wire EDM, coated wire, WEDM system, wire materials, taper cutting

* Corresponding author: D. Ghodsiyeh. Department of Mechanics and Aerospace, Politecnico. di Torino, 10129 Torino, Italy. E-mail: danial.ghodsiyeh@gmail.com.

INTRODUCTION

Wire Electrical Discharge Machining (WEDM) is a thermo-electrical process in which material is eroded by series of sparks between the workpiece and the wire electrode (tool). In normal wire EDM, the workpiece and wire are immersed in a dielectric fluid (that depending upon the application can be deionised water or oil), which also acts as a coolant and flushes away debris. The movement of the wire is controlled numerically to achieve the desired three-dimensional shape and high accuracy of the workpiece. Wire EDM was first introduced to the manufacturing industry in the late 1960s. The development of the process was the result of seeking a technique to replace the machined electrode used in EDM. In 1974, D.H. Dulebohn applied the optical-line follower system to automatically control the shape of the component to be machined by the WEDM process. By 1975, its popularity was rapidly increasing, as the process and its capabilities were better understood by the industry. It was only towards the end of the 1970s, when computer numerical control (CNC) system was added to WEDM and brought about a major evolution of the machining process. As a result, the broad capabilities of the WEDM process were extensively exploited for any through-hole machining to the wire, which has to pass through the part to be machined. The common applications of WEDM include the fabrication of the stamping and extrusion tools and dies, fixtures and gauges, prototypes, aircraft, medical parts, and grinding wheel form tools.

WEDM is probably the most exciting and diversified machine tool developed for tool, die, mould, and metalworking industries in the last fifty years, and has numerous advantages. In this process, there is no contact between workpiece and the electrode, thus materials of any mechanical properties (hardness, brittleness or abrasiveness) can be cut as long as they can conduct electricity. Whereas the wire does not touch the workpiece, so there is no physical pressure imparted on the workpiece and amount of clamping pressure required to hold the workpiece is minimal. Although electrical conductivity is an important factor in this type of machining, some techniques can be used to increase the efficiency in the machining of low electrical conductive materials. The Spark Theory on the wire EDM is basically the same as the vertical EDM process. Sparks require the existence of a distance between electrode and workpiece, which is called the gap, and is filled with the dielectric. In Spark Theory application of electrical pulse creates an intense electrical field at the point where surface irregularities provide the narrowest gap between the workpiece and the wire. This occurrence results in formation of a high conductivity bridge in the medium across the gap. The increase of the voltage or decrease of the gap between the workpiece and the electrode cause vaporization and ionization of dielectric in the high conductivity bridge and formation of a plasma channel between the two surfaces. A powerful magnetic field is then generated due to further ionization caused by the high intensity of current. This increases both the temperature and pressure in the plasma channel. Although the spark duration is some micro seconds, a small amount of materials from both the electrode and the workpiece at the point of spark contact are still melted and vaporized by the extremely high temperature of the spark. Many sparks can be observed at one time due to the fact that actual discharges can occur more than one hundred thousand times per second.

Discharge duration can be variable; however, it can be measured in terms of microseconds. The heat of each electrical spark is estimated around 15,000° to 21,000° Fahrenheit. Consequently, part of the specimen material melts and vaporises, generating craters on the surface of the workpiece, which is removed in the form of debris by dielectric flushing [1]. This process is recently used in aerospace, nuclear and automotive industries, to machine precise, complex and irregular shapes in various difficult-to-machine materials. In addition, WEDM offers high cutting speed and surface finish, for example the typical cutting rates in case of WEDM are 300 mm^2/min for a 50 mm thick D2 tool steel and 750 mm^2/min for 150 mm thick aluminium, and surface finish is as fine as 0.04-0.25μm Ra which is quite good [2]. Due to the improved wire positioning and machining accuracy WEDM process is also being used to machine a wide variety of miniature and micro-parts in metals, alloys, sintered materials, cemented carbides, ceramics and silicon. These characteristics make WEDM a process that has remained as a competitive and economical machining option fulfilling the demanding machining requirements imposed by the short product development cycles and the growing cost pressures.

THE WEDM PROCESS

A wire EDM machine has many elements in common with other machine tools. For instance, Structural elements and Computerized Numerical Control (CNC) do not differ too much from those of other manufacturing equipments. A wire EDM system comprises of four major parts that are separately described in the following paragraphs. These elements are:

1) CNC
2) Power Supply
3) Wire drive system and Automatic Wire Threading (AWT)
4) Dielectric System

Computerized Numerical Control (CNC)

WEDM positioning systems usually consist of a 2-axis CNC table, and in some cases, an additional multi-axis wire positioning system. 2-axis machines can perform straight and taper cuts while 4 ½-axis machines have the ability to position the upper wire guide automatically depending on thickness of material. The numerical control system offers the capabilities of scaling, mirror imaging, rotation, axis exchange and assist programs. These enable the operator to produce entire family of parts from a single program without need of editing the program. Mirror imaging is used in cases of symmetrical workpieces, and scaling is useful while working with "shrink factors" for plastic cavities or extrusion dies. Assist programs are used to find the edge of parts, align the wire vertically, and perform centring routines that are useful for operator during set up process. Other CNC characteristics are technology of preventing wire breaks, background editing and graphic displaying of the programs while the machine is running. In addition, a digitizer may be used to obtain X and Y coordinates of shapes that are not defined geometrically.

One of the most important features that are set by the CNC is offset. Programs are written for the centre of the tool (wire) to follow the outline of the part. Imagine you are using a 0.010 inch diameter wire and it cuts a 0.012 inch slot with the power settings provided for the particular material. A 0.006 inch offset is needed to put the part "on-size" with respect to the clockwise or counter clockwise direction of cutting.

“Machine intelligence” which is primarily important in WEDM machines is applied by some programmes including technological data for optimization of cutting different materials and thicknesses, strategies for improvement of accuracy in corner cutting, cures to avoid wire breakage and intelligent selection of EDM parameters for situations of degraded erosions (such as stepped parts, large thickness parts, taper cutting, etc.).

Positioning of Wire

The most unique feature of the CNC is that it must operate in an adaptive control mode to always insure the consistency of the gap between the wire and the workpiece. When wire is in contact with the workpiece or when a small piece of material fills the gap and causes a short circuit, the positioning system must recognize the condition and back along the programmed path to maintain the proper cutting gap condition. Machine movement is accomplished with precision lead screws with recirculating ball bearings on all axes that are driven by AC motors. Once a while the position of machine must be checked and any errors or backlashes have to be corrected by pitch error compensation that is permanently stored in the computer memory.

Power Supply

Power supplies for WEDM machines are different in design and technology. When these machines were first introduced in the United States, they were equipped with power supplies that could achieve machining rate of less than one square inch per hour. The most significant differences between the power supplies used for WEDM and those for the conventional EDM are the frequency of the pulse and the current. To achieve the smoothest finished surface by WEDM, the pulse frequency should be maintained high (1 MHz). Such a high frequency ensures that each spark removes as little amount of material as possible, leading to reduction of the crater sizes. Current carrying capability is limited by the diameter of the wire used in cutting operation. Due to this limitation, WEDM power supplies are rarely built to deliver currents more than 20 Amp. There are two types of power supplies, which are pulse type and capacitor discharge models. Pulse type power supplies require fewer adjustments and are easier to operate; however, capacitor discharge models offer some cutting advantages on certain materials.

Wire Drive System and Automatic Wire Threading (AWT)

Wire drive system continuously delivers new wire under constant tension to the worktable. Constant wire tension is important to prevent problems such as machining streaks, taper, vibration marks, and wire breaks.

To ensure wire straightness, a number of preparation stages are added to wire delivery systems. After the wire leaves the supply spool, it passes through several wire feeds and wire removal capstan rollers. This leads to protect the eroding zone from any disturbing influences created by the wire supply. Changing part contour produces different cutting conditions requiring the drive system to modify the speed of cutting.

Automatic wire thread (AWT) is a system that automatically provides thread through start hole, with approximately 100% reliability. When wires with low tensile stress resistance are used, it is much simpler and more reliable to use AWT rather than manual threading. Most AWT systems heat, draw and guide the wire by high pressure flushing water or air. AWT systems provide the guides with much longer life, and therefore lower cost per hour and downtime. Cutting and threading the wire are automatically controlled by codes in the program. When there is a wire breakage during machining process, the machine returns to the start point, re-threads the wire and move through the program path to the position where the wire broke, then it powers up, and continues cutting. Some of EDM machines can also rethread the wire through the slot. In a wire break situation, the end of the wire is clamped and the supply wire is drawn back.

Dielectric System

The dielectric system consists of the water reservoir, filtration system, deionization system, and water chiller unit. The dielectric plays a dual role as both an insulator and a conductor. Before the discharging, the deionized water acts as an insulator, and allows the electrical potential between the wire and the workpiece to be built up to a certain intensity, then the dielectric breaks down and forms an electrical conductive path which is known in EDM as the "Discharge Channel." The energy of the spark is transferred from the wire to the workpiece in order to remove metal through this conductive path. The role of the Discharge Channel is crucial in assuring that each discharge has the same effect on cutting speed, surface finish and slot width. Thus, maintaining a constant condition of the dielectric is essential to obtain consistent results by wire EDM process.

There are different types of dielectrics, but deionized water is mainly used due to three reasons: low fire hazard, low viscosity, and high cooling rate. In addition, high pulse frequencies can be achieved in deionized water. The dielectric filtering and deionizing system play key roles in preventing excessive wire breakage. Ionization occurs rapidly because water is not insulator, and when the voltage is turned off, water still retains current. Resins help to maintain the conductivity level of the water.

Due to material type, the desired level of conductivity that should be maintained for a given application may vary. Excessive wire breakages may occur during machining process in cases that the conductivity level is too high. Two major methods are mainly used in order to reach the dielectric to the workpiece. In first method there are upper and lower nozzles, which make a water jet through the gap between the wire and the workpiece. Second method is submerged machining, and it is extremely useful for applications with poor flushing conditions such as irregular shaped parts, cutting large taper angles, laminations, giant workpieces, tubes, workpieces with undercuts and cutting very close to the edge of the workpiece. Over the past few years, dielectric flushing pressures have been increased up to 300 psi (20 bar) in order to increase cutting speed.

Filtering Systems

In de-ionized water dielectric systems, the water is recycled to decrease operating costs. This is accomplished by filtering the collected water with disposable paper filters, and after filtration, the water resistively is corrected by passing through a mixed-bed deionizer cartridge. Special additives can be added to the water to avoid rust formation on the parts surfaces. In case of rust formation, an extra polishing operation is generally required to remove the oxides.

Paper cartridge filters and mineral filters are two main types of filtering systems. Paper cartridge filters are replaceable and can be used for 200-300 working hours depending on the EDM process, water volume, etc. Filters assure a consistent EDM fluid quality, and uniform process condition to avoid blockage of rinsing nozzles, control resin consumption, prevent sediment in the cooling and supply system, and to reduce corrosion deposits.

Mineral filter systems in wire EDM machines do not require filter media replacement which is the unit taking dirty water from the machine filtering to a 3 micron cleanliness level in order to supply clean water for machining. When the filter vessel reaches the cleaning capacity, as detected by a pressure switch, a backwashing cycle starts and clean filtered water is supplied to the machine dielectric tank. With this feature the machine always has a supply of clean water.

Deionizing Subsystem

The deionizing subsystem consists of a pump, control system and a deionizing container, which contains deionizing resin that removes the dissolved contaminations from the water. The level of conductivity of the water in the clean tank of the dielectric system is monitored by the control system, which activates the pump forcing water to pass from the clean tank through the deionizing container and return to the clean tank. The mentioned parts can be identified in Figure 1.

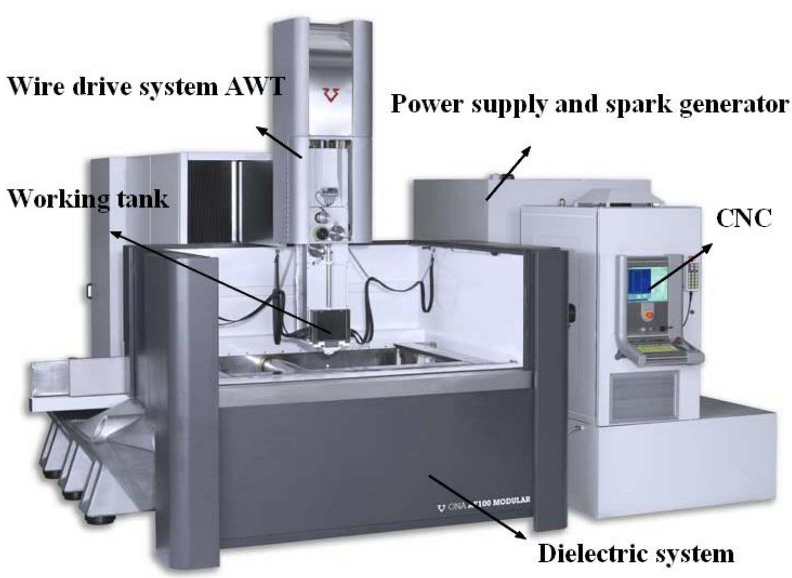

The photograph shows an ONA® AF100 wire EDM machine [3].

Figure 1. Main systems of a WEDM machine.

WEDM TYPES

The WEDM process can be divided into three main types including dry, near dry and normal WEDM. Also, the process parameters of all types of WEDM can be divided into two different categories of electrical and non-electrical parameters. The difference between different types of WEDM is in dielectric. As it was mentioned before, in normal WEDM dielectric fluids are used to fill the gap between wire and workpiece, but dielectric system is usually complicated and costly. Recently, some WEDMs are performed in the gas mediums.

Dry and Near-Dry Wire Cut

Dry WEDM is conducted in a gas environment without using dielectric liquid. Another new method has been also introduced in WEDM that is called near dry wire cut that liquid dielectric fluid is replaced by the minimum quantity of liquid to the gas mixture.

To better understanding of the process the fundamentals of dry WEDM are briefly discussed in the following. Electrical discharge is a process that occurs when a pulse current passes through a dielectric material between two electrodes.

This current is the result of a plasma channel formed by a series of electron collisions, which are excited by a strong electric field between the two electrodes, and the atoms of the medium. When the applied voltage is not significantly varied, the length of the gap between the two electrodes where the discharge occurs depends on the breakdown voltage (strength) of the dielectric fluid. The gap is smaller when the dielectric has a higher strength. Since the dielectric strengths of gases are much lower than those of dielectric liquids, the gap length of the electrical discharge is much higher in gases than in dielectric liquids. Electrical discharge in gases is the major mechanism of a dry WEDM process.

As described by DiBitonto et al., [4], the high density of a liquid is the main reason for its higher energy and plasma pressure compared to gas discharges. Therefore, a low MRR can be observed for WEDMing in gases.

However, since the energy intensity is low, electrical discharge in gases generates shallower craters with smaller volumes, resulting in a higher quality surface-finish. In addition, in dry WEDM, high pressure gases (injection or suction) are provided to cool down and flush away melted material, and necessary gases (e.g., oxygen) are supplied to the working gap.

In dry WEDM, vibration of the wire electrode is minimal due to the negligible process reaction force, the gap distance is narrower and no corrosion occurs in workpiece during machining. Some other advantages of dry WEDM are better straightness, and shorter gap length. These characteristics can improve the accuracy and surface quality of the workpiece during cutting. The main drawbacks of dry WEDM are lower material removal rate compared to conventional WEDM and more generation of streaks. Increasing the wire winding speed and decreasing the actual depth of cut can improve these weaknesses. Dry WEDM is also used for micro-WEDM with high-pressure air injection and thin workpiece. Figure 2 shows the dry micro-WEDM system.

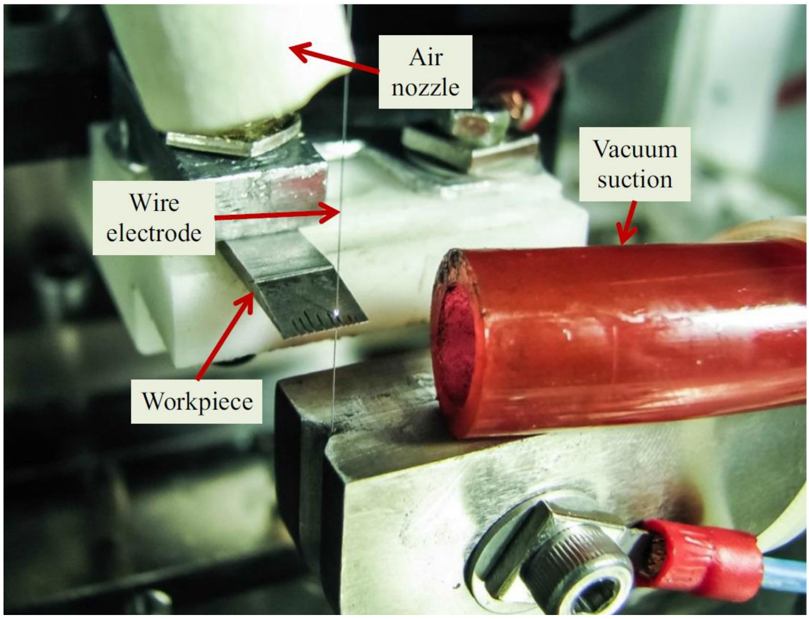

Figure 2. Dry micro-WEDM system [5].

WEDM Electrical Parameters

Major electrical parameters in WEDM are pulse on time, pulse off time, peak current, gap voltage, servo feed rate and servo voltage. These are briefly described in following.

Pulse on Time and Pulse Off Time

Electrical discharge machining must occur (on time) and stop (off time) alternately throughout machining process. During the on time, the voltage is applied to the gap between the workpiece and the electrode (wire), while no voltage is placed during the off time.

Consequently, electric discharge occurs only for the duration of the on time. To have a long duration of electric discharge, it is possible to select the great value for the on time; however, it may cause a short circuit and wire breakage. To avoid such a problem, the off time must be inserted between two on times as it is shown in figure 3. These parameters have the greatest effect on the surface roughness of the workpiece.

Peak Current

Basically, the most important machining parameter in WEDM is peak current. It refers to the amount of power used in process and is measured in unit of amperage. During each pulse on time, the current increases until it reaches a pre-set level that is expressed as the peak current. In both die sinking and wire EDM processes, the maximum amount of amperage is governed by the surface area of the cut.

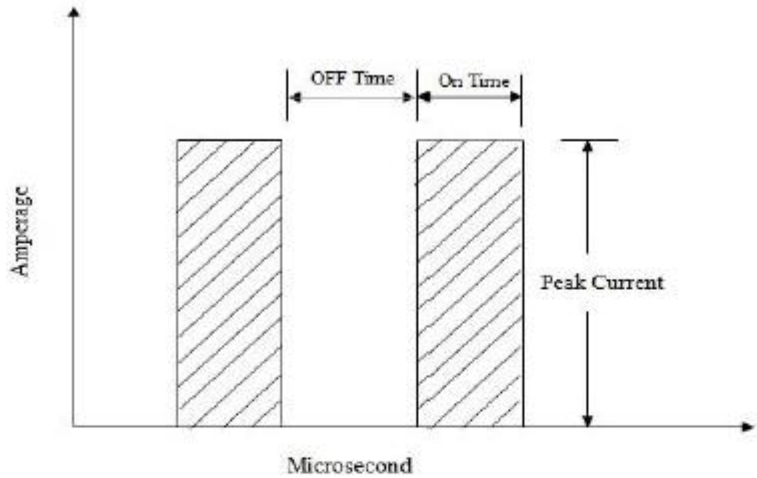

Figure 3. Pulse on time and off time.

Higher amperage is used in rough operations and in cavities. Peak current have the greatest effect on the material removal rate of the machining.

Gap Voltage

Gap or open circuit voltage specifies the supply voltage to be placed in the gap. The greater values of this parameter lead to larger electric discharge energies; however, normally these factors are not independent. In the other words as the gap voltage increases the peak current also increases. In some WEDM machines, both of these factors refer to machining voltage.

Servo Voltage

Servo voltage (SV) is used for controlling advances and retracts of the wire. During machining, the mean machining voltage varies depending on the state of the machining between the workpiece and the electrode. SV establishes the reference voltage for controlling advances and retracts of the wire. If the mean machining voltage is higher than the set voltage level, the wire advances, and if it is lower, the wire retracts (to be precise, the work table advances or retracts instead of wire).

Therefore, increasing SV value makes the gap between the workpiece and the electrode wider. Higher values of SV also decrease the number of electric sparks, stabilize electric discharge and slow down the machining rate. When a smaller value is set for the SV, the mean gap becomes narrower, leading to an increase in the number of electric sparks. It can speed up the machining rate; however, the state of machining at the gap may become unstable, resulting in wire breakage.

Servo Feed Rate

Servo feed rate (SF) specifies the feed rate of the table during machining. Usually, the WEDM machines select this factor automatically with respect to the SV, but it also can be set manually where machining table has constant speed independent to the SV. So, both servo voltage and servo feed rate can affect the feed rate as it is illustrated in figure 4.

WIRE EDM NON ELECTRICAL PARAMETERS

Major WEDM non-electrical parameters are dielectric flow rate, dielectric type, wire tension and wire speed.

Dielectric Flow Rate

Dielectric fluid is required in order to stabilize electric discharge and perform efficient cooling and chip removal. The deionized water is typically used as a dielectric fluid in WEDM machines because it has friendly environmental characteristics. Immersion flushing and spray or jet flushing are commonly used as flushing methods. In immersion flushing method, water jets upper and lower of the workpiece are flushing the water inside the gap. The dielectric pressure is measured in units of bar and depending on the type of WEDM machine it can be up to 20 bar. Dielectric flow rate significantly affects material removal rate and surface roughness especially for the workpieces with low thermal conductivity.

Wire Speed or Wire Feed

Wire speed shows the feed rate of the wire in WEDM. During WEDM cut, the wire is continuously advanced between spools to present a constant diameter wire to the job. As the wire speed increases the wire consumption and in result the cost of machining increase. The wire speed is measured in the terms of meter per minute, and it highly depends on type of wire. A normal wire speed in typical machining is as high as 10 (m/min). This factor has the greatest effect on the wire wear ratio. In low wire speeds, wire wear ratio significantly increases which can cause wire breakage especially in rough machining.

Wire Tension

Wire tension is the factor that controls the wire tightness in WEDM. When the wire tension is high enough, the wire stays straight otherwise wire drags behind as it is illustrated in figure 5. This parameter is generally mentioned in wire characteristics by company in the unit of grams. Theoretically within considerable range, an increase in wire tension can increase the cutting speed. The higher tension decreases the wire vibration amplitude and hence decreases the cut width, so that the speed is higher for the same discharge energy.

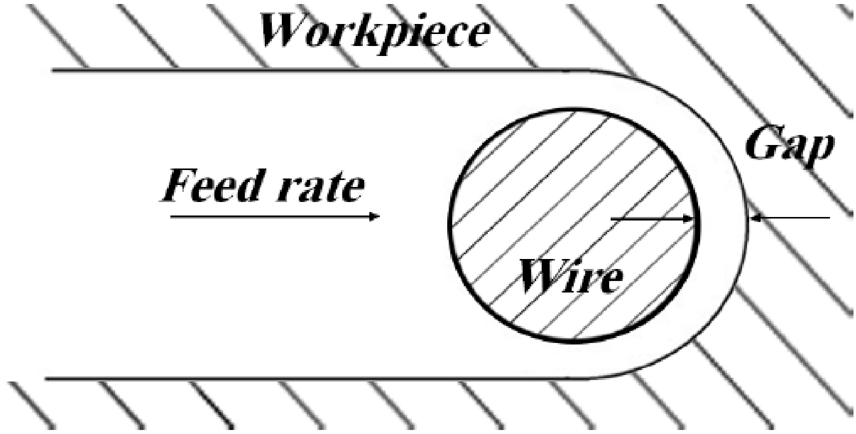

Figure 4. Feed rate and gap size in wire EDM.

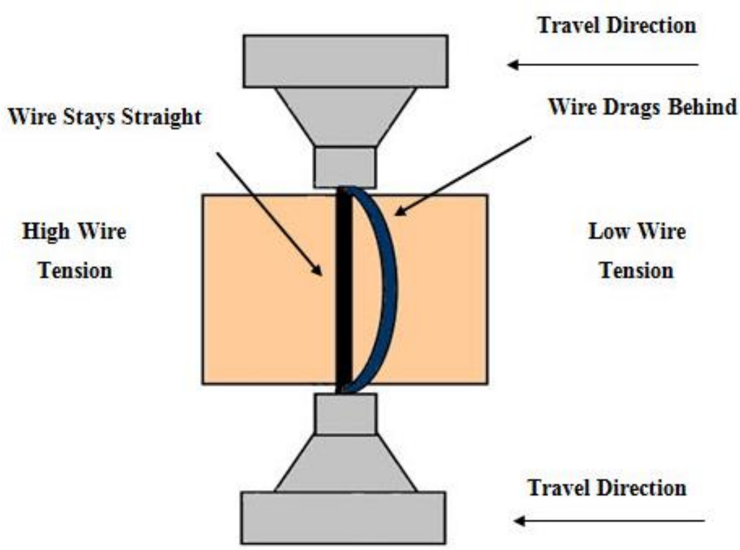

Figure 5. Relationship between drag and wire tension.

However, if the applied tension exceeds the tensile strength of the wire, it leads to wire breakage. Wire tension has the greatest effect on three dimensional accuracy characteristics in WEDM. Proper wire tension increases machining accuracy, production time and wire lifetime, and meanwhile it also reduces machine downtimes.

It is a well-known fact that WEDM process has various process variables, complexity and stochastic nature. Cause and effect diagram is shown in Figure 6 to identify the process parameters that may affect the machining characteristics of WEDM machined parts [6].

How EDM Wire Is Made

The process of manufacturing EDM wire is much more complex than most of users imagine. In this part method of producing brass wire and coating are briefly reviewed.

The manufacture of brass EDM wire can be divided into the following steps:

- Casting
- Rolling
- Preliminary Drawing
- Finish Drawing
- Spooling
- Packaging

Casting

As brass is an alloy of zinc (usually in the form of cast zinc ingots) and copper (usually in form the of copper cathode plates), at first the raw materials are mixed in the correct weight proportions. Then the mixture is placed in a crucible, and heated by resistance elements. The continuous casting method is used to produce best quality EDM wires.

This is a continuous process in which molten material is poured from the pot into a reservoir in a water cooled graphite mould, containing passages to transform the molten metal into a solid rod. The rod (around 16mm diameter) is cooled in air and then coiled in order to form a large reel.

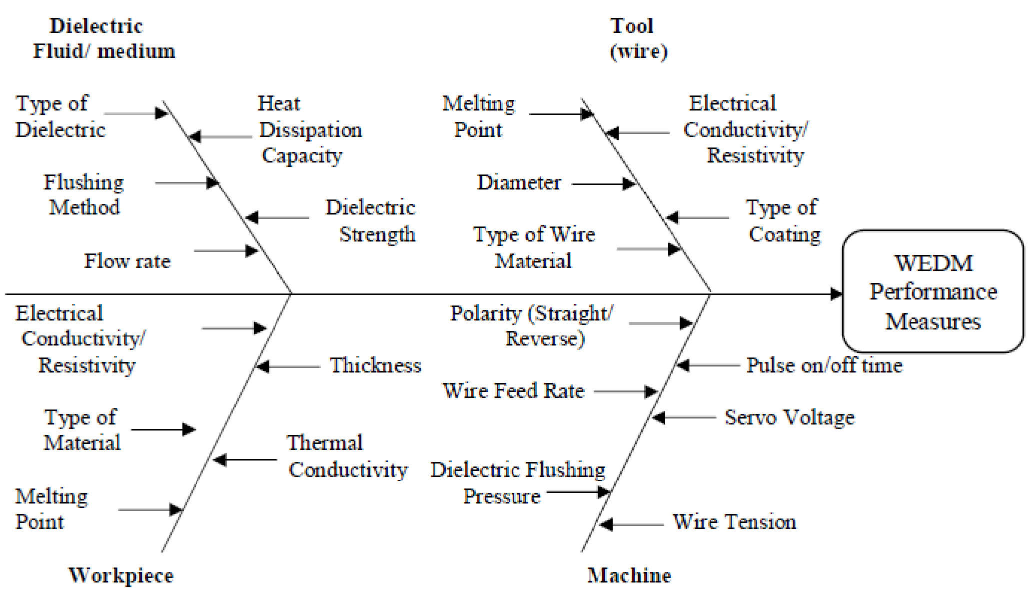

Figure 6. Cause and effect diagram for wire EDM parameters.

Rolling

After rolling mill, cross sections of the huge coils are reduced to a size that is suitable for the first drawing operations. Manufacturer selects actual shape of the cross section, and among different shapes a modified square is one of the most common cross sections.

The wire shape also can be customized in order to increase the material removal rate. Figure 7 shows some of the different wire shapes. The cross section is reduced from 16mm to 8mm by passing through a series of rolling devices. The wire is strictly deformed during the rolling process which makes the hardness increase. After that in a large furnace, the reels are heated up to the re-crystallization temperature and then slowly cooled in order to soften the material to enable further processing.

Preliminary Drawing

During this process, the square wire is pulled through series of ten to twenty draw dies. Special lubricant is also used, so that the cross section diameter decreases to 0.9 mm. Quality of the finished product tightly depends on the speed of drawing, the amount of reduction between each die, type of lubricant, geometry of the draw die openings and the draw die material. Due to application of wire additional annealing steps may also be added to the process. The output product of this stage is called “Redraw Wire.”

Finish Drawing

This stage is used by manufacturer to change the wire diameter from 0.9 mm to finished size. Since output of this process is the finished product, all parameters of finish drawing operation need to be tightly controlled.

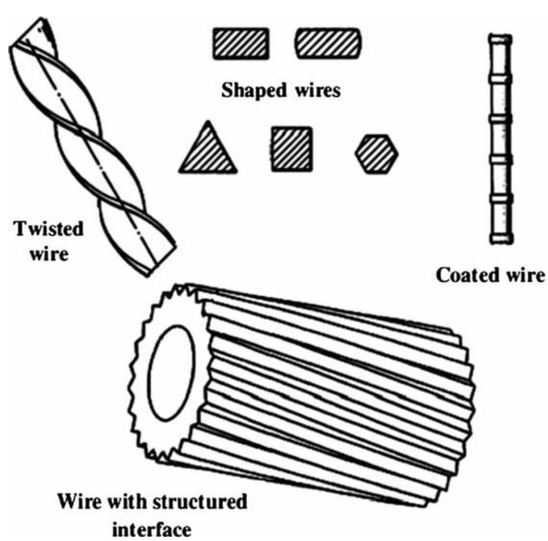

Figure 7. Customized wire shapes [7].

By reduction of cross section of the wire, brass powder may be produced in microscopic flaws of the draw die surfaces, which must be filtered from the lubricant. Therefore, conditioning and maintenance of the drawing lubricant is crucial during the finish drawing. The lubricant temperature must be precisely controlled during this process as the great portion of the heat of this stage is absorbed by lubricant.

In the finish drawing operation, the inserted materials for all the draw die stations are natural or artificial diamonds. Since there are no intermediate heat treatments in the finish drawing process out coming wire is hard and brittle. Consequently, an annealing process; which varies by manufacturer and the wire application; is done as soon as finishing drawing operations is done to bring the wire to the desired conditions of hard, half hard or soft temper.

Spooling

This is one of the most important stages of producing EDM wires. Not only a large amount of produced wires are rejected because of improper spooling, but also the spools themselves need to be exactly inspected. It is the most critical operation in the spooling process to set the traverse reversal points in the way that they exactly match the flanges of the spool. If these reversal points are set beyond the flange location, the wire climbs up upon itself at each reversal, often causing machine stopping overwraps.

Another process variable that is important to have a successful unwinding of the wire when the spool is finally installed on the wire machine is spooling winding tension. If it is set too high, the axial forces may develop on layers of the wire, and can cause the flanges of the spool to break off, usually long after the spool is packaged and shipped. If the spooling tension is set too low, the adjacent coils can shift due to shocks in transit, and result in an overwrap spool before it is even removed from the box.

Packaging

The aim of wire packaging is not only to protect the wire from oxidation and corrosion, but also to protect the spool from impact damages. Wire manufacturers maintain the wire from oxidation and corrosion by one of these three ways of adding a desiccant package to the wire box in order to absorb moisture, shrinking a plastic sleeve around the spool barrel and a portion of the flange, or inserting the entire spool in a plastic or foil bag, then removing all the air, and finally sealing the bag. The latter method obviously provides the best protection of wire. At this point, it should be noticed that after each stage of producing the wire a sample is taken to the testing laboratory so the metallurgical integrity and grain size can be checked. For example surface properties, diameter, strength, elongation and cleanliness of the wire samples are precisely checked before the spooling operations [8].

Coated Wires

It is usually thought that coating a wire is done at the end of wire production procedure, which is generally not true. Coating process is done before final drawing operations.

In manufacturing process of coated wires, additional plating and heat treating steps are essentially required in comparison to what is described previously. There are three basic types of coated wires all based on a zinc layer: zinc Coated, Heat Treated zinc Coated, and Multiple Layered Heat Treated zinc Coated.

There are two different methods used to coat the 0.9 mm redraw wire with zinc: Hot Dip and Electroplating. From economical point of view, Hot Dip method is the best one while it is difficult to control coating thickness and preventing pin holes during this process as the wire passes through a molten bath of zinc and it sticks to the wire and then solidifies.

In the Electroplating method very precise control of coating thickness is possible as the zinc ions in the bath are plated onto the surface of the wire during passage of the wire through a chemical plating bath while an electric current is imposed upon it. The wire makes numerous forward and backward passes through a bath of more than 100 feet long.

WIRE PROPERTIES

When wire EDM was first introduced, the main problem was wire material because this material should have lots of properties. The main physical properties of EDM wires include high values of conductivity, tensile strength, elongation, melting point, straightness, flush ability and cleanliness.

Conductivity

A high conductivity rate is important because it means the wire can carry more current, which equates to a ‘hotter’ spark and increased cutting speed. In the other hand, low wire conductivity results in voltage drop and energy loss over the distance from the power feed to the cutting point. This is significant to consider that the peak current of most modern power supplies often exceeds 100 amps so the wire must be capable of carrying this amount of amperage. Conductivity is often expressed as a percentage of International Annealed Copper Standard (IACS), which is a unit for electrical conductivity of metals and alloys relative to standard annealed copper.

Tensile Strength

It indicates the ability of the wire to withstand the tension imposed upon it during cutting process in order to make a vertically straight cut. EDM wires are considered “hard” at tensile strengths of 900 MPa or above, “half hard” at tensile strengths around 490 MPa, and “soft” at tensile strengths below 440 MPa.

Hard wires are used in most of cases, while half hard and soft wires are used for taper cuts where the taper angle is greater than 5° since a hard wire resists bending at the guide pivot and cause inaccurate taper cutting. Half hard and soft wires are often unsuitable for automatic threading unless the machine is specifically designed to work with such wires.

Elongation

This describes how much the wire plastically deforms just before it breaks. The wire with higher elongation can bear more force. It could also be stated that elongation relates to how brittle the wire is. Usually, hard wires have considerably less elongation than half hard wires. A brittle wire may break at the first overload condition, while a more ductile wire is expected to accept a temporary overload. Since EDM wires operate in hostile environments under high tension and get attacked by thousands of sparks at their cross section, elongation is an important property. Elongation is measured in percent of gauge length used in a standard test.

Melting Point

It is preferred that the wire electrode be resistant to being melted too quickly by electric sparks. Also, low melting point increases wire wear significantly which leads to wire breakage.

Straightness

This can help wire to stay straight. It is seldom specified but is critically important especially for successful auto threading and cutting thicker workpieces.

Flush Ability

Better flush ability leads to faster wire cut and decreases the chance of wire breakage. As it was mentioned, this property is very important for cutting low thermal conductivity materials.

Cleanliness

Wire can become “dirty” due to contamination by residual metal powder left over from the drawing process, drawing lubricant, or added paraffin to the wire by some manufacturers prior to spooling. Dirty wires result in clogged guides, power feeds and slipping belts or rollers. Wires ranging in diameter from 0.02 to 0.36 mm are generally available for WEDM. An increase in diameter due to residual contamination raises pulse energy supplied to the working gap, thus leads to increasing the overall material removal rate [9].

DIFFERENT WIRE MATERIALS

As the science of wire manufacturing has developed, a variety of new wire materials and types have become available.

Each type has distinct characteristics, so the user has a variety of choices. Selection of the ideal wire is a critical basis for achieving successful operation that many parameters such as greater taper angles, thicker workpieces, automatic wire threading, and long periods of unattended operation affect it.

Evolution of EDM wire electrode can be divided in to two main parts consisting technologies from using copper to the widely employed brass wire electrodes and from brass wire electrodes to the latest coated wire electrodes. Pure copper was used for wire electrodes in the early 1970s but accuracy and strength were insufficient.

In the second half of the 1970s, brass wire started to be used instead of pure copper wire. Copper wire electrodes coated with zinc were first introduced for high speed cutting in 1980, and brass wire electrodes coated with zinc were developed and utilized in the following year for high precision cutting. Afterward, core materials of stainless wire coated with copper were made. By increasing zinc concentration and adding titanium and aluminium to brass wire electrodes new types of wires were developed offering higher cutting speed due to improvement of heat resistance especially during cutting thick materials.

Nowadays, brass wire electrodes are extensively used as WEDM tools. However, there is an expanding demand for wire electrodes with superior performance to the conventional brass wire electrodes. High performance wires such as coated, composite, and diffusion-annealed wires are characterized by high conductivity and spark ability. These are generally zinc-coated wires with a copper-brass alloy or steel core; the brass contains either a small amount of chromium or high concentration of zinc.

Copper

Copper was the first material used in wire EDM. Although conductivity of copper is excellent, low tensile strength, high melting point and low vapour pressure severely limits its application. Nowadays, practical use of copper is restricted to old machines with power supplies designed for copper wire.

Brass

When manufacturers of early WEDM were looking for better performance, brass was the first alternative to copper. Brass EDM wire is a combination of copper and zinc, typically alloyed in the range of 63-65% Cu and 35-37% Zn.

Higher vapour pressure, higher tensile strength and lower melting point are all significant results of the addition of zinc. The zinc in the brass wire vaporizes during the cutting process, which helps the wire cool and delivers more energy to the workpiece.

Also, some zinc particles that are not filtered out of the dielectric fluid may remain in the gap between the electrode and the workpiece to help the gap ionization and cutting process. Brass quickly became the most widely used electrode material for general-purpose wire EDM. Today, it is commercially available in a wide range of tensile strengths and hardness [7].

Aluminium-Brass

Small percentage of aluminium added to a brass wire creates a special alloy wire (65Cu33Zn2Al) with improved tensile strength up to 1,200 MPa without adversely affecting elongation. These wires are also less prone to breakage in comparison with other types of plain brass wires.

Steel

A force opposite to the machining direction is created in the machined sections of the wire electrode due to electric discharge. Also, Electrostatic and electromagnetic forces are created on the wire electrode. Because of these forces and the wire vibrations, the actual wire position differs from the programmed position, leading to problems of accuracy and precision. For instance at the corners, deviations from the programmed outline produce round corners instead of the desired sharp corners. Consequently, plain molybdenum or tungsten wires form due to the high tensile strength (> 1,900 MPa).

As these wires were expensive and their flush ability was poor, a high strength pearlite steel wire with over 0.06% carbon content and a coat of copper free zinc was developed. The result was improved precision and accuracy with ability to increase mechanical load.

Molybdenum

In some limited applications where very high tensile strength is required, this type of wire is used to provide a reasonable load carrying capacity for EDM wires with small diameters of 0.1 mm or less.

Both high melting point and tensile strength are momentous characteristics of molybdenum wires. Using this wire has some drawbacks such as low electrical conductivity, very low flush ability and being very expensive. In addition, it is very abrasive to power feeds and wire guides. Finally, it is often difficult to auto thread this wire.

Tungsten

Tungsten wire is often an economical alternative for molybdenum wire in diameters of 0.05 mm and smaller because in comparison with molybdenum wire, it has greater tensile strength and melting point. Tungsten wire is dramatically preferred in high precision works with wire EDM machines, as it requires small inside radius in the range of 0.025-0.1 mm. Due to low load carrying capacity of brass and coated wires in these sizes, they are not practical.

Hence, molybdenum and tungsten wires are used. It should be noticed that because of the limited conductivity, high melting point, low vapour pressure and slow cutting tendency, this wire is not suitable for very thick workpieces.

MolyCarb

MolyCarb is a composite wire which molybdenum wire is coated with a mixture of graphite and molybdenum oxide. Therefore, flushing characteristics are highly improved. This wire provides significant advantages in small diameter works.

Single-Layer Coated Wires

The next step was the development of coated wires; sometimes called plated or “stratified” wires; since brass wires could not be efficiently fabricated with any higher concentration of zinc. Coated wires typically have a core of brass or copper for conductivity and tensile strength, and are electroplated with a coating of pure or diffused zinc for enhanced spark formation and flush characteristics.

Originally, coated wires are called “speed wire” due to their ability to cut at significantly higher metal removal rates. To suit various applications and machine requirements, these wires are now available in a wide variety of coating materials, core materials, tensile strengths and coating depths. Coated wires currently represent the optimum choice for top performance; although they are more expensive than brass wire.

In other words, in order to combine the conductivity of a copper core with the flush ability of zinc, copper wire coated with zinc was commercially produced. It has no current application because when sparks penetrate the thin zinc coating, the cutting rate slows to the sluggish pace of pure copper wire. Another attempt to present more zinc to the cutting surface of wire was zinc coated brass wire. This wire consists of a thin (around 5 microns) zinc coating over a core of brass. Material removal rate and integrity of nickel based superalloy and titanium alloy were examined during wire EDM process, and an increase in productivity of about 40% for nickel based superalloy and about 70% for titanium alloy were obtained by replacing standard uncoated brass wire with diffusion-annealed brass core coated wire under the same operating conditions. Furthermore, in terms of recast layer thickness, by machining with coated wire for both roughing and trim operations about 25% thinner recast for nickel based superalloy and about 40% thinner for titanium alloy were produced [10].

With regards to various researches the cutting speed of the zinc coated wire is about twice of the brass wire because the exterior zinc coating of the electrode has a lower melting temperature than the core of brass [11]. In the presence of a pulse, zinc is evaporated acting as a heat sink, which in turn reduces the wire temperature and improves efficiency of the WEDM process. In addition, the evaporation of coating layer increases the gap size and results in better debris removal that deteriorates the surface roughness and the sparking gap [12].

Double-Layer Coated Wires

In US different inventions have been made to improve coated wires especially in terms of speed. For instance US Patent No. US4968867 discloses a wire electrode with a core of copper, silver, aluminium, or alloys, having relatively high thermal conductivity and a coating layer formed by a low boiling point material.

This wire electrode also has an outermost brass layer with high mechanical strength. It has certain characteristics such as, vibration damping, heat transfer and breakage resistivity that ultimately increase machining speed.

Multi-Layer Coated Wires

As it was mentioned before US is frontier in terms of wire EDM and their other important invention is patent No. US4341939, which mainly increases machining speed by eliminating the short circuits that can decrease machining efficiency.

To be more exact it rapidly changes the transformation of non-erosive short-circuited electrical discharges into electro-erosive effective discharges. The wire should be coated with at least one thin layer of a non-metallic material with a sufficient thickness to provide a semi-conductive effect when the film is in contact with the workpiece.

When a few volts are applied between the wire and workpiece, the film completely becomes conductor by electrical and/or thermal breakdown, thus the applied voltage rises to about 100V. The metallic coating is preferably made of zinc and is subjected to an oxidizing thermal or electrolytic treatment such that on the surface of the metallic layer a thin film of zinc oxide is formed [7].

Diffusion-Annealed Coated Wires

Zinc has a low melting point, and it is only plated on the surface of the wire core. The intensity of the spark discharge tends to blast the zinc layer off the wire core. Thus, a coating with high zinc content and relatively high melting point results in good adhesion to the wire core. All these effects can be achieved by heat-treating process of the zinc coated wire called diffusion annealing.

Diffusion is the process whereby atoms diffuse from areas of high concentration to areas of lower concentration. The zinc atoms diffuse into the brass, and the copper atoms from the brass diffuse into the zinc, leading to transformation of the zinc coat into a high-zinc brass alloy which has a relatively high melting point, and is metallurgically bonded to the core material [7].

Brass Wire Phases

Figure 8 represents the different phases of brass alloy used in EDM wires which are alpha, beta, gamma, and epsilon phases. The melting point of alpha phase is approximately 910°C at its highest commercially feasible zinc content of 35-39 wt% (weight percentage); beta phase with the melting point of about 890°C in a diffusion-annealed coating with a typical 40-53 wt% zinc content has the next highest melting point; the melting point of gamma phase is 800°C in a diffusion annealed coating with a typical 57-70 wt% zinc content; and epsilon phase has the lowest melting point which is approximately 550°C in a diffusion annealed coating with a typical 85 wt% zinc content.

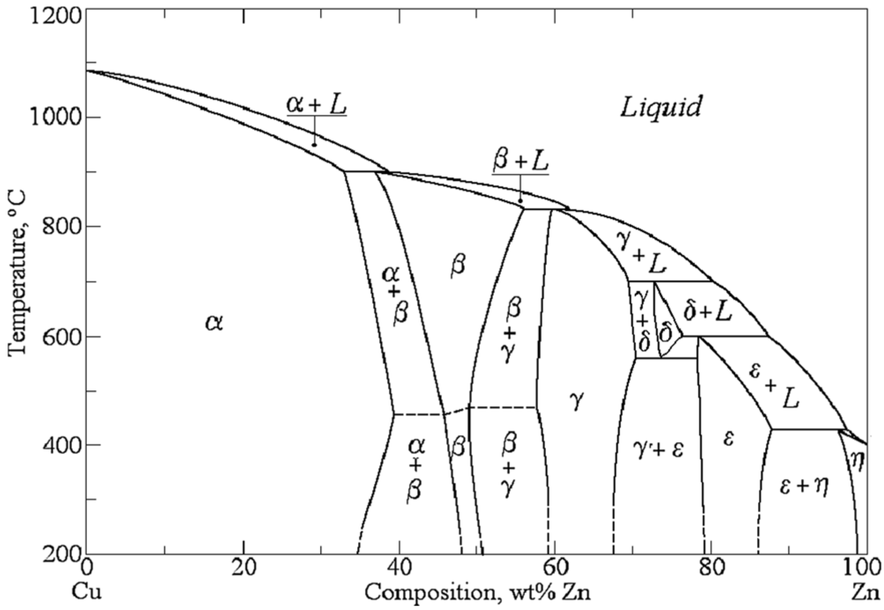

Figure 8. Cu-Zn phase diagram [7].

Beta Phase Wires

The X-type wire is a pure copper core coated by a beta brass. The main advantage is the combination of high copper conductivity with coherent zinc-rich coating, and disadvantages are the tensile strength equivalent to half hard brass combined with poor straightness and high cost relative to brass wires.

This kind of wire produces significant productivity gain in aerospace alloys such as Inconel and Titanium. D-type wire consists of a beta brass coating over a copper core alloyed with 20% zinc. It combines improved conductivity of the 80% Zn to 20% copper core, a coherent zinc-rich coating, and relatively high tensile strength (800N/mm2). Although this wire is very expensive, it produces significant productivity gain in virtually all materials and on many different machines.

Gamma Phase Wires

Gamma phase brass has higher zinc content than beta phase brass. As it is very brittle, the gamma coating thickness is usually limited to less than 5 microns because thicker coatings may fracture and strip off in the final drawing process.

Due to the brittleness, the gamma phase brass actually fractures during the final drawing process, producing a discontinuous surface.

This wire increases the cutting speed by improving flush ability as the wire passes through the cut, enhancing water flow and scouring debris from the gap. The discontinuous surface has the problem of being slightly dirtier than other zinc-coated wires.

Epsilon Phase Wires

The epsilon phase has a lower melting point considered as a disadvantage in comparison to beta or gamma phase. The higher zinc content of the epsilon phase offsets some of its disadvantages, so that these coatings match the performance of beta phase coatings while being competitive with gamma phase coating performance. Therefore, epsilon phase coatings provide similar cutting performance but at a lower manufacturing cost than either beta or gamma phase.

Fine Wires

Generally, the wire diameters are in the range of 0.006-0.012 inches. High precision works on wire EDM machines, require small inside radiuses and wire diameters in the range of 0.001-0.004 inches. Since brass and coated wires are not practical due to their low load carrying capacity in these sizes, molybdenum and tungsten wires are used.

It should be noticed that due to limited conductivity, high melting points and low vapour pressure, they are not proper for very thick workpieces, and tend to cut slowly. Only a few scientific works have been dealing with WEDM cuttings by using wires with diameters below 50µm. The materials of these fine wires are tungsten with high tensile strength and melting temperature and brass coated steel wire. Typical ultra-thin wire diameters are 20, 25, 30 and 50µm. These wires can be used to produce micro parts with WEDM.

Table 1 includes technical recommendations of use of different wires for WEDM.

Table 1. Recommendations of use of different types of wire for WEDM

Wire type	Available sizes (mm)	Tensile strength (N/mm^2)	Elongation (%)	Cutting speed	Cutting accuracy	Taper-cutting (> 7º)	Automatic threading
Diffused Zn coated Cu wire	0.30 0.25	500	1	✓✓	✓	✓	✓
Annealed Zn coated Cu wire	0.25	450	1	✓	×	✓✓	×
Diffused Zn coated Brass (CuZn10)	0.30 0.25	690	1	✓✓	✓✓	✓	✓
Zn coated Brass (CuZn36)	0.30/0.25 0.20/0.15 0.10	900	1	✓✓	✓✓	×	✓✓
Zn coated Brass (CuZn36)	0.30/0.25 0.20	500	18	✓	✓✓	✓✓	×
Brass (CuZn36)	0.25	1,000	1	✓✓	✓✓	✓	✓✓
Brass (CuZn36)	0.30/0.25 0.20/0.15	500	18	✓	✓	✓	×
Brass (CuZn37)	0.30/0.25 0.20/0.15	400	25	×	✓	✓✓	×
Mo coated Molybdenum Oxide Graphite	0.20/0.15 0.10/0.05 0.03	1900	5	✓	✓✓	✓	×

×: Not recommended, ✓: Recommended, ✓✓: Strongly recommended.

DIFFERENT PROCESS RESPONSES

Major WEDM performance measurements are material removal rate, cutting speed, surface roughness, kerf width (sparking gap) and wire wear ratio. Different types of wire EDM inaccuracies such as wire lag and wire deviation are also parts of WEDM performance measurements. Moreover, different kinds of surface integrity parameters such as white layer thickness, heat affected zone and the surface crack density are characteristics of all types of EDM process performance measurements.

Material Removal Rate and Cutting Speed

For most users WEDM is the matter of speed and accuracy. Cutting speed has primary importance during the rough cut. Although speed should be expressed in terms of length divided by time, this is not a practical measure of material removal rate in WEDM since it is strongly dependent on part thickness. This is the reason why it is commonly accepted to measure the machining with material removal rate in mm3/sec. Lots of attempts have been done to maximize the material removal rate and cutting speed by different approaches because these factors can considerably increase economic benefits of WEDM.

Generally, MRR is obtained by the following equation:

$$MRR = (W_b - W_a)/(Tm \times p)\ (mm^3/sec) \tag{1}$$

where W_b and W_a are respectively weights of workpiece before and after machining (gr). Tm is machining time (sec) and ρ is the density of workpiece material (gr/mm^2). The rate of material removal depends on amount of current of each discharge, frequency of the discharge, wire material, workpiece material and dielectric flushing conditions. Increasing the peak current can increase the energy of each discharge, producing wider and deeper craters that cause higher material removal rate. Increasing pulse on time can also increase the duration of each discharge, leading to rise of material removal rate.

The material removal rate in WEDM increases initially with the decrease of pulse off time. However, at a very short pulse off time, the gap becomes unstable which causes a reduction in the machining rate. Discharge current, pulse duration, and dielectric flow rate and their interactions play significant roles in rough cutting operations for maximization of MRR [13].

The physical, metallurgical, and electrical properties of the workpiece material also influences the cutting process, for instance low melting point of the material can increase the cutting speed. Higher values of thermal conductivity and specific heat capacity of machined material decrease the efficiency of WEDM. Furthermore, thermal conductivity and specific heat are the most significant factors of workpiece which can determine MRR and volume of heat affected zone.

The various potential factors affecting the WEDM performance measurements are divided into five major categories: different properties of the workpiece material and dielectric fluid, machine characteristics, adjustable machining parameters and component geometry [14].

Surface Roughness

Surface roughness is significantly affected by the pulse on time, peak current and the cutting speed. There is an inverse relationship between surface roughness and the cutting speed. Pulse on time is the most significant factor that affects surface roughness, and its increase causes an increase of surface roughness because of “double sparking” phenomenon which produces a poor surface finish [15]. In the other words, double sparking and localized sparking become more frequent as the pulse on is raised. Cutting parameters affect the size of eroded craters (diameter and depth) on wire electrode. Larger sizes of craters on the wire increase the risk of wire rupture and also result in poor workpiece surface quality and machining accuracy. Increasing the pulse duration, peak current, and wire speed increase the crater size, whereas excess dielectric flushing pressure reduces the crater size [16]. Roughness can be measured by a profilometer that can be in contact or optical. A roughness value can either be calculated on a profile (line) or on a surface (area). Among profile roughness parameters Ra is more common which is arithmetical mean of the sums of all profile values.

Kerf Width and Sparking Gap

Kerf width and sparking gap are illustrated in figure 9, and they refer to the amount of the material that is wasted during machining. They can determine the dimensional accuracy of the finishing part and the internal corner radius of the product in WEDM operations.

Following equation determines the sparking gap value:

$$\text{Sparking gap (mm)} = (\text{average of kerf width} - \text{diameter of wire})/2 \tag{2}$$

There are some conflict reports about influences of pulse off time duration, peak current and dielectric flushing pressure, on kerf width. For example Parashar et al., (2010) [17] investigates the effects of WEDM parameters on kerf width while machining stainless steel, and it was presented that pulse on time and dielectric flushing pressure are the most significant parameters, while gap voltage, pulse off time and wire feed are the less significant parameters affecting the kerf width. In another research Tosun et al., (2004) [18] performed an investigation on the level of importance of the machining parameters on the kerf width, and he claimed that the gap voltage and pulse duration also were the high effective parameters whereas wire speed and dielectric flushing pressure were less effective factors. According to this research gap voltage is about three times more important than the pulse duration for controlling the kerf width.

Wire Wear Ratio

Minimizing the wire wear ratio is important as this parameter can considerably prevent the wire rupture phenomena. Wire wear ratio (WWR) is obtained by the following equation:

$$WWR = WWL/IWW \tag{3}$$

where WWL is the wire weight loosed after machining and IWW is the initial wire weight. Experimentally, increasing pulse duration and peak current increase the WWR whereas increasing wire speed and dielectric fluid pressure decrease it. The high WWR is always accompanied by high MRR and high Ra value.

Analysing the Wire Rupture and Wire Wear Topography

High peak current and increased spark frequency may cause wire rupture. Topology of wire after EDMing workpiece represents that the wire wear significantly increases with rising peak current and pulse on time. In addition, there is a high risk of wire breakage when wire wear increases [19].

Wire Lag and Wire EDM Inaccuracy

Wherever there is the need to generate complex geometry with tight tolerances, WEDM is very useful. Geometrical inaccuracies are completely unacceptable in this condition. Minimizing the wire lag is important because it can produce geometrical inaccuracy; however, still there is a lack of information about this phenomenon.

More researches about wire lag can improve the accuracy in contour cutting with wire EDM. The wire lag phenomenon is illustrated in figure 10. It is usually measured using Profile Projector by measuring the projection image [20]. In case of orthogonal corners, there is the simple solution of over travel method, however; it is complicated when cutting along a curve is desired. The effects of different WEDM parameters on wire lag during rough cut and trim cut process present that pulse on time, pulse off time and pulse peak current during rough cutting; and also pulse peak voltage, wire tension, servo spark gap set voltage, during trim cutting are the significant factors.

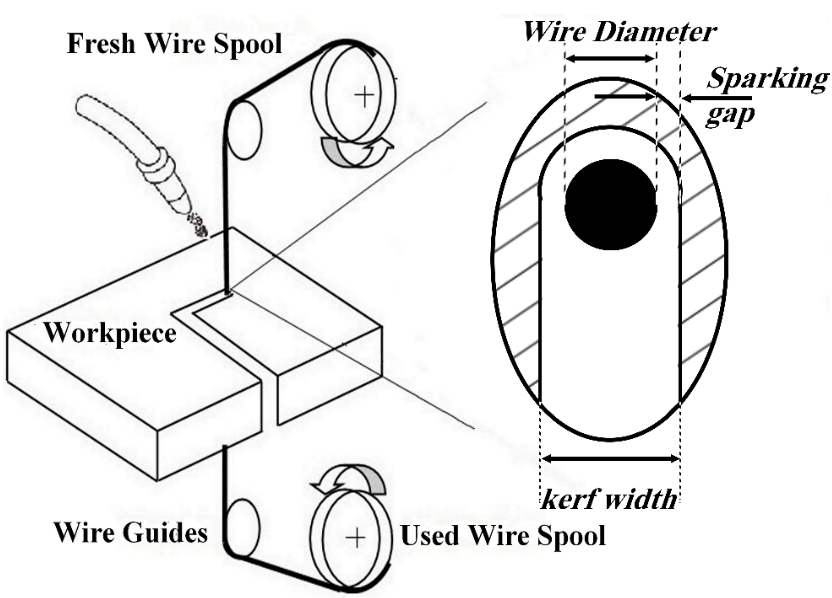

Figure 9. Kerf width and Sparking Gap.

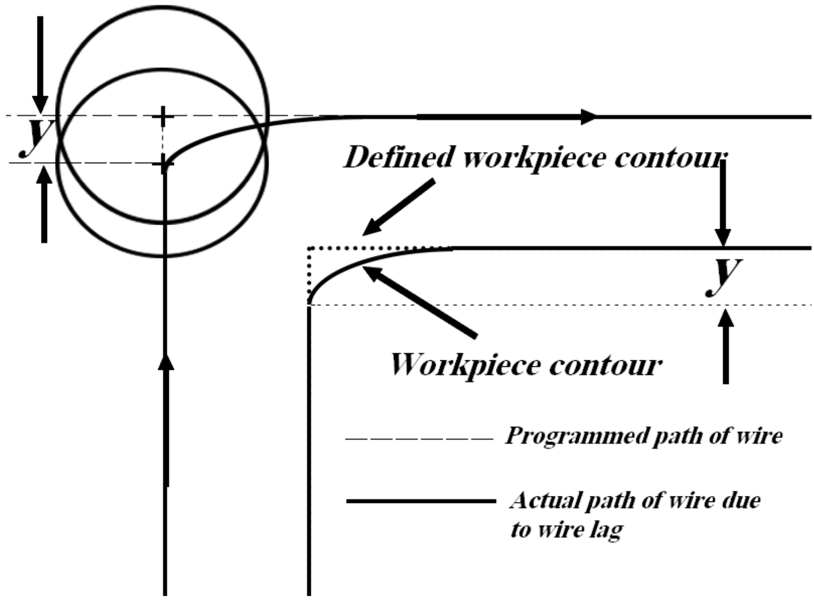

Figure 10. Wire lag phenomenon during wire EDM.

The linear dimensional error, flatness error and perpendicularity error caused by WEDM inaccuracies compared with CNC end milling reveal that the dimensional accuracy achievable in wire cut electrical discharge machining is not as high as anticipated, and its precision level is far less than CNC end milling [21]. Furthermore, wire tension has the greatest effect on three dimensional accuracy characteristics in WEDM, and as it increases dimensional accuracy in WEDM also increases.

Surface Integrity

Although WEDM is among the best choices for cutting "superhard" materials and complex shapes, the major problem is huge thermal stress produced in the process. This thermal stress is created by energy discharge in the bombarded sparks of sample surface during machining process. This stress causes three major phenomena on the surface of specimen, including white or recast layer, surface crack and heat affected zone.

In WEDM each spark makes a small portion of the workpiece melt. While a portion of this molten material is flushed away with dielectric, the remaining part resolidifies rapidly to form a surface layer, known as recast or white layer. This white layer is in direct contact with the environment, and the micro cracks are mostly restricted to this layer. The white layer at the surface of the workpiece machined by WEDM is extremely susceptible to fatigue failure. Below the recast layer, there is Heat Affected Zone (HAZ) which; depending on the chemical mixture of the workpiece; can be a composition of several secondary layers. The HAZ may also contain an altered microstructure, tensile stresses, micro cracks, impurities and other undesirable features, subjected to premature part failure under operation [22].

The intense heat generated with each discharge during machining results in severe local temperature gradients on the machined surface.

During discharge cessation, surface layers cool quickly, developing a residual tensile stress sufficient to produce cracks on the machined surfaces. Among these surface defects, cracking is the most significant as it reduces material resistance to fatigue and corrosion, especially under tensile loading condition. Crack formation is usually associated with plastic deformation and the development of high thermal stresses exceeding the fracture strength. The formation of a micro crack is not only influenced by the setting machining parameters, but also depends on several material properties such as tensile strength, thermal conductivity, thermal expansion coefficient and Young's modulus. The subsurface cracks of WEDM machined samples indicate that the material is amorphous either in free form or in compound form. The formation of a micro crack is generally accompanied due to rapid cooling and heating by dielectric fluid. The heating and cooling processes increase the yield stress, and the plastically deformed material during heating builds up the tensile stresses, which leads to crack formation.

The increases of pulse on time and peak current lead to intense heat conditions on the workpiece, and develop surface cracks in the material. Researches show that increasing pulse on time and peak current develops the surface cracks. To improve the surface integrity of the WEDM process, the surface roughness, white layer thickness and surface crack should be considered. High quality surface integrity can enhance the fatigue strength, corrosion and wear resistance of the workpiece. Through investigation of the effects of different parameters on surface characteristics of Ti6Al4V, it was observed that more uniform surface characteristics are obtained with coated wire electrode [23]. Furthermore, pulse off time is the most affecting parameter in formation of a layer consisting of a mixture of oxides, and a considerable reduction in the formation of oxides is obtained with a lower value of pulse of time. Effects of process parameters on the formation and characteristics of recast layer expose that in term of recast layer the peak discharge current and pulse on time are the driving parameters in order to determine average recast layer thickness and pulse off time, and wire diameter does not displays a significant effect on the recast layer thickness.

Material Transfer

Investigations reveal the migration of tool elements (wire) and dielectric fluid elements to the workpiece surface. For instance, the residuals of copper, carbon and zinc can be detected in the machined samples using zinc coated brass wire which may be due to the melting, evaporation and resolidification of the brass wire electrode. In addition, as a result of high process temperature oxidation of workpiece is observed. For instance, after WEDMing of titanium alloys different types of titanium dioxide such as (TiO_2), ($TiO_{0.325}$), and Ti_2O_3 were formed in the workpiece. The migration of copper to the surface of work material during machining with WEDM may improve the lubricity of the workpiece [24].

TAPER CUTTING

Wire electro discharge machining (WEDM) has become one of the most popular processes for producing precise geometries in hard materials such as those used in the tooling industry. Taper cutting involves the generation of inclined ruled surfaces, and it is especially important in the manufacturing of tooling requiring draft angles.

In this case, the angle is achieved by applying a relative movement between the upper and the lower guides, as shown in Figure 8. The maximum angle that can be obtained is a function of the workpiece thickness and the mechanical behaviour of the wire. Depending on the machine angles as high as ±30 can be cut in a workpiece of thickness 400mm, but this is an upper limit and the angle is usually limited for parts of high thickness.

Accuracy in WEDM is recognised as the research lines key for the next years, since the requirements of tolerances and roughness imposed by industries such as tool making or micromechanics are growing day by day. The mechanics of the process must be analysed in order to achieve better understanding of the inaccuracy causes. When the wire is subjected to tensile stress, the induced deformation depends on different factors such as the cutting condition (whether for rough or finish cutting), the geometry of workpiece and the mechanical properties of the wire. In the case of taper cutting, the deformation caused by the rigidity of the wire in generation of a given angle is also of primary importance. The wire deformation during cutting leads to deviations in the inclination angle of machined parts. This fact causes dimensional errors and loss of tolerances that can lead to the rejection of high added value tooling. In taper cut machining value of the error depends on aspects such as the distance between upper and lower guides, the stiffness of the wire, the geometry of the guides and the forces exerted during the cutting process.

Furthermore, with proper choose of machining parameter and stiffness of wire, angular error can be reduced to less than 3′45″ in 75% of cases [25]. Figure 11 shows the difference between Vertical cutting and Taper cutting in WEDM.

MICRO WEDM

The origin of micro machining technology; which is effectively used in modern manufacturing industries; is in the techniques of manufacturing of microsystems developed in the 1990s. Micro WEDM is recognized as an effective machining technique used in a wide range of applications namely automotive, aerospace, electronics, telecommunications, and healthcare of micro feature with micro and nano level surface finish.

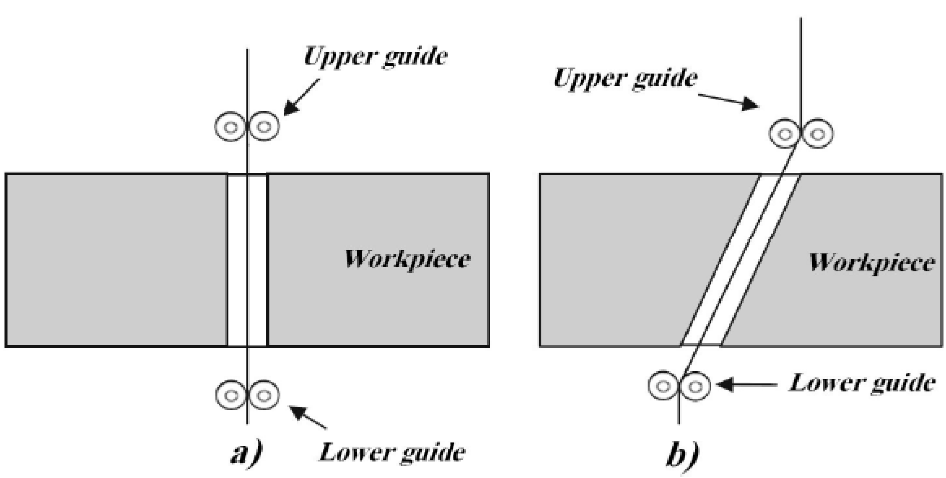

Figure 11. Wire EDM cutting: (a) Vertical cutting, and (b) Taper cutting.

Micro WEDM is conceptually similar to macro WEDM process. it is recognized as an effective machining technique used in micro parts machining for difficult-to-cut materials using micro wire tools (brass, copper and zinc coated copper wire with diameter range from 0.02 mm to 0.05 mm) with advantages of high machining efficiency, precision and low cost. In fact, absolute tolerances of about 1 μm, a surface finish as low as Ra 0.05 μm, a minimum wall thickness of 10 mm and slots of 40 μm width are usual values in this type of product. Cutting speed is no longer a critical issue, ranging in values of about 1 mm^2/min. Part thickness is usually limited to about 3 mm with wire of 30 μm diameter, increasing up to 5 mm when 50 μm diameter wire is used. The first noteworthy point is the ratio between wire diameter and gap width. This ratio is about 10:1 in the case of conventional WEDM, and is reduced to 5:1 in the case of thin WEDM. Implications of this fact include a lower ability of the wire to stand thermal loads, a lower wire rigidity and strength to stand variations of axial load. Moreover, machine precision, and the effect and compensation of heat sources are also very important.

A new family of discharge and pulse generators has been developed for thin wire EDM. Discharge energy must be limited to a minimum in order to prevent wire breakage due to thermal load and wire deformation. Minimum values of discharge energy in conventional WEDM machines equipped with transistor type (FET) generators are about 1.5 μJ, value imposed by pulse on time, the discharge current and the voltage, which is excessive for micromachining applications. The alternative is the use of relaxation type circuits, in which a condenser controls the energy. Also, pulse generator with ability to provide high frequency is essential in micro WEDM [26].

WEDM APPLICATIONS

Traditional machining processes, such as turning, grinding, drilling, milling, etc. remove material by chip formation, abrasion, or micro-chipping. These processes are not satisfactory, economical, or possible to use for machining of advanced materials in many cases for different reasons. First of all normally hardness and strength of these materials are very high and presence of abrasive reinforcing particles reduces tool life while conventional machining.

In addition, usually producing components with complex shapes, high surface finish and dimensional tolerance are not possible with these types of machining. As it was mentioned before, WEDM provides an effective solution for producing these types of components. Brief overview of capability of the WEDM process in the machining of most widely used difficult-to-machine materials including metal matrix composites (MMCs) and titanium alloys are presented in this section.

Modern Tooling Applications

WEDM has been gaining wide acceptance in the machining of the various materials used in modern tooling applications. Several investigations show the machining performance of WEDM in the wafering of silicon and machining of compacting dies made of sintered carbide.

The feasibility of using cylindrical WEDM for dressing a rotating metal bond diamond wheel used for the precision form grinding of ceramics has also been used and the results show that the WEDM process is capable of generating precise and intricate profiles with small corner radius [27].

Metal Matrix Composites

Metal matrix composites (MMCs) are new advanced materials with properties of light weight, high specific strength, good wear resistance and a low thermal expansion coefficient. These materials are extensively used in industry. Greater hardness and reinforcement makes machining with traditional techniques be difficult. Among the different material removal processes, WEDM is considered as an effective and economical tool in the machining of modern composite materials. During WEDM machining of MMCs an accurate and efficient machining performance is achievable. Several comparative studies [28] have been made between WEDM and laser cutting in the processing of metal matrix composites (MMC), carbon fibre and reinforced liquid crystal polymer composites.

These studies showed that WEDM yields better cutting edge quality and has better control of the process parameters with fewer workpiece surface damages. However, it has a slower MRR for all the tested composite materials. Table 2 represents some EDMed and WEDMed metal matrix composites applications in industries [29].

Aeronautical Alloys

Aeronautic alloys, also called superalloys, are metallic alloys for elevated temperature service, usually based on group VIII elements of the periodic table, where resistance to deformation and stability are primary requirements.

Titanium, Inconel and Nimonic alloys are three famous superalloys widely used in different industries. WEDM is one of the best and sometimes the only choice for machining these materials.

Table 2. EDMed and WEDMed metal matrix composites applications

Metal matrix composites	Industrial application
Cobalt matrix with hard tungsten carbide particles	Carbide drills
Steel reinforced with boron nitride	Tank armors
Aluminium boron carbide matrix	Driveshaft
Monofilament silicon carbide fibers in a titanium matrix	F-16 fighting falcon (jet’s landing gear)
Al_2O_3-SiO_2/AC4C	Vane, Pressure side plate of oil pressure vane pump
SiCw/7075	Joint of aerospace structure
Al_2O_3, CF/Al-alloy	Cylinder liner
SiCw/Al-17%Si-4%Cu alloy	Rotary compressor vane

Titanium and its alloys are newly developed advanced materials. This material has a relatively high melting temperature, low thermal conductivity and high electrical resistivity compared to other common materials. Combination of high strength to weight ratio, excellent mechanical properties, corrosion resistance, high elastic stiffness and low density has made titanium alloy the best choice for many critical applications. Reports indicate that it has been widely used in aerospace, military and commercial applications. But at the same time, these characteristics especially low thermal conductivity, low modulus of elasticity and high chemical reactivity of titanium make titanium extremely difficult to machine by conventional machining operations. Low thermal conductivity does not allow the heat generated during machining to dissipate quickly from the tool edge, and high chemical reactivity of titanium alloys destroys the upper layer of the cutting tool besides resulting in cratering and premature tool failure during conventional machining. The best way for machining this material and its alloys is unconventional machining, EDM and WEDM in particular. Although WEDM is among the best choices for cutting titanium, a major problem is huge thermal stress produced in the process. Low thermal conductivity reduces heat dispersion which makes thermal stresses penetrate deeply in the material. Therefore, depth of HAZ produced by WEDM machining depends on thermal conductivity of workpiece and for titanium is significantly larger than most of other commercial materials. This problem can altered microstructure and impose tensile stresses to the workpiece and cause premature failure under operation. The solution to this problem can be WEDM machining with low pulse on time and high flushing pressure.

Nickel base superalloys are extensively used in high temperature applications such as gas turbines, electric power generation equipment, nuclear reactors and high temperature chemical vessels. Inconel 601 and 718 are two famous high nickel content superalloys possessing high strength at elevated temperatures and resistance to oxidation and corrosion. These are examples of an alloy that can be easily machined by WEDM, and this process is widely used for machining them [30]. Nimonic alloys have elevated mechanical properties in extreme temperatures such as resistance to corrosion and retention of strength, which make them valuable in many industries. Because of high specific strength, they are extensively used for the manufacturing of aeroengine components.

In high temperatures most of metals begin to crack, deform and corrode. Nimonic alloys are famous for the maintaining their mechanical properties such as impact strength, yield strength, and hardness in temperatures as high as 1100°F. Hence, these alloys are useful in industries where product damages may occur due to erosion or abrasion of the material or where an aesthetic appearance is necessary. The chemical composition of nimonic alloys ranges from 38 to 76 wt% nickel, up to 27 wt% chromium and 20 wt% cobalt. Other elements such as tungsten (W), tantalum (Ta) and molybdenum (Mo) may be added in order to increase the strength and oxidation properties [28].

Notch wear occurs due to work hardening of the material at the tool nose. Disastrous fracture of the entire inset edge occurs because of the work hardened layer and burr formation. High strength is maintained during machining at high temperatures, which prevents the plastic deformation causing chip formation. Production of hard and continuous chip leads to the reduction of the cutting speed by seizure and cratering. Due to the poor thermal diffusivity of the nimonic alloy high temperature is generated at the tool tip, producing tool wear. There is localization of shear in the chip during machining of nimonic alloys, which produces abrasive edges.

During nimonic alloys machining, the hottest spot is the tool tip, while in case of steels machining; it is at some distance from the cutting tip/edge, resulting in rapid tool wear [6]. Therefore, WEDM is also one of the best alternatives that commonly used for machining this superalloy.

REFERENCES

[1] Ghodsiyeh, D., Golshan, A., Shirvanehdeh, J. A., (2013). Review on current research trends in wire electrical discharge machining (WEDM). *Indian J. Sci. Tech.* 6(2), 154-168.
[2] Kumar, R., Singh, S., (2012). Current Research Trends in Wire Electrical Discharge Machining: An Overview. *Int. J. on Emerging Technol*. 3(1), 33-40.
[3] ONA NX MODULAR: Large die sinking edm machines, Retrieved from: www. onaedm.com Accessed 2015-03-15.
[4] DiBitonto, D. D., Eubank, P. T., Patel, M. R., Barrufet, M. A., (1989). Theoretical models of the electrical discharge machining process: A simple cathode erosion model. *J. Appl. Phys.* 66, 4095-4103.
[5] Hoang, K. T., Yang, S. H., (2015). Kerf analysis and control in dry micro-wire electrical discharge machining. *Int. J. Adv. Manuf. Technol.* 78, 1803-1812.
[6] Goswami, A., Kumar, J., (2014). Optimization in wire-cut EDM of Nimonic-80A using Taguchi's approach and utility concept. *Eng. Sci. Technol., International Journal.* 17, 236-246.
[7] Maher, I., Sarhan, A. A. D., Hamdi, M., (2015). Review of improvements in wire electrode properties for longer working time and utilization in wire EDM machining. *Int. J. Adv. Manuf. Technol*. 76, 329-351.
[8] Kern, R., (2013). *The art and science of making EDM* wire. Retrieved from: http:// www.edmtodaymagazine.com/.
[9] Kern, R., (2013). *EDM wire primer*. Retrieved from http://www.edmtodaymagazine. com.
[10] Antar, M. T., Soo, S. L., Aspinwall, D. K., Jones, D., Perez, R., (2011). Productivity and workpiece surface integrity when WEDM aerospace alloys using coated wires. *Procedia Engineering* 19, 3-8.
[11] Poro´s, D., Zaborski, S., (2009). Semi-empirical model of efficiency of wire electrical discharge machining of hard-to-machine materials. *J. Mater. Process. Technol*. 209, 1247-1253.
[12] Golshan, A., Ghodsiyeh, D., Izman, S., (2015). Multi-objective optimization of wire electrical discharge machining process using evolutionary computation method: Effect of cutting variation. *Proc. IMechE Part B: J Engineering Manufacture*; 229(1), 75-85.
[13] Singh, H., Garg, R., (2009). Effects of process parameters on material removal rate in WEDM. *Journal of Achievements in Materials and Manufacturing Engineering* 32, 70-74.
[14] Yu, P. H., Lee, H. K., Lin, Y. X., Qin, S. J., Yan, B. H., Huang, F. Y., (2011). Machining Characteristics of Polycrystalline Silicon by Wire Electrical Discharge Machining. *Mater. Manuf. Processes*. 26(12), 1443-1450.

[15] Sarkar, S., Mitra, S., Bhattacharyya, B., (2005). Parametric analysis and optimization of wire electrical discharge machining of γ -titanium aluminide alloy. *J. Mater. Process. Technol*. 159, 286-294.

[16] Kanlayasiri, K., Boonmung, S., (2007). Effects of wire-EDM machining variables on surface roughness of newly developed DC 53 die steel: Design of experiments and regression model. *J. Mater. Process. Technol*. 192-193, 459-464.

[17] Parashar, V., Rehman, A., Bhagoria, J. L., Puri, Y. M., (2010). Kerfs width analysis for wire cut electro discharge machining of SS 304L using design of experiments. *Indian J. Sci. Tech.*, 3, 369-373.

[18] Tosun, N., Cogunb, C., Tosun, G., (2004). A study on kerf and material removal rate in wire electrical discharge machining based on Taguchi method. *J. Mater. Process. Technol*. 152, 316-322.

[19] Kumar, A., Kumar, V., Kumar, J., (2013). Investigation of machining parameters and surface integrity in wire electric discharge machining of pure titanium. *Proc. IMechE Part B: J Engineering Manufacture*, 227 (7), 972-992.

[20] Puri, A. B., Bhattacharyya, B., (2003). An analysis and optimisation of the geometrical inaccuracy due to wire lag phenomenon in WEDM. *Int. J. Mach. Tools Manuf*. 43, 151-159.

[21] Islam, M. N., Rafai, N. H., Subramanian, S. S., (2010). An Investigation into Dimensional Accuracy Achievable in Wire-cut Electrical Discharge Machining. *Proceedings of the World Congress on Engineering* Vol. III, 1-6.

[22] Newton, T. R., Melkote, S. N., Watkins, T. R., Trejo, R. M., Reister, L., (2009). Investigation of the effect of process parameters on the formation and characteristics of recast layer in wire-EDM of Inconel 718. *Mater. Sci. Eng. A* 513-514, 208-215.

[23] Ghodsiyeh, D., Golshan, A., Izman, S., (2014). Multi-objective process optimization of wire electrical discharge machining based on response surface methodology. *J. Braz. Soc. Mech. Sci*. 36(2), 301-313.

[24] Kumar, A., Kumar, V., Kumar, J., (2014). Surface integrity and material transfer investigation of pure titanium for rough cut surface after wire electro discharge machining. *Proc. IMechE Part B: J Engineering Manufacture*, 228(8), 880-890.

[25] Plaza, S., Ortega, N., Sanchez, J. A., Pombo, I., Mendikute, A., (2009). Original models for the prediction of angular error in wire-EDM taper-cutting. *Int. J. Adv. Manuf. Technol.* 44, 529-538.

[26] Sivaprakasam, P., Hariharan, P., Gowri, S., (2014). Modeling and analysis of micro-WEDM process of titanium alloy (Ti-6Al-4V) using response surface approach. *Eng. Sci. Technol., International Journal* 17, 227-235.

[27] Ho, K. H., Newman, S. T., Rahimifard, S., Allen, R. D. (2004) "State of the art in wire electrical discharge machining (WEDM)." *Int. J. Mach. Tools Manuf*. 44, 1247-1259.

[28] Lau, W. S., Yue, T. M., Lee, T. C., Lee, W. B., (1995). Un-conventional machining of composite materials. *J. Mater. Process. Technol.* 48(1-4), 199-205.

[29] Garg, R. K., Singh, K. K., Sachdeva, A., Sharma, V. S., Ojha, K., Singh, S., (2010). Review of research work in sinking EDM and WEDM on metal matrix composite materials. *Int. J. Adv. Manuf. Technol*. 50, 611-624.

Ramakrishnan, R., Karunamoorthy, L., (2008). Modeling and multi-response optimization of Inconel 718 on machining of CNC WEDM process. *J. Mater. Process. Technol*. 207, 343-349.

In: Electrical Discharge Machining (EDM)
Editor: M. P. Jahan
ISBN: 978-1-63483-591-6

Chapter 3

EDM MODELLING AND SIMULATION

U. Maradia* and K. Wegener
Institute of Machine Tools and Manufacturing,
ETH Zurich, Zürich, Switzerland

ABSTRACT

EDM processes due to their complexity require a large number of control parameters. On the machine tool manufacturers side, this means hundreds of hours of experimentation to build an optimised parameter database, whereas on the user side, it requires skilled machine operators for today's ever changing product requirements ranging from size, materials and required surface finishes. The modelling of EDM processes is thus not only relevant to understand the gap phenomena but it is also required to increase the competitiveness of EDM process in the manufacturing industry. This chapter provides the state-of-art knowledge on the EDM modelling of single discharges and multiple discharge process, including the associated experimental techniques needed for better understanding of the involved phenomena.

Keywords: EDM, process modelling, material removal, electrode wear

INTRODUCTION

Electrical discharge machining (EDM) is based on the erosive effect of electric discharges on the electrode surfaces. Since the erosion on one of the electrode is higher compared to the other, the electrode with lower erosion is used as a tool electrode and the other is used as the workpiece. Each electric discharge, mainly spark-arc discharge causes a crater on the electrode surfaces and applying a series of sparks results in erosion over the frontal surfaces of the electrodes as shown in Figure 1. In order to achieve the desired surface quality and precision in the smallest possible time, one uses multiple steps or strategies during erosion of a cavity.

* Corresponding author: U. Maradia. E-mail: maradia@inspire.ethz.ch.

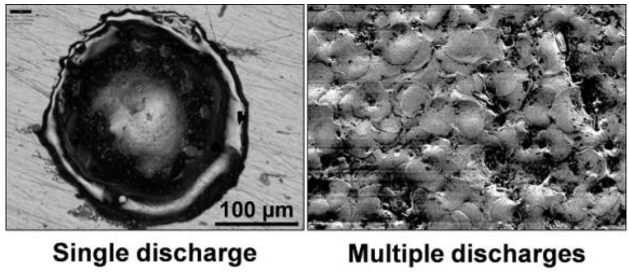

Figure 1. Left: an erosion crater generated by a single discharge on steel workpiece; Right: a series of pulsed discharges leading to erosion of the surface.

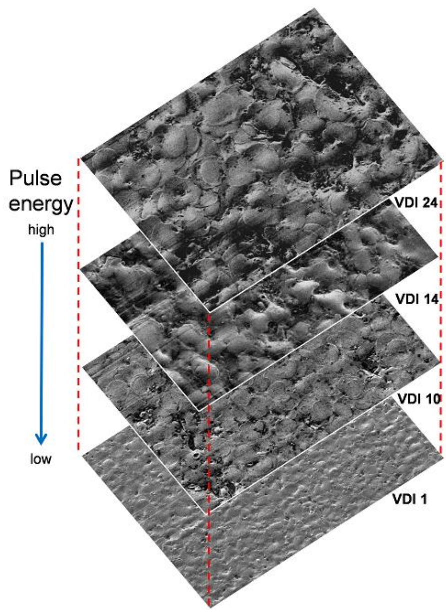

Figure 2. Effect of different discharge energies on the crater size and the resultant surface quality. With decreasing discharge energy, roughness of the eroded surface decreases.

Here, large discharge energies in *mJ* range are applied during roughing leading to large crater volumes and thus high material removal rates (MRR). For semi-finishing and finishing steps, decreasingly smaller discharge energies in *µJ* range are applied until the desired surface quality is achieved as seen in Figure 2. Since the smaller discharge energies result in smaller craters and thus lower MRR, only a last few hundred microns of erosion is performed by these steps. For the discharge energies in a few hundred *mJ* range, transistor type pulse generators are used, whereas for smaller discharge energies relaxation type or capacitor pulse generators are used. Examples of the typical electrical signals of these different pulse types are shown in Figure 3.

Over the time, EDM has been developed into several main task specific variants namely die-sinking EDM, wire EDM and drilling EDM. The types of pulses used during erosion are dependent on the specific requirements of erosion job and the variant. For example, transistor type pulses are mainly used for roughing in die-sinking EDM and in drilling EDM.

Relaxation capacitor pulses are used for finishing in die-sinking EDM, for wire-EDM and for micro-EDM drilling and micro-EDM milling.

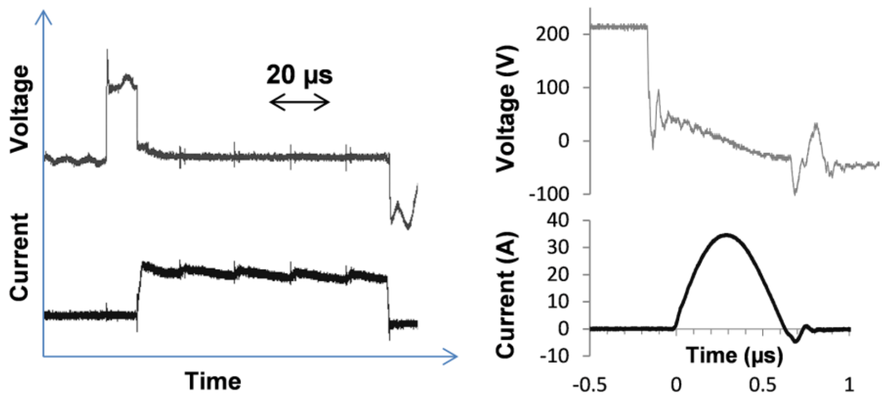

Figure 3. Voltage and current waveform examples for a single pulsed discharge generated by transistor pulse generator (left) with 5.4 A, 100 V ignition voltage and relaxation pulse generator (right).

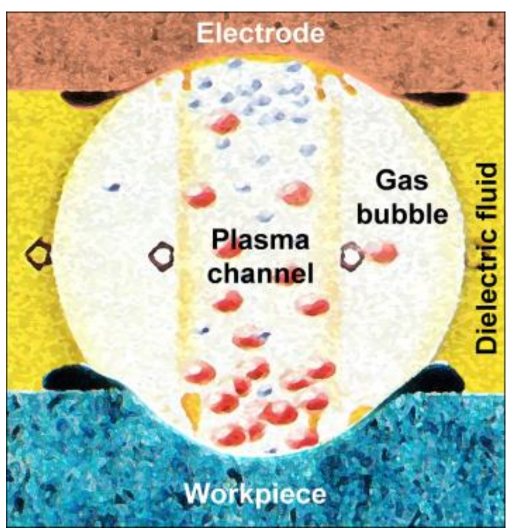

Adapted from GF AgieCharmilles SA.

Figure 4. Depiction of the electric discharge phenomena in EDM. Here, electrode (+) and workpiece (-) are separated by a small gap filled by dielectric fluid.

Thus, understanding of both pulse types is essential. Also, transistor type pulses with *mJ* energies have pulse duration ranging from a few micro seconds to a few hundred micro seconds, whereas relaxation capacitor type pulses usually have pulse durations below a microsecond down to a few nanoseconds. Additionally, the dielectric fluid is different depending on the EDM variant and application, where oil is typically used for die-sinking and de-ionised water is used in wire-EDM and drilling EDM.

OVERVIEW OF EDM GAP PHENOMENA

When the electrode and workpiece are separated by a small gap filled with dielectric oil, deionised water or gas; the application of high voltage between these two electrodes (tool, workpiece) results in ionisation of the dielectric fluid. This leads to forming of streamers, which establish a plasma channel between the electrode and workpiece (see Figure 4), usually at a spot where the electrostatic potential is strongest, due to micro peaks, small metallic debris and micro-bubbles in the gap. The time from the application of the ignition voltage U_i in the gap region till the breakdown is called delay time t_d in EDM (see Figure 3).

Upon the establishment of the electrical conductive plasma channel, the ignition voltage drops and current passes through the plasma channel, thus closing the electric circuit. The voltage during the discharge remains at a certain value range, called discharge voltage U_e or burning voltage. The current conduction through the resistive plasma channel results in Joule heating and the energy is released from the plasma channel to the surrounding, i.e., tool electrode, workpiece and dielectric through radiative, conductive and convective losses. This leads to vaporisation of the liquid to form a gas bubble surrounding the plasma channel. The plasma channel expands with time through ionisation of the surrounding gas, whereas the gas bubble expands due to the instantaneous pressure generated during the breakdown, plasma radiation and kinetic energy.

The heat flux from plasma into the electrodes leads to melting and vaporisation of the material. Upon termination of pulse current, the plasma channel extinguishes rapidly, resulting in the open electric circuit loop. A part of the molten material on the electrode surfaces is flushed away by the gas bubble implosion and dielectric fluid jets impinging upon it and the rest of the molten material is re-solidified. The dielectric fluid quickly de-ionises during the open electric circuit condition. After sufficient time t_p, another voltage pulse is applied between the inter-electrode gap. This time duration between two pulses is called pause time or interval time. Thus, using consecutive pulse discharges, erosion is achieved in all variants of EDM. It must be noted that the capacitor type pulses have sinusoidal current form and the peak intensity and duration is dependent on the chosen capacitance, capacitor charging voltage-current and time. EDM process modelling is a complex task due to the involved multi-physics at multi-time scales. The single discharge phenomena in EDM consist of solid, liquid, gas and plasma states confined within a few hundred micrometres region and occur at the time scales ranging in micro- to nano-seconds. The involved thermodynamics, plasma physics - chemistry, magneto-hydrodynamics and fluid dynamic effects require several simplifications in order to model and simulate the process. A generalised model for EDM processes according to Hinduja and Kunieda [1] is shown in Figure 5 (left). Also, the research and understanding of the EDM fundamentals is well summarised by Kunieda et al., [2] and Kunieda [3].

Apart from the physical or mechanistic modelling summarised by Dhanik et al., [4], phenomenological models developed in EDM are compiled by Mohd Abbas et al., [5] and shown in Figure 5 (right). In the following section, physical process modelling of single discharges is presented, followed by the modelling of multiple discharges with respect to the EDM variant specific issues in process modelling. A short overview of the phenomenological modelling techniques for EDM is provided at the end.

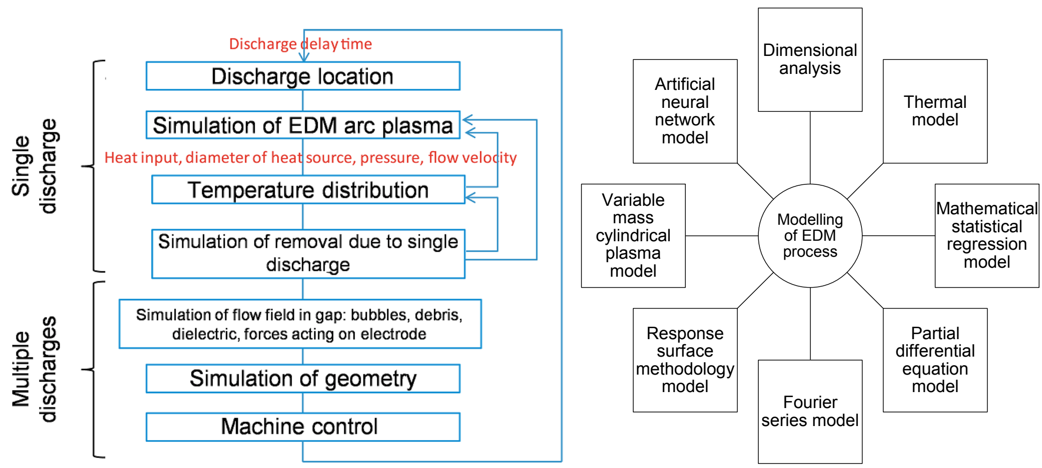

Figure 5. Left: generalised model for EDM processes according to Hinduja and Kunieda [1]; Right: Overview of EDM process model approaches from literature compiled by Mohd Abbas et al., [5].

SINGLE DISCHARGE

For EDM, the interest in process modelling mainly lies in the crater simulations, since it defines the main process outputs, namely material removal rate, electrode wear and surface roughness. However, since the crater is generated due to the heat flux from plasma, it is also necessary to understand the plasma conditions.

A schematic overview of a single discharge for modelling is shown in Figure 6 (left). Here, the fractions F_c, F_a, F_p of total discharge energy E are shown to be distributed into cathode, anode and plasma / dielectric respectively. Also, different plasma channel radii r_a and r_c are considered for anode and cathode respectively.

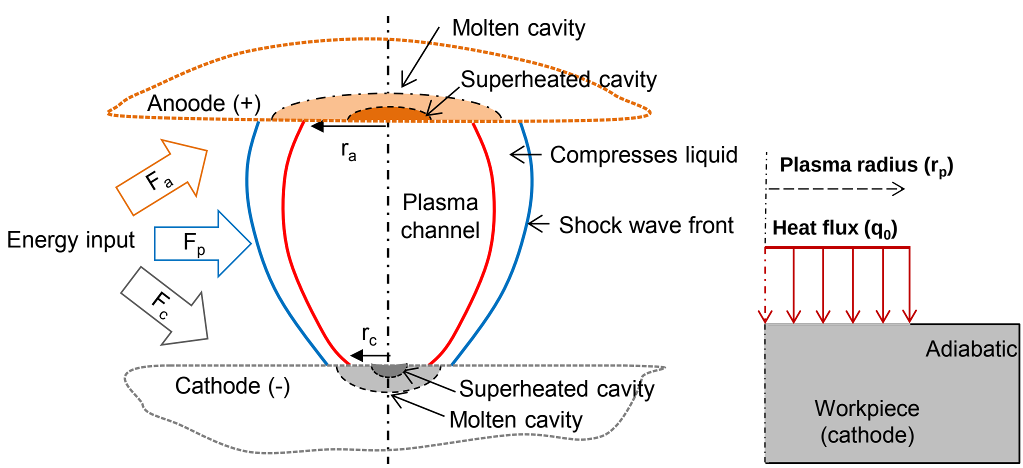

Figure 6. Left: schematics of the thermo-physical model of a single discharge in EDM adapted from Yeo et al., [6, 7]; Right: boundary conditions for temperature distribution simulations in workpiece.

In order to simulate the temperature distribution in anode and cathode, several boundary conditions and assumptions are required, as seen in Figure 6 (right). It is seen that for the temperature distribution simulations in electrodes, mainly plasma or heat source radius, heat flux or heat source temperature and heat flux profile are required. Once the molten material region is simulated, its removal mechanism also needs to be understood.

Thus, present section first shows the modelling technique of discharge plasma, followed by plasma-material interactions, which deal with temperature distribution simulations and material removal mechanism.

Discharge Plasma

The discharge plasma during a single discharge has three distinct phases, i.e., ignition or breakdown, propagation and extinction. The ignition or the breakdown phase is mainly interesting for the inter-electrode gap and the delay time, especially for developing the dielectric oil. While larger inter-electrode gaps result in lower precision of the eroded cavity, longer delay times also result in unproductive times during erosion. Discharge breakdown occurring in gas along with the associated physical phenomena have been studied thoroughly, especially for the discharge gaps larger than 1 mm as summarised by Meek and Craggs [8] and Raizer [9], along with the widely accepted theory of streamers to explain the discharge breakdown in gas by Loeb and Meek [10]. On the other hand, breakdown mechanism in liquid is still disputed as reviewed by Kolb et al., [11]. Also, for gaseous dielectric media, Paschen's law overestimates the required breakdown voltage. Breakdown in microgaps filled with liquid is investigated by Schoenbach et al., [12]. Schulze et al., [13, 14] analysed the pre-ignition stage in EDM using high-speed imaging. The debris particles in discharge gap lead to an increase in gap width, however discharge breakdown in EDM is found to be probabilistic by Kunieda and Takanobu [15]. The role of debris particle and gas bubbles in the discharge gap is further investigated in Schumacher [16] to understand the discharge breakdown behaviour. The debris distribution and gas bubble growth are well summarised in Kunieda et al., [2]. Recently Gatto et al., [17] provided the experimental proof of the bridges of debris in small hole drilling, which affects the spark ignition process.

Eckman and Williams [18] analysed the physical theory concerning the state and dynamics of the ionised column for first micro second after the arc formation, where arc radial growth, column pressure, temperature, and electron density were calculated for discharge plasma in liquid nitrogen dielectric. Eubank et al., [19] developed a variable mass cylindrical plasma model with water as dielectric, where plasma radius, temperature and pressure are calculated by considering plasma enthalpy, mass density and inclusion of the heats of dissociation and ionisation. Radiation from plasma is considered as the main mechanism of heat dissipation from the plasma into the dielectric and electrodes. Hayakawa [20, 21] carried out magneto-hydrodynamics analysis of a steady state arc in gas, with plane-plane copper electrode configuration. Thermo-physical properties of the plasma such as electromagnetic field, temperature, pressure and velocity distributions were calculated, an example of which is shown in Figure 7 (left).

A model of single discharges in deionised water for micro-EDM has been recently presented by Mujumdar et al., [22]. Using a global model consisting of plasma chemistry, power balance and bubble dynamics, various outputs such as plasma composition, temperature, plasma size, pressure and heat flux are calculated. Average electron density of 8.9×10^{17} cm^{-3} and electron temperature of 6817 K are predicted.

In terms of the experimental analysis of discharge plasma, Albinski et al., [24] used photomultipliers and using the relative intensities of two Fe I spectral lines, determined the EDM plasma temperature at about 8,000 K - 10,000 K. Pillans et al., [25] used a fibre optic to detect arcing through plasma and measured the temperature ranging from 30,000 K down to 9,000 K. A first detailed analysis of EDM discharge plasma was carried out by Descoeudres [23], where both time-resolved and spatially-resolved optical plasma spectroscopy was performed. Examples of the acquired time- and space-resolved spectra of EDM discharges are shown in Figure 7 (centre, right).

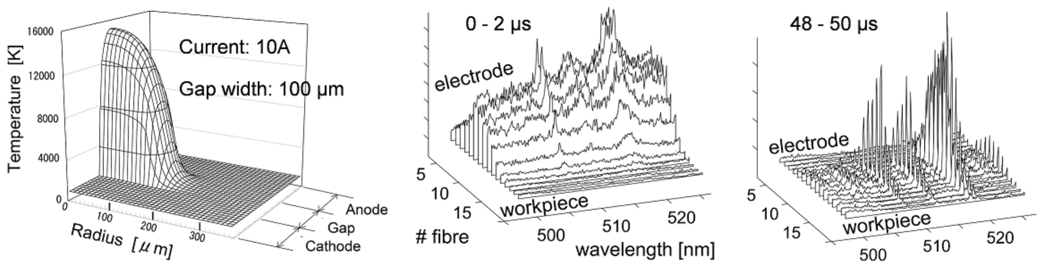

Figure 7. Left: temperature distribution in electrode and gap obtained by magnetohydrodynamics analysis [20]; Centre, Right: measured spatial and time resolved spectra of 12 A discharges in oil between copper anode and steel cathode with elapsed time from discharge breakdown of 0 µs - 2 µs and 48 µs - 50 µs [23].

Plasma temperature of about 8000 K and electron density in order of 10^{17} - 10^{18} have been determined which relates to the cold dense plasmas, as the coupling factor of EDM plasmas is 0.33. Nagahanumaiah et al., [26] characterised the plasmas in micro-EDM, where the capacitance type pulses are used. Electron density in order of 3.5×10^{18} cm^{-3} and plasma temperature between 5000 K - 8000 K with an average of 6170 K have been determined. Also, the plasma coupling parameters is determined to be 0.475 apart from the observation of broadened H_β spectral line. Kanmani Subbu et al., [27] characterised the plasma in dry-EDM, where electron density of 10^{13} - 10^{14} cm^{-3} and plasma temperature of 4,000 K ± 500 K has been determined, suggesting the ideal plasma. It must be noted that for all the mentioned work in EDM plasma characterisation, thousands of discharges have been considered and average plasma values have been calculated, since the emitted light signal from a single discharge is weak.

Recently, Braganca et al., [28] used optical emission spectroscopy and semi-empirical resistive plasma model to understand the effect of gap size, pulse duration and current on electrode density of single discharges, which was determined to be in order of 10^{16} - 10^{17} cm^{-3}. Kanemaru et al., [29] observed the bubble dynamics by applying double-pulsed micro-discharges. Here, the plasma generated by a second pulse within the bubble resulted from the first discharge is also analysed.

In order to better understand and interpret the discharge plasma spectrum, recently spectrum simulations have been performed by Hollenstein [30]. It is shown that using the commercial simulation software such as PrismSpectra, one may simulate the discharge plasma spectra with the inputs such as electron density, electron temperature, atomic composition and plasma size. The simulations may be useful for element spectral line identification, analyse the opacity of the plasma, ionisation of the plasma, contribution of the different plasma components, etc. An example of the spectrum simulation is shown in Figure 8. Using the measured properties by experimental analysis from the above mentioned authors, Adineh et al., [31] calculated thermodynamic and radiative properties of plasma excited in EDM in liquid nitrogen dielectric, where the net emission co-efficient method has been used as explained in [32]. The modelling and simulation of plasma opens up a new way to increase the understanding of EDM plasma, such as the cooling effect in a plasma due to increasing iron vapour content, as shown by [31].

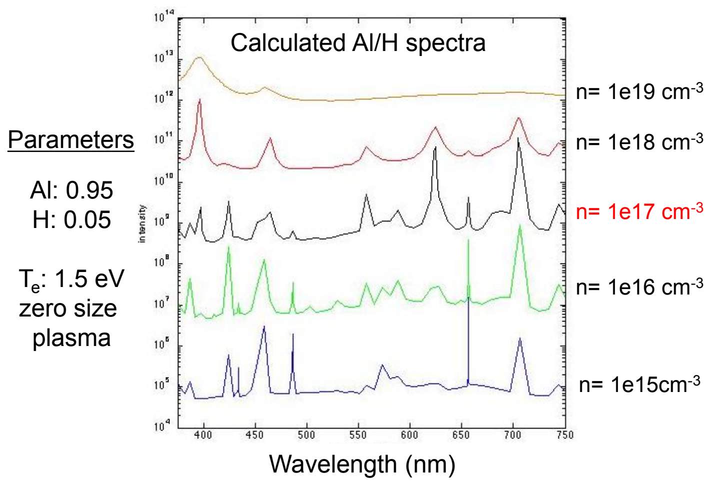

Source: Hollenstein [30].

Figure 8. Analysis of the effect of electron density on the resulting plasma spectrum of a discharge between aluminium (Al) electrodes in dielectric hydrocarbon oil.

Plasma As Heat Source

As mentioned before, for erosion crater simulations, boundary conditions such as plasma or heat source radius, flux or temperature and flux profile are required. In order to determine these conditions, one may either directly analyse the plasma or take the approach of inverse analysis, where the plasma properties, thus boundary conditions are derived through analysis of the erosion craters.

One of the first theoretical models for spark channel in large gaps and its expansion were first presented by Drabkina in 1951, later improved by Braginskii [33]. While Drabkina used instantaneous energy release which forms a cylindrical region of pressure discontinuity at whose boundary, shock is formed; Braginskii used hot expanding channel to act as piston to compress the gas in front of it thus leading to shock in surrounding compressed gas, forming a thin shell where ionisation takes place. Skvortsov et al., [34] used electrical and optical measurements and provided experimental studies for expansion of a spark channel in liquid. Underwater experiments on wire explosion led Robinson [35] to simulate electric discharge in water using finite difference method. Zahn et al., [36] proposed a theoretical hydrodynamic shock wave propagation model using Rankine-Hugoniot boundary conditions to explain expanding cylindrical wavefront emanating from expanding spark channel of high current and voltage observed by several authors using techniques such as laser Schlieren, shadowgraph photography, etc. However, most of these studies were concentrated to high voltage, high current and large gap discharges resulting in overestimation of the plasma radius for EDM.

For low current, low voltage discharges in small gaps as in the case of EDM, Eubank et al., [19] proposed a variable mass plasma expansion model. From the underwater exploding wires experiments, they defined plasma radius r_p (in µm) expansion over time t (in µs) as

$$r_p = 0.788 \cdot t^{3/4} \tag{1}$$

Pandey and Jilani [37] assumed that the channel growth rate is limited by a minimum surface temperature inside the heat source, in order to evaporate metal during the entire pulse duration. As it has been observed by Utsumi [38] for vacuum arcs that the cathode spot temperature remains nearly constant and equal to the boiling temperature T_b of the cathode material, Pandey and Jilani [37] considered that in EDM, the cathode spot temperature remains equal to the boiling temperature and derived

$$T_b = \frac{E \cdot F_c \cdot 10^6}{k \cdot r_p \cdot \pi^{3/2}} \cdot tan^{-1}\left[\frac{4 \cdot a \cdot t \cdot 10^6}{{r_p}^2}\right]^{1/2} \tag{2}$$

Note that here the energy density Q has been replaced with the discharge energy E and the units are normalised. Here, T_b is boiling point temperature in K, r_p is heat source radius in m, k is thermal conductivity in W/m·K, a is thermal diffusivity in m^2/s, t is pulse duration in µs, E is total discharge power in W and F_c is cathode energy fraction.

One of the first systematic experimental measurements of plasma expansion using high-speed imaging in EDM were performed by Descoeudres et al., [39], shown in Figure 9. Using a fibre bundle, high-speed imaging camera and band-pass filter for hydrogen spectral line H_α, measurement of the plasma region were performed. It was found that the plasma develops rapidly upon breakdown and the visible light emission region and ionised hydrogen region are almost similar. Kojima et al., [40] used high speed imaging up to one million frames per second and used spectroscopy to determine EDM arc plasma diameter in gas and correlated to the discharges in oil. It was observed that the discharge crater expands much slowly compared to the arc plasma channel. Also, an empirical relation of the plasma radius is expressed as

$$r_p = 0.85 \cdot 10^{-3} \cdot t^{0.35} \cdot {i_e}^{0.48} \tag{3}$$

Here, r_p is in m, t is in s, i_e is discharge current in A.

Using transparent SiC and Ga_2O_3 single crystal electrodes and inverse heat conduction simulations, Kitamura and Kunieda [41] found that the plasma diameter is larger than the heat source diameter. However, Maradia et al., [42] used high-speed imaging to determine the gas bubble and plasma expansion for different currents and electrode-workpiece materials and found that the gas bubble and plasma region vary depending on the anode and cathode material properties.

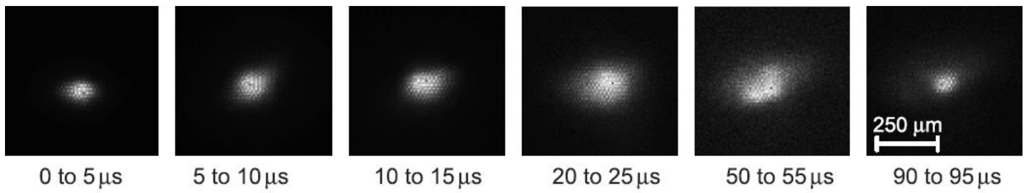

Source: Descoeudres et al., [39].

Figure 9. Plasma images at different times during the discharge (5μs exposure, variable delay after breakdown; 24 A, 100μs, water). The images are normalized in intensity. Each image is obtained during a different discharge.

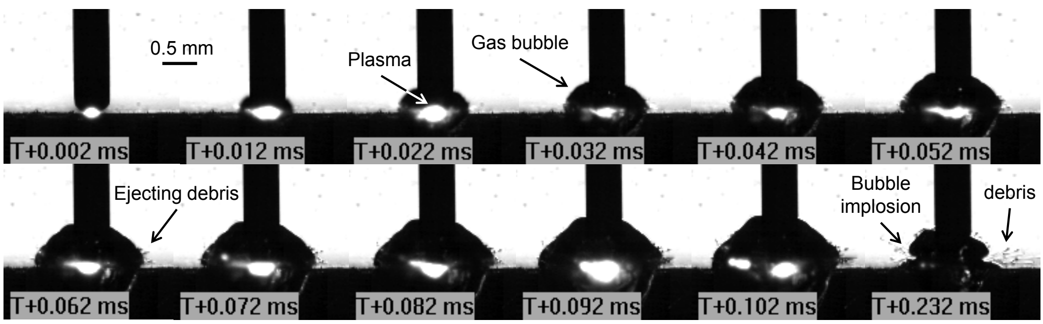

Figure 10. High-speed imaging of gas bubble and plasma expansion at 200,000 fps. A single discharge with 20A and 100µs is generated in dielectric oil between Ø 0.5 mm graphite electrode (anode) and steel 1.2343 workpiece plate (cathode).

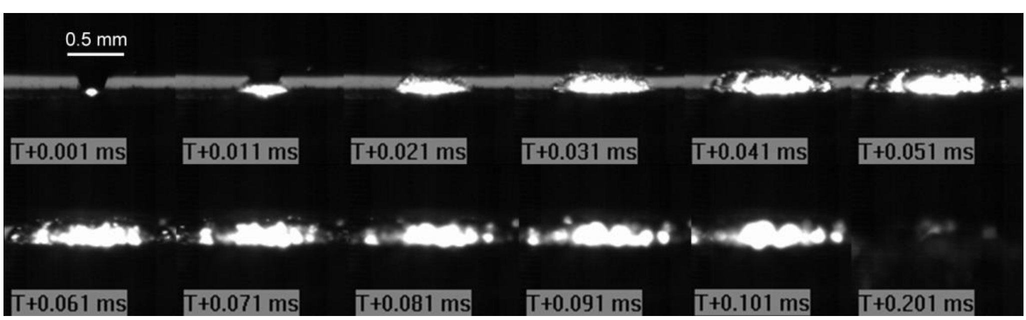

Figure 11. High-speed imaging of gas bubble and plasma expansion at 200,000 fps. A single discharge with 20A and 100µs is generated in dielectric oil between Ø 5 mm graphite electrode (anode) with a micro peak and steel 1.2343 workpiece plate (cathode).

Thus, the use of high resistivity transparent materials may lead to slightly different behaviour compared to the conventional EDM materials. In fact when considering the light-emission region, the excitation energy difference for different workpiece material elements must also be taken into account.

Some examples of the high-speed images for 20A discharges with 100 µs duration for different electrode configurations are shown in Figure 10 and Figure 11. It is seen that the plasma region or the light-emission region may be ambiguous due to the obstruction and reflection from the gas bubble. A method combining a high repetition rate imaging and a short pulse laser as an illumination source has been developed by Tanabe et al., [43], where example of 30 A discharge images with a band-pass filter (532 nm) to block the plasma light is shown in Figure 12. Heat flux profile is also important for the crater simulations. Using the high speed imaging, Descoeudres et al., [39] found that the light intensity is highest in the discharge centre as shown in Figure 13.

Also, using spatially-resolved light emission spectroscopy of plasma they found that the electron density is slightly higher in the discharge centre, whereas the electron temperature remained almost constant. Kitamura and Kunieda [41] found that the heat flux is not uniform in the plasma because the lower temperature in the circumferential area in plasma results in a significant drop in the degree of ionisation. For crater simulations, mainly uniform heat flux distribution and Gaussian heat flux profiles are considered as discussed later. Heat flux q_0 is a fraction F of the total discharge energy E over the heat source area.

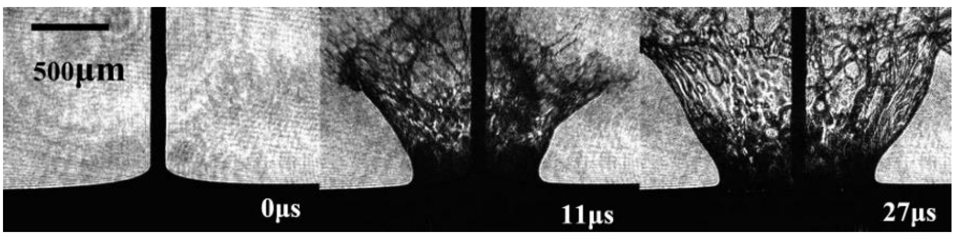

Figure 12. Typical oil blow-off in a single discharge with negative electrode polarity acquired using a novel method by Tanabe et al., [43].

For uniform distribution of heat flux over the discharge spot, heat flux q_0 is given by

$$q_0 = \left(\frac{E \cdot F}{\pi \cdot {r_p}^2}\right) \tag{4}$$

where the total discharge power E is given by

$$E = U_e \cdot I \cdot t \tag{5}$$

An example of Gaussian heat flux profile is defined by Joshi and Pande [44] as

$$q(r) = \frac{4.57 \cdot E \cdot F_c}{\pi \cdot {r_p}^2} \cdot exp\left[-4.5 \cdot \left(\frac{r}{r_p}\right)^2\right] \tag{6}$$

Here, r is the distance from heat source centre. Since discharge voltage U_e and current I can be measured using an oscilloscope, one mainly needs to determine r_p and the fractions of total discharge energy entering the anode F_a and cathode F_c.

Energy distribution into the gap is a complex phenomenon and almost no theoretical models exist in EDM to determine anode and cathode energy fractions. Some theoretical work exists and remains active research topic in arc discharges as seen from Benilov [45] and Heberlein et al., [46]. In electric discharges, electrons are seen as simply falling from the plasma into the anode because of its higher electrical potential, whereas the cathode has to develop very efficient emission mechanisms to extract electrons from the metal into the plasma, which is considered mainly to be thermionic field emission for the arc discharges. The voltage jump is mostly localised near the electrodes, in the anode and cathode layer, as seen in Figure 14.

As Descoeudres [23] summarises, the discharge organises itself in such a way as to create a strong electron emission from the cathode. The cathode spot is heated by the ion bombardment coming from the ionisation layer of cathode layer, leading to evaporation and melting, thermionic emission and in some cases thermal runaway. The electrons coming from the cathode are crucial to create a high ionisation in the ionisation layer, producing the ions that will heat the cathode. This coupled ion-electron production is the sustaining mechanism of the arc discharge. Thus, energy balance at cathode involves ion bombardment, smaller contributions from Joule heating, atom and electron bombardment, recombination in the cathode and plasma radiation.

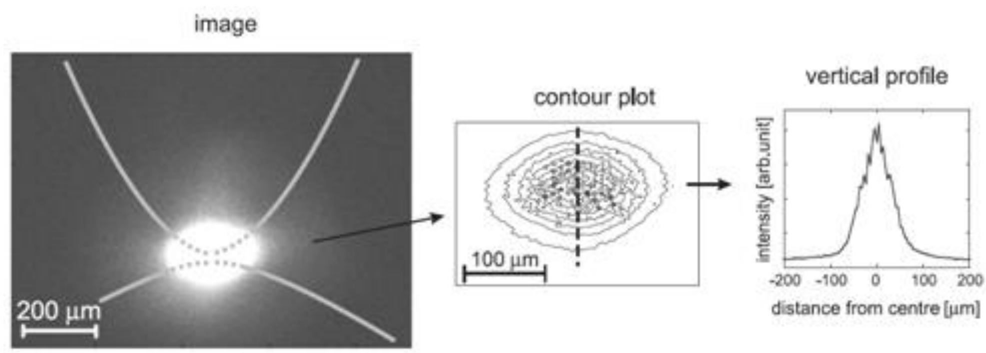

a b c

Source: Descoeudres et al., [39].

Figure 13. (*a*) Typical plasma image (5μs exposure, 5μs delay after breakdown; 24 A, 100μs, oil). The position of the electrodes is drawn. (*b*) Contour plot of (*a*). (*c*) Intensity profile of (*a*) along the vertical axis.

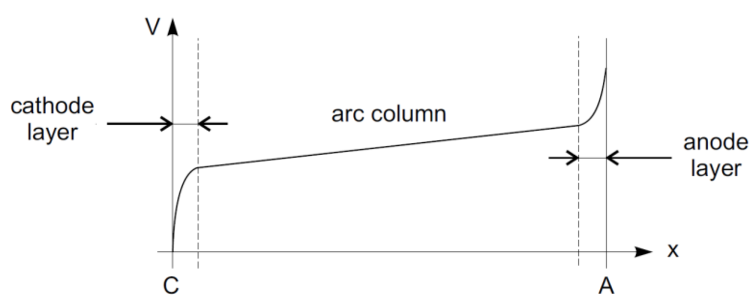

Figure 14. Schematic profile of electrical potential in an arc [23].

Energy is dissipated mainly by electron emission and heat conduction in the electrode, along with a small fraction by evaporation, surface radiation and droplet emission. Similarly, the situation at the anode is also complex, where the current is considered to be distributed over a larger surface compared to the cathode. The metal vapour from the anode can be ionised in the anode layer due to a space charged region. Energy is brought to the anode by the electron flux and recombination with ions in the anode, whereas the energy is dissipated through evaporation and heat conduction. In the arc column itself, a large quantity of the discharge power is dissipated by Joule effect, heat conduction and radiation.

Due to the high complexity of energy balance in discharges, experimental techniques are employed in EDM for anode and cathode energy fraction determination. This mainly involves temperature measurements in anode and cathode, analysis of the melt zone of the discharge craters and then performing inverse heat conduction simulations to determine the heat input.

König et al., [47] measured the temperature of electrodes and dielectric fluid to determine the energy distribution, whereas Xia et al., [48] measured temperature of electrodes and compared with the calculated results to obtain energy distribution. They found that the energy fraction into anode is always higher than into cathode, with values ranging from 0.40 - 0.48 and 0.25 - 0.34 respectively, both for single and multiple discharges.

Similar approach has been taken by Revaz et al., [49], where using a high resolution and fast response temperature measurement device shown in Revaz et al., [50], reverse simulation is performed to calculate energy fraction, which was found to be 0.10 for a single discharge and 0.15 for the multiple discharges. Using different current emission mechanisms and cathode space charge characteristics, and on basis of the spot current density values including electronic and ionic contributions, a model for relative power dissipation in EDM discharges is presented by Perez et al., [51].

Singh [52] used temperature measurement and simulations to determine the effect of current, pulse duration, materials and polarity and found the energy fraction into cathode ranging from 0.06 - 0.268, where it is shown that the energy fraction values are time dependent. Zhang et al., [53] performed metallographic analysis of the erosion craters to determine the melt zone and using heat conduction simulation, determined the energy input into anode and cathode. Based on the crater analysis for melt front and heat conduction simulations, Maradia et al., [42] shown that the energy fraction is also dependent on thermal properties of the anode and cathode material. An overview of the energy distribution into anode and cathode from nanosecond to millisecond scale discharge durations is shown in Figure 15. It is shown that for short discharge durations, most of the energy is dissipated into the plasma and dielectric, whereas for longer discharge duration, when the plasma becomes self-sustaining, most of the energy is dissipated into the anode and cathode.

Plasma Material Interactions

Once the boundary conditions such as heat source radius, heat flux profile and heat flux are known, one may calculate the temperature distribution in anode and cathode using the heat conduction theory. Such simulation provides estimation of the melt region in the electrodes, however erosion craters are in reality smaller than the molten material region. The difference in the molten volume and the eroded crater volume is termed as plasma flushing efficiency (PFE).

Temperature Distribution

Temperature distribution in the electrode due to the heat flux from plasma is calculated using the heat conduction theory or Fourier's law by

$$\frac{\partial^2 T}{\partial x^2}+\frac{\partial^2 T}{\partial y^2}+\frac{\partial^2 T}{\partial z^2}+\frac{\dot{q}}{k}=\frac{1}{\alpha}\cdot\frac{\partial T}{\partial t} \tag{7}$$

Here, T is the temperature, x, y and z represent the Cartesian coordinate system, q is the rate of internal energy generation per unit volume (Joule effect), k is the thermal conductivity, t represents time and α is the thermal diffusivity defined by

$$\alpha=\frac{k}{\rho\cdot c_p} \tag{8}$$

where ρ is mass density and c_p is specific heat at constant pressure. Carslaw and Jaeger [54] have provided analytical solutions for different spatial configurations.

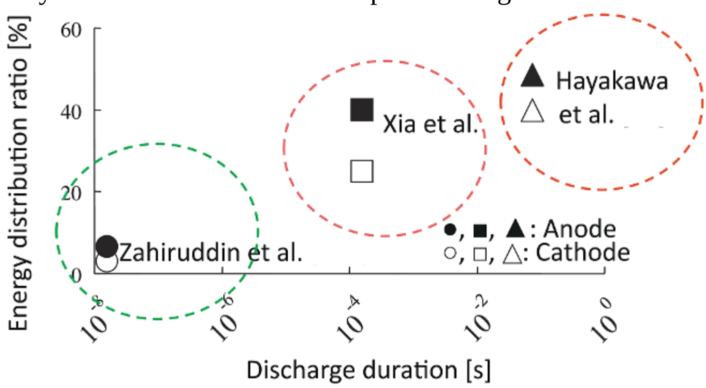

Taken from Hinduja and Kunieda [1].

Figure 15. Energy distribution into anode and cathode.

Another common approach for heat conduction simulation is using the numerical methods. Here, heat equation for FEM is described as

$$\rho C_p\left(\frac{\partial T}{\partial t}\right)+\rho C_p\overline{u}\cdot\nabla T=\nabla\cdot(k\nabla T)+Q \tag{9}$$

with the boundary condition for general inward heat flux defined by

$$-\overline{n}\cdot(-k\nabla T)=q_0 \tag{10}$$

and the boundaries without heat flux are considered adiabatic, with the thermal insulation defined as

$$-\overline{n}\cdot(-k\nabla T)=0 \tag{11}$$

In addition to the above mentioned symbols, ***u*** is velocity vector and ***n*** is the normal outwards vector on the boundary. Q is thermal energy generated per unit volume and q_0 is the heat flux vector per surface area from the plasma channel.

A first comprehensive physico-mathematical model of material removal in cathode and anode has been provided by Van Dijck [55], based on the theories proposed by Zolotykh [56, 57] and Zingerman [58]. A time dependent circular heat source is used to analytically calculate temperature in cathode and anode with energy fractions (F_a, F_c) of 0.5. The heat source, i.e., the plasma was considered to expand such that the centre temperature on the cathode surface remains about 200°C - 300°C higher than its boiling temperature, due to the consideration of average gas bubble pressure. Here, temperature dependent properties of material and latent heats of vaporisation and melting were not considered. Joule heating, radiation and convection effects were found to be negligible compared to the heat conduction into the electrode with plasma as the heat source.

Yeo et al., [59] compared the five well-cited models from Snoeys, Van Dijck, Beck, Jilani and DiBitonto, and found that simulated results using the DiBitonto’s model yielded closest approximation to the measured crater geometries, especially for the discharge energies larger than 1.2 mJ. DiBitonto et al., [7] used a point heat source and photoelectric effect in cathode erosion model, where discharge power instead of the surface temperature and energy fraction of 0.183 entering into the cathode are considered. Also, temperature dependent properties of materials are included, while ignoring the latent heat of vaporisation and melting, as their contribution is considered to be less than 2% on simulation results.

An anode erosion model was presented by Patel et al., [60], belonging to the same group as DiBitonto, where a time dependent circular heat source according to Equation (1) and Gaussian-distributed heat flux is considered. Using the energy fraction entering into anode F_a = 0.08, rapid melting of the anode material (copper) and subsequent re-solidification of the material for longer discharge times leading to low wear has been simulated.

It is seen that for the heat conduction simulations, different boundary conditions are used by different authors, which has been found to exert a significant influence on the calculation of boiling and melting point isothermal surfaces, as mentioned by Kunieda et al., [2] from Xia [61]. An overview of the used energy fraction values and some of the important concepts by different authors for erosion crater simulations are presented in Table 1.

Since different researchers have used different boundary conditions to simulate the molten region in the anode and cathode, a common framework for boundary conditions is lacking.

A brief list of different boundary conditions has been summarised here:

- *Heat conduction:* Analytical solution, numerical methods such as finite element method (FEM) and Finite difference method (FDM). Additional consideration of Joule effect.
- *Heat source:* Point heat source, constant radius disc heat source, disc heat source expanding with time, discharge energy (time, current), heat source radius based on the measured crater radius, based on the constant boiling temperature condition.
- *Heat flux:* discharge power, heat source temperature, constant energy fractions, time-dependent energy fractions.
- *Heat flux profile:* equilibrium profile, Gaussian distribution.

- *Material properties:* Average material properties, Temperature dependent material properties, consideration of latent heat of fusion and vaporisation.

In general, it is found that for the discharge durations longer than 20 μs, anode craters are smaller compared to the crater on cathode. Since longer discharge durations are used for roughing in die-sinking EDM using the transistor type generators, the electrode polarity is kept positive (anode) and the workpiece polarity is kept negative (cathode).

For the long pulse durations, the erosive effect on anode is believed to be reduced due to protective carbon layer generation. For the discharge durations shorter than 20 μs, typical for relaxation type generator or the capacitance pulses used in wire-EDM, finishing in die-sinking EDM and micro-EDM, anode removal amount is greater than cathode as shown by Xia et al., [48] and Yeo et al., [6].

In order to explain this effect, variation of the energies distributed into cathode and anode based on discharge duration by the T-F emission (combined temperature and electric field emission) is proposed.

Table 1. Erosion crater simulations by different authors and the used energy fractions F_c and F_a

Authors	Concept	F_c (%)	F_a (%)
Van Dijck [55]	Thermo-physical model with disc heat source	50	50
Pandey and Jilani [37]	Constant cathode boiling temperature condition	50	50
DiBitonto et al., [7]	Point heat source with photoelectric effect	18.3	-
Patel et al., [60]	Disc heat source with photoelectric effect	-	8
Xia et al., [48]	Temperature measurements: single, multiple sparks	25 - 34	40 - 48
Revaz et al., [49]	Temperature measurement: single, multiple sparks	10 - 15	
Zahiruddin and Kunieda [62]	Micro-EDM with small energy discharges, T_{ON}: 70 ns	-	10.37
Singh [52, 52]	Temperature measurements: multiple sparks	6 - 27	-
Zhang et al., [63]	Gaussian heat source, validated for single craters	44	-
Shabgard et al., [64]	Gaussian heat source, plasma flushing efficiency	4 - 9	4 - 36
Zhang et al., [53]	Metallographic analysis of craters to derive energy input	42 - 60	36 - 50
Maradia et al., [42]	Expanding disc heat source, different electrode and workpiece materials, single spark analysis	15 - 45	28 - 36

Source: Maradia et al., [42].

Another hypothesis is that due to smaller mass, electron impingement on anode is faster than the ion bombardment on the cathode surface, however for low current arcs in small gaps, as in the case of EDM, no theoretical proof has been presented so far for either of the hypotheses. The capacitive pulse discharges with low energies are also investigated due to their use in micro-EDM and wire-EDM. While most of the boundary conditions remain similar to the long duration discharges, energy distribution has been found to be different.

Zahiruddin and Kunieda [62] compared the removal efficiencies between macro EDM discharges and micro EDM discharges, where energy fraction of 0.10 was found for the micro EDM discharges, compared to 0.34 suggested by Xia et al., [48] for macro-EDM.

It was found that higher power density in micro-EDM led to higher removal efficiency (PFE). Dhanik and Joshi [65] provided a comprehensive model of capacitor type pulses with discharge energies below 100 µJ, by considering the plasma model and pre-breakdown phenomena.

Yeo et al., [6] developed electro-thermal models for anode and cathode erosion in micro-EDM, and validated simulated craters with the discharge crater measurements, shown in Figure 16. Singh and Ghosh [66] proposed that for very short pulse durations, electrostatic forces are more important for the material removal compared to the thermal melting.

Since wear of wire in wire-EDM is less relevant, only anode model has been presented by Spur and Schönbeck [67]. Recently, Weingärtner et al., [68] analysed influence of the assumptions on simulation results as seen in Figure 17, and found that the latent heat of vaporisation and melting significantly affects the results for wire-EDM, as also shown by Escobar et al., [69] and Joshi and Pande [44] for die-sinking EDM.

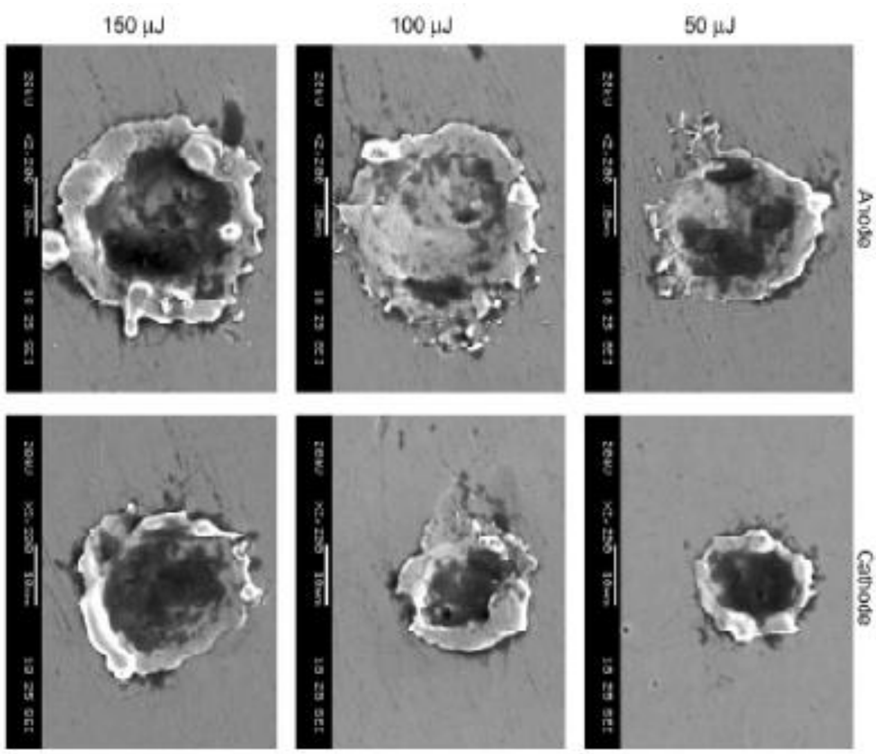

Source: Yeo et al., [6].

Figure 16. SEM images of the micro-craters on anode and cathode generated by different discharge energies. Anode is AISI 4140 alloy steel and cathode is pure tungsten.

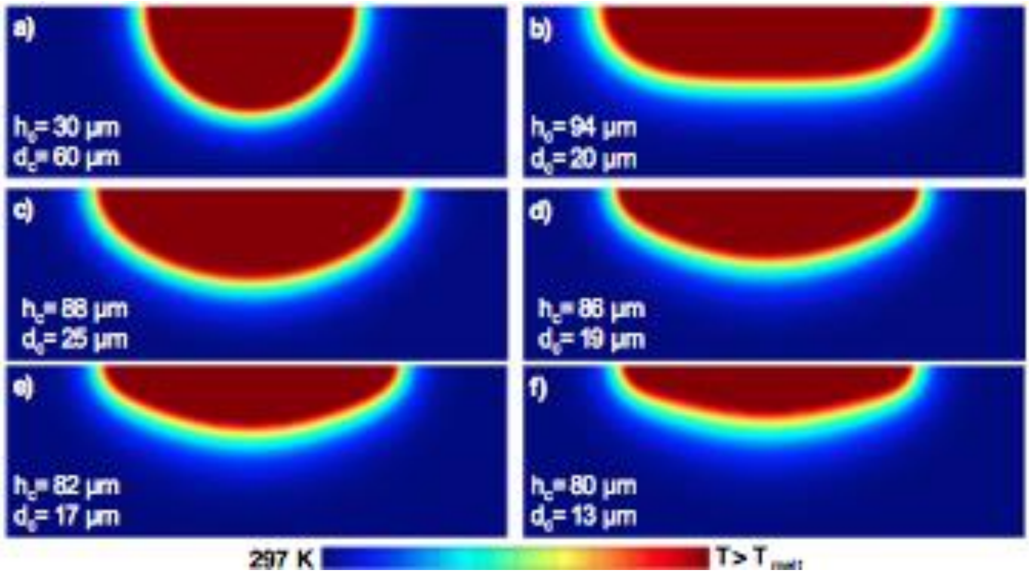

Source: Weingärtner et al., [68].

Figure 17. Influence of different types of boundary conditions on temperature simulations in Aluminium anode: a) point heat source; b) disc heat source; c) time dependent heat source; d) + temperature dependent material properties; e) + latent heat of fusion; f) + latent heat of vaporization.

Removal Mechanism

Once the molten region is simulated, the next step is to determine the amount of molten material actually removed from the discharge region. The forces required to eject the molten material from electrode were calculated by Van Dijck [55] considering the electrostatic, electromagnetic, hydraulic, aerodynamic forces and boiling of superheated metal.

It was proposed that in the beginning phase of a discharge, material removal takes place by the electromagnetic forces due to high current densities and the boiling of superheated metal due to large pressure drop. At the end of a discharge, a second pressure drop leads to further material removal due to boiling of superheated metal. The simulated results were compared with both single and multiple discharges. The ratio of ejected to melted volume, also known as plasma flushing efficiency (PFE) was found within 1% to 10%. Van Dijck [55] and DiBitonto et al., [7] considered that most of the metal removal occurs due to boiling of the superheated molten mass in the craters at the end of discharge because boiling of superheated metal is prevented by the bubble pressure during the discharge. Hockenberry and Williams [70] proposed that after the discharge termination, during the bubble collapse, the gas bubble is fragmented and the liquid jets penetrating the bubble impinge upon the electrode crater to eject the molten metal. In order to understand the crater formation, Samela and Nordlund [71] and Timko et al., [72] used the particle-in-cell (PIC) method in spark-material interaction through ion bombardment, shown in Figure 18.

It is shown that the huge fluxes of energetic ions can form craterlike damage on the surface and lead to sputtering of large atom clusters. The craters have a complex shape that can be explained by the strong non-equilibrium heating of the material due to energetic ions accelerated in the plasma sheath potential. Yang et al., [73, 74] used molecular dynamics (MD) simulations to simulate crater generation in micro-EDM. While the space and time domains used in these methods are extremely small, mainly limited by the computational power, crater formation is well understood using these methods.

It is inferred that for lower power density, material is removed by vaporisation, whereas for higher power densities, bubble explosion plays the dominant role and the material is removed in the form of clusters. Witz et al., [75] considered the Marangoni effect, where using surface tension driven convection, rim formation around the craters is explained. Tao et al., [76] simulated realistic crater morphology by incorporating both molten and solid materials using the volume of fraction method.

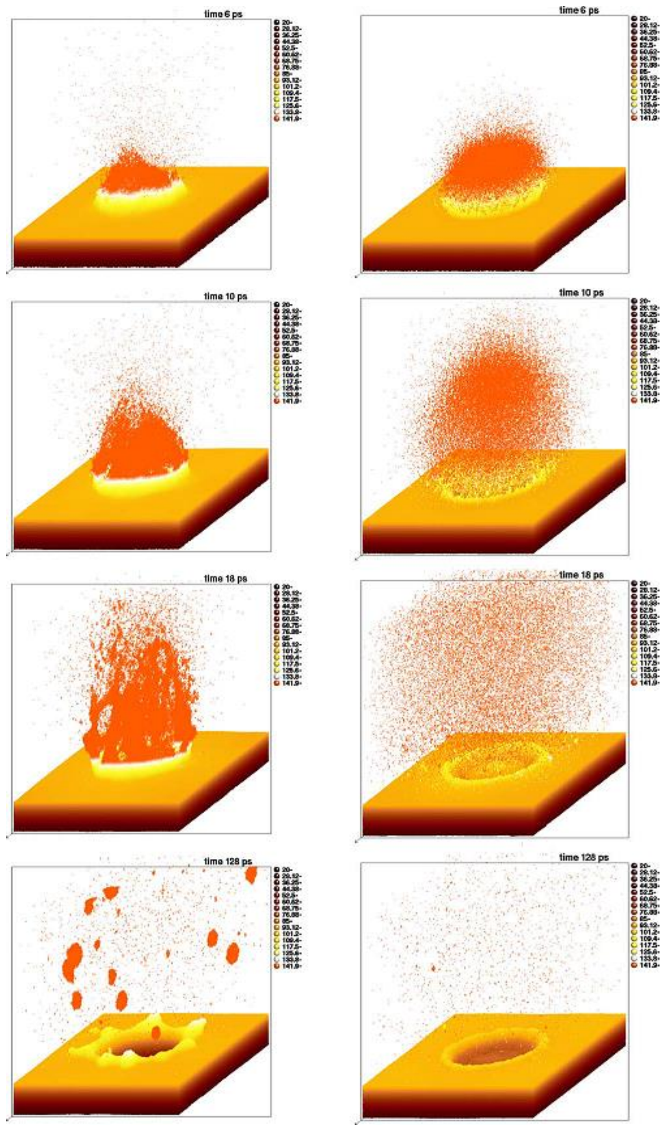

Source: Timko et al., [72].

Figure 18. Snapshots of the time development of cratering by arcs. Left: crater produced by energetic plasma ion flux obtained from dc plasma simulations. Right: crater produced by nonballistic (thermal) energy deposition but depositing the same amount of energy as in the plasma ion case.

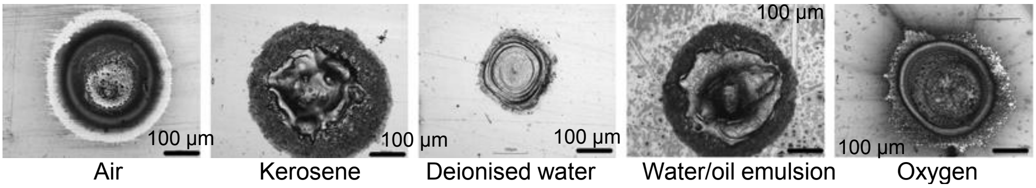

Figure 19. Comparison of the external appearance of craters formed in different dielectrics for 105 µs pulse duration by Zhang et al., [83].

Apart from the theoretical approaches, various experimental techniques are used to further understand the removal mechanism, such as high-speed imaging, X-ray analysis, crater analysis, force measurements, etc. As reported in [1, 2] from various sources, X-ray analysis showed that 85% of the material removal occurs during the discharge duration, whereas material removed per pulse in air is almost equal to that in liquid when the discharge duration is longer than 100 µs. Takezawa et al., [77] observed that the timing of the material removal is after the discharge end, where a low melting temperature (47°C) alloy is used for analysis. Hayakawa et al., [78] analysed relationship between the occurrence of material removal and bubble expansion. Similarly, Maradia et al., [79] used high-speed camera observation and found that material removal occurs while the generated bubble is expanding and at the end of discharge, as also seen in Figure 10. Here, the effect of pressure drop causes cavitation like effect on molten metal. Mesyats [80] observed micro-explosions on cathode resulted from the plasma-material interactions. Akematsu et al., [81] used acoustic emission signals to detect cavitation occurrence times for discharges in air and in liquid. Tamura and Kobayashi [82] measured impulse forces generated by motion of a bubble in single discharge, and found a negligible effect on the craters.

Instead, they found the effect of polarity to be dominant for crater geometry. Zhang et al., [83] analysed the effect of gaseous and liquid dielectric for single discharge crater generation and found that water-oil emulsion resulted in higher removal due to high pressure generated over the discharge spot, compared to gaseous dielectrics.

An example of the discharge craters generated in different dielectrics is shown in Figure 19. Similar results are also reported by Yoshida et al., [84]. From the above presented discussion on the single discharge modelling, it is seen that the erosion crater simulations are largely based on some assumptions for heat source boundary conditions.

Also, quantitative description of the material removal mechanism is lacking. Thus, crater simulations rely on the key assumptions of values for energy balance (F_c, F_a) and plasma flushing efficiency (PFE) under different discharge conditions.

MULTIPLE DISCHARGES

As discussed, mainly two types of discharges are simulated, namely discharges with large energies and long durations (transistor type) and for low energies and short pulse durations (relaxation capacitor type). In practice, multiple discharges are used for EDM, where some conditions differ from the single discharges, such as flushing of dielectric, gas bubble dynamics and debris particles. Thus, simply applying the single discharge analysis is not sufficient for the actual process modelling. Also, since electrode configuration, flushing mechanism and dielectric media differ for different EDM variants, typical aspects regarding the multiple discharge process modelling are addressed according to the main EDM variants.

Die-Sinking EDM

In die-sinking EDM, complex electrode geometries are used to erode cavities where flushing is usually performed using jump cycles for modern die-sinker machines. Due to this mechanism, flushing of dielectric is intermittent, leading to periodic removal of gas bubble and debris from the discharge region. Thus, gas bubble dynamics plays a greater role in die-sinking compared to the other EDM variants. In this section, material removal rate (MRR), electrode wear, surface quality and geometry prediction are addressed.

Material Removal

Typically cathode erosion is simulated for material removal in die-sinking roughing operation. Before comparing the single discharge and multiple discharge process simulations; gas bubble dynamics, debris movement and discharge location are analysed.

Hockenberry and Williams [70] used high-speed imaging to analyse the gas bubble in EDM, where recently Wang et al., [85] and Kitamura et al., [86] used transparent materials like PMMA and SiC to observe the EDM gap phenomena during multiple discharge process, especially gas bubble and debris movement. The later authors also analysed the spark distribution in gap and classified the sparks occurring in liquid, in gas and on gas-liquid interface.

It was found by Kitamura et al., [87] that probability of discharge occurrence per unit area was highest at the boundary between liquid and bubble, compared to discharges in bubble or in liquid. Also, the probability of discharge occurrence through debris particles located at this boundary generated by the last discharge was highest. Hayakawa et al., [88] analysed the machining properties at gas-liquid interface, as the gas bubble occupy most of the cavity after a certain time of erosion.

They found that the material removal rate is nearly zero after the machining liquid is completely replaced by the gases. Hayakawa et al., [89] also observed flying debris scattered from the discharge point and recently analysed a relationship between the occurrence of material removal and bubble expansion using high-speed imaging in [78]. Shervani-Tabar et al., [90] and Zhang et al., [91] used numerical methods to study the dynamics of gas bubble in EDM. Pontelandolfo et al., [92] used computational fluid dynamics (CFD) and particle image velocimetry (PIV) in order to study the effect of flow during flushing in die-sinking EDM as shown in Figure 21. It was found that the presence of bubbles increases the evacuation of debris particles from the discharge gap.

Liao et al., [93] have performed similar analysis in order to determine the optimal jump motion and height for the efficient removal of the bubbles and debris from the discharge gap. Wang and Han [94] simulated debris and bubble movement for consecutive pulse discharges, an example of which is shown in Figure 22.

It is seen that the gas bubble and debris accumulation and their distribution in the discharge region affect the discharge location and discharge phenomena as discussed by Schumacher [16, 95]. While the debris accumulation reduces the dielectric strength of the dielectric oil, accumulation of debris on the gas bubble boundaries leads to high probability of discharge at these locations and larger gap width compared to the single discharge setup. The larger gap width leads to lower gas bubble and plasma region diameters.

While simulation of gas bubble and debris movement in the discharge gap is interesting, the ulterior motive is to analyse the effect of material removal capability of discharges in the multiple discharge process. More precisely, discharges generated in liquid, gas bubble and on the boundary of the gas bubble may results in different crater removals.

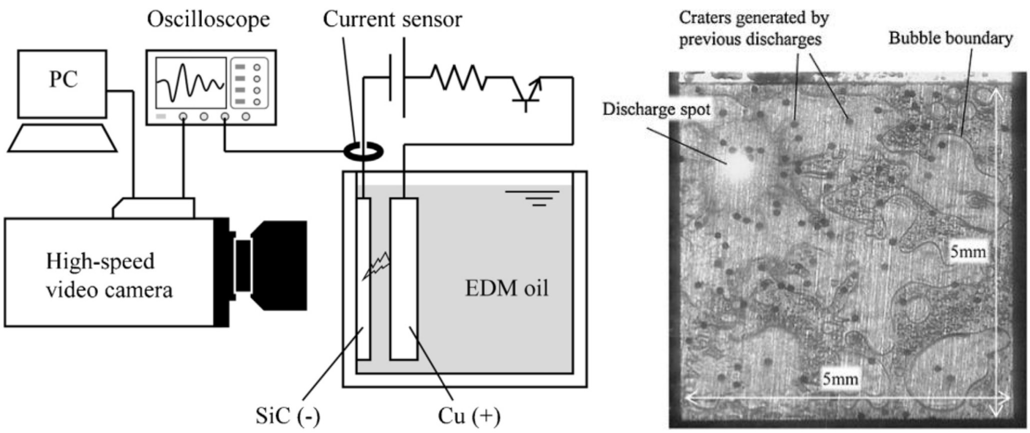

Figure 20. Left: schematic view of experimental setup where a transparent electrically conductive SiC electrode is used for high-speed observations; Right: Example of an image acquired at the 100th discharge in the gap between SiC and Copper electrodes.

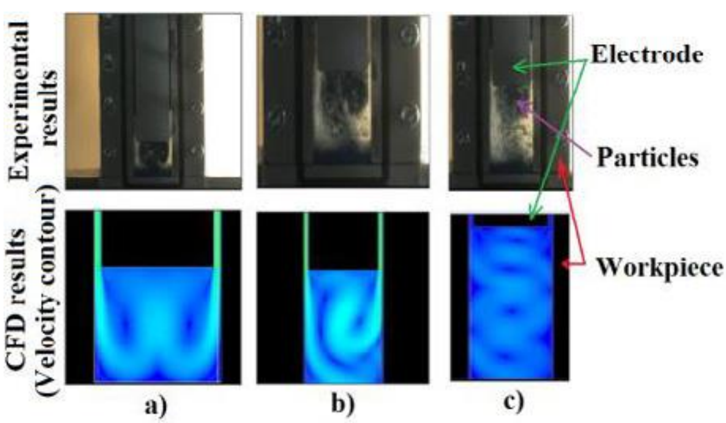

Source: Pontelandolfo et al., [92].

Figure 21. Particle hydrodynamics in sinking EDM: comparison of experimental and CFD results for a) beginning of the ascending period with the formation of a couple of vortexes, b) instability of the vortexes during the ascending period, c) unstable vortexes aligned horizontally for high velocity.

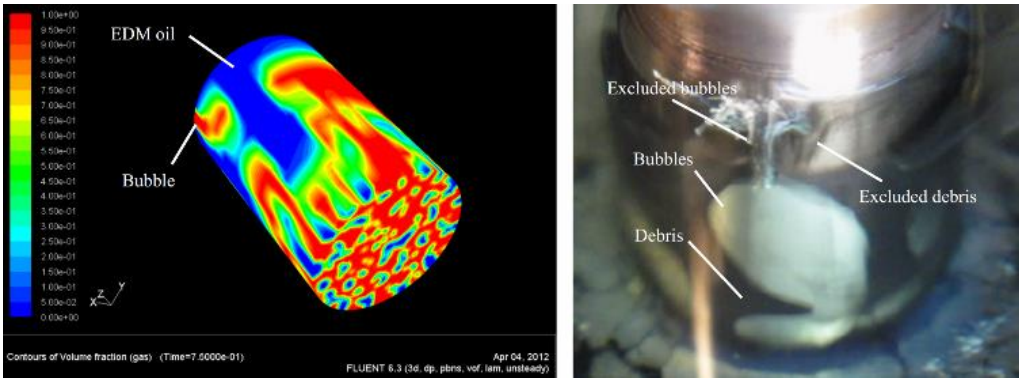

Figure 22. Simulation results and experimental observation of the bubble and debris movement by Wang and Han [94].

A systematic comparison of the single discharge crater volumes and the mean crater volumes derived from the multiple discharge process is performed by Maradia et al., [96]. Erosion craters on steel 1.2343 workpiece by 20A single discharges are simulated, where the energy fraction F_c is found to be about 0.45 when using graphite electrodes and 0.20 when using copper electrodes, assuming 100% PFE. For multiple discharge process, it is proposed that the re-solidified rim or bulge around the crater must also be removed by the subsequent craters. Thus, effective crater volume from a single discharge is the difference of eroded crater volume V_- and the re-solidified volume around the crater V_+. With such consideration, the effective crater volume V_e is simulated using F_c of about 0.20 for the graphite electrodes and 0.13 for copper electrodes. Furthermore, mean crater volume V_m is calculated from the erosion of cavities using thousands of discharges. It is found that the F_c values required to simulate V_m is between 0.08 to 0.15 in the case of graphite electrode and 0.10 to 0.25 for copper electrodes. Thus, it can be seen that for the same discharge parameters, a large variation in the used energy fraction values occur. Additionally, it was also shown that the mean material removal per discharge is much lower in the case of micro scale electrodes with projection area below 1 mm^2 compared to the macro scale electrodes with surface area above 10 mm^2. This effect is called the scaling effects in EDM. In order to understand this scaling effect, the effects of electrode projection area, erosion depth and electrode materials on material removal rate are analysed.

It is found that while the discharge frequency remains almost constant for different electrode projection areas, the material removal per discharge strongly reduces when the electrode area becomes small. Also, for small electrodes, higher material removal per spark is observed when eroding at the depth below 1 mm, compared to the higher depths. However, since 100% PFE is assumed for the simulations, the variation in the F_c values is not precise. Thus, one must consider both the PFE and F_c to understand the effects in multiple discharge process. The energy fraction F_c mainly depends on the energy balance in a discharge, which is strongly affected by the electrode-workpiece materials as shown by Maradia et al., [42]. The energy balance also affects the gas bubble diameter and the implosion instances, thus plasma flushing efficiency PFE. Also, the type of dielectric itself affects the flushing efficiency as analysed by Zhang et al., [83].

Thus, one must consider both the discharge state and gas bubble dynamics for calculation of F_c and PFE. In order to understand the decrease in these two variables for multiple discharge process, Maradia et al., [79] used high-speed imaging in near-real erosion conditions. While the transparent electrode technique as mentioned before allows better observation of the process, there are several simplifications and deviations from the real erosion process. For example, the erosion region is an open cavity from sides, as opposed to a closed cavity typical for die-sinking EDM.

Also, high resistivity transparent material is used, which may also vary the gas bubble dynamics and plasma characteristics. In the case of near-real erosion conditions, the erosion cavity is tightly sealed between two glass plates as shown in Figure 23.

While it allows the process observation using conventional EDM electrode and workpiece materials, the process is carried out in a closed cavity, where the dielectric flow and the gas bubble escape path is restricted, simulating real erosion like pressure drop conditions. Also, process observation can be carried out during the erosion begin or during the steady-state. The obvious draw back similar to the transparent electrode method is its limitation to observe only thin electrodes. Also, one may not see the plasma and crater diameter expansion.

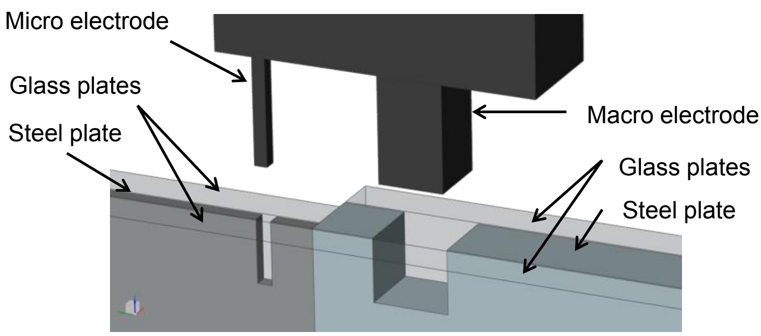

Figure 23. Near real-erosion process conditions for high-speed observations used by Maradia et al., [79].

Using the above mentioned setup, Maradia et al., [96] also observed that the discharges take place inside bubble, liquid or at their interface, as shown in Figure 24. However, it was also observed that in the small gaps, the gas bubbles merge to form larger gas bubbles, increasing the buoyancy forces for their removal from the discharge gap, apart from the pressure generated by the bubbles and discharge breakdowns around them.

Also, the debris are transported with these bubbles out of the discharge region. It is also observed that in the case of micro electrodes, a single bubble becomes large enough to fill the complete cavity and the bubble implosion does not take place, as the bubble is simply lifted away from the discharge region into the work tank. Such observation may explain much lower mean crater volume for the multiple discharge process due to the reduction of PFE.

In order to understand the role of gas bubble implosion on the crater generation, especially during the multiple discharge process, Maradia et al., [42] generated single discharges inside a cavity filled with hydrocarbon oil, as shown in Figure 25. Using the same discharge parameters, craters are generated with air as dielectric. It is shown that the crater generated inside the cavity filled with oil are more identical with the craters generated in air as dielectric, compared to the craters generated in oil on a flat workpiece surface. Thus, it is inferred that PFE indeed decreases during the multiple discharge process, where the discharges occur inside the gas bubbles along with the lack of gas bubble implosion instances.

Apart from the plasma flushing efficiency PFE, Maradia et al., [96] showed that the plasma state also differs in the case of multiple discharge process. Since the micro scale cavities are mostly completely filled by the gas bubbles, the plasma has higher metallic vapour compared to the plasma generated in dielectric oil. This is shown by the plasma spectroscopy performed in near real-erosion conditions as shown in Figure 26.

It is seen in the discharge plasma spectrum that the ratio of the intensity of Fe spectral line to the hydrogen H_α spectral line is higher in the case of erosion using a 1 mm diameter graphite electrode.

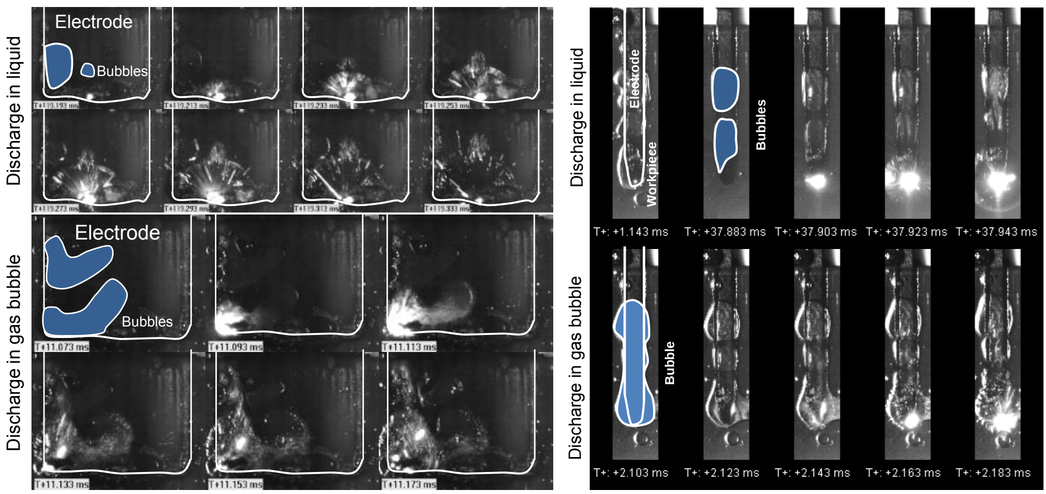

Source: Maradia et al., [96].

Figure 24. Gas bubble dynamics and discharges in near real-erosion like process conditions observed using high-speed imaging for a rib electrode with 5 mm width (left) and a micro electrode with 0.25 mm side length (right).

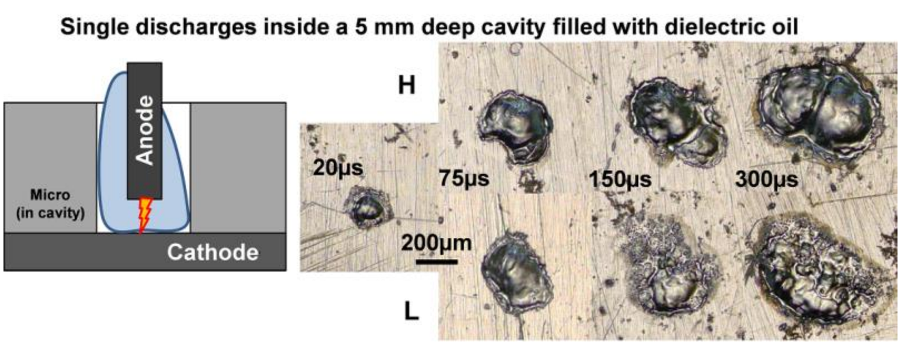

Figure 25. (Continued).

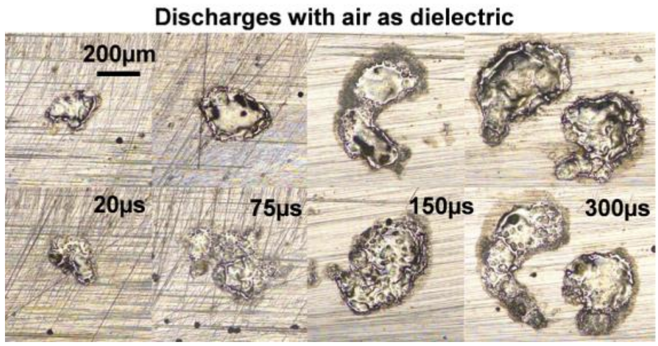

Source: Maradia et al., [42].

Figure 25. Top: craters generated on steel cathode plane using 20 A discharges with Ø1 mm graphite anode inside a 5 mm deep cavity filled with dielectric oil. Bottom: craters generated on steel cathode by 20 A discharges using Ø1 mm graphite anode with air as dielectric.

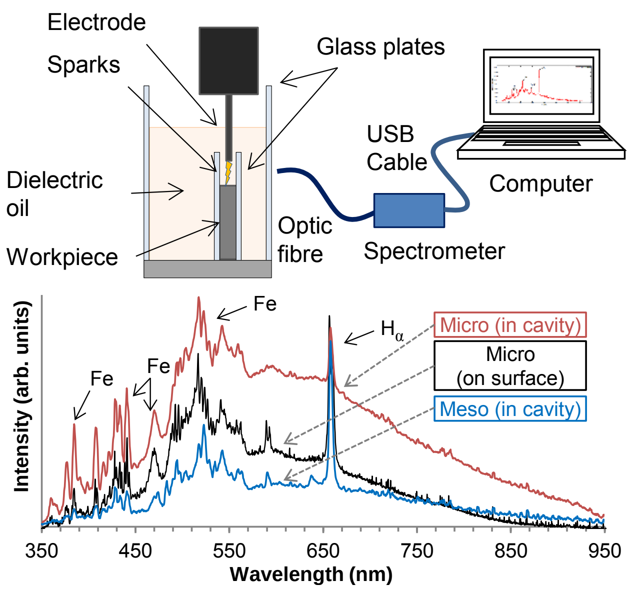

Source: Maradia et al., [96].

Figure 26. Top: light emission spectroscopy of discharge plasma in near real-erosion conditions for multiple discharge process. Bottom: plasma light emission spectrum for different electrode areas.

A reversal in the scenario is observed for the erosion using a 3 mm diameter electrode. It is know that the higher metal vapour in the plasma causes cooling and may thus lead to different energy balance in the gap, requiring further adjustment to F_c values used for simulations. Thus, one needs to know the gas bubble dynamics and debris distribution in order to predict the discharge location. Also, the medium in which discharge takes place is important. Estimation of these conditions may lead to some prediction of the plasma state to determine F_c and PFE for MRR prediction.

Electrode Wear

Xia et al., [48] and Natsu et al., [97] explained that even though high energy is distributed into anode, for longer discharge durations, a protective carbon layer on the anode surface is responsible for lower removal on the anode.

It was observed that, for single discharges higher anode fraction is measured compared to multiple discharge process, where the protective layer gradually builds up. Higher boiling point temperature of carbon reduces the anode erosion, thus also electrode wear. Mohri et al., [98] investigated time dependence of Ø10 mm copper electrode wear in sinking EDM with 8 A, where they observed higher corner wear during the beginning of erosion and lower wear on the frontal face of electrode.

It was observed that edge portion is not covered with a black carbon layer as opposed to the frontal region. Mohri et al., [99] investigated the carbon layer, which was identified as turbostratic carbon through the X-ray diffraction technique. It was proposed that carbon cracked from hydrocarbon oil precipitated at the electrode surface with a decrease in temperature along with the ejected workpiece debris.

Further, the workpiece debris such as iron, nickel and chromium support the carbon build-up process as the known catalysts. The reason of rapid wear on the edges was explained by a lack of carbon precipitation at the region with large curvatures. Also, through single discharge analysis, it was mentioned that the long duration pulses increase the amount of carbon. As opposed to the observations from Mohri et al., [99] and Murray et al., [100] for the copper electrodes, Itoh [101] and Klocke et al., [102] observed deposits concentrated mainly on the edges and corners of macro graphite electrodes.

Maradia et al., [103] analysed the carbonaceous layer built up on the graphite electrodes (anode) during the erosion in meso-micro scale, as shown in Figure 27. Using micro- Raman spectroscopy it was determined that the built up layer is similar to the diamond like carbon (DLC), a type of amorphous carbon. As opposed to conventionally believed pyrolytic carbon structure, DLC has much lower thermal conductivity.

A thermal model of the low wear conditions is provided, including the conditions for the carbonaceous layer build-up. It is proposed that when the electrode material temperature is below its boiling or sublimation temperature and above the hydrocarbon oil vaporisation temperature, low thermal wear and condensation of carbon vapour in this region takes place. The simulated pulse duration values where the complete micro scale electrode surface would be covered with such layer are compared to the experimental results of wear. It is shown that the low thermal conductivity of DLC layer on the electrode protects it against thermal wear.

Kunieda and Kobayashi [104] used spectroscopic measurement of copper vapour density to verify if the protective carbon layer is responsible for lower tool wear ratio.

Copper electrodes with Ø2 mm diameter were used to erode steel in hydrocarbon oil with 20 A, 40 A and different pulse durations (20 µs to 100 µs) to generate a carbon layer.

These electrodes were then used to make single discharges in gas and spectroscopic measurements were performed to observe relative vapour density of the copper spectral lines. Also, X-ray micro analysis is performed over the electrode surface with the carbon layer to analyse temporal evolution of main workpiece and electrode elements as shown in Figure 28. It was proposed that the higher copper vapour density in the discharge beginning prevents carbon formation / adhesion.

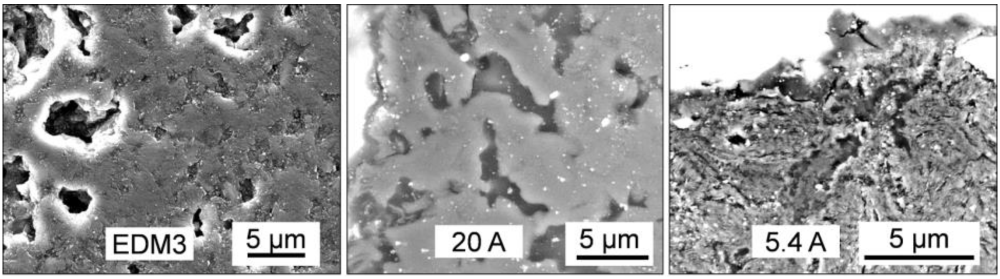

Source: Maradia et al., [103].

Figure 27. Comparison of the microstructure of base graphite Poco EDM3 (left), built-up layer by erosion with 20 A (centre) and with 5.4 A (right) on the graphite electrodes.

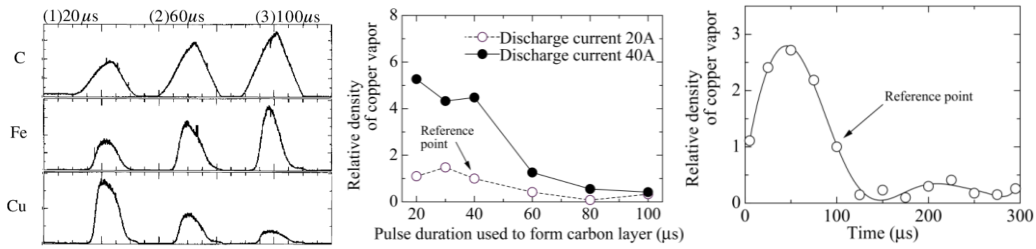

Source: Kunieda and Kobayashi [104].

Figure 28. Left: temporal element evolution on a copper electrode analysed using X-ray micro analysis; Centre: relative density of the copper vapour from plasma radiance dependent on the carbon layer thickness; Right: relative density of copper vapour evolution over the discharge duration.

Maradia et al., [42] used time-resolved plasma spectroscopy to map the evolution of plasma species during a single discharge in oil. It was seen that the copper spectral lines have high intensity during the discharge beginning, which reduce with increasing pulse duration as shown in Figure 29. The erosion crater analysis shows that the eroded crater volume decrease with time on copper anode, whereas carbonaceous deposits are observed on the discharge spot for longer pulse durations, which has been simulated in [103].

It is seen that the protective carbonaceous layer reduces the anode wear during the multiple discharge process. Generation of such layer with lower thermal conductivity may alter the energy balance and plasma expansion, resulting in lower heat flux q_0. Here, individual changes in the energy fraction F_a and heat source radius r_p remain unclear.

Surface Quality

In terms surface quality, the surface roughness, re-solidified layer and residual thermal stresses are of primary interest. Izquierdo et al., [105] used thermal model and simulated multiple sparks using FEM to simulate surface roughness with an error below 6% as shown in Figure 30.

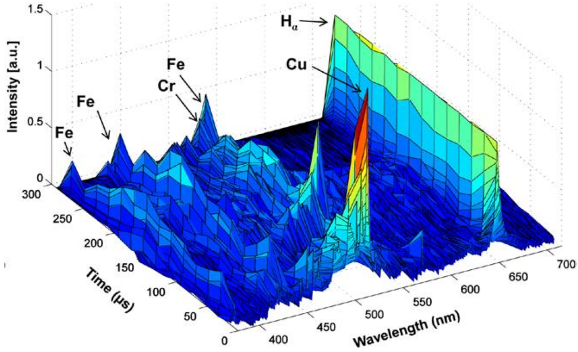

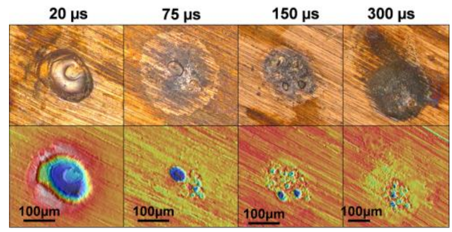

Source: Maradia et al., [42].

Figure 29. Left: time resolved spectra of a 20 A single discharge, acquired at 20 μs interval with 19 μs exposure time and normalized to the H_α peak. The discharge is generated between a steel cathode and a copper anode. Right: discharge craters generated by 20 A single discharges on copper anode using a Ø1 mm steel cathode.

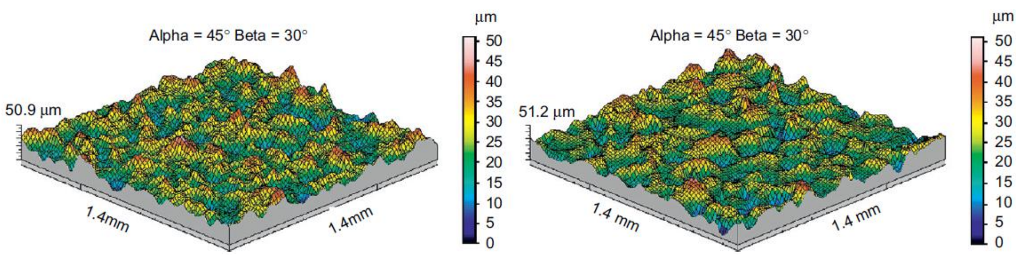

Figure 30. Comparison between simulated (left) and measured (right) surfaces from Izquierdo et al., [105]. The mean error between the measured and simulated values is less than 6%.

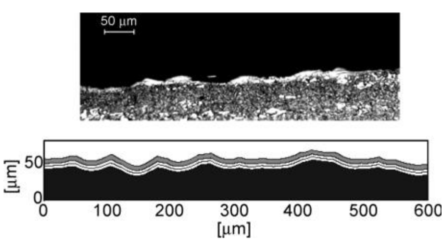

	Measured	Predicted
Recast Layer [μm]	5. 06	6. 1
Heat affected zone [μm]	5. 22	7. 7

Source: Izquierdo et al., [106].

Figure 31. Left: observed and simulated profiles of the white layer and heat affected zone. Right: predicted and measured average thicknesses of recast layer and heat affected zone.

The spark distribution function is derived from the consecutive pulse experiments. The model was further enhanced by the ability to predict thermally affected layers in [106] as seen in Figure 31. Salonitis et al., [107] provided similar thermal model to predict surface roughness, however analytical approach was taken by them. Kansal et al., [108] simulated erosion with powder mixed dielectric, where it was inferred that the powder in dielectric led to craters with a larger radius but shallow depths. Kurnia et al., [109] developed a thermal model for estimation of surface roughness in micro-EDM and found a good agreement with the measured results. Kiran and Joshi [110] developed surface roughness model by extending the single discharge simulations to predict surface roughness and included the role of debris for the simulations. Somashekhar et al., [111] and Tan and Yeo [112] simulated overlapping multi-sparks in micro-EDM.

Das et al., [113] provided a FEM based calculation of microstructure and residual stresses. Pérez et al., [114] analysed the metallurgical properties of steel influenced by heat from the electric discharges using thermal simulations. Murali and Yeo [115] used FEM and Yang et al., [116] used molecular dynamic simulations to analyse the residual stresses in micro-EDM. Typically, single crater simulations are extended to multi-discharge process by including the spark distribution function over the surface for surface finish simulations.

Geometry Prediction

The modelling of individual aspects in EDM is interesting to understand the underlying mechanisms and also for the process parameter optimisation based on them. Geometry prediction on the other hand may use modelling and simulation capabilities in actual erosion conditions and machine control.

It basically unifies all the different aspects to simulate the multiple discharge process. Here, starting with the breakdown and discharge location prediction, the crater simulation, discharge location distribution over the surface based on the gas bubble and debris movement, consideration of different discharge types based on their location and the effect of intermittent flushing effects on debris and gas bubbles in the discharge region may be considered.

Tricarico et al., [117] performed geometrical simulation of die-sinking EDM process by considering 2D electrode and workpiece geometries as shown in Figure 32. Here, thermo-physical interactions are not considered for the simulation of material removal and electrode wear. Morimoto and Kunieda [118] used a voxel model and based on the probabilistic calculation of the discharge delay time for each voxel, discharge location is predicted as shown in Figure 33. Here, material removal and electrode wear per discharge, gas bubble volume and debris size for the model input are derived from the experimental analysis.

Using the reverse simulation in sinking EDM as presented by [119], Kunieda et al., [120] demonstrated that using the electrode shape derived from the reverse simulations having an oversize equal to the predicted wear, the eroded cavity shape closer to the target shape can be achieved as shown in Figure 34.

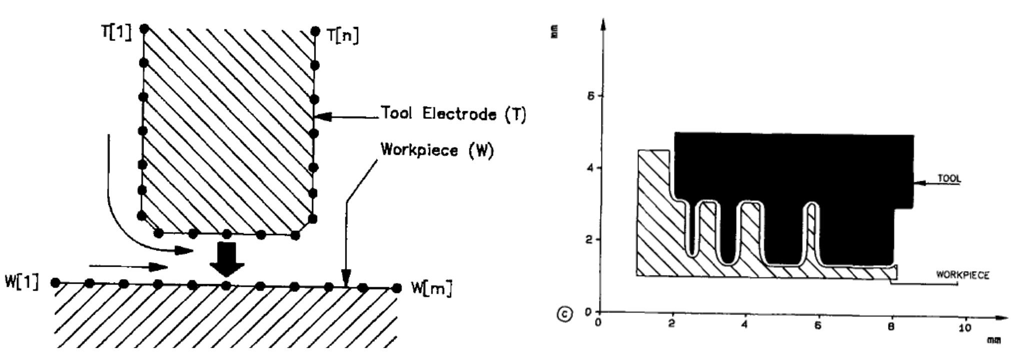

Source: Tricarico et al., [117].

Figure 32. Left: 2D surface model for geometric simulation. Right: an example of tool wear and workpiece removal simulation.

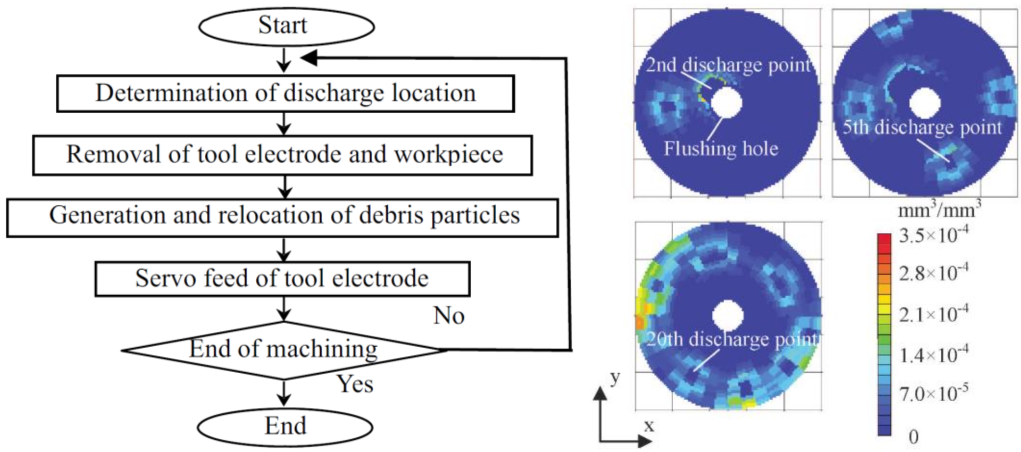

Source: Morimoto and Kunieda [118].

Figure 33. Left: discharge location searching algorithm. Right: distribution of debris concentration.

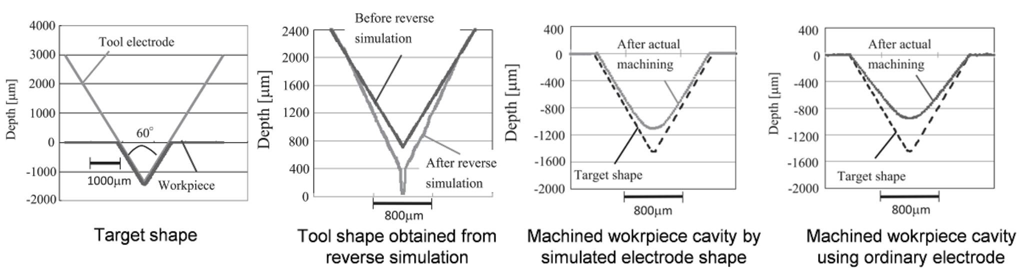

Figure 34. Example of reverse simulation in die-sinking EDM, where an oversized electrode shape derived from the simulations results in a better form conformity of the eroded cavity [120].

For high aspect ratio electrode and micro-electrodes, the process forces may lead to vibration of the electrode, leading to geometric deviations in the eroded cavity. Adachi et al., [121] calculated bubble oscillation in plane-plane electrode configuration and calculated the reaction forces by bubble formation, whereas Klocke et al., [122] measured the forces induced by the single discharges to be within a few Newton. Klocke et al., [123] measured the force signal and analysed the deflection of slender electrodes as shown in Figure 35. It was shown that the electrode deflection highly depends on fluid viscosity and on discharge frequencies equivalent to the electrode's natural frequencies. Also, discharge force signals were found to be effective for the description of hydrodynamic effects in the working gap for µs range.

Wire EDM

In wire-EDM (WEDM), a travelling wire electrode is used to cut 2D-2.5D geometries. Since fresh wire is continuously fed for erosion, electrode wear is not so relevant in WEDM. Also, since the discharge region is open at least on the upper and lower ends of the workpiece where the wire is fed, continuous feeding of deionised water co-axial to the wire ensures better flushing conditions compared to the die-sinking EDM.

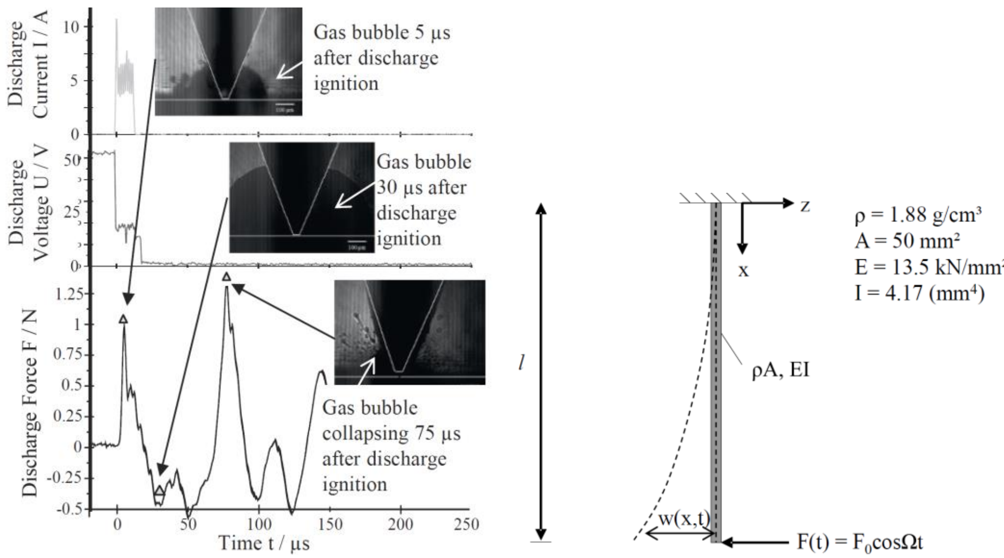

Source: [123].

Figure 35. Left: measurement of single discharge forces on the force sensor. Right: modelling of a graphite electrode as a cantilever beam excited periodically by discharge forces.

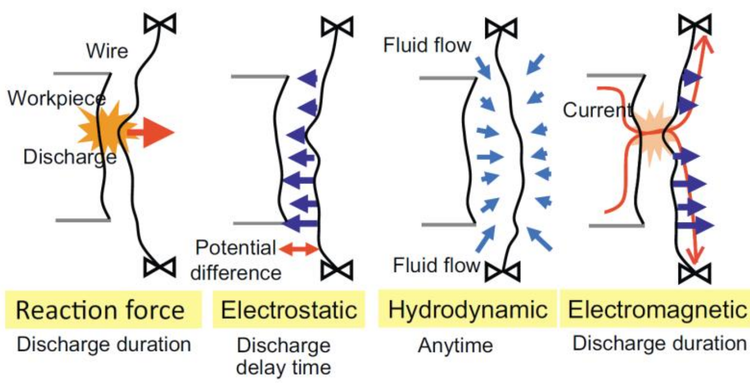

Source: Hinduja and Kunieda [1].

Figure 36. Forces acting on a wire electrode during erosion.

Thus, material removal rate in multiple discharge process can be simulated using the single discharge analysis and additional consideration of discharge frequency during the erosion process. The use of wire electrode however poses its own set of problems, where the forces acting on wire cause wire vibrations, deflection and wire breakage.

Apart from the temperature rise in the wire due to discharges, the main forces acting on a wire electrode are considered to be discharge reaction force, electrostatic force, electromagnetic force and hydrodynamic forces, as summarised in Figure 36.

In order to illustrate how sensitive a free stretched wire is to external forces, wire deflection was calculated based on a model proposed by Dauw and Beltrami [124]. The general differential equation of motion for a wire of length l in a plane along the z axis, assuming no time dependent phenomena influence the wire and neglecting the wire bending moments can be written as

$$F_D \frac{\partial^2 y}{\partial z^2} = q_y \tag{12}$$

Here, F_D is the wire pre-tensioning force and q_y is an external force. Solving Equation (12) for z = $l/2$, the maximum deflection of the wire can be calculated by

$$y_{(l/2)} = \frac{q_y \cdot l^2}{8 \cdot F_D} \tag{13}$$

Figure 37 shows maximal wire deflections calculated for free stretched wires using a pre-tensioning force of F_D = 25 N. When an external force q_y of 1 N is applied to the free stretched wires of length 60 and 110 mm, the maximum deflections are 18 µm and 60 µm respectively. While Kinoshita et al., [126] used mechanical method for wire vibration measurement, Dauw and Beltrami [124] used optical sensor method for wire position detection.

The compensation of wire drag reduces errors in machining accuracy, especially for contours and sharp corners. Yamada et al., [127] analysed wire displacement with normal vibration modes. Wire displacement was measured during real machining of a thin plate and the displacement was compared with the simulated modal analysis. Obara et al., [128] analysed single discharge force reaction and found that the vibrating wire behaviour is more complex than the simple low frequency mode due to superposition of stepwise waves from multiple discharges. Mohri et al., [129] developed a dynamic wire vibration model where impulsive force measured through impulse response by a single discharge was used. Puri and Bhattacharyya [130] presented an analytical approach for wire vibration modelling and showed dependence of vibrations on the discharge frequency and workpiece height.

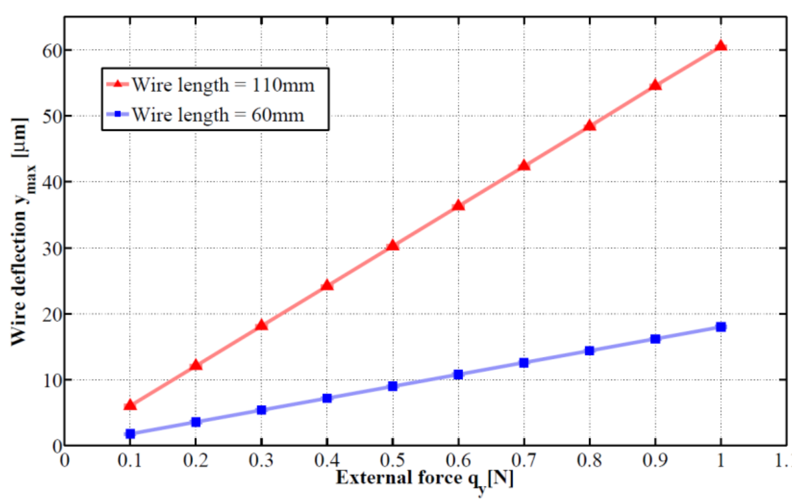

Source: Weingartner [125].

Figure 37. Calculated deflection of free stretched wires of lengths l = 60 mm and 110 mm under external forces q_y = 1 N and wire pre-tensioning force of F_D = 25 N.

Altpeter and Perez [131] presented an aggregation of the wire modelling in terms of vibration and the methods to deal with damping of wire vibrations at high frequency and slackness control at low frequency. Currently, wire pre-tension and wire-position sensors are mainly used to reduce wire vibration and drag during the erosion process.

The fluid flow and the debris motion in ED-Machined kerf were analysed by Okada et al., [132], where they used CFD simulation and compared the results with the observation by high-speed imaging. It was shown that a stagnation area with little flow velocity around the wire reduces debris exclusion efficiency in this region.

An example of the CFD simulation and the observed flushing effect on the wire cut surface is shown in Figure 38. Based on this method, optimisation of nozzle flushing for smooth debris exclusion is presented in [133]. The influence of the jet conditions on the wire deflection based on CFD analysis of the force is reported in [1]. Haas et al., [134] used experimental test rig and CFD analysis as shown in Figure 39 and developed a nozzle concept with rapid prototyping for high thickness workpieces.

Tomura and Kunieda [135] used a 2D FEM program to analyse the electromagnetic field by taking into account the electromagnetic induction as shown in Figure 40. It was found that the static electromagnetic force is attractive and permeability of the workpiece materials has a significant influence on the static force.

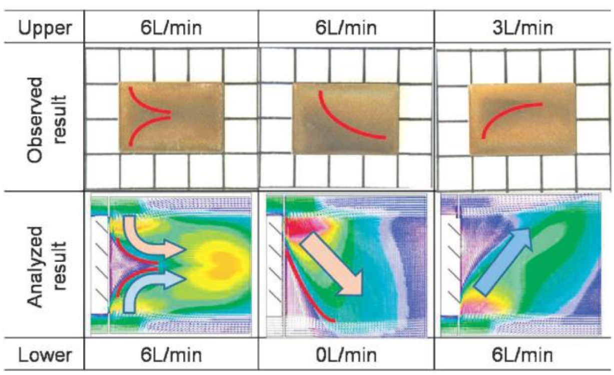

Figure 38. Wire EDMed surfaces and CFD analysed flow fields from Okada et al., [132].

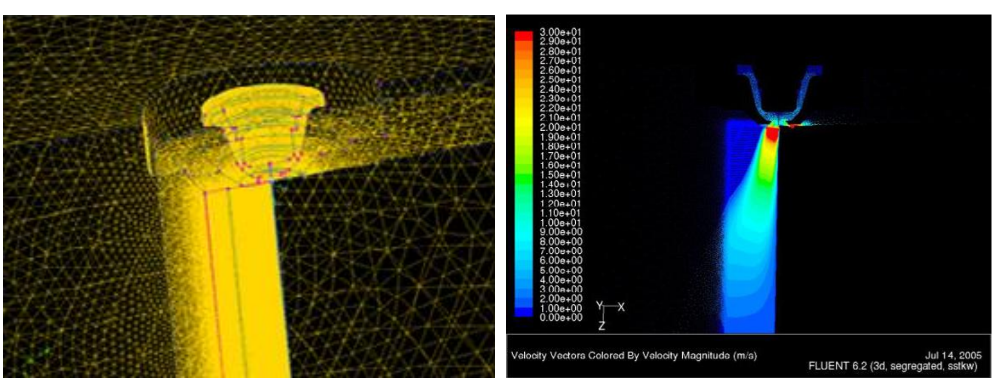

Source: Haas et al., [134].

Figure 39. Left: meshed CFD model with upper nozzle for jet flushing and workpiece. Right: dielectric jet in machining conditions with velocity vectors coloured by velocity magnitude in m/s.

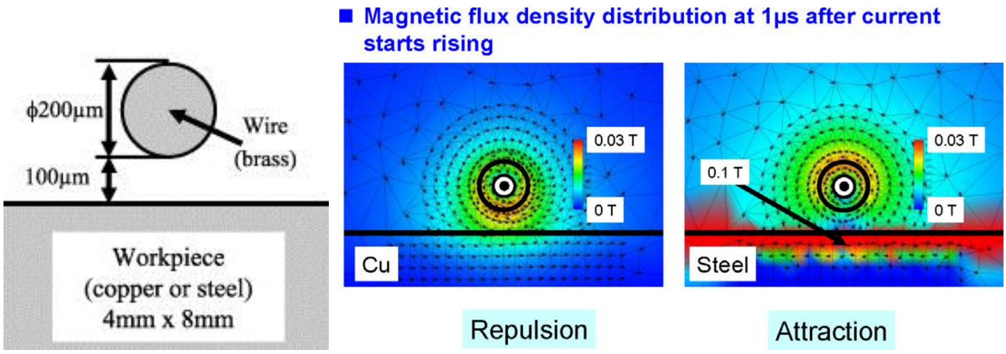

Source: [1, 135].

Figure 40. Left: model setup for electromagnetic analysis. Right: simulation of electromagnetic field.

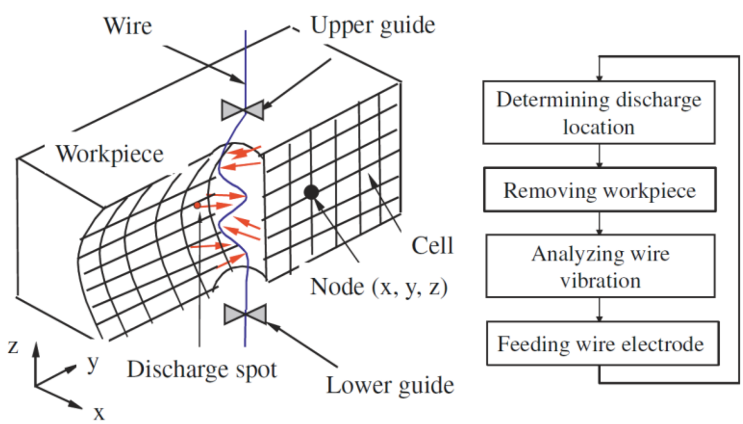

Figure 41. Geometrical simulation of wire EDM from [1, 137].

Dynamic electromagnetic force has been found to be repulsive and dependent on the electrical conductivity of the workpiece material. As mentioned in [1], the magnitude of electrostatic and electromagnetic forces are found to be dependent on the discharge energy. The analysis of wire impedance considering electromagnetic fields generated around the wire electrode is presented by Hada and Kunieda [136] which may help to consider impedance effect while programming the current pulses. Geometrical simulation of wire EDM is performed by Han et al., [137], where calculation of wire vibration is performed considering the forces applied to the wire. Determination of the discharge location is carried out based on the gap width between workpiece and wire, then removal at this location is applied. The concept is shown in Figure 41. Thermal load on the wire is one of the main reasons for wire breakage or rupture during the erosion, leading to increased downtimes in production. While pretension is applied to the wire electrode to reduce vibrations, the rise in temperature at discharge spots reduces its tensile strength, leading to wire breakage.

Jennes et al., [138] and Dekeyser et al., [139] used a thermal model as shown in Figure 42 to calculate thermal load on the wire electrode. They found that for non-uniformly distributed discharges the wire breakage is less frequent, however when the discharges occur in clusters on specific regions of the wire, thermal load on the wire in this region increases leading to wire rupture.

Based on the thermal models, the measured pulse frequency and the discharge location detection on a wire using differential current and voltage signals, several researchers provided adaptive control methods such as [140, 141] in order to reduce wire rupture by reducing the discharge energy when the thermal load on a wire is critical. Recently, Okada et al., [142] and Weingärtner et al., [143] used high-speed imaging to observe discharge distribution on the wire electrode as shown in Figure 43 and Figure 44 respectively.

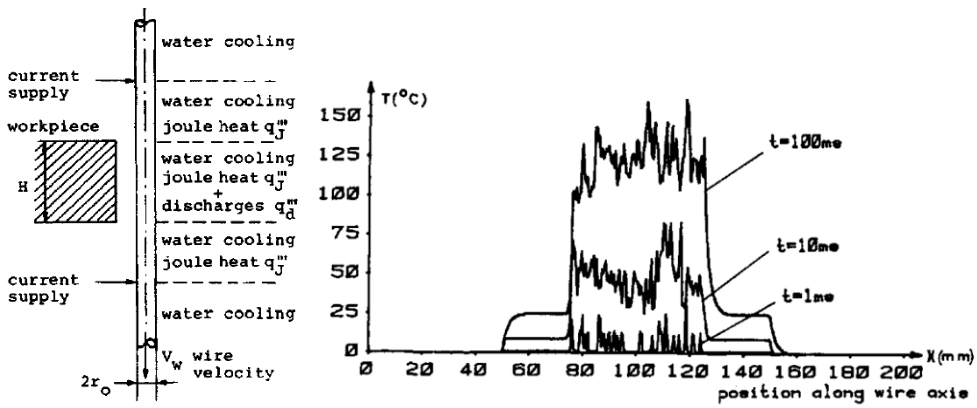

Source: Jennes et al., [138].

Figure 42. Left: layout of thermal model of wire in the workpiece vicinity for analytical approach. Right: calculated wire temperature for randomly distributed discharges.

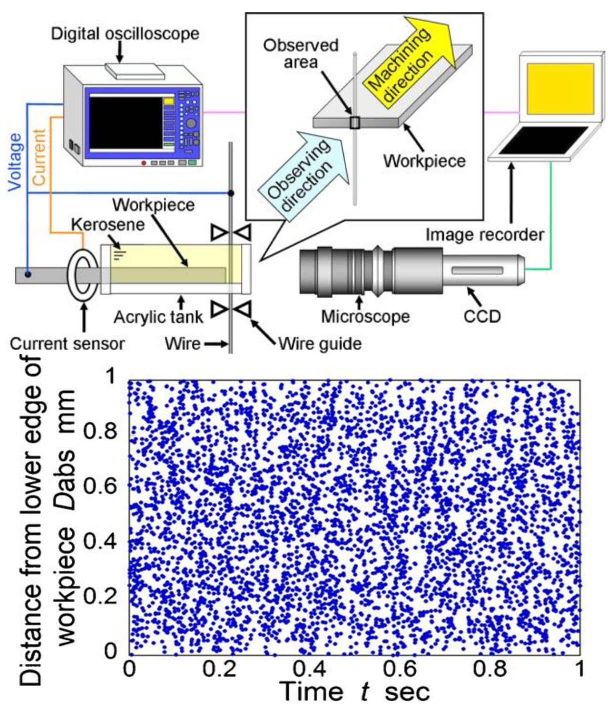

Taken from Okada et al., [142].

Figure 43. High-speed observation system of wire EDM and spark location on the wire electrode during erosion.

Such experimental technique help to determine spark distribution function for modelling of thermal loads on wire electrodes. In order to reduce the wear of wire electrode (cathode), various electrode materials and their coatings are analysed by Perez et al., [144].

A model for the relative power dissipation in EDM discharges has been developed by taking into account the different current emission mechanisms and cathode space-charge characteristics by [51]. The model explained the low cathode dissipation in materials like Zn, which present the highest electronic current densities and the lowest fraction of ionic current, which leads to power balance which reduces the losses at the cathode and enhances the anode erosion. For the micro wire-EDM, thin wire electrodes are used, where the process forces are measured by Klocke et al., [145]. An application of wire EDM is dressing of metal bonded grinding wheels as shown in [143]. Here, the use of high rotating velocities of grinding wheels results in relative motion between the spark channel and the workpiece surface. The simulation of such discharges is performed by Weingärtner et al., [68] as shown in Figure 45. Here, a moving time dependent expanding disc heat source is used to simulate the erosion craters. As a side note, such technique is also used for simulation of sliding arc spots to reduce electrode wear in sinking-EDM by [146].

Drilling and Milling EDM

In EDM drilling, simple cylindrical shaped rotating electrodes are used, where depending on the electrode diameter; inner cooling channels are used to supply pressurised deionised water as dielectric. Dry EDM uses similar concept where instead of deionised water, different gases are used as dielectric. Using similar process parameters as in the case of micro drilling EDM, electrode motion in XYZ is used combined with the uniform wear method developed by Yu et al., [147] for precision machining of 3D micro cavities (see Figure 46) in micro-EDM milling. The main modelling aspects in drilling EDM are tool wear, geometry prediction, MRR and surface quality. In micro-EDM milling, electrode wear compensation and geometry prediction are important aspects.

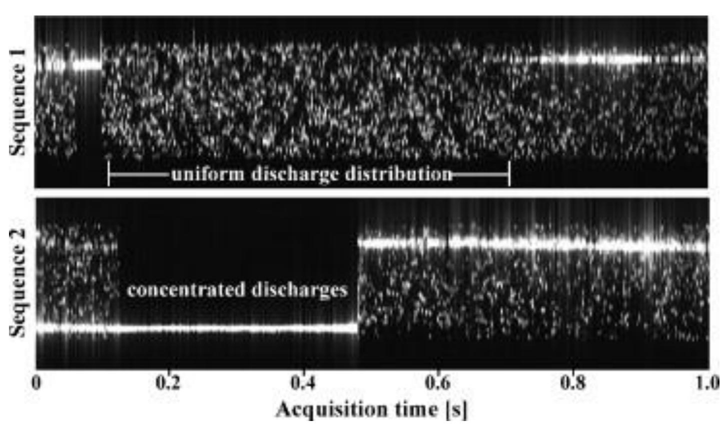

Source: Weingärtner et al., [143].

Figure 44. Discharge mapping over a wire electrode using high-speed imaging. Different scenarios of uniform discharge distribution and concentrated discharges on a single region on the workpiece are seen.

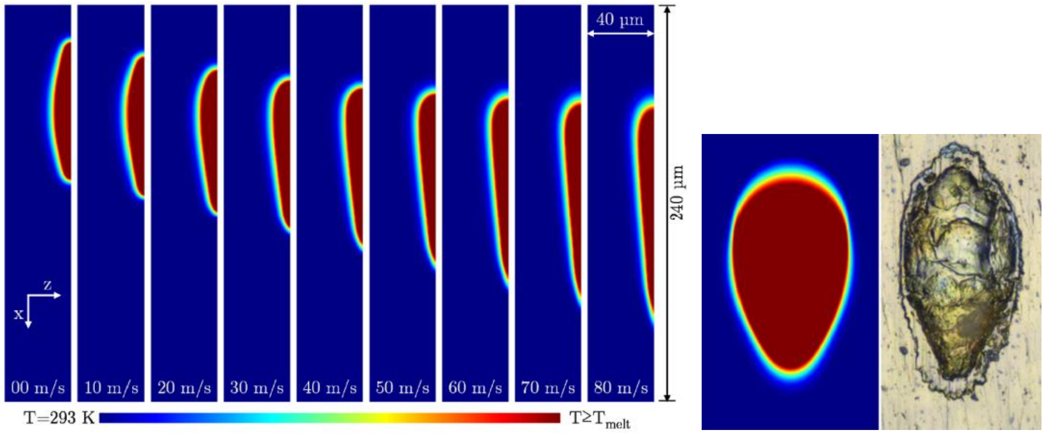

Source: [125].

Figure 45. Left: influence of the relative speed on simulated single discharges in brass (cross section view, peak current = 73 A, time = 1.25 µs). Right: comparison between simulated and measured craters, 80 m/s (top view).

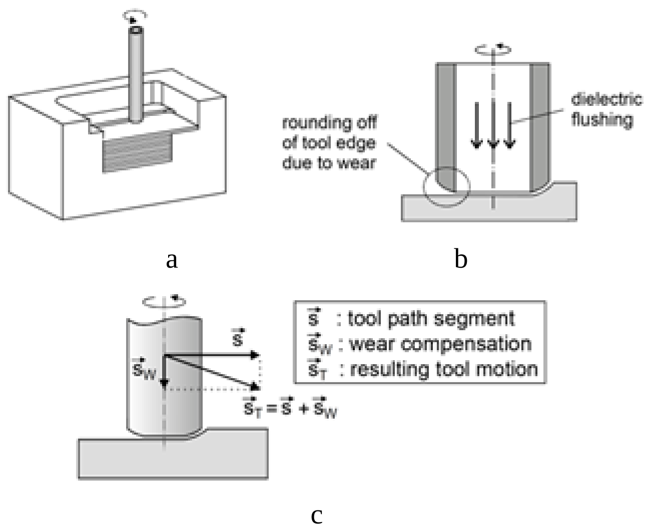

Figure 46. (a) Layer-by-layer milling EDM using a tubular electrode; (b) small layer thickness and electrode wall thickness to retain the electrode shape; (c) downward-motion vector to compensate electrode wear along the tool path [148].

Wear Compensation

A two-dimensional geometric simulation model for EDM drilling with electrode rods is developed by Jeong and Min [149]. Here, using a point heat source model, material removal volume per discharge and the relative tool wear were used to accurately predict the change of tool and workpiece geometries during the machining. The simulated and experimentally measured geometric shapes were compared as shown in Figure 47. The developed model was used off-line for the end and corner wear compensation with error less than 3%.

For micro-EDM milling, Yu et al., [150] presented a model for surface profile generation taking into account the effect of electrode wear.

Heo et al., [151] developed a virtual EDM simulator to simulate the electrode profile after micro-EDM milling and surface geometries of the workpiece as shown in Figure 48.

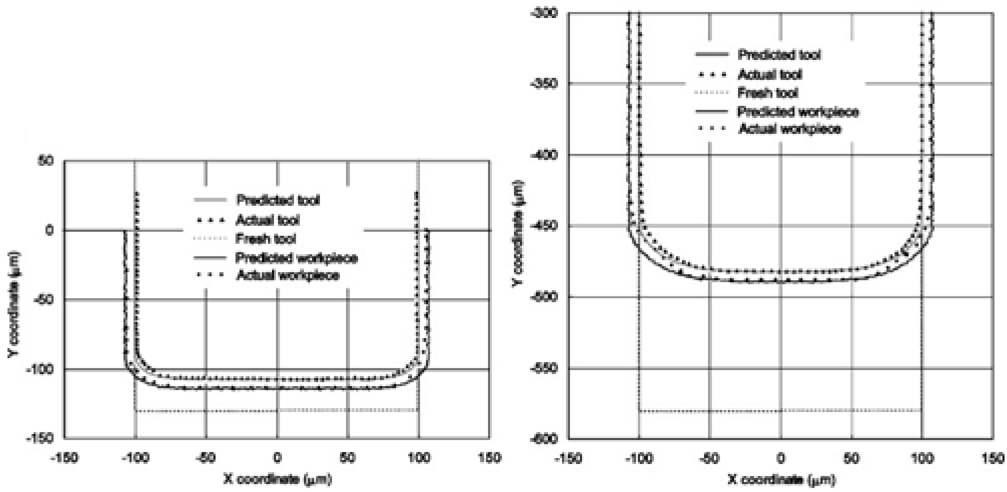

a b

Source: Jeong and Min [149].

Figure 47. Comparison between actual machined and simulated tool and workpiece: (a) when the drilling depth is 130 μm and (b) when the drilling depth is 580 μm.

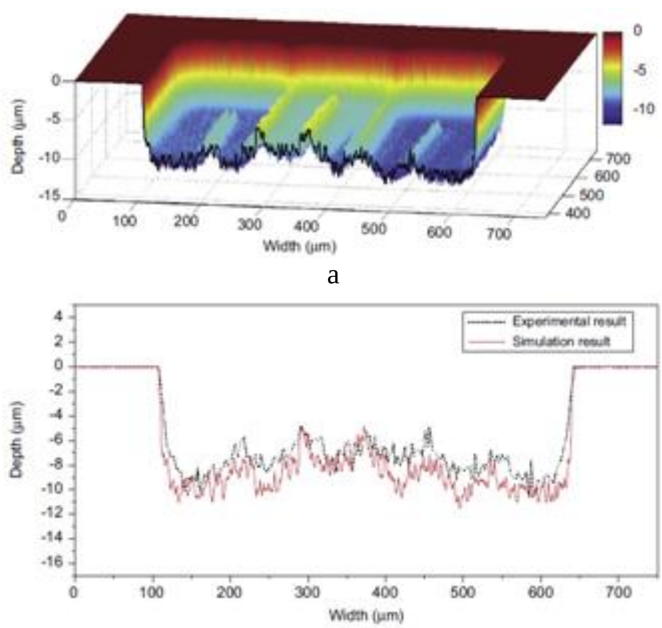

a

b

Source: Heo et al., [151].

Figure 48. Workpiece surface generation simulation in micro-EDM milling: (a) graphical cross-sectional view generated by simulator (solid line shows the contour of cross-section edge); (b) comparison of the real machined and the simulated surface profiles.

Bleys and colleagues [148, 152] developed a real-time wear compensation based on pulse analysis. It was found that using the pulse analysis, wear per discharge could be determined, however slight error in the estimation could lead to the errors in depth, which was then solved by combined wear compensation, which uses real time wear sensing and periodical measurement of the electrode to adjust the wear correction factor. Real time compensation is furthermore either based on full discharge pulse discrimination as used by Aligiri et al., [153] or based on discharge counting and statistical treatment of the discharge population. In the former method, theoretical electro-thermal model, number of discharge pulses and pulse discrimination are used to correct tool wear for micro-EDM drilling.

The later method is developed for both the material removal per discharge [154] and tool wear per discharge [155], where periodic electrode wear length measurements for the wear correction are required to achieve better form accuracy. Jung et al., [156] proposed a model based control considering the real-time pulse monitoring and pulse frequency.

Ivanov et al., [157] and Kozak et al., [158] developed two mathematical models for frontal and lateral electrode shape deformation (see Figure 49), to show the effect of electrode shape deformation on micro-EDM milling accuracy, apart from the effect of variation in the volumetric wear ratio [159].

Material Removal

Compared to die-sinking EDM, the flushing conditions in drilling and milling EDM are efficient due to high pressure flushing through the electrode cooling holes. In order to improve flushing and debris removal from the discharge region in micro-holes, helical micro-tool electrodes are used as shown by [160, 161], however no modelling exists to predict or prove the increase in flushing efficiency. Kunieda et al., [162] developed EDM in gas, where higher material removal is obtained with increased concentration of oxygen. This technique was further expanded for 3D milling using gas as dielectric in [163].

It is proposed that chemical reaction between gas and workpiece material due to its oxidation results in higher material removal rate. Roth [164] calculated the thermal energy of sparks in different gases for different workpiece materials along with the reaction energies from oxidation. It was shown that the energy from the oxidation is not significant compared to the heat flux from plasma.

However, oxidation of debris particles resulted in electrically non-conductive particles. It is proposed that such particles between the electrode and workpiece reduce short circuits and improve overall material removal conditions in the gap.

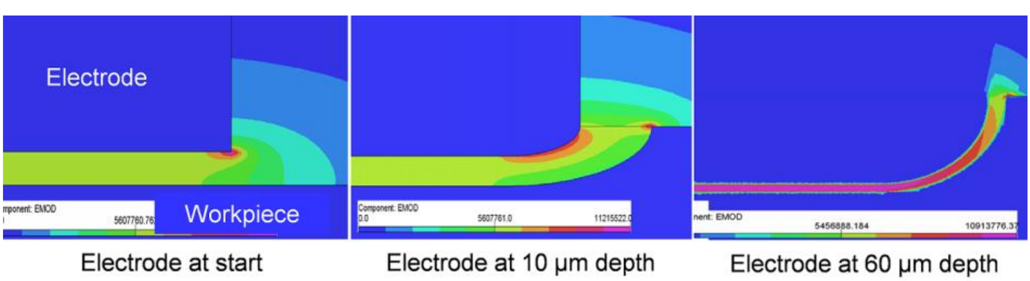

Figure 49. Electric field strength |E| (V/m) in the discharge gap region at different erosion times from Ivanov et al., [157].

Jahan et al., [165] used low frequency vibration in micro-EDM drilling and presented an analytical approach to explain how workpiece vibration improve the process performance. It is found that workpiece vibration aids debris removal and dielectric circulation, resulting in improved overall flushing conditions, which has been also found by [166] using FEM simulations. Shervani-Tabar and Mobadersany [167] performed a numerical study of the dielectric liquid around the gas bubble in ultrasonic EDM conditions. Lin and Lee [168] analysed magnetic field-assisted EDM, where increase in process stability due to better removal of debris was suggested. Joshi et al., [169] applied pulsating magnetic field in dry EDM to increase productivity. Govindan et al., [170] explained the effects in magnetic field assisted EDM using mathematical modelling and experimentation. Application of external magnetic field around the dry EDM plasma is considered to cause confinement of the plasma channel and reduction in mean free path of electron. Here, an analytical model for predicting the effect of Lorentz forces on the crater radius and depth is used as shown in Figure 50. It is found that the magnetic field assistance reduced crater diameter and increased the crater depth.

Material Deposition

EDM can also be used for generating 3D micro structures in air using metal deposition mode as shown by [171, 172]. An example of the deposited steel micro-cylinder is shown in Figure 51. Hayakawa et al., [173] and Wang et al., [174] used temperature simulations to predict the process parameters for the deposition process. Chi et al., [172] used particle-in-cell (PIC) method to computationally study the forming mechanism of the micro-3D spiral structures as shown in Figure 52. The simulation results showed that the electromagnetic field in the discharge field is time constant in the clockwise direction and the moving track of the deposition particles in this electromagnetic field is in a helix shape, while the path of the discharge points in the electrode is in a similar helix with the same outer radius.

PHENOMENOLOGICAL MODELS

Phenomenological models are also called empirical models, statistical models, data-driven models or black box model in which a mathematical model is constructed based on the experimental data only without any insights into the physical system [175].

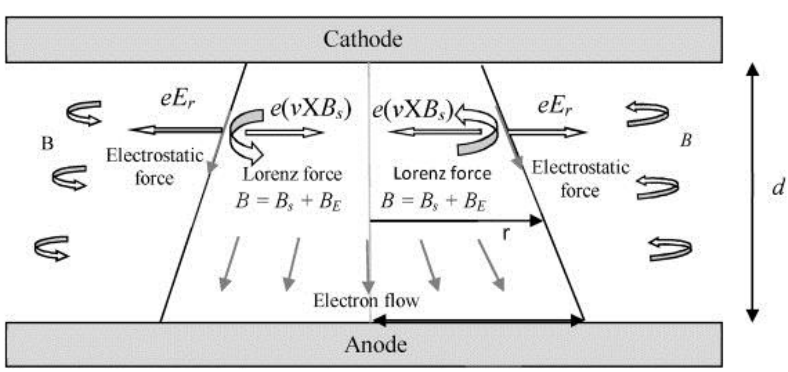

Figure 50. A schematic showing effect of magnetic field on the flow of electrons in dry EDM [170].

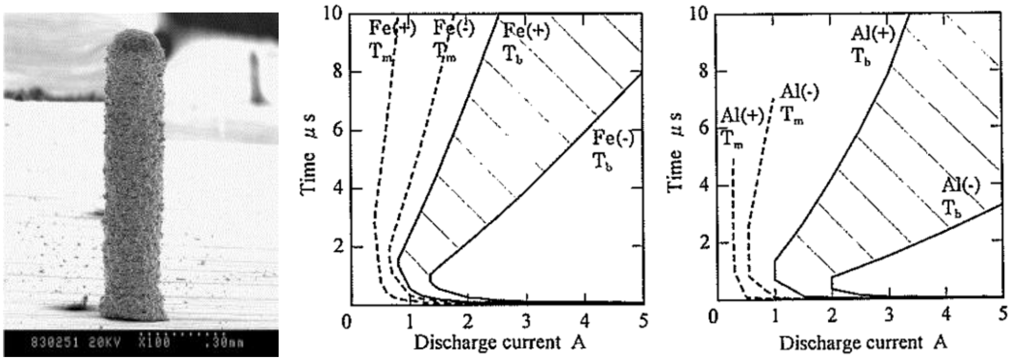

Figure 51. Left: micro-cylinder fabricated by EDM deposition process [171]. Calculated results of the suitable discharge conditions for the deposition process from Hayakawa et al., [173]. Calculated suitable conditions for iron anode-cathode (centre) and aluminium anode-cathode (right) are shown.

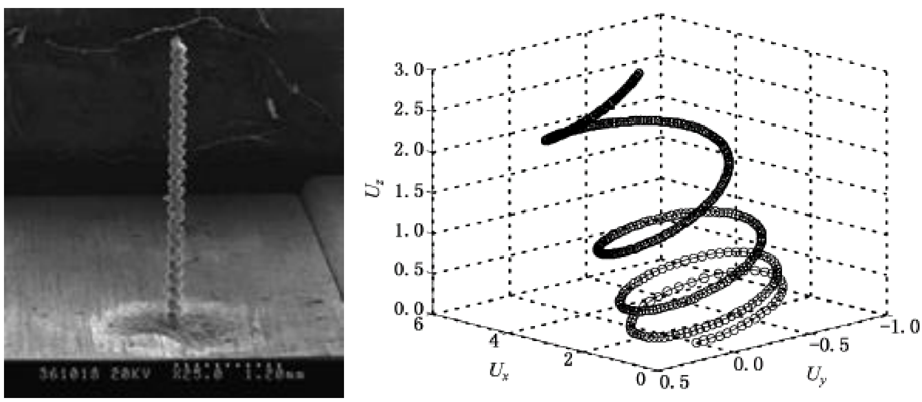

Source: Chi et al., [172].

Figure 52. Left: micro scale 22-circle spiral structure generated using EDM deposition in air. Right: simulated movement trace of particles in the discharge channel.

Actually, most of the theoretical models in EDM currently use one or other fitting parameters, where an *ab initio* approach seems unfeasible due to the sheer complexity and scale of the involved phenomena. Many researchers have provided statistical models based on the experimental analysis. Some approaches are briefly mentioned here without providing specific details and it is far from an extensive list. Dimensional analysis has been used for modelling wear, material removal and surface finish by [176-179]. Models based on neural-networks, artificial neural networks (ANN), Neuro-fuzzy approach, recurrent neural networks and genetic algorithms are also developed in EDM [180-185]. Response surface methodology (RSM) has been used to model EDM process outputs in [186-190]. Additionally, various regression models and optimisation methods with least square theory, ANOVA analysis with Taguchi method, particle swarm optimisation, auto-regressive model, fuzzy logic, grey relational analysis and bee colony algorithm are also developed. Although such models give an overview on the dependence of the process outputs on input parameters, their intrinsic reliance on the experimentation poses mainly two challenges:

1) Since the experimental setup and conditions vary based on a number of factors such as machine type, electrode-workpiece materials, dielectric, etc. their applicability is mostly limited to the particular setup. To find the co-efficient and constants used for the model for different erosion conditions requires further experimentation.
2) Over the years, machine tool manufacturers have developed a number of control and protection algorithms, some of which can be turned off by the users, whereas some cannot be changed by the users. For example, arc control algorithm stops the current pulses when an arc is supposedly detected by the machine control. This may lead to a number of changes, such as different pulse duration, pause duration, etc. Such considerations are not always taken into account during the experimental analysis. This is also true for the validation of theoretical models using the multiple discharge process. Thus, care must be taken to thoroughly know the functioning of the machine control.

CONCLUSION AND OUTLOOK

A comprehensive overview of the theoretical models and simulation in EDM is presented in this chapter. Modelling of single discharge phenomena have been divided into discharge plasma and plasma-material interactions. The main purpose of discharge plasma simulations is to derive boundary conditions for the erosion crater simulations. Extension of single discharge simulation to multiple discharge process is classified according to the main variants of EDM, namely die-sinking, wire-EDM and drilling-milling EDM. Following are some important conclusions from the chapter, which also help outline the future work needed for EDM modelling and simulation.

- Light-emission spectroscopy is found to be important tool to investigate plasma in EDM, where simulation of spectra can open a new way to derive plasma properties and verify the results derived from spectroscopy. Some development in the EDM plasma modelling is observed, however further work is needed for simulation of some important plasma properties, such as plasma radius and flux profile.
- Energy balance in the discharge gap is one of the most important aspects for EDM modelling, however almost no theoretical model exists for its determination. Since energy input into cathode and anode are required to predict material removal and tool wear, effort is required to develop energy balance model which can take into account electrode materials and discharge power. Developments in arc plasma physics need to be explored for their applicability in EDM.
- Once the boundary conditions for heat source are available, temperature distribution simulation in electrode materials is straightforward. The advances in computational power already allow consideration of temperature dependent material properties and latent heats for precise simulations.
- Although superheating as the material removal mechanism is widely accepted mechanism, a quantitative simulation capability to determine plasma flushing efficiency in EDM is still lacking. There is however an increasing consensus that the material removal by a single discharge takes place during the discharge itself.

However, the effect of gas bubble implosion on material ejection remains still unquantified.

- The material removal differences for anode and cathode, especially for different time scales remains unclear. Further investigation is required to understand and simulate this effect. Also, the conditions for protective carbon layer deposition on the anode have been simulated. However, the effect of cathode material and carbon microstructure on the deposition process has not yet been considered in the model.
- A simulation tool for the multiple discharge process solely based on the theoretical approach is lacking. Apart from the single discharge modelling, this would require macroscopic understanding of the gas bubble and debris dynamics. This may eventually lead to online process simulation and aid adaptive control process.

References

[1] Hinduja, S., Kunieda, M., (2013). Modelling of ECM and EDM processes. *CIRP Annals-Manufacturing Technology* 62(2), 775-797.

[2] Kunieda, M., Lauwers, B., Rajurkar, K. P., Schumacher, B. M., (2005). Advancing EDM through Fundamental Insight into the Process. *CIRP Annals - Manufacturing Technology* 54(2), 64-87.

[3] Kunieda, M., (2010). Advancements in Fundamental Studies on EDM Gap Phenomena. *Proceedings of the 16th International Symposium on Electromachining*, pp. 15-23.

[4] Dhanik, S., Joshi, S. S., Ramakrishnan, N., Apte, P. R., (2005). Evolution of EDM process modelling and development towards modelling of the micro-EDM process. *Int. J. Manufacturing Technology and Management* 7(2/3/4), 157-180.

[5] Mohd Abbas, N., Solomon, D. G., Fuad Bahari, M., (2007). A review on current research trends in electrical discharge machining (EDM). *International Journal of Machine Tools and Manufacture* 47(7–8), 1214-1228.

[6] Yeo, S. H., Kurnia, W., Tan, P. C., (2007). Electro-thermal modelling of anode and cathode in micro-EDM. *Journal of Physics D: Applied Physics* 40(8), 2513.

[7] DiBitonto, D. D., Eubank, P. T., Patel, M. R., Barrufet, M. A., (1989). Theoretical models of the electrical discharge machining process. I. A simple cathode erosion model. *Journal of Applied Physics* 66(9), 4095-4103.

[8] Meek, J. M., Craggs, J. D., (1978). *Electrical breakdown of gases*. Wiley, New York.

[9] Raizer, Y., (1991). *Gas discharge physics*. Springer-Verlag, Berlin.

[10] Loeb, L. B., Meek, J. M., (1941). *The mechanism of the electric spark*. Stanford University Press.

[11] Kolb, J. F., Joshi, R. P., Xiao, S., Schoenbach, K. H., (2008). Streamers in water and other dielectric liquids. *Journal of Physics D: Applied Physics* 41(23), 234007.

[12] Schoenbach, K., Kolb, J., Xiao, S., Katsuki, S., Minamitani, Y., Joshi, R., (2008). Electrical breakdown of water in microgaps. *Plasma Sources Sci. T*, 17(2), 024010.

[13] Schulze, H.-P., Läuter, M., Wollenberg, G., Storr, M., Rehbein, W., (2001). Investigation of the pre-ignition stage in EDM, *Proceedings of the 13th International Symposium for Electromachining* ISEM XIII, pp. 141-152.

[14] Schulze, H. P., Wollenberg, G., Lauter, M., Storr, M., Rehbein, W., (2003). Measurement equipment for investigation of the influence of viscosity of dielectric working fluids on spark erosion, *Dielectrics and Electrical Insulation, IEEE Transactions on*, 10(6), pp. 985-993.

[15] Kunieda, M., Takanobu, N., 1998, Factors Determining Discharge Location in EDM, *International Journal of Electrical Machining*, 3, pp. 53-58.

[16] Schumacher, B., 1990, About the role of debris in the gap during electrical discharge machining, *CIRP Annals-Manufacturing Technology*, 39(1), pp. 197-199.

[17] Gatto, A., Bassoli, E., Denti, L., Iuliano, L., (2013). Bridges of debris in the EDD process: Going beyond the thermo-electrical model. *Journal of Materials Processing Technology* 213(3), 349-360.

[18] Eckman, P. K., Williams, E. M., (1960). Plasma dynamics in an arc formed by Low-voltage sparkover of a liquid dielectric. *Appl. Sci. Res.* 8(1), 299-320.

[19] Eubank, P. T., Patel, M. R., Barrufet, M. A., Bozkurt, B., (1993). Theoretical models of the electrical discharge machining process. III. The variable mass, cylindrical plasma model, *Journal of Applied Physics* 73(11), 7900-7909.

[20] Hayakawa, S., (1998). *Study on EDM phenomena through Thermal-Fluids Analysis of Arc Plasma*, PhD thesis (in Japanese), Tokyo University of Agriculture and Technology.

[21] Hayakawa, S., Yuzawa, M., Kunieda, M., Nishiwaki, N., (2001). Time variation and mechanism of determining power distribution in electrodes during EDM process. *International Journal of Electrical Machining* 6, 19-25.

[22] Mujumdar, S. S., Curreli, D., Kapoor, S. G., Ruzic, D., (2014). A Model of Micro Electro-Discharge Machining Plasma Discharge in Deionized Water. *Journal of Manufacturing Science and Engineering* 136(3), 031011.

[23] Descoeudres, A., (2006). *Characterization of Electrical Discharge Machining Plasmas*, PhD thesis, EPF Lausanne, Switzerland.

[24] Albinski, K., Musiol, K., Miernikiewicz, A., Labuz, S., Malota, M., (1996). The temperature of a plasma used in electrical discharge machining. *Plasma Sources Science and Technology* 5(4), 736.

[25] Pillans, B. W., Evensen, M. H., Taylor, H. F., Eubank, P. T., Ma, L., (2002). Fiber optic diagnostic techniques applied to electrical discharge machining sparks. *Journal of Applied Physics* 91(4), 1780-1786.

[26] Nagahanumaiah, Ramkumar, J., Glumac, N., Kapoor, S. G., DeVor, R. E., (2009). Characterization of plasma in micro-EDM discharge using optical spectroscopy. *Journal of Manufacturing Processes* 11(2), 82-87.

[27] Kanmani Subbu, S., Karthikeyan, G., Ramkumar, J., Dhamodaran, S., (2011). Plasma characterization of dry μ-EDM. *Int. J. Adv. Manuf. Technol.* 56(1-4), 187-195.

[28] Braganca, I. M. F., Rosa, P. A. R., Dias, F. M., Martins, P. A. F., Alves, L. L., (2013). Experimental study of micro electrical discharge machining discharges. *Journal of Applied Physics* 113(23), 233301-233314.

[29] Kanemaru, M., Sorimachi, S., Ibuka, S., Ishii, S., (2011). Single bubble generated by a pulsed discharge in liquids as a plasma microreactor. *Plasma Sources Science and Technology* 20(3), 034007.

[30] Hollenstein, C., (2013). *Optical emission spectroscopy of cold and high density aluminium plasmas*, Unpublished Presentation, CRPP, EPFL, Switzerland.

[31] Adineh, V. R., Coufal, O., Zivny, O., (2012). Thermodynamic and Radiative Properties of Plasma Excited in EDM Process Through N2 Taking Into Account Fe. *Plasma Science, IEEE Transactions on* 40(10), 2723-2735.

[32] Adineh, V. R., 2012, Net Emission Coefficient of Plasma Excited in the Electrical Discharge Machining Through Liquid Nitrogen Dielectric Medium, Plasma Science, *IEEE Transactions on*, 40(3), pp. 853-862.

[33] Braginskii, S., (1958). Theory of the development of a spark channel. *SOVIET PHYSICS JETP-USSR* 7(6), 1068-1074.

[34] Skvortsov, Y. V., Komelkov, V., Kuznetsov, N., (1961). Expansion of a spark channel in a liquid. *Soviet Physics-Technical Physics* 5(10), 1100-1112.

[35] Robinson, J. W., (1973). Finite-difference simulation of an electrical discharge in water. *Journal of Applied Physics* 44(1), 76-81.

[36] Zahn, M., Forster, E. O., Kelley, E. F., Hebner Jr, R. E., (1982). Hydrodynamic shock wave propagation after electrical breakdown. *Journal of Electrostatics* 12(0), 535-546.

[37] Pandey, P. C., Jilani, S. T., (1986). Plasma Channel Growth and the Resolidified Layer in Edm. *Precis. Eng.* 8(2), 104-110.

[38] Utsumi, T., (1971). Measurements of cathode spot temperature in vacuum arcs. *Applied Physics Letters* 18(6), 218-220.

[39] Descoeudres, A., Ch, H., Wälder, G., Perez, R., (2005). Time-resolved imaging and spatially-resolved spectroscopy of electrical discharge machining plasma. *Journal of Physics D: Applied Physics* 38(22), 4066.

[40] Kojima, A., Natsu, W., Kunieda, M., (2008). Spectroscopic measurement of arc plasma diameter in EDM. *CIRP Annals - Manufacturing Technology* 57(1), 203-207.

[41] Kitamura, T., Kunieda, M., (2014). Clarification of EDM gap phenomena using transparent electrodes. *CIRP Annals - Manufacturing Technology* 63(1), 213-216.

[42] Maradia, U., Hollenstein, C., Wegener, K., (2015). Temporal characteristics of the pulsed electric discharges in small gaps filled with hydrocarbon oil. *Journal of Physics D: Applied Physics* 48(5), 055202.

[43] Tanabe, R., Kusano, H., Ito, Y., (2008). High-speed imaging system for observation of discharge phenomena, *28th International Congress on High-Speed Imaging and Photonics*, pp. 71260-71269.

[44] Joshi, S. N., Pande, S. S., (2010). Thermo-physical modeling of die-sinking EDM process. *Journal of Manufacturing Processes* 12(1), 45-56.

[45] Benilov, M. S., (2008). Understanding and modelling plasma–electrode interaction in high-pressure arc discharges: A review. *Journal of Physics D: Applied Physics* 41(14), 144001.

[46] Heberlein, J., Mentel, J., Pfender, E., (2010). The anode region of electric arcs: A survey. *Journal of Physics D: Applied Physics* 43(2), 023001.

[47] König, W., Wertheim, R., Zvirin, Y., Roren, M., (1975). Material removal and energy distribution in electrical discharge machining. *Annals of the CIRP* 24(1), 95-100.

[48] Xia, H., Kunieda, M., Nishiwaki, N., (1996). Removal amount difference between anode and cathode in EDM process. *International Journal of Electrical Machining* 1, 45-52.

[49] Revaz, B., Witz, G., Flukiger, R., (2005). Properties of the plasma channel in liquid discharges inferred from cathode local temperature measurements. *Journal of Applied Physics* 98(11), 113305-113306.

[50] Revaz, B., Flükiger, R., Carron, J., Rappaz, M., (2005). A device for measurements of the temperature response to single discharges with high local resolution and fast response time. *Sensors and Actuators A: Physical* 118(2), 238-243.
[51] Perez, R., Rojas, H., Walder, G., Flükiger, R., (2004). Theoretical modeling of energy balance in electroerosion. *Journal of Materials Processing Technology* 149(1–3), 198-203.
[52] Singh, H., (2012). Experimental study of distribution of energy during EDM process for utilization in thermal models. *International Journal of Heat and Mass Transfer* 55(19-20), 5053-5064.
[53] Zhang, Y. Z., Liu, Y. H., Shen, Y., Li, Z., Ji, R. J., Cai, B. P., (2014). A novel method of determining energy distribution and plasma diameter of EDM. *International Journal of Heat and Mass Transfer* 75, 425-432.
[54] Carslaw, H. S., Jaeger, J. C., (1959). *Conduction of heat in solids*, Oxford: Clarendon Press.
[55] Van Dijck, F., (1973). *Physico-mathematical analysis of the EDM process*, PhD Thesis, Katholieke University, Leuven, Netherlands.
[56] Zolotykh, B., (1960). The mechanism of electrical erosion of metals in liquid dielectric media. *Soviet Physics - Technical Physics* 4(12), 1370-1373.
[57] Zolotykh, B., (1970). Phänomenologische Theorie der Funkenerosiven Massbearbeitung. *International Symposium for Electromachining*, pp. 185-191.
[58] Zingerman, A., (1959). Regarding the problem of the volume of molten metal during electrical erosion. *Soviet Physics-Solid State* 1(2), 255-260.
[59] Yeo, S. H., Kurnia, W., Tan, P. C., (2008). Critical assessment and numerical comparison of electro-thermal models in EDM. *Journal of Materials Processing Technology* 203(1–3), 241-251.
[60] Patel, M. R., Barrufet, M. A., Eubank, P. T., DiBitonto, D. D., (1989). Theoretical models of the electrical discharge machining process. II. The anode erosion model. *Journal of Applied Physics* 66(9), 4104-4111.
[61] Xia, H., (1995). *Study on Factors Affecting Electrode Wear Ratio and Improvement of Machining Characteristics in EDM Process*, PhD Thesis (in Japanese), Tokyo University of Agriculture and Technology.
[62] Zahiruddin, M., Kunieda, M., (2012). Comparison of energy and removal efficiencies between micro and macro EDM. *CIRP Annals-Manufacturing Technology* 61(1), 187-190.
[63] Zhang, Y., Liu, Y., Shen, Y., Li, Z., Ji, R., Wang, F., (2013). A New Method of Investigation the Characteristic of the Heat Flux of EDM Plasma. *Procedia CIRP* 6(0), 451-456.
[64] Shabgard, M., Ahmadi, R., Seyedzavvar, M., Oliaei, S. N. B., (2013). Mathematical and numerical modeling of the effect of input-parameters on the flushing efficiency of plasma channel in EDM process. *International Journal of Machine Tools and Manufacture* 65(0), 79-87.
[65] Dhanik, S., Joshi, S. S., (2005). Modeling of a single resistance capacitance pulse discharge in micro-electro discharge machining. *J. Manuf. Sci. Eng*. 127(4), 759-767.
[66] Singh, A., Ghosh, A., (1999). A thermo-electric model of material removal during electric discharge machining. *International Journal of Machine Tools and Manufacture* 39(4), 669-682.

[67] Spur, G., Schönbeck, J., (1993). Anode Erosion in Wire-EDM – A Theoretical Model. *CIRP Annals - Manufacturing Technology* 42(1), 253-256.

[68] Weingärtner, E., Kuster, F., Wegener, K., 2012, Modeling and simulation of electrical discharge machining, *Procedia CIRP*, 2(0), pp. 74-78.

[69] Escobar, A. M., Lange, D. F. d., Castillo, H. I. M., Gutiérrez, F. G. P., (2013). Influence of Modeling Assumptions on the Simulated EDM Performance. *Proceedings of the ASME 2013 International Mechanical Engineering Congress and Exposition*, pp. V08CT09A079-V008CT009A079.

[70] Hockenberry, T. O., Williams, E. M., (1967). Dynamic Evolution of Events Accompanying the Low-Voltage Discharges Employed in EDM. *Industry and General Applications, IEEE Transactions on* IGA-3(4), 302-309.

[71] Samela, J., Nordlund, K., (2008). Atomistic Simulation of the Transition from Atomistic to Macroscopic Cratering. *Physical Review Letters* 101(2), 027601.

[72] Timko, H., Djurabekova, F., Nordlund, K., Costelle, L., Matyash, K., Schneider, R., Toerklep, A., Arnau-Izquierdo, G., Descoeudres, A., Calatroni, S., Taborelli, M., Wuensch, W., 2010, Mechanism of surface modification in the plasma-surface interaction in electrical arcs, *Physical Review B*, 81(18), p. 184109.

[73] Yang, X., Guo, J., Chen, X., Kunieda, M., (2010). Study on Influences of Material Micro-Structure in Micro-EDM by Molecular Dynamics Simulation. *Proceedings of the 16th International Symposium on Electromachining*, pp. 717-720.

[74] Yang, X., Guo, J., Chen, X., Kunieda, M., (2011). Molecular dynamics simulation of the material removal mechanism in micro-EDM. *Precision Engineering* 35(1), 51-57.

[75] Witz, G., Revaz, B., Flukiger, R., (2005). *Heat transfer and Marangoni effect in the electron discharge machining (EDM) process*, COMSOL Multiphysics User's conference, Paris.

[76] Tao, J., Ni, J., Shih, A. J., (2012). Modeling of the Anode Crater Formation in Electrical Discharge Machining. *Journal of Manufacturing Science and Engineering* 134(1), 011002-011002.

[77] Takezawa, H., Kokubo, H., Mohri, N., Horio, K., Yanagida, D., Saito, N., (2007). A study on single discharge machining with low melting temperature alloy. *Proceedings of the 15th International Symposium on Electromachining*, ISEM XV, pp. 69-73.

[78] Hayakawa, S., Sasaki, Y., Itoigawa, F., Nakamura, T., (2013). Relationship between occurrence of material removal and bubble expansion in electrical discharge machining. *Proc. CIRP* 6, 174-179.

[79] Maradia, U., Knaak, R., Boos, J., Boccadoro, M., Stirnimann, J., Wegener, K., (2013). EDM process analysis using high-speed imaging. *Proceedings of the 13th International Conference of the European Society for Precision Engineering and Nanotechnology*, pp. 39-42.

[80] Mesyats, G. A., (1984). Microexplosions on a cathode aroused by plasma-metal interaction. *Journal of Nuclear Materials* 128-129(0), 618-621.

[81] Akematsu, Y., Kageyama, K., Mohri, N., Murayama, H., (2007). Effect of Discharge Current on the Occurrence Time of Cavitations. *Proceedings of the 15th International Symposium on Electromachining*, pp. 105-109.

[82] Tamura, T., Kobayashi, Y., (2004). Measurement of impulsive forces and crater formation in impulse discharge. *Journal of Materials Processing Technology* 149(1–3), 212-216.

[83] Zhang, Y. Z., Liu, Y. H., Shen, Y., Ji, R. J., Li, Z., Zheng, C., (2014). Investigation on the influence of the dielectrics on the material removal characteristics of EDM. *Journal of Materials Processing Technology* 214(5), 1052-1061.

[84] Yoshida, M., Hanaoka, D., Flynn, B., McGeough, J., (2011). Observation of craters formed by single pulse discharge by stacking cross sectional shapes: comparison of craters in liquid and air. *Proceedings of the Institution of Mechanical Engineers, Part B: Journal of Engineering Manufacture*, pp. 1311-1318.

[85] Wang, J., Han, F., Cheng, G., Zhao, F., (2012). Debris and bubble movements during electrical discharge machining. *International Journal of Machine Tools and Manufacture* 58(0), 11-18.

[86] Kitamura, T., Kunieda, M., Abe, K., (2013). High-speed imaging of EDM gap phenomena using transparent electrodes. *Proc. CIRP* 6(0), 314-319.

[87] Kitamura, T., Kunieda, M., Abe, K., (2015). Observation of relationship between bubbles and discharge locations in EDM using transparent electrodes. *Precision Engineering* 40(0), 26-32.

[88] Hayakawa, S., Sudo, Y., Omiya, K., Itoigawa, F., Nakamura, T., (2007). Machining Properties of Electrical Discharge Machining at Gas-Liquid Interface. *Proceedings of the 15th International Symposium on Electromachining*, pp. 87-91.

[89] Hayakawa, S., Doke, T., Itoigawa, F., Nakamura, T., (2010). Observation of Flying Debris Scattered from Discharge Point in EDM Process. *Proceedings of the 16th International Symposium on Electromachining*, pp. 121-125.

[90] Shervani-Tabar, M. T., Abdullah, A., Shabgard, M. R., (2006). Numerical study on the dynamics of an electrical discharge generated bubble in EDM. *Engineering Analysis with Boundary Elements* 30(6), 503-514.

[91] Zhang, Y., Liu, Y., Ji, R., Zheng, C., Shen, Y., Wang, X., (2013). Transient dynamics simulation of the electrical discharge-generated bubble in sinking EDM. *Int. J. Adv. Manuf. Technol.* 68, 1707-1715.

[92] Pontelandolfo, P., Haas, P., Perez, R., (2013). Particle hydrodynamics of the electrical discharge machining process. Part 2: Die sinking process. *Proc. CIRP* 6, 47-52.

[93] Liao, Y. S., Wu, P. S., Liang, F. Y., (2013). Study of debris exclusion effect in linear motor equipped die-sinking EDM process. *Proc. CIRP* 6, 123-128.

[94] Wang, J., Han, F. Z., (2014). Simulation model of debris and bubble movement in consecutive-pulse discharge of electrical discharge machining. *Int. J. Mach. Tool. Manuf.* 77, 56-65.

[95] Schumacher, B. M., (2004). After 60 years of EDM the discharge process remains still disputed. *Journal of Materials Processing Technology* 149(1–3), 376-381.

[96] Maradia, U., Wegener, K., Boccadoro, M., Knaak, R., Stirnimann, J., (2013). Investigation of the scaling effects in meso-micro EDM. *Proceedings of the ASME 2013 International Mechanical Engineering Congress and Exposition*, Americal Society of Mechanical Engineers, pp. V02BT02A038-V002BT002A038.

[97] Natsu, W., Kunieda, M., Nishiwaki, N., (2004). Study on influence of inter-electrode atmosphere on carbon adhesion and removal amount. *International Journal of Electrical Machining* 9, 43-50.

[98] Mohri, N., Suzuki, M., Saito, N., (1995). Time dependence of electrode wear in EDM. *Proceedings of the 11th International Symposium for ElectroMachining*, Lausanne Switzerland, pp. 447-454.

[99] Mohri, N., Suzuki, M., Furuya, M., Saito, N., Kobayashi, A., (1995). Electrode Wear Process in Electrical Discharge Machinings. *CIRP Annals - Manufacturing Technology* 44(1), 165-168.

[100] Murray, J., Zdebski, D., Clare, A. T., (2012). Workpiece debris deposition on tool electrodes and secondary discharge phenomena in micro-EDM. *Journal of Materials Processing Technology* 212(7), 1537-1547.

[101] Itoh, T., (1994). Method and apparatus for sink-type electrical discharge machining with control of pyrographite buildup, *US Patents* 5,369,239.

[102] Klocke, F., Schwade, M., Klink, A., Veselovac, D., (2013). Analysis of material removal rate and electrode wear in sinking EDM roughing strategies using different graphite grades. *Proc. CIRP* 6, 163-167.

[103] Maradia, U., Boccadoro, M., stirnimann, J., Kuster, F., Wegener, K., (2015). Electrode wear protection mechanism in meso-micro EDM. *Journal of Materials Processing Technology* 223, 22-33.

[104] Kunieda, M., Kobayashi, T., (2004). Clarifying mechanism of determining tool electrode wear ratio in EDM using spectroscopic measurement of vapor density. *Journal of Materials Processing Technology* 149(1–3), 284-288.

[105] Izquierdo, B., Sánchez, J. A., Plaza, S., Pombo, I., Ortega, N., (2009). A numerical model of the EDM process considering the effect of multiple discharges. *International Journal of Machine Tools and Manufacture* 49(3–4), 220-229.

[106] Izquierdo, B., Sanchez, J. A., Plaza, S., Ortega, N., Pombo, I., (2010). On the Characterization of the Heat Input for Thermal Modelling of the EDM Process. *Proceedings of the 16th International Symposium on Electromachining*, pp. 27-32.

[107] Salonitis, K., Stournaras, A., Stavropoulos, P., Chryssolouris, G., (2009). Thermal modeling of the material removal rate and surface roughness for die-sinking EDM. *Int. J. Adv. Manuf. Technol.* 40(3), 316-323.

[108] Kansal, H., Singh, S., Kumar, P., (2008). Numerical simulation of powder mixed electric discharge machining (PMEDM) using finite element method. *Mathematical and Computer Modelling* 47(11), 1217-1237.

[109] Kurnia, W., Tan, P., Yeo, S., Tan, Q., (2009). Surface roughness model for micro electrical discharge machining. *Proceedings of the Institution of Mechanical Engineers, Part B: Journal of Engineering Manufacture*, pp. 279-287.

[110] Kiran, M. P. S. K., Joshi, S. S., (2007). Modeling of Surface Roughness and the Role of Debris in Micro-EDM. *Journal of Manufacturing Science and Engineering* 129(2), 265-273.

[111] Somashekhar, K. P., Panda, S., Mathew, J., Ramachandran, N., (2013). Numerical simulation of micro-EDM model with multi-spark. *Int. J. Adv. Manuf. Technol.* 76, 83-90.

[112] Tan, P., Yeo, S., (2008). Modelling of overlapping craters in micro-electrical discharge machining. *Journal of Physics D: Applied Physics* 41(20), 205302.

[113] Das, S., Klotz, M., Klocke, F., (2003). EDM simulation: finite element-based calculation of deformation, microstructure and residual stresses. *Journal of Materials Processing Technology* 142(2), 434-451.

[114] Pérez, R., Carron, J., Rappaz, M., Wälder, G., Revaz, B., Flükiger, R., (2007). Measurement and Metallurgical Modeling of the Thermal Impact of EDM Discharges

on Steel. *Proceedings of the 15th International Symposium on Electromachining*, pp. 17-22.

[115] Murali, M. S., Yeo, S.-H., (2005). Process Simulation and Residual Stress Estimation of Micro-Electrodischarge Machining Using Finite Element Method. *Japanese Journal of Applied Physics* 44(7A), 5254-5263.

[116] Yang, X., Han, X., Zhou, F., Kunieda, M., (2013). Molecular Dynamics Simulation of Residual Stress Generated in EDM. *Procedia CIRP* 6, 433-438.

[117] Tricarico, C., Delpretti, R., Dauw, D., (1988). Geometrical simulation of the EDM die-sinking process. *CIRP Annals-Manufacturing Technology* 37(1), 191-196.

[118] Morimoto, K., Kunieda, M., (2009) Sinking EDM simulation by determining discharge locations based on discharge delay time, *CIRP Annals - Manufacturing Technology*, 58 (1), pp. 221-224.

[119] Kunieda, M., Kowaguchi, W., Takita, T., 1999, Reverse simulation of die-sinking EDM. *CIRP Annals-Manufacturing Technology* 48(1), 115-118.

[120] Kunieda, M., Kaneko, Y., Natsu, W., (2012). Reverse simulation of sinking EDM applicable to large curvatures. *Precision Engineering* 36(2), 238-243.

[121] Adachi, Y., Yoshida, M., Kunieda, M., (1997). Study on Process Reaction Force Caused by Bubble Formation in EDM. *Journal of The Japan Society of Electrical Machining Engineers* 31(67), 23-30.

[122] Klocke, F., Garzón, M., Dieckmann, J., Klink, A., (2011). Process force analysis on sinking-EDM electrodes for the precision manufacturing. *Production Engineering* 5(2), 183-190.

[123] Klocke, F., Garzon, M., Braun, C., Dieckmann, J., (2013). Analysis of Sinking EDM Electrode Deflection Measurements for the Manufacturing of High Aspect Ratio Cavities. *Procedia CIRP* 6, 151-156.

[124] Dauw, D. F., Beltrami, I., (1994). High-Precision Wire-EDM by Online Wire Positioning Control. *CIRP Annals - Manufacturing Technology* 43(1), 193-197.

[125] Weingartner, E., (2013). *On-machine wire electrical discharge dressing of metal bonded grinding wheels*. Diss., Eidgenössische Technische Hochschule ETH Zürich, Nr. 20835, 2012.

[126] Kinoshita, N., Fukui, M., Kimura, Y., (1984). Study on Wire-EDM: Inprocess Measurement of Mechanical Behaviour of Electrode-Wire. *CIRP Annals - Manufacturing Technology* 33(1), 89-92.

[127] Yamada, H., Mohri, N., Saito, N., Magara, T., Furutani, K., (1997). Modal analysis of wire electrode vibration in wire-EDM. *International Journal of Electrical Machining* 2, 19-24.

[128] Obara, H., Ishizu, T., Ohsumi, T., Iwata, Y., (1998). Simulation of wire EDM. *VDI BERICHTE* 1405, 99-108.

[129] Mohri, N., Yamada, H., Furutani, K., Narikiyo, T., Magara, T., (1998). System Identification of Wire Electrical Discharge Machining. *CIRP Annals - Manufacturing Technology* 47(1), 173-176.

[130] Puri, A. B., Bhattacharyya, B., (2003). Modelling and analysis of the wire-tool vibration in wire-cut EDM. *Journal of Materials Processing Technology* 141(3), 295-301.

[131] Altpeter, F., Perez, R., (2004). Relevant topics in wire electrical discharge machining control. *Journal of Materials Processing Technology* 149(1–3), 147-151.

[132] Okada, A., Uno, Y., Onoda, S., Habib, S., (2009). Computational fluid dynamics analysis of working fluid flow and debris movement in wire EDMed kerf. *CIRP Annals - Manufacturing Technology* 58(1), 209-212.

[133] Fujimoto, T., Okada, A., Okamoto, Y., Uno, Y., (2012). Optimization of Nozzle Flushing Method for Smooth Debris Exclusion in Wire EDM. *Key Engineering Materials* 516, 73-78.

[134] Haas, P., Pontelandolfo, P., Perez, R., (2013). Particle Hydrodynamics of the Electrical Discharge Machining Process. Part 1: Physical Considerations and Wire EDM Process Improvement. *Procedia CIRP* 6, 41-46.

[135] Tomura, S., Kunieda, M., (2009). Analysis of electromagnetic force in wire-EDM. *Precision Engineering* 33(3), 255-262.

[136] Hada, K., Kunieda, M., (2013). Analysis of Wire Impedance in Wire-EDM Considering Electromagnetic Fields Generated around Wire Electrode. *Procedia CIRP* 6, pp. 244-249.

[137] Han, F., Kunieda, M., Sendai, T., Imai, Y., (2002). High Precision Simulation of WEDM Using Parametric Programming. *CIRP Annals - Manufacturing Technology* 51 (1), 165-168.

[138] Jennes, M., Snoeys, R., Dekeyser, W., (1984). Comparison of Various Approaches to Model the Thermal Load on the EDM-Wire Electrode. *CIRP Annals - Manufacturing Technology* 33(1), 93-98.

[139] Dekeyser, W., Snoeys, R., Jennes, M., (1985). A thermal model to investigate the wire rupture phenomenon for improving performance in EDM wire cutting. *Journal of Manufacturing Systems* 4(2), 179-190.

[140] Kinoshita, N., Fukui, M., Gamo, G., (1982). Control of Wire-EDM Preventing Electrode from Breaking. *CIRP Annals - Manufacturing Technology* 31(1), 111-114.

[141] Lauwers, B., Kruth, J.-P., Bleys, P., Van Coppenolle, B., Stevens, L., Derighetti, R., (1998). Wire rupture prevention using on-line pulse localisation in WEDM. *Proceedings of the 12th International Symposium for Electromachining*, pp. 203-213.

[142] Okada, A., Uno, Y., Nakazawa, M., Yamauchi, T., (2010). Evaluations of spark distribution and wire vibration in wire EDM by high-speed observation. *CIRP Annals - Manufacturing Technology* 59(1), 231-234.

[143] Weingärtner, E., Roth, R., Kuster, F., Boccadoro, M., Fiebelkorn, F., (2012). Electrical discharge dressing and its influence on metal bonded diamond wheels. *CIRP Annals - Manufacturing Technology* 61(1), 183-186.

[144] Perez, R., Chiriotti, N., Demellayer, R., Flükiger, R., Zryd, A., (2001). Investigation of physical processes in wire-EDM by means of single and multiple discharge measurements and analysis. *Proceedings of the 13th International Symposium for Electromachining*, ISEM XIII, Bilbao, Spain, pp. 9-11.

[145] Klocke, F., Lung, D., Thomaidis, D., Antonoglou, G., (2004). Using ultra thin electrodes to produce micro-parts with wire-EDM. *Journal of Materials Processing Technology* 149(1–3), 579-584.

[146] Kunieda, M., Kameyama, A., (2010). Study on decreasing tool wear in EDM due to arc spots sliding on electrodes. *Precision Engineering* 34(3), 546-553.

[147] Yu, Z., Masuzawa, T., Fujino, M., (1998). Micro-EDM for three-dimensional cavities-development of uniform wear method. *CIRP Annals-Manufacturing Technology* 47(1), 169-172.

[148] Bleys, P., Kruth, J. P., Lauwers, B., (2004). Sensing and compensation of tool wear in milling EDM. *Journal of Materials Processing Technology* 149(1–3), 139-146.
[149] Jeong, Y. H., Min, B.-K., (2007). Geometry prediction of EDM-drilled holes and tool electrode shapes of micro-EDM process using simulation. *International Journal of Machine Tools and Manufacture* 47(12–13), 1817-1826.
[150] Yu, Z., Kozak, J., Rajurkar, K., (2003). *Modelling and simulation of micro EDM process. CIRP Annals-Manufacturing Technology* 52(1), 143-146.
[151] Heo, S., Jeong, Y. H., Min, B.-K., Lee, S. J., (2009). Virtual EDM simulator: Three-dimensional geometric simulation of micro-EDM milling processes. *International Journal of Machine Tools and Manufacture* 49(12–13), 1029-1034.
[152] Bleys, P., Kruth, J.-P., Lauwers, B., Zryd, A., Delpretti, R., Tricarico, C., (2002). Real-time tool wear compensation in milling EDM. *CIRP Annals-Manufacturing Technology* 51(1), 157-160.
[153] Aligiri, E., Yeo, S. H., Tan, P. C., (2010). A new tool wear compensation method based on real-time estimation of material removal volume in micro-EDM. *Journal of Materials Processing Technology* 210(15), 2292-2303.
[154] Bissacco, G., Tristo, G., Hansen, H. N., Valentincic, J., (2013). Reliability of electrode wear compensation based on material removal per discharge in micro EDM milling. *CIRP Annals-Manufacturing Technology* 62(1), 179-182.
[155] Bissacco, G., Hansen, H. N., Tristo, G., Valentincic, J., (2011). Feasibility of wear compensation in micro EDM milling based on discharge counting and discharge population characterization. *CIRP Annals - Manufacturing Technology* 60(1), 231-234.
[156] Jung, J. W., Jeong, Y. H., Min, B.-K., Lee, S. J., (2008). Model-based pulse frequency control for micro-EDM milling using real-time discharge pulse monitoring. *Journal of Manufacturing Science and Engineering* 130(3), 031106.
[157] Ivanov, A., Ferri, C., Petrelli, A., (2007). Micro EDM - identification and analysis of two sources of natural tolerance. *Proceedings of the 8th International Conference and Exhibition on Laser Metrology, Machine Tool, CMM and Robotic Performance*, pp. 25-28.
[158] Kozak, J., Ivanov, A., Al-naemi, F., Gulbinowicz, Z., (2007). EDM Electrode Wear and its Effect on Processes Accuracy and Process Modelling. *Proceedings of the 15th International Symposium on Electromachining*, pp. 81-86.
[159] Dimov, S., Popov, K., Bigot, S., Ivanov, A., Pham, D. T., (2007). A study of micro-electro discharge machining electrode wear. *Proceedings of the Institution of Mechanical Engineers, Part C: Journal of Mechanical Engineering Science*, pp. 605-612.
[160] Hung, J.-C., Lin, J.-K., Yan, B.-H., Liu, H.-S., Ho, P.-H., (2006). Using a helical micro-tool in micro-EDM combined with ultrasonic vibration for micro-hole machining. *Journal of Micromechanics and Microengineering* 16(12), 2705.
[161] Plaza, S., Sanchez, J. A., Perez, E., Gil, R., Izquierdo, B., Ortega, N., Pombo, I., (2014). Experimental study on micro EDM-drilling of Ti6Al4V using helical electrode. *Precision Engineering* 38(4), 821-827.
[162] Kunieda, M., Yoshida, M., Taniguchi, N., (1997). Electrical Discharge Machining in Gas. *CIRP Annals - Manufacturing Technology* 46(1), 143-146.

[163] Kunieda, M., Miyoshi, Y., Takaya, T., Nakajima, N., ZhanBo, Y., Yoshida, M., (2003). High Speed 3D Milling by Dry EDM. *CIRP Annals - Manufacturing Technology* 52(1), 147-150.

[164] Roth, R. A., (2014). *Trockene Funkenerosion*, Diss., Eidgenössische Technische Hochschule ETH Zürich, Nr. 22025.

[165] Jahan, M. P., Saleh, T., Rahman, M., Wong, Y. S., (2010). Development, Modeling, and Experimental Investigation of Low Frequency Workpiece Vibration-Assisted Micro-EDM of Tungsten Carbide. *Journal of Manufacturing Science and Engineering* 132(5), 054503.

[166] Singh, J., Walia, R., Satsangi, P., Singh, V., (2011). FEM modeling of ultrasonic vibration assisted work-piece in EDM process. *International Journal of Mechanic Systems Engineering* 1(1), 8-16.

[167] Shervani-Tabar, M. T., Mobadersany, N., (2013). Numerical study of the dielectric liquid around an electrical discharge generated vapor bubble in ultrasonic assisted EDM. *Ultrasonics* 53(5), 943-955.

[168] Lin, Y.-C., Lee, H.-S., (2008). Machining characteristics of magnetic force-assisted EDM. *International Journal of Machine Tools and Manufacture* 48(11), 1179-1186.

[169] Joshi, S., Govindan, P., Malshe, A., Rajurkar, K., (2011). Experimental characterization of dry EDM performed in a pulsating magnetic field. *CIRP Annals - Manufacturing Technology* 60(1), 239-242.

[170] Govindan, P., Gupta, A., Joshi, S. S., Malshe, A., Rajurkar, K. P., (2013). Single-spark analysis of removal phenomenon in magnetic field assisted dry EDM. *Journal of Materials Processing Technology* 213(7), 1048-1058.

[171] Peng, Z., Wang, Z., Dong, Y., Chen, H., (2010). Development of a reversible machining method for fabrication of microstructures by using micro-EDM. *Journal of Materials Processing Technology* 210(1), 129-136.

[172] Chi, G., Wang, Z., Xiao, K., Cui, J., Jin, B., (2008). The fabrication of a micro-spiral structure using EDM deposition in the air. *Journal of Micromechanics and Microengineering* 18(3), 035027.

[173] Hayakawa, S., Ori, R. I., Itoigawa, F., Nakamura, T., Matsubara, T., (2001). Fabrication of microstructure using EDM deposition. *Proceedings of the 13th International Symposium for Electromaching*, Bilbao, pp. 783-793.

[174] Wang, Y.-k., Xie, B.-c., Wang, Z.-l., Peng, Z.-l., (2011). Micro EDM deposition in air by single discharge thermo simulation. *Transactions of Nonferrous Metals Society of China* 21, Supplement 2, s450-s455.

[175] Velten, K., (2009) *Mathematical modeling and simulation: introduction for scientists and engineers*, John Wiley and Sons.

[176] Jeswani, M. L., (1979). Dimensional analysis of tool wear in electrical discharge machining, *Wear* 55(1), 153-161.

[177] Wang, P.-J., Tsai, K.-M., (2001). Semi-empirical model on work removal and tool wear in electrical discharge machining. *Journal of Materials Processing Technology* 114(1), 1-17.

[178] Tsai, K.-M., Wang, P.-J., (2001). Semi-empirical model of surface finish on electrical discharge machining. *International Journal of Machine Tools and Manufacture* 41(10), 1455-1477.

[179] Yahya, A., Manning, C. D., (2004). Determination of material removal rate of an electro-discharge machine using dimensional analysis. *Journal of Physics D: Applied Physics* 37(10), 1467.

[180] Tsai, K.-M., Wang, P.-J., (2001). Comparisons of neural network models on material removal rate in electrical discharge machining. *Journal of Materials Processing Technology* 117(1–2), 111-124.

[181] Mandal, D., Pal, S. K., Saha, P., (2007). Modeling of electrical discharge machining process using back propagation neural network and multi-objective optimization using non-dominating sorting genetic algorithm-II. *Journal of Materials Processing Technology* 186(1–3), 154-162.

[182] Joshi, S. N., Pande, S. S., (2011). Intelligent process modeling and optimization of die-sinking electric discharge machining. *Applied Soft Computing* 11(2), 2743-2755.

[183] Spedding, T. A., Wang, Z., (1997). Study on modeling of wire EDM process. *Journal of Materials Processing Technology* 69(1), 18-28.

[184] Indurkhya, G., Rajurkar, K., (1992). Artificial neural network approach in modeling of EDM process, *Proceedings of Artificial Neural Networks in Engineering (ANNIE'92) Conference*, St. Louis, Missouri, US, pp. 15-18.

[185] Tsai, K.-M., Wang, P.-J., (2001). Predictions on surface finish in electrical discharge machining based upon neural network models. *International Journal of Machine Tools and Manufacture* 41(10), 1385-1403.

[186] Pradhan, M., Biswas, C., (2009). Modeling and Analysis of process parameters on Surface Roughness in EDM of AISI D2 tool Steel by RSM Approach. *International Journal of Mathematical, Physical and Engineering Sciences* 3(1).

[187] Chiang, K.-T., (2008). Modeling and analysis of the effects of machining parameters on the performance characteristics in the EDM process of Al2O3+ TiC mixed ceramic. *Int. J. Adv. Manuf. Technol.* 37(5-6), 523-533.

[188] Gopalakannan, S., Senthilvelan, T., Ranganathan, S., (2012). Modeling and Optimization of EDM Process Parameters on Machining of Al 7075-B 4 C MMC Using RSM. *Procedia Engineering* 38, 685-690.

[189] Puri, A. B., Bhattacharyya, B., (2005). Modeling and analysis of white layer depth in a wire-cut EDM process through response surface methodology. *Int. J. Adv. Manuf. Technol.* 25(3), 301-307.

[190] Hewidy, M., El-Taweel, T., El-Safty, M., (2005). Modelling the machining parameters of wire electrical discharge machining of Inconel 601 using RSM. *Journal of Materials Processing Technology* 169(2), 328-336.

In: Electrical Discharge Machining (EDM)
Editor: M. P. Jahan

ISBN: 978-1-63483-591-6

Chapter 4

SURFACES IN ELECTRICAL DISCHARGE MACHINING

Bülent Ekmekci**, Nihal Ekmekci and Hamidullah Yaşar
Department of Mechanical Engineering, Bülent Ecevit University, Zonguldak, Turkey

ABSTRACT

Electrical discharge machining (EDM) involves complex physical phenomena and produces distinctive microstructures on the machined surfaces. Therefore, an obvious characterization is crucial to determine the resultant surface quality and functionality. The industry has realized the importance of EDM'ed surface quality. However, many issues including machining parameters and the mechanisms cannot be addressed due to the complexity. Improving the resultant surface quality with deliberate surface treatments during machining is the critical issue to provide an economic and precise alternative. Therefore, enhancement of the surface quality by applying other proper techniques with EDM and/or by arranging the working parameters will continue as a primary research interest. Understanding surface topographical features, properties of re-solidified and heat affected layers, residual stresses, their relation with the working parameters and the materials became a vital concern. This work presents a comprehensive study on machined surface properties and mechanisms participating in EDM. Moreover, future trends and possible research directions are suggested in the light of the research literature.

Keywords: Electrical Discharge Machining, EDM, surface integrity

INTRODUCTION

Electrically conductive and difficult to cut materials could be machined in complex geometries by using Electrical Discharge Machining (EDM). Electrical parameters can be quickly set in a widespread range during machining, and this feature gives the opportunity of controlling the surface integrity. Significant technological developments and attracting

* Corresponding author: Bülent Ekmekci. E-mail: bekmekci@hotmail.com.

concern for EDM expand its usage as a valuable nontraditional machining process. Nowadays, EDM has a broad range of applications.

It is indispensable and involves the core facilities in mold and die industry. Adaptation of the process for the micro-scale production expands its capabilities to complicated microstructure generation in hard materials. The number of advanced electrical discharge machines increase progressively and now, it is usual to come across with an EDM machine for routine machine shop and tool room applications.

The amount of energy released during EDM affects the surface quality and damage of the machined parts. Open gap voltage, pulse-on duration, pulse-off time and pulse current are the easily controlled parameters. Material properties as thermal conductivity, specific heat, electrical resistance, melting and boiling temperatures of electrodes, composition, and size of the removed material or added powders in dielectric liquid affect the process and surface integrity. Therefore, advocating the process by improving a systematic identification of the relationships between the properties of the surface has been taken as a principal direction in research facilities. Surface quality in terms of topography, microstructural changes, residual stresses and consequent influences such as cracking has been investigated by many researchers for a variety of applications such as wire, micro, and powder mixed EDM.

Consequently, surface topographical features and sub-surface properties studied through the research literature and presented with the emphasis on the evolved mechanisms.

SURFACE TOPOGRAPHY

While reducing the inter-electrode gap by a servo system, an open gap voltage (100-400 V) is supplied to the electrodes. This result in an electrical field in the gap and the field is strongest at a minimum distance. Meanwhile, the electric field intensity increases as the tool electrode move towards the work material. The electrical field intensity exceeds the dielectric strength of the gap at a particular distance (~10 μm). The dielectric liquid breaks, the open gap voltage suddenly decreases (~30 V) and current starts to flow in a small resistance discharge channel. Electrons and polarized ions strike to both electrode surfaces. The collision process transfers the kinetic energies of the atomic particles in the form of heat and pressure. The spot temperatures at the local discharge area of the electrodes increase for the short pulse duration. The estimated heat transfer is around 10^{17} W/m^2 and such high intensity of heat boost the temperatures over 20000ºC [1]. Such extreme temperatures are unexpected for any other known machining process. Therefore, the electrode materials melt, vaporize and even ionize at the local discharge area. The plasma channel continues to expand during the pulse period and result in a decrease in current density. The channel pressure is also high and prevents evaporation of the superheated material in the melted cavity. The channel pressure decreases suddenly at the end of the pulse period followed by an intense explosion of the superheated cavity.

Meanwhile, the rushing back dielectric liquid fills the volume occupied by the plasma channel. Then, both electrode surfaces cools down abruptly as well as the exploded material (debris) in dielectric liquid. Finally, circulation system flushes away the debris particles to keep similar gap properties for the next discharge. The debris particles on the other hand usually have hollow spherical and irregular geometries with a characteristic range of sizes depending on machining parameters. So, the next discharge generates a microscopic crater on both of the electrode surfaces. By driving one electrode towards the other, under successive discharges with high frequencies will remove the work material gradually. Finally, a complementary form of the tool electrode will be obtained on the work material surface. EDM'ed surfaces own a dull appearance due to an arbitrary distribution of overlying craters (Figure 1a). Sparking results in ridges, which could come from the molten material flow while discharging. A closer look also designates globules and pockmarks presumably formed due entrapped gasses escaping from the molten material and then suddenly solidified (Figure 1b). The complex geometrical features and consequent splashes over the craters also designate the traces of molten material ejection.

Pulse-on duration and current dominates the size of the craters produced as well as the thermal characteristics of the material and the dielectric liquid composition. Many thousands of sequentially applied discharges per second lead corresponding work material texture and surface finish. Produced crater volume depends on the pulse energy used during machining. Pulse-on duration and pulse current have distinctive characteristics on produced crater diameter and depth. As a rule of thumb, increasing the pulse-on duration allows the discharge channel to expand and result in relatively big craters. On the other hand, pulse current mainly reflects the depth of the craters produced. Such a simple reasoning gives a sense of the relation between surface roughness and the used electrical parameters. However, the shapes of the craters deviate from the circularity and rely on the electrode polarity. For example, during the liquid dispersal time, anode craters represent a circumferential rim due to rising molten metal and take a circular form regardless of the crystal orientation. Instead, the cathode craters diverge from the circularity and expose the crystal faces symmetry [2]. The craters produced on different types of materials usually represent similar geometries. The difference is only the size variation for different materials [3]. The craters diverged from circularity when elevated pulse energy levels used during machining. For example, application of low pulse energies under 50 μJ leads circular craters with better-defined rim [4]. Surface roughness also can be taken as a rough estimation of produced craters. A sudden increase in surface roughness is essential with respect to increasing in pulse energy under fine and moderate machining conditions followed by saturation in rough machining conditions.

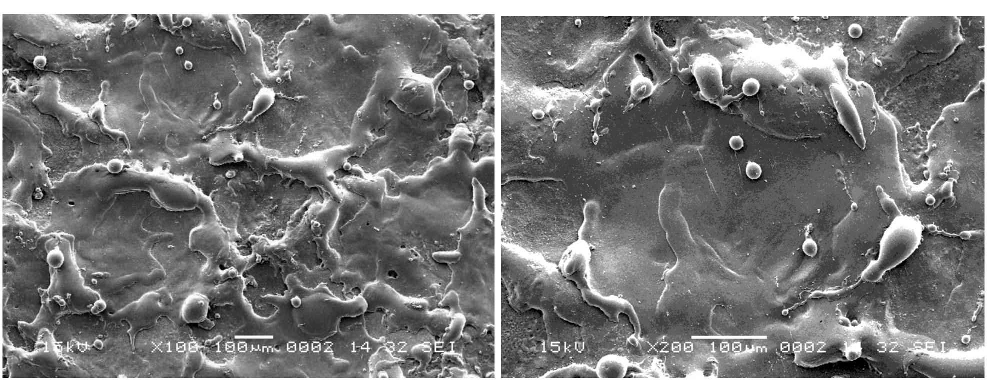

a b

Figure 1. Craters, global appendages and pockmarks on EDM'ed surface of DIN 1.2738 steel. a) A General view. b) A Magnified view.

The diversity of topological features in different combinations of dielectric liquid and tool electrode material reveals different modes of phenomena depending on the availability of carbon sources during machining [5]. For example, if machining in deionized water and using copper tool electrode leads a surface with none or rare occasion’s appendages attached to the rims (Figure 2a). When the tool electrode is graphite, the appendages develop on the surface (Figure 2b). Replacing the electrode with copper and machining in the hydrocarbon-based dielectric liquid result in an intense increase in such attachments ascending upward (Figure 2c). Continuing the experiment with both carbon based tool electrode and dielectric liquid will not alter the result when compared with the previous case (Figure 2d). These results are the indication of the material interface during EDM.

Tool electrode and/or dielectric liquid release small atoms like carbon and trigger the boiling process in the melted cavity while discharging. Then the cavity suddenly froze at the end of discharge duration. The generated features are excellent descriptions of sudden closure and subsequent pressure decrease at the end of pulse duration.

Extreme temperature and pressure variations during machining produce a variety of imperfections on the surface. Surface cracks are uncomplimentary examples that significantly decrease the material fatigue and corrosion resistance [6, 7]. Hence, the cracking mechanisms in EDM have impelled interest for scientists. This way, it would be possible to figure out the proper operational situations for crack-free surface generation.

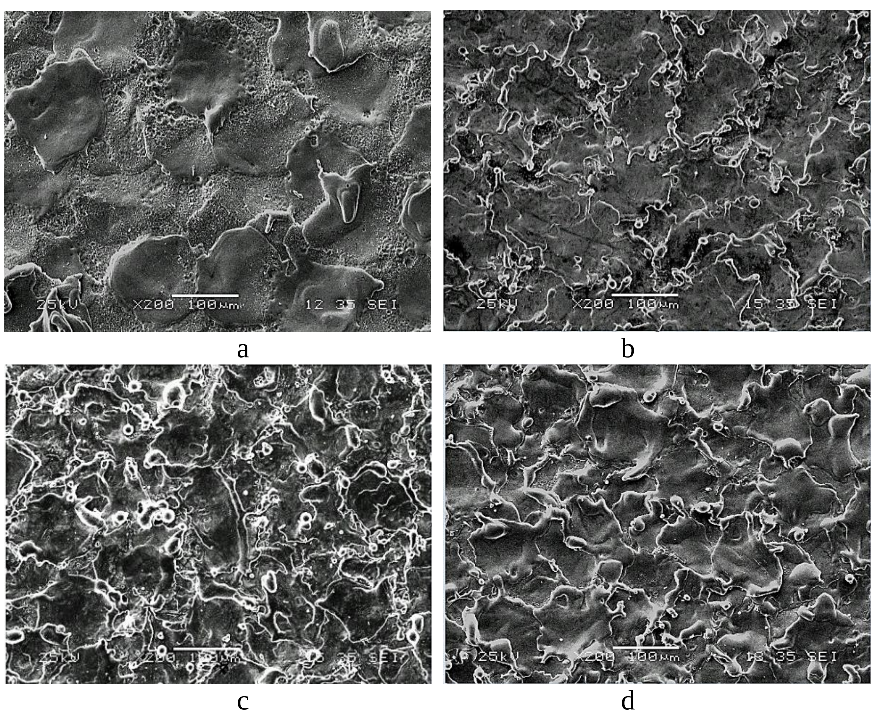

[a]Copper tool electrode in water dielectric liquid.
[b]Graphite tool electrode in water dielectric liquid.
[c]Copper tool electrode in kerosene dielectric liquid.
[d]Graphite tool electrode in kerosene dielectric liquid.

Figure 2. EDM’ed surface of DIN 1.2738 Steel Specimen (I_{av} = 8A, t_p = 8μs).

Pulse duration, current, work material, and dielectric liquid properties are the main factors determining the cracking probability of the resultant surfaces. Solidification of melted cavities in extreme rates generates high contraction stresses, in some circumstances, beyond the fracture strength of the work material [8]. Melted layer contracts more than the base material and yields high stress during solidification [9].

Surface cracking probability increases especially when using high pulse-on durations and low pulse currents during machining [10]. It is in accordance with the simple reasoning given previously. High pulse-on durations lead large diameter craters and low pulse current result in a thin melted portion underneath which produce a high gradient of stress. The usual appearances of a crack network produced by EDM (Figure 3) reveal closed loops around crater edges and perpendicular crosses in the craters. Continued cracks over the overlapped craters imply propagation due to subsequent discharges.

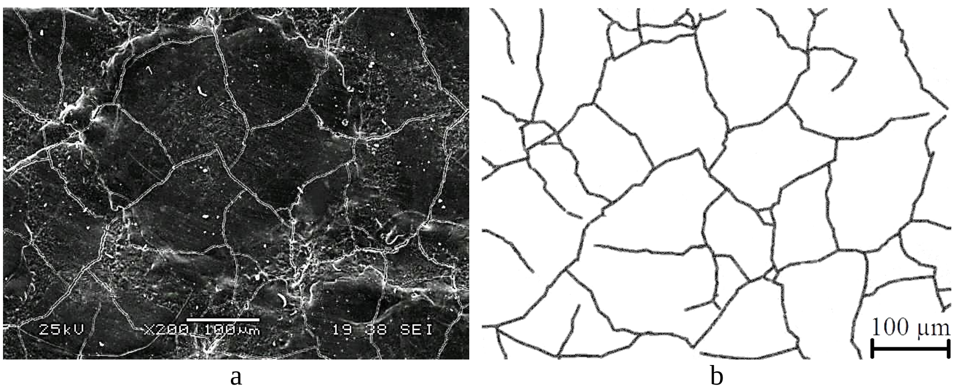

Figure 3. An example of a cracked surface in EDM. a) The SEM image. b) Visualization of the cracking network after edge detection.

However, such nearly patterned crack network formation cannot describe the whole cracking mechanism encountered during EDM. The interactions with the dielectric liquid and the tool electrode became important aspect to describe some different types of cracks encountered. Therefore, several questions come up with the sub-surface characteristics such as the depth of re-solidified and heat affected layers, microstructural changes, metallurgical transformations and so on.

SUB-SURFACE MICROSTRUCTURE

Former studies on different steel grades indicated a high resistance section to a variety of acids over the heat affected layer. In fact, this is the melted and then solidified part of the material. Additionally, this section is heavily interacted with dielectric and tool electrode during machining. Therefore, it is not a surprise to encounter with different alloying elements within the layer. The layer is observed regardless of the machining conditions utilized such as dielectric liquid, tool electrode and released pulse energy [11] and harder than the structures achievable by quenching [2]. Researchers defined the structure as ledeburite of a hypoeutectic white cast iron or completely austenitic surface tracked by an austenite-cementite matrix when machining in hydrocarbon-based dielectric liquid [12].

The carbon intensity rigorously increased within the layer as nine times greater than the bulk material [13]. Such an increase is only possible by carbon migration from the tool electrode and/or dielectric liquid. A variety of re-solidified layer microstructure is etched by using unconventional metallographic reagents [14]. For example, a typical solidification microstructures on EDM plastic mold steel samples indicates four discernible sublayers. The top most layer consists large columnar grains oriented downward.

Similar grains are also visible in opposite direction growing over the featureless layer. The thin featureless layer exhibits some occasion of dendritic features projecting upwards (Figure 4a). Sometimes directions of the columnar grains are somehow disturbed over the featureless layers and reveal the complicated nature of the thermal cycles (Figure 4b). The piled segments clearly identify multilayer structures and subsequent heating effects due to intersecting layers (Figure 4c). The re-solidified layer thickness increases due to molten metal expulsion onto a re-solidified structure that produced previously. The result is a modified microstructure generated due to the subsequent heat treatments of the outermost layers (Figure 4d).

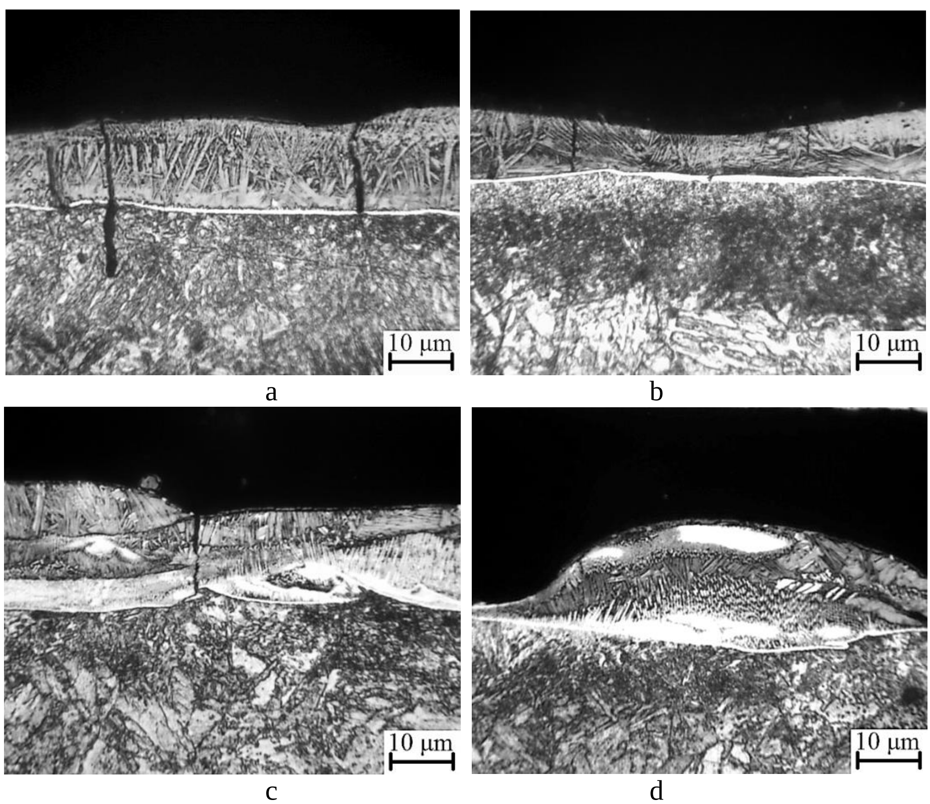

[a]Dendrite structures over featureless layer and cracks.
[b]Columnar grains and over tempered section.
[c]Multilayer structures at piled segments.
[d]Subsequent thermal effects during solidification.

Figure 4. Sections of EDM'ed DIN 1.2738 steel surfaces (I_{av} = 25A t_p = 400 μs).

The usual composition of the re-solidified structure contains martensite and a variety of carbides in austenite matrix. The amount of martensite increases and carbide decreases gradually as with respect to increasing the depth. The innermost sublayer is thin and featureless suggesting carbon migration from the dielectric liquid is insufficient to form carbides. Therefore, this layer has less amount of retained austenite, rather uniform, and free from complex iron carbides [10]. Dendrite formations at some sections above are the signs of solidification interface confrontation.

The molten pool solidifies by conduction from the base and by convection from the topmost. The temperature variation could be considered higher than the variation in the substrate due to convection. The intermediate sub-layer solidified towards both interfaces, and the thin featureless layer is the portion of the material melted just after discharge and re-solidified due to conduction from the base [15].

The re-solidified structure followed by heat affected layers that moderately disturbed due to carbon migration both from the dielectric and/or the tool electrode. The tempered microstructure usually followed by an over tempered region and the total thickness increases correspondingly with the discharge energy. This layer usually includes larger and more rounded second phase particles than the base and sometimes harder than the re-solidified layer [14]. When machining single-phase materials, a plastically deformed zone underlies the heat affected layer without undergoing phase transformations [16]. The thickness of this zone is ranging between few tens and a hundred micrometers depending on the pulse energy used during machining. Cracks can extend into the base material when brittle materials machined under severe conditions [17].

The re-solidified structure defined as the composition of martensite and some dissolved carbides in austenite matrix. Interstitial atoms such as carbon fixed in the crystal structure due to the insufficient duration of time to diffuse out. To identify carbon migration phenomena during EDM, retained austenite, dielectric liquid, electrode material, residual stress, microstructural constitutes and their interrelations became an interesting issue [18]. The high quantity of residual austenite is essential (> 40%) when machining is carried out using hydrocarbon-based dielectric liquid. The amount decreases abruptly (Figure 5a) with respect to depth and signifies saturation of the surface with carbon unrelatedly to the material type of the tool electrode. However, replacing the tool electrode with copper and machining in deionized water result in a peak in the re-solidified structure (Figure 5b). It is signifying the uncompleted transformation due to carbon diffusion from the base material. Finally, replacing again the tool electrode with graphite and machining in water dielectric liquid inhibits the peak formation. A gradual distribution with a moderate increase in retained austenite due to carbon uptake from the tool electrode is developed in the re-solidified structure (Figure 5c).

Sectional examinations using unconventional etching reagent revealed the microstructure of the affected layers when machining in a hydrocarbon-based liquid. However, the re-solidified structure still resistant to the unconventional etching agents when machining in water dielectric liquid (Figure 6a). This result suggests the structural homogeneity of the re-solidified layer composed of fine martensite matrix (Figure 6b). Dissolved carbides developed over the structure when using the graphite tool electrode.

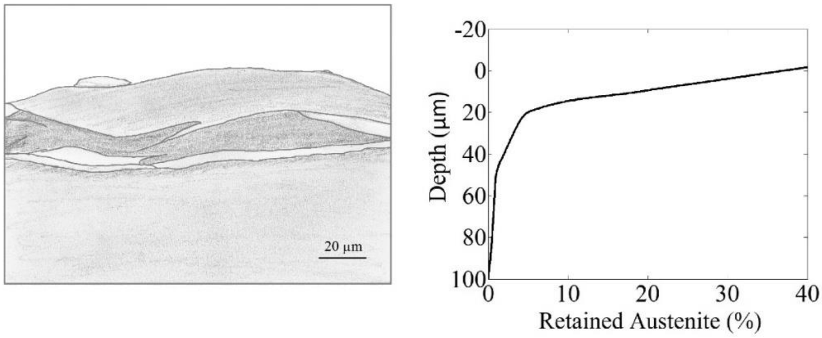

a

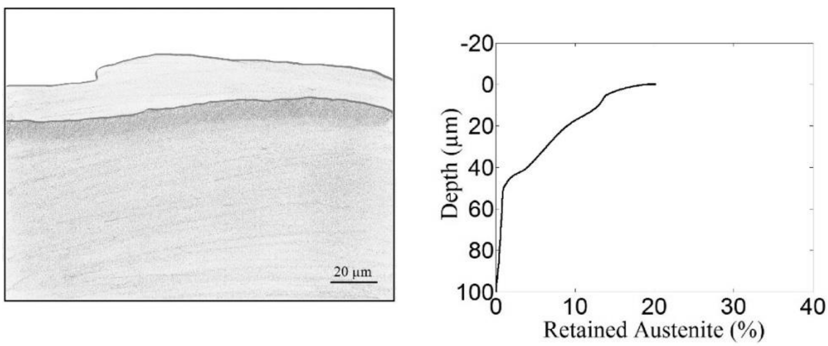

b

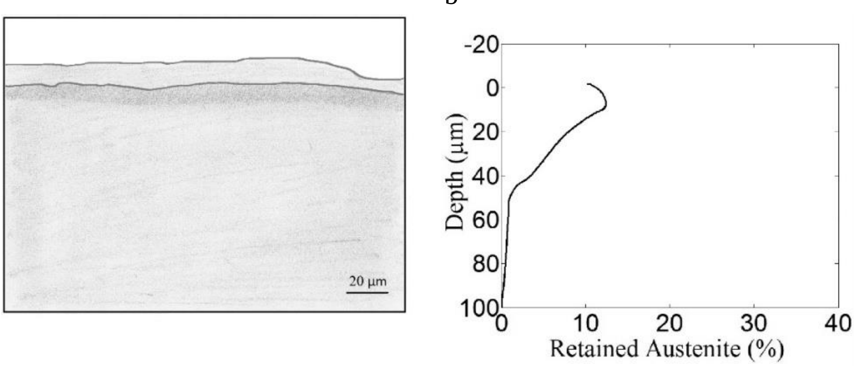

c

[a]Graphite tool electrode in kerosene dielectric liquid.
[b]Graphite tool electrode in water dielectric liquid.
[c]Copper tool electrode in water dielectric liquid.

Figure 5. Variation of retained austenite in EDM'ed surfaces.

Studies on ferrous alloys exposed various morphological structures in the sub-surface correlated with the used dielectric liquid and electrode materials. Similar reasoning is also pronounceable for other metallic materials. For example Ti and its alloys, which are used widely in aerospace and biomedical applications, are difficult to machine materials. Therefore, EDM has been applied to manufacture these materials beside traditional techniques.

The surface topography is much more similar to ferrous alloys when Ti-6Al-4V EDM in water dielectric liquid (Figure 7a). However surface cracking is a severe problem even under fine machining conditions. Micro cracks usually stay within the re-solidified structure and indicate a similar crack network pattern as in the ferrous alloys. Machining in hydrocarbon-based dielectric liquid considerably altered the surface topography due to increased amount of molten material (Figure 7b) during machining. The sectional analysis also confirmed the increase in re-solidified layer thickness. The main difference in re-solidified layer composition is the formation of oxides (TiO_2) in water and carbides (TiC) in kerosene dielectric liquid.

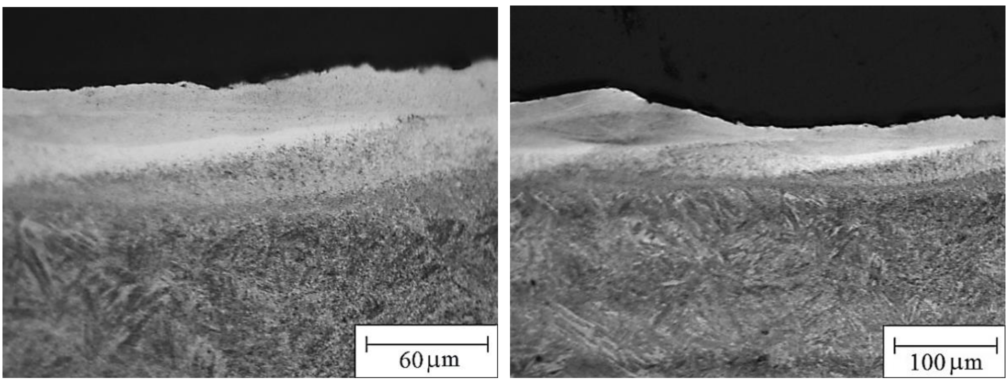

a b

[a]A General view.
[b]A Magnified view.

Figure 6. Section analysis of EDM'ed DIN 1.2738 steel using copper tool electrode in deionized water dielectric liquid (I_{av} = 12A, t_p = 1600 µs).

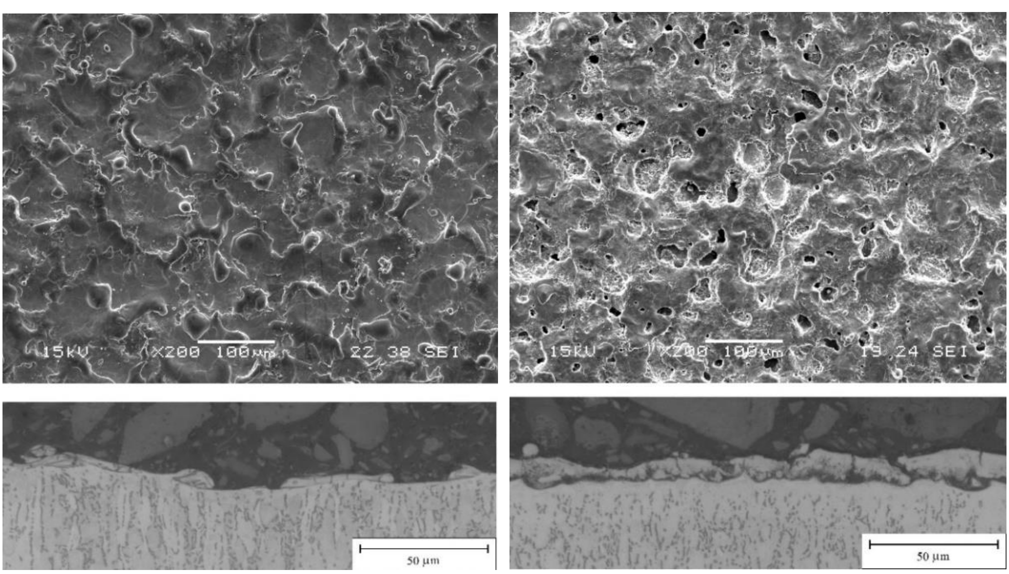

a b

[a]Machining in deionized water dielectric liquid.
[b]Machining in hydrocarbon based dielectric liquid.

Figure 7. EDM'ed Ti-6Al-4V surfaces and its sections (I_{av} = 7A, t_p = 6 µs).

Furthermore, using distilled water as dielectric results in a relatively higher potential for micro cracks development [19]. Electrode material also has an obvious effect on the re-solidified layer composition. Complex carbides such as $Ti_{24}C_{15}$ [20] detected over the surface. Several parameters affect the nature of the EDM. In the light of the previous studies, it can be concluded that surface morphologies, microstructures, mechanical properties such as residual stress distribution, hardness, cracking are all interrelated with the dielectrics and electrode materials.

RESIDUAL STRESSES AND HARDNESS

Residual stresses are a function of materials processing history and continually formed if regions of a material are subject to inhomogeneous plastic deformation. Formation of a renewed state of equilibrium due to strain incompatibilities results in stresses without the action of external loads. The addition of residual stresses on to the existing stress state diverges the conditions for strength if not taken into consideration during the mechanical design stage. The base material around a melted cavity acts as a stiff body while high shrinkage rates progressed during solidification. Additionally, shock waves generated due to the electrical discharges successively impose residual stresses on work material. An EDM surface shaped by randomly distributed overlapping craters over the whole surface. Each discharge leaves an axisymmetric crater including a biaxial stress field in the substrate. Additionally, transverse stresses could not generate on the surface since the primary source is thermal nature. Nearly equal stress fields for each crater result in a biaxial stress state that has equal magnitudes in each direction. Therefore, only one directional measurement of residual stress is acceptable by a realization of the biaxial field.

Low amount of residual stress just over the surface rises rapidly and forms a peak reaching up to material’s tensile strength. The location of the maximum stresses is usually between the heat affected and re-solidified layers. Later, the stresses decrease quickly to the relatively low values of compressive stresses level in the parent material. Different phases present in the re-solidified and heat affected layers mainly does not affect the distribution of residual stress. Measurements using X-Ray diffraction method specified significant amount of residual stresses approaching the fracture strength of the material beneath the machined surface. The intensity of the peak is nearly unrelated to the discharge energy provided during machining [21]. The increase in discharge energy increases the depth of heat affected layers and re-solidified layer thickness. Consequently, the peak residual stress shifts to a deeper location. This result could be associated to surface cracking with an increase in pulse energy. However, machining of dual phase and micro-alloyed steel specimens under similar conditions indicate comparatively low peak stresses in dual-phase steels. This result shows the influence of transformational stresses between different phases generated during re-solidification. Since, the mechanical strength of both materials are approximately same.

Microcracks are essential for a number of examples. The formation of peak residual stresses is usually attributed to the microcrack formation near the surface [13] or the cavities generated in the re-solidified layer [22]. Residual stress relaxed over a period for some instances without altering the pattern. Diffusion of carbon atom around dislocations is the main reason for the relaxation. It is worthy of notice; stress relaxation phenomenon cannot be verified for all machined samples even after several days. Such, unlike behavior could not be explained reasonably, although the trivial microstructural differences. Comparisons of residual stresses on austenitic non-hardenable and martensitic hardenable steels reveal a wider profile for martensitic ones. Moreover, surface stress relaxation is observed even under fine machining conditions for non-hardenable steels [23].

A qualitative relationship with respect to the machining parameters for residual stress is presented for EDM in deionized water using layer removal method [5]. Further, the study is extended using the case of machining in hydrocarbon-based dielectric liquid [24] with a suggestion of a semi-empirical model. The primary output also confirmed the independence of residual stress distribution pattern with respect to the electrical parameters such as pulse duration and current. The only source of pattern disruption appears in the case of surface cracking due to relaxation. Removal of the stressed layers revealed a unit amplitude shape function for the all analyzed samples.

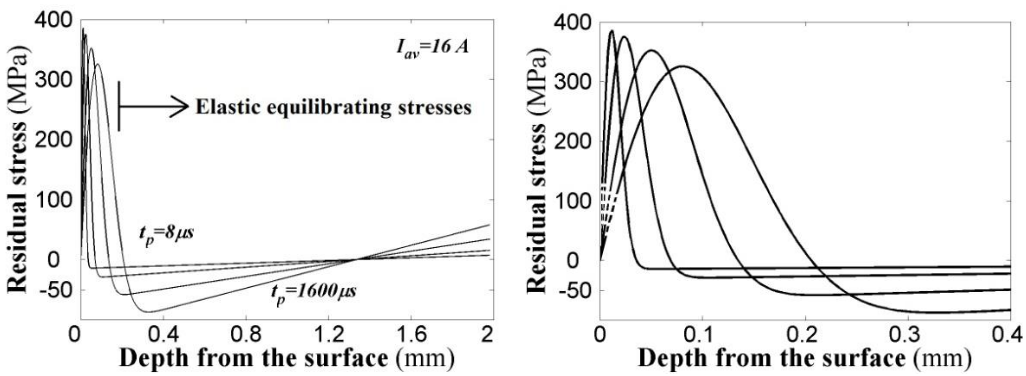

a b

[a]Residual stress distributions in two mm thick samples.
[b]Residual stress distribution in the heat affected layers.

Figure 8. Results of residual stress measurements using layer removal method for plastic mold steel sample EDM'ed using copper tool electrode in deionized water.

Three different coefficients characterize the function that relies on the properties of the materials. Gauss Distribution using two Gaussian peaks defines the unit function, with the same amplitude and pulse width but opposite center location. Interestingly, the amplitude coefficient scaled the unit function over the experimental results and leads a power functional relationship for pulse energy. Moreover, the coefficients are related with the operational conditions e.g., electrode material type. For instance, location of the peak stresses shifted to a deeper position and widened if machining in carbon based dielectric liquid and tool electrode. Two distinct regions as plastically deformed and elastic equilibrating stresses respectively describe the residual stress distribution through a sample (Figure 8a). It also describes how compressive stresses developed in the unaffected portion of the material. A closer look at the residual stress (Figure 8b) also indicates the peak stress variation with respect to electrical parameters. The peak value slowly decreases as the pulse energy increases during machining. The zero stress on the surface is due to the surface topographical features, such as appendages where the stresses are self-equilibrated and loosely connected to the machined surface. Microhardness of the re-solidified layer is usually much more than the bulk material.

Migration of carbon atoms from tool electrode and/or the dielectric liquid or even carbon diffusion from the base leads such an increase. For example, if interstitial free steel is machined using the copper tool electrode in deionized water, micro hardness slightly increases in the re-solidified layer.

However, machining in a hydrocarbon-based dielectric liquid results in a re-solidified layer structure, which is much harder than the base (Figure 9). The re-solidified layer thickness is relatively low, and the peak hardness is slightly high for the hardenable steels when dielectric liquid is water. Moreover, micro hardness deviations in the re-solidified layer are relatively low when compared to samples machined in hydrocarbon-based dielectric liquid.

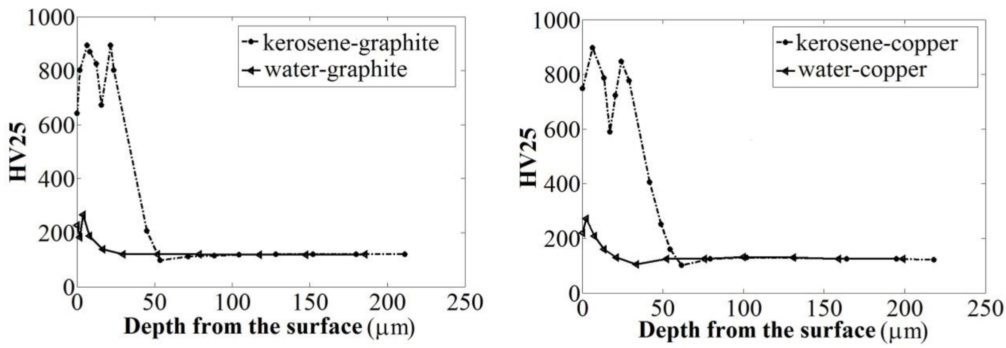

a b

[a]Micro hardness variations when using graphite tool electrode.
[b]Micro hardness variations when using copper tool electrode.

Figure 9. Micro hardness variation of EDM'ed interstitial-free steel samples under different dielectric liquid and tool electrode combinations.

MICRO CRACKS

The re-solidified layer consists of various microscopic metallurgical layers depending on the machining conditions [14, 25-27]. The molten material shrinks more than the unaffected parent material during solidification of a melted cavity. Cracking occurs when stresses go beyond the material's ultimate tensile strength [6, 25, 28]. Former studies [13, 17, 25, 26, 28] revealed that the increase in the pulse energy also increases surface cracking probability. However, pulse energy increase does not always lead cracking. In fact, a severe cracking network appears on the surface when using low pulse currents and high pulse-on durations [9]. High pulse currents primarily lead deeper craters with comparatively thicker re-solidified segments that are the result of molten metal ejection to the rims at the end of a discharge. In this way, induced transformational stresses could be equilibrated in the re-solidified structure during solidification. Increasing pulse-on duration decreases the ejection rate and leads broader and shallow craters. The molten metal at middle section becomes thin and dissipates heat rapidly. Then, the re-solidified layer cools quickly and shrinks faster than the parent material. Moreover, surface cracking probability increases for work materials that have low thermal conductivities [29] and high carbon content [5].

Surface cracks originate from the surface and penetrate down to the re-solidified layer, and most of them are terminated over the heat affected layers in the solid state. However, in some instances cracks may cross over the affected layers and penetrate up to the parent material [5, 30-32]. In addition, there are several instances of miniature cracks usually placed around crater rims and/or on spherical or formlessly shaped add-ons. Such cracks are distributed over the surface unsystematically and have extra low penetration depths. Therefore, cracks could be classified with these three distinctive characteristics [10] as surface, penetrating and miniature. The number of penetrating cracks dramatically increases if machining pre-quenched work material in deionized water. These cracks follow crater rims (Figure 10a) with forming closed loops and, therefore, could be visualized by relatively constant intervals in the sectional analysis. The machined surface exhibits similar closed loop arrangements around the rims when machining in hydrocarbon-based dielectric liquid.

However, there are additional radial cracks on the surface that have relatively low widths of openings (Figure 10b). Cracks forming closed loops penetrate into the underlying material to some extent whereas radial ones stop at the interface among the re-solidified and heat affected layers. The result is the approximate distribution of intervals for penetrating cracks with a number of occasions of non-penetrating ones among them.

Machining in carbon based dielectric and tool electrode heavily influences the re-solidified microstructure and result in diverse metallurgical phases. Cracks inside the re-solidified layer are the indication of excessive stresses development due to the ingredients of carbon causing elevated transformational tensile stresses. On the other hand, penetrating cracks are the consequence of highly localized stresses produced around the rims. Moreover, the existence of re-solidified debris globules inside a penetrating crack (Figure 10a) is the indication of occurrence in early stages of the solidification process.

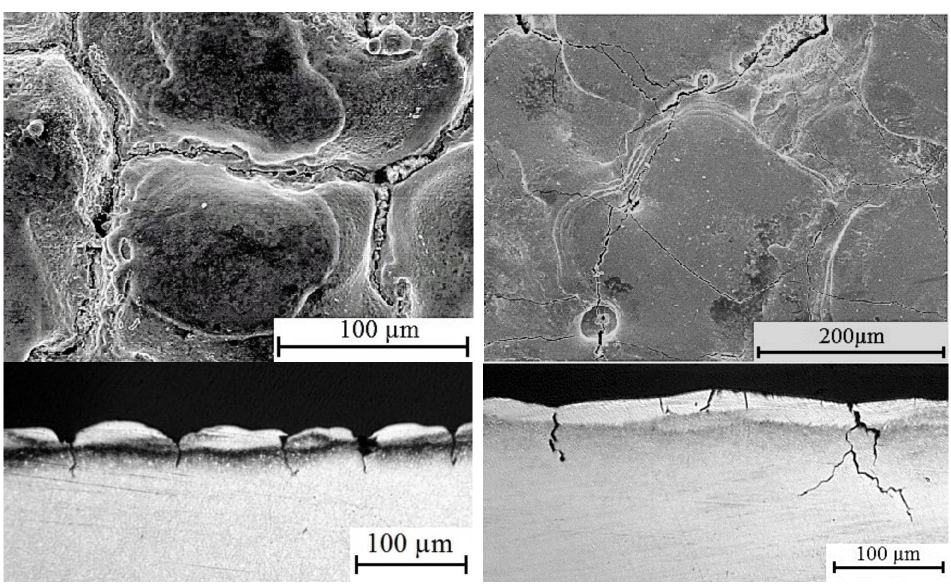

a b

[a]EDM in water dielectric liquid (I_{av} = 6 A, t_p = 100 µs).
[b]EDM in kerosene dielectric liquid (I_{av} = 6 A, t_p = 400 µs).

Figure 10. Surface topography and sections of EDM'ed quenched roll steel samples.

After an electrical discharge, the melted cavity is quenched quickly from the surface. Meanwhile, the parent material acts as a heat sink and cools the cavity in an opposed direction due to conduction. Therefore, the material is in a liquid phase when two solid-liquid interfaces progress respectively. The flow of dielectric liquid makes the temperature gradient at the surface higher than the base. A thin shell appears on the molten cavity and utilizes highly localized stresses around the rim due to shrinkage. Thus, a crack originated from the rims and penetrated through the parent material. Meanwhile, the shell expands and finally integrates with the solidification front growing from the base. Hence, if there are additional produced transformational stresses due to carbon uptake from dielectric liquid or tool electrode, surface cracks develop and remain in the re-solidified structure.

The pathways of penetrating cracks designate relevance with the temperature isotherms and explain the occurrence of parallel cracks encountered in machining of pre-quenched work materials (Figure 11). These cracks track the temperature isotherms of the melted cavity during solidification. Crack tip originated from the rim, tracked the temperature gradient and turned parallel to the work material's surface under the cavity. It also explains the possibility of thermal cracking. Moreover, the crack paths continue to spread into the parent material due to the influences of nearby discharges. In this case, crack tips guided to the opposite side.

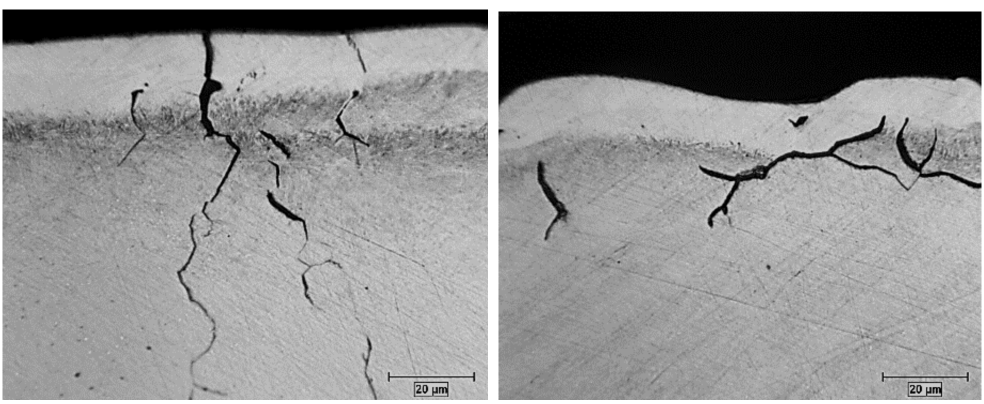

a b

[a]I_{av} = 6 A, t_p = 400µs in kerosene dielectric liquid.
[b]I_{av} = 6, t_p = 25 µs in kerosene dielectric liquid.

Figure 11. Micro-crack paths followed in EDM'ed quenched roll steel sub-surfaces.

MICRO-EDM

Essentially micro-EDM is a consequent adaptation of conventional EDM to produce mainly micro scaled parts. The main difference is the power supply, which generates nanosecond duration pulses. This results in low discharge energies (~µJ) and small craters (~0.05-500 µm^3) on the surface. Therefore, axes accuracy and resolution is improved down to micrometers and equipped with tool fixtures to handle delicate electrodes. Nowadays, such machines also have the opportunity to form a micro tool by the use of a wire dressing unit.

Micro-EDM serves several benefits in micro scale part production. The non-contact nature of machining induces very low forces both on the electrode and the work material. It reduces mechanical stress and vibrations during machining. It is possible to use delicate tool electrodes with diameters down to few micrometers. Thus, micro-EDM provides machining of complicated structures to any conductive material. Such as complicated micro-cavities for micro mold and die manufacturing, drilling micro holes with diameters down to a couple microns, and classical features widely faced in macro production on a micron scale. Producing high aspect ratio micro holes, differences in entry and outlet diameters, surface integrity aspects, shape deformations and possible improvements are considered as primary research propensity in the field. Firstly, a micro hole is drilled approximately in 100 μm with an aspect ratio of 10 in 2 minutes [33]. Then, positive tool polarity is suggested to reduce tool electrode wear and sparking gap to improve the profile geometry [34]. Small amplitude movements of the tool electrode substantially increase the aspect ratio of drilled micro holes up to 18 [35]. Using a micro feeding mechanism increases the aspect ratio to 20 [36]. The entry and outlet diameter difference is reduced approximately to 2 μm for a 150 μm diameter micro hole to a depth of 500 μm [37]. Aspect ratios bigger than 20 is obtained for holes having diameters smaller than 0.1 mm in sheets [38]. Fabrication reverse tapered holes are possible [39] and it is feasible to use magnetic fields to obtain higher aspect ratios [40]. Application of ultrasonic vibrations on a helical micro-tool electrode during machining of a micro-holes significantly decrease the inter-electrode gap distance, taper problem and machining time [41].

Formerly micro-EDM is classified as a non-destructive technique due to lack of time to heat material adequately for short pulses. This way, the basis for material removal is attributed to the electrostatic forces developed during discharging [42]. However, the formation of a heat damaged layer is indispensable due to fast thermal cycles even for a pulse-on durations around 50 ns [43]. Therefore, imperfections such as micro cracks are also essential in micro-EDM applications. Thus, estimation structural morphology and heat damaged layer thickness became an important matter. Application of unconventional etching procedures reveals the microstructure of the re-solidified layer under an optical microscope. An example a drilled blind micro-hole sections (Figure 12) show the re-solidified structure from several regions.

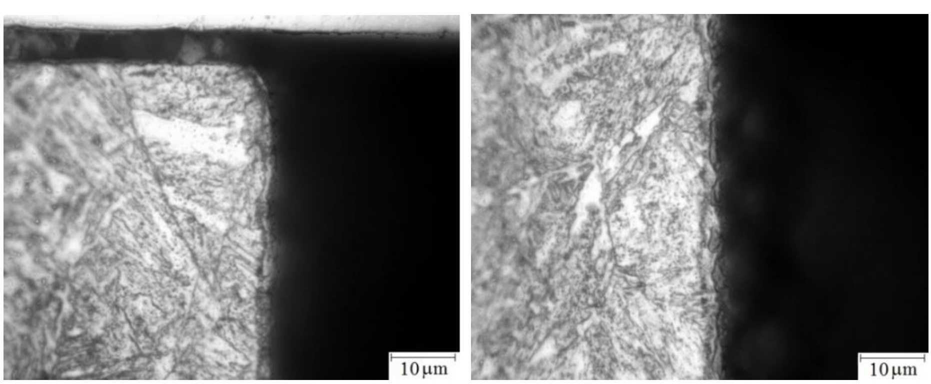

a b

Figure 12. (Continued).

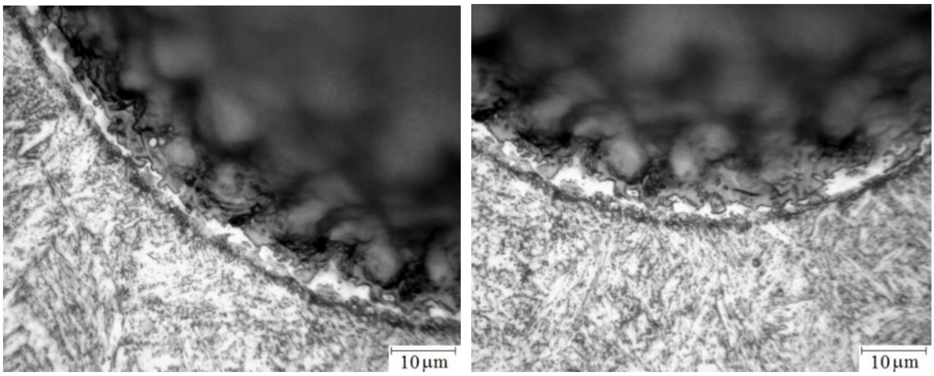

c d

[a]The entrance. [b]The parallel walls. [c]The tip corner. [d]The end tip.

Figure 12. Several sections of a blind micro hole in plastic mold steel drilled using micro-EDM.

The re-solidified structure is reflecting the carbon migration from cracked dielectric liquid. Traces of austenite, martensite, and complex carbides are the indication of process similarity with conventional applications. The main difference is the reduced thicknesses of affected layers. However, the gap distance is so small and produces difficulties in keeping the inter-electrode gap clear especially during high aspect ratio drilling. So, surfaces are affected with respect to drilling depth due to altered dielectric liquid circulation conditions. Thus, comparative analysis of different sections such as parallel walls and tip reveals variation with respect to sublayer thicknesses in the re-solidified layer. The total layer thickness increases as in conventional applications and reflects a power functional dependency with the pulse energy. Moreover, heat affected layer thicknesses are fairly uniformly distributed over the parallel wall sections. However, hole tips indicate piled re-solidified structures with deformed shapes and susceptible to microcrack formation. Careful examinations on re-solidified layer revealed instances of surface cracks particularly at these piled sections and extent over the re-solidified structure (Figure 13). Micro crack generation over the micro-EDM'ed surface is noteworthy and implies a different mechanism for surface cracking.

The tool wear limits the precision of micro-EDM process and is usually visualized at the end tip [44]. Corners receive a higher potential for discharging and wear accelerate at these sections. The gap twirled due to forced vortex, and debris particles follow its streamlines, and the tool electrode expands the inter-electrode distance. A tapered nose forms under adequate flushing conditions at the end tip. Otherwise, debris starts to accumulate at tip section during machining.

Then, the piled particles establish electrical conductivity with the work material. After that, machining experiences among the piled structure and the tool. Finally, the end tip diverges from its usual nose geometry. The successive accumulation of melted particles onto the current layer forms the re-solidified layer. This results in succeeding heat treatments and growth in the layer. Consequently, contraction stress repeatedly develops during solidification and generates stress exceeding material mechanical strength.

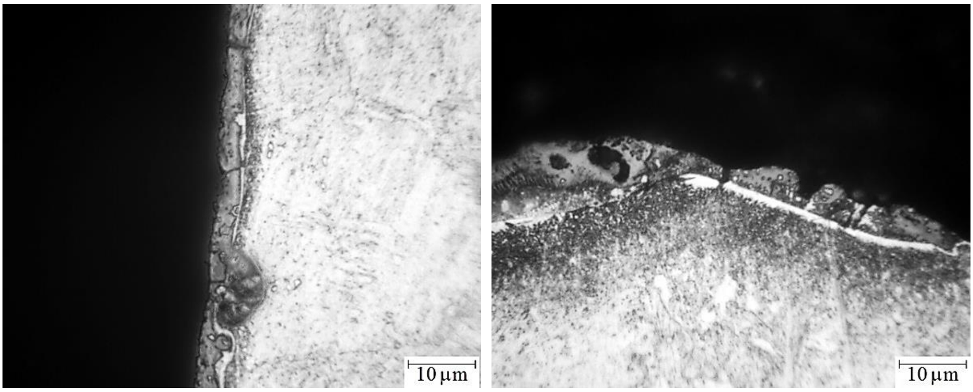

a b

[a]Micro-cracks in the parallel wall section.
[b]Micro-cracks in the end tip.

Figure 13. Micro-cracks in a blind micro-hole section produced during micro EDM.

The main reason of retained austenite is the increase in carbon content in the re-solidified layer and approved the microsegregation from carbon migration. Carbon cumulates in a fine region and allows a thorough stabilization of austenite. Therefore, martensitic zone lays beneath the austenite. The fine features are the consequence of microsegregation under instant non-equilibrium freezing. Deviation of the re-solidified layer thickness is related to pulse energy as in conventional process. The re-solidified structure progressively grows in regard to pulse current and produces a thick molten cavity. High pressures while discharging drives the molten material to the rims and leads deviation in re-solidified layer thickness. However, increasing pulse-on duration leads a thin molten section that allows sufficient time for interactions with hydrocarbon-based dielectric liquid. Therefore, it is not a surprise to encounter with increased thickness of carbon enriched layer.

POWDERS IN DIELECTRIC LIQUID AND SINTERED TOOL ELECTRODES

Metallic powder, as well as carbon powder additive in kerosene dielectric fluid, improves the discharging conditions and the quality of the machined surface. Moreover, the rise in the amount of powder additives in dielectric liquid enhances the machining rate [45]. However, increasing the concentration beyond a limit results in machining instabilities due to short circuits. Fine graphite powder addition in kerosene dielectric liquid decreases the breakdown voltage and increases the gap distance [46]. Silicon powder addition in dielectric liquid gives a corrosion resistant surface [47]. Aluminum and graphite powder additives by using particular pulse current and durations produce improved surface finish [48].

The critical point is the electrical properties of the gap when discharge takes place. Suspended particles increase the probability of electrical discharges due to decreased dielectric liquid strength [49]. The addition of silicon powder in dielectric liquid improves the surface finish of a tool steel [50]. Moreover, the addition of aluminum and silicon carbide powders improve the material removal rate [51]. Similarly both conductive and inorganic oxide additives decreases the tool wear rate and increase the material removal rate [52]. Moreover, silicon powder mixture in kerosene dielectric liquid produces smoother surfaces due to the smaller craters produced on the surface [53]. The mirror finish is also possible by using aluminum powder additives [54]. Aluminum and SiC powders additives in kerosene dielectric liquid improve the dielectric liquid circulation due to increased discharge gap when titanium alloy is used as a work material [55]. Density, size, electrical and thermal conductivity of the additives also influence the situations in discharging. For example, using smaller size powder additives result in an increase in material removal rate and a decrease in the tool wear rate during machining [56]. However, application of low discharge current and pulse-on duration decreases the gap and cause difficulties in the clearance preservation. Therefore, the capacitive effect is detracted, and the ignition is delayed [57]. The observed results on machining efficiency and surface roughness could not be explained by the non-additive case and implied that material mechanism is somehow different from the conventional machining mechanism [58]. One of the major research concern about the subject is surface roughness after EDM. On the purpose of improving surface roughness, several of add-ons included dielectrics are used especially in past decades.

With multiwall carbon nanotubes in dielectric using graphite electrode at least 50% of improvement on surface roughness can be achieved on AISI D2 tool steel in comparison with pure kerosene dielectric [59]. TiC layer is formed on the surface of the work material when using titanium powders in hydrocarbon-based dielectric liquid. The measured hardness of the deposited layer was around 2000 HV [60]. Manganese powder addition in a dielectric liquid increases the microhardness of the work material surface up to 73% without micro-crack formation [61]. Moreover, machining rate is improved by 26.85% with 12 g/l of fine graphite powder mixing in dielectric [62]. Metal matrix composites could also be machined to achieve improved corrosion resistance, wear resistance and surface roughness [63].

The amount of powders in dielectric liquid, mixing characteristic, produced vapor bubbles while discharging, and surface texture disturb the discharge locations in EDM. On the other hand, added powder creates additional breakdown regions in dielectric liquid [64]. Electrophoresis results in movement of added particles in the gap and some circumstances, particles lineup and link the gap for a very short period just before discharging. The quick expansion the plasma channel ruins the particles lineated in the vicinity of a discharge spot. Moreover, vapor bubbles grow and full with dissociated gasses from the dielectric liquid. Therefore, it is right to add the ruining potential of the bubbles just after the discharge period. By the way, most of the chains remain persistent away from this discharge spot and another strike produced at the proximate location after a pause time [65]. Suspended particles placed close the discharge channel expansion boundaries vaporized and even ionized. The ions also collide with both electrode surfaces together with the ions from the tool electrode and dielectric liquid. Such material transfer to the machined surface surely happens at severe temperatures which resulting incomplete decomposition of the material. However, under definite machining conditions, suspended particles nearby the discharge channel start to drift and diffuse on the surface without signs of disintegration (Figure 14). This result indicates the different mechanisms evolved during the process. Dielectric liquid and the suspended particles charge to the melted cavities and sometimes diffuse into the molten pool just before solidification at the end of an electrical discharge. Dielectric liquid and the interactions with the work material affect the resultant surface.

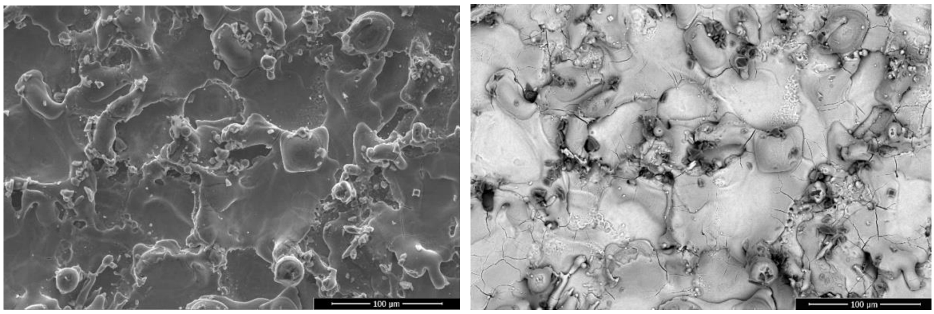

a b

[a]Secondary SEM image. [b]Back scattered SEM image.

Figure 14. Powder mixed EDM'ed surface images of Ti-6Al-4V using 20 g/l SiC powder suspension in water dielectric liquid (I_{av} = 2 A, t_p = 25 µs).

For example, carbon uptake from dielectric liquid activates boiling, and such boiling will dislocate particles directed to the melted cavity just before solidification [5]. Another positive impact of suspended particles during machining is the absence of penetrating micro cracks.

Therefore, the way that how the particles prevent cracking during discharging is also an important concern. The mechanical action of the particles plays a dominant role as well as changing discharge conditions. The melted cavity cools quickly from the surface as a result of convection and from the bottom material as a result of conduction and bump by fine particles. Thus, if the particles have enough energy to distort the continuity of the formed shell on the melted cavity, localized stresses cannot develop on the rims. Then, the shell thickness increases and finally combines with the substrate. If the products of tool electrode, dielectric liquid and added powders infiltrate the re-solidified layer while discharging, microcracks within the re-solidified layer develop due to high transformational stresses. Thus, it is not a surprise to come up with a cracked surface when using high pulse-on durations and low pulse current during machining in powder mixed EDM.

In EDM process, electrode wear and deformation problem are primarily considered in terms of total cost of operation. High melting temperature, good electrical and heat conductivity are desirable for the tool electrode. That is why there are several types of the electrode that made of different material such as graphite, copper and copper alloys and fabricated using conventional machining methods.

Besides conventional machining methods, various techniques are available to fabricate the electrodes in complex geometries with reduced cost. The powder metallurgy process frequently comes across in the literature for tool electrode alternatives. In this technique, the powders are first mixed then compressed under pressure and sintered at different temperatures. A porous specimen could be obtained using high temperatures than is machined to the required shape or soldered as tips.

Several configurations sintered ZrB_2, TiSi with Cu tested as tool electrodes in terms of machinability in EDM [66]. Although, TiSi is well bonded with the Cu matrix without porosity or significant defects, it is not recommended as an EDM tool electrode because of high wear rates. Low sintering temperatures result in poor bonding, and hence thermal stress leads spalling during machining.

Reduction in porosity in selective laser sintering decreases the electrode wear and increases the material removal rate [67]. Copper with 15% titanium carbide (TiC) sintered electrodes provides reduced wear and improves removal rates considerably [68]. Fast, simple, low-cost electrode fabrication is possible by blending copper powders contained resin with chromium powders at low pressure (20 MPa) and temperature (200°C) in a hot mounting machine. Cr is distributed uniformly in the Cu matrix and migrated to work material surface during EDM. So, machined surface corrosion resistance increases [69]. Laser sintered tool electrodes provide the preferable surface finish. Such electrodes consist of steel powder as base material, polyester as a binder, and the phosphate as a strengthener [70]. Titanium carbide electrode tips lead thinner re-solidified layer structure on work material surface when compared to sintered copper electrode tips in ultrasonic assisted cryogenically cooled EDM [71]. Using a multi-layer electrode composed of titanium (Ti) and graphite (Gr) with the same dimensions results in the formation of a TiC layer and reduces micro-crack formation on nickel work material surface [72].

DISCUSSION

The re-solidified layer is the top-most and heavily interacted layer with dielectric liquid and the tool electrode in EDM. The influences on the surface properties dominated the resultant quality by means of its microstructure and deterioration. Complicated mechanisms evolved in the processes supply the elements of the tool electrode and dielectric liquid to the surface. The typical result is a harder re-solidified structure over the heat affected layers. Excessive temperature gradients lead residual stresses and consequent cracking which is the primary negative output of the process.

From this respect increasing the quality of the surface by a proper mixture of the operational parameters to suppress such adverse effects will be continuing core trend for researchers in EDM. There is a significant endeavor to recognize the phenomena to explore the relationship between surface quality and machining parameters.

However, there are still particular occasions that are not apparently identified in the literature. Therefore, the interfaces of electrical discharge, electrode surfaces, and dielectric liquid will continue as a primary research interest in the near feature.

The possibility of surface alloying by the process is an important concern. Therefore, powder additives in dielectric liquid with a variety of material combinations gather a substantial interest. The powder particles produce several breakdown regions in dielectric liquid and hence creating higher discharge probabilities. Moreover, decrease in dielectric strength [49] and interactions with the suspended particles alter the resultant surface quality [73]. The subject suggests the viability of the process to produce functional surfaces. An alternative way for surface alloying might be the use of composite electrodes and has possible extensions for further research. Hybridization of the process gives the opportunity to handle extraordinary materials with appropriate quality and machining rate. Examples include the arrangements of EDM with laser and ultrasonic machining [74-77]. Such combinations probably lead exclusive surface features. However, the knowledge is about the elemental stage, and further research is foreseeable in the area.

The surface of micro-EDM parts are similar, but features are in reduced sizes when compared with the conventional EDM [43]. Therefore, it is natural to express the similarity of the mechanisms evolved in the micro-EDM process. Deformations and also interactions with the dielectric liquid go through the stages that are similar to conventional EDM applications. High surface qualities with tight tolerances are predictable with application nanosecond duration pulses during drilling a micro hole. However, resultant tip geometry deploys from the classical shape indicating debris particles plays an important role [78]. Similar results presented in the literature, and the reason usually attributed to the stochastic nature of the process. Application of pulse durations in the order of nanoseconds results in fine debris particles. The tool electrode rotation generates a forced vortex at the micro-hole tip. Debris particles piled under the action of the fluid vortex and create proper electrical conductivity with the work material. Then, form a gradual cone at the tip where electrical conductivity occurs between the work material and the cone build by debris particles. This result in stable machining conditions between the cone and the rotating tool electrode. As a result, debris particles function as a work material and a fraction of debris go through the discharge processes again. The tool electrode is machined in the complementary shape of the piled debris geometry.

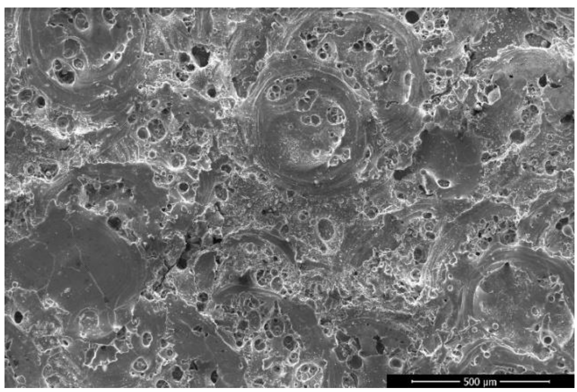

a

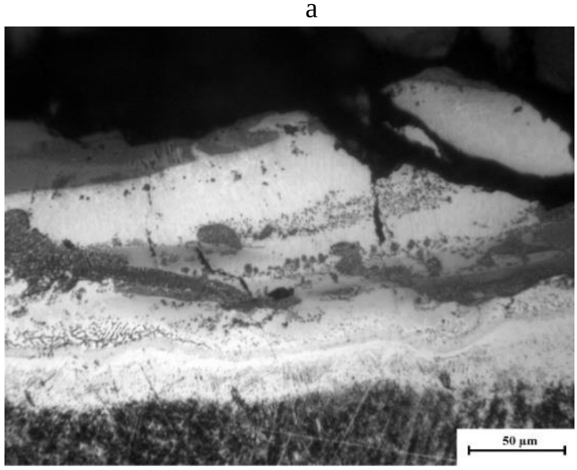

b

[a]The subdivisions of discharge channels, I_{av} = 2 A, t_p = 100 µs, 5 g/l SiC powder in water.
[b]Re-solidified and heat affected layers, I_{av} = 42 A, t_p = 100 µs, 20 g/l SiC powder in water.

Figure 15. The resultant effects of secondary discharges in SiC powder mixed EDM of Ti-6Al-4V surfaces.

Adding powders in dielectric liquid and controlling the fluid flow at the inter-electrode gap indicate the possibility of tools made of particles. Generating a controlled electromagnetic field in a magnetically dielectric fluid might be the plausible choice for the further improvement of the process. For example, properly feed particles over the tool electrode under controlled electromagnetic field can prevent the tool wear.

Electrical discharges exhibit different constructions under the action of suspended particles in a dielectric liquid. Single cylindrical heat source model cannot describe most of the surfaces textures generated by powder suspended EDM [79]. The main discharge channel is separated into a number of secondary discharges since suspended particles in the gap increased the number of breakdown zones. Therefore, additional material transfer mechanisms are generated during powder mixed EDM and dominated the resultant surface properties. Discharge channel heats the particles nearby. Then, the particles flush back and finally diffuse into the melted cavity. The interesting result is the fastness of the collision process under definite operational conditions that lead penetrated particles on work material surface.

This result yields the significance of a suspended particle around a discharge channel and designating a high dependency with the amount of powders in dielectric liquid. Low powder concentrations lead surfaces with plenty of pocks on the surface. It is an indication of main discharge channel subdivisions into secondary discharges due to suspended powders (Figure 15). The increase in breakdown zones boosts the number of sub-discharges and the probability of particles being nearest to a discharge boundary. Such a mechanism implies a controlled means of deliberate alloying [73].

CONCLUSION

The resultant surface quality and the interrelation with the materials maintain as a vital matter and need further understanding of the process. Many novel technologies such as powder additives in dielectric liquid and use of sintered tool electrodes hold a brilliant potential particularly concerning deliberate alloying and functionalization of the surfaces in a straightforward manner. Despite the noteworthy developments, some of the principle aspects are still under clouds and understanding the machining mechanism in detail will remain the key factor to discover the complicated interrelationship of different process parameters for further developments.

ACKNOWLEDGMENTS

The authors acknowledge the sincere thanks to The Bülent Ecevit University Research Program for the grants given on the subject, which otherwise the work would not be initiated.

REFERENCES

[1] McGeough, J. A., Rasmussen, H., (1982). A macroscopic model of electro-discharge machining. *Int. J. Mach. Tool Des. Res*. 22(4), 333-339.

[2] Lloyd, H. K., Warren, R. H., (1965). Metallurgy of spark-machined surfaces. *J. Iron and Steel Ins*. 203, 238-247.

[3] Radhakrishnan, V., Achyutha, B. T., (1980). Study of the surface formed in EDM using relocation technique. *IE (I) Journal-ME*. 60, 217-222.

[4] Wong, Y. S., Rahman, M., Lim, H. S., Han, H., Ravi, N., (2003). Investigation of micro-EDM material removal characteristics using single RC-pulse discharges. *J. Mater. Process. Technol.* 140, 303-307.

[5] Ekmekci, B., Elkoca, O., Erden, A., (2005). A comparative study on the surface integrity of plastic mold steel due to electric discharge machining. *Metall. Mater. Trans. B* 36, 117-124.

[6] Thomson, P. H., (1989). Surface damage in electrodischarge machining. *J. Mater. Sci. Technol*. 5, 1153-1157.

[7] Abu Zeid, O. A., (1997). On the effect of electrodischarge machining parameters on the fatigue life of AISI D6 tool steel. *J. Mater. Process. Technol*. 68, 27-32.

[8] Lee, H. T., Rehbach, W. P., Tai, T. Y., Hsu, F. C., (2004). Relationship between electrode size and surface cracking in the EDM machining process. *J. Mater. Sci.* 39, 6981-6986.

[9] Lee, H. T., Tai, T. Y., (2003). Relationship between EDM parameters and surface crack formation. *J. Mater. Process. Technol.* 142, 676-683.

[10] Ekmekci, B., (2009). White layer composition, heat treatment, and crack formation in electric discharge machining process. *Metall. Mater. Trans. B* 40, 70-81.

[11] Crookall, J. R., Khor, B. C., (1974). Electro-discharge machined surfaces. *Proceedings of 15th International Machine Tool Design and Research Conference, Macmillan*. 331-338.

[12] Massarelli, L., Marchionni, M., (1977). Morphology of spark-affected surface layers produced on pure iron and steels by electro discharge machining. *Metal. Technol*. 4, 100-105.

[13] Rebelo, J. C., Diaz, A. M., Kremer, D., Lebrun, J. L., (1998). Influence of pulse energy on the surface integrity of martensitic steels. *J. Mater. Process. Technol*. 84, 90-96.

[14] Lim, L. C., Lee, L. C., Wong, Y. S., Lu, H. H., (1991). Solidification microstructure of electrodischarge machined surfaces of tool steels. *J. Mater. Sci. Technol*. 7, 239-248.

[15] Ekmekci, B., Ekmekci, N., (2012). Assessment of heat affected zones with a finite element model in electrical discharge machining. *The 15th International Conference on Machine Design and Production* June 19-22, Pamukkale, Denizli, Turkey.

[16] Bucklow, I. A., Cole, M., (1969). Spark Machining. *Met. Rev*. 3, 103-118.

[17] Lee, L. C., Lim, L. C., Narayanan, V., Venkatesh, V. C., (1988). Quantification of surface damage of tool steels after EDM. *Int. J. Mach. Tool. Manu.* 28, 359-372.

[18] Ekmekci, B., (2007). Residual stresses and white layer in electric discharge machining (EDM). *Appl. Surf. Sci*. 253, 9234-9240.

[19] Chen, S. L., Yan, B. H., Huang, F. Y., (1999). Influence of kerosene and distilled water as dielectrics on the electric discharge machining characteristics of Ti–6A1–4V. *J. Mater. Process. Technol.* 87(1-3), 107-111.

[20] Çaydaş, U., Hasçalık, A., (2007). Electrical discharge machining of titanium alloy (Ti–6Al–4V). *Appl. Surf. Sci.* 253(22), 9007-9016.

[21] Mamalis, A. G., Vosniakos, N. M., Vacevanidis, N. M., Junzhe, X., (1988). Residual stress distribution and structural phenomena of high-strength steel surfaces due to EDM and ball-drop forming. *CIRP Ann. Manuf. Technol.* 7, no. 1, 531-535.

[22] Kruth, J. P., Bleys, P., (2000). Measuring residual stress caused by wire EDM of tool steel. *Int. J. Electl. Mach*. 5, No. 1, 23-28.

[23] Ghanem, F., Braham C., Sidhom, H., (2003). Influence of steel type on electrical discharge machined surface integrity. *J. Mater. Process. Technol*. 142, 163-173.

[24] Ekmekci, B., Tekkaya, A. E., Erden, A., (2006). A semi-empirical approach for residual stresses in electric discharge machining (EDM). *Int. J. Mach. Tool. Manu.* 46, 858-868.

[25] Lee, L. C., Lim, L. C., Wong, Y. S., Lu, H. H., (1990). Towards a better understanding of the surface features of electro-discharge machined tool steels. *J. Mater. Process. Technol*. 24, 513-523.

[26] Lim, L. C., Lee, L. C., Wong, Y. S., (1992). Towards crack minimization of EDMed surfaces. *J. Mater. Process. Technol*. 32, 45-54.

[27] Huang, C. A., Tu, G. C., Yao, H. T., Kuo, H. H., (2004). Characteristic of the rough-cut surface of quenched and tempered martensitic stainless steel using wire electrical discharge machining. *Metall. Mater. Trans. A* 35, 1352-1357.

[28] Mamalis, A. G., Voaniakos, G. C., Vaxevanidis, N. M., (1987). Macroscopic and microscopic phenomena of electro-discharge machined steel surfaces: an experimental investigation. *J. Mech. Work. Tech.* 15, 335-356.

[29] Lee, L. C., Lim, L. C., Wong, Y. S., Fong, H. S., (1992). Crack susceptibility of electro-discharge machined surfaces. *J. Mater. Process. Technol*. 29, 213-221.

[30] Lin, Y. C., Hwang, L. R., Cheng, C. H., Su, P. L., (2008). Effects of electrical discharge energy on machining performance and bending strength of cemented tungsten carbides. *J. Mater. Process. Technol.* 206, 491-499.

[31] Guu, Y. H., Ti-Kuang Hou, M., (2007). Effect of machining parameters on surface textures in EDM of Fe-Mn-Al alloy. *Mater. Sci. Eng. A*. 466, 61-67.

[32] Bhattacharyya, B., Gangopadhyay, S., Sarkar, B. R., (2007). Modelling and analysis of EDMED job surface integrity. *J. Mater. Process. Technol.* 189, 169-177.

[33] Masuzawa, T., Tsukamota, J., Fujino, M., (1989). Drilling of Deep Microholes by EDM. *CIRP Ann. Manuf. Technol*. 38, 195-198.

[34] Her, M. G., Weng, F. T., (2001). Micro-hole machining of copper using the electro-discharge machining process with a tungsten carbide electrode compared with a copper electrode. *Int. J. Adv. Manuf. Tech.* 17, 715-719.

[35] Yu, Z. Y., Rajurkar, K. P., Shen, H., (2002). High aspect ratio and complex shaped blind micro holes by micro EDM. *CIRP Ann. Manuf. Technol*. 51, 359-362.

[36] Li, Y., Guo, M., Zhou, Z., Hu, M., (2002). Micro electro discharge machine with an inchworm type of micro feed mechanism. *Precis. Eng*. 26, 7-14.

[37] Yan, B. H., Wang, A. C., Huang, C. Y., Huang, F. Y., (2002) Study of precision micro-holes in borosilicate glass using micro EDM combined with micro ultrasonic vibration machining. *Int. J. Mach. Tool. Manu*. 42, 1105-1112.

[38] Kaminski, P. C., Capuano, M. N., (2003) Micro hole machining by conventional penetration electrical discharge machine. *Int. J. Mach. Tool. Manu*. 43, 1143-1149.

[39] Diver, C., Atkinson, J., Helml, H. J., Li, L., (2004) Micro-EDM drilling of tapered holes for industrial applications. *J. Mater. Process. Technol.* 149, 296-303.

[40] Yeo, S. H., Murali, M., Cheah, H. T., (2004). Magnetic field assisted micro electro-discharge machining. *J. Micromech. Microeng*. 14, 1526-1529.

[41] Hung, J. C., Lin, J. K., Yan, B. H., Liu, H. S., Ho, P. H., (2006) Using a helical micro-tool in micro EDM combined with ultrasonic vibration for micro-hole machining. *J. Micromech. Microeng*. 16, 2705-2713.

[42] Sing, A., Ghosh, A., (1999). A termo-electric model of material removal during electric discharge machining. *Int. J. Mach. Tool. Manu*. 39, 669-682.

[43] Ekmekci, B., Sayar, A., Öpöz, T. T., Erden, A., (2009), Geometry and surface damage in micro electrical discharge machining of micro-holes. *J. Micromech. Microeng*. Number 10, 19.

[44] Öpoz, T. T., Ekmekci, B., Erden, A., (2009). An experimental study on the geometry of microholes in microelectric discharge machining. *Mater. Manuf. Process*. 24, 1236-1241.

[45] Erden, A., Bilgin, S., (1980). Role of impurities in electric discharge machining. *Proceedings of 21th International Machine Tool Design and Research Conference*, Macmillan, London, 345-350.

[46] Jeswani, M. L., (1981). Effects of the addition of graphite powder to kerosene used as the dielectric fluid in electrical discharge machining, *Wear*. 70, 133-139.

[47] Mohri, N., Saito, N., Higashi, M. A., (1991). A new process of finish machining on free surface by EDM methods. *CIRP Ann. Manuf. Technol*. 40, 207-210.

[48] Narumiya, H., Mohri, N., Saito, N., Otake, H., Tsnekawa, Y., Takawashi, T., Kobayashi, K., (1989). EDM by powder suspended working fluid. *Proceedings of 9th International Symposium for Electromachining*, Nagoya. 5-8.

[49] Schumacher, B. M., (1990). About the role of debris in the gap during electrical discharge machining. *CIRP Ann. Manuf. Technol*. 39, 197-199.

[50] Kobayashi, K., Magara, T., Ozaki, Y., Yatomi, T., (1992). The present and future developments of electrical discharge machining. *Proceedings of Second International Conference on Die and Mould Technology*, Singapore. 35-47.

[51] Yan, B. H., Chen, S. L., (1994). Characteristics of SKD11 by complex process of electric discharge machining using liquid suspended with aluminum powder. *Journal of Japan Institute of Metals*. 58, 1067-1072.

[52] Ming, Q. Y., He, L. Y., (1995). Powder-suspension dielectric fluid for EDM. *J. Mater. Process. Technol*. 52, 44-54.

[53] Uno, Y., Okada, A., (1997). Surface generation mechanism in electrical discharge machining with silicon powder mixed fluid. *Int. J. Electl. Mach*. 2, 13-18.

[54] Wong, Y. S., Lim, L. C., Rahuman, I., Tee, W. M., (1998). Near-mirror-finish phenomenon in EDM using powder-mixed dielectric. *J. Mater. Process. Technol*. 79, 30-40.

[55] Chow, H. M., Yan, B. H., Huang, F. Y., Hung, J. C., (2000). Study of added powder in kerosene for the micro-slit machining of titanium alloy using electro-discharge machining. *J. Mater. Process. Technol.* 101, 95-103.

[56] Tzeng, Y. F., Lee, C. Y., (2001). Effects of powder characteristics on electro discharge machining efficiency. *Int. J. Adv. Manuf. Tech*. 17, 586-592.

[57] Pecas, P., Henriques, E. A., (2003). Influence of silicon powder mixed dielectric on conventional electrical discharge machining. *Int. J. Mach. Tool. Manu*. 43, 1465-1471.

[58] Zhao, W. S., Meng, Q. G., Wang, Z. L., (2002). The application of research on powder mixed EDM in rough machining. *J. Mater. Process. Technol*. 129, 30-33.

[59] Prabhu, S., Vinayagam, B. K., (2009). Effect of graphite electrode material on EDM of AISI D2 tool steel with multiwall carbon nanotube using regression analysis. *International Journal of Engineering Studies* 1 (2), 93-104.

[60] Furutani, K., Saito, H., Suzuki, M., (2009). Influence of electrical conditions on performance of electrical discharge machining with powder suspended in working oil for titanium carbide deposition process. *Int. J. Adv. Manuf. Tech*. 40(11-12), 1093-1101.

[61] Kumar, S., Singh, R., (2010). Investigating surface properties of OHNS die steel after electrical discharge machining with manganese powder mixed in the dielectric. *Int. J. Adv. Manuf. Tech.* 50, 625-633.

[62] Kumar, A., Maheshwari, S., Sharma, C., Beri, N., (2010). Realizing potential of graphite powder in enhancing machining rate in AEDM of nickel based super alloy 718. *Proc. Int. Conf. Advances in Mechanical Engineering*. 50-53.

[63] Hu, F. Q., Cao, F. Y., Song, B. Y., Hou, P. J., Zhang, Y., Chen, K., Wei, J. Q., (2013). Surface properties of SiCp/Al composite by powder-mixed EDM. *Procedia CIRP*. 6, 101-106.

[64] Luo, Y. F., (1997). The dependence of interspace discharge transitivity upon the gap debris in precision electro-discharge machining. *J. Mater. Process. Technol*. 68, 121-131.

[65] Kunieda, M., Yanatori, K., (1997). Study on debris movement in EDM gap. *Int. J. Electl. Mach*. 2, 43-49.

[66] Zaw, H. M., Fuh, J. Y. H., Nee, A. Y. C., Lu, L., (1999). Formation of a new EDM electrode material using sintering techniques. *J. Mater. Process. Technol*. 89-90, 182-186.

[67] Dürr, H., Pilz, R., Eleser, N. S., (1999). Rapid tooling of EDM electrodes by means of selective laser sintering. *Computers in Industry* 39, 35-45.

[68] Li, L., Wong, Y. S., Fuh, J. Y. H., Lu, L., (2001). EDM performance of TiC copper-based sintered electrodes. *Mater. Des*. 22, 669-678.

[69] Tsai, H. C., Yan, B. H., Huang, F. Y., (2003). EDM performance of Cr/Cu-based composite electrodes. *Int. J. Mach. Tool. Manu.* 43, 245-252.

[70] Zhao, J., Li, Y., Zhang, J., Yu, C., Zhang, Y., (2003). Analysis of the wear characteristics of an EDM electrode made by selective laser sintering. *J. Mater. Process. Technol*. 138, 475-478.

[71] Srivastava, V., Pandey, P. M., (2013). Study of ultrasonic assisted cryogenically cooled EDM process using sintered (Cu–TiC) tooltip. *J. Manuf. Process*. 15, 158-166.

[72] Hwang, Y. L., Kuo, C. L., Hwang, S. F., (2010). The coating of TiC layer on the surface of nickel by electric discharge coating (EDC) with a multi-layer electrode. *J. Mater. Process. Technol*. 210, 642-652.

[73] Ekmekci, B., Ulusöz, F., Ekmekci, N., Yaşar, H., (2015). Suspended SiC particle deposition on plastic mold steel surfaces in powder-mixed electrical discharge machining. *Proc. Inst. Mech. Eng., B J. Eng. Manuf.* 229(3), 475-486.
[74] Kremer, D., Lhiaubet, C., Moisan, A., (1991). A Study of the effect of synchronizing ultrasonic vibrations with pulses in EDM. *CIRP Ann. Manuf. Technol*. 40, 211-214.
[75] Yan, B. H., Chen, S. L., (1994). Effect of ultrasonic vibration on electrical discharge machining characteristics of Ti–6Al–4V alloy. *Journal of Japan Institute of Light Metals*. 44, 281-285.
[76] Jia, Z. X., Zhang, J. H., Ai, X., (1997). Study on a new kind of combined machining technology of ultrasonic machining and electrical discharge machining. *Int. J. Mach. Tool. Manu*. 27(2), 193-197.
[77] Aspinwall, D. K., Dewes, R. C., Burrows, J. M., Paul, M. A., (2001). Hybrid high speed machining (HSM): system design and experimental results for grinding/HSM and EDM/HSM. *CIRP Ann. Manuf. Technol*. 50(1), 145-148.
[78] Ekmekci, B., Sayar, A., (2013). Debris and consequences in micro electric discharge machining of micro-holes. *Int. J. Mach. Tool. Manu*. 65, 58-67.
[79] Rehbein, W., Schulze, H. P., Mecke, K., Wollenberg, G., Storr, M., (2004). Influence of selected groups of additives on breakdown in EDM sinking. *J. Mater. Process. Technol*. 149, 58-64.

In: Electrical Discharge Machining (EDM)
Editor: M. P. Jahan
ISBN: 978-1-63483-591-6

Chapter 5

ULTRASONICALLY AIDED ELECTRICAL DISCHARGE MACHINING

Daniel Ghiculescu*
Polytehnic University of Bucharest, Bucharest, Romania

ABSTRACT

This chapter deals with a hybrid machining process called electrical discharge machining aided by ultrasonics, i.e., vibration with ultrasonic frequency of tool-electrodes or workpieces simultaneously with electrical discharge machine finishing and micro-machining. Specific phenomenology is described, and as a result, optimization conditions of working parameters aimed at machined surface roughness, minimization of volumetric relative wear (precision maximization), and maximization of machining rate are presented. Experimental data are also presented and connected with finite element method modeling of the material removal mechanism. Some innovative solutions regarding the equipment are depicted, which are used as ultrasonically aided micro-electrical discharge machining, based on granted patents.

Keywords: Ultrasonic vibration, electrical discharge machining, finishing, micro-machining

INTRODUCTION

The hybrid processes approached in the frame of this chapter, i.e., ultrasonically aided electrical discharge machining, are highly developed concentrated energy (nonconventional) machining. It benefits from the advances of both processes, which are combined and lead to synergy, as detailed below. The actual major trend of ultra-miniaturization led to the development of micro-technologies generating surfaces with dimensions in the range of 1-999 μm, and nano-technologies creating surfaces with dimensions ranging from 1-999 nm [1]. Generally, the precision of non-conventional technologies is placed at 1 nm order of

* Corresponding Author: Daniel Ghiculescu, Email: daniel.ghiculescu@upb.ro

magnitude when machining by chemical-mechanical polishing (CMP) and laser polishing [2], and surface roughness, Ra at 0.1 nm, i.e., angstrom (Å) order of magnitude, in case of electrochemical machining (ECM), CMP and laser polishing [2, 3, 4, 5, 6]. Nonetheless, the productivity, which is generally a drawback of nonconventional machining, is at the same level as the conventional one, e. g. ECM against milling, 10^5 mm^3/min [3].

In this background, the micro-electrical discharge machining (μEDM) and its finishing variant encounter frequent degenerations of the removal process due to a very narrow working gap (several μm) affecting the machining rate, volumetric relative wear/precision and surface quality. In these cases, the machining rate is of 0.1 mm^3/min of magnitude, volumetric relative wear is 15 – 40%, and the machined surface roughness, Ra = 0.05-0.2 μm. Ultrasonic aiding (μEDM+US) can lead to spectacular improvement of all the above-mentioned parameters, if some optimization conditions are fulfilled.

Specific Phenomenology of Electrical Discharge Machining Aided by Ultrasonics

The ultrasonics aiding, i.e., longitudinal vibrations of electrode-tool, normal on the machined surface with ultrasonic frequency of finishing electrical discharge machining (EDM+US) aims to eliminate the specific instability of the process and increases its performances of precision, surface quality and machining rate.

Under normal conditions, EDM finishing occurs in a very narrow working gap (μm order of magnitude), which determines frequent short-circuits and difficult evacuation of removed particles, affecting volumetric relative wear and implicit precision of the machined surface. Controlled cavitational phenomena, ultrasonically induced within the gap, could solve these problems and improve the related technological performances mentioned above [7, 8, 9, 10]. Starting from the analysis of phenomena strongly related to volumetric relative wear, some technological solutions are described in order to improve machining precision [11].

Working Parameters Influencing Electrode Wear

Precision of machined surface is directly related to electrode wear and also to one of the main EDM output parameters, volumetric relative wear (ϑ), defined by:

$$\vartheta = V_e / V_p \ [\%], \tag{1}$$

where: V_e is volume eroded from the electrode during machining [mm^3]; V_p - volume removed from workpiece during machining [mm^3].

In EDM processes, current density within the plasma channel (J) produced by discharge determines the anode/cathode ratio and consequently, the volumetric relative wear (ϑ), according to F. Van Dijck and R. Snoeys's model [12].

Power dissipated on cathode surface P_c can be determined with the relation:

$$P_c=(i_{c+})(U_c+U_{i+}-\Phi_{i+}) - (i_{c-})\Phi_e \ [W], \tag{2}$$

where: i_{c+} is ionic current [A]; i_{c-} – electronic current [A]; U_c – potential fall at cathode [V]; U_{i+} – ionization potential of positive ions [V]; Φ_{i+} , Φ_e – extracting tension corresponding respectively to cathode metal and electronic emission [V]; $(i_{c-})\Phi$ factor contributing to cathode cooling due to electronic emission [W].

Power dissipated at anode (P_a) can be determined from the following relation:

$$P_a = P_{tot} - P_c - P_{col} \text{ [W]}, \quad (3)$$

where: P_{tot} is power corresponding to a discharge, respectively:

$$P_{tot} = W_e / t_i \text{ [W]}, \quad (4)$$

where: W_e is discharge energy [J]; P_{col} – power dissipated in plasma channel, estimated lower than 1% from P_{tot} [12] ; t_i – pulse time [s].

A qualitative synthesis of working parameters influencing anode/cathode distribution power is presented in Figure 1. At short discharge times, the plasma channel does not have sufficient time to develop and thus, discharge energy is reported on the small transversal section of the plasma channel, resulting in high current density. In this case, the electronic current (i_{c-}) is dominant due to its lower extraction tension (Φ), and therefore a growing currents ratio (i_{c-} /i_{c+}) is produced. In relation (2), the factor $(i_{c-})\Phi$ has high values, ionic current (i_{c+}) is low and thus, taking into account relations (2, 3), the anode/cathode power ratio (P_a/P_c) grows.

This is an important aspect, and the polarity effect must be analyzed. As the finishing mode is characterized by low pulse time, it is advantageous to work with negative polarity (the tool is the cathode), resulting in low density J within the plasma channel. Moreover, relaxation pulses, usually used in this case, can attain a superior quality of surface due to the crater shape, which is flatter than in cases of commanded pulses [10].

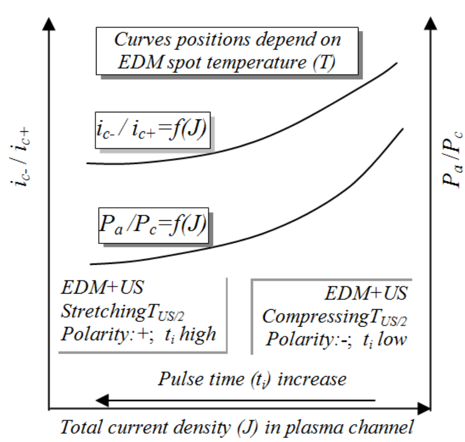

Figure 1. Qualitative variation of working parameters influencing electrode wear [11].

When commanded pulses are used, having greater pulse durations, the plasma channel has time to develop, decreasing the density J. Ratio (P_a/P_c) becomes low, positive polarity is advantageous, taking into account tool wear and implicit precision. These phenomena are involved in the EDM+US process, as it will be further detailed.

Flushing pressure (p_{fl}) is another parameter related to wear ϑ. High flushing pressure determines easier evacuation of gas bubbles from the working gap and thus, inertia forces of the dielectric liquid with high purity degrees restrict development of the plasma channel, producing high J density. When working with positive polarity, the P_a/P_c ratio increases and implicitly, great ϑ values are recorded.

The pause time (t_o) also influences ϑ. For small values of t_o, inertia forces of dielectric liquid are low due to its pollution and plasma channel extents, thus density J is decreased with consequences to related working parameters, mentioned above. But at a too small t_o, the EDM finishing process could degenerate in continuous arcs due to the very narrow gap, specific to finishing modes [13].

In addition, the importance of tool material characteristics must be mentioned; electrode material has lower wear during the EDM process than workpiece material, being proportional with the C_{PZ} coefficient - Palatnik and Zingermann's criterion involving its thermo-physical characteristic [10].

Phenomena Influencing Electrode Wear during Discharge

The pressure in the gas bubble, developed around the plasma channel produced by discharge, limits the transversal section of the plasma channel, influencing density (J) inside it.

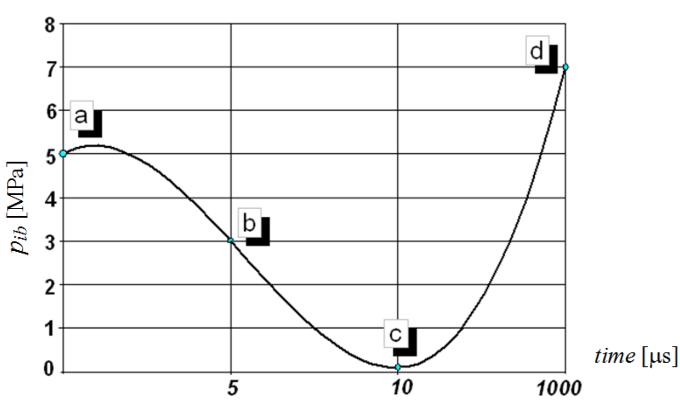

Figure 2. Pressure variation within the gas bubble for a pulse time of 10 µs, EDM finishing [11].

As shown in Figure 2, gas bubble dynamics comprise four stages:

a) *initial stage* is characterized by very high pressure (p_{ib}) in the gas bubble due to great inertial forces of dielectric liquid, which are opposed to bubble development;
b) *development stage* - pressure p_{ib} lowers gradually because of bubble volume growing;
c) *intermediate stage* – sudden fall of inner pressure p_{ib} due to the pulse end;

d) *final stage* of bubble implosion – great increase of inner pressure p_{ib} as a result of adiabatic gas compression and distended gas elastic.

In Figure 2, p_{ib} values for a particular case are presented. Other researchers such as D. Kremer, C. Lhiaubet [8], I. Anton [14], and K. Isuzugawa [15], reported relatively close values corresponding to these development stages of the gas bubble.

These four stages lead to corresponding phases of volumetric relative wear dynamics, considering the polarity effect.

The analysis below corresponds to working with tool *positive polarity*:

1) in this phase, corresponding to stage (a) the great values in the gas bubble determine high values of density J in the plasma channel. Therefore the anode-cathode ratio (P_a/P_c) has great values and thus the electrode wear grows.
2) in this phase, matching stage (b), the density J is lower due to p_{ib} inner pressure decrease; thus the P_a/P_c ratio has low values and consequently, electrode wear is lowered.
3) (c) sudden fall of p_{ib} at the final pulse determines a quick boiling, mainly in workpiece material - the main mechanism of removal process at EDM [12] – and low volumetric relative wear because material couple was selected taking into account Palatnik and Zingermann's criterion.
4) (d) at classic EDM, the probability of removing material through the bubble implosion is very low because this moment is very far in time from the pulse end, unlike at EDM+US, when bubble implosion occurs at each end of the oscillation period. The hydraulic forces cannot remove a great volume of material because it is already solidified at this moment. Cavitational phenomena due to bubble implosion can remove material, and relative wear ϑ, difficulty quantified, is assessed as high.

The analysis of working with tool *negative polarity* highlights:

1) in the first phase (a), because of p_{ib} high values, current density J is high, P_a/P_c ratio grows, determining low tool wear.
2) in the bubble development phase (b), inner pressure p_{ib} gets low values as well as density (J); due to P_a/P_c ratio diminishing, electrode wear increases. The analysis of phases (3') and (4') does not emphasize the polarity effect, the observations from above being correct for negative polarity too.

To conclude, positive polarity produces low wear electrode, when bubble development is sufficient (phase b) and negative polarity determines low wear at short pulse times (phase a). The analysis of gaseous and hydrodynamics phenomena are in agreement with the Van Dijck - Snoeys model, experimentally confirmed [13].

If the results from classic EDM phenomena analysis are transferred to the specific mechanism of ultrasonically aided EDM, the solution of the pulse generator, synchronized with the time intervals when current density is high or low, becomes very effective in reducing relative wear ϑ.

Carbon Layer Depositing

Carbon depositing, as a surface layer on an electrode-tool when using dielectric liquid consisting of hydrocarbons with a high content of carbon, is a known phenomenon. Taking into account a very high melting point of this deposited material, it is necessary to analyze this phenomenon in connection to tool wear.

Mohri et al. revealed an interesting occurrence, studying on-line the wear of frontal plate zones of electrodes [16]. The total wear on this region is lower at the beginning of machining and increases gradually up to a value that depends on machining and material conditions.

At the start, the plate region wear becomes negative as a result of carbon deposits on this area, determined by cracking reactions of dielectric liquid with hydrocarbon content during EDM because it is about $10{,}000^{o}$ C around the plasma channel.

Experimentally, at finishing/superfinishing modes with low machining time of 10-15 min., we noticed very low volumetric wear ϑ, even negative [13].

After these first phenomena, the depositing process begins to balance the EDM material removal process. On electrode edges, the wear dynamics is explained by the fact that carbon deposits are not apparent as long as their radii are very small. The depositing process occurs as machining progresses and the edges become more round.

Moreover, at carbon steel machining, carbon adheres very well on the electrode surface in some cases and in other cases, it is very easily removable. X-ray analysis suggests that in the first case, the carbon layer is turbolayered, i.e., laminated layers of bidimensional carbon crystals with random phase. At machining of steels with high carbon content, the adhering process is considered to be the result of carbon precipitation, similar to the graphite precipitation phenomenon at steel cast.

The carbon layer depth is proportional with equivalent carbon content from workpiece material and hence with electrode wear. But when machining materials with relative high content of Ni or Cr, the electrode wear is very low even if their carbon content is reduced. It is considered that elements like Ni, Cr, Fe have a catalyzing role in carbon precipitation [17].

We also consider a strict connection between temperatures during the EDM process and carbon depositing. In different phases of the EDM+US process, we emphasize some phenomena that sustains carbon deposition and consequently reduces electrode wear, a hypothesis in agreement with our experimental results.

On this basis, technological solutions are elaborated to increase dimensional precision.

Phenomena at Ultrasonically Aided Electrical Discharge Machining Influencing Electrode-Tool Wear

An oscillation period T_{US} at EDM aided by longitudinal vibrations (normal on machined surface) of the electrode-tool comprises two semiperiods with distinctive cavitational phenomena influencing electrode wear, synthesized in Figure 3.

The graph values are calculated with relations (5) and (6), experimentally confirmed [13].

In the first semiperiod lasting from 0 to 25 μs (at used frequency of 20 kHz), the *compression* of dielectric liquid from the frontal working gap is produced, with capillary phenomena occurring.

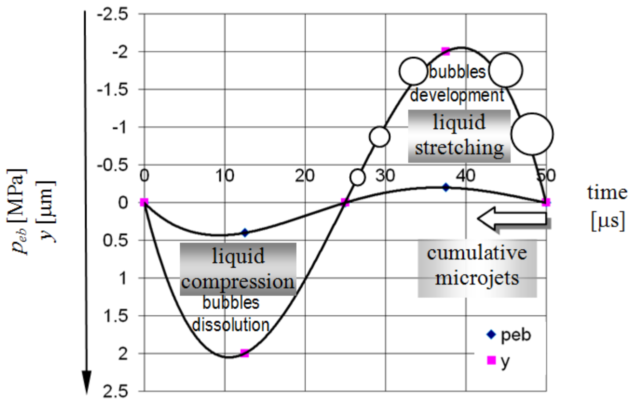

Figure 3. Cavitational phenomena ultrasonically induced at EDM+US [11, 20].

Thus, gas bubbles resulting from previous electrical discharges are dissolved when elongation y is positive, due to acoustic pressure (p_{ac}) created within the frontal gap, determined with relation [7]:

$$p_{ac} = 2\pi \cdot f_{US} \cdot A \cdot \rho \cdot c_s \text{ [Pa]}, \tag{5}$$

where: f_{US} is the ultrasonic oscillations frequency on normal direction [Hz]; ρ - dielectric liquid density [kg/m^3]; A – ultrasonic oscillation amplitude [m]; c_s – sound velocity in dielectric liquid [m/s].

To produce cavitation, p_{ac} must be greater than the cavitation threshold that depends on existent conditions [13]. In our experimental research, cavitation was obtained using f_{US} = 20 kHz, A=1…2 μm in dielectric liquid with density ρ=840 kg/m^3.

During compression, inertial forces of dielectric hydraulic are great and they restrict development of plasma channel. Hence, discharges occurring within the first semi-period are characterized through great current density (J) in the plasma channel. When working with *positive polarity*, density J determines high electrode wear.

However, the volumetric relative wear defined with relation (1) can be maintained in suitable limits even in this semi-period. The solution could be machining with *negative polarity*. In this case, high values of density J within the plasma channel determine low values of electrode wear because cathode power P_c is reduced.

The second semi-period, lasting from 25 to 50 μs at 20 KHz frequencies, produces *stretching* of dielectric liquid from the frontal working gap, explained by relation (6). Total hydrostatic pressure (p_{ht}) is equal with pressure from the gas bubble exterior (p_{eb}), surrounding the plasma channel and determined by:

$$p_{eb} = p_{ac} \sin \omega t + p_h \text{[MPa]}, \tag{6}$$

where: $\omega=2\pi f_{US}$ [s^{-1}]; p_h is local hydrostatic pressure [MPa], considered 0.1 MPa.

Thus, dielectric pressure from the working gap becomes negative and the volume of gas bubbles resulting from a previous electrical discharge grows to a value corresponding to high dielectric pressure at the end of an oscillation period. At this moment, *cumulative microjets* are produced, resulting from implosion of gas bubbles from a working gap. This phase is characterized by pressures of 100 MPa order of magnitude, much higher than those from phase (d) at classic EDM, producing low values of relative wear ϑ due to great material volume removed by additional ultrasonic aid.

During the stretching semiperiod, discharges could be produced mainly in predominant gaseous medium due to gas bubble development (Figure 3). In these conditions, current density within the plasma channel is very low, decreasing electrode wear when working with positive polarity.

Implosion of gas bubbles in cumulative microjets phase produces a temperature of around 10,000 C. These secondary phenomena intensify cracking reactions in dielectric liquid, increasing carbon deposits on tool surfaces and consequently, a decrease of tool wear [10].

Luminescent phenomena also takes place during the second semi-period, according to K. Negiski [14]. When gas bubble walls are still close (at around 1/5 from developing time), electric discharges occur between opposite walls, locally ionizing the working medium and contributing to carbon deposits on surface tools by liquid cracking reactions.

Comparison between Gas Bubble Life Duration at Classic and Ultrasonic Aided Electrical Discharge Machine Finishing

The plasma channel formed during discharge between the surfaces of tool and workpiece at EDM, with temperatures at approximately 10,000^{o}C, determines the vaporization of dielectric liquid from the working gap and of electrode-tool and workpiece materials involved in the electrical discharge machining (EDM) process. Consequently, it creates a gas bubble around the plasma channel.

At the first view, this is a secondary phenomenon, but it governs the access of hydraulic forces of dielectric liquid from the working gap to material melted by discharge. Many models of EDM like [12], much later confirmed by Schulze's et al. research, based on high speed framing camera [18, 19] proved that the life duration of gas bubbles forming around the plasma channel lasts much longer than the pulse time, which leads to lower efficiency of the EDM process.

Ultrasonic aiding of EDM finishing limits life duration of gas bubbles to an ultrasonic oscillation period, which is usually 25 and 50 µs usually at frequency of 40 and 20 kHz, respectively, of longitudinal vibrations of electrode tool. This is the result of cavitational phenomena ultrasonically induced within the working gap, which, in case of EDM finishing/micro-machining, is less than 10 µm [20].

A basic model is the Van Dijck's one [21], which in the case of 1 A discharge current and 10 µs pulse time predicts that bubble life duration is around 180 µs. The validation of models attempting to evaluate the life duration is a difficult problem under conditions where these phenomena occur at micrometric dimensions within the working gap. Amazing progress was achieved using a high speed framing camera (HSFC) with 10^5 and 10^6 frames/s, beginning in the 1980s. Kremer et al. [8] and many other researchers used this camera type. A special arrangement must be made in order to visualize the bubble evolution during discharge, i.e., the electrode must be pointed, or have reduced dimensions (µm order of frontal part).

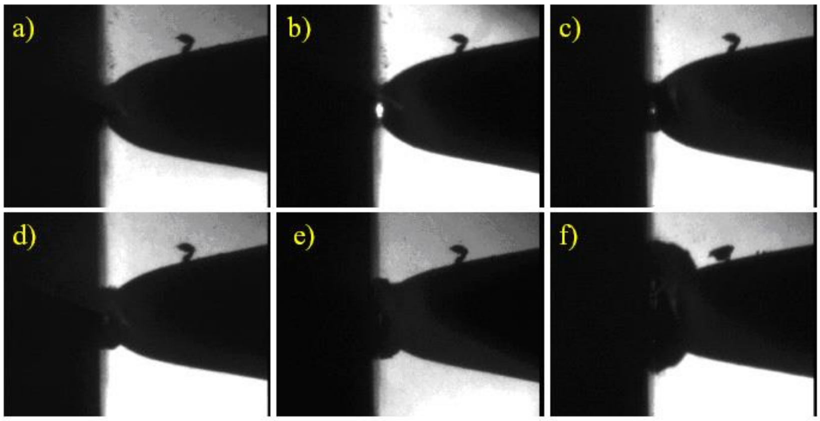

Figure 4. Images of gas bubble formed at EDM with following parameters: maximum current 25 A, pulse time 6 μs, working gap 15 μm, hydrocarbon dielectric liquid [18].

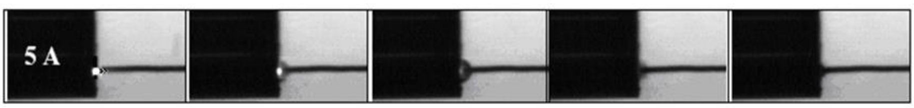

Figure 5. Images of gas bubbles formed at EDM finishing with following parameters: pulse time 10 μs, working gap 15 μm, hydrocarbon dielectric liquid [18].

At EDM finishing and micro-machining, at around 1A discharge currents, HFSC determined that the gas bubble is much bigger than the plasma channel and EDM spots, in the order of 0.1 mm [18]. In Figure 1.4, a gas bubble evolution is presented with the following stages: (a) pre-ignition; (b) dielectric medium breakdown (discharge); (c) evolution during discharge; (d) evolution after 3 μs; (e) evolution after 6 μs; (f) evolution after 120 μs.

One can notice that the gas bubble provided by a single discharge is still in the working gap even after 120 μs from the dielectric medium breakdown, i.e., it lasts 20 times more than the pulse time. After the bubble collapse, no material removal is achieved because it is already solidified; only a clearing of the working gap is completed.

The real relative dimensions of the gas bubble could be evaluated in Figure 1.5, where comparative evolutions of the gas bubble are presented. End values of interest regarding the current are 5 A. The gas bubble increases after the pulse end and reaches a radius of around 0.6 mm.

In real processes comprising successive discharges, the life duration of the gas bubble formed around the plasma channel could be shortened by the following electrical discharge due to the pressure created by the new plasma channel development. The phenomenon of successive discharge placements in relatively close spaces was reported by several researchers, using specialized equipment to locate discharges, like Kojima et al. [22], Ydreskog [23], and Fuzhu et al. [24].

The sucession of discharges, due to the decreased dielectric capacity of working medium, has the capacity to remove a great amount of material from the same zone, and stops only after the corresponding frontal gap grows to a value that determines the growth of electrical resistance, due to the higher value of s_F. The following discharges move to another zone, under the criterion of minimum frontal gap (s_F), the cycle of successive discharges being resumed. This phenomenon is also explained by the proximity where the next discharge occurs, which is determined by high conductivity of the working medium, resulting in an ionization state generated by the previous discharge.

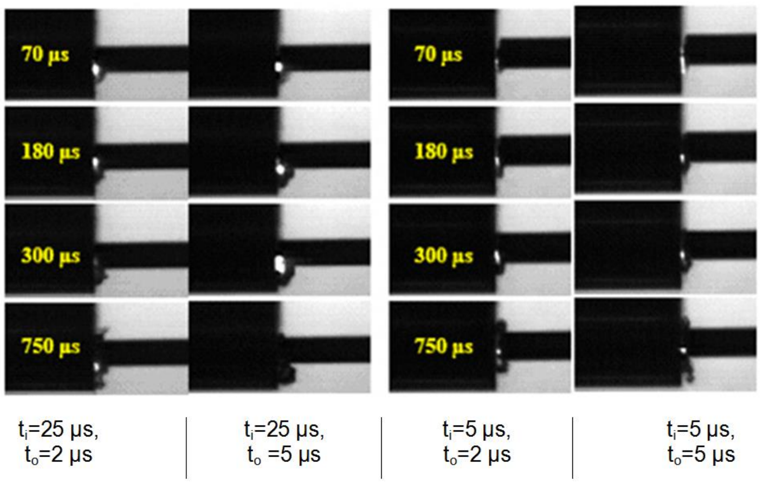

Figure 6. Images of gas bubbles resulted at EDM with different pulse time (t_i) and pause time (t_o), current I=5A, frontal gap s_F=10 µm [19].

The working dielectric liquid capacity cannot be restored if the pause time is not sufficient [20]. As one can see in Figure 6, after the pause time (t_o) ranged between 2 and 5 µs, the gas bubble formed when working with parameters corresponding to finishing still exist in the working gap, even after 750 µs.

The shortened life of the gas bubble is strongly dependent on ignition delay time (t_d); its dependence from other process parameters can be described as:

$$t_d \sim \frac{s_F^{\ 3}}{\kappa \cdot u_0^{\ 2}} \tag{7}$$

where: κ is electrical conductivity of working liquid; u_o - ignition voltage, generally, a constant of EDM generator.

In the analyzing relation (7), it can be noticed that delay time is very sensitive to κ. In case of finishing, this could be expressed in relative long t_d, more than 100 µs as our experimental data pointed out, due to low electrical conductivity. This is the result of low energy discharge, specific to finishing and micro-machining. So, in this case, at classic EDM, the life time of gas bubbles could last a long time after the pulse end, since the next discharge can destroy the gas bubble formed by the previous discharge, and consequently a great amount of material could already be solidified by the time that hydraulic forces could access the EDM spot [20].

At EDM+US, the bubble evolution is described by Figure 3, where one can notice that capillary phenomena are produced in two semiperiods: liquid compression (bubble dissolution in dielectric liquid) and liquid stretching (bubble development) until cumulative microjets stage occurs. At each final oscillation period, which lasts 50 µs when working with 20 kHz ultrasonic frequency, a collective implosion of bubbles from the gap is produced due to the increase of pressure from the exterior of bubble p_{eb}.

Beside gas bubbles created around the plasma channel, specific to the EDM process, previously described, there are gas bubbles developed from numerous cavitational nuclei (in the order of millions) existing in the gap. Both types of bubbles are the subject of cavitational phenomena during the stretching semi-period. Consequently, huge pressure, of 100 MPa order is developed, and shock waves parallel to the machined surface, leading to roughness, is decreased by removing micro-peaks with low shear resistance.

The implosion time τ located at the end of each oscillation period is calculated with relation [14]:

$$\tau = R_m \sqrt{\frac{3\rho}{2p_h}} \int_{\beta}^{1} \frac{\beta^{\frac{3}{2}}}{(1-\beta)[\beta^2 + (\beta+1)\dfrac{1+3\sigma}{p_h R_m}]} d\beta \qquad \text{[s]}, \tag{8}$$

where: $\beta = R_f/R_m$; R_m and R_f are maximal radius before contraction and final radius after contraction [m]; σ – superficial tension [N/m], p_h - local hydrostatic pressure [Pa].

In the specific case of total shut-down of gas bubble (β=0), Rayleigh provided the relation for calculation of implosion time τ [14]:

$$\tau = 0.915 R_m \sqrt{\frac{\rho}{p_h}} \quad \text{[s]}. \tag{9}$$

When using usual dielectric liquid oil, with a density of 840 kg/m^3, when working with a maximum finishing gap of 0.01 mm and local pressure p_h of 0.1 MPa, the bubble implosion time was determined as τ =0.84 µs. In this time interval, besides huge pressure, a high temperature of around 10,000^{o}C is developed. Thus, each bubble implosion has an equivalent effect of an EDM finishing discharge, which can be considered as an added material removal mechanism.

The pressure decrease within the working gap in stretching the semiperiod also contributes to the melting and boiling point, decreasing the machined material. Cumulating the effects of thermal mechanism of classic EDM and ultrasonic cavitational phenomena, the technological performances were significantly improved. Experimental data will point this out below.

The plasma channel development is stopped by the huge pressures deployed during the cumulative microjets stage (see Figure 3). This phenomenon could affect tool wear and implicit machining when working with positive polarity due to the polarity effect; in this case, the current density inside the plasma channel is very high.

Theoretically, the dynamics of bubble gas implosion is explained by adiabatic compression and then elastic relaxation of gas from the bubble located within compression, which determined cavitational erosion. This complex phenomenon occurs through two mechanisms [14]: a) shock waves; b) microjets.

In different cases, one of both mechanisms is apparent, but their effects are cumulative. Under specific conditions of ultrasonically-aided electrodischarge micro-machining (µEDM+US), the ultrasonically induced cavitational phenomena present particularities because they occur between two solid walls, i.e., frontal surfaces of electrode-tool and machined workpiece. Moreover, the distance between these two walls (the working frontal gap, s_F), have low values comparable to gas bubble dimensions. For this reason, the results could not be extrapolations of other phenomena produced under totally different conditions like: a single wall, two walls placed at great distance from one another, etc.

Shima et al. experimentally determined the pressures created after discharges between an electrode and a solid surface separated by distance L; They concluded that pressure values depend on ration L/R_m. Deshkunov and Kuvshinov reached the same conclusion concerning the implosion speed of gas bubbles and microjets orientation. If the distance L is great, then the microjets are perpendicular on the walls. On the contrary, if the ratio $L/2R_m=1$, then the interface liquid-vapors have maximum speed on a plane parallel to the solid walls. The bubbles are divided and microjets occur with a speed of 10,000 m/s order. After a great deal of experiments were carried ou5 by different researchers concerning the pressure and speed generated by cavitation, the results had a large variation depending on real conditions under which the experiments took place. After implosion, the pressure travels concomitantly with the compression wave, having sound velocity in the respective medium and decreasing in inverse proportion with the distance [14].

Generally, the pressures produced by gas bubble implosion under conditions close to EDM+US micro-machining/finishing, had values greater than 10 MPa with speeds larger than 80m/s. The corresponding stagnation pressures were in 10 MPa order lasting around 1 µs.

Optimization of Working Parameters

An increase of dimensional precision by volumetric relative wear (ϑ) was decreased up to 50% [13], based on optimization conditions concerning technological input parameters. These conditions resulting from previously presented analyses are:

1) Minimization of flushing pressure and pause time t_o still avoiding degeneration of the EDM process; t_o is strongly related to maximization of discharge number within an oscillation period [10];
2) Short time pulses must be used when working with negative polarity and relaxation pulses, advantageous in EDM finishing by producing flat craters, i.e., low roughness (R_a); in order to not damage the crater margins that are very sensitive to cavitational shock waves. The power supply of the ultrasonic chain must be 30% lower than that used for commanded pulses, which produces deeper craters [10].
3) When using positive polarity, long commanded pulses must be utilized; they must be located within stretching semi-period; on the contrary, when negative polarity is used, short commanded pulses must be used inside the compressing semi-period;
4) The carbon depositing layer is favored by long time pulses and intensification of cavitational effect through increasing power supply of acoustic chain (P_{cUS}); this is in contradiction with condition (2); therefore an optimum must be found experimentally, depending on real working conditions; P_{cUS}=70W was appropriate in

our experimental research when using relaxation pulses, and 100W for commanded pulses [10];

5) Machining high carbon steels alloyed with Ni, Cr facilitates tool protection by carbon depositing; this is the case of high hardness steels machined by EDM.

Conclusions Concerning Phenomenology and Technological Solutions

The study of complex specific phenomenology of EDM+US material removal mechanisms determined technological solutions, aiming at improving the main output parameters of the finishing process: precision / volumetric relative wear, surface quality / machined surface roughness, and machining rate. All these mentioned parameters are deficient at classic EDM finishing due to very difficult machining conditions resulted from the narrow working gap, less than 10 µm, generating frequent degeneration of the process. The analysis of cavitational phenomena ultrasonically induced in the working gap explains possibilities (solutions) to reduce machining instability, to ameliorate evacuation of removed particles from the sinuous working gap resulted at the complex surfaces generation to protect the tool, thus reducing its wear and therefore precision, to improve machined surface quality by reducing its roughness and resolidified material layer (white layer), significantly augmenting the machining rate by the effect of ultrasonic removal, assuring take-away of melted material by discharge. Decreasing volumetric relative wear (ϑ) can be achieved by a dedicated pulse generator and computer control of deformations through the Finite Element Method (FEM) – Figure 7. The Computer Integrated Machining (CIM) system achieves simulation of machining under process stability, and then components of the technological system can be optimized in the CAD/CAE phase, and finally machined with maximum precision by CNC machines. This system is capable of reducing known EDM+US technology and lack of flexibility derived from needed resonance conditions – equality between frequencies of ultrasonic transducer and horn.

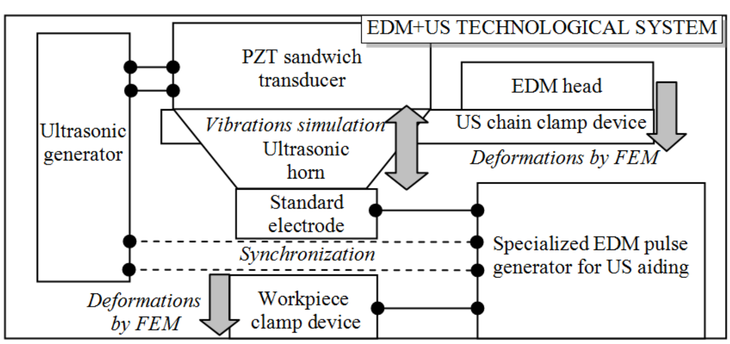

Figure 7. Architecture of CIM system for EDM+US [11].

The analysis of the removal mechanism at EDM+US emphasizes some technological solutions in order to increase the precision of machined surfaces through relative electrode wear. The main solutions could be:

- Decreasing the power supply of the acoustic chain, with the ultrasonic pressure situated over the cavitation threshold;
- Synchronization of commanded pulses with tool oscillation semiperiods;
- Working as much as possible with frontal flat surfaces of standard electrodes and 3D CNC for generating complex surfaces.

Using speed frame cameras, the duration of gas bubbles formed around the plasma channel at micro-machining and finishing EDM was determined. The results confirmed early theoretical classic models such as Van Dick's, which highlighted that bubble life-time is much longer than pulse time.

At classic EDM, by the time of the bubble collapse, the hydraulic forces could not remove the workpiece material melted by discharge because it is already solidified, leading to poor efficiency of the process.

At ultrasonic aided EDM, the gas bubbles from the working gap collapse after each stretching semi-period, e.g., 25 μs when working with 20 kHz ultrasonic frequency, contributing to spectacular growth of the machining rate. The experimental data proved that high pressure of the cumulative microjets stage can even stop the discharge, and hydraulic forces of dielectric liquid can remove the melted material. Therefore, the attempt to synchronize the pulses with the stretching semi-period could be very useful in terms of machining rate, and volumetric relative wear.

Experimental Data at Electrical Discharge Machining Aided by Ultrasonics

Some of the most significant experimental data obtained by research relates to the development of electrical discharge machining aided by ultrasonics, with working modes of finishing and micro-machining; these are presented below.

Analysis of Technological Performances

The main (output) technological parameters that were statistically studied, and characterize the electrical discharge process, are: *machining rate* (V_W), representing the removed volume in time unit, *volumetric relative wear* (ϑ), representing the ratio of worn volume of tools and removed volume from the workpiece, and *machined surface roughness* (R_a).

Relations used for calculation of parameters V_W and ϑ are [25]:

$$V_W = v_p / t_{mach} \text{ [mm}^3\text{/min]}, \tag{10}$$

where: v_p is removed volume from the workpiece [mm^3]; t_{mach} - machining time [min].

$$\vartheta = 100 \, (v_e / v_p) [\%], \tag{11}$$

where: v_e is worn volume of electrode-tool [mm^3].

The removed volume from the workpiece and the worn volume of the electrode-tool are determined with relations:

$$vp = 1000 (mip - mfp) / \rho p[mm3], \tag{12}$$

where: m_{ip} is the initial mass of the workpiece to be machined [g]; m_{fp} - final mass of the machined workpiece [g]; ρ_p - density of the workpiece material [g/cm^3].

$$v_e = 1000 (m_{ie} - m_{fe}) / \rho_e [mm^3], \tag{13}$$

where: m_{ie} is the initial mass of the electrode [g]; m_{fe} - final mass of the electrode [g];

ρ_e - density of electrode material [g/cm^3].

The values of the above-mentioned masses were determined by weight using an analytical balance with superior limits of 80g and precision of 10^{-4}g.

Roughness (Ra) of the frontal and lateral machined surfaces were determined by measuring using a Taylor-Hobson surface instrument, and it is the result of crater depths generated by discharges during the EDM material removal process.

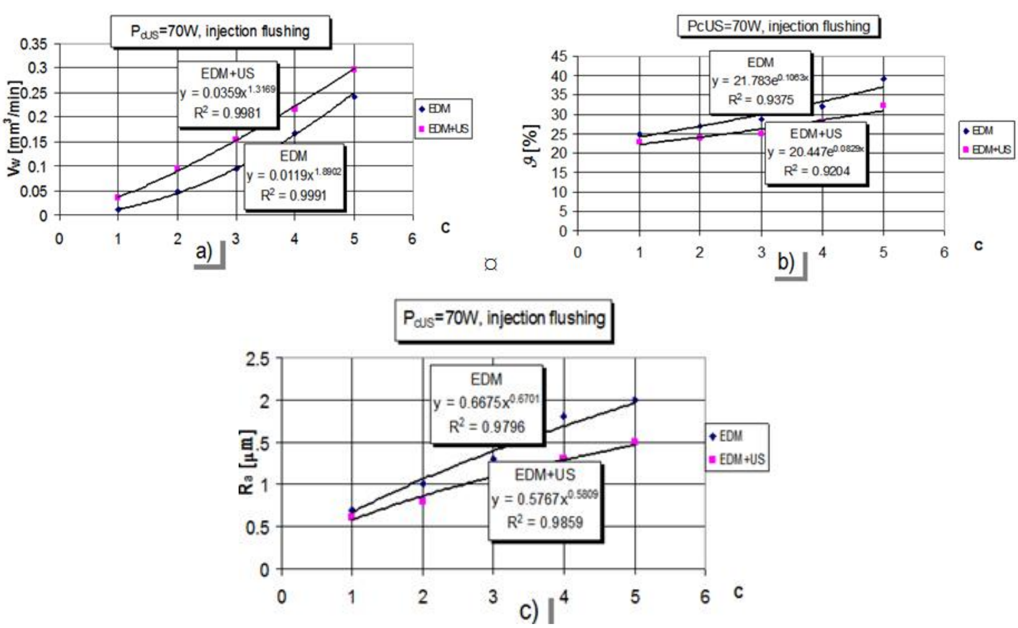

Figure 8. Output technological parameters at EDM and EDM+US finishing with relaxation pulses, 30 mm electrode diameter [26]. a) machining rate (V_W) vs. capacity steps (C). b) volumetric relative wear (ϑ) vs. capacity steps (C). c) surface roughness (Ra) vs. capacity steps (C).

Comparative EDM and EDM+US finishing tests with different current steps (I), pulse (t_i), and pause times (t_o), in case of commanded pulses, and capacity steps and supply currents for relaxation pulses were carried out mainly on ELER 01 machines from the Nonconventional Technologies Laboratory of the Faculty of Engineering and Management of Technological Systems, “Politehnica” University of Bucharest. The longitudinal (normal on machined surface) ultrasonic vibrations of electrodes were provided by a generator with a consumed power (P_{cUS}) up to 400 W on ultrasonic chains and a vibration frequency (f_{us}) within the range of 19…21 kHz.

The results obtained with relaxation pulses are presented in Figure 8:

Analyzing the parameters from Figure 8, it can be noticed that the major improvement induced by ultrasonic aid is more apparent at higher discharge energies, i.e., higher capacity steps. The energy (W_e) produced by the relaxation (dependent) generator based on capacitors battery is determined with the relation:

$$W_e = \frac{1}{2} C \cdot U^2 = \frac{\varepsilon \cdot S \cdot U^2}{2 \cdot s_F} \text{ [J]}, \tag{14}$$

where: C is generator capacity [F]; U - gap voltage [V]; ε - permittivity [F/m]; S - frontal surface of electrode-tool [m^2]; s_F - frontal gap [m].

Nevertheless, when using dependent pulses, their correlation with ultrasonic elongation of a tool (in this case) or a workpiece is difficult to achieve, so the improvement of technological parameters is not at an optimum level.

Due to the long period of capacitors loading and very short pulse durations, the probability of no discharges within the stretching semiperiod is very high and therefore, the effect of cumulative microjets stage on the material removal mechanism cannot be exploited [27]. Another disadvantage is given by the capacitor effect, formed by frontal surfaces of the electrode-tool and the machined workpiece (see relation 14), which limits the surface to be machined. At higher surfaces (S), the discharge energy is increased and therefore the obtained roughness (Ra) too. Nevertheless ultrasonic aiding can attenuate this effect by decreasing roughness by removing the peaks of micro-geometry due to ultrasonically induced shockwaves [28].

When using commanded pulses at EDM and EDM+US finishing, the variation of output technological parameters was comparatively presented after being statistically processed in Figure 9. As it can be observed, the significant improvement of the machining rate and volumetric relative wear was obtained at a higher duration of pulse time (more than 12 µs).

This can be explained by higher probability of pulse time overlapping on cumulative microjet stages, which determines the increase of removed volume from the workpiece.

At the end of the discharge, which is stopped by the cumulative microjet stage, the hydraulic forces of dielectric liquid can find workpiece material in a liquid state. So melting is the main thermal mechanism of material removal at EDM+US against boiling in case of classic EDM. Volumetric relative wear decreases when removed material grows (see relation 1.11). At lower pulse time (less than 12 µs), the improvement of machined surface roughness (Ra) by ultrasonic aiding is more apparent.

This is the effect of lower crater depths as a result of discharged energy decreases, and removal of micro-geometry peaks by ultrasonically induced shock waves, parallel with the machined surface, i.e., along the working gap. The results mentioned above were obtained using the experimental setup presented in Figure 10. The positions indicate the following elements of technological system: 1 - work head of ELER 01 machine; 2 - nodal flange; 3 - hose for lateral flushing; 4 - workpiece; 5 - device for clamping and orientation of the workpiece; 6 - electrical connections to the ultrasonic generator; 7 - reflecting bushing; 8 - sandwich PZT transducer for 20 KHz frequency; 9 – radiant bushing; 10 – ultrasonic horn; 11- electrode-tool.

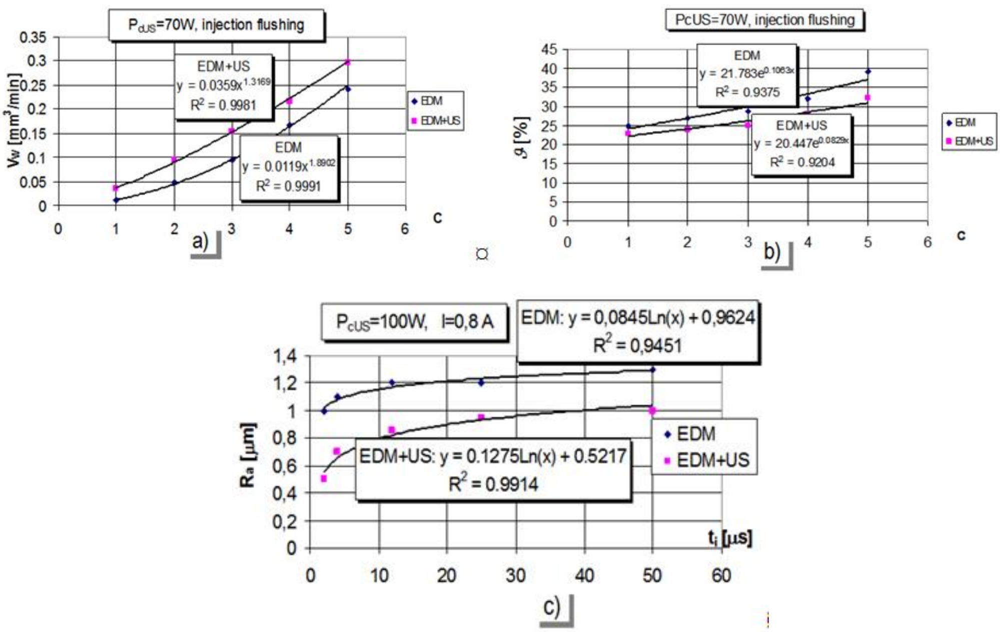

Figure 9. Output technological parameters at EDM and EDM+US finishing with commanded pulses, electrode diameter 30 mm, lateral flushing on ELER 01 machine [29]. a) machining rate (V_W) vs. pulse time (t_i) . b) volumetric relative wear (ϑ) vs. pulse time (t_i). c) surface roughness (Ra) vs. pulse time (t_i).

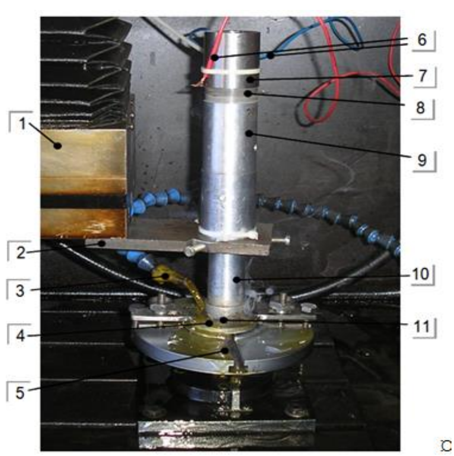

Figure 10. Experimental setup for EDM and EDM+US comparative finishing tests on ELER 01 machine.

Pilot comparative experiments of EDM and EDM+US micro-drilling on ELER 01 Romanian machine with specialized generator, the following parameters were used: 0.8 A current step, with cylindrical electrode-tool of 0.8 mm diameter from copper, X210Cr12 steel workpieces, consumed power on acoustic chain, P_{cUS}=100 W, ultrasonic frequency f_{US}=40 kHz, only with random overlapping of EDM pulses on cumulative microjets stage. The experimental setup is presented in Figure 11, where the positions indicate the following elements of technological system: 1 - clamping and orientation device of ultrasonic chain; 2 - assembling rod; 3 - nodal flange; 4 - radiant bushing; 5 - ultrasonic horn; 6 - clamping device of electrode-tool; 7 - electrode-tool; 8 - hose for lateral flushing; 9 – guiding device of electrode-tool; 10 – machined workpiece; 11- bracket for workpiece clamping; 12- worktable of ELER 01 machine.

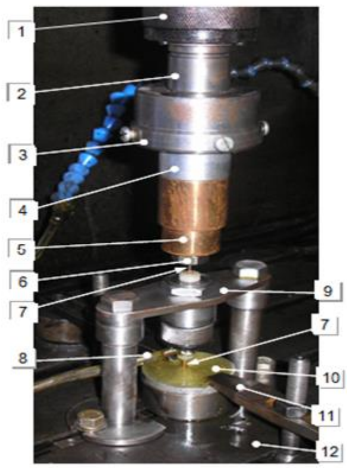

Figure 11. Experimental setup at EDM and EDM+US comparative micro-machining tests on ELER 01.

The used working parameters led to energy discharges situated at superior limits of micro-machining. Ultrasonic assistance is more appropriate for utilization of tools with transversal dimensions located at superior dimensional range of micro-machining, aimed at minimization of their deformations at ultrasonically induced cavitation. Moreover, commanded pulses were used because of their capacity to be easily-controlled in relation to tool elongation during T_{US}, and also with discharge energy determined with relation [25]:

$$W_e = \int_0^{t_i} u_e(t) \cdot i_e(t) \cdot dt \ \text{[J]}, \tag{15}$$

where: $u_e(t)$ [V], $i_e(t)$ [A] - time dependent voltage and current during pulse time t_i [µs].

All the output technological parameters of micro-EDM - machining rate (a), volumetric relative wear (b), and machined surface roughness (c) - were improved by US aid against classic EDM in the same working conditions, at certain finishing modes using different specific equipment as it is exemplified in Figure 10. These are based on several optimization conditions of input working parameters [25].

The results presented in Figure 12 emphasize the following assumptions:

- Roughness (Ra) increase can be kept under control at pulse time increase by the effect of micro-peaks removal due to ultrasonic shock waves oriented along the machined surface. More comprehensible roughness improvement by ultrasonic aiding was recorded in pulse time range 8-12 µs;
- Volumetric relative wear (ϑ) improvement is more evident at pulse time increase, which is strongly dependent by workpiece material removal, greater at longer pulse time, determining higher probability of pulse time overlapping on cumulative microjets stage;
- Machining rate (V_w) is more obvious with at longer pulse time, when the cumulative microjets stage can stop – as the visualizations on oscilloscope during experiments pointed out - the discharge and removed material in liquid state are overlapping on pulse time.

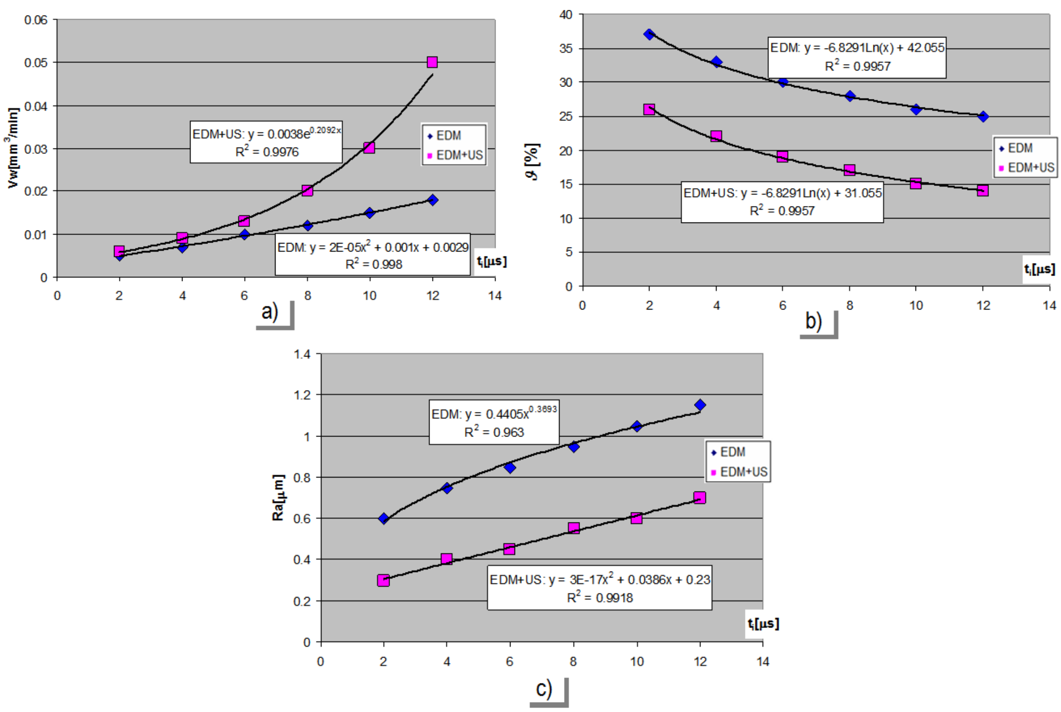

Figure 12. Comparative pilot experimental data at EDM and EDM+US micro-drilling with random pulses overlapping on cumulative microjets stage; X210Cr12 workpiece; electrode-tool of 0.8 mm diameter from copper, lateral flushing on ELER 01 [30] a) machining rate (V_W) vs. pulse time (t_i). (b) volumetric relative wear (ϑ) vs. pulse time (t_i). (c) surface roughness (Ra) vs. pulse time (t_i).

Analysis of Machined Surface Micro-Geometry

A selection of experimental data was achieved concerning machined surface micro-geometry comparatively obtained at classic EDM and EDM+US. These results are strongly connected to machined surface quality, which is an objective of utmost importance at finishing and micro-machining. In synthesis, the crater dimensions obtained at EDM and EDM+US finishing are comparatively presented [31, 32], using both commanded pulses and relaxation ones – Figure 13. The zones subjected to ultrasonic removal are pointed out, i.e., the margins of craters. The improvement of ultrasonic assistance in terms of surface quality is very apparent in case of both types of pulses. Micro-electrical discharge machining, using ultrasonic longitudinal vibrations (normal on machined surface) of an electrode with frequency 20 kHz, amplitude 2 µm were achieved on Romanian installation ELER 01 [33, 34, 35].

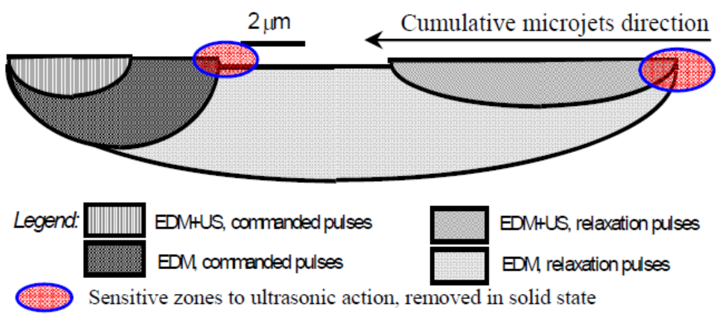

Figure 13. Comparison of crater mean dimensions in transversal section experimentally determined at EDM and EDM+US finishing [32].

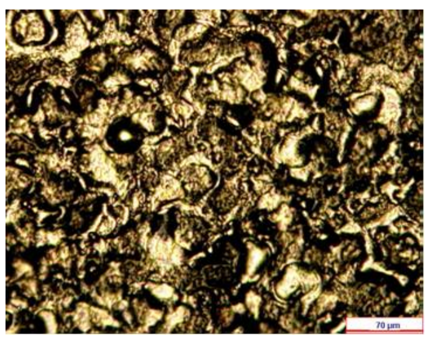

Figure 14. Micro-topography of EDMed surface with Ra=0.8 µm at I=0.8A, t_i=6µs, t_o=4µs, positive (tool) polarity [35].

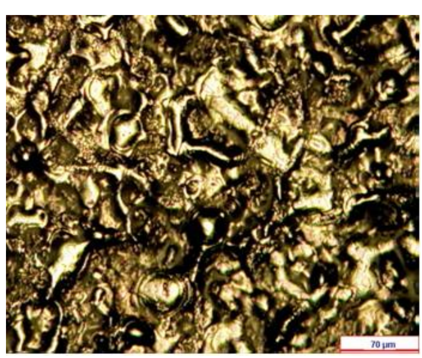

Figure 15. Micro-topography at EDM+US with Ra=0.45 µm at I=0.8A, t_i=6µs, t_o=4µs, positive (tool) polarity, P_{cUS}=100 W [35].

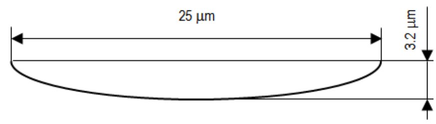

Figure 16. Mean dimensions of craters at micro-EDM, I=0.8A, t_i=6µs, t_o=4µs, positive polarity [35].

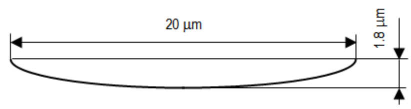

Figure 17. Mean dimensions of craters at micro-EDM+US, I=0.8A, t_i=6µs, t_o=4µs, positive polarity, P_{cUS}=100 W [35].

Some experimental results in comparison with classic EDM, under the same working conditions are presented below. Samples from X210Cr12 steel were machined with a specialized generator, using cylindrical electrode-tool diameter of 0.8 mm from copper. The images of machined micro-topography (Figure 14, 15) were obtained using a Reichert Univar microscope and Buehler OmniMet Enterprise specialized software from "Politehnica" University of Bucharest, Faculty of Material Science. The correspondent profiles of micro-craters obtained on the basis of their mean dimensions are presented in Figure 16 and Figure 17.

From these pilot experiments, it can be observed that the effect on the cumulative microjets stage, respectively the ultrasonic shock waves oriented along the working gap, parallel to machined surface is very apparent at micro-machining by decreasing the obtained surface roughness by almost 50% in comparison with classic micro-EDM in the same working conditions.

It must be mentioned that dimensions of machined surfaces are located at a superior range of micro-machining in order to prevent inherent deformations of tools due to great ultrasonic pressure developed inside the working gap.

Analysis of Ultrasonic Chains Dimensions and Own Frequencies

Although there is spectacular improvement of EDM+US technological improvement in comparison with classic EDM, EDM+US technology has a significant drawback due to the lack of flexibility. This is derived from the critical technological condition to be fulfilled when ultrasonic chain works at resonance, which supposes equality between the frequencies of the main components of the ultrasonic chain: ultrasonic transducer and ultrasonic horn that include the electrode-tool as an integrated part or similar workpiece.

The analysis of ultrasonic chain dimensions and its own frequency is absolutely necessary at: initial stage, during the iterative process of its dimensional adjusting and finally achieving resonance conditions. All are in strong correlation with application of the finite element modelling of ultrasonic chain and working at certain dimensions, as will be presented below. The results of the above-mentioned analysis provide important data concerning traceability of ultrasonic chain quality.

Different shapes of ultrasonic chains used for EDM+US finishing comprise both variants related to vibrated object and integrated in ultrasonic horn: (a) electrode-tool; (b) workpiece.

In case (a), the components of an ultrasonic chain are presented in Figure 18. A transducer assembly is presented in detail in Figure 19. Its own frequency is considered an entry date. Subsequently the ultrasonic horn was dimensioned and machined in a CIM environment.

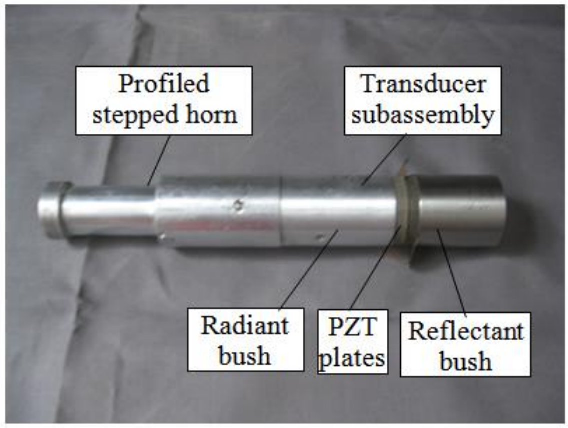

Figure 18. Ultrasonic chain assembly used at EDM+US finishing [36].

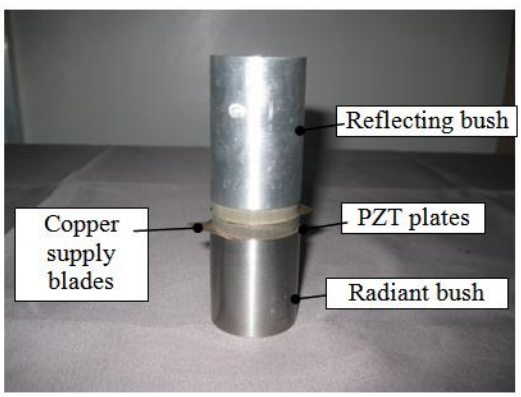

Figure 19. Transducer subassembly used in ultrasonic chain for EDM+US finishing [37].

The transducer assembly provided by the Institute of Solid Mechanics of the Romanian Academy (figure 19) has their own *series frequency* f_{tr}= 20.1 kHz – of interest for this type of application – [38], and the output diameter of the radiant bush was D_b=39 mm.

In this case, the horn made from 1045 steel (ASTM) with characteristics, Young's modulus, $E=2.1 \cdot 10^{11}$ Pa, density ρ = 7850 kg/m^3, the entry frequency of the horn was f_{o1}=19.0 kHz lower than that of the transducer f_{tr}. Thus, the values of physical parameters were: the wave length, λ=0.26188 m, wave number, α=23.06951 m^{-1}. A preliminary calculation provided the lengths of stepped horn from Figure 1.18: the entry step length, l_1=65.02 mm; the output step length, l_2=69.35 mm. The entry diameter of the horn was equal with that of the radiant bush, D_1=39 mm.

Based on these data, after some iterative stages consisting in adjusting dimensions and using finite element modelling strategy, which will be presented underneath, the final dimensions of the ultrasonic horn were obtained (Figure 20), satisfying resonance conditions. The tool path for machining on the CNC lathe is shown in Figure 21.

Fabrication on classic machine-tools is highly time-consuming because resonance condition supposes fabrication of ultrasonic horn at longer length, corresponding to lowering its own frequency, followed by several lengths of shortening, increasing its own frequency until the equality between the frequencies of transducer and ultrasonic horn is attained.

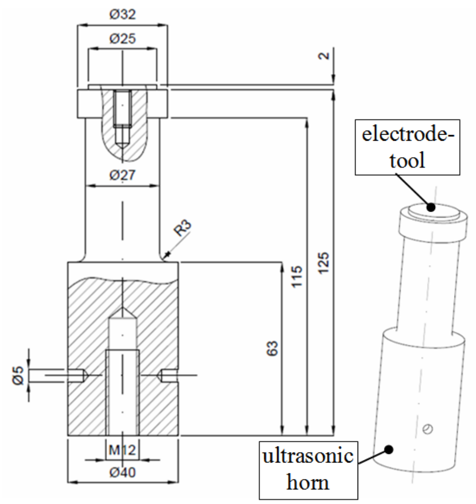

Figure 20. The profiled stepped horn with integrated electrode-tool [36].

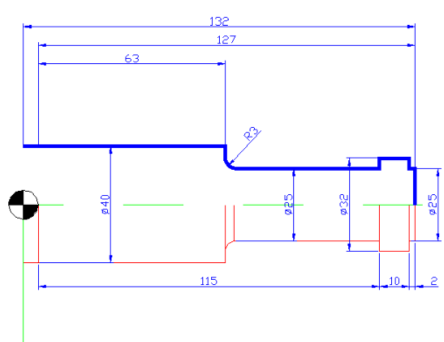

Figure 21. The horn stepped profile and the generated NC path [36].

Using CAM applications and CNC lathe, the resonance condition was attained in shorter time than when using usual classic machines, which contributes to increasing flexibility of EDM+US technology.

This is not only based on lengths shortening but some other constructive solutions of ultrasonic horn, like modifications of fillet radius, steps diameters, and holes machined inside the horn, also involving finite element method modelling.

Conclusions Concerning Analysis of Experimental Data

Some synthetic conclusions are presented resulting from experimental data, which also supports further research directions concerning the technological output performances of EDM+US finishing and the micro-machining process:

- The variation of machined surface roughness, volumetric relative wear, and the machining rate against discharge duration emphasized that all these main technological parameters were significantly improved even on classic machines-tools by vibrations of the electrode-tool with ultrasonic frequency, oriented on the machined surface;
- Using commanded pulses against relaxation pulses determined more visible improvement of the main technological parameters, especially at higher pulse time, based on the possibility of superior control of discharges in terms of duration, moment of delivery and current peak; this is in connection with a main research direction, synchronization of pulse time and ultrasonic elongations of electrode-tool / workpiece through probability increase of pulse time on cumulative microjets stage, taking full advantage of this cavitation effect ultrasonically induced in the work gap;
- The above-mentioned improvements were obtained by application of some optimization conditions of input working parameters. The key-parameter was consumed power on the ultrasonic chain (P_{cUS}), whose optimum value was experimentally determined. This also satisfies exceeding of cavitation threshold, specific to concrete working conditions. As a comparative EDM and EDM+US study micro-topography pointed out, the deeper craters profile when machining with commanded pulses required an increase of 30% of parameter P_{cUS} against the corresponding value from using relaxation pulses.
- The major drawback of EDM+US, lack of flexibility, which is imposed by resonance conditions within ultrasonic chain, integrating electrode-tool / workpiece, was improved by fabrication of ultrasonic horns, specific to each machine in a Computer Integrated Environment. This is a major research direction, which is strongly supported by finite element modelling methodology applied especially in the case of complex profiled ultrasonic horns.

CHARACTERIZATION OF MICRO-ELECTRICAL DISCHARGE MACHINING AND SOLUTIONS FOR TECHNOLOGICAL PERFORMANCES IMPROVEMENT THROUGH ULTRASONIC AIDING

Micro-machining defines the processes that achieve products in the range of 1 to 999 μm, according to the CIRP committee of Physical and Chemical processes. The present trend of ultra miniaturization of mechanical components led to µEDM applications at microscopic mechanical components and devices. In this respect, the µEDM technology is helpful for conventional precision machining as well as for micro-components fabrication like micro-moulds, micro-inserts, and in general, filigree structure up to 5 µm [39].

For this type of machining, the energy must be minimized and consequently, also the size of the gap at a width of 1 µm. A specific EDM strategy was applied in current research that permits setting of a minimized discharge gap. Working with increments of under 1 µm of the feed system, which are effectuated gradually, after a short delay (sample time), as the gap increases, this µEDM requirement is attained.

A large range of products can be achieved like fuel injector valves, parts and components for medical devices, fiber optic connectors, micro-moulds, stamping tools, micro-electronic parts, etc. [40, 41].

Micro-EDM is considered a very flexible machining process due to its different variants. Three versions of big industrial applications are micro-die sinking, micro-wire electrical discharge machining and micro-electrical discharge drilling. The other micro-EDM variants with less industrial relevance are micro-electrical discharge milling, micro-electrical discharge grinding, and micro-wire electrical discharge grinding [42, 43].

At present, micro-die sinking is mostly used in single or small series production, mainly in fabrication of tools for micro-embossing or micro-injection moulding. Minimal structure widths that can be achieved by micro-die sinking ranges between 20 µm and 40 µm. Channels of around 20 µm and corner radii of 10 µm at aspect ratios of up to 25 can be produced. Deviations of contouring accuracies are of ±1 µm [44].

At micro-ED drilling, the rotating or stationary pin electrode is moved axially into the workpiece. Conventional electrodes for micro-ED drilling made from cemented carbide are available with diameters down to 45 µm [39]. Smaller dimensions for electrodes down to 2.5 µm are also available [43]. Special clamping systems also made from cemented carbide or ceramics are needed for the exact guiding and positioning of the electrode [42].

Compared to classic EDM, micro-EDM is focused on the following items [42], synthesized in Figure 22:

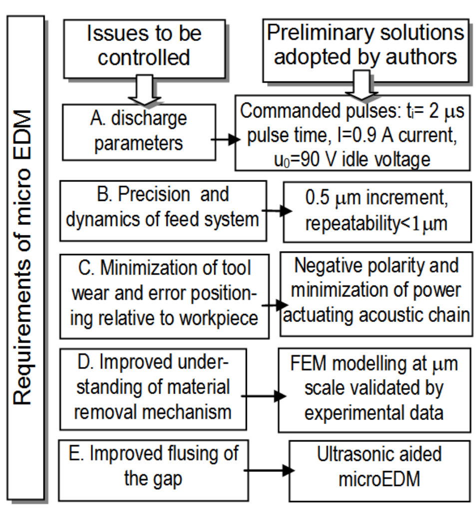

Figure 22. Specific issues addressed at micro-EDM [45].

A. Strict control of discharge parameters: frequency of discharge (pulse and pause time), level of the energy input, (current, voltage and pulse time) - the minimum discharge energy of 0.1 μJ is obtainable, which determines a very small material removal at one single discharge and an extremely small gap width ranging from 1 to 5 μm [46].
B. High precision control of the motion of the electrodes - in case of actual installations, the feed is achieved through a servo system with the highest sensitivity and positional accuracy of 0.5 μm on the X, Y and Z axes movement [47].
C. Requirements concerning the wear of the electrodes and compensation for the wear - since μEDM operates at very short discharge durations from t_i = 10 ns to t_i = 2.5 μs [43], the tool electrode is usually charged as the cathode to reduce tool electrode wear [48]. This is explained by the polarity effect, which is also included in Van Dijck's model [49]; even graphite, cemented carbides or tungsten-copper (very thermally and mechanically resilient) are used for tool electrodes, the relative wear can be over 30%; this is extremely visible at machined surfaces with edges and corners due to increased electric field intensity [42].
D. Improved understanding of the μEDM removal process and the factors that affect it, like material properties, thermal conduction of the workpiece, melting and recasting processes, and their effect on the surface finish/integrity - this is an objective for present and further research by undertaking FEM studies at micrometer scale, validated by experimental data concerning the material removal mechanism;
E. Improved flushing of the gap, evacuation of the removed particles from the process - this is in strong correlation with gap size and working of the dielectric unit. Taking into account the gap width of several μm, a filtering capacity under 1 μm is recommended.

The issue of dielectric liquid must also be considered. Dielectric oil with lower viscosity, $\nu \leq 1.8 \cdot 10^{-6}$ m^2/s (appropriate for gap width with μm order of magnitude), is used in the micro-die sinking process [42]. In comparison to dielectric oil, deionized water contributes to a higher surface quality and material removal rate [48]. These could be explained by the following phenomena: density of the water is lower, allowing the development of the plasma channel and consequently, a lower energy density on EDM spot; the water has higher conductivity determining a greater gap size and therefore an improved evacuation of the removed particles from the gap. In order to avoid the secondary effect of electrolysis, negative polarity is recommended aiming at achievement of additional anodic dissolution to the workpiece.

In respect with requirement (E), several improved flushing modes have yet to be analyzed. The following modes of direct flushing strategies could be used: lateral flushing (a), injection flushing (b) and suction flushing (c); b and c variants are more expensive when using the tubular electrodes - very high costs under 0.1 mm diameter. Injection or suction through workpiece is difficult to apply at very small dimensions of μm level. Flushing through the electrode is in most cases impossible because of the small electrode dimensions.

Indirect flushing strategies must be approached, which consist in relative motion between the tool electrode and the workpiece, simultaneously with the tool feed. The relative motion can be a periodic high frequency vibration or a rotary motion of the tool electrode. Thus, at μ-ED drilling, the electrodes have rotations up to n = 2000 rot/min [50, 51, 52] in order to obtain higher accuracies in roundness, higher aspect ratios and higher material removal rates.

These results are similar to those of planetary motion at EDM. Additionally, the effectiveness of the flushing is increased by a translatory vibration with amplitude between 4 μm and 20 μm and a frequency of 50 - 300 Hz [42]. Nevertheless experimentally, it was demonstrated that low frequency vibrations are inferior to ultrasonic ones in terms of machining rate [53]. Ultrasonic aiding μEDM can also be considered a very effective indirect flushing strategy.

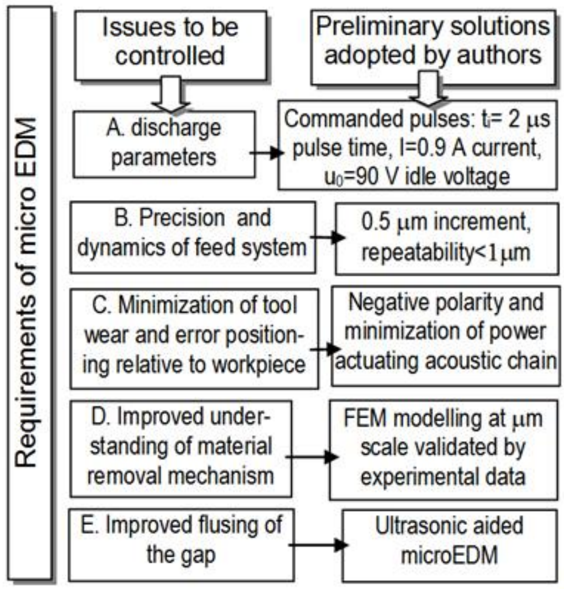

Figure 23. Weaknesses of micro-EDM and solutions for improvement [54].

This up-to-date variant of the EDM process, micro-EDM, is so called because it utilizes low discharge energies approximately in the range of 10^{-9} – 10^{-5} J to remove small volumes of material of around 0.05 – 500 μm^3 [43]. Even a single discharge can be used.

The micro-EDM process features two very important disadvantages (Figure 23): The first one is a rather slow machining process – (A). The material removal rate is relatively low compared to other machining and micro-machining processes. This is due to the low machining rate given by general conditions of EDM occurring especially to the very narrow working gap (under 5 μm), characteristic of μEDM, leading to process instability. It is also a serial process (successive discharge), while silicon fabrication processes for example, are parallel. Lithography and their etching parallel nature makes them more productive [43].

The second weakness is high tool wear, leading to shape inaccuracies, i.e., lack of machining precision – (B).

Several solutions to improve the machining rate were undertaken (Figure 23). The solutions carried out in connection with ultrasonically aided EDM were written in italics. A research direction was to drill multiple holes with multiple electrodes. In 1991, Higuchi et al. developed a pocket-size EDM system [55]. Drilling one at a time instead of hundreds or thousands of holes was clearly inefficient. The pocket-sized EDM permits many clamping systems to be placed on a large part, thus drilling several holes at the same time. More recently, other attempts to use multiple electrodes at micro-EDM were reported, obtaining a raised machining rate [56, 57, 58].

However, the attempt to increase the number of electrode-tools working in parallel does not necessarily lead to proportional augment of the machining rate due to an increased number of short-circuits and consequently, corresponding retracts of the electrode-tool. An optimum number of tools working in parallel to increase the machining rate is needed, strictly in connection with real working conditions.

Other solutions could be indirect flushing produced by rotary movement of the electrode-tool. Ultrasonic aiding micro-EDM (μEDM+US) is also included in this type of approach. But μEDM+US is more than that due to an additional mechanism, the material removal mechanism produced by ultrasonically induced cavitation. It dramatically reduces the gas bubble life around the plasma channel at the most half-period of ultrasonic oscillations and consequently, could remove material in liquid state. The hydraulic material removal occurs too, determined by high pressure resulting from the collective implosion of gas bubbles from the gap, which is of tens MPa order [25].

H. Huang at al. achieved a spectacular increase of the machining rate, up to 60 times, μEDM+US of micro-holes in Nitinol, an intelligent material from Ni and Ti alloy, which keeps its shape after deformation and reheating [59]. J.C. Hung at al. combined ultrasonic vibration with rotary movement of electrode-tool at micro-holes achieved by μEDM [60].

Nevertheless, ultrasonic aiding supposes additional costs to achieve the chains and the generator, which could be covered at higher volume of fabrication than at classic EDM.

The main methods for prevailing over shape inaccuracies introduced by tool wear are more precise position of the tool [61] or better compensation of tool wear [62].

Another approach to improve the accuracy of micro-EDM is to use a more accurate method of tool fabrication like LIGA, an alternative micro-fabrication process combining deep X-ray lithography, plating-through-mask and molding. This enables the highly precise manufacture of high aspect ratio micro-structures with large structural height ranging from hundreds to thousands of micrometers thickness, which are difficult to be achieved with other manufacturing techniques [56].

Several machines performing micro-EDM exist on the market today. Most of them use RC circuits capable of producing pulses as short as 10 nano-seconds. It is obvious that by using this type of pulse, very low discharge energy can be produced. On the other hand, relaxation pulses cannot be controlled in terms of delivery moment, which makes them unacceptable for US aided – synchronization, the current pulse with stretching semiperiod of ultrasonic oscillation. The lowest values of static pulse durations, which are more suitable for US aiding, are 2.5 μs in the state of the art [29].

Another key-parameter addressing shape accuracy is feed system dynamics. This also affects the entire process, evaluated by machining rate, relative volumetric wear and surface roughness. All actual installations provide submicrometer values for resolution and 1 μm for position precision and repeatability [43].

The tool drawbacks affecting the machining rate can be produced by high pollution of dielectric liquid from the gap. So, dielectric unit is also a very important element that has an influence on accuracy if the feed system has inappropriate dynamics. If a polluted dielectric with particles comparable with the gap size is provided, short-circuits can occur. Therefore it is recommended that μEDM installation must be equipped with a dielectric liquid unit with submicronic filtering capacity.

FINITE ELEMENT MODELLING APPLIED TO REMOVAL PROCESS MODELLING OF ELECTRICAL DISCHARGE MACHINING AIDED BY ULTRASONICS AND ULTRASONIC CHAIN FUNCTIONING

The material removal mechanism modelled by the finite element method comprised two principal components: thermal and ultrasonic. The first component, the dynamics of the thermal front within the workpiece during tbe EDM process is able to provide solutions for improvement of the machining rate and volumetric relative wear. The second one, the effect of ultrasonic mechanical removal on workpiece material in a solid state is strongly related to decreasing surface roughness. Ultrasonic chain modelling is of the utmost importance for flexibility improvement of EDM+US technology.

Thermal Finite Element Modelling Applied to Removal Process Modelling of Electrical Dischage Machining Aided by Ultrasonics

Some critical aspects of thermal finite element modelling (FEM) of the material removal mechanism, extracted from several papers [63-67], are emphasized. In this context, the influence of dimensional variation of the plasma channel and the surrounding gas bubble radii must be taken into account to increase precision of finite element models at micro-machining, respectively at micro-EDM+US. An illustrative generic evolution of the two elements at μEDM is comparatively depicted in Figure 24:

The time dependent (t) parameters of interest in the frame of thermal modelling are presented in Figure 25, where: r_{pc} (t) - radius of plasma channel, which is narrowed at cathode zone; r_{As} (t) - anode spot radius produced by plasma channel on the anode surface; r_{Cs} (t) - analogous cathode spot radius; r_{gb} (t) - radius of gas bubble; r_{Agb} (t) – gas bubble radius on anode surface; r_{Cgb} (t) – homologous radius on a cathode spot. These elements are critical, since they determine the main boundary conditions of the model, and consequently have a strong influence on FEM results.

The removed volume by discharge from the anode and cathode materials is bordered by boiling isothermal in the case of classic EDM. This assumption is supported by the overheating model in different variants.

The model of overheating – applied in this chapter – with 200-300 K above the normal boiling temperature means that EDM spot temperature on anode/cathode, in contact with the plasma channel, cannot exceed the limit mentioned above [21].

Regarding the plasma channel evolution, there are different relations through which the plasma channel radius could be calculated [67].

Patel, Barrufet, Eubank, and DiBitonto, (1989) considered that the discharge channel radius can be estimated using the following relation [68]:

$$r_{dc}\left(t\right) = K \cdot t^{n}, \tag{16}$$

where: t is pulse duration; K, n - empirical constants with the following values, K=0.788 and n=0.75.

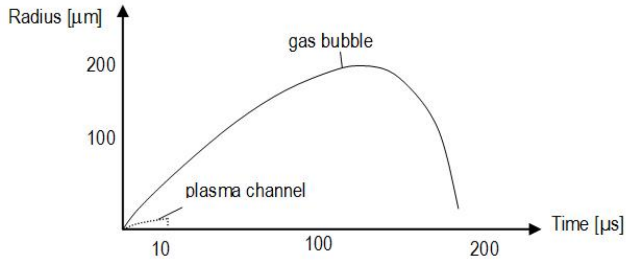

Figure 24. Plasma channel and gas bubble qualitative evolution at micro-machining [29].

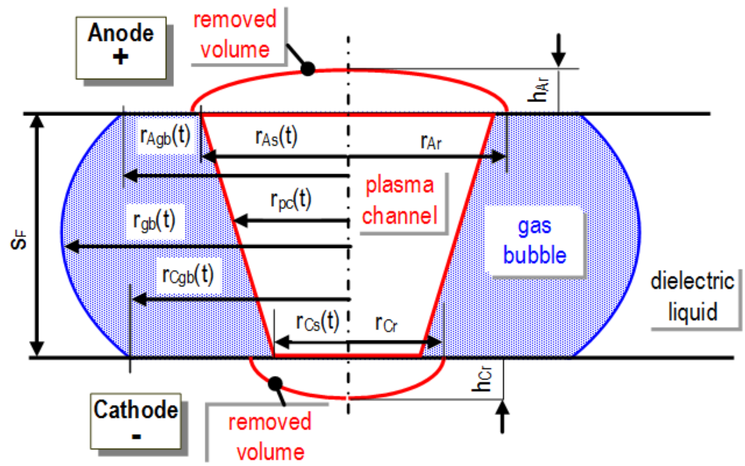

Figure 25. Modelling parameters at µEDM removal mechanism [66].

In this context, the above-mentioned authors considered for the first time (1993) that quantitative evidence supports that superheating is the dominant mechanism at EDM [69].

Shuvra et. al. (2003) pointed out that plasma radius varies with time as the following relation shows [70]:

$$r_{dc} = k \cdot t^{\frac{3}{4}}, \tag{17}$$

where: t is the pulse duration [µs]; k – proportionality constant.

More recently, Marafona and Chousal (2006) concluded that the discharge channel radius (r_{dc}) is proportional to the discharge current, pulse duration, workpiece materials, dielectric liquid properties and proportionality constants and indices (depending on gap size), according to the following relation [71]:

$$r_{dc}(t) = K \cdot Q^m \cdot t^n, \ [\mu m] \tag{18}$$

where: Q is the discharge current [A]; t – pulse duration; m, n, K – empirical constants that take into account working conditions mentioned above.

Salonitis et. al. (2007) considered the following relation to compute discharge channel radius [72]:

$$r_{sp} = 2040 \cdot I^{0.43} \cdot t_{on}^{0.44}\text{, [µm]} \tag{19}$$

where: I is the current [A]; t_{on} - the pulse on time [µs].

Some of relations presented above were used in this actual FEM modelling of material removal mechanism at µEDM aided and unaided by ultrasonics under specified conditions.

The first approach was the time dependent radius variation given by Patel et al.. Therefore, the relation (16) was converted in the following one, needed for the compatible measure units used in the time dependent thermal module of Comsol Multiphysics modelling of channel radius (r_{ch}) variation:

$$r_{ch} = 0.024942 \cdot t_i^{0.75}\text{, [m]} \tag{20}$$

where: t_i is pulse time [s].

The parameters utilized in the frame of this approach (similar in the following models) are presented in Figure 26 as they were defined in global definitions:

Parameters

Name	Expression	Value	Description
lp	10[mm]	0.01 m	workpiece dimension
acr	5e-6	5.0E-6	axis x dimension of crater
bcr	3.2e-6	3.2E-6	axis y dimension of crater
rms	0.15e-6	1.5E-7	radius of resolidified material
rch	0.024942*ti^0.75	0	radius of plasma channel
ti	0	0	pulse time
rbg	0.1[mm]	1.0E-4 m	radius of gas bubble

Figure 26. Parameters used at time variation of plasma channel modelling of micro EDM [67].

Another approach was made starting from the Kiyoshi Inoue’s assumption, that the variation of radius r_{ch} can be expressed like [75]:

$$r_{ch} = k \cdot \sqrt{t_i}\ \text{[µm],} \tag{21}$$

where: t_i is pulse time [µs].

The previous relation was converted in the suitable form for Comsol modelling as follows [67]:

$$r_{ch} = 0.0014 \cdot \sqrt{t_i} \text{ [m]}, \tag{22}$$

where: t_i is pulse time [s].

Generally, the results obtained from FEM – detailed below - concerning the volume of the crater produced by a single discharge in the last case were even reported closer to the reference data (experimental data presented above), in comparison with the previous modelling approaches.

The influence of time dependent plasma channel, and gas bubble radii within the removal mechanism was studied by a strategy with the logical scheme from Figure 27.

Regarding the gas bubble dynamics, when working with step current I=10A, pulse time t_i=10 µs, and atmospheric pressure, the gas bubble radius was determined at maximum extension of 0.9 mm at 100 µs from the pulse start [12].

For machining conditions relatively close to the ones of present study, this model is confirmed by high speed framing camera (HSFC) [10]. The gas bubble volume is determined mainly by the current step, and secondly by pulse time. Some data provided in [18, 19] led to the variation of the gas bubble radius from Figure 28:

The dimensions from Figure 16 and 17 are taken as reference for FEM modelling validation.

Comsol Multipysics, Heat Transfer in Solids, Time Dependent with Parametric Sweep as pulse time were used to determine positions of the thermal front in X210Cr12 steel produced by discharge in the case of both variants of classic and ultrasonic aided EDM.

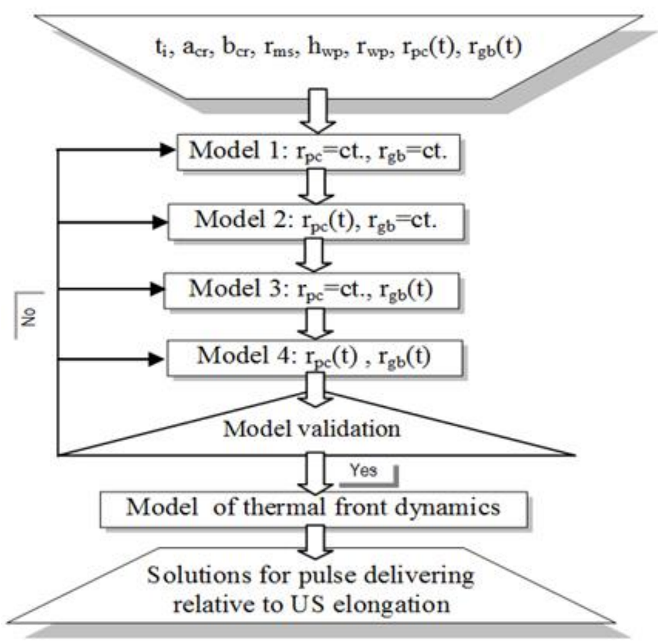

Figure 27. Scheme of the approached strategy at FEM modelling with time dependent radii of plasma channel and gas bubble [66].

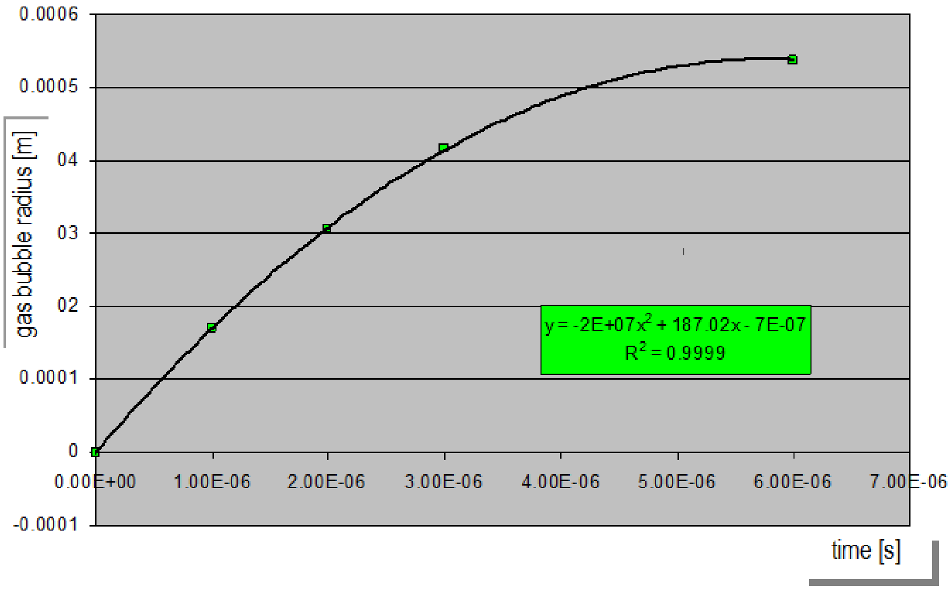

Figure 28. Gas bubble radius variation extrapolated from experimental data provided by HSFC at 0.8 A current step [66].

Parameters

Name	Expression	Value	Description
rwp	5[mm]	0.005 m	radius of workpiece
hwp	10[mm]	0.01 m	height of workpiece
rms	1e-6	1.0E-6	radius of solidified material
acr	12.5e-6	1.25E-5	a semiaxis of crater
bcr	3.2e-6	3.2E-6	b semiaxis of crater
ti	0	0	pulse time
rgb	-2e7*ti^2+187.02*ti+7e-7	7.0E-7	radius of gas bubble
rpc	0.004695*ti^0.5	0	radius of plasma channel

Figure 29. Parameters defined for time dependent radii of gas bubble and plasma channel model [66].

The parameters defined in global definitions for the most complex model (4) are shown in Figure 29, all representing the corresponding dimensions of items on cathode spot (positive polarity), based on mathematical models issues previously presented.

The dimensional space 2D/axis symmetric is used and creates the initial microgeometry resulted from previous discharges during the EDM process, characterized by parameters a_{cr}, b_{cr}, and r_{ms}; the last one is due to resolidified material melted by discharge on the craters borders, specific to positive polarity and commanded pulses.

The moving mesh with free triangular elements, much finer in spot adjacent zone, needed to time dependent radii of plasma channel and gas bubble, is presented in Figure 30, with its corresponding statistics.

Constant 3473 K temperature on the cathode spot, (circle with r_{pc} radius), thermal isolation on area covered by gas bubbles (circle with r_{gb} radius), and convection cooling on workpiece periphery immersed in dielectric liquid with 313K were considered for boundary conditions (Figure 31).

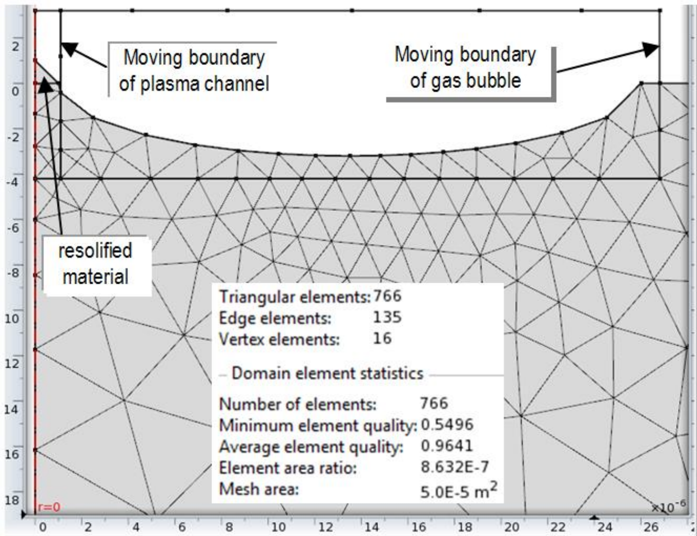

Figure 30. Geometry and mesh at time dependent radii of plasma channel and gas bubble modelling of EDM / EDM+US [66].

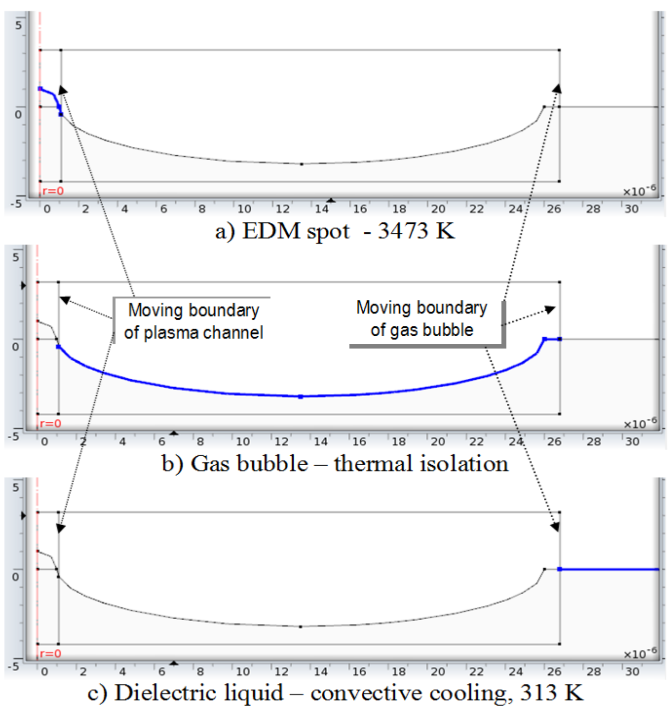

Figure 31. Boundary conditions at model with time dependent radii of plasma channel and gas bubble [66].

The boundary conditions are similar at simpler models (1, 2, 3) from Figure 27 enable to exert the corresponding influence on material removal mechanism. The FEM results of the first model with constant radii of plasma channel and the gas bubble provided the position of boiling thermal after a single discharge as it presented in Figure 32.

The results of next stage modelling with time dependent radius of plasma channel are presented in Figure 33.

In case of model (2) with time dependent radius of plasma channel, it can be observed that boiling isothermal margins, which determine the crater size at classic EDM size, are closer to reference data, i.e., 12.5 µm, than boiling isothermal margins determined at Model (1), difference between models being more than 1 µm.

The next stage following the approached strategy of modelling, is the time-dependent radius of gas bubble. Its FEM results are presented in Figure 34. As one can see, in the case of time dependent radius of the gas bubble, the crater margins defined by the position of boiling isothermal are only a little closer (difference in submicron range) to that of constant radius of plasma channel and gas bubble. So, the influence of parameter, time dependent radius of bubbles gas is very limited on volume removed by a single discharge.

The modelling stage before validation in the frame of approached strategy is both time dependent radius of plasma channel and gas bubble, whose FEM results are presented in Figure 35.

It can be observed that in a case of final model with both time dependent radii of plasma channel and gas bubble, the margins of boiling isothermal is closest to the crater mean dimensions from reference experimental data. So this model was validated. Even so, the influence of time dependent parameter of gas bubble radius is insignificant, visible only as 0.01 µm order of magnitude. The influence of time dependent parameter of plasma channel radius is more significant, observable at 1 µm order of magnitude.

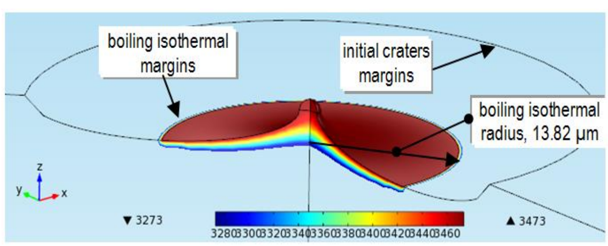

a) 3D image of boiling isothermal

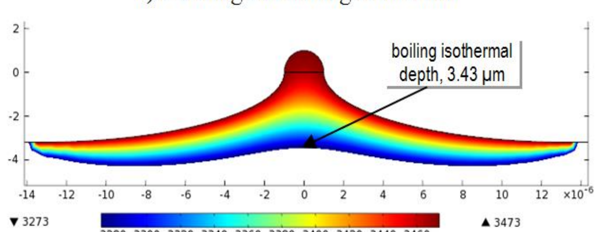

b) Transversal section of boiling isothermal in plane xz

Figure 32. Position of 3273 K boiling isothermal at Model (1) of constant plasma channel and gas bubble radii at pulse end of t_i=6 µs, r_{pc}=12.5 µs, r_{gb}=0.5 mm [66].

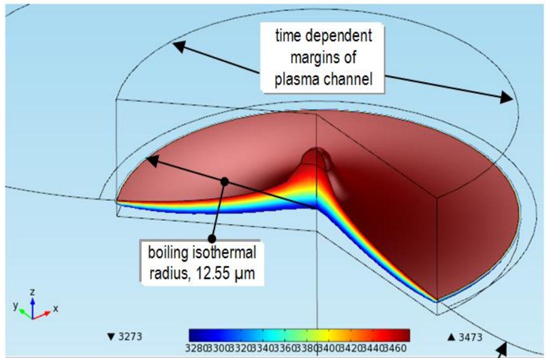

a) 3D image of boiling isothermal

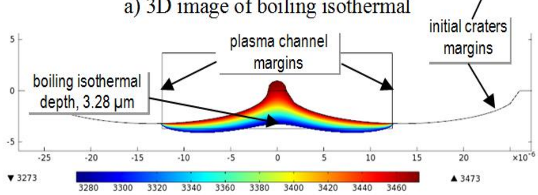

b) Transversal section of boiling isothermal in plane xz

Figure 33. Position of 3273 K boiling isothermal at Model (2) with time dependent radius of plasma channel at pulse end of t_i=6 μs [66].

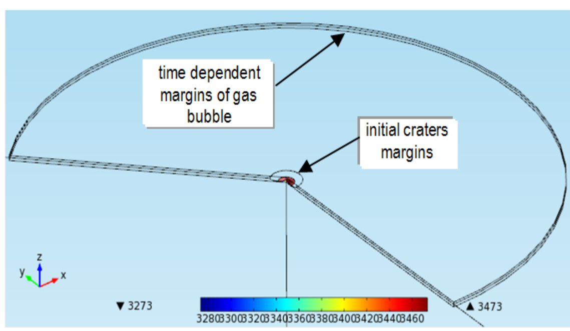

a) 3D image of boiling isothermal

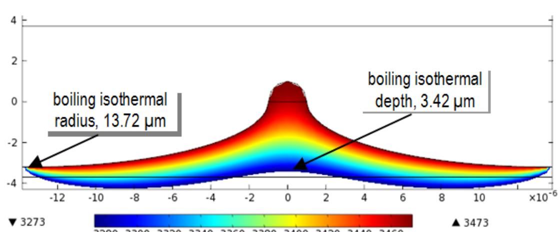

b) Transversal section of boiling isothermal in plane xz

Figure 34. Position of 3273 K boiling isothermal at Model (3) with time dependent radius of gas bubble at pulse end of t_i=6 μs [66].

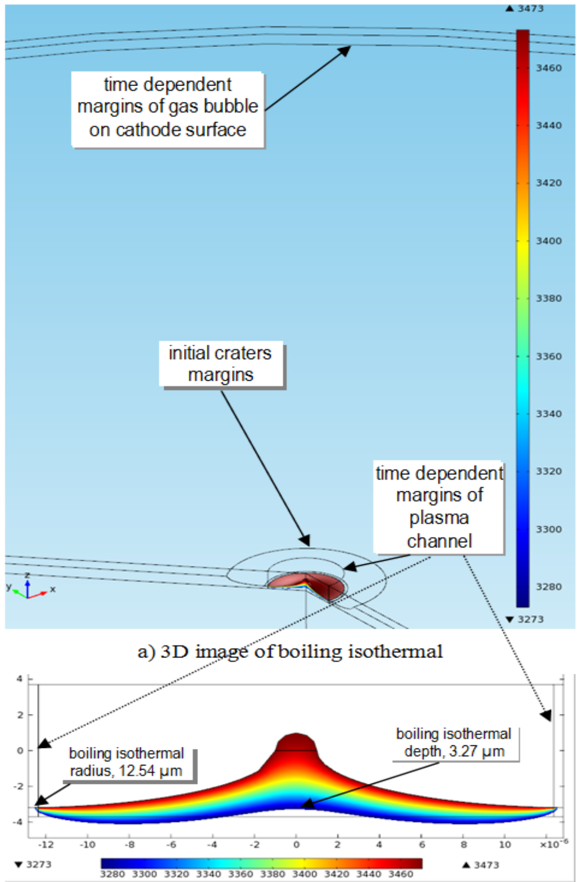

Figure 35. Position of 3273 K boiling isothermal at Model (4) with time dependent radii of plasma channel and gas bubble at pulse end of t_i=6 μs [66].

These results pointed out the importance of $r_{ch}(t)$ at micro-machining modelling, and $r_{gb}(t)$ at under micro-machining modelling.

For pulse delivering appropriate moments relative to ultrasonic oscillations, the dynamics of thermal front has to be addressed. The validated model with both time dependent radii of the plasma channel and gas bubble was used. The positions of boiling isothermal at classic micro-EDM were presented at different moments, during pulse time in Figure 36.

As it can be observed, most parts of the removed volume is already overheated in the very early stage of pulse time at classic EDM, a shock heating occurring in this case.

The positions of melting isothermal (1683K for X210Cr12 steel) at micro-EDM+US were presented in Figure 37, as relevant for the strategy of overlapping on cumulative microjets stage. It can be noticed that significant volume can be removed by hydraulic forces at micro-EDM+US even within a time interval less than 1 μs as the gas bubble is collapsed and the workpiece material is still in liquid state.

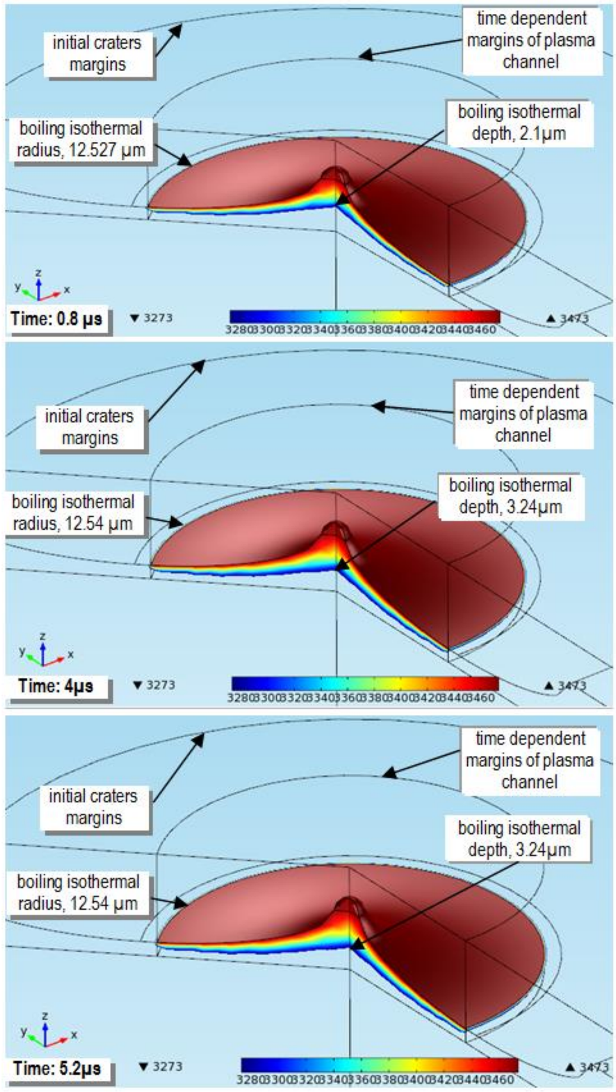

Figure 36. Relevant thermal front dynamics at microEDM [66].

Mechanical Hydraulic Finite Element Modelling Applied to Material Removal Mechanism Due to Ultrasonics at Micro-Machining

The specific EDM surface with multiple craters generated by previous micro-discharges was considered for process modelling with Comsol Multiphysics, using the module Solid Mechanics in time dependent variant.

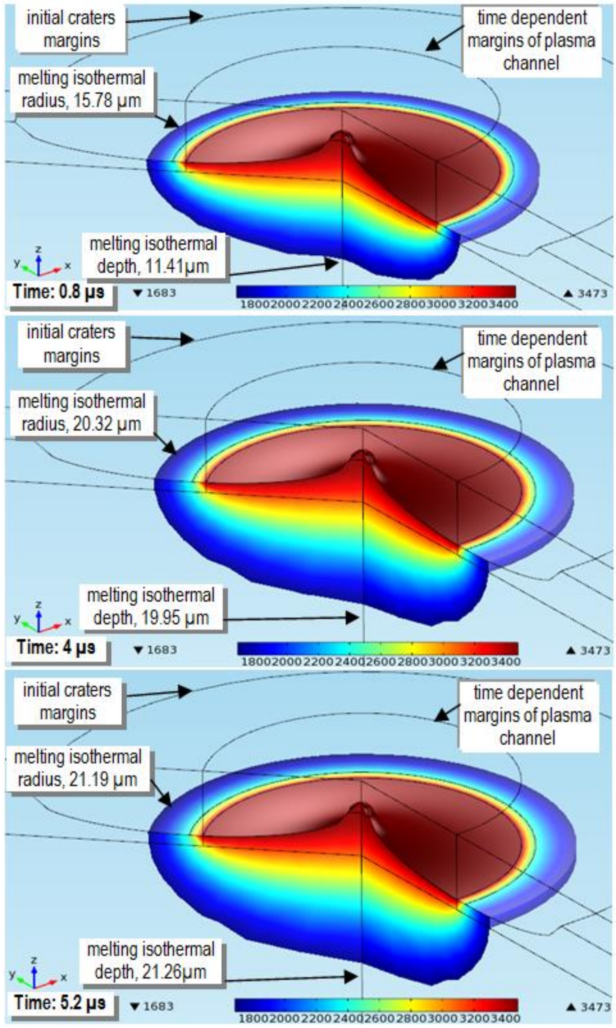

Figure 37. Relevant thermal front dynamics at microEDM+US [66].

The workpiece material was D3 (UNS T30403), corresponding to X210Cr12, whose properties were taken from the Comsol library and completed with needed mechanical properties for the module that was applied. The meshing was the same as that used at thermal modelling previously presented, conceived as multiphysics models.

Some experimental data concerning EDM drilling of micro-hole represented references for modelling validation. The following working parameters were used: static pulse duration t_i=2µs, pause time t_0= 2µs, positive polarity, current step I=0.5A, consumed power P_{cUS}=100 W, on plane surface machining. The following reference data were synthesized: for classic µEDM – crater depth 3 µm, crater radius 3.7 µm; for µEDM+US - crater depth 1.6 µm, crater radius 3.2 µm.

Parameters

Name	Expression	Value	Description
lp	10[mm]	0.01 m	workpiece size length
rmh	50e-6	5.0E-5	micro-hole radius
hmh	0.2[mm]	2.0E-4 m	micro-hole depth
acr	3.7e-6	3.7E-6	initial craters radius
bcr	3e-6	3.0E-6	initial craters depth
rms	0.25e-6	2.5E-7	radius of solidified material
hmcr	0.19[mm]	1.9E-4 m	position of micro-peak
pus	130[MPa]	1.3E8 Pa	ultrasonic pressure
tus	1e-6	1.0E-6	ultrasonic load time interval

Figure 38. Parameters defined for ultrasonic hydraulic mechanical removal at a micro-hole with 50 μm radius and 200 μm depth machined by EDM+US.

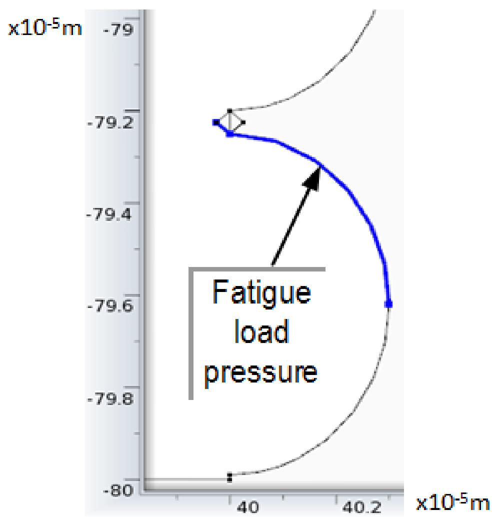

Figure 39. Boundary condition type as ultrasonic pressure fatigue load on one flank of crater profile.

The parameters used for modelling are defined in Figure 38, representing the microgeometry from frontal and lateral working gap resulted from machining of a micro-hole with radius 50 μm and depth 200 μm.

Several types of boundary conditions were adopted: fixed constraint at the inferior part of the workpiece placed on the machine worktable, and a vertical fixing force was used against it. A boundary pressure created by cumulative microjets of 100 MPa in each ultrasonic period, on one flank of the microgeometry peak produced by previous discharges (craters) was considered as a fatigue load, as it is presented in Figure 39.

The fatigue loads oriented along the lateral gap, produced by cumulative microjets stages can contribute to microhole lateral roughness decrease (Figure 40. a) - in limits of ultimate tensile strength at fatigue pulsing cycles [76] - but higher pressure (higher P_{cUS}) can increase the roughness (Figure 40. b), confirmed by experimental data. An optimum value for P_{cUS} has to be determined experimentally; in this case, P_{cUS}=100 W.

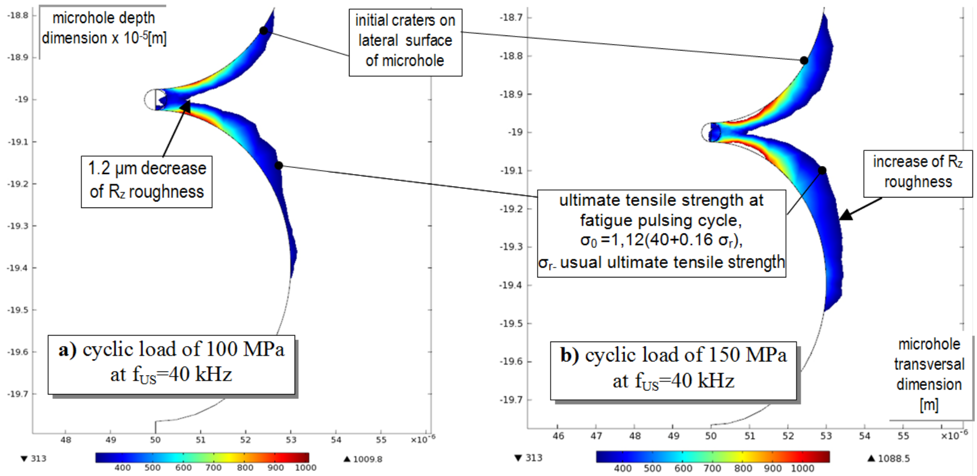

Figure 40. Von Mises stress [MPa] produced by cumulative microjets at EDM+US micro-drilling [77].

In case of relaxation pulses use (flatter craters), P_{cUS} power must be lower with around 30% than in case of commanded pulses (deeper craters) as experimental data presented above indicated. Other models for much bigger microholes, e.g., with radius of 0.49 mm and depth of 1 mm gives similar results concerning the decrease of lateral roughness of the machined surface. But the ultrasonic pressure needed to be applied to the flanks of the microcraters profile was higher [78].

Finite Element Modelling Applied to Ultrasonic Chains Working Simulations

The *sine qua non* conditions of resonance - equality between assemblies of transducer (f_{otr}) and ultrasonic horn (f_{oh}) - mainly in case of complex shape ultrasonic horn, is an intricate and time consuming process, containing several iterative stages (horn dimensional adjustment – own frequency measurement). This is a technologic task, justified on relative great volumes of fabrication, and consequently showing lack of flexibility of EDM+US technology.

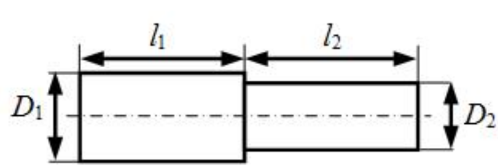

Figure 40. Shape and dimensions of usual cylindrical stepped horn.

But FEM modeling of ultrasonic chains facilitates the resonance condition obtaining. In this chapter, a conic shape horn - leading to low cost manufacturing mainly by conventional machining against other complicated curve profiles - that integrates the tool for the micro-holes is approached.

Coupling FEM with Computer Aided Machining (CAM) of the horn becomes of the utmost interest nowadays; new shapes of ultrasonic horn appropriate for diverse applications are being achieved [79], taking into account the unique character of the horn shape in relation to types of machining [80].

A preliminary dimensioning was carried on for a usual cylindrical stepped horn, standing as entry data for FEM modelling of complex profiled horn, integrating the tool to be axially vibrated during micro-drilling by EDM+US. Some known relations were used.

The upper (l_1) and lower (l_2) steps lengths in case of a cylindrical horn (Figure 40), after Merkulov and Kharitonov [81], are equal with:

$$l_1 = 1.5 / \alpha \text{ [m]}, \tag{23}$$

$$l_2 = 1.6 / \alpha \text{ [m]}, \tag{24}$$

where α is the wave number calculated with relation:

$$\alpha = 2\pi / \lambda \text{[m}^{-1}\text{]}, \tag{25}$$

and λ is the wave length calculated as it follows:

$$\lambda = \frac{c}{f} = \frac{1}{f}\sqrt{\frac{E}{\rho}} \text{ [m]}, \tag{26}$$

where f is the oscillation ultrasonic frequency [Hz]; c - ultrasound velocity within a solid material [m/s]; E - Young's modulus of horn material [Pa], ρ - density of horn material [kg/m^3].

The previous dimensional conditions lead to amplification (K), which is equal with:

$$K = \left(\frac{D_1}{D_2}\right)^2, \tag{27}$$

where: D_1, D_2 are the entry and the output diameter of the stepped horn [m], Figure 40.

The transducer assembly provided by the Institute of Solid Mechanics of the Romanian Academy - IMSAR (Figure 41) has the own series frequency f_{otr}= 40805 Hz – entry data for this application type [82]. Its radiant bush, which joints the concentrator, has output diameter D_b=35 mm. In case of our horn made from 1045 steel, the needed characteristics are: E=2.1x10^{11} Pa, ρ = 7850 kg/m^3. Its entry frequency for calculation was f_{o1}=40.0 kHz, lower than that of the transducer f_{otr}. Therefore, values of physical parameters from the above relations are: λ = 0.1293 m,

α =48.5674 m^{-1}. So, resulted steps lengths are: l_1=30.885 mm; l_2=32.944 mm. The horn entry diameter is D_1= D_b=35 mm.

Comsol Multiphysics with the Structural Mechanics module, and the Eigenfrequency submodule were used for FEM modeling and simulation of a complex ultrasonic horn, which includes the tool and its clamping at the horn end, an antinodal point under conditions of standing waves.

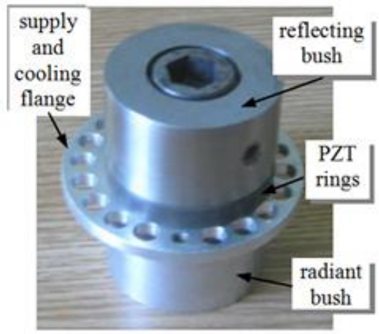

Figure 41. IMSAR 40 kHZ transducer.

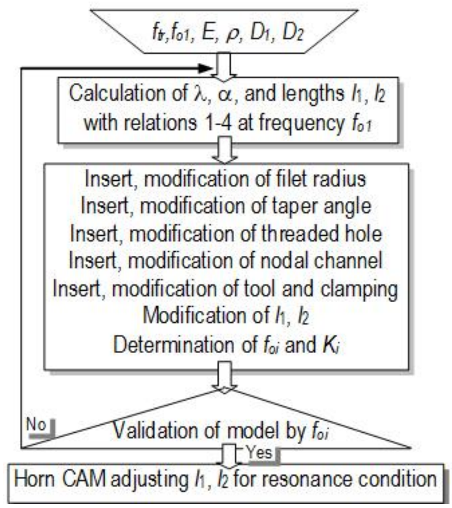

Figure 42. Logical scheme of FEM modeling strategy applied to complex horn with tool integrated.

▾ Parameters

Name	Expression	Value	Description
l1	30.885[mm]	0.03089 m	upper step length
r1	17.5[mm]	0.0175 m	upper step radius
l2	32.944[mm]	0.03294 m	lower step length
r2	10[mm]	0.01 m	lower step radius
rr	r1-r2	0.0075 m	fillet radius at steps jonction
ModulE	2.1e11	2.1E11	1045 steel Young's modulus

Figure 43. Defined parameters for initial stage.

Using FEM modeling strategy, only one constructive parameter of horn geometry was introduced or changed in each stage, aiming at control of its own frequency f_{oi} and amplification K_i, and thus having a permanent feedback.

More than 20 modeling stages of strategy were covered, whose generic logical scheme is presented in Figure 42.

Figure 42. Logical scheme of FEM modeling strategy applied to complex horn with tool integrated.

The modeled horn geometry was created using 2D axis symmetric space, using defined parameters like those presented in Figure 43 for the first stage.

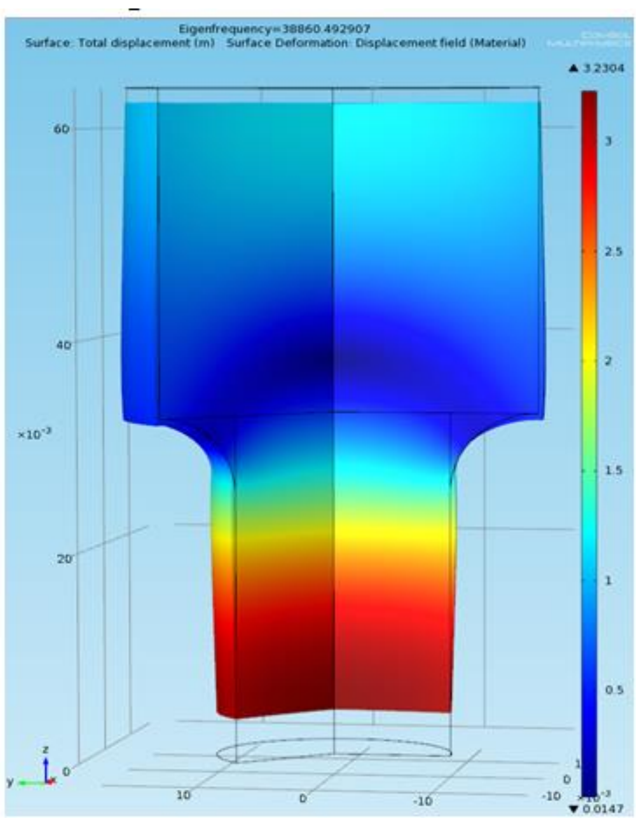

Figure 44. Own frequency and displacements at initial stage.

The needed material properties were provided by Comsol Library and were adjusted for real (measured sound velocity) 1045 steel used for horn and real copper 99.5 for tool.

The physics boundary conditions for horn eigenfrequency were set on free for all geometry limits. The mesh was set on extrafine, with more than 2000 elements for final models and average quality around 0.96 on a 0-1 scale.

In the initial stage, the horn's own frequency, 38.86 kHz, and its amplification, 3.23 (in direct relation with relative displacements) are presented in Figure 44, in correspondence with parameters previously defined. In the next stages, other constructive elements of complex conical shape horn were introduced step by step, like filled radius between exterior surfaces, taper angle, cavities and threaded holes that increased the horn's own frequency. Other elements like nodal channel, tool and threaded stud insertion decreased the horn's own frequency.

In the final stages, for resonance condition, the step lengths were increased: l_1=37.385 mm and l_2=39.444 mm; von Mises stress was decreased at pointed inner surfaces through their radii increase, according to prior running models; the position of the nodal channel was changed to z=48.6 mm, for adjusting displacement of the nodal point due to previous constructive changes (Figure 45).

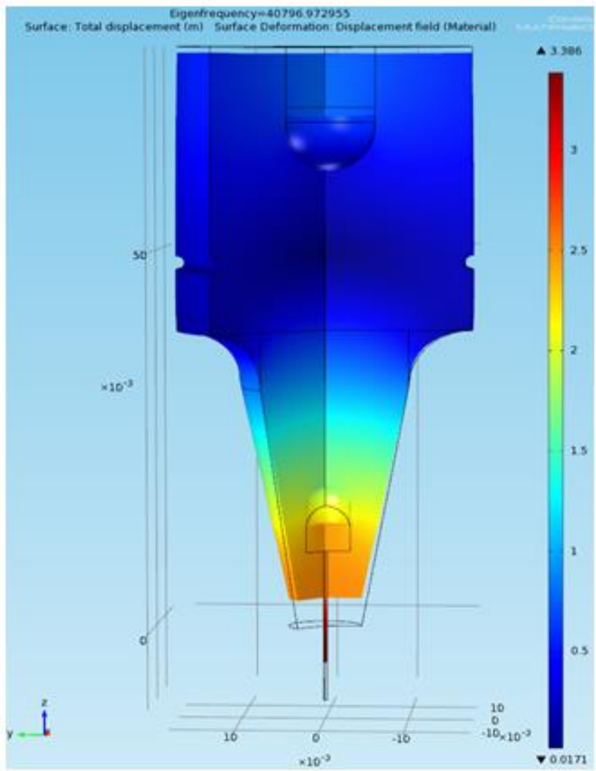

Figure 45. Own frequency and displacements at initial stage.

The strategy of complex horn was finalized through CAM machining its final version resulted from FEM, whose own real frequency proved to be very close under entry frequency f_{otr}= 40805 Hz. Only fine adjustments of step lengths by their reduction were executed for resonance.

FEM results indicated that positioning of clamping elements at the horn end in the antinode point led to proper working of the ultrasonic chain - the tool appropriate for micro-drilling through EDM exerted very low influence on its own frequency of horn assembly. Such CAE-CAM approached strategy proved its capacity to improve flexibility of μEDM+US technology.

Conclusions Regarding Finite Element Modelling Applied to Ultrasonically Aided Electrical Discharge Machining

Some synthetic conclusions are presented below resulting from FEM of material removal mechanism:

- The results of modelling of gas bubble influence are in agreement with experimental data, showing a high increase of ultrasonic contribution to the EDM machining rate and surface quality.
- At classic microEDM, long life duration of gas bubbles from the gap makes boiling the main material removal mechanism with a consequently low machining rate. After bubble collapse, the melted material is long ago resolidified.
- At microEDM+US, in order to take advantage of the shortened bubble life by ultrasonic assistance, the collective bubbles implosion must occur within 0.5 μs from the pulse end. However due to the pressure decrease during stretching semi-period inside the gap, the removed volume grows. This synchronization between discharges and tool elongation could increase the machining rate more than 5 times in comparison with classic EDM.
- A strategic approach can be considered in order to improve the main output technological parameters at micro-electrodischarge machining aided by ultrasonic longitudinal vibrations of the electrode-tool. This is based on Finite Element Analysis results validated through experimental date, consisting mainly of two solutions:

1) Overlapping relative long commanded pulse on cumulative microjets phase, i.e., collective implosion of the gas bubbles from the gap ultrasonically induced in order to remove the material in the melted state;
2) Actuate with optimum value of the acoustic chain to remove material in solid state, i.e., the peaks of microgeometry, but also maintaining the stability of the machining process.

- The correlation between crater dimensions and the machining rate at EDM+US is strongly related to the degree of overlap between pulse time and the cumulative microjets stage. The probability of overlapping gives roughly the increase of machining rate at EDM+US in comparison with EDM. There are also a lot of factors that have influence on this parameter, due to the random character of EDM process that influences the machining rate.
- A relevant model of plasma channel development is very difficult to achieve because this is strongly dependent on the characteristics of the EDM generator, and the profile of discharge energy delivered. The plasma channel radius is dependent not only on pulse time but also on the variation of energy density delivered on the EDM spot.
- From modelling of influence exerted on material removal mechanism by time dependent radii of plasma channel and gas bubbles, it resulted that the first parameter

must be taken into account at microEDM modelling, but the second parameter has to be considered at submicronic machining models.

- FEM modelling of thermal front development emphasized that at classic microEDM, shock heating is produced, most of the crater volume being overheated in the early stage of the discharge. At microEDM+US, any overlap of pulse time on the cumulative microjets stage could be very efficient in terms of machining rate.

SOME INNOVATIVE SOLUTIONS REGARDING THE EQUIPMENT FOR ULTRASONICALLY AIDED EDM

Some innovative solutions were adopted at construction of dedicated equipment for microEDM+US. They are addressing some elements of technological systems: ultrasonic chains, integrating tools or workpieces, clamping devices of ultrasonic chains, orientation of ultrasonic chains and consequently, the relative position between the tool and the workpiece, aiming at assuring precision and machined surface quality.

The device for ultrasonic aiding of wire electrodischarge machining can be easily mounted on any WEDM machine in order to improve: machining rate, precision, and surface quality [83]. Its novelty consists in: vibrations in the deionized water (dielectric liquid) to produce cavitation and not of the wire or workpiece as previous solutions do; shortening the distance between cavitation place and working zone by device leaning for decrease of pressure losses; cavitation occurs within a hopper that allows high acoustic pressure (amplitude) **-** no contact with the wire or workpiece.

The main device elements are presented in Figure 46:

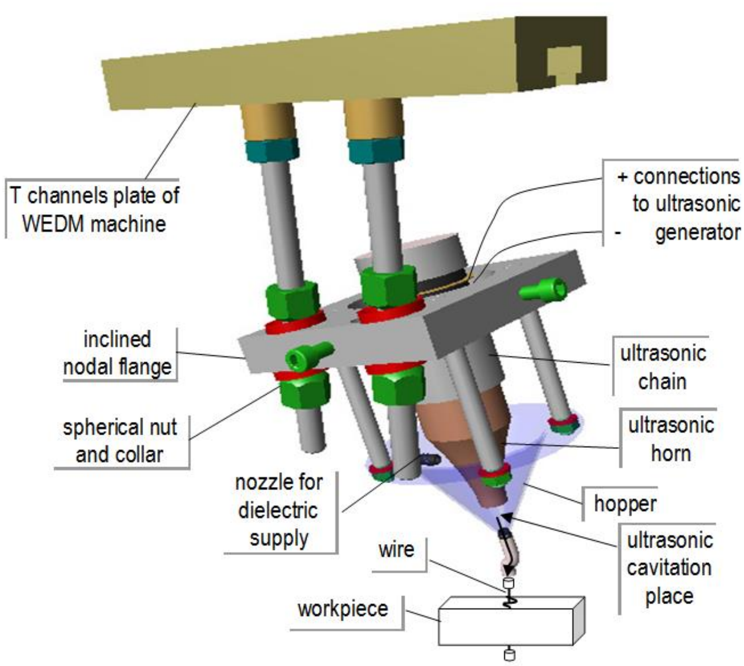

Figure 46. Device for ultrasonic aiding of wire electrical discharge machining.

The novel solutions have the following advantages: precision increase due to good evacuation of particles from the gap through high acoustic pressure ultrasonically induced, thus avoiding instability of the WEDM process; the relative position between the wire and the workpiece is not modified by oscillations since any component of the acoustic chain has no contact with wire – workpiece couple; simple construction with no holes within the acoustic horn, an additional reason to easily get the resonance – equality between frequency of the acoustic horn, with PZT transducer subassembly; device inclination contributes to decrease of pressure losses; quality increase due to cumulative microjets orientation, parallel to machined surface and along the wire; reduction of surface roughness and white layer.

The equipment for ultrasonic aided electrical discharge machining of micro-slots is presented in Figure 47-51 [84]. The main subassemblies are presented in Figure 47. The equipment is easily assembled on any EDM machine, as it can be seen in Figure 48, using T channels plates. In Figure 49, some details are shown of clamping and orientation device of tool ultrasonic chain, achieving inclination, perpendicularity, and angular position of tool. A similar device for the workpiece is presented in Figure 50, which accomplishes the workpiece inclination and perpendicularity. In Figure 51, the device for the high pressure dielectric supply is presented.

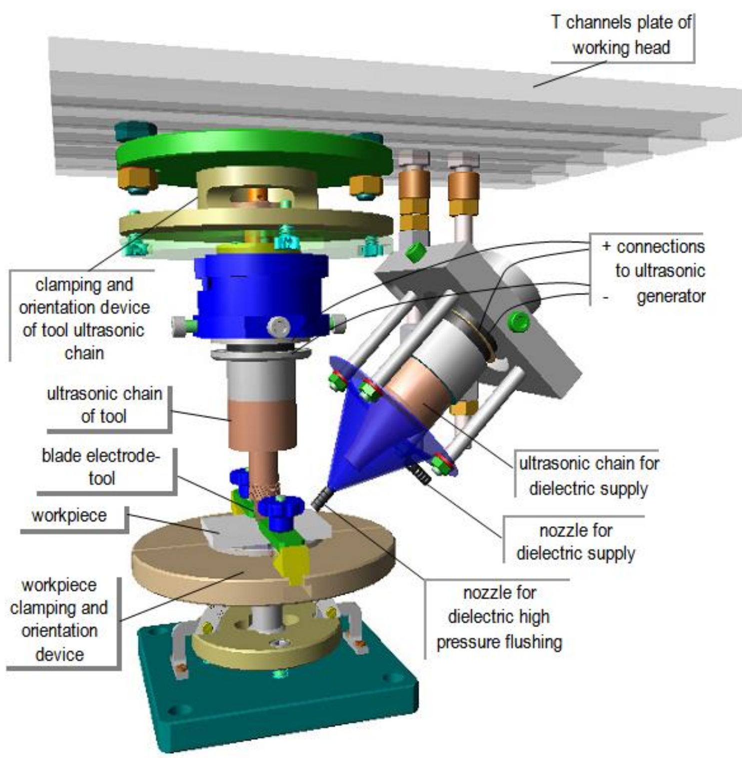

Figure 47. The main subassemblies of equipment for ultrasonic aided electrical discharge machining of micro-slots.

When machining microslots under classic conditions, EDM instability occurs due to a very narrow working gap. Ultrasonic aiding, through high pressure of dielectric supply due to ultrasonic cavitation, improves removed particles evacuation from the gap reducing short-circuits, and consequently the main technological parameters, mainly machining rate and surface quality. Its specific construction leads to several advantages: under some optimization conditions of working parameters, it can increase the machining rate up to 500% compared to classic EDM; no holes for flushing inside the workpiece or electrode-tool is needed; achieving great inclination of pierced and unpierced micro-slots; adjusting perpendicularity and angular position of the electrode-tool relative to the workpiece.

Figure 48. The equipment for ultrasonic aided electrical discharge machining micro-slots on ELER 01 machine.

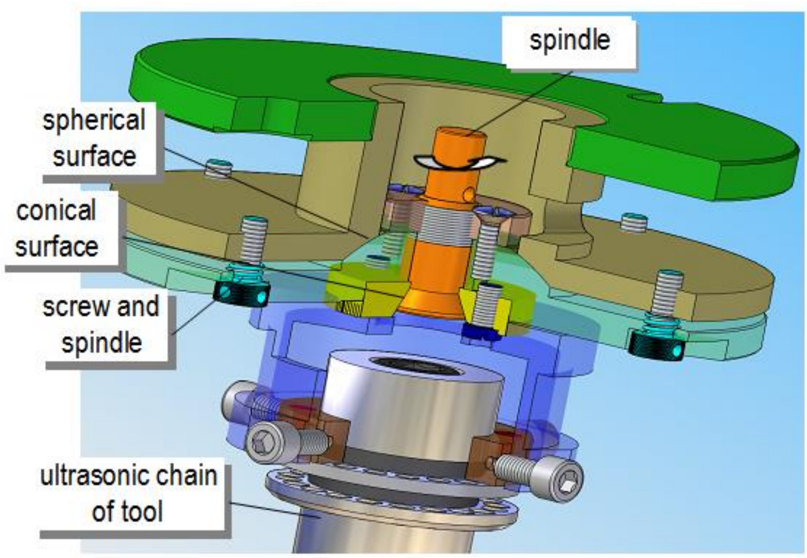

Figure 49. The details of clamping and orientation device of tool ultrasonic chain.

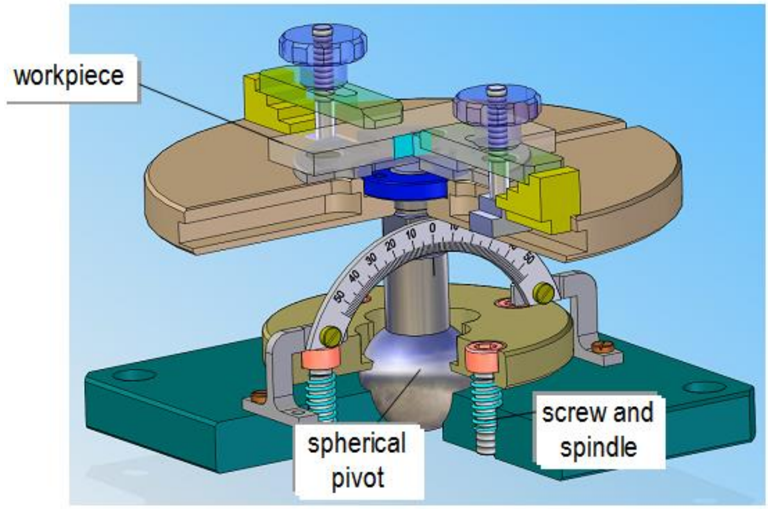

Figure 50. The details of clamping and orientation device of workpiece.

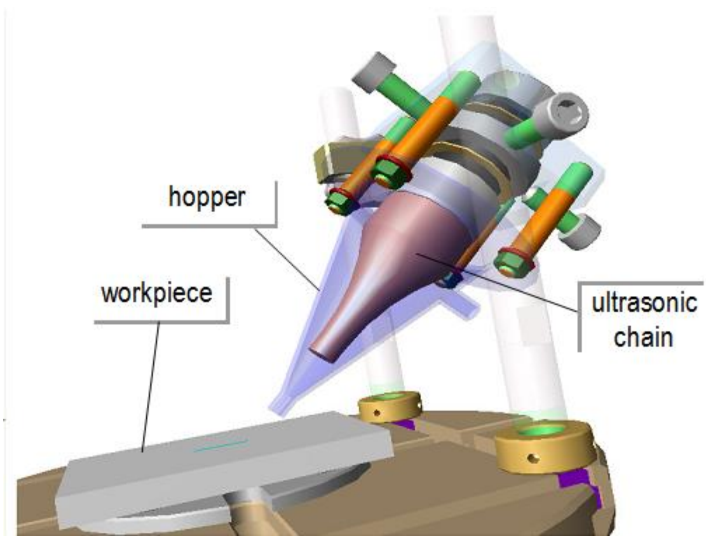

Figure 51. The device for high-pressure dielectric supply.

The novelty of equipment consists in: cumulating the effects produced by vibrations of ultrasonic chain including the electrode-tool and of ultrasonic chain for dielectric supply action at workpiece level; high-pressure supply of dielectric liquid within working zone through cavitational effect produced by an ultrasonic chain that vibrates within a hopper; simultaneous inclination and rotation both of the blade electrode-tool and the workpiece.

The variant of equipment appropriate for EDM+US deep micro-slots is presented in Figure 52-54 [85]. The main subassemblies of the equipment are show in Figure 52. Taking into account the susceptible deformations of the blade electrode-tool during the machining process, a guiding subassembly is conceived (Figure 53), comprising two semi-skates with low friction coefficient, and channels for lateral flushing.

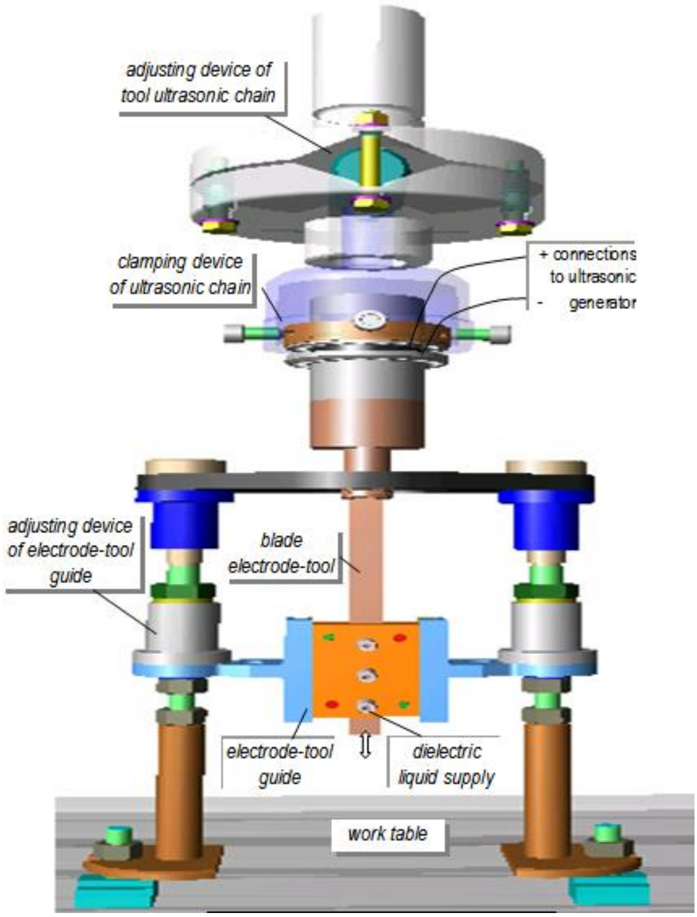

Figure 52. The main subassemblies of equipment for ultrasonic aided electrical discharge machining deep micro-slots.

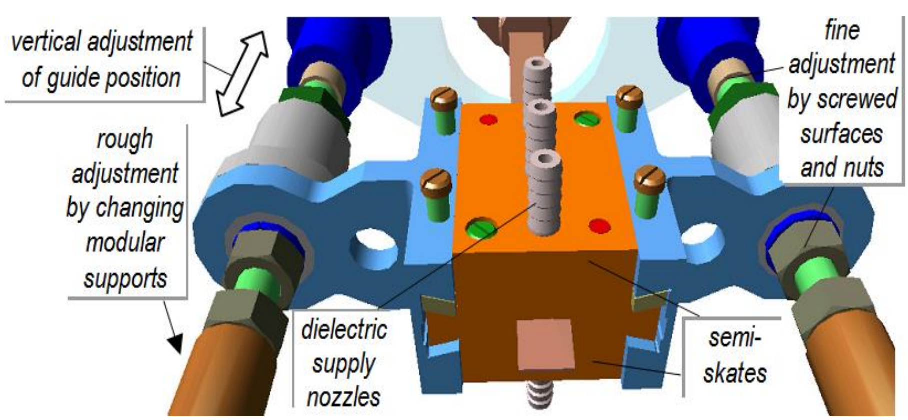

Figure 53. The details of tool guiding subassembly.

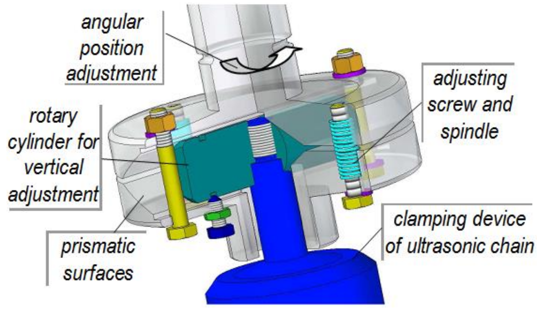

Figure 54. The details of device for orientation of ultrasonic chain.

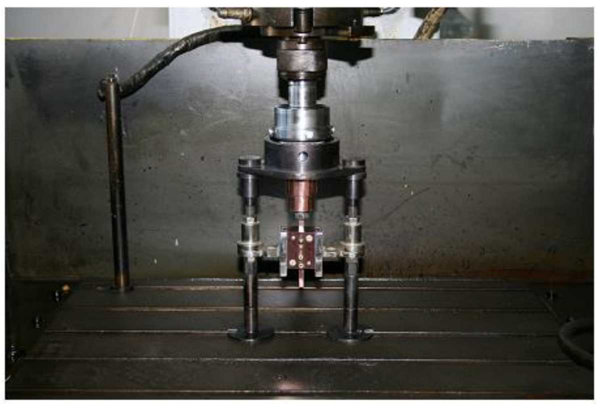

Figure 55. The equipment for ultrasonic aided electrical discharge machining, deep micro-slots on ELER 01 machine.

The guide position of the tool-electrode guide can be roughly and finely adjusted in a vertical direction in order to obtain the optimum position of the tool against the machined surface.

The details concerning adjusting device of ultrasonic chain containing the tool is presented in Figure 54. Thus, the angular position as well as the vertical position of the electrode-tool can be achieved, assuring the needed micro-machining precision.

The equipment can be easily assembled on any EDM machine as it is presented in Figure 55. The construction of equipment led to some advantages: machining deep micro-slots without the necessity of providing holes for dielectric flushing inside the workpiece of the electrode-tool; growing machining precision, mostly at great depths, by passing the electrode-tool through the guiding assembly above or beneath the workpiece; appropriate flushing with dielectric liquid of the lateral side of the electrode-tool, through several flushing holes achieved inside the guide; it assures the adjustment of perpendicularity of longitudinal axis of the blade shaped electrode-tool against the frontal surface of the machined workpiece, and the angular position of the electrode-tool in the frontal plane of the machined workpiece.

In conclusion, several patented solutions were presented regarding micro-EDM+US technological systems.

The critical elements of these types of equipment address two main issues: ultrasonic chain and tool-guiding. Ultrasonic chains are introduced in equipment constructions in order to assure ultrasonic longitudinal oscillations of the electrode-tool, and high pressure of the dielectric supply in the working gap due to the ultrasonically induced cavitational effect. Since the electrode-tool is subjected to deformations affecting the precision of micro-machining, the adopted solutions aim at electrode-tool guiding, and precise orientation of both the electrode-tool and the workpiece.

REFERENCES

[1] Masuzawa, T., Tonshoff, H.K., (1997). Three-dimensional micromachining by machine tools. *Annuals of the CIRP* 46(2), 621-628.

[2] Yatsui, T., Hirata, K., Nomura, W., Tabata, Y., Ohtsu M., (2008). Realization of an ultra-flat silica surface with angstrom-scale average roughness using nonadiabatic optical near-field etching. *Applied Physics B* 93(1), 55-57.

[3] Marinescu, N.I, Ghiculescu, D., (2005). Electrochemical Machining Technologies and Connected Processes. Treatise (in Romanian), Printech, ISBN 973-718-380-0, Bucharest.

[4] Marinescu, N.I,, Chivu, C., Ghiculescu, D., Herman, R., Ivan, M., Marinescu, R. D., Măniuț, P., Nanu, A., Nanu, D., Obaciu, Gh., Pisarciuc, C., Popa, L., Sârbu, F.A., Țîțu, M., (2006). Treatise of Nonconventional Technologies (in Romanian), Vol IV, Electrochemical Machining, Printech, ISBN 973-718-613-3, Bucharest.

[5] Obaciu, Gh, Klocke, F., Marinescu, N.I., Ivan, M., Sarbu, F., Ghiculescu, D., (2009). Metallic Materials Machining by Electrochemical Erosion, Transilvania University of Braşov, ISBN 978-973-598-499-1.

[6] Pokropivny, V., Lohmus, R., Hussainova, I., Pokropivny, A., Vlassov, S., (2007). Introduction to Nanomaterials and Nanotechnology, Tartu University Press, ISBN 978-9949-11-741-3.

[7] Kavtaradze, O., Lipceanski, A., (1989). Research of hydrodynamics process mechanisms in working gap under influence of ultrasonic oscillations applied on tool. *Electronnaia Obrabotka Materialov,* p. 52-54.

[8] Kremer, D., Lhlaubet, C., Moisan, A., (1991). A study of the effect of synchronizing ultrasonic vibrations with pulses in EDM. Available from: http:// http:// www.cirp.net/ Accessed: 2008-05-25.

[9] Sundaram, M., Pavalarajan, G., Rajurkar, K., (2006). A Study on Process Parameters of Ultrasonic Assisted Micro EDM Based on Taguchi Method, Available from: http:// www.springerlink.com/content/ Accessed: 2008-05-25.

[10] Ghiculescu, D., (2004). Nonconventional Machining (in Romanian), Printech, ISBN 973-652-975-4, Bucharest,

[11] Ghiculescu, D., Marinescu, N.I., Jitianu, G., Seritan, G., (2009). On precision improvement by ultrasonics-aided electrodischarge machining. Estonian Journal of Engineering, p. 24-33, ISSN 1736-7522 (electronic), ISSN 1736-6038 (print).

[12] Van Dijck, F., Snoeys, R., (1975). Theoretical and Experimental Study of the Main Parameters Governing the Electrodischarge Machining Process. *Mecanique* 301-302, 9-16.

[13] Marinescu, N.I, Amza, Gh, Deaconescu, A. Deaconescu, T., Ghiculescu, D., Herman, R., Lăcătuș, E., Mălaimare, G., Nanu, A., Nanu, D., Oancă, O., Obaciu, Gh., Popa, L., Safta, V.I., Safta, V. Ionel, Tulcan, L., (2004). Treatise of Nonconventional Technologies (in Romanian), Vol. VIII, Machining by erosion with ultrasonic waves, Bren, ISBN 973-648-385-1, Bucharest.

[14] Anton, I., (1984). Cavitation (in Romanian), Vol. 1, 2, Romanian Academy.

[15] Isuzugawa, K., Tsuji, M., Horiuchi, M., (1989). High-Speed Photographic Study of Spark-Induced Shock Waves in Water. ISEM 9, 289-292.

[16] Mohri, N., Suzuki, M., Furuya, M., Saito, N., (1995). Electrode Wear in Electrical Discharge Machining. *Annals of the CIRP* 44(1), 165-168.

[17] Suzuki M., Mohri, N., Saito, N., Ozaki Y., (1992). Thermal Machinability and Electrode Wear Material in EDM. *Proceedings of the 2nd International Conference on Die & Mould Technology*, p. 403-412.

[18] Schulze, H.-P., Wollenberg, G., Herms, R., Mecke, K., (2004). Gas bubble morphology in small working gaps at spark erosion. Annual report Conference on Electrical Insulation and Dielectric Phenomena, Boulder, Colorado, USA, 16-20, October, p. 534 – 537.

[19] Schulze, H.-P., Wollenberg, G., Mecke, K, Trautmann, H.-J., (2006). Propagation of Gas Bubble at Spark Erosion in Small Working Gap. IEEE Proceeding of ICPADM 2006, Bali, Indonesia, p. 665-668.

[20] Ghiculescu, D., Schulze, H.P., Marinescu, N., (2009). Comparison between gas bubble life duration at classic and ultrasonic aided edm finishing. *Academic Journal of Manufacturing Engineering* 7(4), 63-68.

[21] Van Dijck, F., Dutré, W., (1974). Heat conduction model for the calculation of the volume of molten metal in electric discharges, Available at: http://http://www.iop.org/EJ/ Accessed: 2008-05-25.

[22] Kojima, H., Kunieda, M., Nishiwaki, N., (1992). Understanding Discharge Location Movements During EDM, ISEM X, p. 144-149, Magdeburg, Germany.

[23] Ydreskog, L., Novak, A., (1989). A Method for EDM Spark Location Detection, Proceedings of ISEM IX, p. 297-300, Nagoya, Japan.

[24] Fuzhu, H, Grangure, P., Kunieda, M., (2008). Improvement in accuracy in potential method for detecting EDM spark locations. *Journal of Materials Processing Technology* 206(1-3), 328-332.

[25] Ghiculescu, D., (2013). Computer Aided Engineering and Manufacturing in the Field of Nonconventional Machining (in Romanian), Printech, ISBN 978-606-521-971-7, Bucharest.

[26] Ghiculescu, D., Marinescu, N.I., Nanu, S. Ghiculescu, Daniela, Kakarelidis, G., (2010). The effect of polarity studied by finite element method at ultrasonic aided micro-electrodischarge machining. Nonconventional Technology Review, no. 4, p. 23-28, ISSN 1454-3087.

[27] Ghiculescu, D., Marinescu, N. I., Popa, L., (2003). Specific Aspects of Surface Microgeometry at Classic EDM Finishing and Aided by Ultrasonics. *Nonconventional Technologies Review*, no. 2, ISSN 1454-3087, p. 10-14.

[28] Ghiculescu, D., Marinescu, N. I., (2001). Atenuation of Capacity Effect at EDM Finishing with Relaxation Generators by Ultrasonic Aiding of Machining Process.

International Conference – TEHNOMUS XI, ISBN 973-9408-95-8, ISBN 973-9408-96-6, p. 433-436, Suceava.

[29] Ghiculescu, D., Marinescu, N.I., Nanu, S. Ghiculescu, Daniela, Kakarelidis, G., (2010). FEM study of synchronization between pulses and tool oscillations at ultrasonic aided microelectrodischarge machining. Nonconventional Technology Review, nr. 3, p. 19-25, ISSN 1454-3087.

[30] Ghiculescu, D., Marinescu N.I, Nanu, S., (2014). Innovative solutions for performances increase at micro-electrical discharge machining aided by ultrasonics. Nonconventional Technologies Review, ISSN: ISSN 2359 – 8646; ISSN-L 2359 – 8646, Vol. XVIII, Nr. 4, p. 9-14.

[31] Ghiculescu, D., Marinescu, N.I., (2009). Gaseous phenomena from the working gap influencing machining rate at ultrasonic aided EDM. Nonconventional Technology Review, nr. 2, p. 36-39, ISSN 1454-3087.

[32] Ghiculescu, D., Marinescu, N.I., **(**2009). Cavitational phenomena and fem modelling at ultrasonic aided EDM. Comparison with classic EDM. Nonconventional Technology Review, nr. 1, p. 11-18, ISSN 1454-3087.

[33] Ghiculescu, D., Marinescu, N. I., (2002). Secondary Cavitational Phenomena Favorizing Finishing Process at Electrodischarge Machining Aided by Ultrasonics. *Revista de tehnologii neconvenţionale*, nr.1, ISSN 1454-3087, p. 32-35.

[34] Ghiculescu, D., Marinescu N.I., Nanu S., Ghiculescu Daniela, (2013). Some aspects of finite element modelling of micro-EDM and ultrasonic EDM with time dependent radius of plasma channel. Nonconventional Technologies Review, No. 2, June, p. 30-35, ISSN 1454-3087.

[35] Ghiculescu, D., Marinescu N.I, Varga, G., Nanu, S., (2014). FEM study of thermal front dynamics at micro-electrical discharge machining aided and not aided by ultrasonics. Nonconventional Technologies Review, ISSN: ISSN 2359 – 8646; ISSN-L 2359 – 8646, Vol. XVIII, Nr. 3, p. 43-48.

[36] Alupei-Cojocariu O. D., Ghiculescu, D., (2014). Computer aided machining of an acoustic horn for ultrasonically aided EDM. Nonconventional Technologies Review, ISSN: ISSN 2359 – 8646; ISSN-L 2359 – 8646, Vol. XVIII, Nr. 4, p. 21-26.

[37] Ghiculescu, D., Marinescu N.I, Varga, G., Nanu, S., (2014). Determination by FEM of ultrasonic horn profile for vibrating the workpiece at EDM assisted by ultrasonics. Nonconventional Technologies Review, ISSN: ISSN 2359 – 8646; ISSN-L 2359 – 8646, Vol. XVIII, Nr. 4, p. 61-66.

[38] Getman, I., Lopatin, S., (2000). Matching of series and parallel resonance frequencies for ultrasonic piezoelectric transducers. Applications of Ferroelectrics, 2000. ISAF 2000. Proceedings of the 2000 12th IEEE International Symposium, Vol. 2, p. 713 – 715.

[39] Rajurkar, K.P., et al., (2006). Micro and nano machining by electro-physical and chemical processes, CIRP Annals – Manufacturing Technology 55(2), 643–666.

[40] Yan, B.H. et al., (1999). Micro-hole machining of carbide by electric discharge machining. *Journal of Materials Processing Technology* 87, 139–145.

[41] Zhang, C. et al., (2000). Precision shaping of small diameter wheels using micro electric discharge truing and holemachining of Al_2O_3 material. *International Journal of Machine Tools & Manufacture* 40, 661–674.

[42] Uhlmann, E., Reohner, M., Langmack, M., (2010). Micro EDM in Qin Yi, Micromanufacturing Engineering and Technology, Elsevier.

[43] Marinescu, R.D., Marinescu, N.I. Purcarea, A., Danalache, F., Ghiculescu, D., (2005). Management in Micro and Nanotechnologies (in Romanian), Printech, Bucharest.

[44] Uhlmann, E., Piltz, S., Doll, U., (2005). Machining of micro/miniature die and moulds by electrical discharge machining – recent development. *Journal of Materials Processing Technology* 167(2-3), 488-493.

[45] Ghiculescu, D., Marinescu, N.I., Nanu, S. Ghiculescu, Daniela, Kakarelidis, G., (2011). Finite element method study on machined shape influence at ultrasonic aided and not aided microelectrodischarge machining. Nonconventional technology Review, nr. 3, p. 33-40, ISSN 1454-3087.

[46] Uhlmann, E., Sascha, P., Schauer, K., (2001). Micro milling of sintered tungsten–copper composite materials. *Journal of Materials Processing Technology* 167(2–3), 402–407.

[47] Koch, O. et al., (2001). Recent progress in micro-electro discharge machining technology – Part 1, Proceeding of the 13th International Symposium for Electro machining ISEM XIII, Bilbao, Spain.

[48] Piltz, S., Grundlagen und Prozessstrategien der Mikrofunkenerosion für die Bearbeitung von Rotationsbauteilen, Fraunhofer IRB Verlag, Stuttgart, 2007.

[49] Van Dijck, F., Snoeys, R., (1975). Theoretical and Experimental Study of the Main Parameters Governing the Electrodischarge Machining Process. *Mecanique*, 301-302, 9-16.

[50] Uhlmann, E., Piltz, S., Doll, U., (2005). Machining of micro/miniature die and moulds by electrical discharge machining – recent development. Journal of Materials Processing Technology, Elsevier.

[51] Ghoreishi, M. M., Atkinson, J., (2001). Vibro-rotary electrode, a new technique in EDM drilling – performance evaluation by statistical modelling and optimisation, Proc. of ISEM XIII, Bilbao, Spain, Vol. II, May 9–11.

[52] Muttamara, A., et al., (2003). Probability of precision machining of insulating Si3N4 ceramics by EDM. *Journal of Materials Processing Technology* 140(1-3), 243-247.

[53] Serepot, V. I., Rudaia, I. D., **(**1990). Method of Electrodischarge Machining Aided by Ultrasonic Vibrations. Electronnaia Obrabotka Materialov 2, 90-92.

[54] Marinescu, N.I., Ghiculescu, D., (2011). Nanu, S. Ghiculescu, Daniela, Kakarelidis, G., Technological parameters comparatively studied by fem at classic and ultrasonic aided microelectrodischarge machining. Nonconventional Technology Review, nr. 3, p. 51-56, ISSN 1454-3087.

[55] Higuchi, T., et al, (1991). Development of pocket-sized electro-discharge machine. Annals of the CIRP 40, 203-206.

[56] Takahata, K., Gianchandani Y.B., (2001). Batch mode micro-EDM for high-density and high throughput micromachining. *Proceedings of the IEEE: MEMS*, p. 72-75.

[57] Takahata, K., Gianchandani, Y.B., (2002). Batch mode micro-electro-discharge machining. *Journal of MEMS* 11(2), 102-110.

[58] Weng, F.-T., Her, M.-G., (2002). Study of the batch production of micro parts using the EDM process. *International Journal of Advanced Manufacturing Technology* 19, 266-270.

[59] Huang, H. et al., (2003). Ultrasonic vibration assisted electro-discharge machining of microholes in Nitinol. *J. Micromech. Microeng.* 13, 693-700.
[60] Hung, J.-C. et al., (2006). Using a helical micro-tool in micro-EDM combined with ultrasonic vibration for micro-hole machining. *J. Micromech. Microeng.* 16, 2705-2713.
[61] Yong, L., et al., (2002). Research of micro electrodischarge machining equipment and process techniques. *Chinese Journal of Mechanical Engineering* 15(2), 177-181.
[62] Wolf, A., et al., (1998). Application of new actuator and vision control systems for micro electro discharge machining. Proceedings of the SPIE, p. 149-158.
[63] Ghiculescu, D., Marinescu, N. I., Jitianu, Gh., Jiga, G., (2010). Finite element analysis of gas bubble influence on ultrasonic aided electrodischarge machining, Proceedings of the 7th International Conference of DAAAM Baltic Industrial Engineering, Edited by: Kyttner, R., Vols. 1 and 2, ISBN: 978-9985-59-982-2, p. 177-182.
[64] Ghiculescu, D., Marinescu, N. I., Nanu, S., (2008). Influence of macro and microgeometry machined surface on ultrasonic aided electrodischarge machining. *International Journal of Material Forming* 1, 1339-1342.
[65] Ghiculescu, D., Marinescu, N. I., Nanu, S. Ghiculescu Daniela, (2012). Multiphysics 3D Finite Element Modelling of Microelectrodischarge Machining Aided by Ultrasonics. Nonconventional Technologies Review 2, 72-77, ISSN 1454-3087.
[66] Ghiculescu, D., Marinescu N.I, Varga, G., Nanu, S., (2014). FEM study of thermal front dynamics at micro-electrical discharge machining aided and not aided by ultrasonics. Nonconventional Technologies Review, ISSN: ISSN 2359 – 8646; ISSN-L 2359 – 8646, Vol. XVIII, Nr. 3, p. 43-48.
[67] Ghiculescu, D., Marinescu N.I., Nanu S., Ghiculescu Daniela, (2013). Some aspects of finite element modelling of micro-edm and ultrasonic EDM with time dependent radius of plasma channel. Nonconventional Technologies Review, No. 2, June, p. 30-35, ISSN 1454-3087.
[68] Patel, R., Barrufet, A., Eubank, T., DiBitonto, D., (1989). Theoretical models of the electrical discharge machining process-II: the anode model. *Journal of Applied Physics* 66, 4104-4111.
[69] Eubank, P. T., Patel, M. R., Barrufet, M. A., Bozkurt B., (1993). Theoretical models of the electrical discharge machining process-III. The variable mass, cylindrical plasma model. *Journal of Applied Physics* 73(11), 7900 – 7909.
[70] Shuvra, D., Mathias, K., Klocke, F., (2003). EDM simulation: finite element-based calculation of deformation, microstructure and residual stresses. *Journal of Materials Processing Technology* 142, 434-451.
[71] Marafona, J., Chousal, J.A.G., (2006). A finite element model of EDM based on the Joule effect. *International Journal of Machine Tools and Manufacture* 46(6), 595-602.
[72] Salonitis, K., Stournaras, A., Stavropoulos P., Chryssolouris G., (2009). Thermal modelling of the material removal rate and surface roughness for die-sinking EDM. *International Journal of Advanced Manufacturing Technology* 40(3-4), 316-323.
[73] Vishwakarma, U. K., Dvivedi, A., Kumar, P., (2012). FEA Modeling of Material Removal Rate in Electrical Discharge Machining of Al6063/SiC Composites. *International Journal of Mechanical and Aerospace Engineering* 6, 398-403.
[74] Khan, A.A., (2011). Role of Heat Transfer on Process Characteristics during Electrical Discharge Machining. Developments in Heat Transfer, Editor M. A. Santos Bernardes.

[75] Inoue, K., (1977). Fundamental of Electrical Discharge Machining, Society of Non – Traditional Technology, Tokyo.

[76] Drobota, V., (1982). Resistance of Materials (in Romanian). Didactic and Pedagogical.

[77] Ghiculescu, D., Marinescu, N. I., Ghiculescu Daniela, Nanu, S., (2013). Aspects of Finite Element Analysis of Microdrilling by Ultrasonically Aided EDM and Related Knowledge Management. Applied Mechanics and Materials, ISSN: 1660-9336, ISBN: 978-3-03785-786-1, Vol. 371, p. 215-219, 17th International Conference on Innovative Manufacturing Engineering, May 23-24.

[78] Ghiculescu, D., Marinescu, N. I., Klepka T., and Carutasu N., (2015). On correlation of pulses and tool elongations at micro-electrical discharge machining aided by ultrasonics. Applied Mechanics and Materials, ISSN: 1660-9336, I, 19th International Conference on Innovative Manufacturing Engineering, May 23-24.

[79] Dudás, I., Kyusojin, A., Varga, Gy., Isobe, H., Oravecz Cs., (2004). Experimental Examination of Propagation of Longitudinal Deformation of Different Shapes of Horn Used at Ultrasonic Machining, 11th International Conference on Tools, Univ. of Miskolc, 09-11, p. 317-324,

[80] Nad, M., (2010). Ultrasonic horn design for ultrasonic machining technologies. Applied and Computational Mechanics 4, 79–88.

[81] Astashev, V.K., Babitsky, V. I., (2007). Ultrasonic processes and machines: dynamics, control and applications, Springer.

[82] Getman, I., Lopatin, S., (2000). Matching of series and parallel resonance frequencies for ultrasonic piezoelectric transducers. Proc. of the 12th IEEE International Symposium, 2, p. 713 – 715.

[83] Ghiculescu, D., Marinescu, N.I., Nanu, S., (2010). Device for ultrasonic aiding of wire electrical discharge machining, RO-123017 Patent.

[84] Ghiculescu, D., Marinescu, N.I., Nanu S., (2012). Equipment for ultrasonic aided electrical discharge machining of micro-slots, RO-126191 Patent.

[85] Ghiculescu, D., Marinescu, N.I., Nanu, S., (2013). Equipment for ultrasonic aiding electrical discharge machining deep microslots, RO-125516 Patent.

In: Electrical Discharge Machining (EDM)
Editor: M. P. Jahan
ISBN: 978-1-63483-591-6

Chapter 6

HYBRID MICRO-EDM/ECM AND ITS APPLICATIONS FOR FABRICATION OF COMPLEX 3D MICRO-STRUCTURES

Minh Dang Nguyen*, Mustafizur Rahman and Yoke San Wong
Department of Mechanical Engineering,
National University of Singapore, Singapore

ABSTRACT

This chapter introduces multiple approaches combining micro-EDM and micro-ECM as hybrid machining to reap the advantages of both processes. Firstly, brief fundamentals of micro-EDM and micro-ECM are shown together with their advantages and challenges. Secondly, multiple attempts to combine them as sequential machining processes to reap both of their advantages are presented. The next section continues with the presentation of a recent approach to combine micro-EDM and micro-ECM in same machining process by using low-resistivity deionized water. Key machining parameters are also characterized for this method. The chapter ends with some applications of hybrid micro-EDM and micro-ECM milling process for fabrication of 3D micro-structures which entail both high dimensional accuracy and good surface finish.

Keywords: Micro-EDM, micro-ECM, hybrid machining

INTRODUCTION

The demands of micro-features and micro-shapes coming from electronics, medical applications, and aviation industries are increasing rapidly [1]. Miniaturization is a vital direction to create smaller and lighter products.

* Corresponding author: Minh Dang Nguyen. Department of Mechanical Engineering, National University of Singapore, Singapore 117576. E-mail: dang@alumni.nus.edu.sg.

The applications widely range from micro-holes for fiber optics, micro-nozzles for jet engines to mold and die for micro-fluidic devices and so on [2]. Therefore, well-established machining processes have been improving to meet the higher requirements for these applications [3]. Special manufacturing processes such as photolithography, focus-ion-beam, and electron-beam-lithography have been demonstrated to be capable of fabricating microstructures. However, such technologies require high expenditure for equipment and routine maintenance activities [4, 5]. On the other hands, many attempts have been made by researchers to develop low-cost machining processes for micro and nano-machining applications. Conventional metal cutting processes such as turning, milling, and grinding could generate surfaces with nano-finish.

Nevertheless, for micro and nano-structures fabrication, sizes of cutting tools as well as machining shapes are limited due to the existence of cutting forces during machining, which is the result of material shearing [3]. Amongst the tool-based machining processes, micro-EDM and micro-ECM emerge to be more effective for micro and nano-machining due to the fact that the cutting force is negligible [6, 7]. During machining, the electrode and workpiece are separated by a fine gap. They are non-contact machining processes so very fine electrode could be used to fabricate intricate micro-shapes and features [8, 9].

Each of these two machining processes has its own advantages as well as limitations. One primary disadvantage of micro-EDM is high surface roughness whereas relatively lower material removal rate and poorer dimensional accuracy are main drawbacks of micro-ECM.

However, surface finish and machining accuracy are both of prime importance for micro-features and products. Hence, there is a need to associate these two processes to reap their strengths and eliminate their adverse effects. This chapter introduces the recent advances of hybrid micro-EDM/ECM and its application for fabrication of complex 3D microstructures.

FUNDAMENTALS

Micro-EDM

EDM is an electro-thermal machining process in which the electro-erosion phenomenon is exploited to remove material from workpiece [10]. During machining, a series of discrete electric discharges is precisely controlled to occur in the fine gap between the electrode and workpiece, which are immersed in dielectric fluid, as illustrated in Figure 1. Each discharge removes a small material amount, forming a discharge crater on the machined surface.

Micro-EDM is the development of EDM for micro-machining [8]. The mechanism of micro-EDM is similar to EDM. However, there are some modifications of EDM to make it suitable for micro-machining. Firstly, micro-EDM is used for fabricating micro-shapes so the electrode used has smaller size (less than 500μm).

Secondly, the discharge energy is lowered (< 100μJ) to reduce the crater size and thus the unit material removal per discharge [7, 11]. For that reason, the RC-type pulse generator is more preferable for micro-EDM because it yields short pulse duration and relatively constant pulse energy [12]. Lastly, more precise movement mechanisms are required to improve the dimensional accuracy [7, 10]. Micro-EDM has wide range of applications, from drilling simple micro-holes to fabricate intricate features of micro-molds and dies [11].

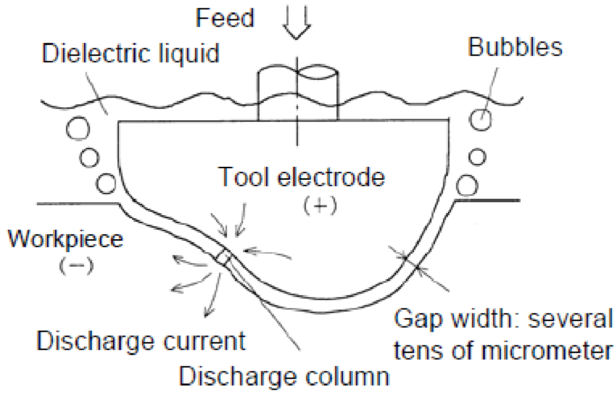

Figure 1. Basic concept of electric discharge machining processes [10].

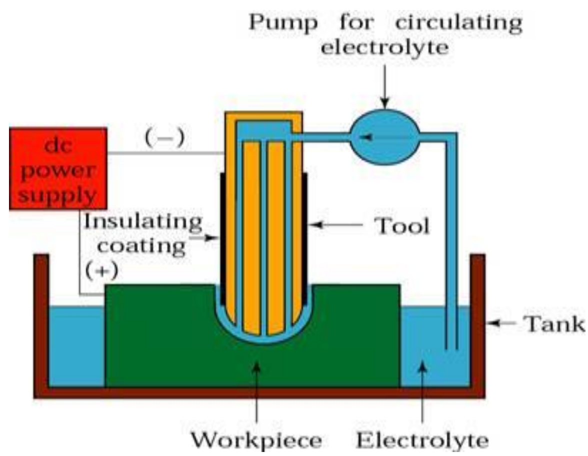

Figure 2. Basic concept of electrochemical machining process [14].

Table 1. Capabilities of micro-EDM [12]

Micro-EDM variant	Geometric complexity	Minimum feature size	Maximum aspect ratio	Surface quality R_a (µm)
Drilling	2D	5 µm	~ 25	0.05 – 0.3
Die-sinking	3D	~ 20 µm	~ 15	0.05 – 0.3
Milling	3D	~ 20 µm	~ 10	0.5 – 1
WEDM	2 ½ D	~ 30 µm	~ 100	0.1 – 0.2
WEDG	Axi-sym.	3 µm	30	0.8

Generally micro-EDM can be classified into five major types of which the capabilities are summarized in Table 1.

Micro-ECM

Electrochemical machining is a material removal process which makes use the dissolution of metal during the electrolysis of electrochemical cell [13]. An illustration of electrochemical machining process is shown in Figure 2.

When a voltage is applied across the anode and cathode immersed in the electrolyte, a current passes through them because the electrolyte acts as a current carrier [14]. The anode is dissolved and the shape of workpiece is approximately the negative image of the tool [15].

The mechanism of micro-ECM is also similar to ECM. However, the dissolution zone must be localized in micro-ECM to assure the dimensional accuracy [7]. As a result, it also requires some modifications such as using smaller electrode size, applying ultra short voltage pulses, lower current and voltage to meet that requirement [9, 15].

In general, micro-ECM can be categorized into four main types [12]:

- Micro-ECM drilling [16]
- Micro-ECM using mask [17, 18]
- Micro-ECM milling [19]
- Die-sinking micro-ECM

Performances of Micro-EDM and Micro-ECM

Table 2 summaries the key advantages and disadvantages of micro-EDM against micro-ECM. These characteristics mainly come from the material removal mechanism of each process. During machining by micro-EDM, material is removed by vaporization and melting. As a result, the machined surface is made up with thermally-damaged layers consisting of the white layer and the heat-affected zones, as can be seen in Figure 3 [20-22]. Micro-cracks and residual stresses are also observed in these distinctive layers [23-26]. Consequently, the fatigue strength of the product is highly reduced. Besides, after each discharge, a small amount of material is removed forming a crater on the surface. The generated surface is thus covered by multiple overlapping discharged craters [27-29]. Therefore, the surface machined by EDM usually has high surface roughness due to its asperity. The topography and roughness of machined surface is mainly constituted by the crater size which is mainly dependent on the discharge energy [30]. On the other hand, the material is removed not only from the workpiece but also from the electrode, which has been known as electrode wear [31, 32]. This influences the machining shape and accuracy, especially in micro-EDM drilling and milling. However, MRR of micro-EDM is considerably higher and its accuracy could be controlled better than micro-ECM [33, 34]. In micro-ECM, the material is removed based on the dissolution of metal from the anode. As a result, the dissolution rate of electrochemical reaction is relatively low.

Table 2. Comparison of micro-EDM and micro-ECM

	Micro-EDM	Micro-ECM
Advantages	Higher accuracy Higher MRR	No tool wear No heat affected zone Good surface finish
Disadvantages	Tool wear Thermally-damaged layers High surface roughness	Lower accuracy Lower MRR

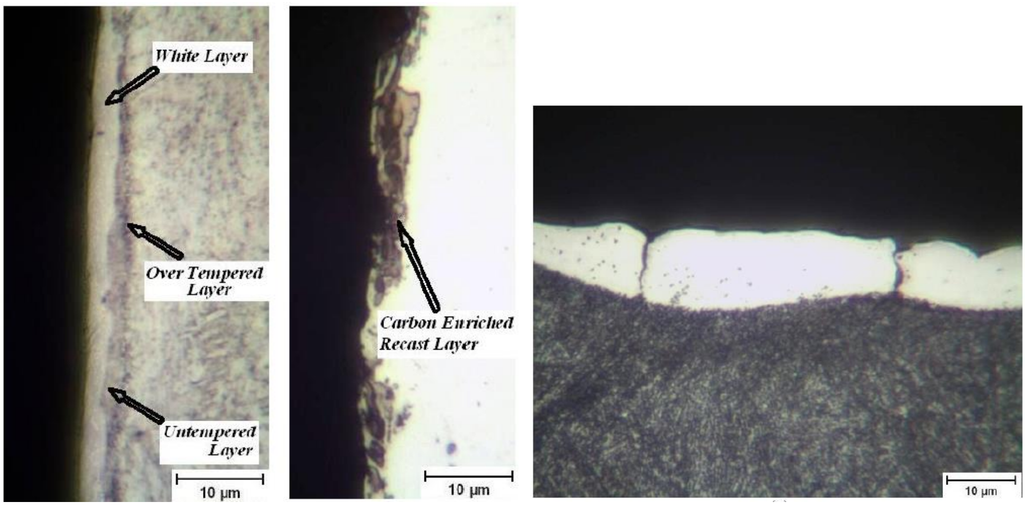

Figure 3. Section observation of micro-EDMed surface [22].

Furthermore, ultra short pulse and low voltage, current must be used in micro-ECM to improve the accuracy by reducing the inter-electrode gap [9, 15, 35]. Due to this reason, the MRR of micro-ECM process is considerably lower than micro-EDM. Although the used power is small, the dissolution could occur in an area larger than the facing zone of the electrode [7].

This effect has been known as stray dissolution, in which the unanticipated material is removed from workpiece, leading to the distortion of machined shapes. Therefore, accuracy is a challenge in micro-ECM.

However, micro-ECM has some valuable advantages. Because the material is removed by electrochemical reaction, the surface generated by micro-ECM is very smooth [7, 12, 36]. In addition, due to the nature of ionic dissolution, there is no thermally affected layer made up on machined surface.

As a result, it is stress-free and there is no burr as well as micro-crack. Furthermore, during the process, only gas evolution occurs at the cathode surface. Consequently, there is no tool wear during machining [37].

SEQUENTIAL MICRO-EDM AND MICRO-ECM

Micro-EDM and Sequential Micro-ECM Using Electrolyte

As discussed above, machined surfaces generated by EDM incur poor surface integrity due to the overlapping of numerous discharge craters and the build-up of distinct thermally-damaged zones. These inherent characteristics are due to the nature of material removal mechanism by using electric sparks. To mitigate this disadvantage, there have been many attempts made to enhance the integrity of EDMed surfaces in recent years.

One of the approach directions is using EDM and ECM as sequential machining processes. The key objectives of these research studies are to reduce the surface roughness induced by overlapping discharge craters and to remove the thermally-damaged zones created during EDM process.

One of the earliest works was carried out to perform the finishing of WEDM products by using ECM [38]. The remaining piece of wire-cut process was used as mate-electrode in the later electrochemical machining step, as illustrated in Figure 4. The $NaNO_3$ electrolyte was pumped to flow through the gap created by WEDM step. Within a few seconds, the maximum surface roughness R_{max} was highly reduced from over 20μm to 2-4μm only. The experiments were also carried out using samples made from SKD11, SKD61, SUS304 and brass. A similar method was also used to smooth the surface made from tungsten carbide [39]. Smooth surface was obtained without the heat-affected zones or cracks.

A specially designed power generator was used to dissolve tungsten carbide. However, it requires the appropriate selection of electrode material for preventing the dissolution from electrode during reverse voltage pulse. In addition, different electrolytes for finishing EDMed surface by ECM have also been investigated [40].

Acidic medium is found to have better smoothing and polishing effects on the surface topography. For environmental aspect, sodium nitrate also yields good polishing rate but the current density must be appropriately set. Another attempt is to smoothen the surface of micro-holes on high nickel alloys machined by micro-EDM by electro-polishing process [41].

Electrolyte solution H_3PO_4 with 85% concentration was used as electrolyte in sequential electro-polishing step with the set-up diagram shown in Figure 5. In view of the high conductivity of electrolyte, only low voltage was applied, from 1V to 5V. After around 5-minute machining time at the electrolytic voltage of 2V, taper and burrs were observed to be reduced and the measured surface roughness dropped from 2.11μm to 0.69μm R_{max}, as shown in Figure 6.

Recently, dilute electrolyte has been used in sequential micro-ECM step to enhance the surface finish of 3D micro-shapes. The surface roughness of hemisphere is found to be reduced from 0.08 μm R_a to about 0.03μm R_a after performing micro-ECM using 0.1M H_2SO_4 electrolyte [34]. Similarly, the surface finish of several 3D metallic micro-structures has also been improved from 0.707 to 0.143μm R_a by using an electrolyte solution consisting of 3%wt $NaClO_3$ [42].

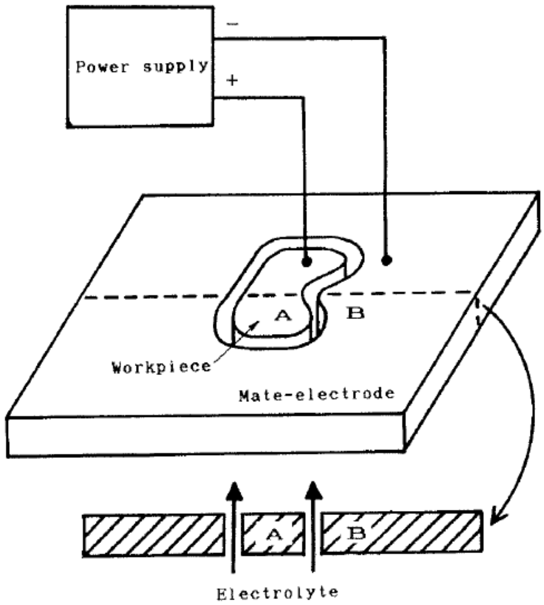

Figure 4. Principle of the Mate-Electrode Method [38].

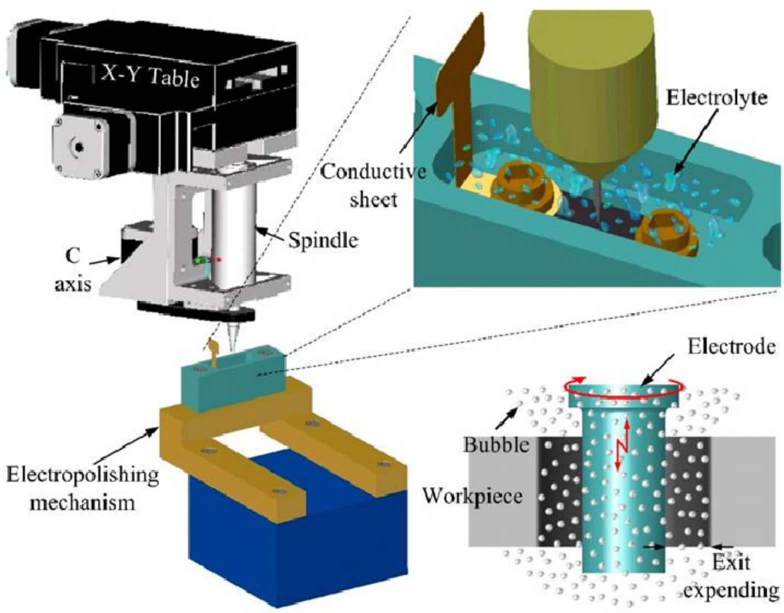

Figure 5. Schematic diagram of electro-polishing after micro-EDM [41].

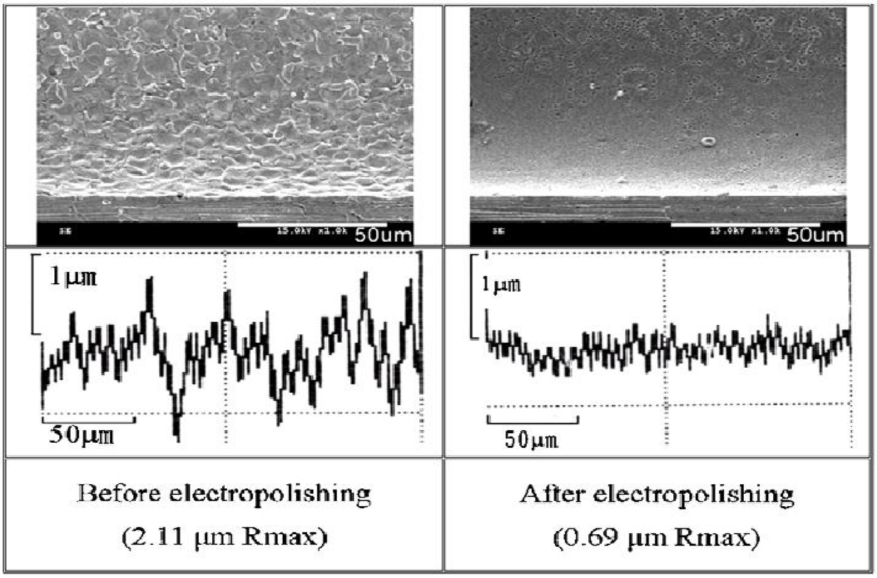

Figure 6. Comparison of electro-discharge machined and electro-polished surface [41].

The electrode was online fabricated using an anti-copying block and it was then used for both micro-EDM and micro-ECM processes. Two different machining fluid supplies were used in the same machining set-up, as shown in Figure 7. It was found that the machining accuracy and machining shape is much better than that of machining by micro-ECM milling only. It also showed that the EDMed recast layer and surface defects are removed completely, as can be seen in Figure 8 and Figure 9. Therefore, the surface quality and integrity of the workpiece is improved, which is better than that of machining by micro-EDM only. The dimensional accuracy can be effectively controlled by using suitable machining conditions and appropriate tool path.

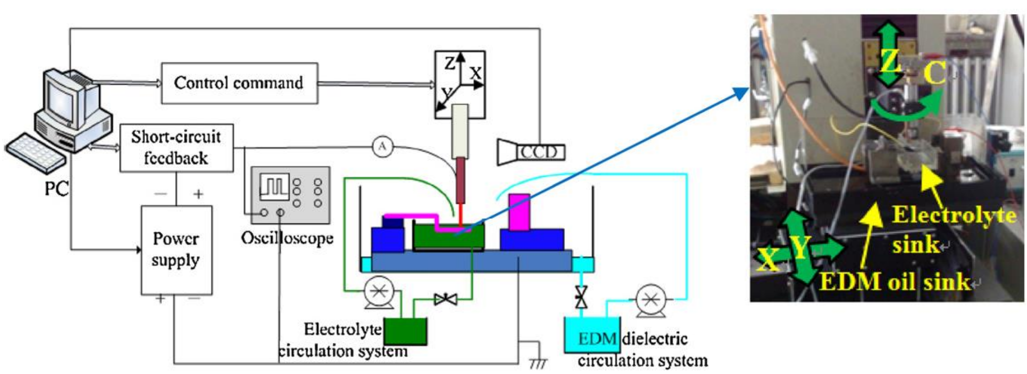

Figure 7. System configuration of micro-EDM and micro-ECM combined machine tool.

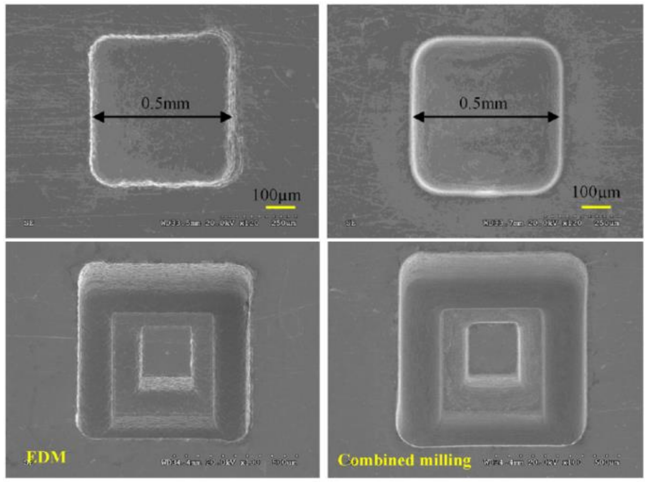

Figure 8. SEM photos of square cavity machined by (a) micro-EDM and (b) combined milling [42].

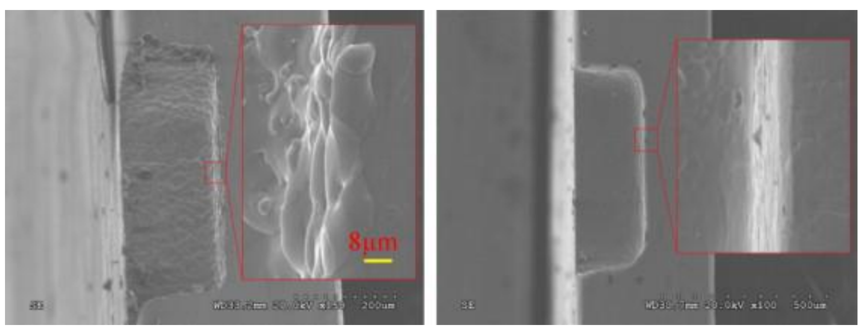

Figure 9. Cross-section and partial enlargement of the micro-cavity [42].

A similar approach using two different machining liquids on the same machine was used to investigate sequential electrochemical–electro discharge process for micro part manufacturing [43]. It showed that the concept of combining EDM and ECM into a sequential process carried out on the same machine tool gives the possibility of minimizing the disadvantages and exploiting the advantages of the ECM and EDM processes. With a properly designed hybrid sequential process, cavity with improved surface finish, machining shape can be obtained together with less electrode wear, as shown in Figure 10 and Figure 11.

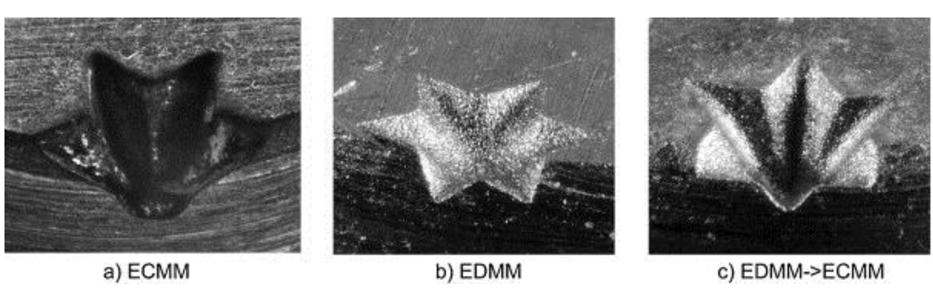

Figure 10. Cavities machined during electrochemical sinking (a), electro discharge sinking (b) and sinking when using the EC/EDMM sequence (c) [43].

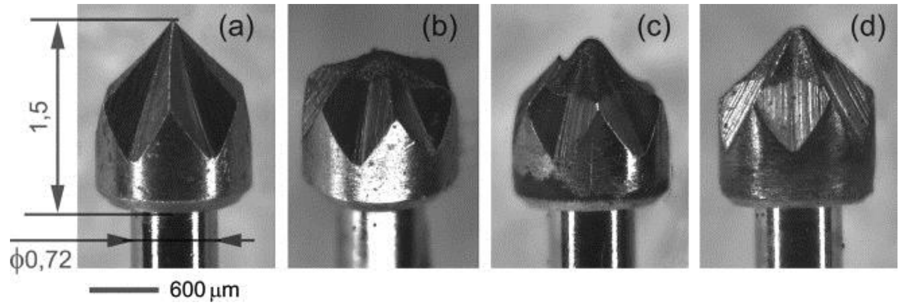

Figure 11. Electrode after electrochemical machining (a), electro discharge machining (b), an improper EC/EDMM sequence (c), a proper EC/EDMM sequence (d) [43].

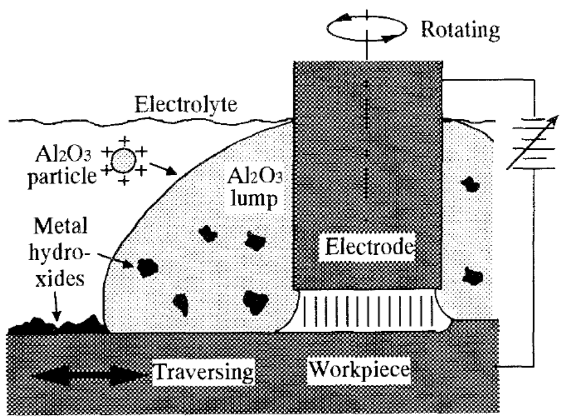

Figure 12. Diagram of machining part around the electrode with Al_2O_3 lump [44].

With a view to further enhancing the integrity of surface generated by micro-EDM, hybrid micro-ECM/lapping has been also used during finishing step. The main objective of these attempts is to associate the dissolution effect of electrochemical reaction and the polishing effect of abrasive grains. One of the earliest researches is reported by Takahata [44].

Fine abrasive grains Al_2O_3 were mixed with colloidal aqueous electrolyte. During machining, beside the metal dissolution by electrochemical reaction, the movement of abrasive grains impacted by rotating electrode increases the efficiency of mechanical polishing, as illustrated in Figure 12. The mirror-like surface with 32nm R_{max} was obtained after 120s machining time, as shown in Figure 13.

Another attempt using similar approach was made to obtain a smoother surface of harden steel after micro-EDM [45]. The abrasive grains Al_2O_3 were also used but with different grain sizes from 2 to 13µm. Surface with 0.06µm R_a was obtained after ECM/lapping process.

It is reported that the surface roughness after ECM/lapping was lower than that after ECM or polishing alone, as shown in Figure 14.

Micro-EDM and Sequential Micro-ECM Using Deionized Water

For micro-application, the product size is small. Therefore, low-conductivity electrolyte is required to localize the dissolution during micro-ECM step [15]. Deionized water is one candidate owing to its slight conductivity. For enhancing the surface finish of micro-pins used for micro-nozzles fabrication, deionized water with 0.6MΩ.cm specific resistivity has been used as a weak electrolyte in a new wire electrochemical grinding process, as illustrated in Figure 15 [15, 36]. The set-up used is similar to wire electro-discharge grinding but the electric discharge is simply replaced by the electrochemical reaction [46]. By applying the voltage of 40V, which is higher than that of normal electrochemical machining, and using low feed speed and large depth of cut, the mirror-like surface was obtained.

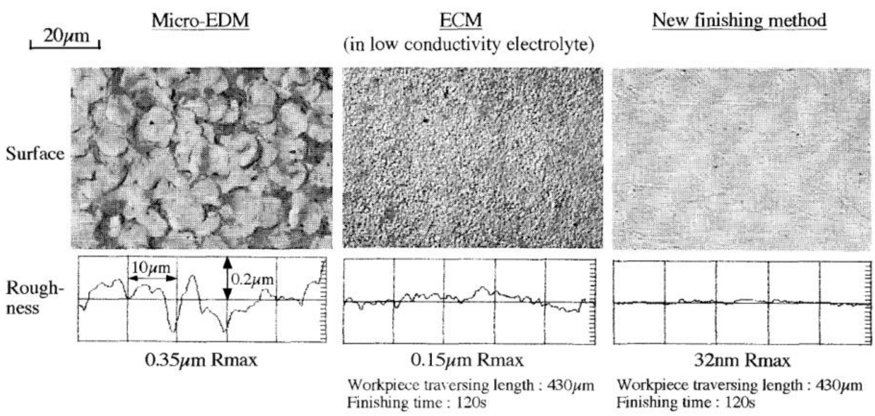

Figure 13. Comparison between machined surfaces [44].

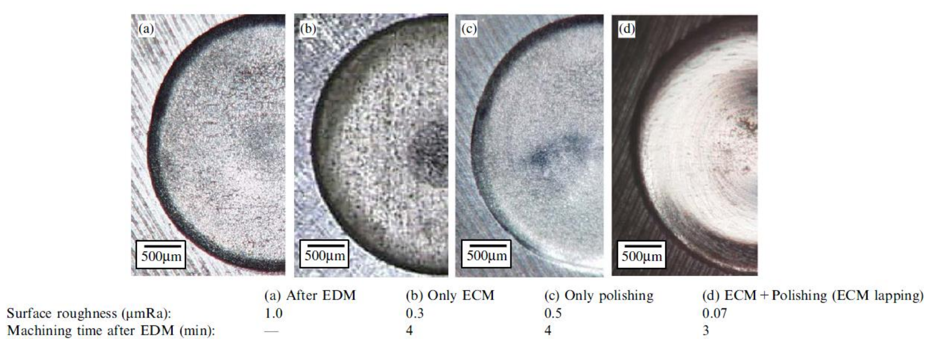

Figure 14. Surface of machined holes [45].

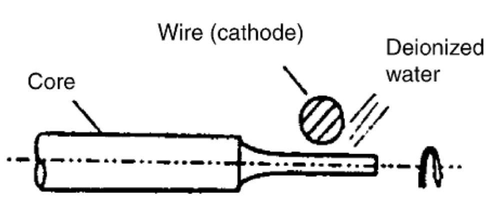

Figure 15. Wire electrochemical grinding process [15].

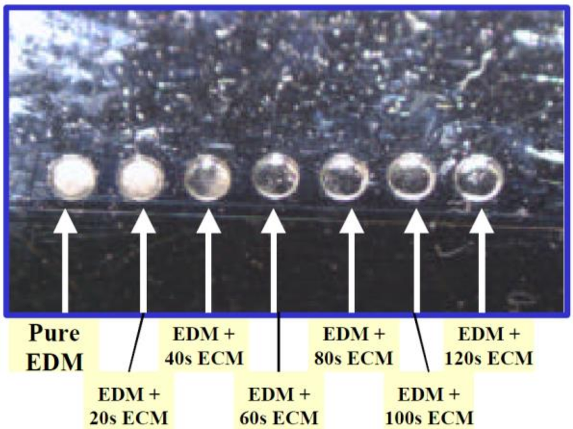

Figure 16. Progressive effect of ECM polishing [47].

Other attempts also used deionized water to reduce the surface roughness of micro-holes during sequential ECM step. Deionized water owning $5\times10^4\Omega$.cm resistivity was used as both the dielectric and the electrolyte for machining micro-holes [47]. After EDM, micro-holes were machined by ECM for a fixed period of time. The average surface roughness R_a decreased from 0.6µm to less than 0.05µm after 60s machining time. The optimum duration for ECM was found to be between 40s and 60s. For higher ECM time, the machining shapes were severely distorted due to the excessive material removal, as shown in Figure 16.

A similar approach was also performed for through micro-holes but with higher resistivity of deionized water, 2MΩ.cm, to prevent the distortion of micro-hole [48].

After 6mins machining time, the surface roughness was significantly reduced from 0.225µm to 0.066µm R_a, as can be seen in Figure 17. It is reported that the usage of deionized water with resistivity as low as 0.1MΩ.cm could lead to the distortion at the entrance and exit of micro-holes due to excessive material dissolution, notwithstanding that its middle area is still covered with discharge craters, as shown in Figure 18.

Another attempt was performed for milling of cavities, as shown in Figure 19 [49].

Surface roughness and hardness were compared for three cases of surfaces machined by micro-EDM using deionized water, by micro-EDM using kerosene, and by finishing in deionized water after micro EDM. Micro grooves and pockets were fabricated by micro EDM milling and electrochemical finish. Figure 20 shows a change of machined surfaces according to different ECM finishing time. As the finishing time increased, craters formed by micro-EDM were removed by ECM and smooth surface was generated. It is observed that smooth surfaces were achieved after about 40 sec finishing time. The pitting structure was seen for early stage of finishing and the grain boundary vanishes for long finishing time situation.

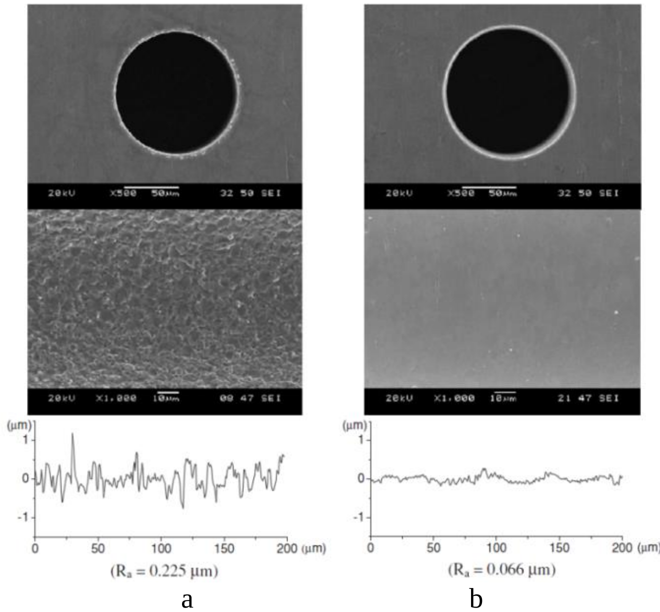

Figure 17. Inner hole surface (a) after micro-EDM, (b) after finishing [48].

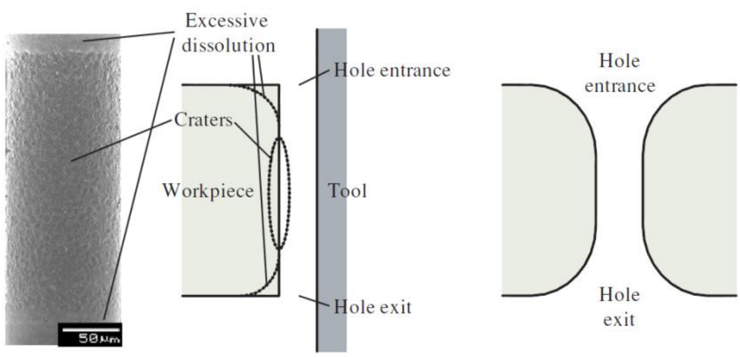

Figure 18. Hole with reverse barrel shape when ECM finishing using 0.1MΩ.cm deionized water [48].

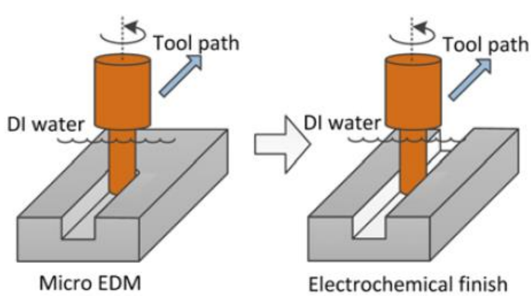

Figure 19. Combination process of micro EDM and electrochemical finish in deionized water [49].

Figure 21 (a) and (b) are images of pockets machining examples after micro EDM milling and after finishing. It is found that high feedrate did not remove pitting surface formed during micro-EDM milling because the ECM finishing time was not long enough.

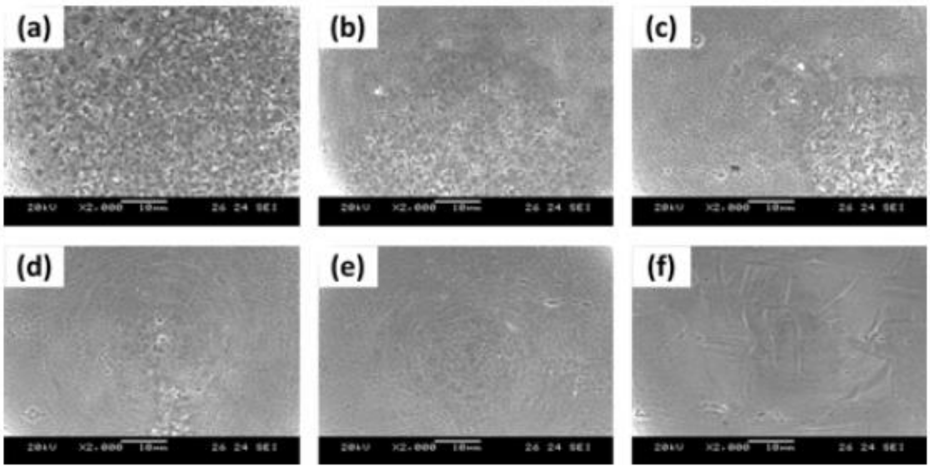

Figure 20. Finished surfaces with voltage of 40 V according to finishing time after micro EDM: (a) 0 sec, (b) 10 sec, (c) 20 sec, (d) 30sec, (e) 40 sec and (f) 180 sec [49].

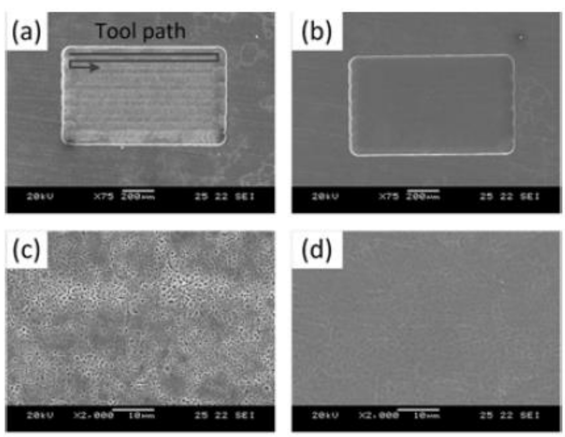

Figure 21. (a) Pocket machining by micro EDM milling in deionized water, (b) pocket machining by electrochemical finishing after micro EDM milling, (c) is machined surface of (a) and (d) is machined surface of (b) finishing [49].

Therefore, low feedrate is required together with proper number of scan for producing fine surface finish. Figure 22 shows surface roughness of machined surfaces according to three cases: micro-EDM in deionized water, micro-EDM in deionized water with finishing, and micro EDM in kerosene. Amongst them, the surface processed by finishing is observed to have lowest surface roughness value of 0.027 μm R_a and 0.15μm R_z. In addition, from hardness test by nano indenter, the hardness in the case of micro EDM in deionized water is similar to that of micro-EDM in deionized water with ECM finishing.

Micro-EDM and sequential micro-ECM using deionized water was also attempted for wire-EDM, as shown in Figure 23 [50]. The fabrication process includes two steps. First, the lenticular shape groove was machined by wire-electrical discharge machining as wire-EDM grooving. Second, electrolytic polishing was performed subsequently to improve the surface finish. This is due to the fact that the surface machined by EDM not adequate for creating a lens pattern mold.

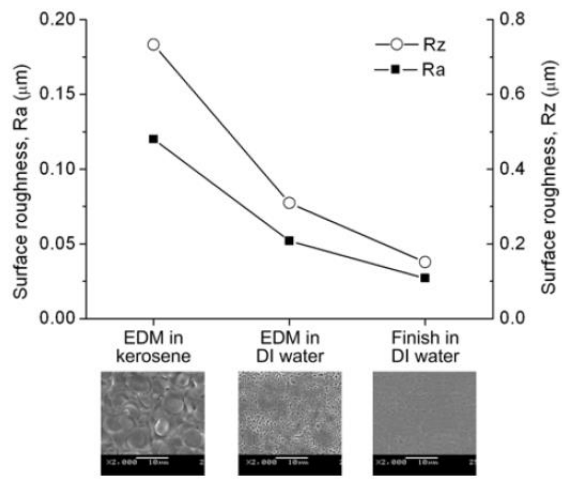

Figure 22. Surface roughness (R_a, R_z) according to three different cases [49].

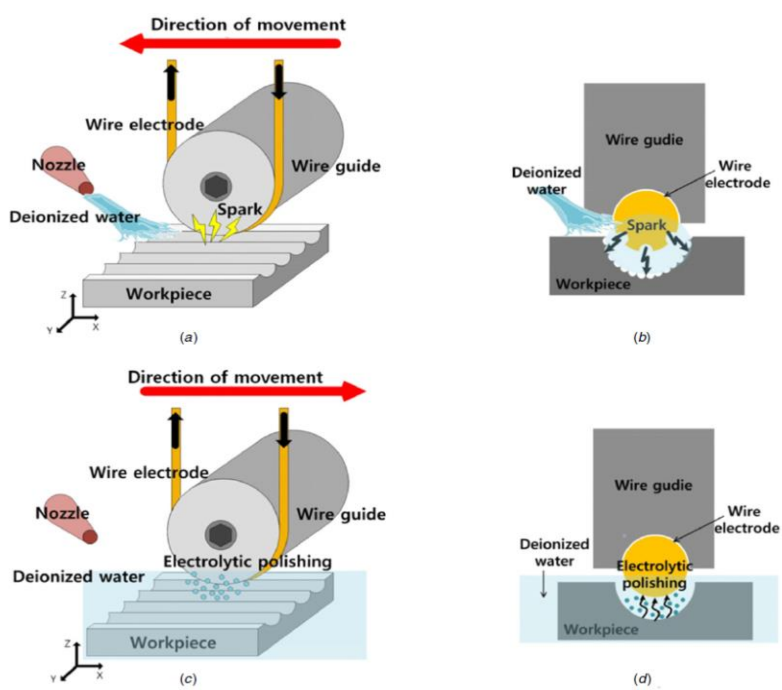

Figure 23. Schematic of WEDM-grooving and electrolytic polishing: (a) WEDM-grooving process, (b) cross-sectional view during WEDM-grooving, (c) electrolytic polishing process, (d) cross-sectional view during electrolytic polishing [50].

Using this multi-step process, a lenticular pattern mold with high surface quality was machined, as shown in Figure 24. Then, the lenticular pattern PDMS lens was successfully produced using this stainless steel mold.

MICRO-EDM USING DEIONIZED WATER AND INHERENT ECM EFFECT

Deionized water is an alternative dielectric fluid to hydrocarbon oil for EDM [51]. It is an environmental-friendly substance that could provide better and safer environment when working with EDM because it does not generate harmful gases such as CO or CH_4. Especially, the special characteristic that makes deionized water superior to hydrocarbon oil is that it brings higher MRR and lower electrode wear.

The earliest attempt to use distilled water in EDM carbon steel was performed by Jeswani [52]. Under the identical machining conditions but high pulse energy (72-288mJ), EDM using distilled water results in higher MRR and lower electrode wear than kerosene.

It is also reported that the surface finish is better but the dimensional accuracy is poor. Then, performance of different water qualities in EDM was also investigated [53]. Tap water ($0.25\times10^4\Omega$.cm resistivity), distill water ($0.32\times10^5\Omega$.cm resistivity) and a mixture of them with 25%-75% ratio were compared.

It was seen that tap water brought highest machining rate.

It also indicated the possibility of zero electrode wear when copper electrode with negative polarity was used in EDM with water. It is also reported that the spark erosion in water has higher thermal stability and thus more power could be input in the discharge [54]. Accordingly, the MRR when water is used as dielectric fluid could be highly increased.

In addition, the comparison of EDM titanium alloy Ti-6Al-4V in kerosene and distilled water was also carried out [55]. MRR was also found to be higher and tool wear was also observed to be less when distilled water was used as dielectric fluid. A similar observation was also obtained when machining micro-slits on titanium alloys [56].

It is found that when dielectric fluid is water, a thin layer of TiO is formed on the machined surface. In contrast, a thick TiC layer is generated when kerosene was used. The melting point of TiC is 3,150°C which is much higher than that of TiO, 1,750°C. Therefore, the TiC requires higher energy density to be removed and thus the MRR when kerosene is used is much lower. It is also observed that the debris size in distilled water is greater but the impulsive force of discharge is less and more stable than in oil medium [55].

Deionized water has also been used for micro-EDM. The ∅0.1mm micro-holes with high aspect ratio were machined on S45C carbon steel [57]. It was observed that using purified water also yielded higher MRR and lower tool wear. Later, a horizontal micro-EDM set-up was built to improve the flushing effect of water to drill deeper micro-holes [58]. Micro-holes obtained from the experiments have the aspect ratio as high as 10.

However, in those studies, high-resistivity deionized water (10^6-$10^7\Omega$.cm) was used to sufficiently suppress electrochemical reaction. It was also mentioned that the reliability and the repetition rate of electric discharge in deionized water are better than oil.

Recently, water has also been used for micro-EDM milling [59]. High resistivity deionized water (12MΩ.cm) was also used to prevent the significant distortion of machining shape due to the excessive unanticipated dissolution. A similar observation of MRR and electrode wear was also obtained. The MRR is observed to be higher and tool wear is found to be lower when machining in deionized water.

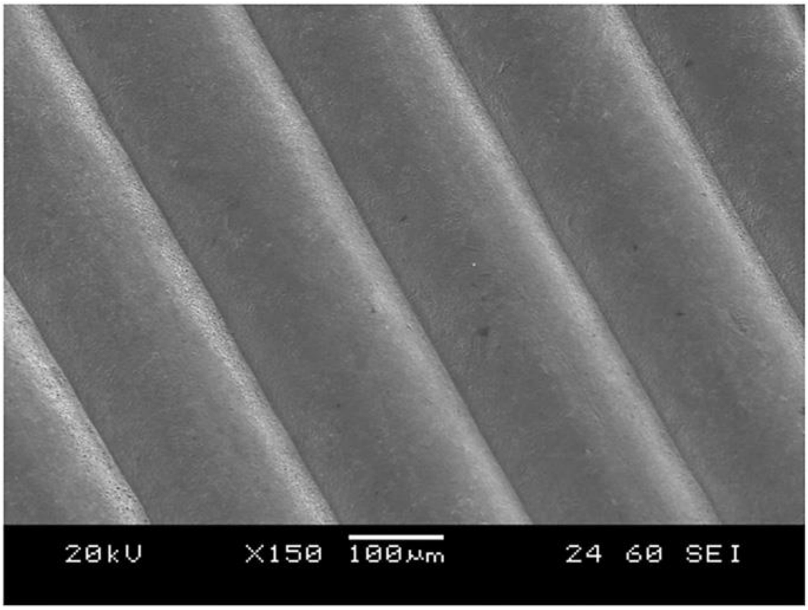

Figure 24. SEM image of the finished lenticular pattern mold [50].

Although deionized water is capable of bringing higher MRR and lower electrode wear, the stray dissolution during machining process deteriorate dimensional accuracy of machined shapes, as can be seen in Figure 25 [58, 59]. Hence, it has been considered as the main drawback of micro-EDM using deionized water. Consequently, many attempts have been made to prevent the excessive dissolution caused by electrolysis in deionized water.

Anti-electrolysis power supplies were designed to reduce the dissolution of workpiece material [60-62]. These power supplies applied AC voltage instead of DC voltage. The polarity of electrode and workpiece was permuted after each pulse to reverse electrochemical reaction. It was observed that the material dissolution was reduced. However, electrode wear was also found to be high since the polarity of electrode was positive for half of the machining time. Therefore, deionized water has been mainly used for wire-EDM because fresh running wire is continuously supplied during machining process [10, 63].

Micro-EDM of tungsten carbide was also carried out in deionized water [63-65]. It was reported that there is significant dissolution of cobalt binder from tungsten carbide although the resistivity of deionized water used was in medium range, 1.6-1.8MΩ.cm.

In order to mitigate this issue, bipolar pulse combined with a modified-shape electrode has been proposed for micro-EDM drilling using deionized water, as shown in Figure 26 [63].

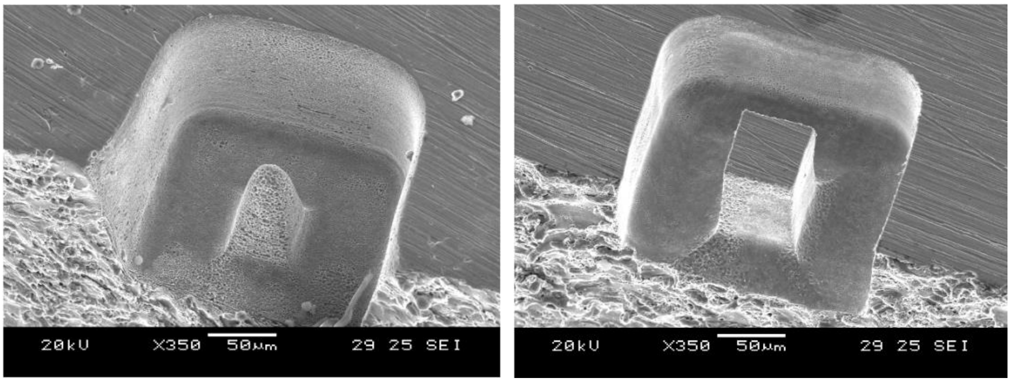

Figure 25. Micro-column fabricated by micro-EDM milling using deionized water with different resistivity: (a) 0.1MΩcm and (b) 12MΩcm [59].

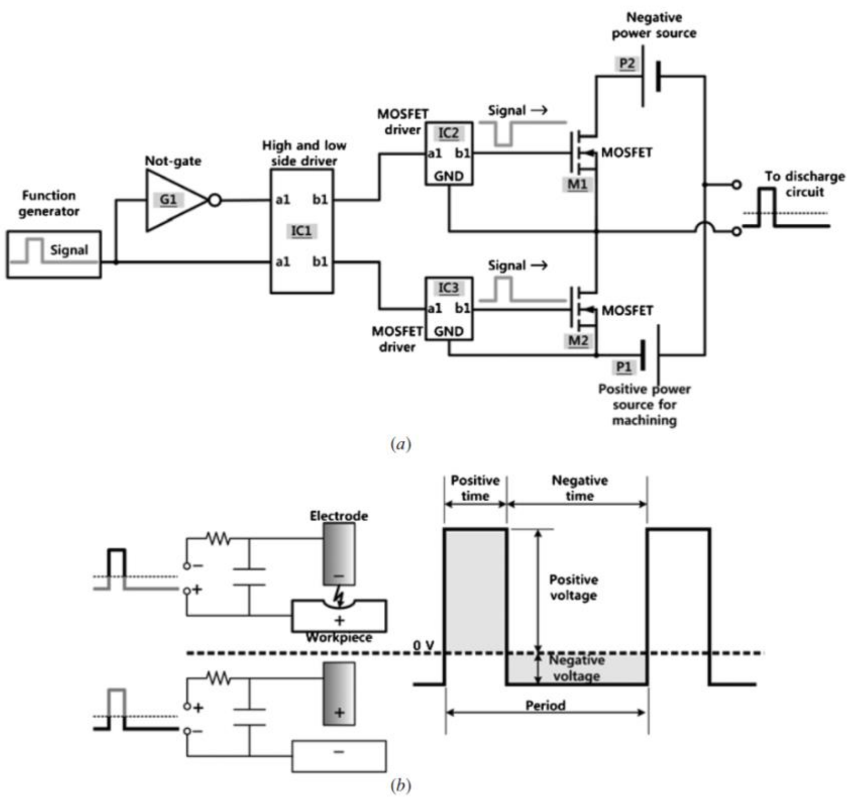

Figure 26. Bipolar pulse generator: (a) schematic of bipolar pulse generator circuit and (b) bipolar pulse waveform [63].

It was found that the electrolytic corrosion is reduced when 125 kHz bipolar pulse with duty factor of 25% and the negative voltage of -20V was used. However, the electrolysis was not fully suppressed. Therefore, electrode with circular cross-section was machined to have rectangular, square and triangular cross-section, as can be seen in Figure 27. In combination with bipolar pulses, the triangular cross-section electrode was found to be most effective among the different electrode shapes in suppressing the unanticipated material dissolution. This is due to the fact that its side area is least compared to the others.

However, because the side area of this electrode type is very small, the MRR is also low and the electrode wear is severe in micro-EDM milling, resulting in the poor machining performance.

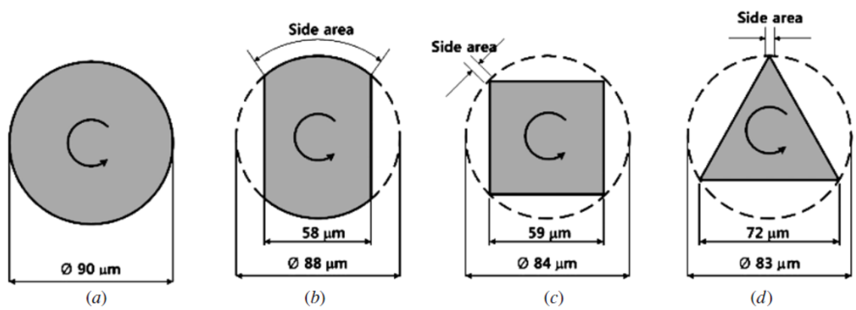

Figure 27. Different types of electrode cross-sections: (a) cylindrical; (b) rectangular; (c) square and (d) triangular [63].

In addition, the triangular-section electrode requires longer time to be fabricated. For that reason, deionized water spray and bipolar pulse combination have been developed for micro-EDM drilling and milling of tungsten carbide [64, 66]. In these researches, deionized water and compressed air are mixed together in form of the mist.

It was then used as the dielectric medium to eliminate the corrosion. Some water drops go into the narrow gap while the other drops on workpiece surface are blown away by the compressed air, as illustrated in Figure 28. As a result, it breaks the continuous electrical path between the electrode and the surface of workpiece adjacent to the machined hole. Consequently, the high-quality micro grooves could be fabricated on WC-Co, as can be seen in Figure 29. Recently, it is also reported that by using bipolar pulses with high frequency, micro-holes without electrolytic corrosion could be also obtained [67].

SIMULTANEOUS MICRO-EDM AND MICRO-ECM DRILLING

This section presents a method to combine micro-EDM and micro-ECM in a single hybrid machining process to reap improved performance for both surface finish and dimensional accuracy by using low-resistivity deionized water, which exhibits both characteristics of a slightly conductive fluid and a dielectric fluid.

Principle

Figure 30 illustrates the principle of SEDCM drilling in low-resistivity deionized water. Short voltage pulses are applied instead of a continuous voltage supply in the conventional micro-EDM using RC-type pulse generator. When the process starts, short voltage pulses are supplied across the electrode and workpiece. Then, the electrode is plunged down to reduce the electrode and workpiece gap, as shown in Figure 30 (a). As soon as the gap meets a critical value, there appears the breakdown of deionized water and the sparks occur as shown in Figure 30 (b). Material is removed by melting and vaporization. Each discharge forms a crater on machined surface. Therefore, the machined surface is covered with numerous overlapped discharge craters and it is rather rough.

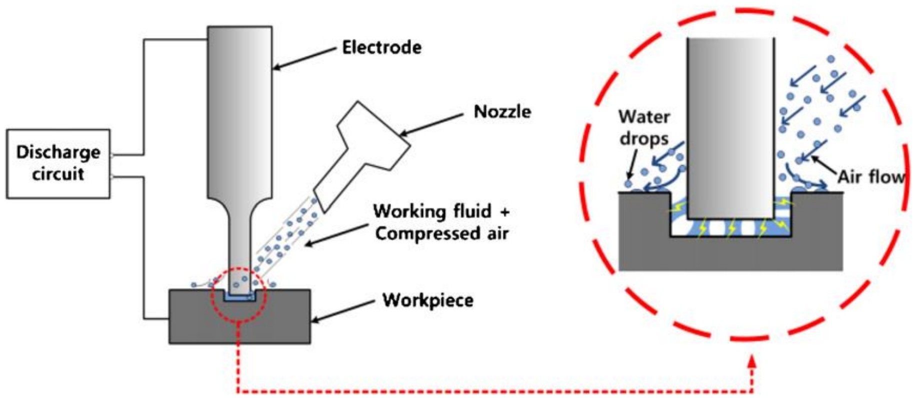

Figure 28. Schematic of spray ED-milling [64].

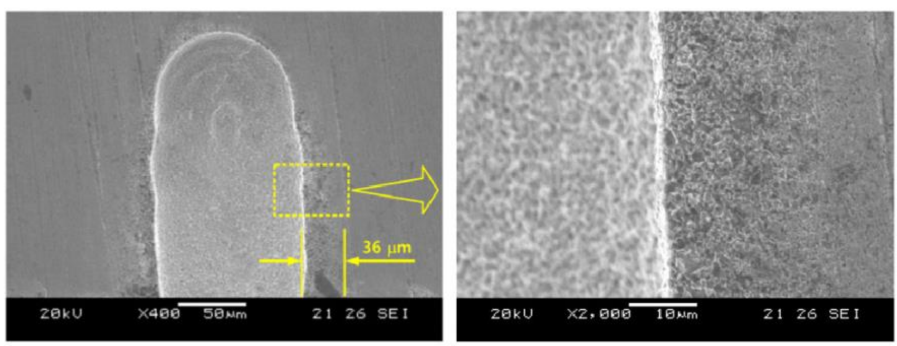

a) With deionized water jet

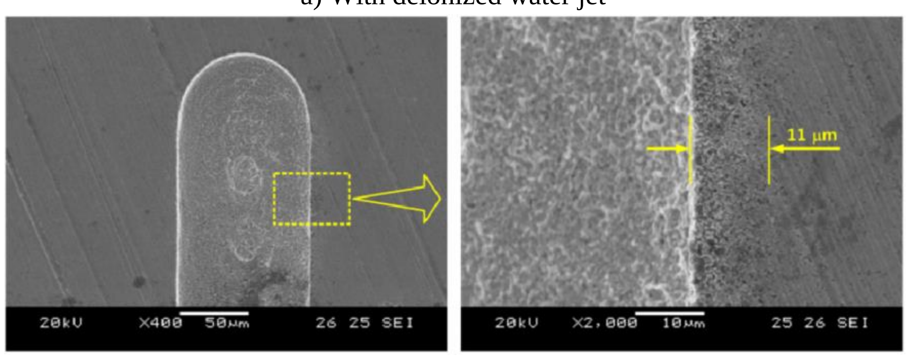

b) With bipolar pulsed power source and a deionized water jet

Figure 29. (Continued).

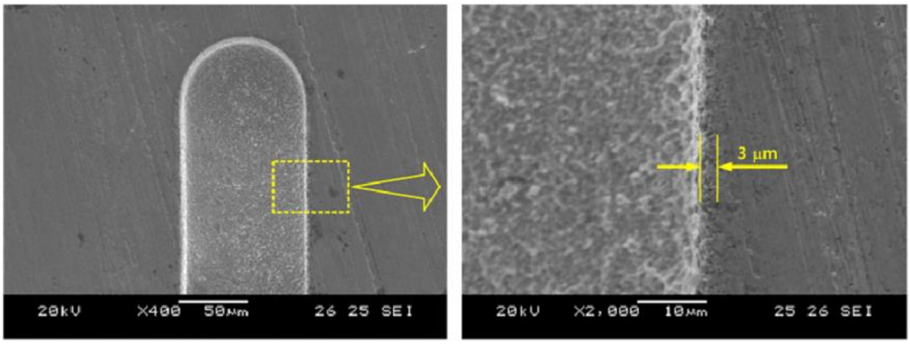

c) With bipolar pulsed power source and an air pressure of 0.3 MPa and a water flow rate of 1 ml min^{-1} (spray ED-milling)

Figure 29. Scanning electron microscopic images of machined slots [64].

After a period of time, the gap between electrode and workpiece increases due to material removal by the sparks and thus no further discharges occur. With the supplied voltage pulses, the electrochemical reaction happens owing to the slight conductivity of deionized water, as illustrated in Figure 30 (c). Anodic dissolution takes place at workpiece surface, producing electrons that are transferred to the cathode by the low-resistivity deionized water which acts as a current carrier. Material is dissolved from the workpiece and thus its surface roughness reduces. Owing to the usage of short voltage pulses, the dissolution of material is localized within a limited distance which is marked with dotted line in Figure 30 (c).

Hence, the machining gap is confined and the machining accuracy could be maintained. After a time period, the electrode is lowered down further through feeding and the cycle repeats, as illustrated in Figure 30 (d).

In order for the electrochemical reaction to have sufficient time to dissolve material, the feedrate must be low enough. In short, this principle simultaneously combines micro-EDM and micro-ECM in a single hybrid machining process with three approaches: low-resistivity deionized water as bi-characteristic fluid, low feedrate to promote electrochemical reaction and short voltage pulses to localize dissolution zone.

The conventional RC-type pulse generator is not suitable for micro-EDM using deionized water due to unanticipated material dissolution, especially in deionized water with low resistivity. It can lead to the severe distortion of machining shape, resulting in poor machining accuracy. Hence, short voltage pulses are required in this method to localize the material dissolution and thus assure the dimensional accuracy.

Figure 31 illustrates the model of the electrochemical cell in terms of circuit elements. When a voltage is supplied across two electrodes immersed in deionized water, electrochemical reaction takes place because deionized water acts as a weak electrolyte. A double layer is formed at the interface of electrodes and electrolyte. It was reported that this electrode-solution interface behaves as a two parallel plate capacitor. For that reason, this interfacial region could be modeled as a capacitor. After the voltage has been applied, this double layer capacitor starts to be charged. The charging time is the product of electrolyte resistance and the capacitance of double layer:

$$\tau = R.C_{DL} = \rho.d_g.C_{DL}$$

where R is resistance of the electrolyte. It depends on the path of the current and can be determined by multiplying the gap distance between anode and cathode (d_g) and the specific resistance of electrolyte (ρ). C_{DL} is the capacitance of double layer.

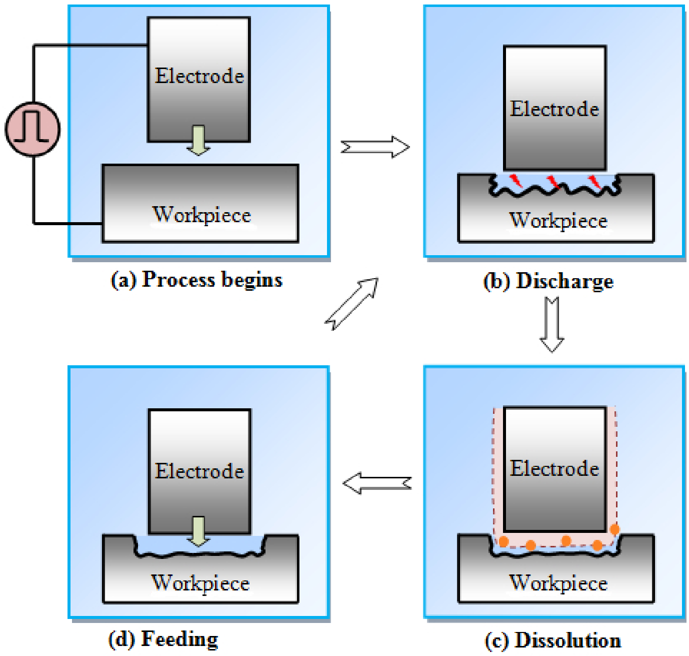

Figure 30. Principle of SEDCM drilling [68].

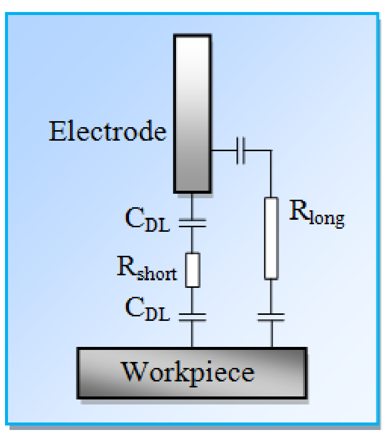

Figure 31. Model of electrochemical cell in terms of circuit elements [9].

This double layer capacitor is considerably charged if the pulse duration (t_{on}) exceeds this charging time constant ($t_{on} > \tau$). The electrochemical reaction rate is exponentially dependent on the potential drop across this double layer capacitor. Therefore, the electrochemical reaction could be localized by controlling the polarization of this double layer capacitor. By using short pulses, the electrochemical reaction only takes place in a confined area.

As illustrated in Figure 31, the double layer capacitor at the bottom of electrode is charged faster than its side surfaces because of different charging time constant caused by various gap distances. The area facing the bottom of electrode has lower resistance (R_{short} < R_{long}) so the double layer is polarized faster and the electrochemical reaction rate is thus higher. By applying adequately short voltage pulse ($t_{long} > \tau > t_{short}$), the double layer is highly polarized at the bottom of electrode whereas it is only weakly polarized at its side surfaces. As a result, the electrochemical reaction could be localized within a certain gap distance.

Capability of SEDCM Drilling

Figure 32 shows the images of fabricated micro-holes at 60 V, using DC regime with two different feedrates: 10 μm/s and 0.2 μm/s. As can be seen in Figure 32(a), for 10 μm/s feedrate, the micro-hole surface is covered with overlapped discharge craters. Especially, the recast material can be seen at its sharp edge. On the contrary, the cylindrical surface of micro-hole machined at 0.2 μm/s feedrate is observed to be smooth and crater-free, as can be seen in Figure 32(b). However, micro-pits appear on the surface near the rim of the micro-hole and the micro-hole diameter is highly expanded. This is caused by the excessive dissolution of material under continuous voltage supplied in low-resistivity deionized water. The 10 μm/s feedrate is rather fast so there is not much time for electrochemical reaction to dissolve the material after the sparks have stopped. In contrast, the 0.2 μm/s feedrate is relatively low. Ionic dissolution can take place on the side surface of machined hole. However, under continuous voltage supply, electrochemical reaction drastically occurs and is not confined. Accordingly, it excessively dissolves the material and increases the electrode and workpiece gap. As a result, machining shape is distorted and thus the machining accuracy deteriorates.

Hence, short voltage pulses were applied instead of continuous voltage supply so as to confine the material dissolution during machining.

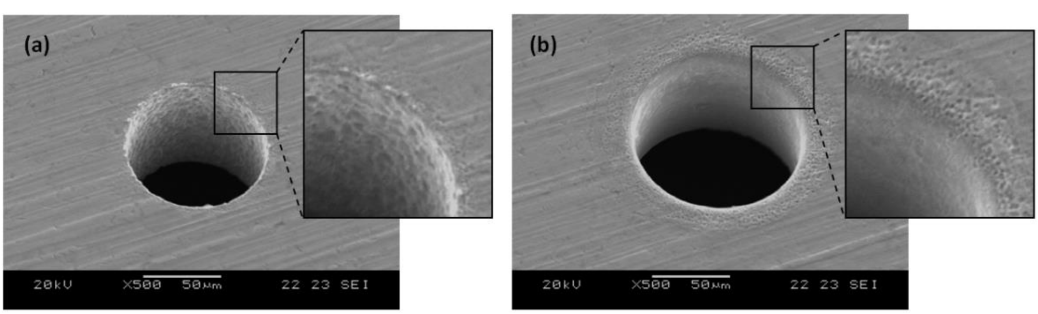

Figure 32. Micro-holes machined using DC regime at 60 V with different feedrate: (a) 10μm/s, (b) 0.2μm/s [68].

Figure 33 shows the image of micro-hole fabricated using pulses at the frequency of 500 kHz with 30% duty ratio and 0.2 μm/s feedrate. The obtained micro-hole is observed to be free of crater on its side surface.

Moreover, there is no significant expansion of diameter as well as the existence of micro-pits adjacent to the rim. This indicates the capability of SEDCM to obtain both good surface finish and high dimensional accuracy.

It also shows that low-resistivity deionized water, low feedrate, and short voltage pulses are three required factors for SEDCM.

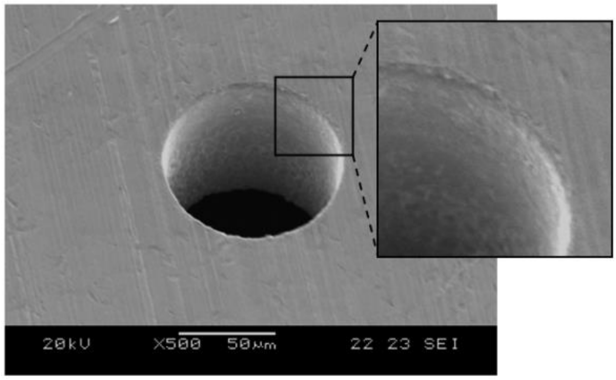

Figure 33. Micro-hole fabricated by SEDCM using 500 kHz pulses with 30% duty ratio at 0.2 μm/s feedrate [68].

Main Requirements of SEDCM Drilling

Short Voltage Pulses

Figure 34 shows the images of micro-holes fabricated using pulses at three different frequencies of 100, 300 and 500 kHz with duty ratio from 15% to 70%. It shows that with smaller duty ratio (or shorter pulse-on time), the diameter of micro-hole has tendency to decrease. Similarly, at higher frequency used, smaller micro-holes are also observed. This can also be seen with the machining gap reduction in Figure 35. This phenomenon could be explained by using the double-layer model. When a voltage pulse is supplied, the double layer starts to be charged.

However, due to the limited pulse width, the double layer is only considerably charged within the area where the distance between electrode and workpiece is less than a certain value. For that reason, the current density and material dissolution rate are significant only in that area. As a result, the electrochemical reaction is localized and the machining gap is confined within that distance. When a shorter pulse-on time is supplied, the machining gap becomes smaller. This explains why the machining gap decreases when a higher frequency as well as smaller duty ratio is used.

It is also found that when the pulse-on time is set to as short as 300 ns, the surface of machined hole is covered with overlapped discharged craters although the same feedrate 0.2 μm/s is used, as seen in Figure 34 (f) and (i). Figure 36 is a magnified view of the micro-hole where the recast material is visible at its edge. Although the 0.2 μm/s feedrate is sufficiently low to promote micro-ECM effect on the machined surface, there is no visible sign of material dissolution in this case. The surface of micro-hole is completely covered with discharge craters. This indicates that electrochemical reaction is localized when voltage pulses are used. In addition, the 300ns pulse-on time is too short so that the localized dissolution distance is even less than the spark gap consisting of critical distance and discharge depth. As a result, the electrochemical reaction is almost suppressed. It shows that short voltage pulses could localize the material dissolution and even suppress the electrochemical reaction when the pulse width is smaller than the critical value. Therefore, the voltage pulses applied in SEDCM must be adequately long to promote the electrochemical reaction within a certain gap distance, not to completely suppress it.

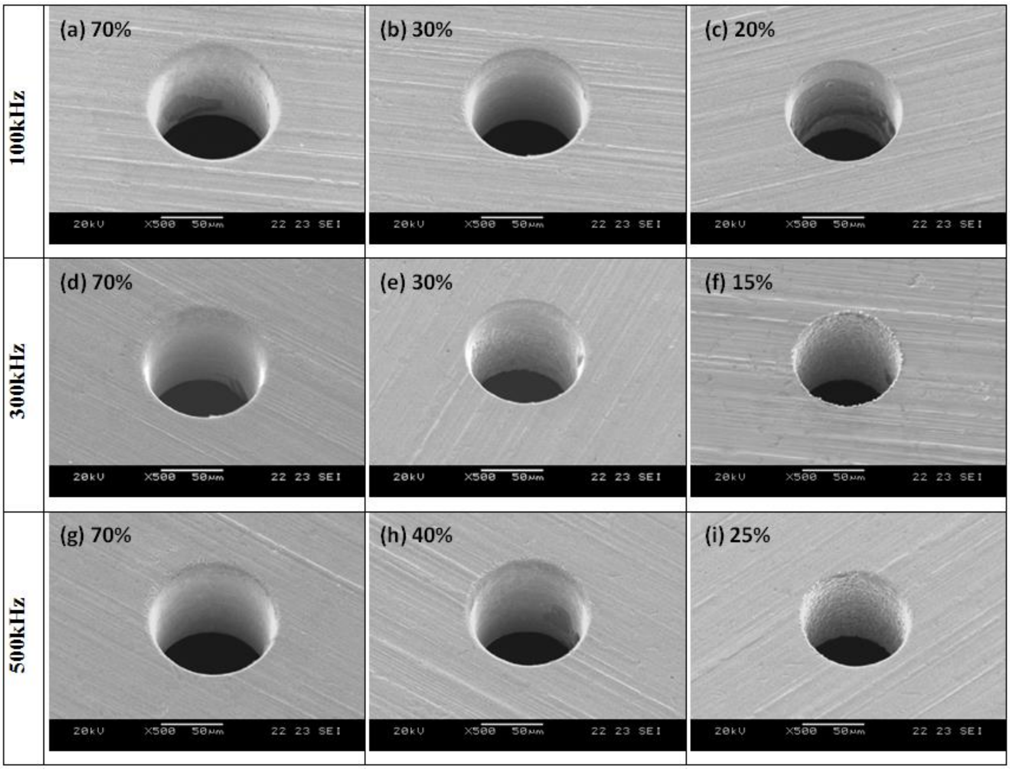

Figure 34. SEM images of micro-holes machined with different pulse frequencies and duty ratio [68].

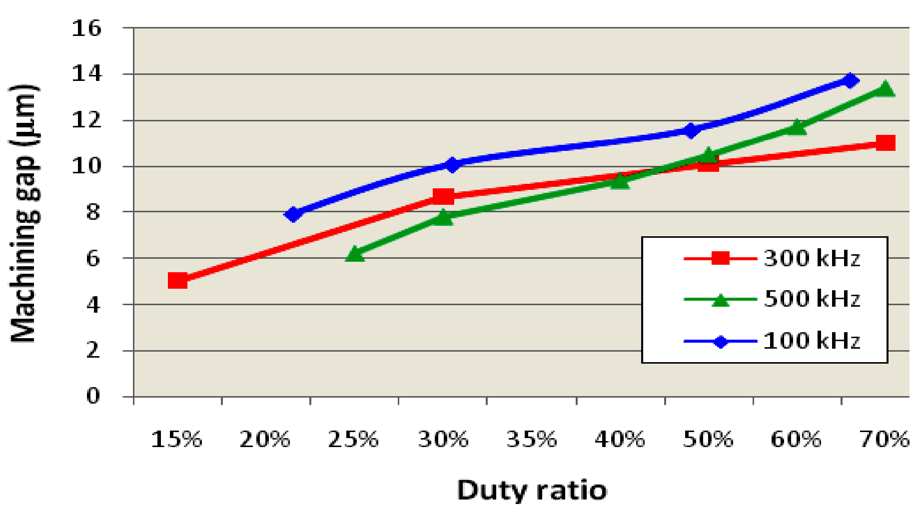

Figure 35. Machining gaps corresponding to different pulse parameters [68].

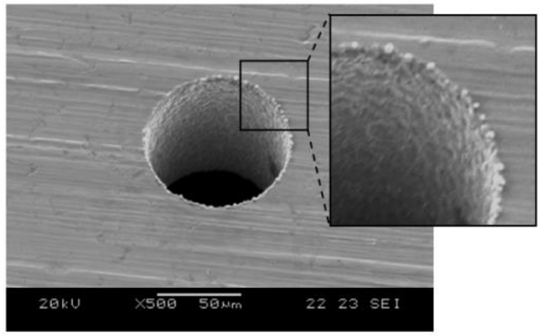

Figure 36. Micro-hole machined using pulses at 300 kHz, 15% duty ratio and with 0.2 μm/s feedrate [68].

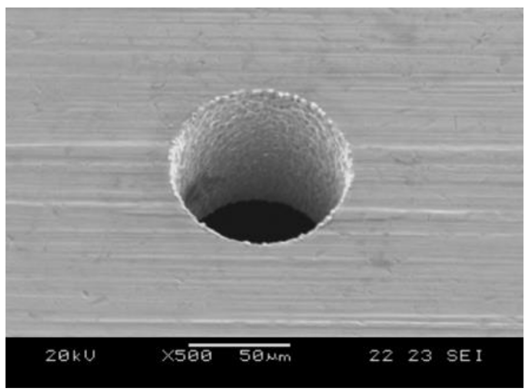

Figure 37. Micro-hole fabricated at 500 kHz, 30% duty ratio and with 1.2μm/s feedrate.

Feed Rate

To indicate the effect of feedrate on the performance of SEDCM, comparison is performed between the micro-holes machined at the same 500 kHz frequency, 30% duty ratio but with two different feedrates: 1.2 μm/s (Figure 37) and 0.2 μm/s (Figure 33). It can be observed that when the 1.2 μm/s feedrate is used, the side surface of machined micro-holes is also completely covered with crater marks. It is different from the micro-hole machined at 0.2 μm/s of which the side surface is seen to be smooth and crater-free. The variation in feedrate is accountable for this phenomenon.

When the electrode moves faster, there is not much time for the electrochemical reaction to happen and dissolve the material from machined surface after the discharge has stopped.

For that reason, the effect of micro-ECM is less and the machined surface is still covered with multiple discharge craters. Accordingly, the machining gap will be smaller and the machining time will be shorter. This shows that feedrate is one of the key elements of SEDCM and selecting the proper feedrate is important to obtain the efficiency of this hybrid machining process.

Modeling of Radial Gap in SEDCM Drilling

As shown above, the uneven material layer after EDM is further removed from machined surface owing to the effect of material dissolution in SEDCM drilling. For maintaining the dimensional accuracy, short voltage pulses are used to localize the dissolution zone. Therefore, additional thickness of material layer removed is important for the final dimension of micro-holes. This section presents the modeling of radial gap in simultaneous micro-EDM and micro-ECM drilling by simulating the thickness of material layer further removed by electrochemical reaction. The analytical model incorporates the double-layer theory, the Butler-Volmer equation and the Faraday's law of electrolysis.

Radial Gap Model

In conventional micro-EDM drilling, the machining gap consists of the critical distance and the discharge depth [69]. However, in SEDCM drilling, a thin layer of material on the lateral surface formed by the electric discharges is further removed to enhance the surface finish of micro-hole, as illustrated in Figure 38.

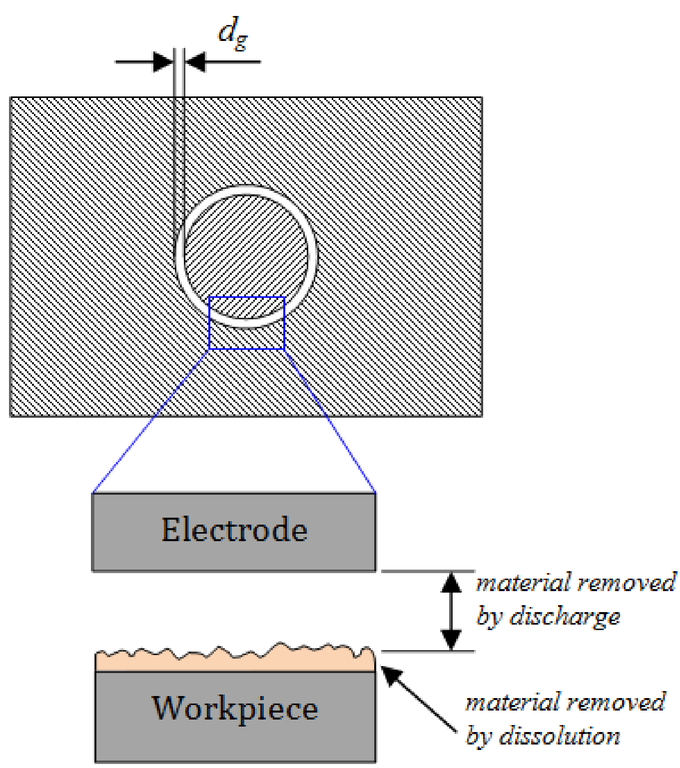

Figure 38. Illustration of the radial gap in SEDCM drilling [70].

For that reason, aside from the critical distance and discharge depth, the radial gap in this hybrid process also includes the dissolution depth which comes from electrochemical reaction.

Therefore, the final radial gap in SEDCM drilling also depends on the thickness of material layer which is further removed. This model focuses on the material dissolution after the discharge to perform the modeling of radial gap. For that reason, the side gap after micro-EDM is considered as the initial gap for material dissolution.

Thanks to the slight conductivity of low-resistivity deionized water, it can be considered as a weak electrolyte. The side gap between electrode and workpiece can be modeled as an electrochemical cell. When a voltage is supplied to two electrodes immersed in deionized water, the ions move towards the electrode surface and the double layer is formed at the interface of the electrode and electrolyte. It was reported that this electrode-solution interface behaves as a two-parallel-plate capacitor [9, 71]. Thus, it is modeled as a capacitor, as shown in Figure 39 [72, 73]. For this model, R_{sol} is resistivity of deionized water. The C_{DL}' and C_{DL}'' are capacitance of double layer at the electrode and workpiece surfaces respectively. The R_F' and R_F'' are the Faradic resistance (or transfer resistance) representing the current density of electrochemical reaction at the surfaces of electrode and workpiece.

Because the thickness of the double layer is significantly smaller than the radial gap, the solution resistance R_{sol} can be expressed as following:

$$R_{sol} = \rho d_g$$

where ρ is the specific resistivity of deionized water and d_g is the electrode-workpiece gap distance.

Polarization of Double Layer Capacitor

Prior to the model development, certain assumptions are made:

- The capacitance of the double layer is constant during machining.
- The transfer resistance and the capacitance of double layer at the electrode-solution and workpiece-solution interfaces are the same ($R_F' = R_F'' = R_F$ and $C_{DL}' = C_{DL}'' = C_{DL}$).
- There is no material dissolution during pulse-off time.
- The roughness of the electrode and workpiece surfaces is neglected in simulating the radial gap distance.

Following the model in Figure 39, the current density going through the workpiece-electrolyte interface includes two different routes: the charging current density i_C (to charge the double layer capacitance C_{DL}) and the Faradic current density i_F (goes through the transfer resistance R_F). The charging current density i_C is given by

$$i_C = C_{DL} \frac{d\eta}{dt}$$

in which t is the time and η is the double layer polarization.

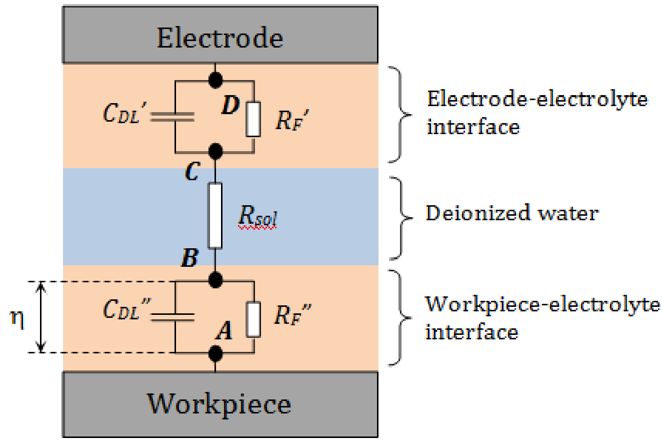

Figure 39. Model of electrode-workpiece side gap in terms of circuit element [70].

The Faradic current density is exponentially dependent on the polarization of the double layers. Therefore, from the Butler-Volmer equation [71], the Faradic current density is

$$i_F = i_o\left[\exp(\alpha z f\eta) - \exp(-\alpha z f\eta)\right]$$

where i_o is the exchange current density at the equilibrium condition, α is the transfer coefficient, z is the number of electrons exchanged during electrochemical reaction and

$$f = F / RT$$

in which F is the Faraday constant, R is the gas constant and T is the absolute temperature.

For application, which exploits the anodic dissolution of metal, the double layer polarization η is considerably high and the cathodic current density is significantly small. Hence, it can be neglected and the Faradic current density going through the transfer resistance R_F could be simplified as following

$$i_F = i_o \exp(\alpha z f\eta)$$

The current density going from A to B in Figure 39 is

$$I_{AB} = C_{DL}\frac{d\eta}{dt} + i_o \exp(\alpha z f\eta)$$

The current density going from B to C is

$$I_{BC} = \frac{U - U_{AB} - U_{CD}}{R_{sol}} = \frac{U - 2\eta}{\rho d_g}$$

where U is the amplitude of the applied voltage pulses.

Since $I_{AB} = I_{BC}$, the following equation can be derived:

$$\frac{d\eta}{dt} = \frac{1}{C_{DL}}\left(\frac{U - 2\eta}{\rho d_g} - i_o \exp(\alpha z f \eta)\right)$$

Now, the polarization of double layer η could be obtained and thus i_F could be calculated.

Dissolution Rate

In order to obtain the dissolution rate, the current density needs to be identified. However, for this process, short voltage pulses are used instead of the continuous voltage. For that reason, the average current density is calculated through the total electric charge per unit area q. For one pulse, the total electric charge per unit area going through the substance could be obtained by integrating the current density i over the pulse-on time t_{on}:

$$q = \int_0^{t_{on}} i_F \, dt$$

The average current density per second could be calculated by dividing the total electric charge by the pulse period t_p as following

$$i_a = \frac{q}{t_p}$$

in which

$$t_p = 1/\ \mathit{frequency}$$

From the Faraday's law of electrolysis [71], the average dissolution rate per second is

$$v = \frac{i_a M}{zF}$$

where M is the molar volume of workpiece material.

Simulation of Radial Gap Distance over Time

The current density is a function of electrode-workpiece radial gap d_g. When the gap increases, the current density is slightly reduced and the dissolution rate is changed as a consequence. Therefore, to simulate the change of radial gap over time, iteration method shown in Figure 40 was used to update the dissolution rate after each time step Δt.

Simulation and Experimental Verification

Simulation parameters are shown in Table 3.

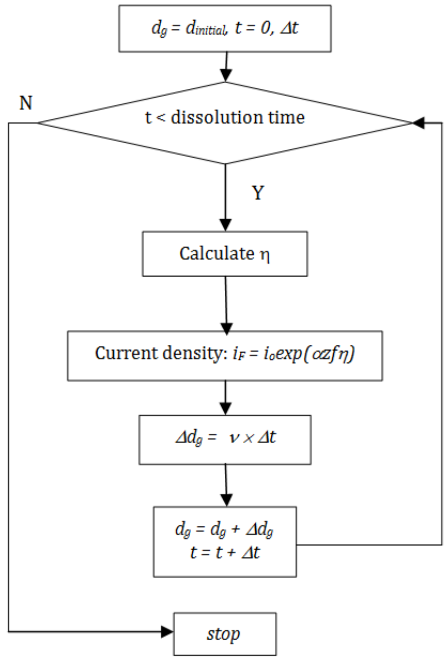

Figure 40. Iterative method to simulate the radial gap over time.

Table 3. Simulation parameters for radial gap distance

Initial gap distance, $d_{initial}$ (μm)	5
Specific conductivity of solution, ρ (MΩcm)	0.4
Double layer capacitance, C_{DL} (μF/cm^2)	0.5
Transfer coefficient, α	0.5
Valency number of ions, z	2
Faraday constant, F (C mol^{-1})	96485
Gas constant, R (J mol^{-1} K^{-1})	8.314
Temperature, T (Kelvin)	298.15
Exchange current density, i_o (μA/cm^2)	70
Pulse amplitude, U (V)	60
Pulse frequency (kHz)	100, 300, 500
Pulse duty ratio	0.15 to 0.9
Molar volume, M (cm^3/mol)	7.11
Time step, Δt (s)	10
Dissolution time (s)	300

Figure 41 shows the predicted data of current density for different duty ratio during one pulse period. Since the frequency is set at 500 kHz, the pulse period is 2 μs. It is noted that during first 0.3 μs, the current density remains steady near zero. Then, it has the quick rise to reach the 0.3 A/cm^2 peak after 0.6 μs. This is due to the double layer charging. When the voltage is supplied, the ions in solution move to the workpiece surface to form the double layer. The Faradic current is exponentially dependent on the polarization of this double layer.

It requires certain time for double layer to be highly charged so the Faradic current remains near zero at the beginning and only increases sharply after 0.3 μs.

When the current density peaks and maintains at 0.3 A/cm^2, it shows that the double layer is fully charged. It can also be seen that with smaller duty ratio, the width of current density profile becomes thinner. After pulse-on time duration, the applied voltage reduces to zero so the current falls off. Furthermore, the dissolution rate is dependent on the total charge transferred during one pulse. As a result, higher duty ratio results in higher dissolution rate, as shown in Figure 41(b).

It is also seen that when the duty ratio is too small, the dissolution rate is negligible because the pulse-on time is too short for double layer to be considerably charged. In this situation, there is no visible effect of material dissolution to improve the surface finish of micro-hole. Figure 42 (a) shows the predicted data of current density for different initial gap distance during one pulse.

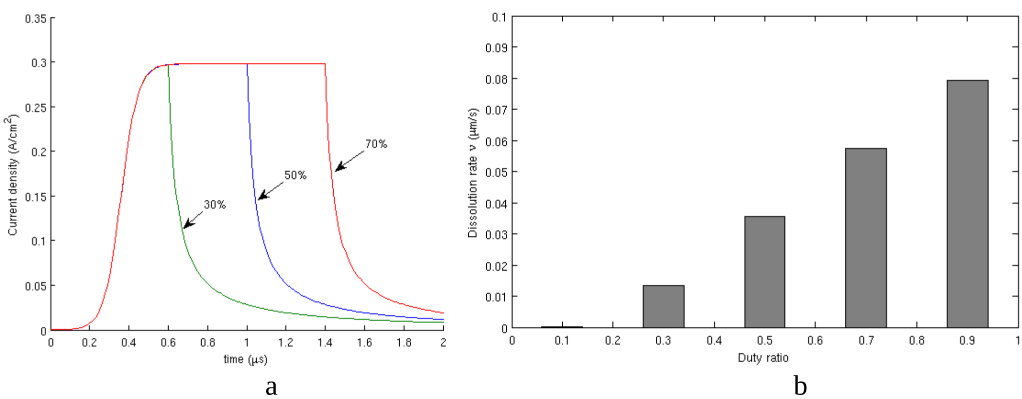

Figure 41. Simulation of current density (a) and dissolution rate (b) for different duty ratios (frequency = 500 kHz, $d_{initial}$ = 5 μm).

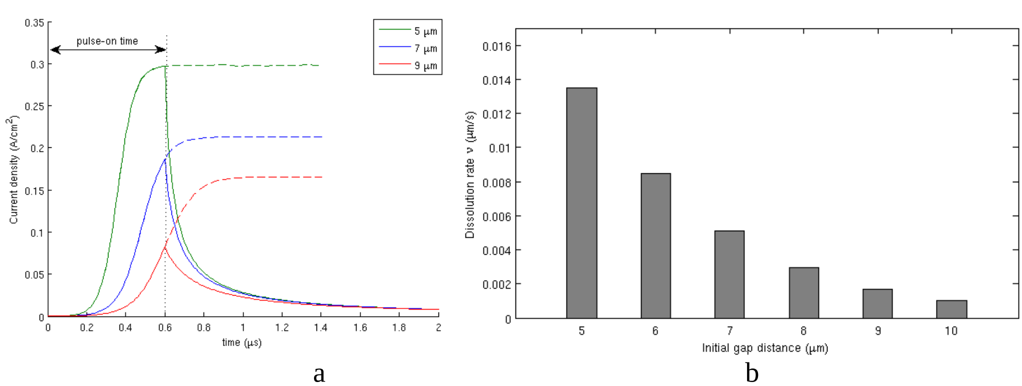

Figure 42. Simulation of current density (a) and dissolution rate (b) for different initial gap distance (frequency = 500 kHz, duty ratio = 0.3).

The pulse frequency and duty ratio are set at 500 kHz and 0.3. It could be observed that the current density can reach the peak for 5-μm gap. It means that the double layer is fully charged.

In contrast, it is seen that for higher gap distance (7 and 9 μm), the current density is smaller and it could not even reach the peak value. This is due to the fact that 0.6 μs pulse-on-time is not sufficiently long for the double layer to be fully charged. As a result, the dissolution rate is significantly smaller for higher gap distance, as indicated in Figure 42 (b). This explains how the material dissolution is localized and the dimensional accuracy is improved when short voltage pulses are used.

Figure 43 compares the experimental and analytical results of radial. It can be observed that there is a reasonable agreement between the predicted data and the experimental results for all the frequencies 100, 300 and 500 kHz. It is in accordance with the aforementioned analysis that the radial gap is increased when higher pulse duty ratio is used. Furthermore, the experimental results also indicate that the radial gap is slightly smaller when frequency is higher.

Electrode Wear in Simultaneous Micro-EDM and Micro-ECM

An attempt to evaluate the electrode wear in Simultaneous micro-EDM and micro-ECM has also been performed.

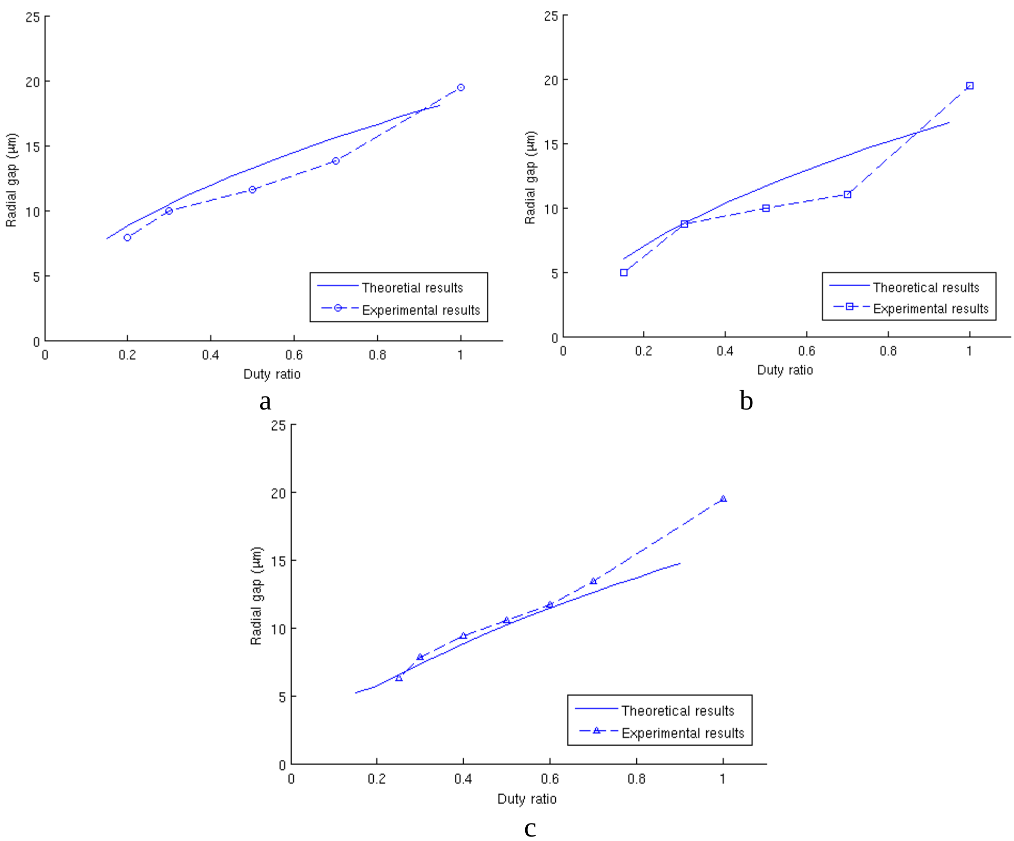

Figure 43. Comparison of experimental data and simulated results of radial gap for different pulse frequencies: (a) 100 kHz, (b) 300 kHz and (c) 500 kHz.

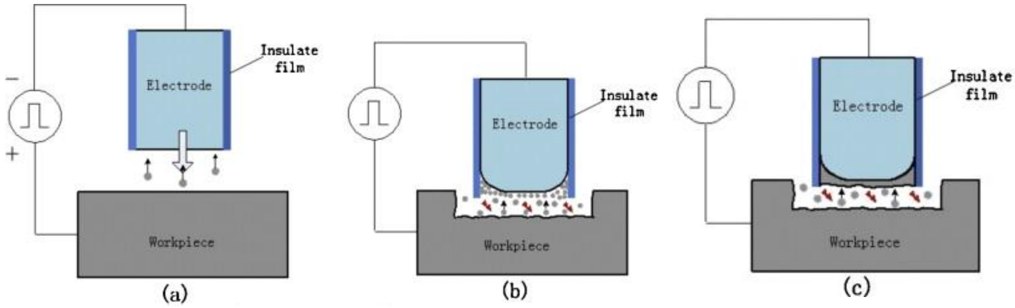

Figure 44. Principle of SEDCM: (a) electrochemical dissolve, (b) discharge and (c) discharge and electro-deposition [74].

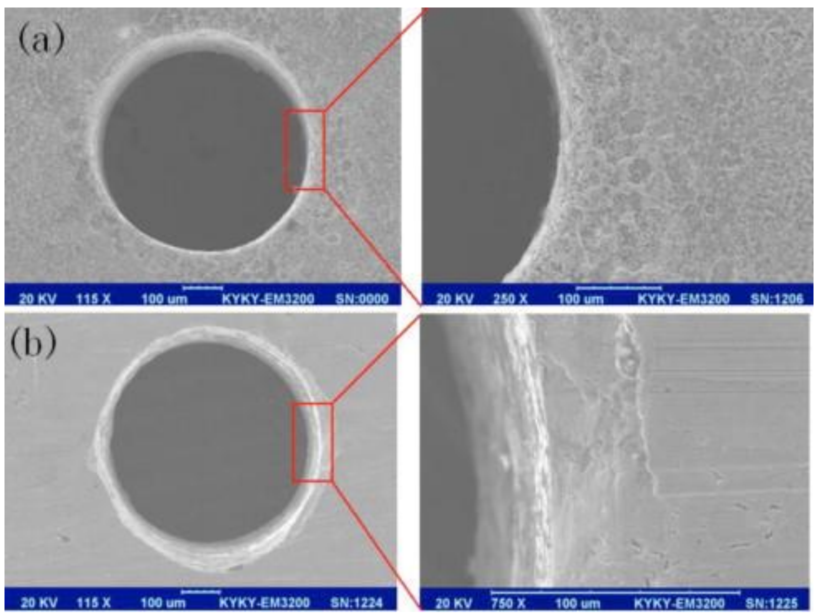

Figure 45. Comparison of holes machined using: (a) naked tool electrode and (b) tool electrode with side-insulation [74].

A similar SEDCM approach but using conductive electrolyte instead of deionized water was carried out [74]. This new method reduces the electrode wear by using electro-deposition and at the same time suppresses excessive electrolytic-erosion by nanosecond voltage pulse and tool electrode with side-insulation, as illustrated in Figure 44. Experimental results show that this new method can suppress excessive electrolytic-erosion effectively as shown in Figure 45 and reduce electrode wear as shown in Figure 46.

SIMULTANEOUS MICRO-EDM AND MICRO-ECM MILLING

Micro-EDM milling is a potential method to fabricate micro-tooling for replication technologies such as micro-injection molding or hot-embossing. This section presents the capability of SEDCM milling for fabrication of intricate micro-shapes with enhanced surface integrity and dimensional accuracy.

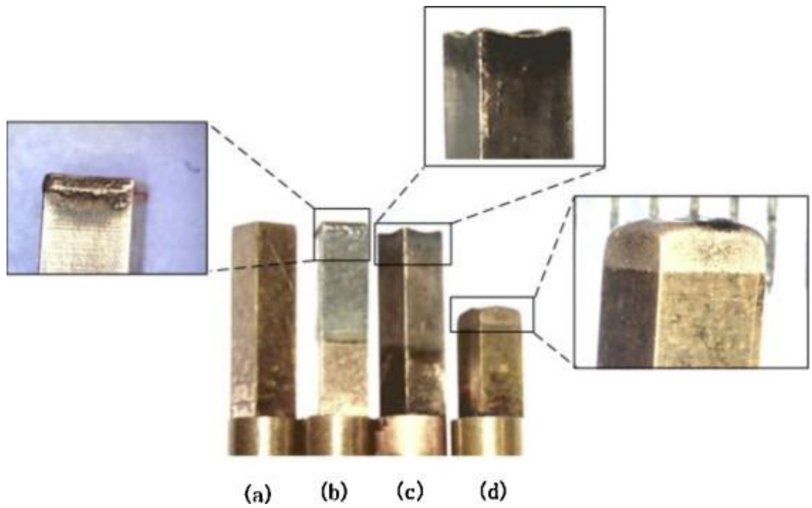

Figure 46. Electrode wear in different machining fluids. (a) Original shape (b) using electrolyte with conductivity 195 µS/cm, (c) electrolyte with conductivity 57 µS/cm and (d) kerosene [74].

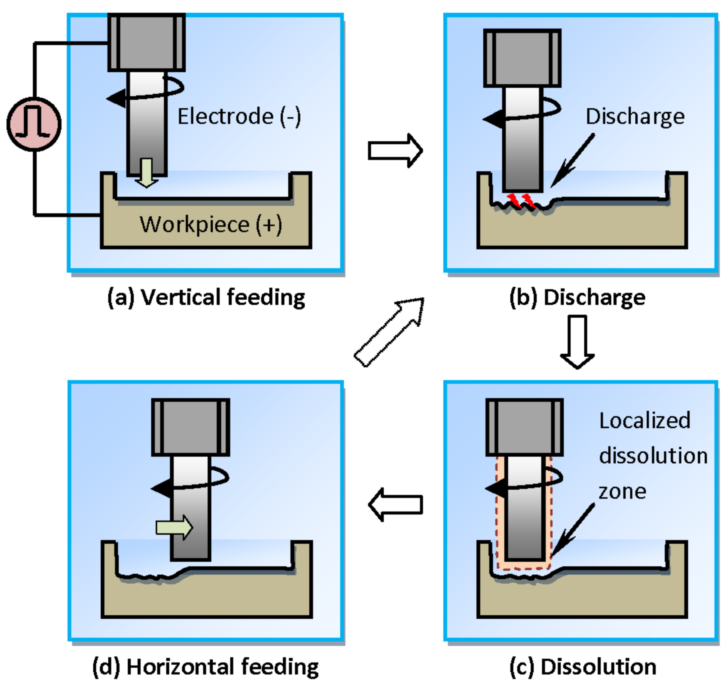

Figure 47. Principle of SEDCM milling [75].

Principle

The mechanism of SEDCM milling is depicted in Figure 47. Material is removed layer-by-layer to maintain the original shape of electrode. Electrode-workpiece gap is filled with low-resistivity deionized water, which exhibits both characteristics of a dielectric fluid and a slightly conductive electrolyte [36, 68].

When the process starts, voltage is applied in terms of short voltage pulses. For each layer, the tool electrode moves down by a specific layer depth, as shown in Figure 47(a). As the inter-electrode gap meets the critical value, the discharge occurs as illustrated in Figure 47 (b). Each discharge forms a crater, and the machined surface is covered with overlapped craters. Due to the removed material, the gap width expands and no further discharge takes place. Then, due to the slight conductivity of deionized water, the voltage pulses initiate a weak electrochemical reaction. Anodic dissolution happens on workpiece surface whereby its roughness is reduced, as shown in Figure 47(c).

In addition, due to the short duration of voltage pulses, dissolution zone is confined within a specific gap width (marked with dotted line) [9]. Hence, the machined shape is maintained, resulting in the improved dimensional accuracy. After that, the electrode moves horizontally following the preset tool path to remove material of the entire layer, as shown in Figure 47(d). The discharge takes place and the cycle is repeated.

Figure 48 illustrates the tool paths used where d is depth of each layer and V_f is the horizontal scanning feedrate. For obtaining the hybrid SEDCM milling, the machining speed needs to be appropriately adjusted and short voltage pulses must be used. In layer-by-layer removal, machining speed is affected by the thickness of each layer and the horizontal scanning feedrate. Therefore, the scanning feedrate, layer depth and voltage pulses are three main factors.

Main Factors of SEDCM Milling

Scanning Feed Rate

Figure 49 shows 5-µm deep micro-slots fabricated using feedrate from 50 to 10 µm/s. The depth of each layer is 0.2 µm and the voltage is applied as 500 kHz pulses with 30% duty ratio. As can be observed in Figure 49 (a), for 50 µm/s feedrate, the machined surface is completely covered with discharge craters. When the feedrate is reduced, it can be seen that there appears a smooth zone wherein the craters vanish. That zone becomes larger as the feedrate is lowered. This is due to material dissolution from machined surface caused by electrochemical reaction. At low feedrate, after the discharge has stopped, deionized water flows into the gap. The small amount of ions in the low-resistivity deionized water could act as a current carrier to facilitate the electrochemical reaction. Material is dissolved to remove recast layer, forming a smoother surface. In contrast, when the electrode moves at a higher feedrate, there is less time for the electrochemical reaction to remove the rough surface. As a consequence, the efficiency of surface finish improvement is reduced and it becomes negligible when the feedrate is as high as 50µm/s, as shown in Figure 49 (a).

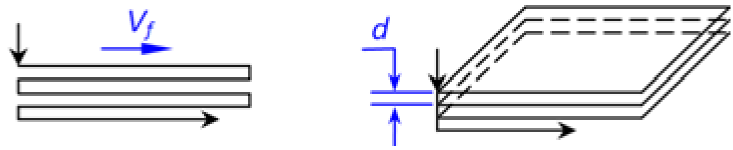

Figure 48. Tool paths to fabricate (a) micro-slots and (b) micro-cavities.

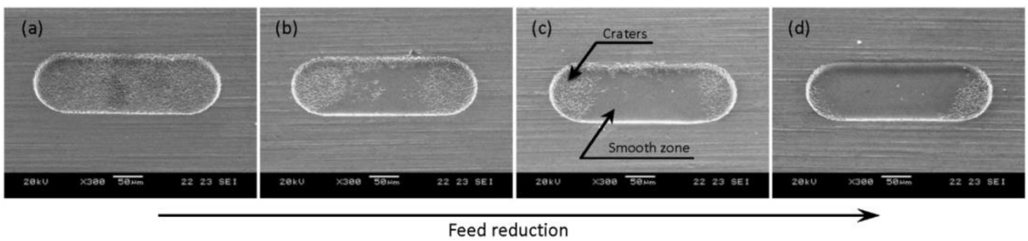

Figure 49. Micro-slots fabricated using short voltage pulses at different scanning feedrate: (a) 50 µm/s, (b) 30 µm/s, (c) 20 µm/s, and (d) 10 µm/s.

This indicates that low feedrate is the requirement for facilitating electrochemical reaction. At 10 µm/s feedrate, the smooth zone is observed to be widespread on most of the machined surface, as exhibited in Figure 49 (d).

However, there are few discharge craters left at the ends of slot. This is due to the lack of ions caused by the difficulty of fresh deionized water in infiltrating into the fine gap after the discharge has stopped. During electrochemical reaction, the electrolyte acts as a current carrier to transfer electrons created during anodic dissolution.

For that reason, lack of electrolyte would result in negligible electrochemical reaction. For improving the replenishment of fresh deionized water in the small gap, the electrode was lifted up a few microns after each layer. However, the effect is observed to be insignificant and the craters still appear at the two ends of the slot.

This is due to the fact that the dissolution zone is localized within a thin gap width owing to the short voltage pulses. The uplift of electrode also increases the frontal gap, resulting in poor efficiency of the electrochemical reaction.

Hence, to allow the replenishment of fresh deionized water into the small gap as well as to maintain that gap width under a certain value, the electrode is dwell at the two ends of micro-slot for few seconds before it starts a new layer. With this technique, the obtained micro-slot is found to be smooth for entire machined area, as shown in Figure 50 (a).

Short Voltage Pulses

Figure 50 (b) shows the micro-slot machined at the same 10 µm/s feedrate but applying continuous voltage supply. Compared with Figure 50 (a) wherein short voltage pulses are used, the machined surface is also observed to be relatively smooth with no visible crater. However, the slot is observed to be significantly enlarged due to the excessive material dissolution. This indicates that the usage of short voltage pulses is a key factor to localize the dissolution zone and thus prevent the machined shape from distortion.

Layer Depth

Figure 51 shows the micro-slots machined using same 10 µm/s feedrate but with higher layer depths, 0.5 µm and 1 µm respectively. It is observed that the discharge craters start to appear when the layer depth is increased. This is a result of the increase of material volume that needs to be removed in every feed.

Accordingly, the discharge has happened for longer duration to remove material, resulting in less machining time for the dissolution. As shown in Figure 51(b), the machined slot is mostly covered with discharge craters when the layer thickness is set to 1 µm. This indicates that small layer depth is also essential factor in SEDCM milling.

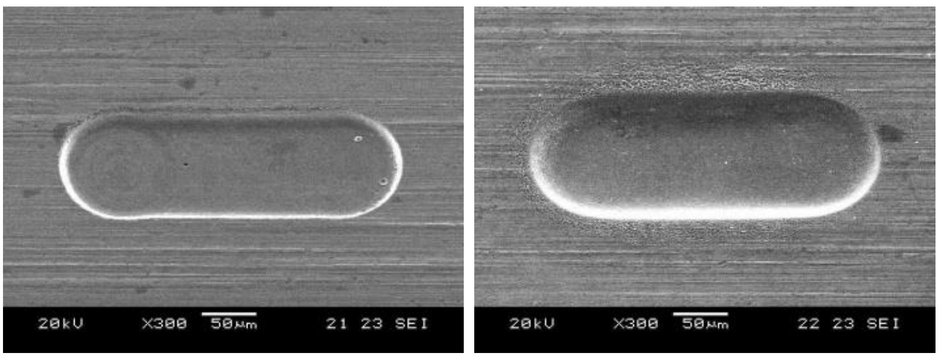

a b

Figure 50. Micro-slots fabricated at 10 µm/s feedrate using different power regimes: (a) 500 kHz voltage pulses and (b) continuous voltage.

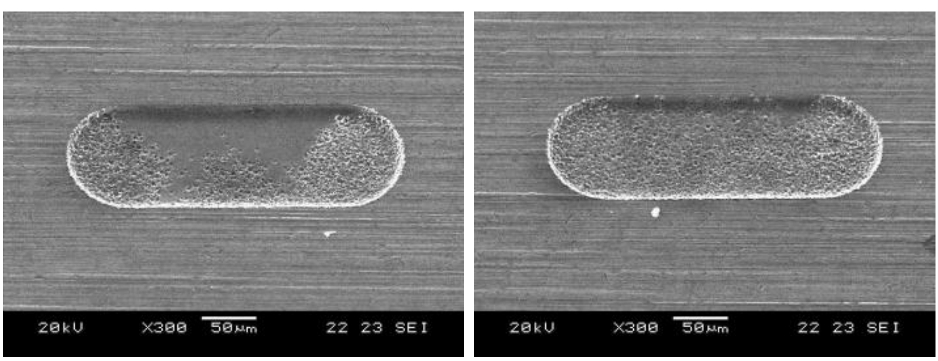

a b

Figure 51. Micro-slots fabricated at feedrate of 10 µm/s with different layer depths: (a) 0.5 µm and (b) 1 µm.

This requirement is also preferable in layer-by-layer removal because thinner layer depth would create surface with better flatness [76].

Performances of SEDCM Milling

Surface Integrity

Figure 52 shows the images of machined micro-slots and shapes. At 50 µm/s feedrate, the machined surface is fully covered with discharge craters and thus it is considered as micro-EDM milling. At 10 µm/s feedrate, the surface of the micro-slot and shape is seen to be smooth, and it represents SEDCM milling. Figure 53 shows the topography of the formed surfaces. Overlapping craters having diameter of 3-4 microns could be observed in Figure 53 (a) whereas a relatively smooth surface with no visible crater is obtained in Figure 53 (b). The surface profiles of these two surface textures are also plotted in Figure 53. For micro-EDM milling (V_f = 50 µm/s), the average surface roughness (R_a) is 142nm whereas for SEDCM milling (V_f = 10 µm/s), the R_a is found to be 22nm only. This shows that SEDCM milling yields better surface finish thanks to the effect of electrochemical reaction.

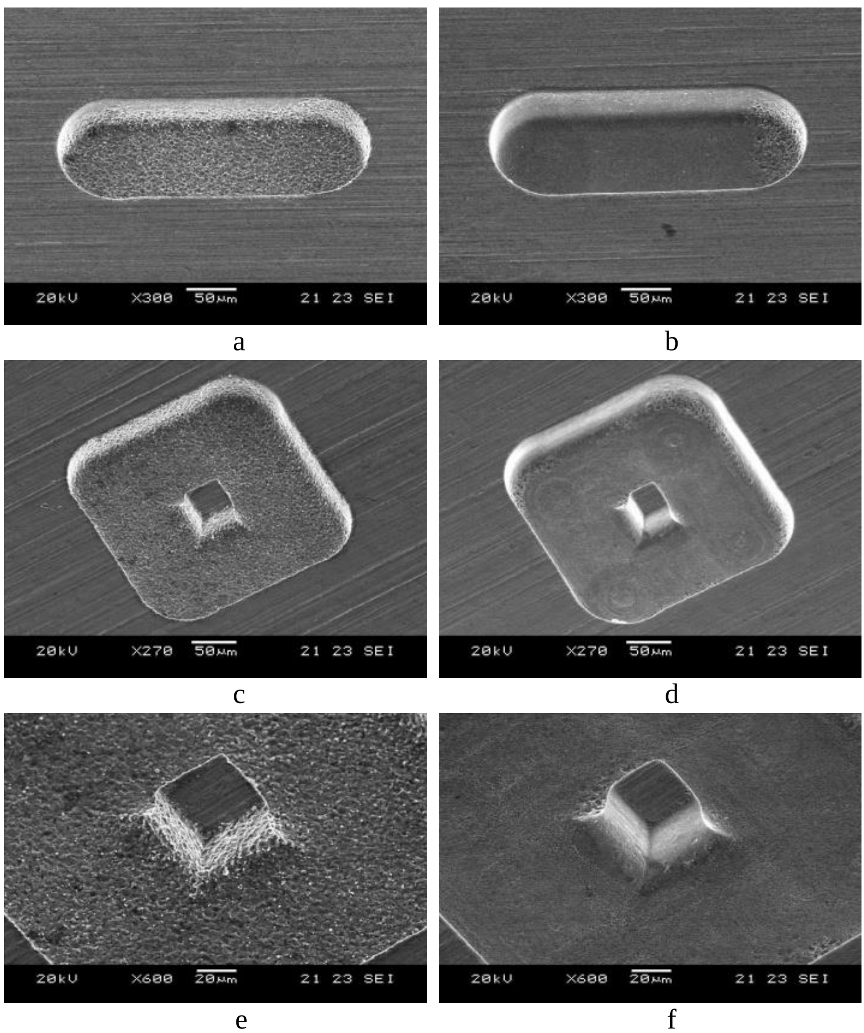

Figure 52. SEM micrographs of micro-slots machined at different feedrate: (a, c, e) 50 µm/s and (b, d, f) 10 µm/s [75].

Dimensional Accuracy

Figure 54 plots the profiles of the micro-slots and micro-shapes fabricated under the two conditions. For SEDCM milling (V_f = 10 μm/s), the width of machined slot is observed to be few microns larger than that of micro-EDM milling (V_f = 50 μm/s).

The slot width in case of SEDCM milling is around 112.99 μm whereas it is about 110.35 μm for micro-EDM milling. It shows that the SEDCM milling brings smoother surface because a thin layer formed by overlapped discharge craters is further removed from machined surface by material dissolution.

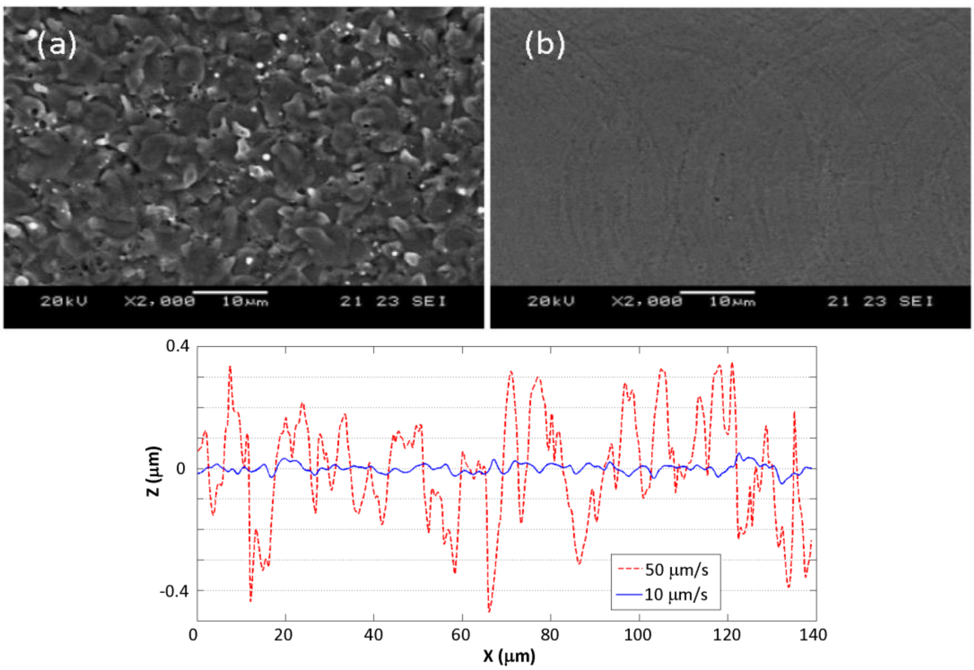

Figure 53. SEM micrographs and profiles of surfaces generated at different feedrate: (a) 50 μm/s and (b) 10 μm/s.

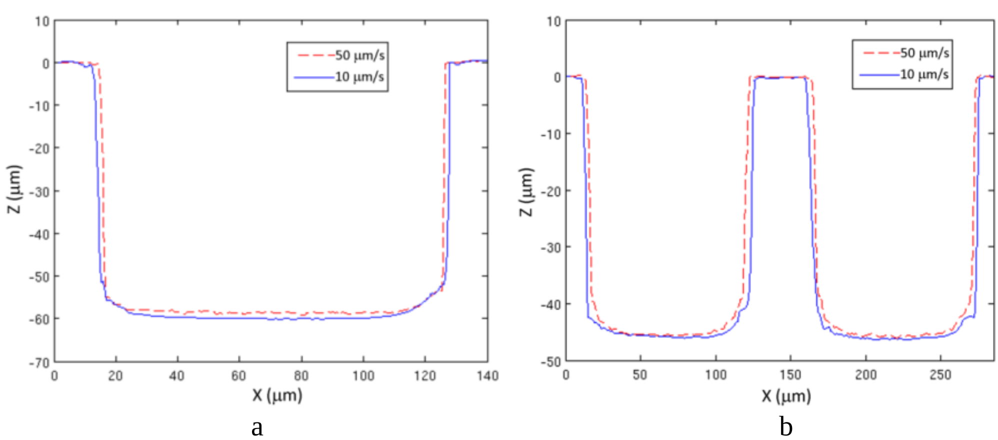

Figure 54. Profiles of micro-slots (a) and micro-cavities (b) fabricated at different feedrate.

In addition, it should be highlighted that the machining shape is still maintained and the dissolution is observed to be confined within micron-thick layer only, whereby high dimensional accuracy could be attained. This advantage is the result of short voltage pulses.

As observed in Figure 55, for SEDCM milling, the shorter the pulse duration, the thinner is the machining gap. At the same 30% duty ratio, the machining gap of SEDCM milling is higher than that of micro-EDM milling by Δg. Therefore, the Δg here indicates the thickness of material layer further removed by electrochemical reaction and it is about 1 ~ 1.5 μm for 30% duty ratio. When the duty ratio increases, the Δg becomes higher.

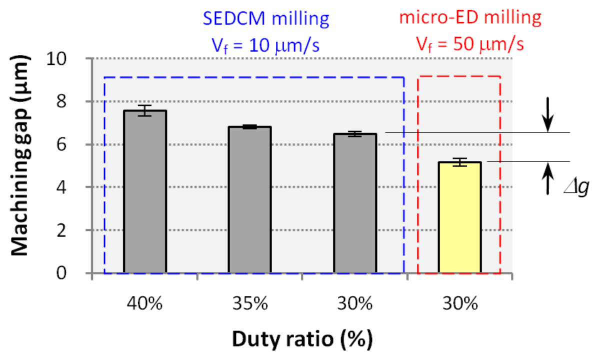

Figure 55. Machining gaps of different machining conditions.

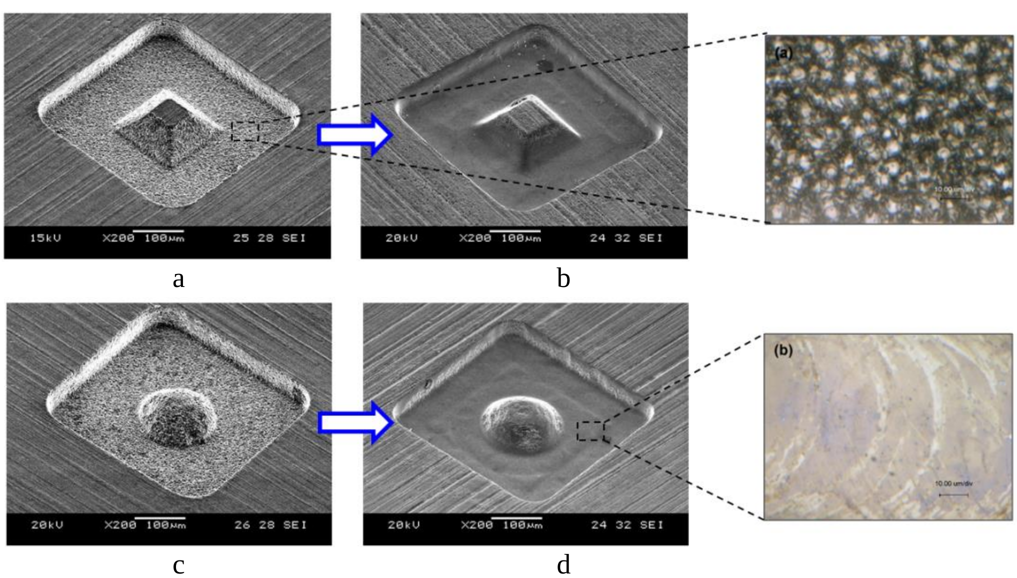

Figure 56. SEM images of 3D micro-cavities fabricated by different machining conditions: (a,c) micro-EDM milling and (b,d) SEDCM milling.

Therefore, it shows that SEDCM milling could enhance the dimensional accuracy by using short voltage pulses to limit the thickness of material layer further removed from the machined surface. Figure 56 shows two further examples of intricate 3D micro-shapes machined by micro-EDM milling and SEDCM milling, demonstrating the feasibility and capability of SEDCM milling process.

CONCLUSION

This chapter gives the comprehensive overview of multiple approaches combining micro-EDM and micro-ECM as hybrid machining to reap the advantages of two processes. The chapter starts with a brief overview of micro-EDM and micro-ECM. Then, multiple attempts to combine micro-EDM and micro-ECM as sequential processes to enhance the performance are presented.

A recent approach to combine micro-EDM and micro-ECM in same machining process by using low-resistivity deionized water is presented in detail. The chapter ends with applications of hybrid micro-EDM and micro-ECM milling for fabrication of 3D micro-structures which have both high dimensional accuracy and good surface finish. This chapter shows that with the proper combination of micro-EDM and ECM as hybrid machining process, it is feasible to fabricate intricate 3D micro-shapes for molds and dies, which entail both good surface finish and high dimensional accuracy.

REFERENCES

[1] Alting, L., Kimura, F., Hansen, H. N., Bissacco, G., (2003). Micro engineering. *CIRP Annals-Manufacturing Technology* 52, 635-657.

[2] Altan, T., Lilly, B., Yen, Y. C., (2001). Manufacturing of Dies and Molds. *CIRP Annals - Manufacturing Technology* 50, 404-422.

[3] Uriarte, L., Herrero, A., Ivanov, A., Oosterling, H., Staemmler, L., Tang, P. T., et al., (2006). Comparison between microfabrication technologies for metal tooling. *Proceedings of the Institution of Mechanical Engineers, Part C: Journal of Mechanical Engineering Science* 220, 1665-1676.

[4] Reyntjens, S., Puers, R., (2001). A review of focused ion beam applications in microsystem technology. *Journal of Micromechanics and Microengineering* 11, 287.

[5] Vieu, C., Carcenac, F., Pepin, A., Chen, Y., Mejias, M., Lebib, A., et al., (2000). Electron beam lithography: resolution limits and applications. *Applied Surface Science* 164, 111-117.

[6] Lim, H. S., Wong, Y. S., Rahman, M., Edwin Lee, M. K., (2003). A study on the machining of high-aspect ratio micro-structures using micro-EDM. *Journal of Materials Processing Technology* 140, 318-325.

[7] Masuzawa, T., (2000). State of the Art of Micromachining. *CIRP Annals - Manufacturing Technology* 49, 473-488.

[8] Masaki, T., Kawata, K., Masuzawa, T., (1990). Micro electro-discharge machining and its applications. *An Investigation of Micro Structures, Sensors, Actuators, Machines and Robots*: IEEE.

[9] Schuster, R., Kirchner, V., Allongue, P., Ertl, G., (2000). Electrochemical Micromachining. *Science* 289, 98-101.

[10] Kunieda, M., Lauwers, B., Rajurkar, K. P., Schumacher, B. M., (2005). Advancing EDM through Fundamental Insight into the Process. *CIRP Annals - Manufacturing Technology* 54, 64-87.

[11] Uhlmann, E., Piltz, S., Doll, U., (2005). Machining of micro/miniature dies and moulds by electrical discharge machining--Recent development. *Journal of Materials Processing Technology* 167, 488-493.
[12] Rajurkar, K. P., Levy, G., Malshe, A., Sundaram, M. M., McGeough, J., Hu, X., et al., (2006). Micro and Nano Machining by Electro-Physical and Chemical Processes. *CIRP Annals - Manufacturing Technology* 55, 643-666.
[13] McGeough, J. A., (1974). *Principles of Electrochemical Machining*. Chapman and Hall London, UK.
[14] Kalpakjian, S., (1997). *Manufacturing Processes for Engineering Materials*. Third Edition ed: Addison Wesley.
[15] Bhattacharyya, B., Munda, J., Malapati, M., (2004). Advancement in electrochemical micro-machining. *International Journal of Machine Tools and Manufacture* 44, 1577-1589.
[16] Kim, B. H., Na, C. W., Lee, Y. S., Choi, D. K., Chu, C. N., (2005). Micro electrochemical machining of 3D micro structure using dilute sulfuric acid. *CIRP Annals-Manufacturing Technology* 54, 191-194.
[17] Madore, C., Piotrowski, O., Landolt, D., (1999). Through-mask electrochemical micromachining of titanium. *Journal of The Electrochemical Society* 146, 2526.
[18] Kern, P., Veh, J., Michler, J. New developments in through-mask electrochemical micromachining of titanium. *Journal of Micromechanics and Microengineering*. 2007; 17:1168.
[19] Kim, B. H., Ryu, S. H., Choi, D. K., Chu, C. N., (2005). Micro electrochemical milling. *Journal of Micromechanics and Microengineering* 15, 124.
[20] Pandey, P. C., Jilani, S. T., (1986). Plasma channel growth and the resolidified layer in edm. *Precision Engineering* 8, 104-110.
[21] Lee, L. C., Lim, L. C., Wong, Y. S., Lu, H. H., (1990). Towards a better understanding of the surface features of electro-discharge machined tool steels. *Journal of Materials Processing Technology* 24, 513-523.
[22] Ekmekci, B., Sayar, A., Öpöz, T. T., Erden, A., (2009). Geometry and surface damage in micro electrical discharge machining of micro-holes. *Journal of Micromechanics and Microengineering* 19, 105030.
[23] Guu, Y. H., Hocheng, H., Chou, C. Y., Deng, C. S., (2003). Effect of electrical discharge machining on surface characteristics and machining damage of AISI D2 tool steel. *Materials Science and Engineering A* 358, 37-43.
[24] Kruth, J. P., Stevens, L., Froyen, L., Lauwers, B. Study of the White Layer of a Surface Machined by Die-Sinking Electro-Discharge Machining. *CIRP Annals - Manufacturing Technology*. 1995;44:169-72.
[25] Ekmekci, B., (2009). White layer composition, heat treatment, and crack formation in electric discharge machining process. *Metallurgical and Materials Transactions B* 40, 70-81.
[26] Bleys, P., Kruth, J. P., Lauwers, B., Schacht, B., Balasubramanian, V., Froyen, L., et al., (2006). Surface and Sub-Surface Quality of Steel after EDM. *Advanced Engineering Materials* 8, 15-25.
[27] Lee, H., Rehbach, W., Tai, T., Hsu, F., (2003). Surface integrity in micro-hole drilling using micro-electro discharge machining. *Materials Transactions* 44, 2718-2722.

[28] Kurnia, W., Tan, P. C., Yeo, S. H., Tan, Q. P., (2009). Surface roughness model for micro electrical discharge machining. *Proceedings of the Institution of Mechanical Engineers, Part B: Journal of Engineering Manufacture* 223, 279-287.
[29] Ekmekci, B., Elkoca, O., Erden, A., (2005). A comparative study on the surface integrity of plastic mold steel due to electric discharge machining. *Metallurgical and Materials Transactions B* 36, 117-124.
[30] Yu, Z. Y., Rajurkar, K. P., Narasimhan, J., (2003). Effect of machining parameters on machining performance of micro EDM and surface integrity. *Proceedings of ASPE Annual Meeting*.
[31] Tsai, Y. Y., Masuzawa, T., (2004). An index to evaluate the wear resistance of the electrode in micro-EDM. *Journal of Materials Processing Technology* 149, 304-309.
[32] Mohri, N., Suzuki, M., Furuya, M., Saito, N., Kobayashi, A., (1995). Electrode Wear Process in Electrical Discharge Machinings. *CIRP Annals-Manufacturing Technology* 44, 165-168.
[33] Rajurkar, K. P., Zhu, D., Mc Geough, J. A., Kozak, J., De Silva, A. K. M., (1999). New developments in electro-chemical machining. *CIRP Annals-Manufacturing Technology* 48, 567-579.
[34] Jeon, D. H., Kim, B. H., Chu, C. N., (2006). Micro Machining by EDM and ECM. *Korean Society Of Precision Engineering* 23, 52.
[35] Kozak, J., Rajurkar, K. P., Makkar, Y., (2004). Selected problems of micro-electrochemical machining. *Journal of Materials Processing Technology* 149, 426-431.
[36] Masuzawa, T., Kuo, C. L., Fujino, M., (1994). A Combined Electrical Machining Process for Micronozzle Fabrication. *CIRP Annals - Manufacturing Technology* 43, 189-192.
[37] Crichton, I. M., McGeough, J. A., Munro, W., White, C., (1981). Comparative studies of ECM, EDM and ECAM. *Precision Engineering* 3, 155-160.
[38] Masuzawa, T., Sakai, S., (1987). Quick Finishing of WEDM Products by ECM Using a Mate-Electrode. *CIRP Annals - Manufacturing Technology* 36, 123-126.
[39] Masuzawa, T., Kimura, M., (1991). Electrochemical Surface Finishing of Tungsten Carbide Alloy. *CIRP Annals - Manufacturing Technology* 40, 199-202.
[40] Ramasawmy, H., Blunt, L., (2002). 3D surface topography assessment of the effect of different electrolytes during electrochemical polishing of EDM surfaces. *International Journal of Machine Tools and Manufacture* 42, 567-574.
[41] Hung, J. C., Yan, B. H., Liu, H. S., Chow, H. M., (2006). Micro-hole machining using micro-EDM combined with electropolishing. *Journal of Micromechanics and Microengineering* 16, 1480.
[42] Zeng, Z., Wang, Y., Wang, Z., Shan, D., He, X., (2012). A study of micro-EDM and micro-ECM combined milling for 3D metallic micro-structures. *Precision Engineering* 36, 500-509.
[43] Skoczypiec, S., Ruszaj, A., (2014). A sequential electrochemical–electrodischarge process for micropart manufacturing. *Precision Engineering* 38, 680-690.
[44] Takahata, K., Aoki, S., Sato, T., (1996). Fine Surface Finishing Method For 3-Dimensional Micro Structures. *An Investigation of Micro Structures, Sensors, Actuators, Machines and Systems*. IEEE.

[45] Kurita, T., Hattori, M., (2006). A study of EDM and ECM/ECM-lapping complex machining technology. *International Journal of Machine Tools and Manufacture* 46, 1804-1810.

[46] Masuzawa, T., Fujino, M., Kobayashi, K., Suzuki, T., Kinoshita, N., (1985). Wire Electro-Discharge Grinding for Micro-Machining. *CIRP Annals - Manufacturing Technology* 34, 431-434.

[47] Campana, S., Miyazawa, S., (1999). Micro EDM and ECM in DI Water. *Proceedings of ASPE Annual Meeting*.

[48] Chung, D. K., Shin, H. S., Kim, B. H., Park, M. S., Chu, C. N., (2009). Surface finishing of micro-EDM holes using deionized water. *Journal of Micromechanics and Microengineering* 19, 045025.

[49] Chung, D., Lee, K., Jeong, J., Chu, C., (2014). Machining characteristics on electrochemical finish combined with micro EDM using deionized water. *International Journal of Precision Engineering and Manufacturing* 15, 1785-1791.

[50] Jong Wuk, P., Ki Young, S., Do Kwan, C., Chong Nam, C., (2013). Fabrication of micro-lenticular patterns using WEDM-grooving and electrolytic polishing. *Journal of Micromechanics and Microengineering* 23, 125034.

[51] Mohd Abbas, N., Solomon, D. G., Fuad Bahari, M. A review on current research trends in electrical discharge machining (EDM). *International Journal of Machine Tools and Manufacture*. 2007;47:1214-1228.

[52] Jeswani, M. L., (1981). Electrical discharge machining in distilled water. *Wear* 72, 81-88.

[53] Jilani, S. T., Pandey, P. C., (1984). Experimental investigations into the performance of water as dielectric in EDM. *International Journal of Machine Tool Design and Research* 24, 31-43.

[54] Konig, W., Siebers, F. J., (1993). Influence of the working medium on the removal process in EDM sinking. *Proceedings of ASME Winter Annual Meeting*. New Orleans, LA, US p. 649-58.

[55] Chen, S. L., Yan, B. H., Huang, F. Y., (1999). Influence of kerosene and distilled water as dielectrics on the electric discharge machining characteristics of Ti-6Al-4V. *Journal of Materials Processing Technology* 87, 107-111.

[56] Lin, C. T., Chow, H. M., Yang, L. D., Chen, Y. F., (2007). Feasibility study of micro-slit EDM machining using pure water. *The International Journal of Advanced Manufacturing Technology* 34, 104-110.

[57] Kagaya, K., Oishi, Y., Yada, K., (1986). Micro-electrodischarge machining using water as a working fluid--I: micro-hole drilling. *Precision Engineering* 8, 157-162.

[58] Masuzawa, T., Tsukamoto, J., Fujino, M., (1989). Drilling of Deep Microholes by EDM. *CIRP Annals - Manufacturing Technology* 38, 195-198.

[59] Chung, D. K., Kim, B. H., Chu, C. N., (2007). Micro electrical discharge milling using deionized water as a dielectric fluid. *Journal of Micromechanics and Microengineering* 17, 867.

[60] Yan, M. T., Lai, Y. P., (2007). Surface quality improvement of wire-EDM using a fine-finish power supply. *International Journal of Machine Tools and Manufacture* 47, 1686-1694.

[61] Yamada, H., Magura, T., Sato, K., Yutomi, T., Kobayashi, K., (1993). High quality electrical discharge machining using anti-electrolysis power source. *EDM Technology* 1, 25-30.
[62] Ukai, Y., Satou, S., (2004). *Power supply system for applying a voltage of both positive and negative polarities in electric discharge machining*. US Patent 6,727,4552004.
[63] Song, K. Y., Chung, D. K., Park, M. S., Chu, C. N., (2009). Micro electrical discharge drilling of tungsten carbide using deionized water. *Journal of Micromechanics and Microengineering* 19, 045006.
[64] Song, K. Y., Chung, D. K., Park, M. S., Chu, C. N., (2010). Micro electrical discharge milling of WC-Co using a deionized water spray and a bipolar pulse. *Journal of Micromechanics and Microengineering* 20, 045022.
[65] Masaki, T., Kuriyagawa, T., (2009). Study of precision micro-Electro-Discharge Machining (3rd Report) - Analysis of micro-EDM process with deionized water. *Journal of The Japan Society of Electrical Machining Engineers* 43, 163-171.
[66] Song, K. Y., Chung, D. K., Park, M. S., Chu, C. N., (2012). Water spray electrical discharge drilling of WC-Co to prevent electrolytic corrosion. *International Journal of Precision Engineering and Manufacturing* 13, 1117-1123.
[67] Chung, D. K., Shin, H. S., Park, M. S., Chu, C. N., (2011). Machining characteristics of micro EDM in water using high frequency bipolar pulse. *International Journal of Precision Engineering and Manufacturing* 12, 195-201.
[68] Nguyen, M. D., Rahman, M., Wong, Y. S., (2012). Simultaneous micro-EDM and micro-ECM in low-resistivity deionized water. *Int. J. Mach. Tool Manu.* 54-55, 55-65.
[69] Kao, C. C., Tao, J., Shih, A. J. Near dry electrical discharge machining. *International Journal of Machine Tools and Manufacture*. 2007;47: 2273-81.
[70] Nguyen, M. D., Rahman, M., Wong, Y. S., (2013). Modeling of radial gap formed by material dissolution in simultaneous micro-EDM and micro-ECM drilling using deionized water. *International Journal of Machine Tools and Manufacture* 66, 95-101.
[71] Bard, A. J., Faulkner, L. R., (2001). *Electrochemical Methods: Fundamentals and Applications* (2nd Edition). Second ed.: John Wiley, New York.
[72] De Abril, O., Gündel, A., Maroun, F., Allongue, P., Schuster, R., (2008). Single-step electrochemical nanolithography of metal thin films by localized etching with an AFM tip. *Nanotechnology* 19, 325301.
[73] Kozak, J., Gulbinowicz, D., Gulbinowicz, Z., (2008). The mathematical modeling and computer simulation of pulse electrochemical micromachining. *Engineering Letter* 16.
[74] Yin, Q., Wang, B., Zhang, Y., Ji, F., Liu, G., (2014). Research of lower tool electrode wear in simultaneous EDM and ECM. *Journal of Materials Processing Technology* 214, 1759-1768.
[75] Nguyen, M. D., Rahman, M., Wong, Y. S., (2012). Enhanced surface integrity and dimensional accuracy by simultaneous micro-ED/EC milling. *CIRP Annals-Manufacturing Technology* 61, 191-194.
[76] Yu, Z. Y., Masuzawa, T., Fujino, M., (1998). Micro-EDM for Three-Dimensional Cavities - Development of Uniform Wear Method. *CIRP Annals - Manufacturing Technology* 47, 169-172.

In: Electrical Discharge Machining (EDM)
Editor: M. P. Jahan
ISBN: 978-1-63483-591-6

Chapter 7

ORBITAL ELECTRO DISCHARGE MACHINING

Harshit K. Dave*[*], *Harit K. Raval and Keyur P. Desai
Sardar Vallabhbhai National Institute of Technology, Surat, India

ABSTRACT

Electro Discharge Machining (EDM) process is the most commonly used non-traditional manufacturing process in industry largely due to its capability to machine any conducting material irrespective of its hardness. It is simple in operation and easy to maintain. However, it has very slow machining rate. Further, tooling cost is high as a dedicated tool is required for every new job with different dimensions. This limitation can be overcome by orbiting the tool along its Z axis i.e., actuating the tool in lateral (XY) plane along with Z axis. It is possible to machine a larger size of cavity with relatively smaller tool electrode by orbital tool actuation at specific orbital radius. There are different strategies of generating orbital tool movement, chief among them being helical part and radial path. It is found that orbital EDM process proves to be efficient relative to cavity sinking process when machining is carried out for deep hole drilling. As compared to cavity sinking process, orbital EDM process provides faster material removal with negligible effect of tool wear and better surface quality at higher depths.

Keywords: EDM, orbital EDM, planetary EDM

INTRODUCTION

Electro Discharge Machining (EDM) process is the most widely used non-traditional manufacturing process in industry due to its capability to machine any conductive material. EDM is a thermal process that uses spark discharges to erode electrically conductive materials.

In EDM, a shaped electrode is used to define the shape of the resulting cavity or hole in the work piece. Typically, such holes are drilled by using a matched electrode with a diameter

[*] Corresponding Author: Harshit K. Dave, E-mail: harshitkumar@yahoo.com

that is slightly smaller than the hole to be drilled. The matched electrode, while capable of creating very small holes, poses a number of problems. Obviously, every hole size needs a separate electrode, making this technique tooling intensive. A second challenge is the supply of the dielectric fluid. For larger sized holes, through flushing can be used in which a hollow electrode can be used to supply the fluid to the bottom of the hole. But for very small sized holes it is difficult to use hollow electrode for fluid supply. As a result, as the depth of the hole increases, the Material Removal Rate (M.R.R.) typically decreases and frequently reduces the quality of the machined surface [1].

A solution to the above mentioned challenge is to decouple the size of the electrode from the size of the hole to be machined. Using an electrode that is significantly smaller than the hole to be drilled, and actuating this electrode on a tool path that will articulate its outer surface on a trajectory equal to the shape of the hole can address both issues addressed simultaneously. This is called orbiting of electrode. In orbital EDM, a standard electrode can be used to drill a wide range of holes while the increased clearance between the hole and the electrode helps getting the dielectric fluid to the bottom of the hole. The use of a small size of standard electrodes instead of matched electrodes for every single hole size drastically reduces tooling efforts. The improved flushing will reduce recasting of removed material, which results in better surface quality [2].

STRATEGIES OF ORBITAL TOOL MOVEMENT

The basic idea behind electrode orbiting is to actuate the electrode on a controlled trajectory. If the orbiting motion is created with a device that allows the radius to be controlled electronically, the motion can be integrated into the EDM machine’s control system. By integrating the orbiting motion into the machine control system, a number of different cutting motions are possible.

Following are different ways in which orbital tool movement can be actuated:

(a) Slicing Movement

In this strategy the required depth is divided into a number of cylindrical slices of thickness t_s, and removes the material contained in each slice by first plunging into the center of the cylinder. This is followed by a linear move outward towards the hole surface. The remaining material is then removed by a single, circular sweep [3]. As shown in Figure 1, first the electrode moves radially outward from center in path 1; it then moves on full circumference along path 2 and comes back to its original position on the circumference; it then moves radially inwards on path 3. Now the electrode plunges inside up to the predefined depth t along path 4. Now electrode follows the same trajectory along path 5 radially outward, 6 circumferentially, 7 radially inward and finally along 8 in downward direction. This is how material is cut using orbital path. The machining parameters that can be varied in this setup are the thickness ts of the slice and the radius r of the orbit. This sequence is illustrated in Figure 1.

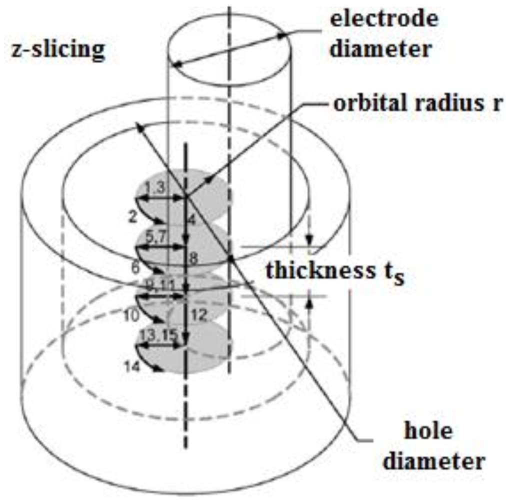

Figure 1. Slicing movement of tool electrode [3].

The main disadvantage in this strategy is that the final side surface is created for defined thickness t_s, there is always a possibility of uneven surface generation on side of the hole. Due to corner wear that may be experienced by the tool electrode, desired final shape of the cavity might not be achieved through this type of movement.

(b) Cylindrical Movement

The second strategy would involve the division of the material to be removed into a center cylinder, which is removed by plunging to the full depth of the hole and cylindrical shells, which are removed by orbits with gradually increasing radii (see Figure 2).

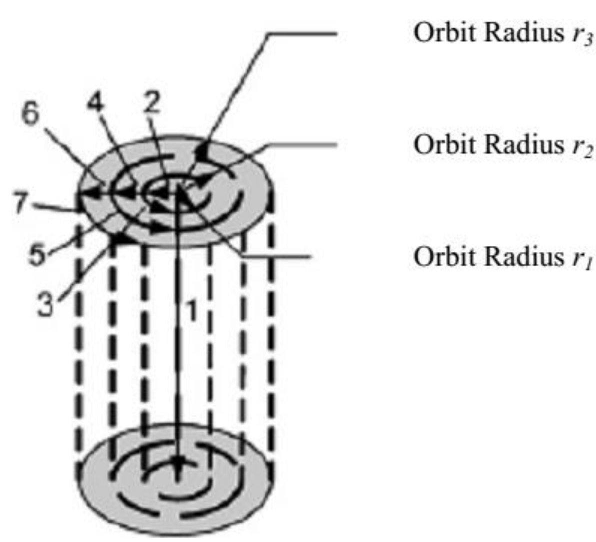

Figure 2. Cylindrical movement of tool electrode [3].

The electrode initially moves up to the full depth required on path 1. Now it moves radially outward along 2 and then along full circumference along path 3. In similar manner, it continues to move along path 4 and 5; 6 and 7; and so on till the cavity of required diameter is generated. In this mode, a substantial portion of the material is removed with the cylindrical surface of the electrode. Hence, there is uniform wear all across the cylindrical surface. However, the wear on the surface will gradually reduce the electrode diameter, which in turn affects the final diameter of the hole. The machining parameters for this setup are the orbital radii. Since the hole will be finished during orbiting, so the cavity generated during plunge cutting will not require good finish. Hence, a larger voltage and current for the plunge cut can be used for faster machining.

Though the surface produced will have relatively low quality surface finish, it is not a big concern because this surface will be eventually removed during the subsequent orbiting.

(c) Helical Movement

In the third strategy a constant feed is given along the axis of the hole along with the orbiting motion. This gives a helical motion that is continued until the final depth of the hole is reached. The parameters that affect this technique are the plunge feed per revolution and the orbital radius. This is illustrated in Figure 3. The possible problem to be encountered in this strategy would be the definition of helical path of movement.

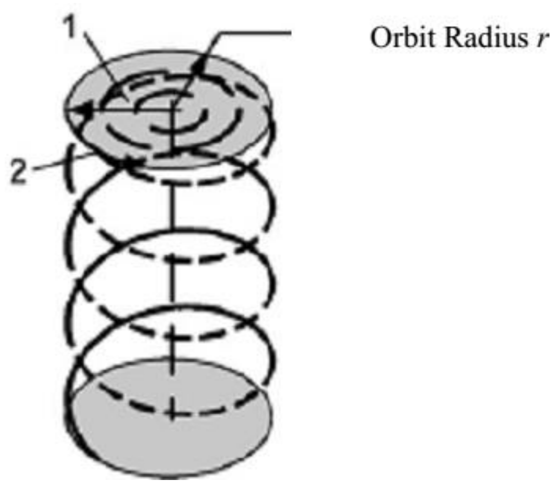

Figure 3. Helical movement of tool electrode [3].

(d) Radial Movement

In this strategy, electrode is plunged to the full depth of hole initially. Then the electrode is moved radially outwards and brought back to center. This is repeated at an angular increment of 5°. Thus, the cavity with desired size is generated after 72 tool travel in radial direction. This is shown in Figure 4.

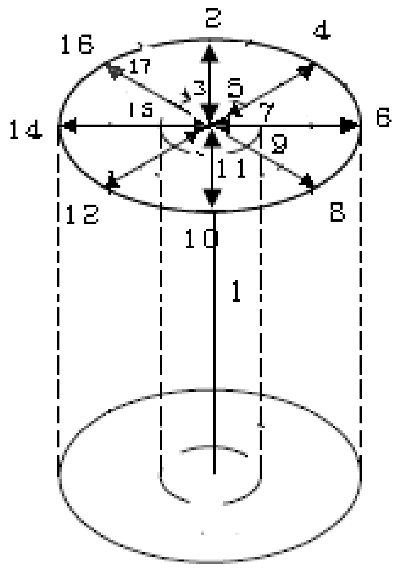

Figure 4. Radial movement of tool electrode.

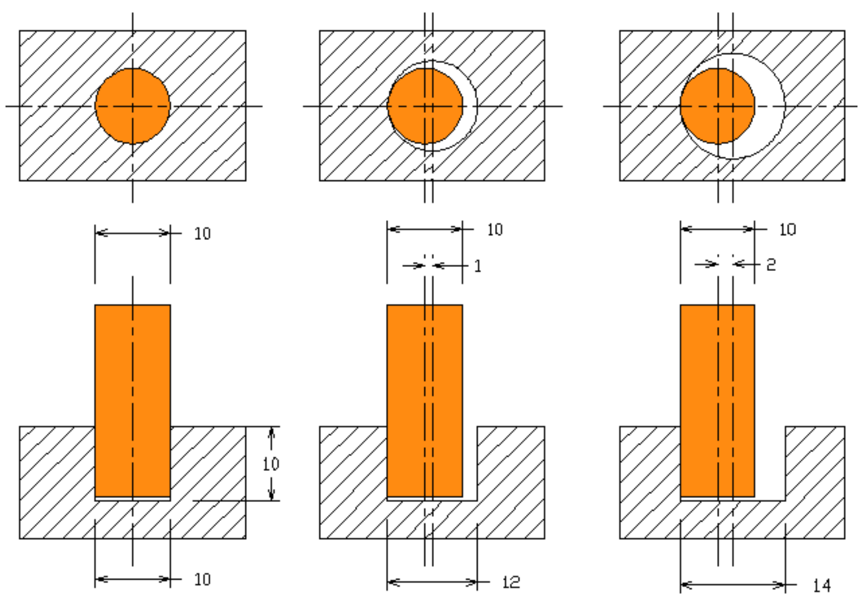

Figure 5. Orbital path traced by electrode with same diameter resulting into different size of cavity.

In this type of strategy, the tool is initially plunged into the work piece to achieve the desired depth. This is shown by path 1 in Figure 4. Just as in cylindrical movement, higher current and voltage can be set for speedy process. Surface finish is not an issue because the surface that will generate at the end of this will be eventually removed in orbital movement. After full depth is achieved, the tool moves radially outwards along the path 2. After the extreme position is reached, the tool returns back radially inside to its original position along the path 3. The next movement is along the radially outward direction at an angle of 5° with the previous direction of movement. Thus, the same movement is repeated 72 times in a circular cavity. As the machining is mostly carried out by the sides of the tool, it can be anticipated that there will be relatively higher side wear.

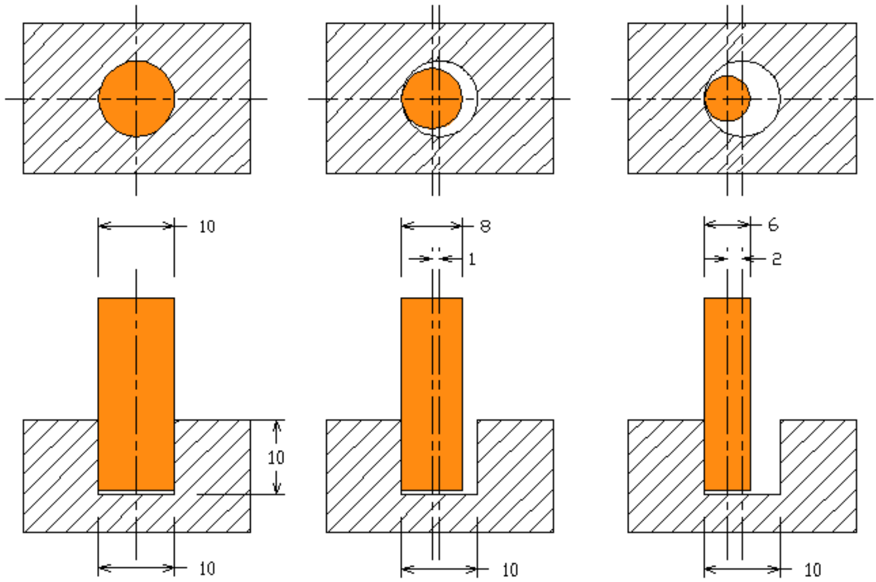

Figure 6. Orbital path traced by different size of tool electrode resulting into same size of cavity.

Generally, orbital tool actuation can be carried out in two different ways, viz. (a) selecting a specific tool diameter and actuating different orbital radius with it resulting into cavity with different diameters and (b) selecting different diameters of tool and actuating different orbital radius with it in such a way that diameter size of final cavity remains constant. The strategies are schematically shown in Figures 5 & 6.

In option (a) when a tool having constant diameter is actuated along different orbital radius, the resulting cavity will have different diameter. This can be understood by Figure 5.

In option (b) it is possible to set the combination of tool diameter and orbital radius in such a way that the machined cavity has same diameter. The diameter of final cavity is kept constant and the tool diameter is varied to provide respective orbital radius. This is shown in Figure 6.

EFFECT ON SURFACE INTEGRITY

Surface integrity has been widely investigated in orbital EDM process. Rajurkar and Royo carried out experiments to study the effect of orbital cutting on surface integrity of EDM Components [4]. They conducted experiments on AISI 4130 work piece using Poco grade EDM-1 tool having 2.54 mm radius and 0.3 mm/sec orbital speed. SEM photographs as shown in Figure 7 are taken for samples under equal machining conditions. Large craters are found on surfaces machined with cavity sinking (without orbital cutting). From Figure 7(a) and (b), it can be noted that the surface quality is inferior when cavity sinking is used while orbital motion produces better surface finish which is evident by the size of craters.

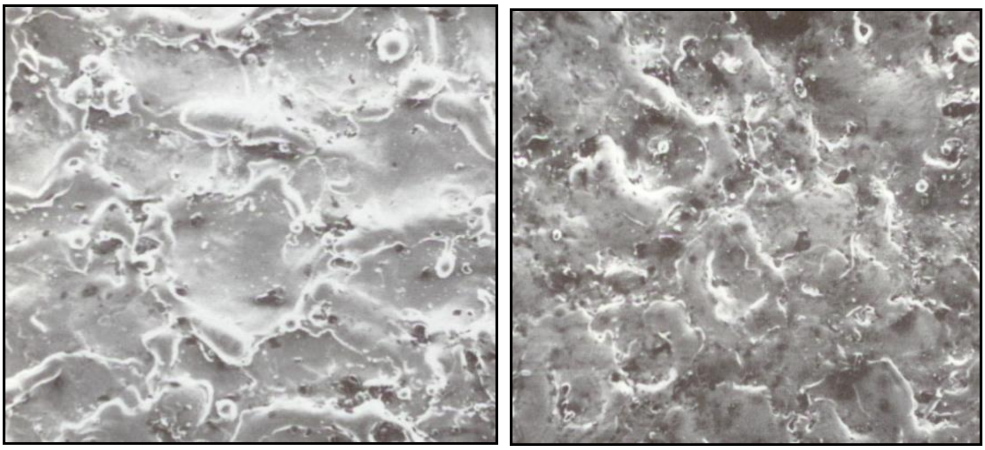

(a) (b)

Figure 7. SEM Photograph of machined surface under (a) Cavity Sinking (b) Orbital Motion [4].

To examine the quality of micro holes, Eberhard Bamberg and Sumet Heamawatanachai drilled three holes with a depth of 500 μm and then dissected them with a wire EDM to expose the machined surfaces [3]. Figure 8 shows the scanning electron microscope (SEM) image of the cross sections, which clearly shows that the surface of the holes drilled with orbiting, are very smooth and uniform throughout the entire length.

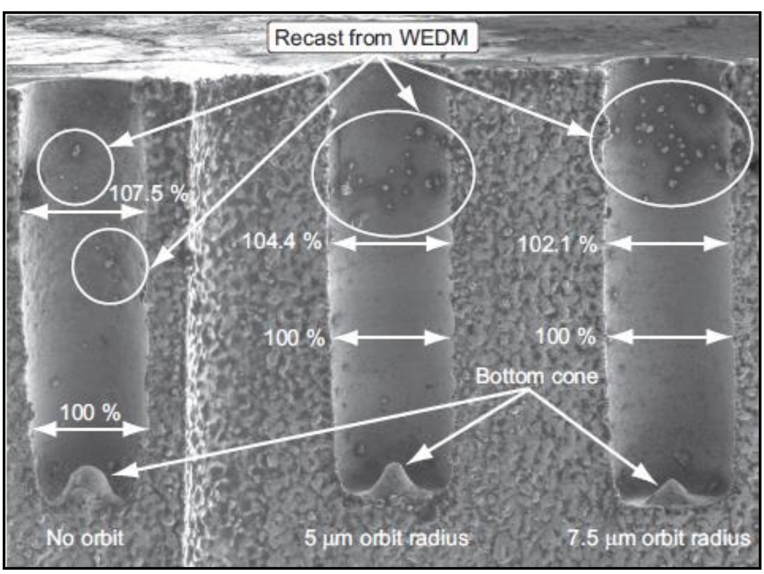

Figure 8. Cross section of 500 μm deep micro holes under different orbital radius [3].

The maximum variation in diameter for the 5 micron orbit hole is measured as 4.4% while the 7.5 micron orbit hole shows only a 2.1% variation. On the other hand, the hole drilled without orbiting has less uniformity and exhibits an increase in surface roughness in the first half of the hole. Also, the maximum variation in diameter was measured as 7.5%.

Some experimental investigations on different modes of orbital movement have been carried out by El Taweel and Hewidy [5]. They found that surface finish can be significantly improved using orbital tool motion relative to cavity sinking process (refer Figure 9).

From the graph shown in Figure 9 it can be noted that there is very small amount of reduction in surface roughness with increase in orbital radius irrespective of orbital speed viz. 10 rpm and 20 rpm. However, under orbital tool actuation, highest surface roughness value is found at the least orbital radius of 0.5 mm and this value of surface roughness is very less than the surface roughness value during cavity sinking process that is the plunge process as termed by the researchers. As suggested in the graph in Figure 9, it can also be understood that with increase in orbital speed there is reduction in surface roughness. Thus, it has been suggested by the researchers that orbital tool actuation can reduce surface roughness to some extent when compared to cavity sinking process [5].

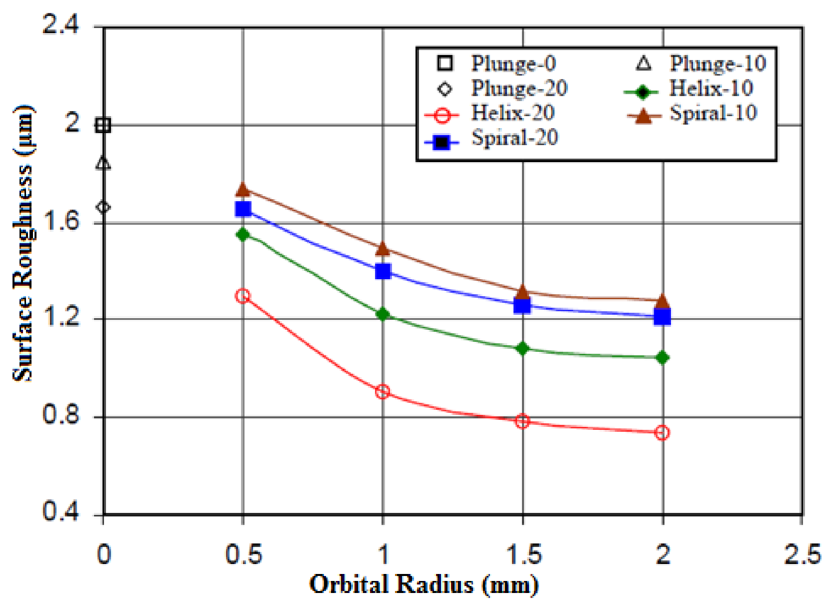

Figure 9. Effect of orbital radius on surface roughness [5].

Dave et al. have studied the effect of variation in orbital radius on surface roughness of Inconel 718., Further, to compare the results with cavity sinking electro discharge machining process, experimental runs have also been performed without actuating tool on orbital path that is by keeping orbital radius as zero. The graphical representation of effect of orbital radius on surface roughness of Inconel 718 at different levels of current and pulse ON time is shown in Figure 10 [6].

From Figure 10(a) and (b) it is found that with increase in orbital radius, surface roughness on machined surface of Inconel 718 reduces initially up to an optimum orbital radius beyond which it begins to rise. It is found that for any current setting or pulse ON time setting, surface roughness on Inconel 718 is minimum at orbital radius of 1.0 mm. Surface roughness values for higher orbital radius is more. Further, it can be noted that surface roughness produced during cavity sinking process is higher than that produced by orbital process.

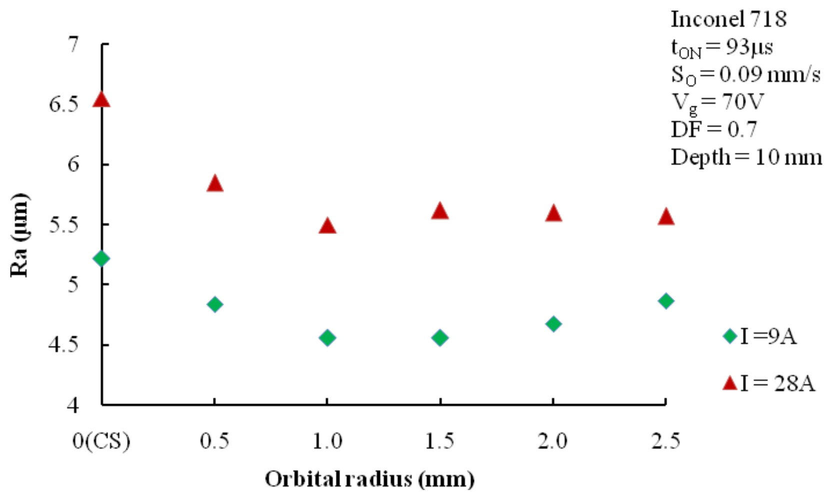

(a)

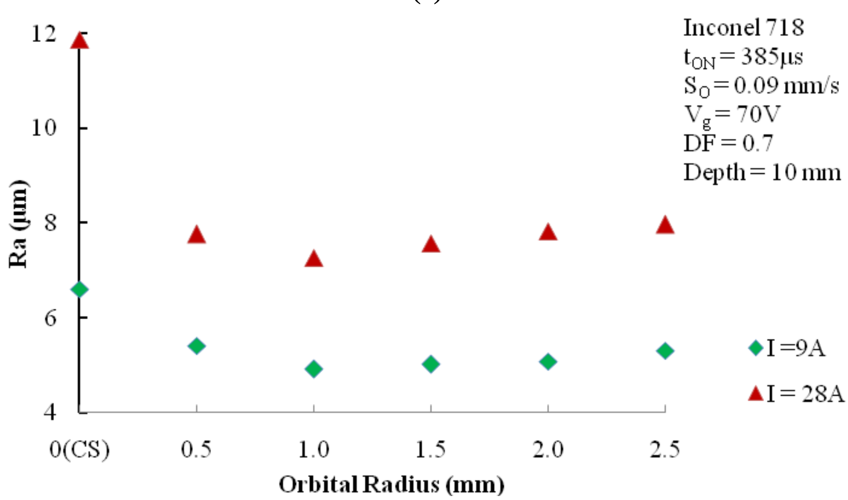

(b)

Figure 10. (a) Effect of orbital radius variation on R_a of Inconel 718 at t_{ON} = 93 µs, (b) 385 µs [6].

Table 1 shows the comparison between the surface roughness produced by cavity sinking process and orbital process at orbital radius of 1 mm. It can be seen that average surface roughness can be reduced up to 38.81% with orbital process under specific machining condition.

Figure 11(a) and (b) shows SEM images of machined surface of Inconel 718 under orbital process at I = 9A, t_{ON} = 93 µs and R_o = 0.5 mm and cavity sinking process.

It can be seen from Figure 11 that under orbital process, a plane surface is formed with shallower craters and almost free from cracks and pockmarks. However deposition of debris particles is visible on the surface. When the machining is carried out with cavity sinking process with similar machining parameters, it can be noted that though the surface largely remains plane but more craters, cracks and pockmarks are visible on the surface.

Table 1. Average Surface Roughness on Inconel 718 at different machining settings [6]

Machining condition	Average surface roughness Ra (μm)		% change
	Cavity sinking process (R_o = 0 mm)	Orbital process with R_o = 1 mm	
I = 9A & t_{ON} = 93 μs	5.22	4.56	12.64%
I = 28A & t_{ON} = 93 μs	6.55	5.5	16.03%
I = 9A & t_{ON} = 385 μs	6.61	4.91	25.72%
I = 28A & t_{ON} = 385 μs	11.88	7.27	38.81%

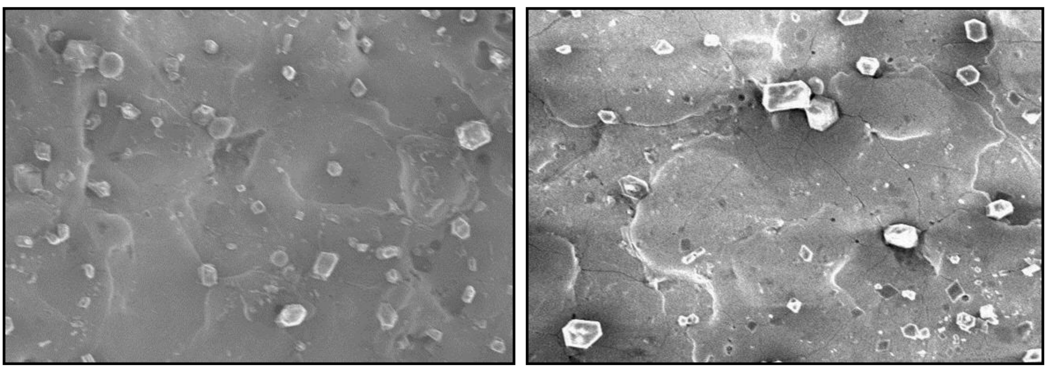

(a) (b)

Figure 11. SEM images (200X) at (a) I = 9A, t_{ON} = 93 μs and R_o =0.5 mm, (b) I = 9A, t_{ON} = 93 μs and R_o = 0 mm [6].

EFFECT ON MATERIAL REMOVAL RATE

Staelens and Kruth studied the influence of orbital speed on Material Removal Rate by using tool electrode with different cross sectional shapes [7]. They found that there exists an optimal speed when Material Removal Rate is observed to have its maximum value. Beyond this speed, Material Removal Rate begins to reduce. This is shown in Figure 12. Further, they noticed a relationship between current and orbital speed. For lower current value, the optimal speed is also less for maximum Material Removal Rate. The graph in Figure 12 shows observations noted at the current value of 16A.

During the experimental investigation Bamberg et al. found that highest MRR is found without orbiting the electrode as shown in Figure 13 [8].

It can be noted from Fig. 13 that material removal rate eventually becomes constant with a very small variability at larger orbit radii, which indicates a much more stable and predictable machining process. Further, in continuation of their work on micro EDM, they made a very significant observation on effect of orbital process and cavity sinking process on material removal rate with respect to machining depth. They found that the material removal rate under orbital process as well as cavity sinking process is same at lesser depth. However, when deeper cavities are machined, orbital process becomes significantly faster than the cavity sinking process due to better flushing conditions.

As part of their experimental investigations on different modes of orbital movement, El Taweel and Hewidy investigated Material Removal Rate under spiral as well as helix mode [5].

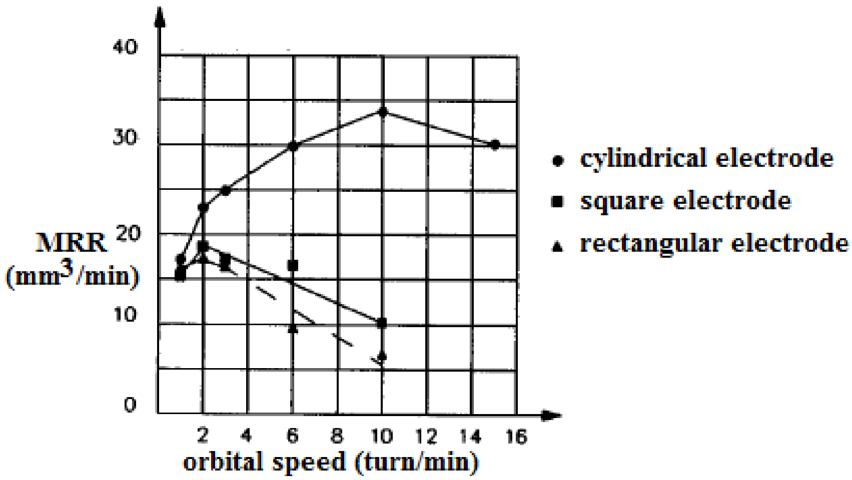

Figure 12. Influence of orbital speed on MRR [7].

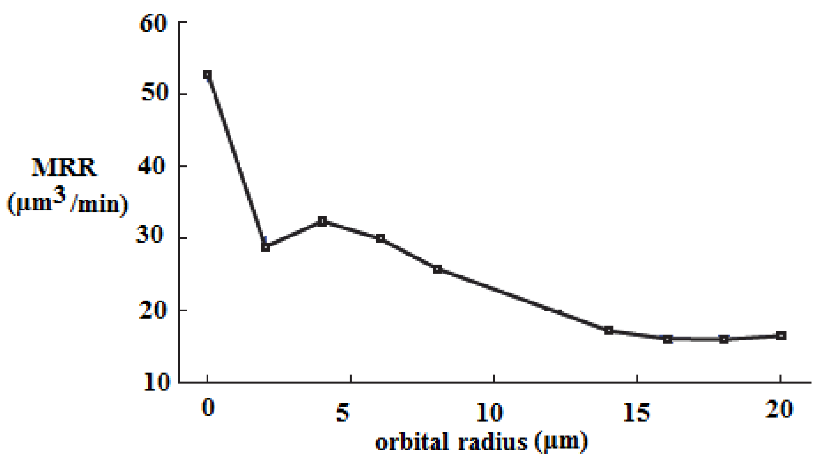

Figure 13. Effect of orbital radius on MRR [8].

As shown in Figure 14, M.R.R. gets reduced with increase in orbital radius. They noted that for a orbital speed of 20 rpm and at orbital radius of 2 mm, the helical tool movement achieved 43% more M.R.R. as compared to spiral movement. However, M.R.R. under any mode of orbiting is found to be less than the MRR recorded under cavity sinking process.

It is worth noting that authors have proposed a semi empirical model [9] and empirical model [10] as shown below for predicting MRR of Inconel 718.

Semi empirical model

$$M.R.R. = 0.7711\left[\frac{I^{0.955}.t_{ON}^{0.109}}{R_o^{0.542}.S_o^{0.0625}.}\right] \tag{1}$$

Empirical model

$$MRR = 0.549\left[\frac{I^{0.885}.V^{0.203}t_{ON}^{0.058}.DF^{0.335}}{R_o^{0.479}.S_o^{0.103}}\right] \tag{2}$$

These models show good match with experimental observations of MRR as shown in figure 15.

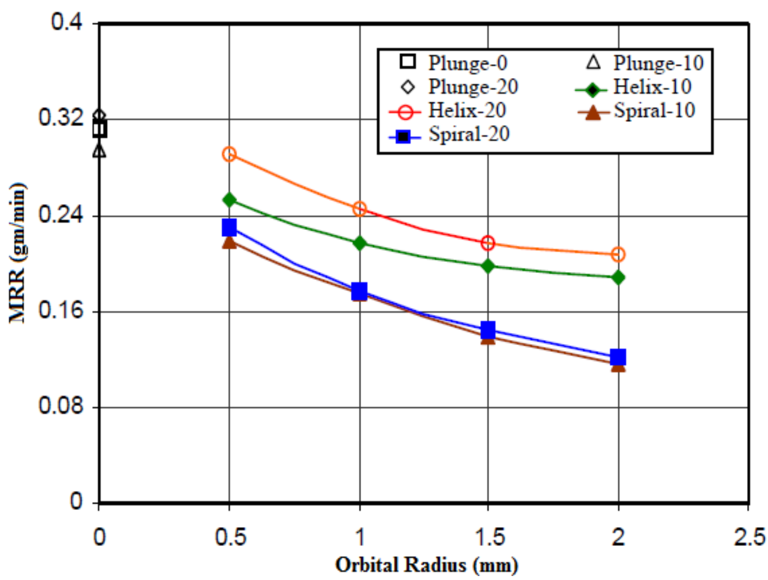

Figure 14. Effect of orbital radius on MRR [5].

It can be seen that while machining Inconel 718, an increase in orbital radius results into substantial reduction in M.R.R. at I = 28A irrespective of the pulse ON time setting. Further, M.R.R. observed under cavity sinking process is less than that observed at under orbital process.

During Orbital tool movement, there is continuous three dimensional motion of tool electrode resulting into continuous flushing of dielectric fluid through the discharge gap area. As a result, an improvement in debris flushing from discharge gap is observed. The debris particles are removed from discharge gap by swirling action. As a result the available discharge energy is not wasted on debris particles but effectively utilized for sparking resulting into improved M.R.R. The maximum M.R.R. under orbital process is observed at the orbital radius of 0.5mm. As orbital radius is increased beyobd 0.5mm, a decline is observed in M.R.R. irrespective of machining conditions. As larger gap is available at higher orbital radius between the surface of work piece and tool, the generation of spark becomes difficult. Further, the sparks the generated are not able to sustain due to continuous movement of tool electrode resulting into lesser heating and vaporization of material.

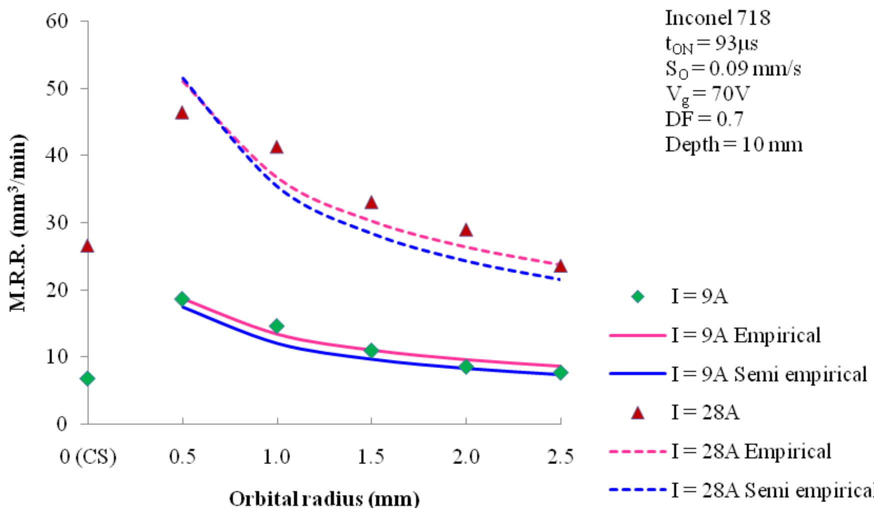

(a)

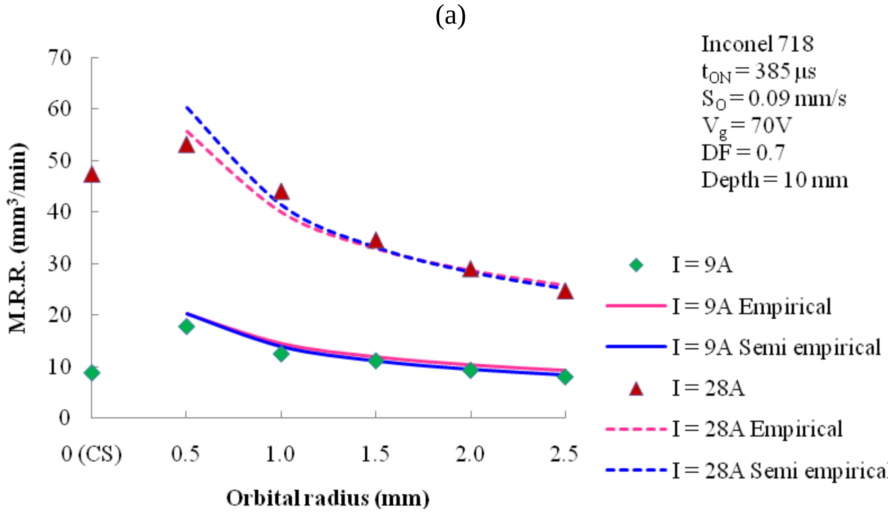

(b)

Figure 15. (a) Effect of orbital radius on M.R.R. of Inconel 718 at t_{ON} = 93 µs, (b) 385 µs.

EFFECT ON TOOL WEAR

Bamberg et al. found that axial wear of orbiting electrodes is found out to be much lower when holes with L/d ratio of 7.5 are drilled, than that of non-orbiting electrodes [3]. This can be understood from the graph shown in Figure 16.

As a result, they observed that the actual depth of the hole is much closer to the desired hole depth. The non-orbiting electrode witnesses maximum 40% axial wear while electrodes that have orbit radius of 5 µm and 7.5µm witness maximum 20% axial wear. Though initially for smaller hole depth, the difference in wear is less but this difference keeps on rising substantially with the increase in hole depth. This may be due to improper flushing in non orbital cutting due to which debris do not get removed easily.

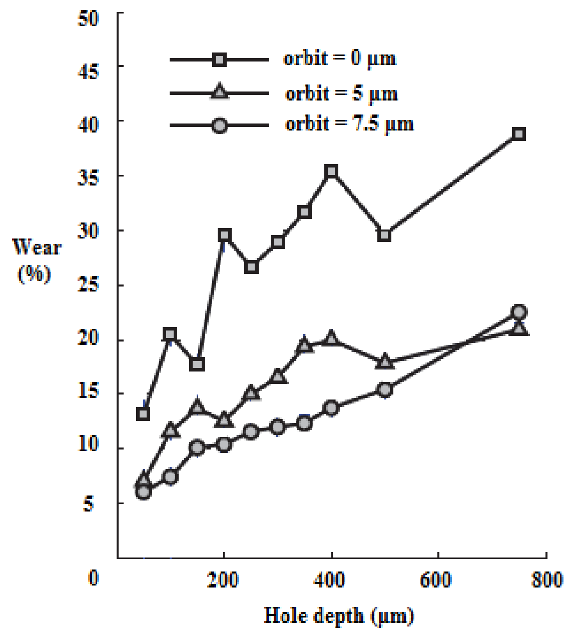

Figure 16. Effect of orbital radius on axial wear at high L/D ratio [3].

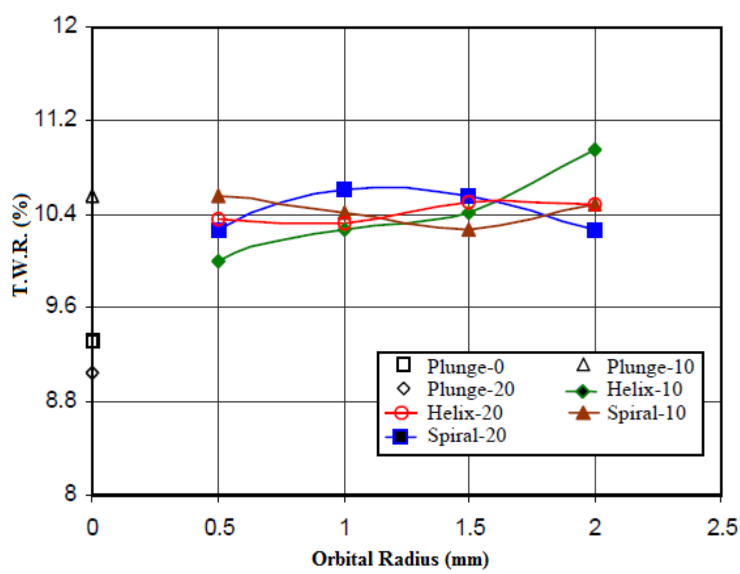

Figure 17. Effect of orbital radius on TWR [5].

El Taweel and Hewidy found that there is no significant effect of increasing orbital radius on Tool Wear Rate (T.W.R.) under helical tool movement [5]. T.W.R. is found to be almost constant as seen in Figure 17. No significant variation in the value of T.W.R. has been recorded with the variation in orbital radius, which is considered in form of tool eccentricity by the researchers. This is very important observation as it is possible to vary the orbital radius under certain critical machining conditions without significantly affecting T.W.R. Hence; same electrode can be used for continuous enlargement of the desired cavity just by increasing the orbital radius.

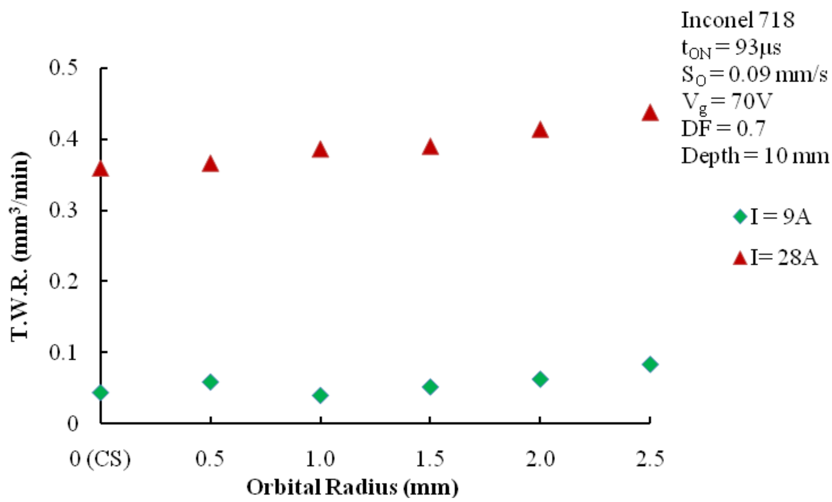

(a)

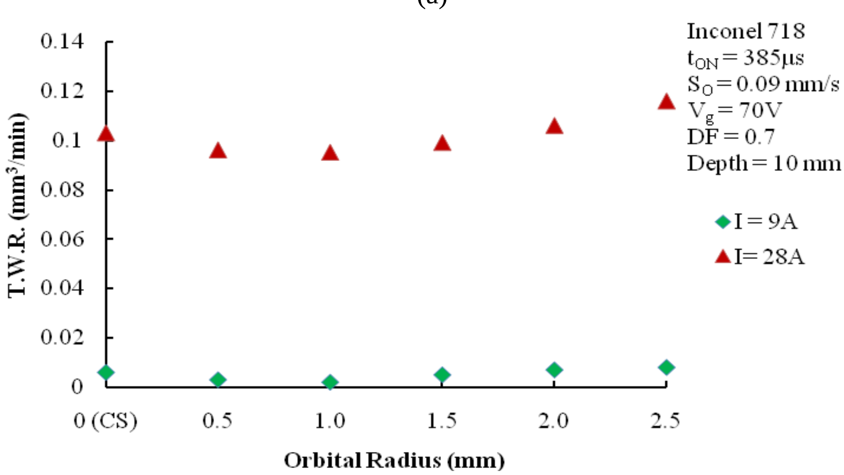

(b)

Figure 18. (a) Effect of variation in orbital radius on TWR of copper electrode while machining Inconel 718 at different current and t_{ON} = (a) 93 µs, (b) 385 µs.

Dave et al. have undertaken the detailed study on tool wear observed on copper electrode while machining Inconel 718 [6]. The effect of orbital radius on T.W.R. of copper electrode on Inconel 718 at different levels of orbital radius has been represented in Figure 18. From these graphs, it can be seen that there is very marginal rise in T.W.R. with increase in orbital radius. The T.W.R. noted at orbital radius of 0.5 mm and 1.0 mm is closely comparable with that under cavity sinking process. When orbital radius increases from 1.0 mm there is rise in T.W.R. also.

The orbital tool movement is actuated along a helical path resulting into a continuous three dimensional motion of tool electrode. Such kinematics conditions result into altered contact parameters between work piece and tool electrode.

Further, continuous tool electrode motion results into continuous and effective flushing of dielectric fluid through the sparking gap area resulting into continuous flushing of the debris removed from work piece as well as tool surface during the sparking time. Hence, the debris that are removed from tool electrode are unable to resolidify and get deposited back on the tool surface resulting into uniform wear on the tool surface.

Further, tool wear conditions have been assessed by the authors (thesis reference) in terms of corner wear on the tool electrode that is measured by observing the tool electrode under scanning electron microscope.

A substantial reduction in corner wear is observed when machining is carried out with orbital process relative to cavity sinking process. The percentage reduction in corner wear that is observed on Inconel 718 during orbital process relative to cavity sinking process is presented in Table 2.

Table 2. Corner wear while machining Inconel 718

Sr. No.	I (A)	t_{ON} (μs)	Corner wear (l_{cw})				% reduction in corner wear
			Orbital process		Cavity sinking process		
			R_o (mm)	l_{cw} (mm)	R_o (mm)	l_{cw} (mm)	
1	9	93	0.5	0.461	0	0.794	41.94%
2	28	93	0.5	0.588	0	1.71	65.61%
3	28	385	0.5	0.341	0	0.96	64.48%
4	28	93	1.5	1.71	0	1.71	0
5	28	93	2.5	2.89	0	1.71	-69%

It is clear from table 2 that corner wear is more under cavity sinking process as compared to orbital process with orbital radius of 0.5 mm as well as 1.0 mm. But when orbital radius is increased to 1.5 mm and 2.5 mm, an increase in corner wear is recorded as compared to the one at orbital radius of 0.5 mm. At higher orbital radius, the effective spark discharge energy available at tool tip is very high as compared to cavity sinking process. Hence, there is overheating of the sharp corners of the tool resulting into excessive wear at the edges.

CONCLUSION

It is possible to actuate tool movement along orbital path with various strategies like helical, radial, cylindrical, slicing etc. During orbiting, machining is carried out not only by bottom surface of the electrode but also by the side surface of the electrode. As larger area is involved in machining process, there is reduction in machining time. This facilitates the use of higher discharge currents and frequencies without damaging the surface finish. While the electrode is inside the hole, it is possible to orbit the electrode and cut with the cylindrical surface of the electrode, which avoids the taper at the entry of the hole. The flushing of the dielectric fluid also becomes less critical under tool orbiting. It is observed that electrode orbiting achieves fine surface finish and electrode wear can be reduced. Further, the roughing and finishing cut can be performed with the same electrode resulting in to cost reduction. Thus, incorporation of orbital strategies in EDM process can result into faster machining with improved surface condition and lesser tool wear.

REFERENCES

[1] Pandey, P.C., Shan, H.S., (1980). *Modern Machining Processes*, first ed. Tata Mcgraw Hill Publishing Co. Ltd., pp. 84-113.

[2] Guitrau, E.P., (1997). *The EDM Handbook*, first ed. Hanser Gardner, Cincinnati, OH, pp. 71–82.

[3] Bamberg, E., Sumet Heamawatanachai, (2009). Orbital Electrode Actuation to improve efficiency of drilling micro holes by micro-EDM. *J. Mater. Process. Technol.* 209, 1826-1834.

[4] Rajurkar, K.P., Royo, G.F., (1989). Effect of R. F. Control and orbital motion on Surface integrity of EDM Components. *J. Mech. Working Technol.* 20, 341-352.

[5] El-Taweel, T.A., Hewidy, M.S., (2009). Enhancing the performance of electrical discharge machining via various planetary modes. *Int. J. Mach. Mach. Mater*. 5(2-3), 308-320.

[6] Dave, H. K., (2012). *Helical path orbital electro discharge machining of Inconel 718 and AISI 304*, Ph.D. Thesis, Sarda Vallabhbhai National Institute of Technology: India.

[7] Staelens, F., Kruth, J.P., (1989). A computer integrated machining strategy for planetary EDM. *CIRP Ann. – Manuf. Technol.* 38 (1), 187–190.

[8] Bamberg, E., Heamawatanachai, S., Dean Jorgensen, J., (2005). Flexural Micro-EDM head for increased productivity of micro holes. In: *Proc. of the annual meeting of the American Society for Precision Engineering*, Norfolk, VA, 82-85.

[9] Dave, H.K., Desai, K. P., Raval, H.K., (2013). Development of semi empirical model for predicting material removal rate during orbital electro discharge machining of Inconel 718. *Int. J. Mach. Mach. Mater*. 13(2-3), 215 – 230.

[10] Dave, H.K., Desai, K.P., Raval, H.K., (2012). Modeling and Analysis of Material Removal Rate During Electro Discharge machining of Inconel 718 under Orbital Tool Movement. *Int. J. Manuf. Syst.* 2(1), 12 – 20.

In: Electrical Discharge Machining (EDM)
Editor: M. P. Jahan
ISBN: 978-1-63483-591-6

Chapter 8

MICRO-ELECTRICAL DISCHARGE MACHINING EMPLOYING POWDER MIXED DIELECTRICS

***G. Kibria*[*1], *I. Shivakoti*[2] *and B. Bhattacharyya*[3]**
[1]Department of Mechanical Engineering, Aliah University, Kolkata, India
[2]Department of Mechanical Engineering, Sikkim Manipal Institute of Technology (SMIT), Sikkim, India
[3]Production Engineering Department, Jadavpur University, Kolkata, India

ABSTRACT

Micro–electro-discharge machining (μEDM), a non-contact machining process that remove material from the workpiece, has been gaining ground as a new alternative method to fabricate micro-structures. Since micro-EDM process is performed into a dielectric fluid, the type of dielectric fluid influences the machining performance criteria. Typically, in EDM, hydrocarbon oil or kerosene is used as the dielectric fluid. However, in micro-EDM, the use of kerosene dielectric creates several problems. These problems include deposition of carbide layer on workpiece surface that reduces material removal rate, adhesion of carbon particles on micro-tool surface that makes the discharge inefficient, formation of harmful vapours such as CO and CH_4 that create toxic environment around the machining area, etc. To promote better micro-machining performances and safe machining environment, experimental investigations are going on employing different non-hydrocarbon based dielectric oils. The oxy-based fluid, i.e., distilled as well as de-ionized water is one of them that can be applied as dielectric liquid during micro-machining in EDM. Several experimental studies on powder-mixed EDM process have been performed by researchers across the globe to investigate their influences on electrical discharge machining performances. The researches include powders of Al, Cr, Cu, graphite, silicon, silicon carbide etc in some of the dielectrics such as kerosene and de-ionized water. The chapter deals with overview of micro-EDM process using conventional dielectric fluids and problems associated with hydrocarbon oil as dielectrics. Moreover, the machining principle of powder mixed EDM process is described. Furthermore, a well planned research study is conducted for exploring the influence of de-ionized water as dielectric during micro-hole machining on Ti-6Al-4V

[*]Corresponding Author: Golam Kibria, E-mail: prince_me16@rediffmail.com

superalloy. Further, boron carbide powder is mixed in dielectric fluid to investigate the influence of mixing powder in dielectrics. The process parameters considered are peak current and pulse-on-time, and the performance parameters are material removal rate, tool wear rate, overcut, diameteral variance in entry and exit and micro-hole circularity. The quality of the machined surface were also examined and analyzed with the aid of various optical and scanning electron microscopic images.

Keywords: Micro-EDM, powder mixed EDM, dielectric fluids, micro-hole, boron carbide additive, Ti-6Al-4V, de-ionized water, circularity

INTRODUCTION

Micro-electrical discharge machining (micro-EDM) is one of the recent and most promising micromachining techniques in precision manufacturing field to fabricate products having geometrically complex profiles with high aspect ratio. These microproducts are difficult as well as costly to manufacture in other conventional and nonconventional machining techniques. In micro-EDM process, any type of conducting materials can be used as the workpiece material regardless of its hardness. Due to the repetitive spark discharge between the tool and workpiece within very small gap, tiny amount of workpiece material is melted and vaporized. As the machining zone is immerged in dielectric fluid, the melted and vaporized materials transform into tiny particles known as debris upon cooling in pulse-off time. This debris is removed from the machining zone by the flushing pressure of the dielectric liquid jet.

Generally, kerosene is used as the dielectric fluid in most of the die-sinking EDM systems; but, the dielectric properties of kerosene are degraded when machining is done for long time. Also, owing to hydrocarbon oil, kerosene decomposes at very high temperature of discharge energy and pollutes the air around the machining setup.

The adhesion of carbon particles on the work surface also restricts the efficient and stable discharge and further reduces the material removal rate (MRR) [1, 2]. Due to these drawbacks and for the sake of industrial safety and ensuring non-polluted environment, investigations are going on using other types of dielectric fluids to overcome the above-mentioned problems. De-ionized water is one of the supplementary dielectrics that can be used efficiently in micro-EDM. Not only that, investigations have been performed by many researchers with powder-mixed dielectrics composed of different size of powder particles with different concentration to explore their effects on the micro-EDM performances and machined surface integrity [3–5]. In spite of some potential results, these types of dielectrics have not been found with wide applications in micro-EDM for modern manufacturing industries due to unsolved fundamental issues related to material removal mechanism by these dielectrics.

Ti-6Al-4V is a widely accepted material for the successful applications in aerospace, automotive, biomedical, and other major industries for its excellent mechanical and thermal properties, outstanding corrosion resistant, and low modulus of elasticity.

Due to some limitations of micromachining of titanium alloy (Ti-6Al-4V) in conventional machining methods, the nonconventional machining processes such as micro-EDM, micro-ECM, and LBM with a number of machining strategies are being utilized to machine these type of materials efficiently and economically.

Experimentations have also been performed using Ti-6Al-4V alloy in micro-EDM by changing the polarity of the electrodes for improving the machining accuracy of straight through micro-hole [6]. The present research study has been performed for micro-electrical discharge machining of Ti-6Al-4V super alloy to investigate the influence of different dielectrics on machining performance characteristics for the successful implementation of micro-EDM process with effective dielectric, which may improve titanium alloy machining efficiency in micromachining domain.

LIMITATIONS OF CONVENTIONAL DIELECTRICS IN MICRO-EDM

It has already been mentioned in the previous research investigation that pure kerosene, which is used as the dielectric liquid in most of the conventional EDM systems, creates several problems while machining, such as degradation of dielectric properties, pollution of air, and adhesion of carbon particles on the work surface etc. All these phenomena obstruct the stable discharge between the two electrodes, i.e., tool and workpiece and further result in lower machining efficiency. Investigation should be made to search out the alternative to kerosene dielectric with other types of dielectrics since the properties of dielectric are the effective machining parameter, which may overcome the above-mentioned problems. An alternative dielectric that can be used efficiently in micro-EDM is de-ionized water instead of hydrocarbon oil, kerosene. The harmful vapors such as CO and CH_4 are liberated while machining using pure kerosene and make the machining environment harmful and toxic [7]. In comparison with it, de-ionized water promotes better and safe machining environment. Also, no carbon deposition occurs, which results in better spark discharge. Further, the rapid cooling and enhanced flushing properties of de-ionized water improve the material removal rate and tool wear rate (TWR) but degrades the machining accuracy [8]. Experimental researches in the direction of comparative study of EDM micromachining using different dielectrics have not been done in an exhaustive manner till date. However, some research studies have been carried out for machining by EDM at higher discharge energies. The investigation on the effect of kerosene and distilled water on MRR/REW as well as surface integrity for Ti-6Al-4V alloy has been performed using higher discharge energies [9]. However, this research study does not report on the influence of powder-mixed dielectric. The experimental investigation using boron carbide powder-mixed dielectrics during micro-hole machining by EDM micromachining process has not been reported as yet. Therefore, the detailed research study and analysis of micro-EDM process characteristics such as MRR, tool wear, overcut (OC), surface topography, and machining time using kerosene and de-ionized water with boron carbide (B_4C) powder at lower discharge energies for micro-hole machining is required immediately. Considering this requirement, the research investigation of micro-hole machining using both dielectrics, i.e., pure kerosene and de-ionized water have been studied and compared while machining of Ti-6Al-4V alloy. Again, some researchers documented that machining debris facilitates the ignition process and further increases the gap size and overall flushing conditions [3]. If there are no debris particles then it can result in arcing owing to the lack of precise feeding mechanism. In addition, more debris leads to uneven and ineffective machining which result in short-circuiting. It is always desirable that some debris particles are present in the machining gap because they provide a great influence over discharge transitivity, gap size, breakdown strength, and deionization [10]. These roles of debris particle are controlled by the mixing of additives in dielectrics having certain characteristics like particle size, its concentration, particle density, and some physical and thermal properties of the powders. Several researchers have explained the actual behavior of the powder particles mixed with dielectrics. Experimentation using Al and SiC powder-mixed kerosene dielectrics to machine titanium alloy (Ti-6Al-4V) by micro-EDM process have shown the effect of these powders on material removal depth, surface quality, tool wear etc. at different powder concentration, and discharge energies [11]. The authors also used SiC mixed water to machine the same alloy material at different polarity setting [12]. A review of electrical discharge machining using several powders such as Al, Cr, Cu, graphite, silicon, silicon carbide etc. mixed in dielectrics has also been done [13]. The paper includes in-depth introduction, the history of PMEDM research issues, and review of research works carried out in this area by researchers across the globe. From the exhaustive review of the past literature on micro-EDM machining of Ti-6Al-4V with additive-mixed dielectric, it is found that no researchers have ever used boron carbide as the additive in the dielectric. Also exhaustive comparative study on the performance of pure kerosene, pure de-ionized water, B_4C mixed kerosene, and de-ionized water has not been performed yet. From the point of view of environmental and economical concerns, the performance of dielectrics other than hydrocarbon oil should be documented immediately to fulfill the demand of high quality and accuracy of micro-features in modern products. In the present experimental study, a new powder additive, i.e., B_4C is mixed in both the dielectrics to investigate the different micro-EDM response criteria, machined micro-hole quality, and surface topography. This B_4C powder has some excellent physical and chemical properties such as high chemical resistance and hardness, excellent wear and abrasion resistant etc. These exceptional characteristics of boron carbide may provide effective and efficient discharge conditions at the machining zone and also enhancement in above-mentioned machining performances. Keeping in view of these requirements and developmental research issue, a well-planned research methodology has been designed considering the direction received from the previous researchers to investigate the influence of B_4C mixed and pure dielectric on various micromachining performance requirements such as material removal rate, tool wear rate, overcut, diameteral variance at entry and exit hole (DVEE) and machined surface topography through various test results and scanning electron microscope (SEM) micrographs.

ROLE OF POWDER PARTICLES IN MICRO-EDM PROCESS

The machining zone consists of dielectric fluid only. When additive particles is mixed with the working fluid and applied at the machining zone, due to the voltage applied between micro-tool electrode and work material, an electric field is created between them. The powder particles in the spark gap get energized and behave in a zigzag fashion. This electric field accelerated the charged particles, which behaves like conductors. Due to this, breakdown of the gap is occurred creating an increase in spark gap. The powder particles come close to each other and assemble themselves in the chain like structures between the electrodes. The chain formation helps in bridging the discharge gap between both the electrodes. Due to this, the dielectric strength of powder mixed working fluid decreases and causes early explosion in the gap. As a result, a series discharge starts under the micro-electrode area near smallest gap zone and material removal takes place from both the electrodes. Simultaneously, the added powder modifies the plasma channel and becomes enlarged and widened. The electrical discharges uniformly distributed among the powder particles at the machining zone and shallow craters are produced on the workpiece surface. The result is the improvement in surface finish of the micro-EDMed surface employing powder mixed dielectric. In Figure 1, the schematic diagram of the discharge pattern between two electrodes is shown during micro-EDM process when powder additives are being employed in the dielectric fluid. During micro-hole machining in EDM employing powder particles mixed in dielectric, the discharge gap consists of additive powders as well as debris produced in erosion of electrode materials. Therefore, the debris concentration and its distribution in the dielectric, formation of bubbles, deionization and surface irregularities of the workpiece as well as the micro-tool electrode determines the stability of the machining process in micro-EDM. The thermo-physical properties i.e., particle size, particle concentration, particle density, thermal conductivity, electrical resistivity, melting point, evaporation point, specific and latent heat etc. of the additive particles play a significant role in discharge transitivity, gap size and breakdown strength of the gap. Electrical and thermal conductive particles such as Al, Cu, graphite etc. can easily distribute themselves uniformly in the discharge gap with the help of electrical field created between electrodes. On the other hand, non-conductive particles like SiC, Al_2O_3 etc. require higher gap voltage and current to arrange themselves in zigzag fashion to improve stable discharge condition. Therefore, sparking efficiency greatly depends on thermo-electrical properties of debris in the gap.

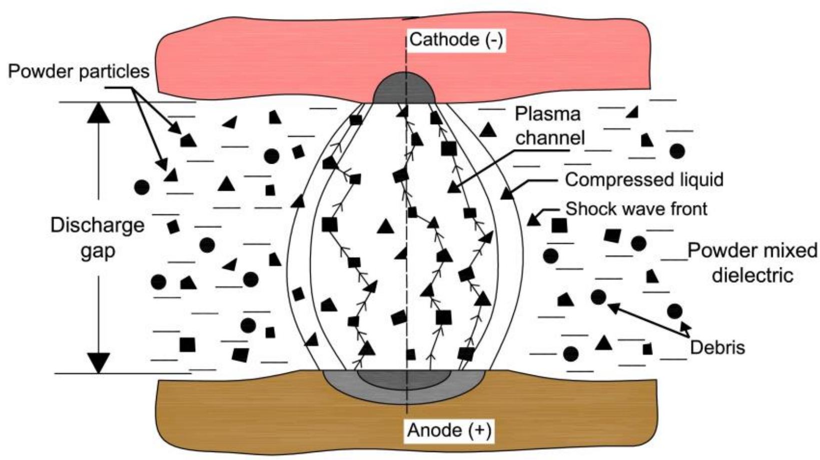

Figure 1. Schematic diagram of discharge using additive mixed dielectric in micro-EDM.

PROCESS PARAMETERS IN POWDER MIXED MICRO-EDM

Powder mixed micro-EDM is associated with various process parameters as these affect the performance measures and quality characteristics of the process in several ways, in both predictable and unpredictable fashion. For a glance view of these process parameters, an

Ishikawa cause–effect diagram was constructed as shown in Figure 2. The important process parameters involved with powder mixed micro-EDM process are discussed hereunder.

Peak Current (I_p)

The average current is the average of amperage in spark gap measured over a complete cycle. This is read on the ammeter during the process. The theoretical average current can be measured by multiplying the duty cycle and the peak current i.e., maximum current available for each pulse from the power supply. The average current is an indication of the machining operation efficiency with respect to rate of material removal. The concept of maximum peak amperage that can be applied to the electrode is an important factor. In micro-EDM process, very high currents are not used as they often lead to thermal damage of the work surface and micro-tool electrode, increase the depth of recast layer, formation of heat affected zone as well as alteration in thermal properties of the machined parts.

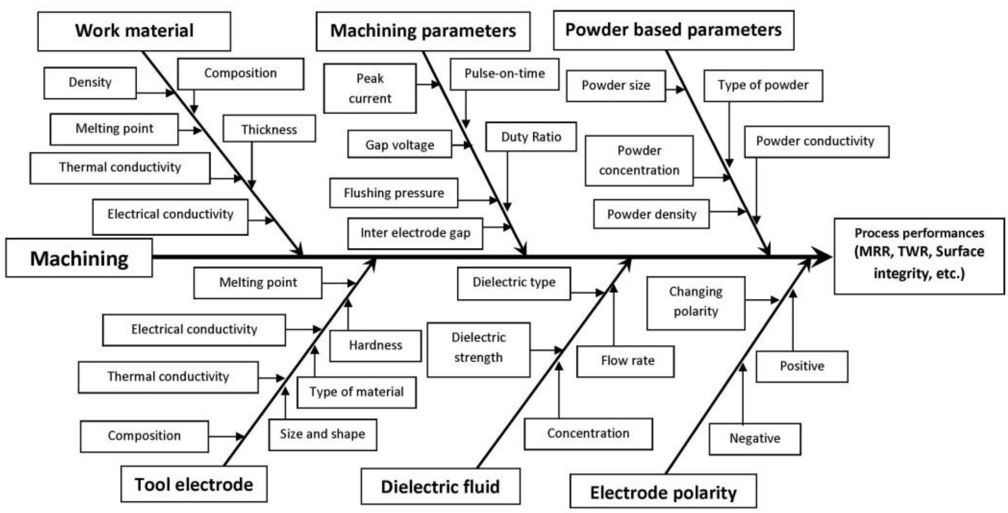

Figure 2. Cause and effect diagram (CED) showing various process parameters and response criteria of EDM process.

Pulse-on-Time (T_{on})

Pulse-on-time is the time period in which pulse discharge energy is supplied to the micro-tool electrode and workpiece to be machined. The actual machining operation i.e., material is removed from workpiece in this period. The spark gap is bridged; the conduction of current and the melting and vapourising of work material takes place. The longer the spark is sustained more is the material removal from workpiece. Consequently the resulting craters will be broader and deeper; therefore the surface finish will be rougher. However, with shorter duration of sparks the surface finish will be better. With a positively charged workpiece, the spark leaves the tool and strikes the work surface resulting in the material removal known as machining. Except roughing operation all the sparks that leave the tool and strike the work surface results in a microscopic removal of particles from it. More sparks produce much more wear, hence, this process behaves quite opposite to normal processes in which the tool wears more during finishing than roughing operations.

Pulse-Off-Time (T_{off})

While most of the machining takes place during pulse-on-time, therefore, during pulse-off-time period in which the supply of pulsed electrical energy is discontinued and the re-ionization of the dielectric takes place. During this off-time the debris are removed from the machining zone and speed up the operation thereby increasing the efficiency of the machining process. The off-time also governs the stability of the process. An insufficient off-time can lead to erratic cycling and retraction of the advancing servo resulting in slowing down the operation cycle.

Gap Voltage (V)

The voltage used is usually a DC power source of 40 to 400 Volts. An AC power source can also be used but it is usually coupled with a DC rectifier. The preset voltage determines the width of the spark gap between the leading edge of the electrode and the workpiece. A high voltage setting increases the gap and hence increases the flushing ability and machining efficiency.

Duty Factor (t)

This is an important parameter in the EDM process. This is given by the ratio of the on time to the total cycle time, as follows:

$$Duty\ \ factor = \frac{Pulse-on-time(T_{on})}{Pulse-on-time(T_{on})+Pulse-off\ -time(T_{off})} \tag{1}$$

If the duty factor is high, the flushing time is very less and this might lead to the short circuit condition and a small duty factor indicates a high off time and low machining rate. Therefore there has to be a compromise between these two depending on the micro-tool used and the workpiece. The value of mostly preferred duty factor is 0.5.

Polarity

Polarity refers to the electrical conditions for determining the direction of the current flow relative to the electrode. The polarity of the electrode can be either positive or negative. Depending on the application, some electrode/work material combinations give better results when the polarity is changed. Generally for graphite electrode, a positive polarity gives better wear condition and negative polarity gives better machining speed.

Inter-Electrode Gap

This is one of the most crucial parameters of the micro-EDM process. The size of the gap between tool and workpiece is governed by the servo control system whose motion is controlled by gap width sensors. They control the motion of the ram head or the quill which in turn governs the gap size. Typical value of the gap size ranges from 0.01 to 0.05 mm. Although gap sizes as small as several hundreds to thousands of micrometers can be obtained, depending on the application, current, voltage, and dielectric medium. To maintain a constant gap size, downward feed rate should be equal to the generation rate of depth during machining. The gap size governs the possibility of sparking and arcing.

Pulse Frequency

This is a measure of the number of times the current is turned on and off. During rough machining the on time is increased significantly for high removal rate and there are fewer cycles per second, hence a lower frequency setting. Finish machining has been carried by shorter pulse-on-time and there are more cycles per second hence a larger frequency setting. Frequency should not be confused with the duty cycle, as this is a measure of efficiency.

Type of Dielectric Fluid

The dielectric fluids used have characteristics of high dielectric strength and quick recovery after breakdown, effective quenching and flushing ability, good degree of fluidity and easy availability. Moreover, different types of dielectic have different composition and viscosity. Generally, in EDM, kerosene dielectric is preferred whereas, in micro-EDM, oxy-based dielectric fluid is used.

One of the most widely used dielectric in micro-EDM is de-ionized water. De-ionized water has several merits for efficient and uniform discharge at the inter-electrode gap and ultimately capability of augmenting the rate of material removal from workpiece.

Nozzle Flushing

Material removal rare, tool wear rate and surface integrity are significantly affected by the type of dielectric and the method of its flushing as efficient flushing removes the debris from discharge gap quickly [14, 15]. Moreover, dielectric flushing should be such that it can deionize the inter electrode gap immediately after the spark has occurred. Different types of flushing mechanisms are proposed by different researchers for conventional EDM process [16]. Some of them are suction through electrode, pressure through electrode, jet flushing, alternating forced flushing, ultrasonic vibration of electrode and rotating electrode flushing.

For micro-EDM, jet flushing is typically used. The dielectric fluid flushes the gaseous and solid debris from the machining zone and maintains the dielectric temperature by acting as coolant also.

Tool Electrode Material

The tool electrode is an integral part of micro-EDM process. In principle, any highly conductive material can be used as micro-tool electrode. Usually, copper, graphite, brass, tungsten and steel materials are used to manufacture micro-tool electrodes for micro-EDM operation. Some criteria which are to be considered for selecting the micro-tool are (i) erosion characteristics, (ii) machining possibilities, (iii) thermal conductivity and diffusivity, (iv) cost and availability, (v) hardness and toughness and (vi) melting temperature. Tungsten is the best material to manufacture micro-tool for micro-EDM as it has high strength, hardness and melting point (3400ºC). However, it is expensive and difficult to machine. Thus, to improve its machinability and usages, it is combined with ductile materials like copper.

Size of Tool Electrode

The size of micro-tool electrode is an important issue for desired machining cavity. Depending upon the end face size and area of the tool electrode, the desired micro-cavities are produced on the workpiece. During micro-EDM drilling, micro-holes are machined using micro-electrodes. However, manufacturing and then clamping a long micro-electrode are the challenging issues. To overcome the clamping problem of micro-tool electrodes, the electrodes are fabricated in situ with high accuracy by micro-electro-discharge grinding process [17, 18].

Type of Powder Particles

Some electrically conductive/ semi-conductive powders are mixed in the dielectric fluid and the mixture is fed in the inter-electrode gap during conventional EDM and micro-EDM processes. This reduces the insulating strength of the dielectric fluid and increases the spark gap between the electrodes. The enlarged spark gap flushes the debris very easily. As a result, the process becomes stable, improving the material removal rate and surface finish [19]. Moreover, there may be some abrasive actions of the powder particles on the machined area that makes the surface quality much better compared to conventional EDM and micro-EDM. Different types of powders have different impact on the EDM process characteristics as some of the powders cannot disperse uniformly and persistently in the discharge gap. Therefore, the selection of powder additive is an important issue during micro-EDM. Researcher have performed a number of experimental investigation in micro-EDM mixing the powders such as aluminium, copper, chromium, graphite, silicon, nickel, SiC, titanium, Span 20, micro-MoS_2, manganese, etc., [13].

Concentration of Powder in Dielectric

Addition of appropriate concentration of powder into dielectric fluid plays a very important role on micro-EDM process criteria such as material removal rate (MRR), tool wear rate (TWR) and surface roughness (SR). The material removal depth reached the maximum value at appropriate concentration. Further increase or decrease in the concentration of the added powder would decrease the MRR.

Shape and Size of Powder Particles

The size and shape of the powder particles affects the machining performances. A large diameter of the powder particle increases the gap but simultaneously decreases the MRR and then increases the SR.

Conductivity of Powder Particles

The electrical as well as thermal conductivity of the added powder directly affects EDM performance. This is because the added powder increases the conductivity of the dielectric fluid and results in the extension of the gap distance.

LITERATURE REVIEW

Powder mixed EDM is also termed as Additive EDM. This innovative technique was introduced in late seventies in technological research. Since its perception, it started to grow for achieving high finish machined surface at high machining rates [10]. A number of researchers have conducted several set of experiments to explore the effects of addition of powder into dielectric on various machining performances in EDM. Experimental and theoretical investigations was performed by Erden and Bilgin [20] to determine the effect of mixing copper, aluminum, iron and carbon in powders in commercial kerosene oil dielectric during machining of brass-steel and copper-steel pairs. The results revealed that the addition of powder improves the breakdown characteristics of the kerosene oil dielectric. Further, it was found that the machining rate increases with increase in the concentration of the added powder. This is due to the decrease in time lags at high impurity concentrations. At excessive powder concentration, the machining process was unstable due to occurrence of short circuits. An investigation was performed by Jeswani [10] to find out the effect of the addition of fine graphite powder mixed in kerosene oil on material removal rate and wear ratio. It was revealed that by addition of 4g/l of fine graphite powder increased the interspace for electric discharge initiation and lowered the breakdown voltage. Due to addition of graphite powder, around 60% increase in MRR and 28% reduction in WR are found out. To study the effects of silicon powder addition in dielectric on machining rate and surface finish, Mohri et al., [21, 22] conducted experimental investigation in EDM and surface roughness of less than 2μm were produced at controlled machining conditions (low discharge current of 0.5–1 A and short discharge time of <3μs).

Narumiya et al., [23] studied the effects of mixing of aluminum and graphite powders into dielectric on surface finish. The surface roughness is obtained as less than 2μm using aluminum and graphite powders having diameter less than 15μm and powder concentration in the ranges of 2 to 15 g/l. Another experimental investigation was conducted by Kobayashi et al., [24] to find the effects of suspended powder in dielectric on MRR and SR. It was revealed that the silicon powder suspended dielectric improved the surface finish of SKD-61 material. Yan and Chen [25, 26] studied the effect of suspended aluminum and silicon carbide powders on EDM of SKD11 and Ti–6Al–4V. The results show that the MRR improved considerably; however, SR increased. The experimental investigation conducted by Ming and He [27] revealed that the conductive and inorganic oxide additives increase the MRR, decrease the TWR and improve the surface quality of the machined surface. Uno and Okada [28] investigated the effect of silicon powder mixing on the surface generation mechanism. The EDM with silicon powder mixed fluid produced glossier surfaces as compared to those produced by conventional EDM with kerosene fluid. Uno et al., [29] mixed nickel powder into working fluid and observed that the suspended powder mixed fluid modifies the surface of aluminum bronze components. A layer is deposited on EDMed surface and the surface becomes abrasion resistant.

Wong et al., [30] studied the effects of fine powders (silicon, graphite, molybdenum, aluminum and silicon carbide) mixed dielectric on MRR, TWR and SR. It was reported that aluminum powder has the ability to render mirror finish surface on SKH-51 workpiece. However, it fails to produce mirror finish surface on SKH-54 material. Moreover, silicon and carbon powders were effective in producing very fine finish surface conditions. Furutani et al., [31] reported that the titanium powder suspended in EDF-K (Mitsubishi oil) of powder of size <36μm and concentration of 50 g/l is responsible for a smooth and thick layer of TiC (thickness of 150 μm with a hardness of 1600 Hv) on surface of carbon steel material. Wang et al., [32] reported the effect of Al and Cr powder mixture in kerosene. It was found that Al and Cr mixture in kerosene fluid enlarges the gap between the tool and workpiece material. Hence, the process efficiency is improved and enhanced the MRR. When small size particles were used, there is higher probability of bridging the gap due to higher suspension effect in the dielectric fluid, which results in good surface finish.

Chow et al., [33] investigated the effects of adding SiC and aluminum powders into kerosene during micro-slit EDM of titanium alloy. The addition of powders to the kerosene results in higher debris removal rate and material removal depth. The added powder particles facilitate the dispersion of discharge into several increments and hence increase the MRR and surface finish. However, the adherence of carbon nuclides attached to the tool electrode surface increases the TWR. Tzeng and Lee [34] investigated the effects of addition of various additives such as Al, Cr, Cu and SiC mixed in the working fluid during EDM of SKD-11 material. The appropriate concentration of powders in the dielectric fluid increased MRR and decreased TWR. It is found that the smallest size of powder particle give highest MRR and lowest TWR. Furutani and Shiraki [35] investigated the effect of addition of molybdenum disulphide powder into the dielectric fluid to deposit a lubricant layer on carbon steel and stainless steel. Compared to traditional EDM, it was found that the surface produced by PMEDM is of lower friction coefficient. Pecas and Henriques [36] reported the influence of silicon powder mixed dielectric on conventional EDM. The results revealed that the operating time and SR decreases by addition of 2 g/l silicon powder into dielectric. The SR varies from 0.09 to 0.57 μm for the area range of 1–64 cm^2.

Zhao et al., [37] studied the machining efficiency and surface roughness during rough PMEDM using Al powder with 40 g/l and 10 mm granularity. The results revealed that the machining efficiency can be highly increased along with better surface finish by selecting proper discharge parameters compared to conventional EDM. Kozak et al., [38] studied the effects of mixing the powder particles into dielectric media and reported that the material removal rate and tool wear rate were decreased. Klocke et al., [39] studied the effect of aluminium mixed dielectric on the machining performances. Using a high speed forming camera, it was found that aluminium mixed dielectric forms larger plasma channel. Moreover, the type and concentration of the aluminium powder into the dielectric have significant effect on performance criteria. Wu et al., [40] studied the behaviour of powder settling by adding a surfactant with aluminium powder in dielectric. The result of surface roughness was achieved as low as 0.2μm due to more apparent discharge distribution in the discharge gap.

Yan et al., [41] investigated the influence of addition of urea into distilled water during EDM of pure titanium material. The experimental results revealed that nitrogen element is decomposed from urea contained dielectric and a hard layer of TiN is formed on the machined surface of workpiece, which in turn results in good wear resistance of the surface. Moreover, MRR and EWR increased with peak current. Kansal et al., [42] investigated for optimization of the process parameters of silicon powder mixed EDM during machining tool steel material. The process performances studied are material removal rate and surface roughness. It is concluded that higher concentration of silicon powder gives improvement in MRR and SR. Yeo et al., [43] compared the EDM process using with and without additive mixed dielectric at low discharge energies of 2.5, 5 and 25 μJ. It was observed that a considerable difference in crater morphology is seen between craters in dielectric with and without the powder. Using powder additive dielectric, more circular shapes with smaller diameter craters and with high consistent depth were produced.

Peças and Henriques [44] investigated the effect of silicon powder suspended in dielectric considering powder concentration and flushing flow rate as process parameters. The results showed that even for small level of powder concentration there is evident amount of reduction in crater depth, crater diameter and the white layer thickness. Moreover, the powder concentration generates better surface morphology. Chow et al., [12] investigated the addition of SiC powder in water for micro slit EDM machining of titanium alloy and it was found that SiC powder suspended in pure water causes a larger expanding-slit and electrode wear than those of using pure water alone. Furthermore, pure water and a SiC powder attain a smaller amount of machined burr than that of using pure water alone. Furutani et al., [45] studied the influence of Ti powder suspended dielectric considering discharge current and pulse duration as process parameters. They concluded that the discharge energy affected the deposit able condition range. TiC could be deposited in the case that both discharge energy and powder density was small. They reported that the hardness of the deposition achieved was 2000Hv. The matrix surface was also hardened.

Kung et al., [46] reported that the material removal rate and electrode wear ratio in powder mixed electrical discharge machining of cobalt-bonded tungsten carbide by suspending aluminium powder in dielectric fluid. They observed that the powder particles disperses and makes the discharge energy dispersion uniform. Prihandana et al., [47] investigated into suspending micro-MoS_2 powder in dielectric fluid during ultrasonic vibration assisted μ-EDM. The results revealed that the addition of MoS_2 micro-powder in dielectric fluid and employing ultrasonic vibration significantly increase the MRR and improves surface quality. Kibria et al., [48] compared different dielectrics such as pure kerosene, pure de-ionized water, boron carbide powder mixed kerosene and boron carbide powder mixed de-ionized water during micro-EDM machining operation. The experimental results revealed that material removal rate is high with de-ionized water dielectric compared to pure kerosene. Moreover, although B_4C additive mixed kerosene has not shown remarkable improvement in MRR, but the mixing of B_4C with de-ionized water shows an excellent increase in MRR due to the efficient distribution of discharge and increase in machining efficiency.

Kumar et al., [49] investigated into manganese powder suspended in dielectric fluid during EDM. The results revealed that significant amount of material transfer takes place from the manganese powder suspended in dielectric fluid to the machined surface under appropriate machining conditions. A significant alteration of the surface composition and properties takes place. It is also reported that percentage of manganese increased to 0.95% from 0.52% and that of carbon to 1.03% from 0.82% that result in increase in the micro hardness. Sharma et al., [50] studied the effect of aluminium powder on the material removal rate, tool wear rate and surface roughness during conventional EDM with reverse polarity considering concentration and grain size of aluminium powder as powder parameters.

Jeswani [8] in 1981 investigated and compared the performances of kerosene and distilled water dielectrics in the range of pulse energy of 72 to 288 mJ. The results revealed that at high pulse energy range, ED machining in distilled water resulted higher MRR and a lower wear ratio than employing kerosene dielectric. Furthermore, it is also revealed that machining accuracy was low using distilled water; however, the surface finish was better. Kruth et al., [51] employed an oil dielectric during EDM and found that the dielectric fluid increases the carbon content in the white layer formed and appears as iron carbides (Fe_3C) in columnar, dendritic structures while machining in water causes a decarbonization. In 1984, Jilani and Pandey [52] studied and compared the influence of distilled water, tap water and a mixture of 25% tap water and 75% distilled water during machining. The tap water gives high machining rate and machining in water has the possibility of achieving zero TWR when using copper tools with negative polarities.

Koenig and Joerres [53] performed machining operation utilizing aqueous glycerine solution as additive in water. The experimental results reported that with long pulse durations, high duty factors, discharge currents, high open-circuit voltages and positive polarity of tool resulted better machining rate employing high concentrated aqueous glycerine solution compared to hydrocarbon dielectrics. Konig and Siebers [54] studied the effects of the working medium on the metal removal process. Utilizing water as dielectric, the erosion process during machining takes place efficiently with higher thermal stability, which further increase in MRR. Tsunekawa et al., [55] studied the surface modification of aluminium using powder compact electrodes (64% Ti and 36% Al) in EDM utilizing kerosene as the working fluid. It is revealed that fine dendritic titanium carbide is precipitated on the machined surface. Further, it is found that the average diameter and alloyed depth of discharge craters increased with increase in pulse width and discharge current.

Chen et al., [56] investigated the influence of kerosene and distilled water on machining rate and surface properties during EDM of Ti-6Al-4V. The results showed that carbide is formed on the workpiece surface while using kerosene. However, oxide is formed on the machined surface using distilled water. Further, it is found that the size of debris produced is greater utilizing distilled water dielectric than using kerosene. In 2004, Leao and Pashby [57] published a review paper of using environmentally friendly dielectric fluids in electrical discharge machining. The reviews showed the feasibility of adding organic compound such as ethylene glycol, polyethylene glycol 200, polyethylene glycol 400, polyethylene glycol 600, dextrose and sucrose in water dielectrics to improve the process performance. Ekmekci et al., [58] studied the residual stresses developed and hardness depth of machined surface in EDM. Stresses increased rapidly with respect to depth, attaining to its maximum value around the yield strength. Then after, it fall rapidly to compressive residual stresses in the core of the material. In 2005, Sharma et al., [59] used electrically conductive chemical vapor deposited diamond as tool electrode during micro-electrical discharge machining utilizing oil and water as dielectrics.

Ekmekci et al., [60] conducted comparative study on the surface integrity of plastic mold steel and the amount of retained austenite phase and the intensity of micro cracks have found to be much less in the white layer of the samples machined in de-ionized water. Kang and Kim [61] studied the effects of EDM process conditions on the crack susceptibility of a nickel-based super alloy. Depending on the dielectric fluid and the post-EDM process such as solution heat treatment, cracks that exist in recast layer formed during machining could propagate into substrate when a 20% strain tensile force was applied at room temperature. However, utilizing kerosene as dielectric, it was observed that carburization and sharp crack propagation along the grain boundary occurred after the heat treatment. Further, using de-ionized water as dielectric the specimen after heat treatment underwent oxidation and showed no crack propagation behaviour.

Chung et al., [62] has investigated micro electrical discharge milling using deionized water. De-ionized water with high resistivity was used to minimize the machining gap. Machining characteristics such as the tool wear, machining gap and machining rate were investigated according to resistivity of de-ionized water. As the resistivity of de-ionized water decreased, the tool wear was reduced, but the machining gap increased due to electrochemical dissolution. Micro hemispheres were machined for the purpose of investigating machining efficiency between dielectric fluids, kerosene and de-ionized water. Lin et al., [63] investigated on the feasibility of micro-slit EDM machining using pure water as the dielectric fluid. Experimental results revealed that pure water could be used as a dielectric fluid and adopting negative polarity EDM machining could obtain high material removal rate (MRR), low electrode wear, small slit expansion, and little machined burr, compared to positive polarity machining.

EXPERIMENTAL DETAILS AND MACHINING CONDITIONS

From the review of past research, it is clear that lot of theoretical and experimental works have been carried out for proper understanding of the basic process of EDM and micro-EDM and also the influence of various types of dielectric fluids on performance criteria during EDM and micro-EDM. Moreover, researchers also applied various type of powder additives mixed in dielectrics during machining difficult-to-cut materials for improving the discharge stability and ultimately improving the material removal rate and accuracy of machining. It is obvious that for improving the machining efficiency in terms of increasing material removal rate and increasing accuracy and also reducing the wear of the tool electrode, new machining strategies should be incorporated in EDM and micro-EDM. Amongst various machining strategies of improving the process performances in EDM and micro-EDM, use of various dielectrics (kerosene, de-ionized water, EDM oil, some additive powders in the dielectric fluid, etc.) has significant contributions for enhancing the yield criteria of machining.

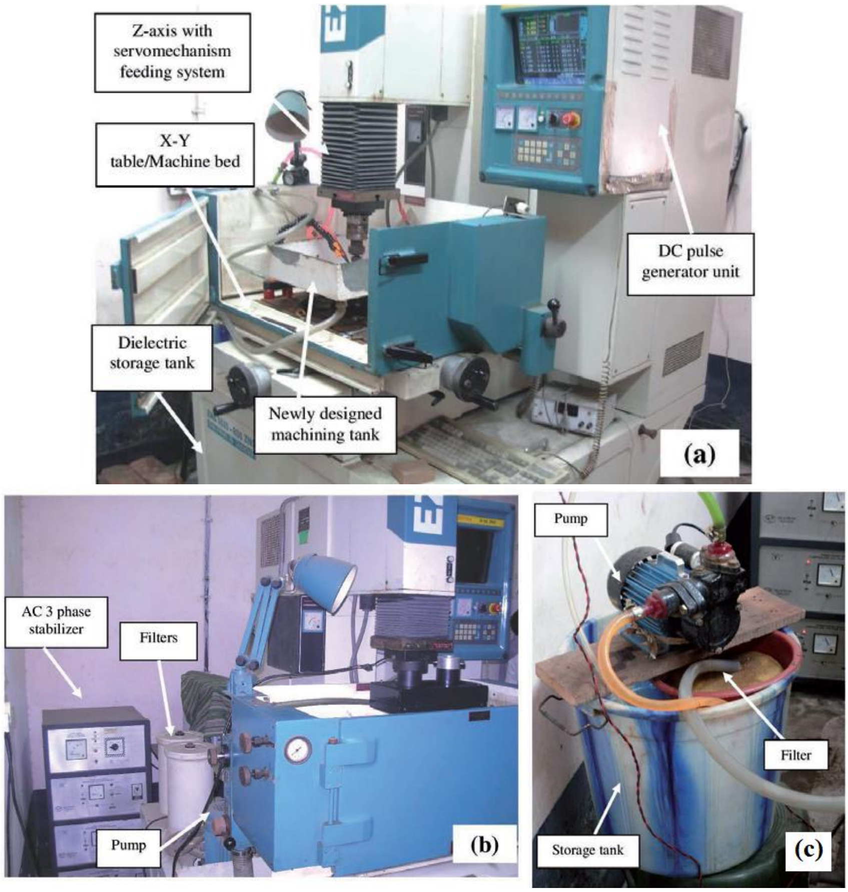

Figure 3. Photographic views of (a) and (b) EMS-5535-R50, ZNC EDM machine (c) External dielectric supply system for circulating de-ionized water.

From the literature review, it is evident that a lot of research investigations were performed to study the effects of water-based dielectrics and also the effects of powder mixed dielectrics. However, these researches are on conventional EDM operation, where the ranges of various process parameters (peak current, gap voltage, pulse duration, flushing pressure, etc) are in higher levels. However, for micro-EDM process, very low discharge energy range is considered and also the levels of various process parameters are scaled downed for machining in micro domains. A very few research activities were conducted by researchers across the globe utilizing water based dielectrics in micro-EDM and also utilizing powder mixed in these dielectrics. It is already known that the type of dielectric plays an important governing role in micro-EDM as different dielectrics have different properties such as dielectric strength, recovery capability after breakdown, quenching and flushing ability, degree of fluidity, composition and availability. Therefore, it is urgently required to conduct an intensive research study during micro-EDM using various types of dielectrics such as kerosene, de-ionized water and also powder additive mixed dielectrics. Keeping in view of the above mentioned requirements, a well planned research activities have been designed considering direction received from the previous researchers to investigate the influence of dielectric on various micro machining requirements such as material removal rate, tool wear rate, overcut and surface quality, etc.

The experiments are performed on a traditional die sinking EDM (model: series 2000, EMS-5535-R50, ZNC EDM machine, Manufacturer: Electronica Machine Tools Pvt. Ltd., Pune, India). This EDM set up is consists of (i) Spark generator unit, (ii) Z axis unit with servo feed mechanism, (iii) X-Y table unit and (iv) Dielectric pumping and filtering unit. Figure 3 (a) and (b) shows the photographic view of the main components of micro-EDM set up used in this experimental study. When experiments are done with dielectric fluid other than kerosene i.e., de-ionized water, powder mixed kerosene, powder mixed de-ionized water, a separate dielectric chamber with separate pump, and pressure-regulating valve and filter were used to circulate the dielectrics without affecting dielectric supply system of the main machine. When machining was done with powder-mixed dielectric, the external filter unit was removed, and a magnetic field was employed to remove the machining debris from the dielectrics. Figure 3 (c) shows the developed external dielectric supply system to supply and circulate dielectrics during micro-EDM experiments.

Table 1. Compositions of Ti-6Al-4V superalloy [48]

Element	Percentage
Aluminium	5.5 to 6.75
Carbon	≤ 0.10
Iron	≤ 0.50
Hydrogen	≤ 0.015
Nitrogen	≤ 0.05
Oxygen	≤ 0.45
Other	< 0.4
Vanadium	3.5 to 4.5
Titanium	Balance

Table 2. Physical and mechanical properties of Ti-6Al-4V [48]

Property	Typical Value
Density (g/cm^3)	4.42
Melting range (ºC±15 ºC)	1649
Specific heat (J/Kg°C)	560
Thermal conductivity (W/m-K)	7.2
Tensile strength (Mpa)	897
Elastic modulus (GPa)	114
Hardness Rockwell C	36

With the advancement of material science different kind of advanced materials of high strength temperature resistance (HSTR) and different kind of supper alloys have been improved in recent times. These materials are widely used in industry for their unique characteristics such as high strength, lightweight, high temperature resistance, and cryogenic property, etc. Titanium super alloy (Ti-6Al-4V) is one of them. The high strength, low weight, outstanding corrosion resistance possessed by titanium and titanium alloys have led to a wide and diversified range of successful applications which demand high levels of reliable performance in surgery and medical applications such as bone and joint replacement, dental implants, cardiovascular devices, surgical instruments as well as in aerospace, automotive, chemical plant, power generation, oil and gas extraction, sports, and other major industries. Through micro-holes were machined on Ti-6Al-4V plates (thickness of 1 mm). Tungsten is the best material to be used as the tool electrode. It has high strength, hardness and it has high melting point of about 3400ºC. However, tungsten is expensive and difficult to give proper shape. Therefore, to provide ductility to tungsten, some elements are mixed and the resulting material is machinable, conductive, strong and wear resistant. Cylindrical shaped tungsten electrodes with flat front of diameter 300 μm were used as tool. Tables 1 and 2 show the chemical compositions and physical as well as mechanical properties of titanium alloy (Ti-6Al-4V), respectively.

As the micro-EDM performances are affected mostly by peak current (Ip) and pulse-on-time (Ton) during machining of Ti-6Al-4V alloy [64, 65], so influence of these two predominant process parameters were considered as the varying parameters keeping other process parameters like flushing pressure (Pr), duty factor (t) as constant during machining with each dielectrics. In the present experimental study, a new powder additive i.e., B_4C is mixed in both the dielectrics to investigate the different micro-EDM response criteria, machined micro-hole quality, and surface topography. This B_4C powder has some excellent physical and chemical properties such as high chemical resistance and hardness, excellent wear and abrasion resistant etc. These exceptional characteristics of boron carbide may provide effective and efficient discharge conditions at the machining zone and also enhancement in above-mentioned machining performances. Electrical resistivity of boron carbide is in the range of 0.1-10 Ω-cm. As B_4C abrasive lie in a transition zone between good conductors and isolators, the potential difference as well as the plasma channel produced in the micron sized inter electrode gap can make the abrasive to conduct thermoelectric power in the machining zone [66, 67]. Boron carbide is characterized by a relatively wide gap in its forbidden band, a low thermal conductivity, and a high thermoelectric power. These properties make it a potentially useful material for high-temperature thermoelectric energy conversion compared to silicon carbide as well as tungsten carbide abrasives. As micro-EDM process uses discharge *energy* in the range of 5–150µJ, so there is a little chance to melt and evaporate the B_4C particles due to discharge in the inter electrode gap. It was observed in the optical measuring microscope that the powder particles comprise of mixture of different shapes and sizes ranging from 8 to 20 µm. When, Boron carbide (B_4C) powder-mixed de-ionized water was applied in the machining zone, most of the particles, which are more than 10 µm in size, get accumulated at the base of machining zone because of self-weight of particles even though a motor driven stirrer was applied to provide turbulence in powder mixed dielectrics in the machining tank. Hence, the effective average particle size that may involve in the machining phenomena at the micro-machining zone ranges from 8 to 10 µm during micro-EDM. Therefore, the average size of B_4C particles, which actively take part in machining, is in the range of 8 to 10 µm. The thermo-physical properties of boron carbide powder are enlisted in Table 3. B_4C powder additive of concentration 4 g/l was added to pure kerosene and deionized water when experimentations were performed with powder-mixed dielectrics. This particular concentration of additive in dielectrics has been selected based on past research studies on powder-mixed dielectrics in EDM [27, 34].

Table 3. Thermo-physical properties of Boron carbide (B_4C) additives [48]

Property	Typical value
Density (g/cm^3)	2.52
Melting point (°C)	2445
Electrical conductivity (at 25°C) (S)	140
Thermal conductivity (at 25°C) (W/m-K)	30-42
Young's modulus (GPa)	450-470
Hardness (Knoop 100g) (kg-mm^{-2})	2900-3580
Specific heat (J.K^{-1}.kg^{-1}) (at 25°C)	950

Table 4. Experimental condition for through hole machining on Ti-6Al-4V alloy

Condition	Description
Workpiece material (anode)	Ti-6Al-4V plate of size 13 mm × 15 mm and thickness of 1 mm
Tool electrode (cathode)	Solid tungsten micro-tool, diameter of 300 µm
Dielectric fluids	Kerosene, de-ionized water
Additive	Boron carbide (B_4C) powder
Average size of additive (µm)	8-10
Powder concentration (g/l)	4
Peak current (A)	0.5, 1, 1.5, 2
Pulse-on-time (µs)	1, 2, 5, 10, 20
Duty factor (%)	95
Flushing pressure (kgf/cm^2)	0.5
Resistivity of pure de-ionized water (megohm-cm)	4.2

In this research investigation, experimentations have been carried out at various peak current settings i.e., 0.5, 1, 1.5, 2 A employing kerosene and deionized water. The details of the machining conditions and other parameter details are enlisted in Table 4. In this research study, micro-EDM characteristics such as material removal rate (MRR), tool wear rate (TWR), overcut (OC), diametric variance in entry and exit (DVEE)/taper and micro-hole circularity were considered as the machining characteristics. Material removal rate was calculated by taking the weight of the workpiece before machining and after machining and dividing the weight difference by time of machining as per Equation 2. Similarly, tool wear rate is calculated by taking the weight of the micro-tool before machining and after machining and dividing the weight difference by time of machining as per Equation 3. A high precision weighing machine (Manufacturer: Mettler Toledo, Switzerland, Least measurable weight = 0.01 mg) is used to measure various weights of workpiece and micro-tools. The overcut of micro-hole machined is measured by diametric difference of the through micro-hole at the entrance and solid micro-tool as per Equation 4. The taper of the through micro-hole is measured by using Equation 5. A high precision measuring microscope (Manufacturer: OLYMPUS, Japan, Model: STM6, minimum measurable dimension = 0.5 μm) is used to measure all the dimensions of micro-hole diameters as well as of micro-tool. The optical photograph of each micro-hole was taken to measure the hole circularity. The circularity was calculated by image processing software ImageJ Version 1.41. This software calculates the circularity of micro-holes according to Equation 6. Experimentation were conducted at various micro-EDM parametric combinations and measured and calculated the performance criteria. The discussion and analysis of various test results are described in the following sections.

$$Material\ removal\ rate\ (MRR) = \frac{Weight\ of\ workpiece\ before\ machining\ (W_B) - Weight\ of\ workpiece\ after\ machining\ (W_A)}{Machining\ time\ (T)} \quad (2)$$

$$Tool\ wear\ rate\ (TWR) = \frac{Weight\ of\ tool\ before\ machining\ (T_B) - Weight\ of\ tool\ after\ machining\ (T_A)}{Machining\ time\ (T)} \quad (3)$$

$$Overcut\ (OC) = \frac{Diameter\ of\ entry\ hole\ (D_{EN}) - Diameter\ of\ tool\ electrode\ (D_T)}{2} \quad (4)$$

$$Taper = \frac{Entry\ hole\ dia.\ (D_{EN}) - Exit\ hole\ dia.\ (D_{EX})}{2 \times Workpiece\ thickness\ (t)} \quad (5)$$

$$Circularity = 4\pi \,/\, \frac{Area\ of\ through\ micro-hole\ (A)}{[Perimeter\ of\ through\ micro-hole\ (P)]^2} \quad (6)$$

RESULTS AND DISCUSSION

In this section, the influence of different dielectrics such as pure kerosene, pure de-ionized water, boron carbide mixed kerosene and boron carbide mixed de-ionized water on different micro-EDM machining process performances such as material removal rate (MRR), tool wear rate (TWR), overcut (OC) and taper of micro-holes are shown and analyzed through various plots based on experimental results varying peak current (Ip) and pulse-on-time (Ton).

Comparative Study of Machining Performance Characteristics Using Kerosene and De-ionized Water

In this section, a detailed comparison of various machining performance characteristics has been performed for the investigation of influence of dielectrics such as kerosene and de-ionized water in micro-EDM for micro machining of titanium alloy (Ti-6Al-4V). Figure 4 depict the comparison of the material removal rate (MRR) using two different dielectrics such as kerosene and de-ionized water varying peak current (Ip) and pulse-on-time (Ton). The material removal rate (MRR) is much more using de-ionized water than the kerosene throughout the considered range of pulse duration and increase of peak current. When machining is done with kerosene, as the dielectric fluid is kerosene which is a chemical compound of carbon and hydrogen, decomposes and produces a layer of titanium carbide (TiC) on the workpiece surface. But, when using de-ionized water, the water decomposes and a layer of titanium oxide (TiO_2) is produced on the machined surface. Since, TiC has a higher melting temperature (3150ºC) than that of TiO_2 (1750ºC), a large discharge energy is required for improving the material removal rate using kerosene. Also, the size of debris formed during machining with kerosene is less compared to machining with de-ionized water, thus improving the material removal rate.

Figure 5 show the comparison of the tool wear rate (TWR) using two different dielectrics such as kerosene and de-ionized water varying peak current (Ip) and pulse-on-time (Ton). It is seen from the figure that the tool wear rate (TWR) is high using de-ionized water compared to machining with kerosene. When using kerosene as the dielectric, it decomposes in the high discharge energy and produces carbon particles that stuck or adhere to the surface of the electrode.

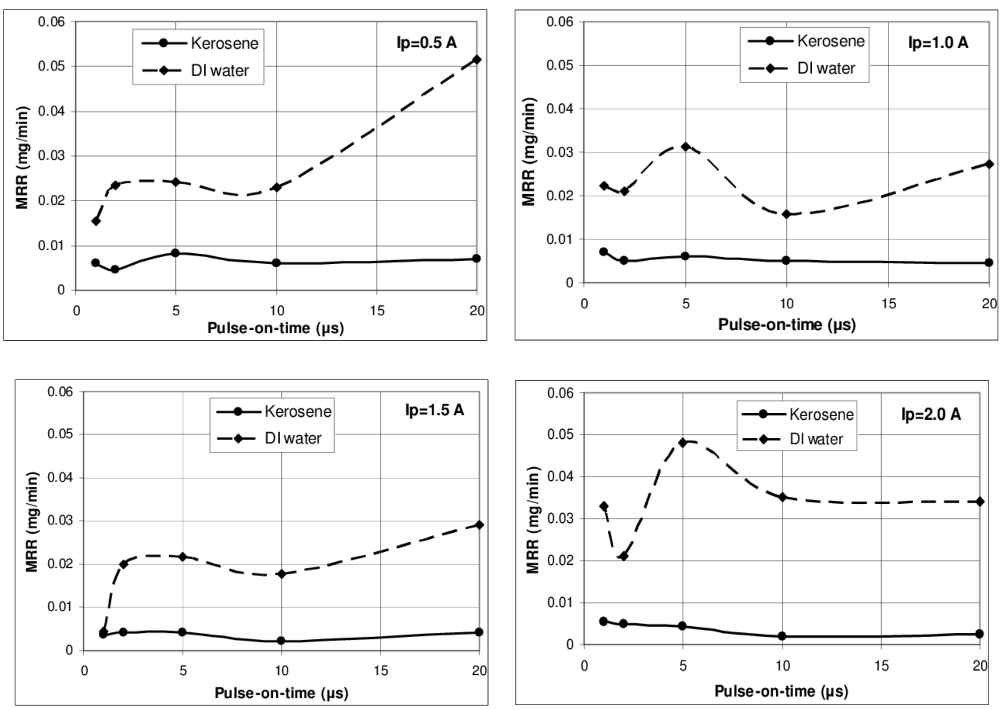

Figure 4. Influence of different dielectrics on the material removal rate (MRR) with varying pulse-on-time (T_{on}).

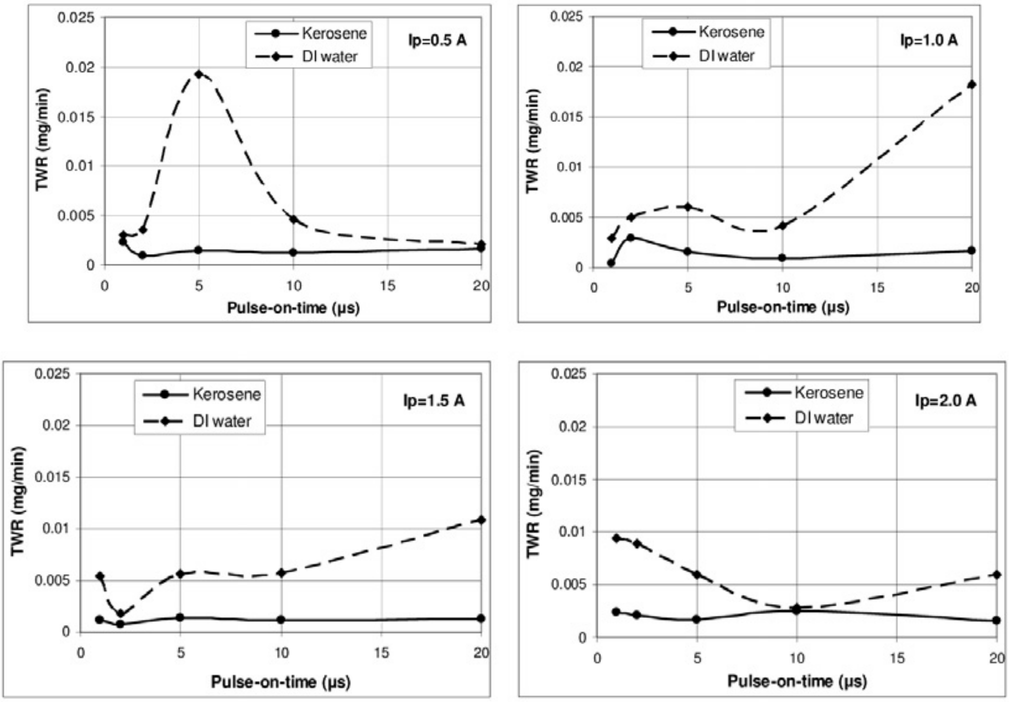

Figure 5. Influence of different dielectrics on the tool wear rate (TWR) with varying pulse-on-time (T_{on}).

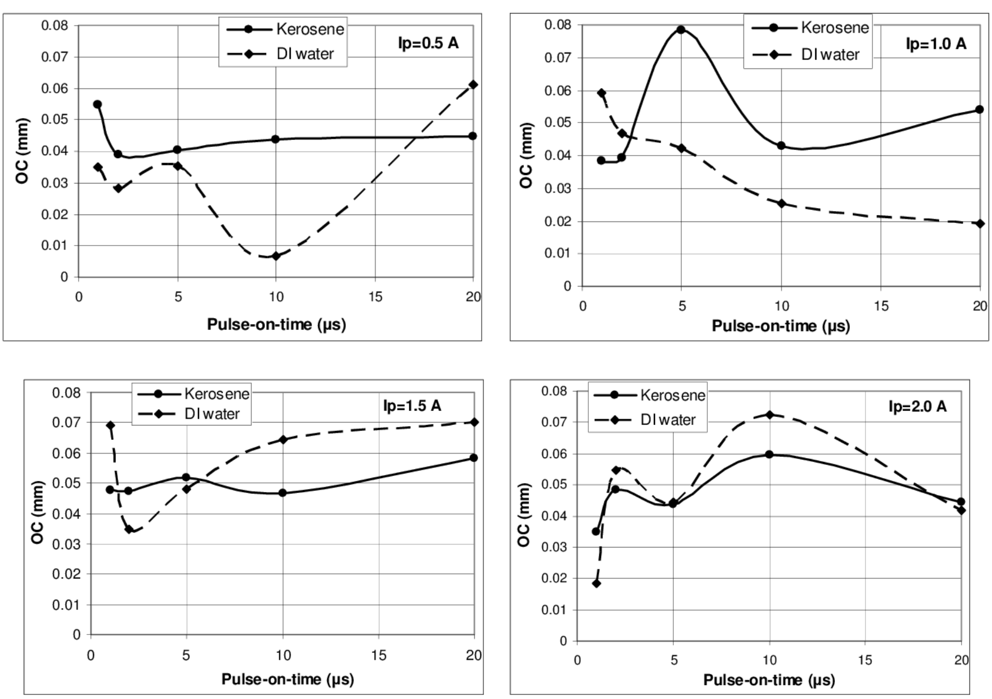

Figure 6. Influence of different dielectrics on the overcut (OC) with varying pulse-on-time (T_{on}).

These carbon particles restrict the rapid wear of the tool. So, the tool wear rate (TWR) is less while using kerosene as dielectric. On the other hand, when using deionized water, no carbon adhere to the tool electrode surface, thus TWR is higher enough with de-ionized water.

Figure 6 show the comparative study of the overcut (OC) using two different dielectrics i.e., kerosene and de-ionized water with varying peak current (Ip) and pulse-on-time (Ton). From the figures, it is clear that the overcut of the machined micro-holes is larger when using de-ionized water for the pulse duration of 1 and 2 μs when machining is done by varying peak current. But, at higher pulse duration the overcut of the micro-holes is larger when using kerosene as the dielectric. When deionized water is used, it releases oxygen decomposed from water. This oxygen influences the machining stability and influence the possibility of debris formation. These debris particles ejected through the short gap of tool surface and micro-hole walls. This phenomena increases secondary sparking, resulting in higher overcut compared to kerosene. But at higher pulse duration, the machining stability and efficiency increases due to more pulses per cycle, resulting higher overcut with kerosene compared to de-ionized water. When the overcut is analyzed with the increase of peak current, it is found that a high peak current results higher overcut with de-ionized water compared to kerosene.

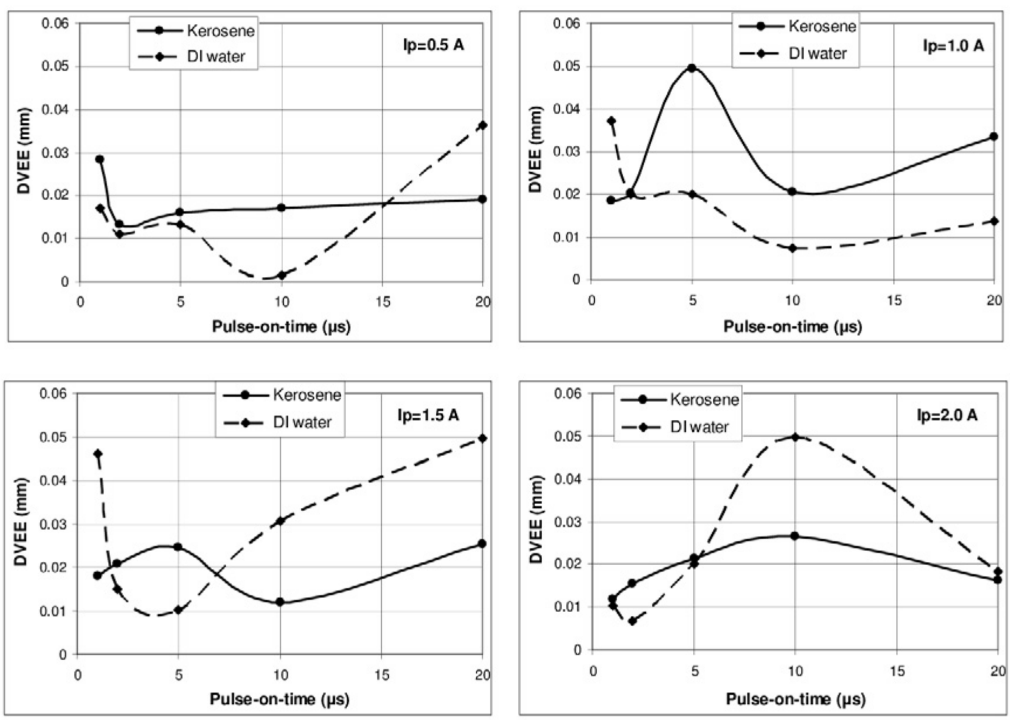

Figure 7. Influence of different dielectrics on the diameter variance between entry and exit (DVEE) with varying pulse-on-time (T_{on}).

Figure 7 show the comparison of the diameteral variance in entry and exit (DVEE) using two different dielectrics i.e., kerosene and de-ionized water with varying peak current (Ip) and pulse-on-time (Ton).

It can be observed from the figures that DVEE of the micro-holes increases at low discharge duration when varying peak current was employed using de-ionized water as dielectric fluid. But, further increase of pulse duration results in decrease of DVEE of the holes with de-ionized water. A straight through micro-hole can be machined at pulse duration of 5 µs and peak current of 1.5 A. On the other hand, DVEE is lower at peak current 0.5 and 1 A employing deionized water compared to kerosene. But, as the peak current increases, the diameter variance increases with de-ionized water. Thus, a straight through micro-hole is not achieved.

Comparative Study of Machining Performance Characteristics Using Kerosene, De-ionized Water and Boron Carbide Mixed Dielectrics

Figure 8 shows the comparative plots of the material removal rate (MRR) using different dielectrics such as pure kerosene, pure de-ionized water and Boron Carbide (B_4C) mixed dielectrics powder for varying pulse-on-time (Ton) at different peak currents (Ip). This figure reveals that MRR is high with de-ionized water than kerosene for all considered settings of pulse duration and peak current during experimentation. Additionally, when machining is done by mixing B_4C powder additives in kerosene dielectric it is clearly seen that MRR increases with the increase of pulse duration at constant peak current of 1.5 and 2 A. Also the MRR with powder mixed dielectrics is larger compared to machining with pure kerosene and de-ionized water at higher pulse duration discharge settings. The increase of MRR with the increase of pulse duration using B_4C mixed kerosene is due to increase of spark discharge time i.e., longer effective machining time per pulse. The presence of boron carbide additive in kerosene further helps in uniform distribution of discharge energy and better conduction of discharge current thereby enabling better machining condition. When B_4C powder was applied to de-ionized water, it is seen that MRR is more using additive compared to pure deionized water at peak current 1.5 and 2 A. The same explanation is applicable here also for the increase of MRR as of additive mixed kerosene.

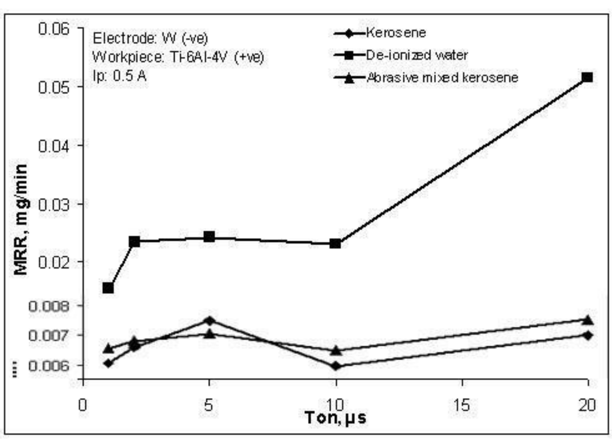

Figure 8. (Continued).

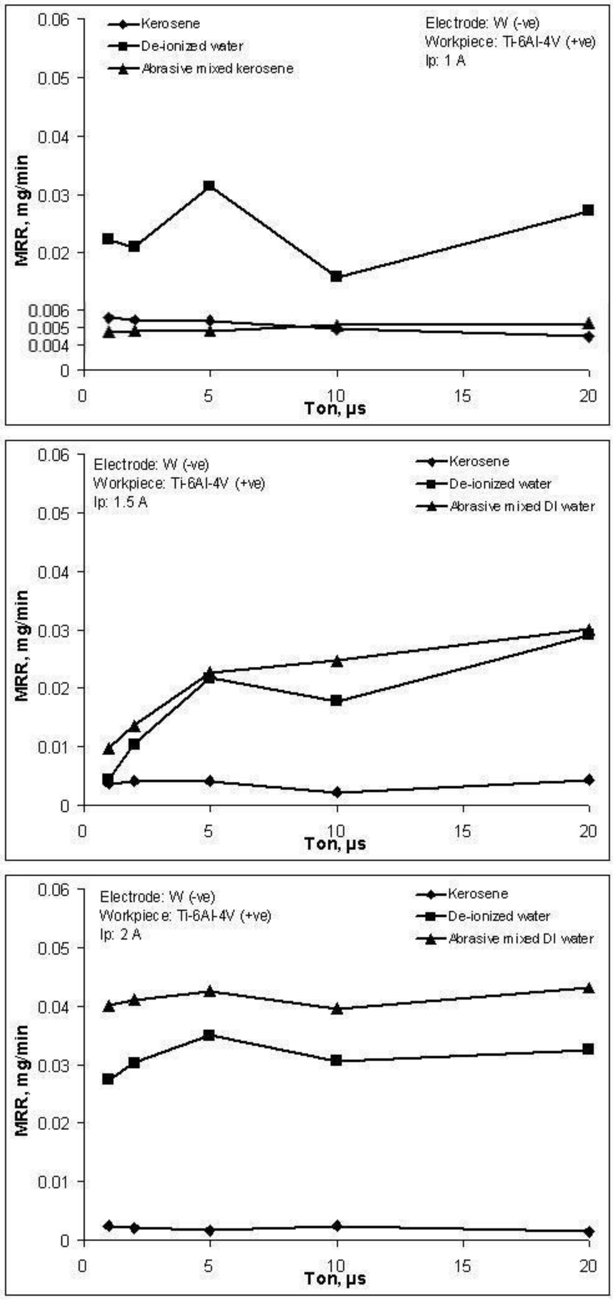

Figure 8. Variation of material removal rate (MRR) with pulse duration (T_{on}) at various fixed peak current (I_p) for different dielectrics [48].

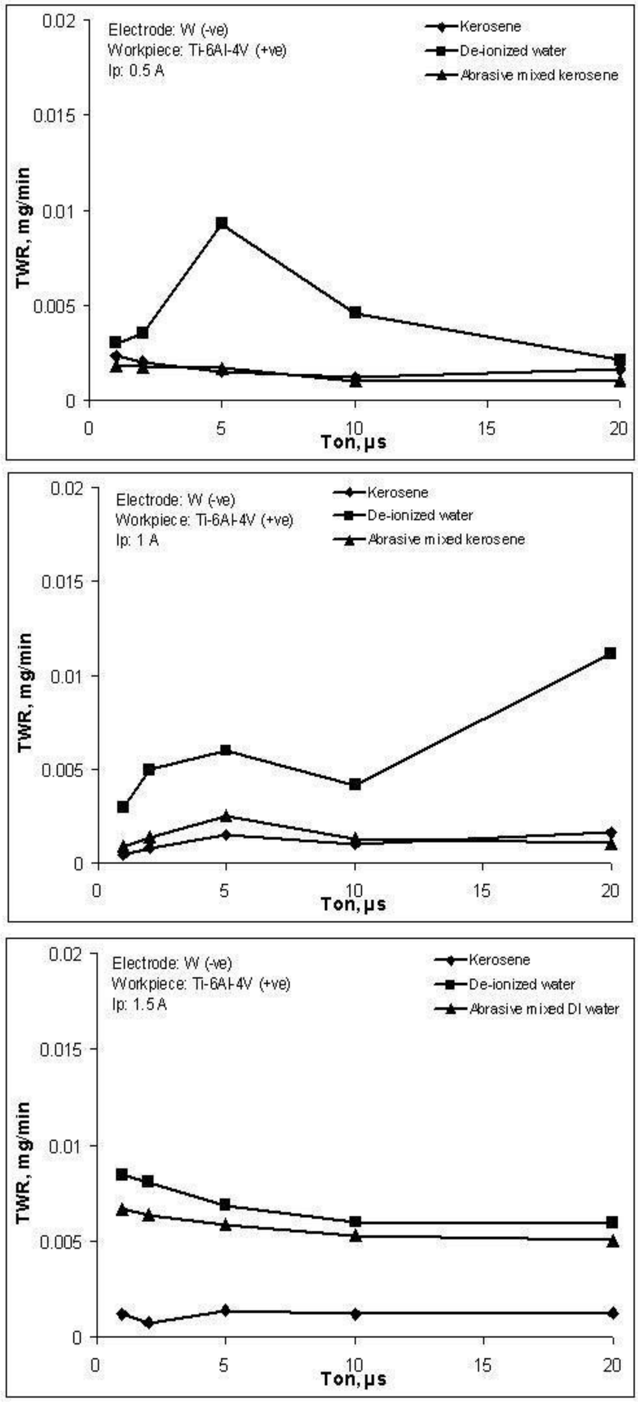

Figure 9. (Continued).

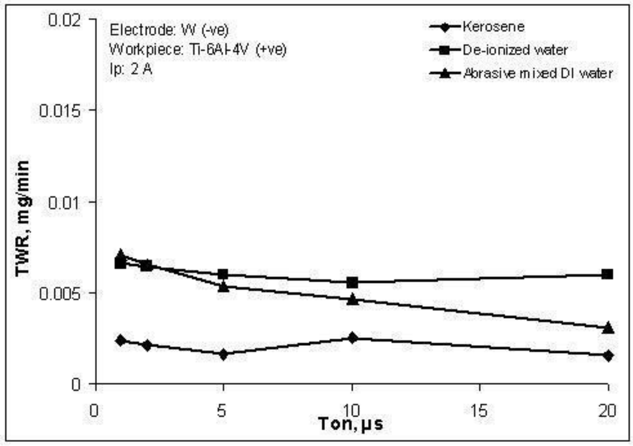

Figure 9. Variation of tool wear rate (TWR) with pulse duration (Ton) at various fixed peak current (Ip) for different dielectrics [48].

In Figure 9, comparative results of tool wear rate (TWR) with pulse duration at different pulse discharge with various constant peak current are shown employing kerosene, de-ionized water and B_4C powder mixed dielectrics. This figure reveals that TWR is high using de-ionized water compared to machining with kerosene dielectric. Furthermore, it is revealed from the same figure that tool wear rate associated with B_4C mixed kerosene is less compared to machining with pure kerosene at peak current of 0.5 and 1 A. When machining is done with boron carbide abrasive mixed kerosene dielectric, the tool wear is less due to the presence of more number of carbon particles evolving from the decomposition of kerosene dielectric as well as boron carbide abrasive in the machining zone. From the same figure, it is observed that at fixed 1 A peak current, tool wear rate is less than at fixed 0.5 A current setting using additive mixed kerosene.

This is due to the fact that the higher discharge energy results in more decomposition of kerosene and it further generates more carbon which in turn adheres onto the tool surface preventing secondary sparking. Although higher peak current i.e., 2A produces more discharge energy, but that results in more current density and subjects the tool electrode under large thermal stresses. The powder mixed de-ionized water results in less tool wear rate at peak current of 2 A compared to 1.5 A due to more deposition of carbon particles from B_4C additives. It is also found that machining combined with boron carbide powder mixed deionized water results in less tool wear compared to pure de-ionized water due to adhesion of carbon particles from boron carbide powder on the tool surface, which restrict tool wear to certain extent.

The comparative plots of overcut (OC) of micro-holes on Ti-6Al-4V employing kerosene, deionized water and B_4C abrasive mixed dielectrics are shown in Figure 10 when pulse duration was varied for different peak current. It is observed from these figures that the overcut of the machined micro-holes is less when dielectric was de-ionized water for peak current setting of 0.5 and 1 A. However, at higher peak current i.e., 1.5 and 2 A, overcut is more in case of de-ionized water compared to pure kerosene dielectric.

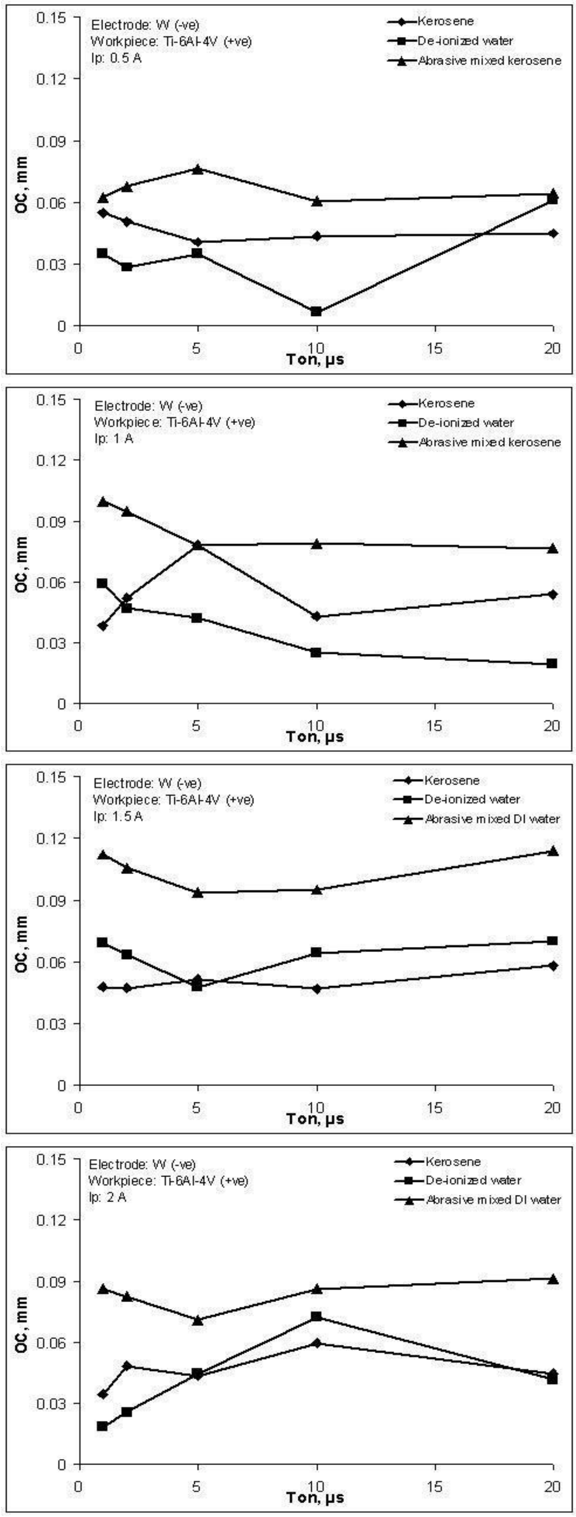

Figure 10. Variation of overcut (OC) with pulse duration (Ton) at various fixed peak current (Ip) for different dielectrics [48].

In addition, when B_4C additive was used in dielectrics, it is found that OC is larger with powder mixed dielectrics compared to pure dielectrics. It is so because the suspended additive particles remove the molten layer from the machining zone and further reduce the possibility of formation of thick white layer, resulting larger OC. It is also revealed that OC decreases with increase in pulse duration while using B_4C suspended kerosene as dielectric. It is due to decrease of overall machining time i.e., faster machining. However, larger OC is found in case of B_4C mixed deionized water as dielectric because of secondary sparking.

Figure 11 shows the comparative plots of diameteral variance at entry and exit (DVEE) using kerosene, de-ionized water and boron carbide powder mixed with these dielectrics. It is found from this figure that DVEE of the micro-holes is lower employing de-ionized water compared to kerosene as dielectric fluid at lower peak current i.e., 0.5 and 1 A. However, at higher peak current i.e., 1.5 and 2 A, DVEE is larger using de-ionized water. It is also found that boron carbide powder mixed kerosene results in large DVEE compared to pure kerosene at low peak current of 0.5 and 1 A. As the machining progresses, the additive boron carbide particles creates more carbon adhesion on the work surface, that further results in lower material removal at exit side of micro-hole and greater variance in entry and exit diameters. But, when B_4C additive mixed de-ionized water is used at higher peak current of 1.5 and 2 A, the powder particles help in uniform distribution of discharge energy which in turn leads to better dimensional accuracy micro-holes compared to pure de-ionized water.

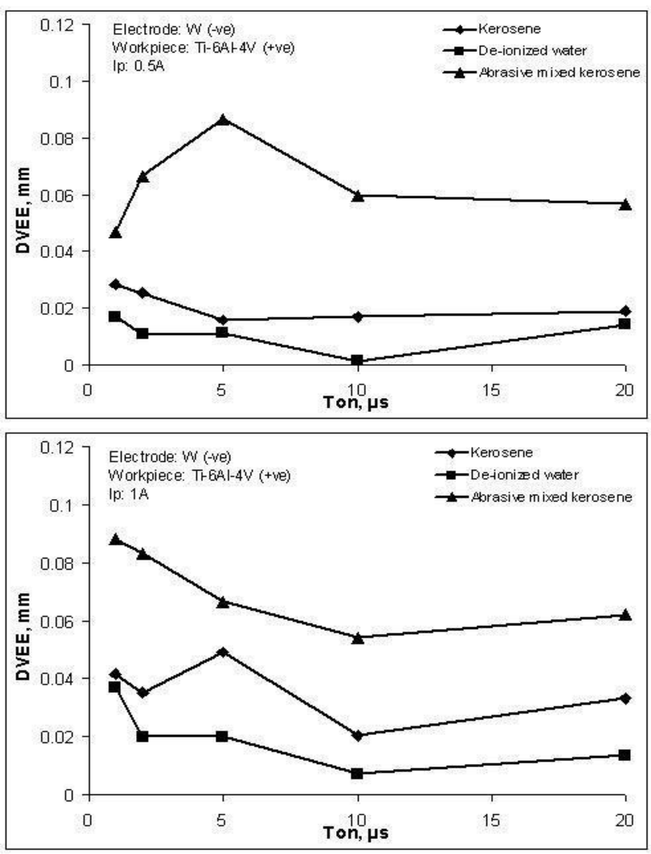

Figure 11. (Continued).

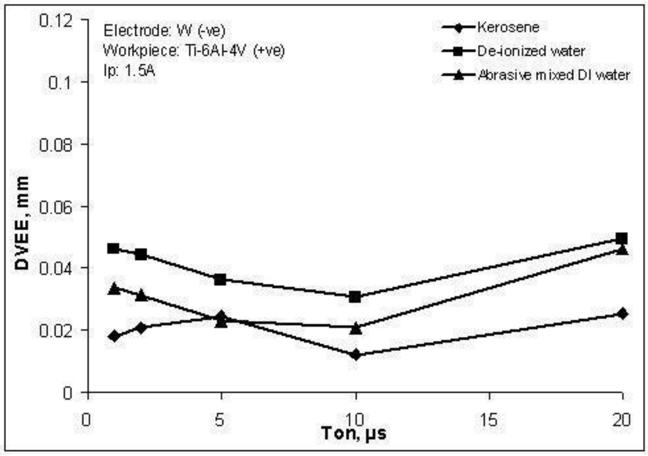

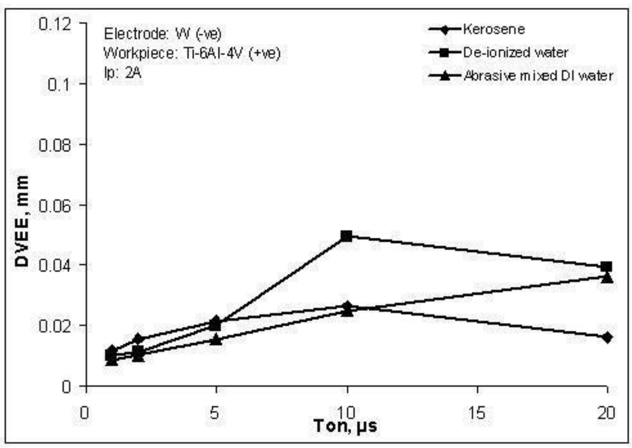

Figure 11. Variation of diameteral variance at entry and exit (DVEE) with pulse duration (Ton) at various fixed peak current (Ip) for different dielectrics [48].

It is a well-known fact that machining time varies when different machining parametric settings are applied for a particular tool-workpiece and machining set-up combination. In this research study, the authors have studied the time required to machine a particular thickness of workpiece (1 mm) by varying two most effective process parameters i.e., peak current and pulse-on-time.

Figure 12 shows the comparison of machining time required in each case for different dielectrics in the research investigation. It can be observed from the figure that at each set of considered machining parameters, pure de-ionized water results in low machining time compared to other dielectrics i.e., kerosene and B_4C mixed dielectrics to fabricate micro-holes in Ti-6Al-4V plate. At low peak current i.e., 0.5 and 1 A, boron carbide mixed kerosene takes longer time for producing through micro-holes than using pure kerosene. Also, when the discharge energy is higher, i.e., at peak current of 1.5 and 2 A, boron carbide powder mixed de-ionized water results in longer machining time than pure de-ionized water. As boron carbide mixed kerosene supplies more carbide particles at the machining zone, so there is more chances of formation of TiC layer on the workpiece surface and consequently requires longer time for machining. Further, as B_4C mixed dielectrics increases the gap size, the distance traveled by the tool will also increase and this results in longer machining time although additive particles encourage the uniform distribution of discharge energy which enables better machining efficiency.

Circularity of a hole is defined as the degree of roundness of a hole. Figure 13 show comparative results of circularity of micro-holes at different machining parametric settings using pure and B_4C mixed kerosene and de-ionised water as dielectrics. From these figures, it is evident that at low current discharges, i.e., 0.5 A and 1 A, high degree of circularity of the micro-holes is found using kerosene than de-ionized water. But, as the peak current increases, i.e., at 1.5 A and 2 A, the circularity value of micro-hole is less using kerosene compared to de-ionised water. At low peak current, i.e., 0.5 and 1 A, the machining rate using kerosene dielectric is less compared to using de-ionised water. Therefore, the possibility of occurring secondary discharge is less with kerosene, which creates uniform and circular micro-hole compared to de-ionised water. However, at peak current of 1.5 and 2 A, the amount as well as size of ejected debris is more due to high discharge energy, which leads to non-uniformity of micro-hole with kerosene.

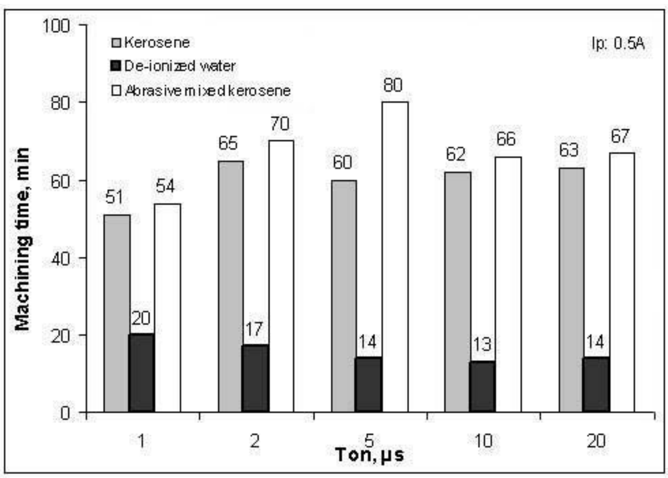

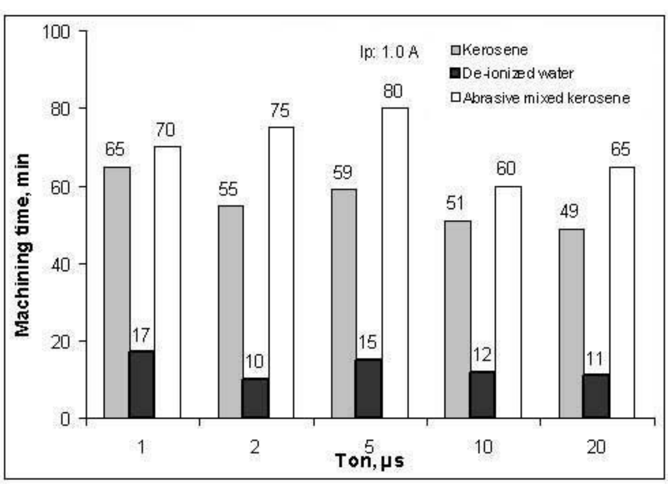

Figure 12. (Continued).

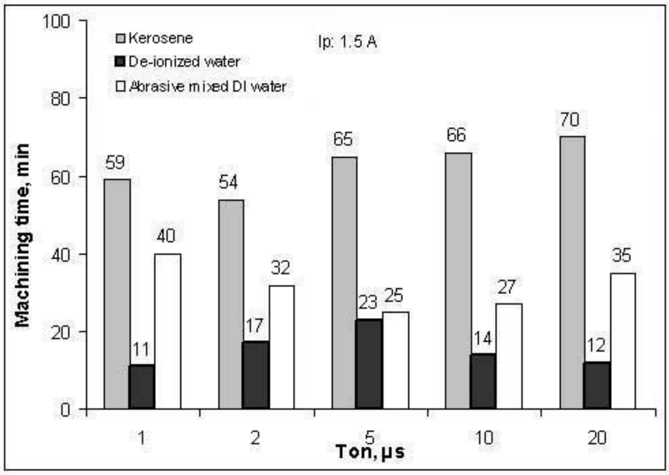

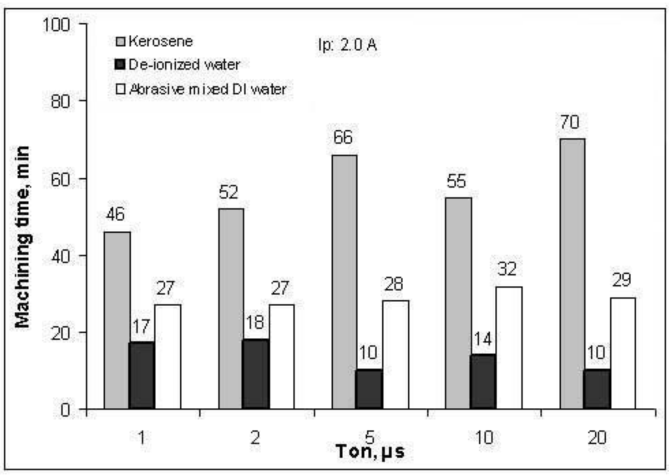

Figure 12. Variation of machining time (MT) with pulse duration (Ton) at various fixed peak current (Ip) for different dielectrics [48].

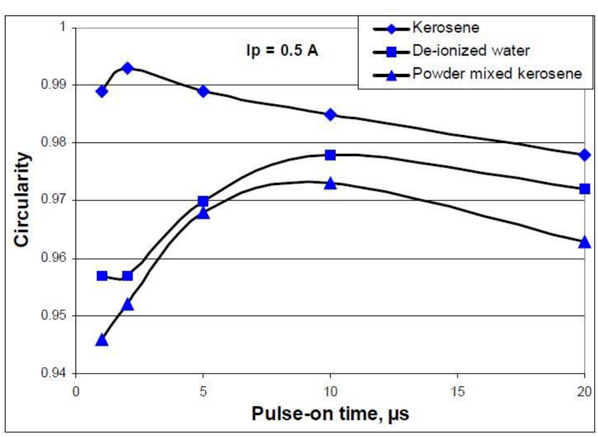

Figure 13. (Continued).

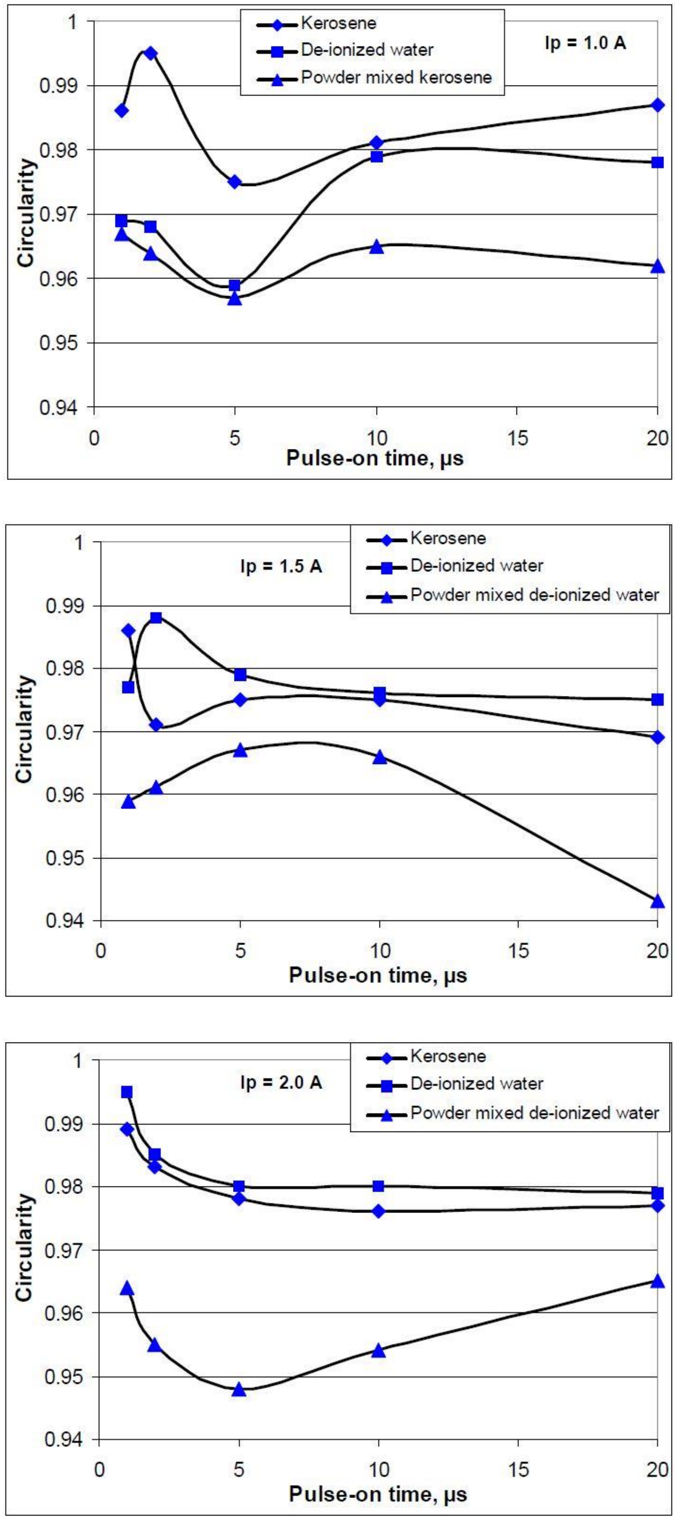

Figure 13. Variation of micro-hole circularity with pulse-on-time at peak current of 0.5, 1.0, 1.5 and 2.0 A using different dielectric fluids [68].

From these figures it is also found that boron carbide powder-mixed kerosene and de-ionized water results in non-uniform micro-hole compared to pure dielectrics in considered parameters settings. Here, the machining gap consists of ejected debris from workpiece as well as boron carbide powders. When these particles try to eject out through the gap of micro-hole wall and surface of micro-tool, the probability of secondary discharges enhanced and the micro-holes become non-uniformly circular. Moreover, the presence of carbide additive in dielectrics further helps in uniform distribution of discharge energy and better conduction of discharge current through the B_4C powder, thereby, enabling better machining condition increasing the amount of debris during machining.

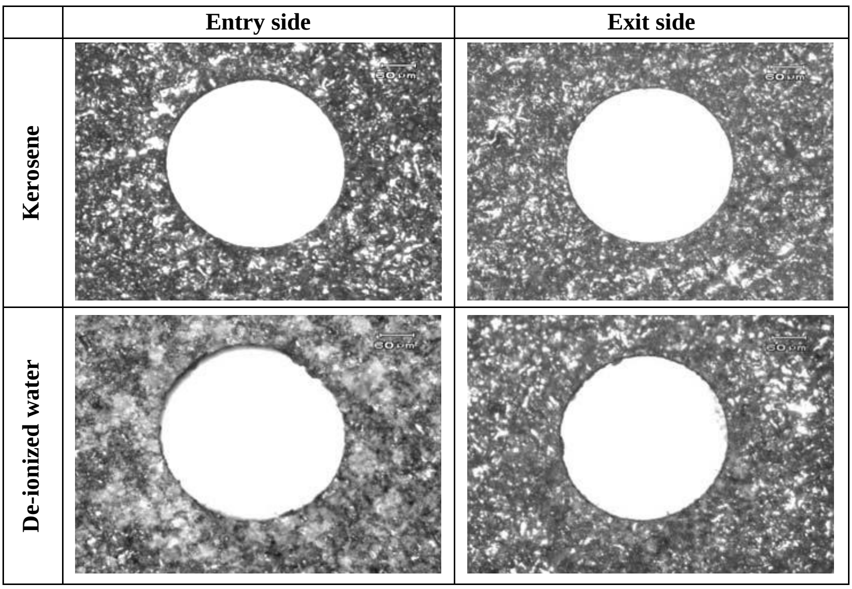

Figure 14. Optical photographs of machined micro-holes with different dielectrics at parametric setting of 1 A/2 μs [48].

Qualitative Study of Micro-EDMed Holes using Optical and Scanning Electron Micrographs

After machining of micro-holes utilizing various type of dielectric fluids, the workpieces were carefully polished, cleaned, and etched with a solution of 2.5 ml of HF acid (40%), 5 ml concentration of HNO_3 and 42.5 ml of de-ionized water for examining the surface topography of micro-holes as well as the recast layer formed on the machined microhole surfaces with the aid of optical and SEM micrographs. Figure 14 shows some optical micrographs of machined micro-holes that were taken using a 10X zoom lens in a precision optical microscope for both pure dielectrics i.e., kerosene and de-ionized water at the machining condition of 1 A peak current and 2 μs pulse duration. It is clear from these figures that kerosene dielectric result in improved quality micro-hole than de-ionized water. Some SEM micrographs of machined micro-holes using B_4C mixed dielectrics are shown in Figure 15. It is confirmed from this figure that employing powder mixed deionized water, accurate micro-holes is produced.

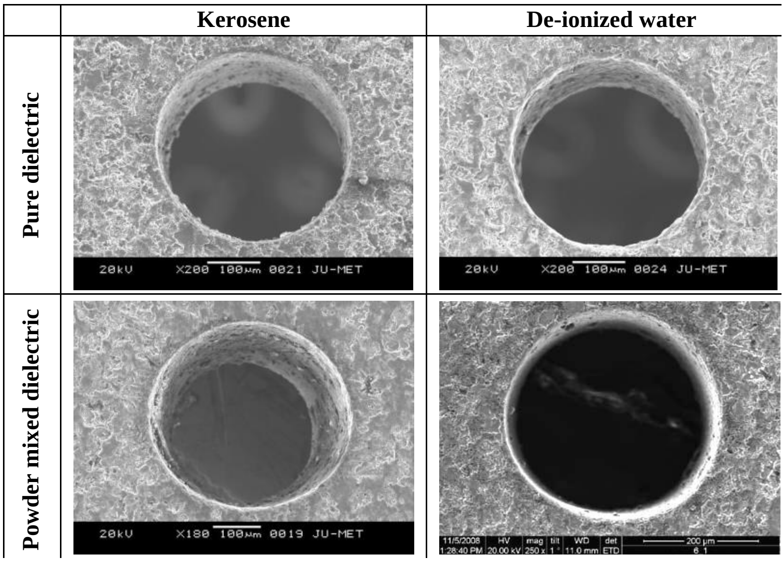

Figure 15. SEM micrographs of machined micro-holes using pure and powder mixed dielectrics [48].

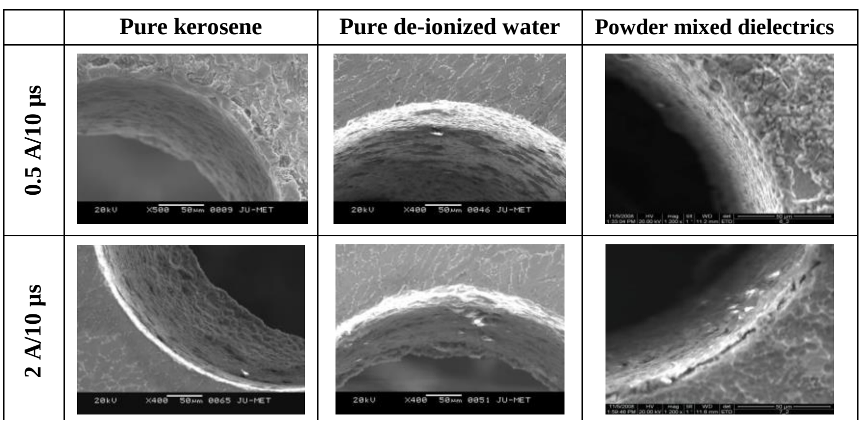

Figure 16. SEM micrographs of surface topography of machined micro-holes using different dielectrics [48].

Figure 16 shows the inner surface topography of the machined micro-holes using pure kerosene, de-ionized water and B_4C mixed in both dielectrics at different process parametric combinations. When machining was done with pure de-ionized water, the inner surface is smoother compared to pure kerosene at the same machining conditions. Also, when micro-holes were produced by adding boron carbide powder in kerosene and de-ionized water dielectrics, B_4C powder mixed de-ionized water results in smoother surface than kerosene at the same machining condition. During machining with kerosene dielectric, it produces titanium carbide (TiC) layer on the machined surface, the energy required to melt it is higher than titanium oxide (TiO_2) layer produced during machining with de-ionized water. These TiC layer restricts smooth and efficient machining. Moreover, when comparing the machining parametric settings with same type of dielectric, it is found that low value of peak current setting generates better surface quality compared to high current setting. It is due to the fact that at low discharge energy, small crater is produced per discharge and this result in better surface finish.

Figure 17 shows the enlarged views of edge of the micro-holes in which the white/recast layer can be seen clearly at two different machining parametric settings employing pure and B_4C mixed kerosene and de-ionized water dielectrics. From these SEM micrographs, it can be clearly observed that the thickness of the white layer is much lower when machining was done using de-ionized water as dielectric compared to machining with kerosene at the same parametric condition. The micrograph also reveals that with the increase of the pulse-on-time, the thickness of the white layer increases. It is due to the fact that as the pulse duration increases, the effective machining time also increases resulting in more production of machining debris. Upon cooling, these debri adhere as well as resolidifies on the work surface. As the cooling rate of deionized water is higher than that of kerosene, the heat is rapidly dissipated from the melted workpiece surface to dielectric water quickly and consequently this results in rapid cooling of workpiece surface. Thus, chances of debris adhering to the work surface is less resulting in lower thickness of the white layer and further get less chances to form thicker white layer. When B_4C additive was mixed in these dielectric liquids, the recast layer formed on the wall of the micro-holes is comparatively low than that for pure dielectrics. The additive particles play an important role to remove the melted portion of the workpiece from the machining zone and restrict the formation of thick recast layer through resolidification of molten material on machined surface.

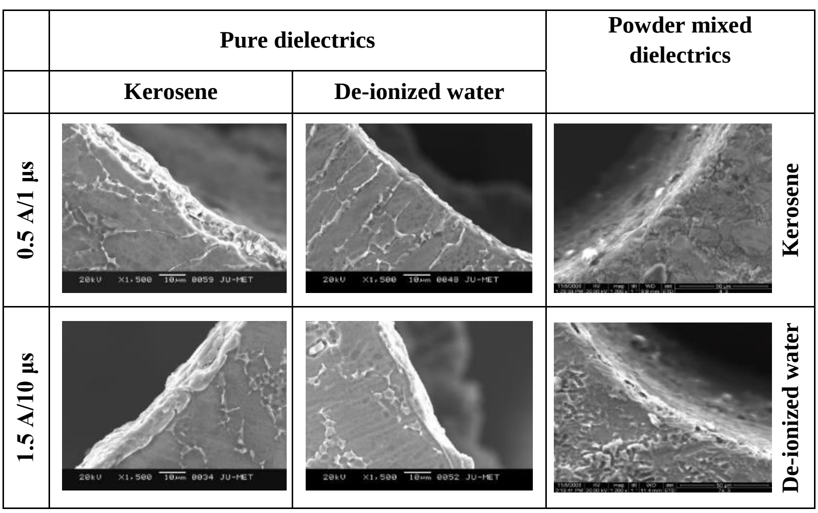

Figure 17. SEM micrographs of white layer of machined micro-hole's walls using different dielectrics [48].

CONCLUSION

From the experimental investigations, it is evident that there is great influence of different dielectrics such as pure dielectrics and additives mixed dielectrics on micro-EDM performance measures such as material removal rate, tool wear rate, overcut, diameteral variance at entry and exit, machined surface integrity and micro-hole accuracy during micro-machining of Ti-6Al-4V superalloy. Material removal rate is high with de-ionized water dielectric compared to pure kerosene. This is due to the formation of oxide (TiO_2) layer on workpiece surface when de-ionized water is used, which melts in lower discharge energy compared to melting of carbide (TiC) formed in case of kerosene. This TiC layer restricts the workpiece material to melt and vaporize during machining. Although B_4C additive mixed kerosene has not shown remarkable improvement in MRR, but the mixing of B_4C with de-ionized water shows an excellent increase in MRR due to the efficient distribution of discharge and increase in machining efficiency. Tool wear is higher with de-ionized water compared to kerosene. Also, TWR is more when B_4C mixed deionized water is used compared to pure kerosene.

Overcut of the micro-hole is less in low discharge energy when using de-ionized water dielectrics when compared to kerosene. However, de-ionized water results in larger overcut at higher discharge energy compared to kerosene. So, the accuracy of the micro-hole is higher at lower peak current and pulse-on-time using de-ionized water and at higher peak current and pulse-on-time using kerosene. Using B_4C additive, the both dielectrics show larger overcut compared to pure dielectrics. The experimental results show that DVEE of the machined micro-holes is less when de-ionized water is used as dielectric compared to kerosene dielectric. However, higher peak current (1.5 and 2A) resulted in larger DVEE using de-ionized water. Mixing of B_4C additive in both dielectrics show an increase in DVEE at low value of discharge current, but B_4C mixed de-ionized water dielectric has resulted comparatively lower DVEE at higher discharge energy compared to pure deionized water.

White layer or recast layer formed is less during machining with de-ionized water compared to pure kerosene. It is also found that with the increase of pulse duration, white layer thickness increases for both the dielectrics. White layer formation using B_4C additive mixed dielectrics is relatively low than pure dielectrics. This is due to quick removal of molten workpiece material from the machining zone. The topography of inner-machined surface is smooth when employing pure deionized water compared to kerosene. The boron carbide mixed de-ionized water also results in smoother surface than additive mixed kerosene. Pure de-ionized water results in excellent machining efficiency in comparison to kerosene as well as B_4C mixed dielectrics. Also, the addition of B_4C abrasive in dielectrics results in more machining time compared to pure dielectrics. The present investigation will open up challenging possibilities for exploring effective applications of titanium based super alloy utilizing micro-EDM technology in the field of precision micro-product manufacturing. However, this area of research still required further investigation for better understanding of the performance of micro-EDM characteristics by controlling other machining parameters such as variation of dielectric flushing pressure in micromachining zone and also mixing other types of additive particles with different sizes and concentrations.

REFERENCES

[1] Kagaya, O.Y., Yada, K., (1986). Micro-electro discharge machining using water as a working fluid-1: microhole drilling. *Precis. Eng.* 8(3), 157–162.

[2] Chow, H.M., Yan, B.H., Huang, F.Y., (1999). Micro slit machining using electric discharge machining with a modified rotary disk electrode (RDE). *J. Mater. Process. Technol.* 91, 161–166.
[3] Luo, Y.F., (1997). The dependence of interspace discharge transitivity upon the gap debris in precision electro-discharge machining. *J. Mater. Process. Technol.* 68, 127–131.
[4] Mohri, N., Saito, N., Higashi, M., (1991). A new process of finish machining on free surface by EDM methods. *CIRP Ann.* 40(1), 207–210.
[5] Narumiya, H., Mohri, N., Saito, N., Otake, H., Tsnekawa, Y., Takawashi, T., Kobayashi, K., (1989). EDM by powder suspended working fluid. *In: 9th International Symposium for Electrode Machining*, 5–8.
[6] Pradhan, B.B., Bhattacharyya, B., (2008). Improvement in microhole machining accuracy by polarity changing technique for microelectrode discharge machining on Ti-6Al-4V. *Proc. Inst. Mech. Eng., B. J. Eng. Manuf.* 222(2), 163–173.
[7] Zhang, Q.H., Du, R., Zhang, J.H., Zhang, Q., (2006). An investigation of ultrasonic-assisted electrical discharge machining in gas. *Int. J. Mach. Tool. Manuf.* 46(12–13), 1582–1588.
[8] Jeswani, M.L., (1981). Electrical discharge machining in distilled water. *Wear* 72, 81–88.
[9] Chen, S.L., Yan, B.H., Huang, F.Y., (1999). Influence of kerosene and distilled water as dielectrics on the electric discharge machining characteristics of Ti-6Al-4V. *J. Mater. Process. Technol.* 87, 107–111.
[10] Jeswani, M.L., (1981). Effect of the addition of graphite powder to kerosene used as the dielectric fluid in electrical discharge machining. *Wear* 70, 133–139.
[11] Chow, H.M., Yan, B.H., Huang, F.Y., Hung, J.C., (2000). Study of added powder in kerosene for the micro-slit machining of titanium alloy using electro-discharge machining. *J. Mater. Process. Technol.* 101, 95–103.
[12] Chow, H.M., Yang, L.D., Lin, C.T., Chen, Y.F., (2008). The use of SiC powder in water as dielectric for micro-slit EDM machining. *J. Mater. Process. Technol.* 195, 160–170.
[13] Kansal, H.K., Singh, S., Kumar, P., (2007). Technology and research developments in powder mixed electric discharge machining (PMEDM). *J. Mater. Process. Technol.* 184, 32–41.
[14] Wong, Y.S., Lim, L.C., Lee, L.C., (1995). Effect of flushing on electro-discharge machine surfaces. *J. Mater. Process. Technol.* 48, 299–305.
[15] Koshy, P., Jain, V.K., Lal, G.K., (1993). Experimental investigations into electric discharge machining with rotating disk electrode. *Precis. Engg.* 15(1), 6-15.
[16] Pandey, P.C., Shan, H.S., (1999). *Modern Machining Process*. Tata McGraw- Hill Publishing Company Ltd, Page 84-113.
[17] Lim, H.S., Wong, Y.S., Rahman, M., Lee, E.M.K., (2003). A study on the machining of high-aspect ratio micro-structures using micro EDM. *J. Mater. Process. Technol.* 140, 318–325.
[18] Jahan, M.P., Rahman, M., Wong, Y.S., Fuhua, L., (2010). On-machine fabrication of high-aspect ratio micro-electrodes and application in vibration-assisted micro-electro discharge drilling of tungsten carbide. *Proc. Inst. Mech. Eng. Part B J. Eng. Manuf.* 224(5), 795–814.

[19] Jahan, M.P., Anwar, M.M., Wong, Y.S., Rahman, M., (2009). Nanofinishing of hard materials using micro-EDM. *Proc. Inst. Mech. Eng. Part B J. Eng. Manuf.* 223, 1127–1142.

[20] Erden, A., Bilgin, S., (1980). Role of impurities in electric discharge machining. *In: Proceedings of 21st International Machine Tool Design and Research Conference*, Macmillan, London, 345–350.

[21] Mohri, N., Tsukamoto, J., Fujino, M., (1988). Surface modification by EDM-an innovation in EDM with semi-conductive electrodes. *In: Proceedings of Winter Annual Meet ASME*. 34, 21–30.

[22] Mohri, N., Saito, N., Higashi, M.A., (1991). A new process of finish machining on free surface by EDM methods. *Annals CIRP* 40(1), 207–210.

[23] Narumiya, H., Mohri, N., Saito, N., Otake, H., Tsnekawa, Y., Takawashi, T., Kobayashi, K., (1989). EDM by powder suspended working fluid. *In: Proceedings of 9th ISEM*, 5–8.

[24] Kobayashi, K., Magara, T., Ozaki, Y., Yatomi, T., (1992). The present and future developments of electrical discharge machining, *In: Proceedings of 2nd International Conference on Die and Mould Technology*, Singapore, 35–47.

[25] Yan, B.H., Chen, S.L., (1993). Effects of dielectric with suspended aluminum powder on EDM. *J. Chin. Soc. Mech. Eng.* 14(3), 307–312.

[26] Yan, B.H., Chen, S.L., (1994). Characteristics of SKD11 by complex process of electric discharge machining using liquid suspended with aluminum powder. *J. Jpn. Inst. Light Met.* 58(9), 1067–1072.

[27] Ming, Q.Y., He, L.Y., (1995). Powder-suspension dielectric fluid for EDM. *J. Mater. Process. Technol.* 52, 44–54.

[28] Uno, Y., Okada, A., (1997). Surface generation mechanism in electrical discharge machining with silicon powder mixed fluid. *Int. J. Elec. Mach.* 2, 13–18.

[29] Uno, Y., Okada, A., Hayashi, Y., Tabuchi, Y., (1998). Surface integrity in EDM of aluminum bronze with nickel powder mixed fluid. *J. Jpn. Soc. Elec. Mach. Eng.* 32(70), 24–31 (in Japanese).

[30] Wong, Y.S., Lim, L.C., Rahuman, I., Tee, W.M., (1998). Near-mirror-finish phenomenon in EDM using powder-mixed dielectric. *Int. J. Adv. Manuf. Technol.* 79, 30–40.

[31] Furutani, K., Saneto, A., Takezawa, H., Mohri, N., Miyake, H., (2001). Accretion of titanium carbide by electrical discharge machining with powder suspended in working fluid. *Precis. Eng.* 25, 138–144.

[32] Wang, C.H., Lin, Y.C., Yan, B.H., Huang, F.Y., (2001). Effect of characteristics of added powder on electric discharge machining. *J. Jpn. Inst. Light Met.* 42(12), 2597–2604.

[33] Chow, H.M., Yan, B.H., Huang, F.Y., Hung, J.C., (2000). Study of added powder in kerosene for the micro-slit machining of titanium alloy using electro-discharge machining. *J. Mater. Process. Technol.* 101, 95–103.

[34] Tzeng, Y.F., Lee, C.Y., (2001). Effects of powder characteristics on electro discharge machining efficiency. *Int. J. Adv. Manuf. Technol.* 17, 586–592.

[35] Furutani, K., Shiraki, K., (2002), Deposition of lubricant layer during finishing process by electrical discharge machining with molybdenum disulphide powder suspended in

working fluid. *In: JSME/ASME International Conference on Materials and Processing*, 468–473.

[36] Pecas, P., Henriques, E.A., (2003). Influence of silicon powder mixed dielectric on conventional electrical discharge machining. *Int. J. Mach. Tools Manuf.* 43, 1465–1471.

[37] Zhao, W.S., Meng, Q.G., Wang, Z.L., (2002). The application of research on powder mixed EDM in rough machining. *J. Mater. Process. Technol.* 129(1-3), 30–33.

[38] Kozak, J., Rozenek, M., Dabrowski, L., (2003). Study of electrical discharge machining using powder-suspended working media. *Proc. Inst. Mech. Eng. Part B J. Engg. Manuf.* 217(11), 1597–1602.

[39] Klocke, F., Lung, D., Antonoglou, G., Thomaidis, D., (2004). The effects of powder suspended dielectrics on the thermal influenced zone by electrodischarge machining with small discharge energies. *Int. J. Mater. Process. Technol.* 149, 191–197.

[40] Wu, K.L., Yan, B.H., Huang, F.Y., Chen, S.C., (2005). Improvement of surface finish on SKD steel using electro-discharge machining with aluminium and surfactant added dielectric. *Int. J. Mach. Tools. Manuf.* 45, 1195–1201.

[41] Yan, B.H., Tsai, H.C., Huang, F.Y., (2005). The effect in EDM of a dielectric of a urea solution in water on modifying the surface of titanium, *Int. J. Mach. Tools. Manuf.* 45(2), 194–200.

[42] Kansal, H.K., Singh, S., Kumar, P., (2005). Parametric optimization of powder mixed electrical discharge machining by response surface methodology. *J. Mater. Process. Technol.* 169, 427–436.

[43] Yeo, S.H., Tan, P.C., Kurnia, W., (2007). Effects of powder additives suspended in dielectric on crater characteristics for micro electrical discharge machining. *J. Micromech. Microeng.* 17, N91–N98.

[44] Peças, P., Henriques, E., (2008). Effect of the powder concentration and dielectric flow in the surface morphology in electrical discharge machining with powder-mixed dielectric (PMD-EDM). *Int. J. Adv. Manuf. Technol.* 37, 1120–1132.

[45] Furutani, K., Sato, H., Suzuki, M., (2009). Influence of electrical conditions on performance of electrical discharge machining with powder suspended in working oil for titanium carbide deposition process. *Int. J. Adv. Manuf. Technol.* 40(11), 1093-1101.

[46] Kung, K.Y., Horng, J.T., Chiang, K.T., (2009). Material removal rate and electrode wear ratio study on the powder mixed electrical discharge machining of cobalt bonded tungsten carbide. *Int. J. Adv. Manuf. Technol.* 40(1-2), 95-104.

[47] Prihandana, G.S., Mahardika, M., Hamdi, M., Wong, Y.S., Mitsui, K., (2009). Effect of micro-powder suspension and ultrasonic vibration of dielectric fluid in micro-EDM processes-Taguchi approach. *Int. J. Mach. Tools. Manuf.* 49(12-13), 1035-1041.

[48] Kibria, G., Sarkar, B.R., Pradhan, B.B., Bhattacharyya, B., (2010). Comparative study of different dielectrics for micro-EDM performance during microhole machining of Ti-6Al-4V alloy. *Int. J. Adv. Manuf. Technol.* 48(5-8), 557-570.

[49] Kumar, S. Singh, R., (2010). Investigating surface properties of OHNS die steel after electrical discharge machining with manganese powder mixed in the dielectric. *Int. J. Adv. Manuf. Technol.* 50(5-8), 625-633.

[50] Sharma, S., Kumar, A., Beri, N., Kumar, D., (2010). Effect of aluminium powder addition in dielectric during electric discharge machining of hastelloy on machining performance using reverse polarity. *Int. J. Adv. Engg. Technol.* 1(3), 13-24.

[51] Kruth, J.P., Stevens, L., Froyen, .L, Lauwers, B., (1995). Study of the white layer of a sur-face machined by die-sinking electro-discharge machining. *CIRP Ann. Manuf. Technol.* 44, 169–72.

[52] Jilani S.T., (1984). Experimental investigations into the performance of water as dielectric in EDM. *Int. J. Mach. Tool. Des. Res.* 24, 31-43.

[53] Koenig, W., Joerres, L., (1987). A aqueous solutions of organic compounds as dielectric for EDM sinking. *CIRP Ann. Manuf. Technol.* 36, 105-109.

[54] Konig, W., Siebers, F.J., (1993). Influence of the working medium on the removal process in EDM sinking. *Am. Soc. Mech. Eng. Prod. Eng. Div.* 64, 649-58.

[55] Tsunekawa, Y., Okumiya, M., Mohri, N., Takahashi, I., (1994). Surface modification of aluminum by electrical discharge alloying. *Mater. Sci. Engg. A.* 174, 193-198.

[56] Chen, S.L., Yan, B.H., Huang, F.Y., (1999). Influence of kerosene and distilled water as dielectric on the electric discharge machining characteristics of Ti–6Al–4V. *J. Mater. Process. Technol.* 87, 107-111.

[57] Leao, F.N., Pashby, I.R., (2004). A review on the use of environmentally friendly dielectric fluids in electrical discharge machining. *J. Mater. Process. Technol.*149, 341-346.

[58] Ekmekci, B., Elkoca, O., Tekkaya, A.E., Erden, A., (2005). Residual stress state and hardness depth in electric discharge machining: de-ionized water as dielectric liquid. *Mach. Sci. Technol.* 9, 39-61.

[59] Sharma, A., Iwai, M., Suzuki, K., Uematsu, T., (2005). Potential of electrically conductive chemical vapor deposited diamond as an electrode for micro-electrical discharge machining in oil and water. *New. Diamond. Front. Carbon. Technol.* 15, 181-94.

[60] Ekmekci, B., Elkoca, O., Erden, A., (2005). A comparative study on the surface integrity of plastic mold steel due to electric discharge machining. *Metall. Mater. Trans. B Process. Metall. Mater. Process. Sci.* 36, 117-124.

[61] Kang, S.H., Kim, D.E., (2005). Effect of electrical discharge machining process on crack susceptibility of nickel based heat resistant alloy. *Mater. Sci. Technol.* 21, 817-823.

[62] Chung, D.K., Kim B.H., Chu, C.N., (2007). Micro electrical discharge milling using de-ionized water as a dielectric fluid. *J. Micromech. Microeng.* 17. 867-874.

[63] Lin, C.T., Chow, H.M., Yang, L.D., Chen, Y.F., (2007). Feasibility study of micro-slit EDM machining using pure water. *Int. J. Adv. Manuf. Technol.* 34, 104-110.

[64] Bhattacharyya, B., Gangopadhyay, S., Sarkar, B.R., (2007). Modelling and analysis of EDMed job surface integrity. *J. Mater. Process. Technol.* 189, 169-177.

[65] Pradhan, B.B., Masanta, M., Sarkar, B.R., Bhattacharyya, B., (2009). Investigation of electro-discharge micromachining of titanium super alloy. *Int. J. Adv. Manuf. Technol.* 41, 1094-1106.

[66] Pierson, H.O., (1996). Handbook of Refractory Carbides and Nitrides: Properties, Characteristics, Processing and Applications, *Noyes Publications*, Westwood, New Jersey, U.S.A.

[67] Luis, C.J. Puertas, I., (2007). Methodology for developing technological tables used in EDM processes of conductive ceramics. *J. Mater. Process. Technol.*189, 301-309.

[68] Kibria, G., Bhattacharyya, B., (2011). Investigation into micro-hole geometrical accuracy during micro-EDM of Ti-6Al-4V employing different dielectrics. *Int. J. Mach. Machinability Mater*. 10(4), 310-325.

In: Electrical Discharge Machining (EDM)
Editor: M. P. Jahan
ISBN: 978-1-63483-591-6

Chapter 9

APPLICATION OF MICRO-EDM IN PATTERNING CONDUCTING POLYMER

Mohammed Muntakim Anwar[1*], Kenichi Takahata[2] and John D Madden[3]

[1]Master of Applied Science, Electrical and Computer Engineering,
University of British Columbia, Vancouver, BC, Canada
[2]Associate Professor, Electrical and Computer Engineering,
University of British Columbia, Vancouver, BC, Canada
[3]Professor, Electrical and Computer Engineering,
University of British Columbia, Vancouver, BC, Canada

ABSTRACT

Conducting polymers have electrochemically controlled electrical conductivity. This feature has enabled them to be used in various sensors, actuators, energy storage devices and organic electronics. Polypyrrole is one of the most commonly used conducting polymers as actuators. High chemical and physical stability, low toxicity of monomer and simple synthesis process make it competitive to other conducting polymer. There has been report of application of Polypyrrole actuators as variable camber foils in underwater vehicle and as medical catheters. Various patterning techniques have been applied for patterning Polypyrrole. These include standard optical lithography, vapor phase chemical polymerization on pre patterned electrodes, self assembled monolayer, laser ablation etc. However, these patterning methods of this polymer have various issues including solubility, precise depth control of ablation, serial processing with limited throughput and cost. Micro Electro Discharge Machining (Micro-EDM) can be a suitable approach for micro patterning Polypyrrole. There has been report of microstructures with surface roughness of 70 nm on Polypyrrole thin film with precise depth control. The application of this patterning method has been extended toward micro patterning thin film of Polypyrrole deposited on commercial medical catheter. Thus Micro-EDM (µEDM) has the capability of creating smart catheters that uses patterned film as integrated actuators.

[*] Corresponding Author: Mohammed Muntakim Anwar, E-mail: muntakimanwar@yahoo.com

This feature of μEDM opens up new possibilities for Polypyrrole and other conducting polymer towards micro device application.

Keywords: Conducting polymer, polypyrrole, micro-EDM, patterning, catheter

INTRODUCTION

Electrical conductivity of conducting polymers can be electrochemically controlled (to be in the orders of 10^4-10^5 S/m) [1, 2]. This notable feature of conducting polymers is advantageous for use in electronics, energy storage, actuation, and packaging [3]. Conducting polymers have the potential to be used as actuators in medical applications such as surgical and diagnostic tools for minimally invasive surgery. This application is possible due to low actuation voltage, high strain, simple structure, and biocompatibility of conducting polymers [4, 5]. Polypyrrole is one of the most commonly used conducting polymer actuators [4] due to high chemical and physical stability, low toxicity of monomer, and simple synthesis process [6, 7].

Polypyrrole actuators have been studied for application as medical catheters [8–10]. Catheter itself is electromechanically inactive. For catheter activation, cylindrical catheters needs to be coated with Polypyrrole and patterned in such a way that it forms a trilayer structure, where two electrodes are electrically isolated and act as the electromechanically active layer [11]. This structure is then submerged in an electrolyte solution that contains mobile negative ions with large immobile positive ion. The catheter is activated when an alternating voltage was applied across the two polymer electrodes, formed on the opposing sides of the cylindrical catheter surface, by causing alternating insertion (expansion) and removal (contraction) of the mobile ions into/from the electrodes. Thus it develops a stress gradient across the polymer/catheter interface resulting in bending of the catheter structure.

Various micromachining techniques have been investigated for conducting polymer patterning. There are some conducting polymers such as polyaniline that can be dissolved in solvents [12] and can be patterned using Standard optical lithography techniques [13]. However, polypyrrole, polythiophene, and other conducting polymers are not soluble. For patterning of these insoluble conducting polymers, selective polymerization techniques in the form of additive and subtractive methods have been adopted. The additive approaches includes vapor-phase chemical polymerization [14], micropatterned self-assembled monolayer (SAM) in combination with micro-contact printing on gold and immersing in the shortchain alkanethiols solution [15] , electropolymerization along with the template assisted approach [16], Electron beam lithography in combination with electropolymerization [17, 18] etc. Besides these additive approaches, subtractive methods such as Dry etching [19], RIE with lithography [12, 13, 20], AFM Lithography were shown to be effective in patterning various conducting polymers [21, 22]. However, the lithographic techniques outlined above involve various steps, have slow etch rates (e.g., 0.3 μm/min [20]) and not suitable for the fabrication of non-planar devices, such as active medical catheters. These constraints can be mitigated using laser ablation. However, laser ablation has low removal rate and can create microcracks in the surface due to thermal damage along with debris deposition [23]. Ultrashort lasers can be an alternative option [24], but it is considered as a challenge in terms of precise depth control and operating costs.

Micro-EDM (μEDM) can be an alternative method for machining Polypyrrole. Although, μEDM has been employed in shaping metals (conductivity in the range of 10^5 – 10^7 S/m [25]), there has been report of shaping ceramics like SiC (conductivity 20 S/m) and B_4C (conductivity 100 S/m) with μEDM [26]. However, the transition zone between stable machining and unstable machining for a low electrically conductive material is very small. Stability regions are identified as discharge current, discharge duration and pulse interval [26]. As polypyrrole and other conducting polymers have higher conductivity than ceramics but lower conductivity than metals, it is worth studying the feasibility of μEDM for patterning these materials. Moreover, it will be able to address the issues like insolubility involved in other patterning techniques. However, there may be concern of thermal damage on the polymer surface associated with patterning using μEDM, as seen in case of polymer patterning using laser methods. However, 100% of the thermal energy generated in μEDM is not transferred into the cathode or anode. For short discharge duration, a larger fraction of the total energy is consumed to generate plasma and increase enthalpy of the plasma [27]. Moreover, the thermal energy transferred to Polypyrrole can lead to instant vaporization rather than melting. As more energy is required for vaporization, most of the thermal energy is used in that process and will carried away by debris [27]. Only 10-15% of the total energy is transferred to cathode and anode [27].These conditions suggest that polypyrrole might be processed by μEDM with minimal thermal damage. But, there is no major improvement in terms of material removal rate, as it is slow similar to other patterning techniques. However, by incorporating batch-mode μEDM processing as demonstrated [28], the issue of slow material removal rate can be resolved. Moreover, using appropriate fixtures, μEDM can be employed for machining non planar surface like polypyrrole coated catheter. Thus, μEDM patterning of Polypyrrole can be used to deal with difficulties associated with other micro-machining techniques and it would enable the application of this material to create many devices such as active catheters.

This chapter reports the feasibility of micro-EDM for high precision, high-quality micropatterning of polypyrrole film, and experimental findings of the process. Fine micromachining of polypyrrole film for a depth of 7.5 mm is demonstrated using 20-mm-diameter electrodes in the presence of EDM oil as dielectric medium. Scaling effects reveals that high structural integrity with smoother and cleaner surfaces can be achieved in polypyrrole using smaller electrodes for finer patterning. Resistive characteristics of the polypyrrole also reveal that the method of coupling polypyrrole with the discharge circuit affects the maching process. The application of the process for active catheter fabrication is also reported.

METHODS

Preparation of Polypyrrole Films

Polypyrrole samples used in this chapter were grown by an electrochemical deposition process using the procedure described by Yamaura et al. [29] Based on this procedure, a solution of 0.06 M pyrrole monomer, 0.05 M tetrabutylammonium hexafluorophosphate and 1% vol. distilled water in propylene carbonate that was bubbled with nitrogen was prepared.

The solution was then chilled to -40°C. Electrochemical deposition of Polypyrrole film on a glassy carbon crucible was achieved using a polished copper counter electrode. A current density of 0.125 mA cm^{-2} was used with eight hours of deposition time. Polypyrrole film with a thickness of 10-15 μm and a conductivity of ~4×10^{4} S m^{-1} was yielded in the process. After drying overnight, the film was peeled off from the crucible to prepare small samples.

Micropatterning Method of Polypyrrole films

A commercially available μEDM system (EM203, SmalTec International Inc., USA) was used for micropatterning of Polypyrrole film. Based on the experimental setup depicted in Figure 1 [30], the samples of polypyrrole film were used as anode and were fixed on the metallic base of the machine using magnets. Tungsten electrodes were used as cathode. Tugsten was shaped into different diameters using WEDG module available in the system. Tungsten was used to drill microholes and to create patterns in the sample by scanning along the lateral axes using the X-Y stage.

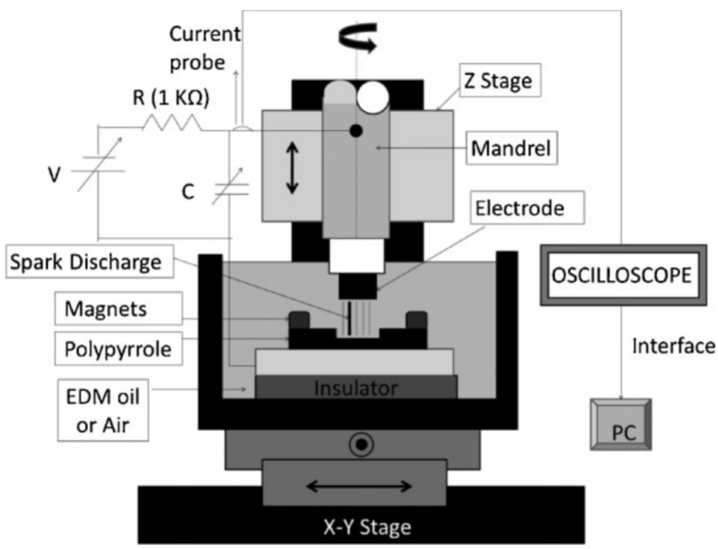

Figure 1. μEDM set-up used for characterization of Polypyrrole [30].

Air was used as dielectric media in both the experiments to verify the feasibility of dry ambient on different μEDM patterning To understand the scaling effects and as well as wet ambient patterning, commercial EDM oil (EDM 185, Commonwealth oil, Canada) was used as the dielectric media to create square patterns of different dimension, using shaped tungsten electrodes of various diameters. Polypyrrole was also connected to conductive surface in three different modes to understand discharge pattern based on connectivity to μEDM circuit. An inductive current probe (CT-1, Tektronix, USA) was inserted in the circuit to measure the discharge currents. The waveforms were captured using Oscilloscope (Infiniium 54845A, Agilent Technologies). The profiles of the square- patterned microstructures were measured using a stylus profilometer (Dektak 150, Veeco Instruments Inc., USA). The images of all the microstructures were captured using Scanning Electron Microscope (Hitachi S3000N).

Preparation of Polypyrrole coated Catheter

Polypyrrole was deposited on a commercial catheter product (Prowler® Select® LP ES Microcatheter, Codman & Shurtleff Inc., USA) of 0.75 mm outside diameter. This deposition was compiled in two steps. In first step, the catheter was dipped in two different solutions in sequence for several times. One of the solutions contained 1.2 g of ferric chloride and 0.1 M of hydrochloric acid, while the other solution comprised of 0.001 M pyrrole and 10 mL of deionized water. This resulted in a thin layer of polypyrrole deposited on catheter. This layer acted a as a seed layer. In second step, this seed layer was used for complete coating of catheter with Polypyrrole using the method described in "Preparation of Polypyrrole films" section.

Micropatterning Method of Polypyrrole-Coated Catheter for Catheter Actuation

A metallic V-groove holder was placed on the metallic base of the μEDM system. The catheter was placed on the V-groove. The surface of the polypyrrole coated catheter was firmly connected to the V-groove mechanically to ensure that the longitudinal surfaces of the polypyrrole films are in contact with V-groove surfaces. In this way, the polypyrrole films on catheter were electrically coupled with μEDM discharge circuit. To eliminate the possibility of vertical misalignment between the V-groove and lateral axis of the μEDM system, machining depth (60 μm) was set to be greater than the thickness of Polypyrrole layer ((~10 μm). Tungsten electrode was laterally scanned to the full length of the catheter to remove Polypyrrole from one side. Then, the catheter was rotated by 180 degree and similarly scanned by tungsten electrode to remove polypyrrole from the other side. The resulting structure comprised of two electrically isolated polypyrrole electrodes on non conductive, non planar catheter. The length of the catheters was 3 mm and 10 mm respectively. The 10 mm long catheter was actuated on an aqueous solution of $NaPF_6$, by using Ag/AgCl as reference electrode and by applying a step voltage of ±8 V across the two polymer electrodes.

RESULTS

μEDM of Polypyrrole Films in Air

To verify the feasibility of μEDM in patterning Polypyrrole film, experiments to create through holes were conducted in air using Voltage (V) of 20-40 V, Capacitance (C) of 10 pf and 300 μm tungsten electrode as cathode. Figure 2 shows the SEM images of the micro-holes [30]. These experiments revealed that discharge pulses are produced using smaller voltages compared to the voltages required to generate discharge for metal machining. This is considered as an important aspect to minimize thermal damage on polypyrrole using μEDM as the machining process. However, when larger voltages are used, the sidewalls of the circular holes become rough and debris adhere near the surrounding area of the micro-holes.

To further extend the study of μEDM process on polypyrrole surface, holes with bottom layers were machined using 150 μm diameter electrode and 5 μm machining depth. The parameters of V of 20-30 V and C of 10 pf were used. From SEM images as depicted in Figure 3 [31], it is evident that micro cracks are formed on the surface. EDX results are computed for particular location in Figure 3 as denoted by A, B and C. The results are shown on Table 1 [31]. EDX results suggest that there is evidence of tungsten on the surface which is melted and adhered to the surface.

To verify the effect of milling μEDM to minimize heat generation in a confined area, similar parameters were used with 100 μm diameter electrode to a scanning length of 200 μm and depth of 10 μm. Figure 4 [30] reveals the SEM images of the microstructures. There is still evidence of micro cracks even at smaller voltages. This suggests that using air as dielectric medium, even with employing movement of electrodes in lateral direction, there is a requirement of flushing the debris to improve structural integrity of the surface. This will remove the debris, which might have created short circuits between tungsten and polyprrole resulting in micro-cracks.

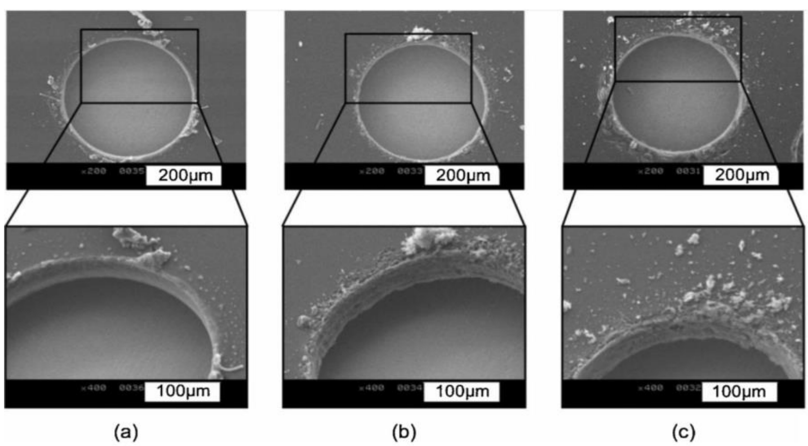

Figure 2. Scanning-electron-microscope (SEM) images of through-holes created using dry μEDM in air with discharge voltages of a) 20 V, b) 30 V, and c) 40 V [30].

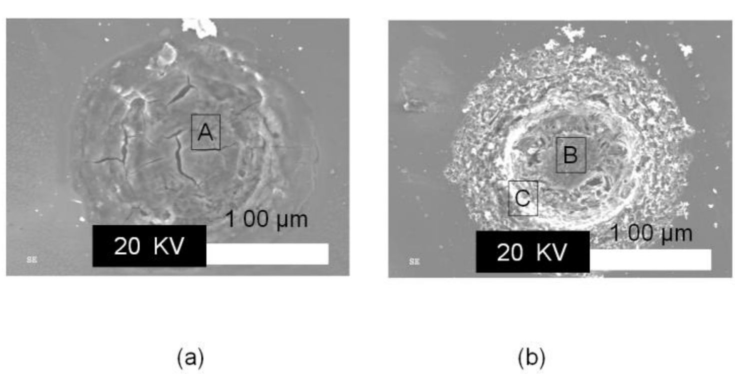

Figure 3. Scanning-electron-microscope (SEM) images of Circular Structures created using dry μEDM in air with discharge voltages of (a) 20 V, and (b) 30 V [31].

Table 1. EDX Analysis on Circular Structure create using dry μEDM in Air [31]

Elements	A	B	C
Carbon	35.86 wt%	31.23 wt%	35.08 wt%
Nitrogen	14.67 wt%	19.64 wt%	13.59 wt%
Oxygen	36.78 wt%	36.09 wt%	36.32 wt%
Fluorine	3.72 wt%	1.51 wt%	0.81 wt%
Phosphorus	8.71 wt%	10.68 wt%	12.34 wt%
Aluminum	0.27 wt%	0.33 wt%	0.20 wt%
Tungsten	0 wt%	0 wt%	1.67 wt%

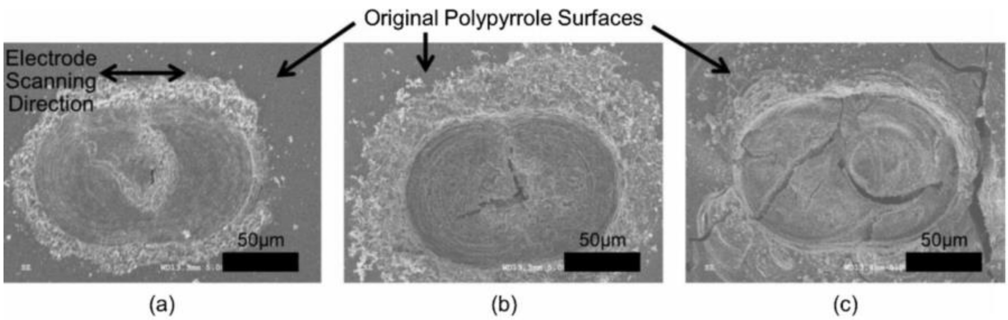

Figure 4. Scanning-electron-microscope (SEM) images of dry μEDM results from dead-ended slot pattern in implemented with discharge voltages of a) 20 V, b) 30 V, and c) 40 V on polypyrrole in air [30].

μEDM of Polypyrrole Films in EDM Oil

Further experiments were conducted using EDM oil as dielectric media. This method provides improved flushing effects, as EDM oil is continuously flushed in the machining area. Thus it carries away debris as well as heat. This minimizes the damage of the workpiece surface and improves structural integrity. Moreover, as a hydrophilic polymer, Polypyrrole does not absorb oil. To verify the effect of EDM oil flushing on polypyrrole surface, samples were immersed in the EDM oil and maching were conducted using different voltage and capacitance. However, there were variations in the parameters from dry EDM. Stable machining was observed while using V of 60 V without an external capacitor. Higher energy resulted in rougher surface, while lower energy resulted in unstable discharge and incomplete machining.

Variation in Material Removal Rate (MRR) with Discharge Energy and Dielectric Media

In order to verify the effect of different energy levels and different dielectric media MRR was computed for micro-holes using air as dielectric media with parameters V of 20, 30, 40 V and C of 10 pf. Similarly MRR was also computed for micro-holes using EDM oil as dielectric media with stable parameter of V of 60 V and C of C_p (Stray capacitance).The discharge energy in µEDM is defined as $(C + C_p)V^2/2$ [32], where C is the capacitance of the circuit, Cp is the parasitic or stray capacitance (C_p in this system is estimated to be ~10 pF) and V is the applied voltage. As shown in Figure 5, the MRR increased with increased energy levels while using air as dielectric medium. However, in case of using EDM oil as dielectric media, discharge energy needed to be increased for stable machining and it resulted in higher MRR. So if the surface damage of polypyrrole can be reduced using EDM oil as dielectric media, it can be applied to pattern polypyrrole for higher MRR.

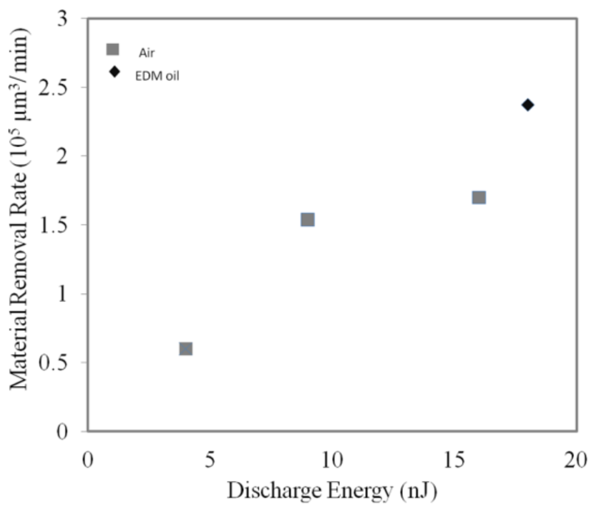

Figure 5. Material removal rates measured in through-hole µEDM of polypyrrole in air and EDM oil with different discharge energy.

Scaling Effects in Polypyrrole Films

Once the stable machining parameters were selected, it was imperative to verify the effect of varied electrode size and patterns on the machining surface. It will provide an insight on the possibility of achieving fine patterns for smaller feature size using µEDM. So for assessing the scaling effects, dead-ended square patterns measuring 300, 150, and 60 µm were machined by scanning 100, 50 and 20 µm electrodes, respectively, in X and Y directions. The electrode feeding depth was 7.5 µm. There was evidence of uniform discharge without any short circuit. There was no evidence of tungsten electrodes on any surface, suggesting negligible electrode wear in the process. From the SEM images of the square patterns as depicted in Figure 6 [30], it can be observed that fine patterns with sharp edges can be obtained in polypyrrole using µEDM process. However, there were evidences of particles adhering to the bottom surfaces while using 100 and 50 µm diameter electrodes. Though the discharge gap measured in all three cases were similar (4.5-6 µm), the bottom surface using 20 µm diameter electrode was much cleaner in comparison. This can be attributed to the fact the when the diameter is larger, discharge induced fluidic forces are less effective to disperse melted particles from the discharge gap [30]. As a result, this melted particle solidifies and adheres to the surface.

The adhered particles may weaken the dielectric breakdown strength and enhance discharge, resulting deeper patterns from the programmed depth. Consequently the surface roughness will also increase. This observation is depicted in Figure 7. This is encouraging in terms of creating fine and smooth micro-patterns with μEDM.

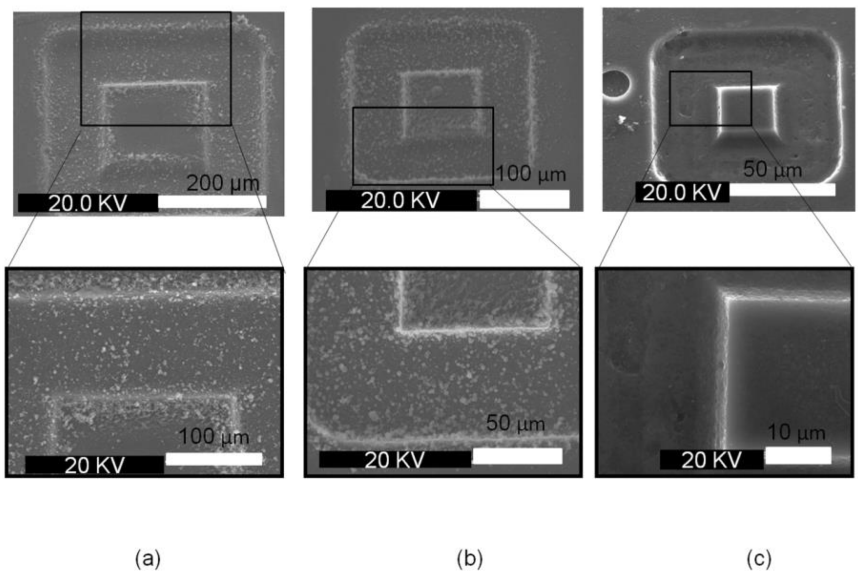

Figure 6. Scanning-electron-microscope (SEM) images of differently sized square patterns created in polypyrrole samples through wet μEDM in the oil using the electrodes with diameters of a) 100 μm, b) 50μm, and c) 20μm [30].

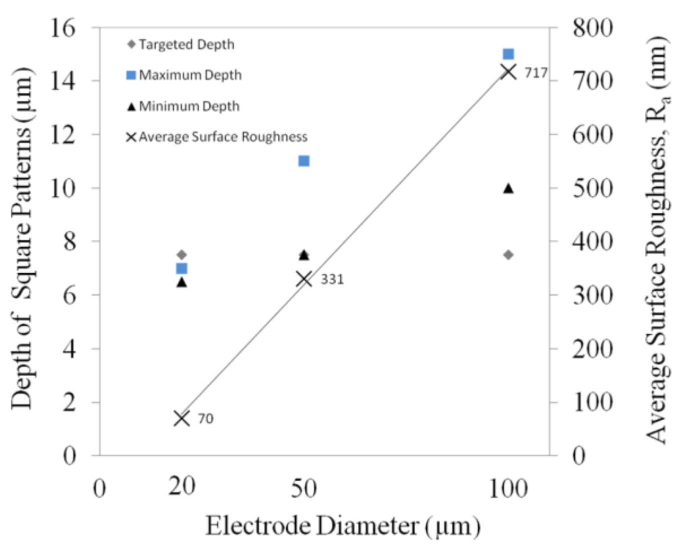

Figure 7. Machined Depth and Average Surface Roughness of square patterns created in polypyrrole samples through wet μEDM in the oil using the electrodes with different diameters.

Resistive Characteristics of Polypyrrole Films

Once it is confirmed that fine micro patterns is achievable using 20 µm diameter electrode , it is imperative to understand whether the removal process of polypyrrole is affected by the coupling of the films to the discharge circuit. This coupling will determine the path of the electron flow during discharge, affecting discharge current. It is important to understand the resistive characteristics of Polypyrrole film before patterning polypyrrole coated cather with µEDM, as the layer of catheter beneath the Polypyrrole film is non conductive. For this reason, polypyrrole was coupled with discharge circuit in two different modes as shown in Figure 8.

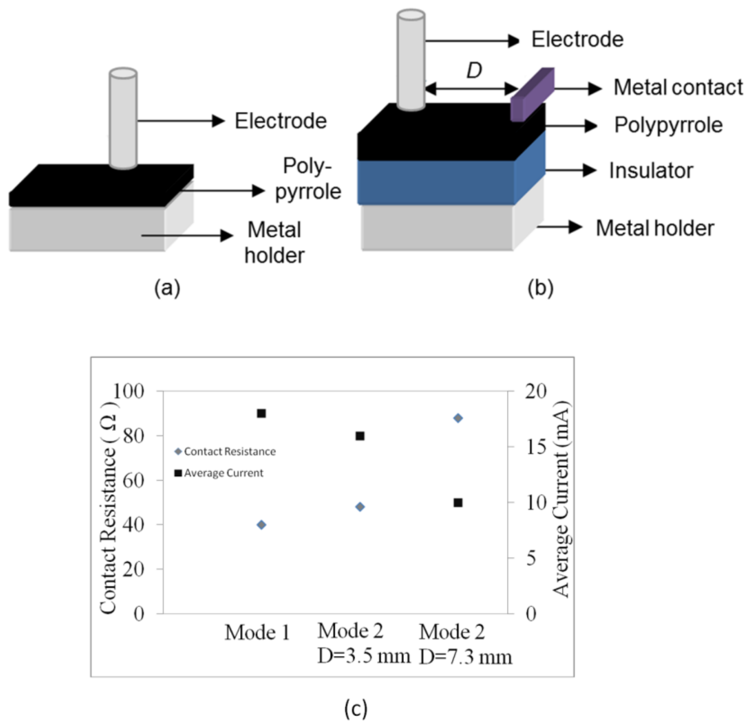

Figure 8. Electrical contacts made with polypyrrole samples: (a, Mode-1) The sample is directly fixed on the metallic base [30], and (b, Mode-2) an insulation layer is present between the sample and the base, and a metal contact is placed on top of the sample away from the electrode location at a distance of D [30], c) Measured contact resistance and average currents for Mode-1 and Mode-2 with D of 3.5 and 7.3 mm.

In Mode-1, polypyrrole was placed on the conductive surface (metal base) directly in the same way as all previous experiments. This will result electrons flowing through the thickness of the material which is around 20-30 µm. So the currents will flow vertically. In the other Mode (Mode 2), a non conductive substrate was placed between the Polypyrrole films and conductive surface. The discharge circuit was completed by using a conductive connector at two different distances (D=3.5 µm and 7.3 µm) from the discharge point. Machining conditions were kept same (60 V and Cp). In these Modes, the current will flow through the connectors to the discharge point in a lateral direction. This mode simulates the condition of polypyrrole coated catheter, where the current in flows radially from the conductive surface to the discharge point. The distance was varied to understand the effect of proximity of the conductor on the discharge current.

Figure 8(c) shows the resistance and currents measured in various Modes. The resistance between electrode and base were measured to be 40 in Mode1, 48 and 88 ohm in Mode 2, for D=3.5 mm and 7.3 mm, respectively. These results are consistent with the measured current of 18 mA, 16 mA and 10 mA in Mode 1, Mode 2 for D=3.5 mm and Mode 2 for D=7.3 mm, respectively. This suggests that if the polypyrrole is connected with the conductive surface vertically, the resistance will be lower and current will flow vertically. However, if there is a presence of non conductive surface between the base and polypyrrole films, the resistance and current will vary according to the location of the conductive connecter. Since the distance between the conductive connector and discharge location in Mode 2 is smaller for D= 3.5 mm, in comparison to D= 7.3 mm, the resistance was lower and consequently the current was higher. From these observations, it can be inferred that the distance between the conductive surface and discharge point on polypyrrole coated catheter needs to be closer for minimizing resistance and generating effective discharge.

μEDM of Polypyrrole Coated Catheter and Catheter Actuation

Based on the resistive characteristics of Polypyrrole, polyrrole coated catheter was placed on a metallic V-groove holder in such way that the longitudinal surface of the Polypyrrole layer is in contact with the surface of the V-groove. This condition is similar to Mode 2, as discussed in the section "Resistive Characteristics of Polypyrrole." During the μEDM process, the current will flow radially from the V-groove surface to the discharge point. In this case, the resistance will be higher and higher energy will be required for machining. To experimentally verify the feasibility of polypyrrole patterning on catheter surface, a polypyrrole coated catheter of 3 mm length, where the thickness of Polypyrrole layer is around 10 μm, was placed on the metallic V-groove.

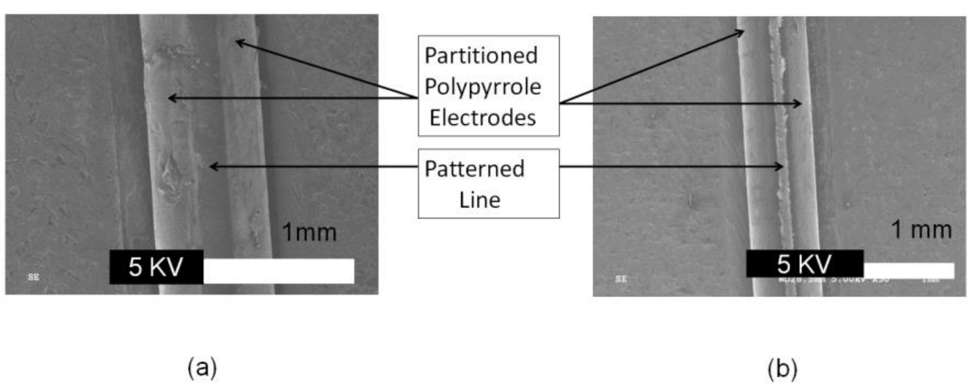

Figure 9. Scanning-electron-microscope (SEM) images of the polypyrrole-coated catheter patterned with Micro-EDM, showing one of the two slots created (the other is located on the backside of catheter) on: (a) 3 mm catheter [30], (b) 10 mm catheter [31].

The contact resistance was measured to be much higher (20.75 Kohm) compared to Mode 2 (48 Ohm for D=3.5mm and 88 ohm for D=7.3 mm). So higher discharge energy was required (120V and 213 pf) for completely removing the polypyrrole along two lines oppositely located along the cylindrical catheter. This created two electrodes which are electrically isolated as confirmed by the 5Mohm resistance measured between them. Once the parameters for effective patterning of polypyrrole coated catheter were identified, it is essential to observe the actuation of such catheters. However, for catheter actuation test, 3 mm length is not sufficient. So, a 10 mm length of polypyrrole coated catheter was patterned using the same parameters described above. Figure 9 shows the sample results for patterning length of 3 mm [30] and 10 mm [31] respectively.

During the actuation test in NaPF6 solutions, the radius of curvature of deflection changed from 10.25 mm to 7 mm [30]. This confirms that µEDM is an effective patterning method for cylindrical surfaces and it is capable to create active catheters.

CONCLUSION

This chapter has demonstrated that µEDM is a stable and effective patterning method for polypyrrole. Dielectric medium has an important effect on surface characteristics of polypyrrole films. Though dry ambient (air) can be used for creating through holes, it leaves debris attached on the surface of the holes with bottom layers. By using EDM oil as dielectric medium, the debris can be flushed effectively that improves structural integrity. In this ambient, stable machining was achieved using 60 V without an external capacitor. Moreover, material removal rate was also higher in this ambient. Tool diameters were varied to create micro-structures of different dimension to study the scaling effects of µEDM. Micropatterning with a smaller diameter (20 µm) electrode illustrated better depth control (6.5 µm -7 µm), close to the targeted depth (7.5 µm) with lower surface roughness (70 nm). The discharge current in this process can be effectively controlled by shortening the the distance between electrode location on polypyrrole films and terminal of the discharge circuit for suitable removal. The application of µEDM has been further extended to create polypyrrole actuator driven catheter. Actuation of a 10 mm catheter has also been demonstrated. The results suggest that µEDM, as a cost effective patterning technique for polpyrrole, will boaden the use of polypyrrole and other conducting polymers in device application. However, further studies are required to improve precision and throughput before µEDM can be adapted as the most effective micromaching method for polypyrrole and other conducting polymers.

REFERENCES

[1] Madden, J.D.W., Peter, G.A., Hunter, I.W., (2002). Conducting polymer actuators as engineering materials. *Proc. SPIE – Smart Structures and Materials: Electroactive Polymer Actuators and Devices*. 176-190.

[2] Angelopoulos, M., (2001). Conducting polymers in microelectronics. *IBM J. Res. Dev.* 45, 57-75.

[3] Skotheim, T., (1986). Handbook of Conducting Polymers. Vol 1 and 2. *Marcel Dekker Inc., New York.*

[4] Madden, J.D.W., Vandesteeg, N.A., Anquetil, P.A., Madden, P.G.A., Takshi, A., Pytel, R.Z., Lafontaine, S.R., Wieringa, P.A., Hunter, I.W., (2004). *Artificial muscle technology: Physical principles and naval prospects IEEE J. Oceanic Eng*. 29, 706-728.

[5] Mazzoldi, A., De Rossi, D., (2000). Conductive polymer based structures for a steerable catheter. *Proc. SPIE – Int. Soc. Opt. Eng*. 3987, 273-280.

[6] Yfantis, D.K., Yfantis, A.D., Lamprakopoulos, S., Depountis, S., Yfantis, C.D., Schmeisser, D., (2006). New environmentally friendly methods – composite coatings based on polypyrroles. *WSEAS Trans. Environ. Dev*. 2, 167-172.

[7] Ramanaviciene, A., Ramanavicius, A., (2002). Application of polypyrrole for the creation of immunosensors. *Crit. Rev. Anal. Chem*. 32, 245-252.

[8] Shoa, T., Munce, N.R., Yang, V.X.D., Madden, J.D., (2009). Conducting polymer actuator driven catheter: Overview and application. *Proc. SPIE Electroactive Polymer Actuators and Devices (EAPAD)*. 7287, 72871J1-72871J9.

[9] Della Santa, A., Mazzoldi, A., De Rossi, D., (1996). Steerable microcatheters actuated by embedded conducting polymer structures. *J. Intelligent Mater. Syst. Struct*. 7, 292-300.

[10] Della Santa, A., De Rossi, D., (1996). Intravascular microcatheters steered by conducting polymer actuators. *Proc. IEEE Eng. Med. Biol*. 5, 2203-2204.

[11] Shoa, T., Madden, J.D., Fekri, N., Munce, N.R., Yang, V.X.D., (2008). Conducting polymer based active catheter for minimally invasive interventions inside arteries. *EMBS 30thAnnual International Conference of the IEEE*. 2063-2066.

[12] Smela, E., (1999). Microfabrication of PPy microactuators and other conjugated polymer devices. *J. Micromech. Microeng*. 9, 1-18.

[13] Jager, E.W.H., Smela, E., Inganas, O., (2000). Microfabricating conjugated polymer actuators. *Science*. 290, 1540-1545.

[14] Nannini, A., Serra, G.J., (1990). Growth of polypyrrole in a pattern: A technological approach to conducting polymers. *J. Mol. Electron*. 6, 81-88.

[15] Collard, D.M., Sayre, C.N., (1997). Micron-scale patterning of conjugated polymers on microcontact printed patterns of self-assembled monolayers. *Synth. Met*. 84, 329-332.

[16] L. Jiang, X. Wang, L. Chi, (2011). Nanoscaled surface patterning of conducting polymers. *Small*. 7, 1309-1321.

[17] Yun, M.H., Myung, N.V., Vasquez, R.P., Lee, C.S., Menke, E., Penner, R.M., (2004). Electrochemically grown wires for individually addressable sensor arrays. *Nano Lett*. 4, 419-422.

[18] Ramanathan, K., Bangar, M.A., Yun, M.H., Chen, W.F., Mulchandani, A., Myung, N.V., (2004). Individually addressable conducting polymer nanowires array. *Nano Lett*. 4, 1237-1239.

[19] Khaldia, A., Plessea, C., Soyerb, C., Chevrota, C., Teyssie, D., Vidala, F., Cattanb, E., (2012). Patterning process and actuation in open air of micro-beam actuator based on conducting IPNs. *Proc. SPIE Electroactive Polymer Actuators and Devices (EAPAD)*. 8340, 83400J.

[20] Smela, E., Kallenbach, M., Holdenried, J., (1999). Electrochemically driven polypyrrole bilayers for moving and positioning bulk micromachined silicon plates. *J. Microelectromech. Syst*. 8, 373-383.

[21] Liu, G.Y., Xu, S., Qian, Y.L., (2000). Nanofabrication of self-assembled monolayers using scanning probe lithography. *Acc. Chem. Res*. 33, 457-466.

[22] Berger, R., Cheng, Y., Forch, R., Gotsmann, B., Gutmann, J.S., Pakula, T., Rietzler, U., Schartl, W., Schmidt, M., Strack, A., Windeln, J., Butt, H.J., (2007). Nanowear on polymer films of different architecture. *Langmuir*. 23, 3150-3156.

[23] Lee, K.K.C., Munce, N.R., Shoa, T., Charron, L.G., Wright, G.A., Madden, J.D., Yang, V.X.D., (2009). Fabrication and characterization of laser-micromachined polypyrrole-based artificial muscle actuated catheters. *Sens. Actuators A*.153, 230-236.

[24] Rizvi, N.H., (2003). Femtosecond laser micromachining: Current status and applications. *RIKEN Rev*. 50, 107-112.

[25] Serway, R.A., (1998). Principles of physics. 2nd ed. *Fort Worth,Texas:London:Saunders College Pub.*

[26] Lauwers, B., Kruth, J.P., Brans, K., (2007). Development of technology and strategies for the machining of ceramic components by sinking and milling EDM. *CIRP Annals – Manufacturing Technolog.* 56, 225-228.

[27] Zahiruddin, M., Kunieda, M., (2010). Energy distribution ratio into micro EDM electrodes. *Journal of Advanced Mechanical Design, Systems, and Manufacturing.* 4, 1095-1106.

[28] Takahata, K., Gianchandani, Y.B., (2002). Batch mode micro-EDM. *Journal of Microelectromechanical Systems*. 11, 102-110.

[29] Yamaura, M., Hagiwara, T., Iwata, K., (1998). Enhancement of electrical conductivity of polypyrrole film by stretching: Counter ion effect. *Synthetic Metals.* 26, 209-224.

[30] Anwar, M.M., Saleh, T., Madden, J.D.W., Takahata, K., (2014). Micropatterning Polypyrrole Conducting Polymer by Pulsed Electrical Discharge. *Macromolecular Materials and Engineering*. 299, 198 – 207.

[31] Anwar, M.M., (2012). A Study on micro-patterning of Polypyrrole using micro-electro-discharge-machining. *M.A.Sc. Thesis, University of British Columbia, Vancouver.*

[32] Masaki, T., Kawata, K., Masuzawa, T., (1990). Micro electro-discharge machining and its applications. *Micro Electro Mechanical Systems Proceedings, IEEE.* 21-26.

In: Electrical Discharge Machining (EDM)
Editor: M. P. Jahan
ISBN: 978-1-63483-591-6

Chapter 10

FABRICATION OF MICRO-GRINDING TOOL BY BLOCK-EDM

Asma Perveen[1*], M. Rahman[2] and Y. S. Wong[2]
[1]Mechanical Engineering Department,
Bursa Orhangazi University, Bursa, Turkey
[2]Mechanical Engineering Department,
National University of Singapore, Singapore

ABSTRACT

Fabrication of microelectrodes with different shapes has become so important due to high demand of industrial products not only with diversified shapes but also of reduced dimensions. In this chapter therefore, the development of an electro-discharge machining (EDM) block electrode method for fabrication of microelectrodes with not only symmetrical sections, e.g., tapered, circularly stepped, rectangular, triangular but also non symmetrical sections have been reported. As a promising branch of EDM technology, several newly developed machining strategies using block electrode have been applied for the fabrication of microelectrodes with different shapes. As the size of the electrode is of micron scale, multi pass machining strategy has been adopted in Block EDM method to reduce the volumetric material removal and thus to reduce possible electrode breakage. This process is especially of significant when the electrode size is of micrometer scale which is proved to be significant. On top of that, this strategy has been found to be feasible for fabricating microelectrodes of various symmetrical, non-symmetrical sections down to a few tens of micrometers. Effect of machining parameters has also been discussed in this chapter. Although, the machining capabilities of these fabricated micro-tools have been extended on both conductive and non-conductive materials utilizing EDM and grinding method, this chapter primarily focuses on its micro-grinding aspect. Therefore, this chapter also contributes to the micro-grinding process of glass and brittle materials using fabricated micro-electorodes. Finally, this chapter will also throw some light on microgrinding and wear mechanism of Polycrystalline Diamond(PCD) microtools.

* Bursa orhangazi University,Mimar Sinan Mh, Mimar Sinan Bulvari,177 Yidirim, Bursa 16310, Turkey
Email:perveen.asma@gmail.com

Keywords: Block EDM, hard and brittle material, micro-electrodes

INTRODUCTION

The demand for fabricated microfeatures on glass and other brittle materials has been rapidly rising for diversified functionalities on optical devices, micro molds and micro fluidics devices due to their attractive features like high strength, wear resistance and good chemical stability [1, 2].

For certain applications, like DNA micro-arrays, glass components with microfeatures are typically produced by photolithography and etching process which is very time consuming and may also involve hazardous chemicals. Hence, it could be an alternative interesting idea to produce these glass micro-features using different mechanical processes [2]. Literature review shows that many researchers have studied glass machining processes which involve single point diamond turning tool [3, 4], conventional grinding wheel [5-11] and milling cutter [12-14]. However, the hardness and brittleness of glass make these mechanically micro machining processes problematic due to the collateral damage resulting from material removal by brittle fracture, cutting force-induced tool deflection or breakage and tool wear [15]. On the other hand, micro tools made of PCD encounter this challenge for micro machining of hard and brittle materials quite successfully. Generally, PCD tool containing micrometer-sized diamond grains is manufactured by sintering process under high temperature and pressure with metallic cobalt. The cobalt fills the interstices between the diamond particles [16, 17]. Besides this, sintered tungsten carbide which is next to diamond in hardness scale is often used to produce these tools components in tool manufacturing industries. These two materials are very popular due to their high hardness and low wear characteristics. Moreover, PCD has added advantage of possessing small diamond grains where each grain acts as one cutting edge. As a result, abrasive material like glass and other brittle materials can be micro-ground by these diamond cutting edges.

Due to heavy industrial demand for the three dimensional complex micro-shapes, fabrication of different shapes tools has got importance rather than commercially available ones. It has two purposes to serve.: firstly,on machine fabrication which minimizes clamping error, secondly freedom of desired shape and size of tool. Several methods are available to meet these requirements. Among these, focused ion beam, mechanical diamond grinding and diamond turning have been most extensively used [18]. However, the fabrication of such tools by diamond grinding gives rise to difficulties, associated with high cost of diamond wheel due to the large consumption of diamond. Moreover, diamond grinding is characterized by significant mechanical and thermal impact on the workpiece, resulting in the formation of split and flaw [19]. As a result, conventional tool fabrication processes including grinding and turning which apply large force on work piece cannot be applied due to low strength of small sized tool [20]. In addition to this, focused ion beam is problematic as it has Gaussian distribution that causes material removal at the axis of beam rather than around the periphery [21]. On the other hand, whereas the efficiency of traditional cutting processes is limited by the mechanical properties of the processed material and the complexity of workpiece's geometry, electro discharge machining is not subjected to such constrains. Now a day, EDM has already been extensively and successfully applied for difficult-to-cut materials [19].

Micro-EDM is suitable because of its low discharge energy which generates smooth surfaces while its negligible forces prevent fragile workpiece from breakage. On the other hand, micro EDM does face two significant challenges: high electrode wear and low material removal. Electrode wear, which results from each discharge removes some material from the electrode, and also degrades geometric accuracy of machined area. However, this effect can be minimized by making micro pockets with uniform wear method as shown by Yu et al. and Pham et al., but this method further compromises the Material removal rate (MRR) [22, 23]. Concerted research efforts have been directed towards the development of fabrication technologies for micro-electrodes using micro-EDM as shown in Figure 1 [24]. Among these technologies, Wire electro-discharge grinding (WEDG) method, mesh method, EDM block method, LIGA and other micromechanical machining methods are commonly practiced. Among these commonly practiced methods, block EDM method has been widely used due to its lower investment cost and easy set up. More importantly, it makes possible on machine-fabrication of electrode which reduces electrode installation cost and dimensional error [25]. In addition to this, with micro EDM technology, there is no direct contact between electrode and work piece, thus eliminating mechanical stress, chatter and vibration problems [26]. Moreover, problems of tool bending, breaking, and strength decrement due to subsurface damages can be solved effectively. As the run out error can be avoided due to on machine fabrication and continue machining using the same micro-electrode, this combination of processes has become very popular and known as hybrid machining. Recently EDM fabrication of micro tool has been a new topic of research in the area of micro-machining because of all these above advantages.

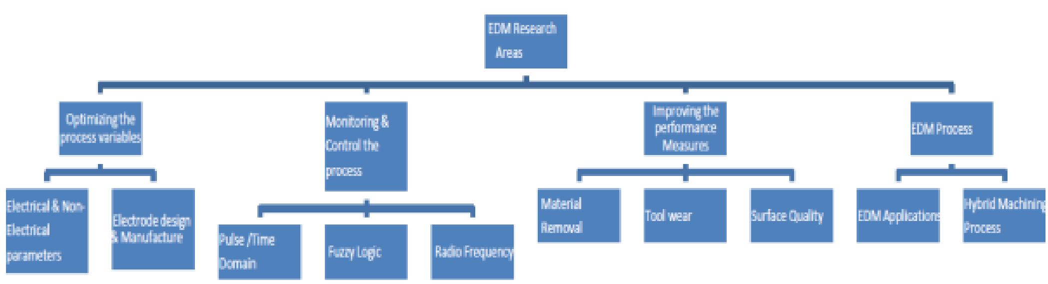

Figure 1. Classification of Major EDM research areas [24].

Block EDM method for fabricating electrodes of various shapes and micro-grinding aspects of those on machine fabricated electrodes have been described in this chapter. This chapter will also encompass the state of art and several relavent techniques of Block EDM process. Apart from these, this chapter will throw some light on the materials, roughness, grinding mechanism and wear of the fabricated electrodes.

POLYCRYSTALLINE DIAMOND (PCD)

PCD is increasingly used in high volume machining due to the superior tool life. PCD is primarily a composite material synthesized from extremely tough intergrown mass of randomly oriented diamond crystals bonded to a tungsten carbide substrate. It is manufactured by sintering together micron sized diamond grains at high pressure and temperature in the presence of a solvent/crystal metal, usually cobalt or cobalt/nickel alloy. During the sintering process, the voids between PCD grains are filled with cobalt binder. As a result, PCD facilitates the fabrication using EDM technology and also works as grinding tool. Unlike cemented tungsten carbide, however individual diamond grain actually is bonded to one another. The result is a tough hard product that will retain its shape and strength if some of the metal matrix is removed. In the case of tungsten carbide, when the binder phase is removed, the tungsten carbide grain breaks away from parent materials and from each other. For PCD, if the matrix is eroded, grains are still held together by the bonding between them which makes it superior over Tungsten carbide for microgrinding technology [27].

Diamond is often used as a cutting tool to machine hard materials such as cemented carbide, glass, silicon and ceramics. Several fabrication processes have been developed for fabrication of PCD tool by researchers which will be discussed later in this chapter. For the diamond coating process, although chemical vapor deposition (CVD) is able to grow a high-quality diamond film on the tool surface, the fabrication cost becomes higher. However, electrodeposited composite coatings have also been extensively employed in various engineering applications due to improved wear resistance, corrosion resistance, dispersion hardening, and self-lubrication. Such electrodeposited composite coatings consist of a metal or alloy matrix containing a dispersion of second phase particles such as diamond, SiC and alumina particles [28, 29].

STATE OF ART OF BLOCK EDM

Significant research efforts have been directed towards the development of fabrication technologies for microelectrodes during past decades. Among these technologies are the wire electro-discharge grinding (WEDG) method [30], the mesh electrode method, the EDM block electrode method, LIGA [31] and the micromechanical machining methods [32, 33]. The EDM block electrode method has already been successfully applied for the fabrication of microelectrodes by Ravi et al.2002. In this method, a precise rectangular conductive block is used as a cutting electrode and a cylindrical rod is used as the workpiece in the EDM process as shown in Figure 2. The microelectrode that needs to be machined is fed against the conductive block.

Generally, due to high wear resistance property, tungsten block is a most convenient choice as cutting block for the tool fabrication. During fabrication using Block-EDM, the cylindrical rod is set in positive polarity and the tungsten block is used as negative polarity as shown by Jahan et al. (2010) [34].

When a voltage is applied between the rod and block, an intermittent spark occurs between the inter-electrodes gap. The spark rises the surface temperature of both the block and the rod to a point where the temperature exceeds the melting point of the both materials. Consequently, a small amount of material is removed from both the electrodes and flushed away from the machining zone using side flushing. Rod material used for micro-grinding purposes is generally polycrystalline diamond (PCD) due to its abrasive characteristics. Since diamond is not an electrically conductive material; the electrical discharges take place between the conductive electrode material and conductive cobalt which works as binder for

PCD rod.Consequently, the conductive cobalt material is removed during the EDM process to expose new or fresh surface of PCD grains for the next grinding process. This removal of cobalt material will leave the space between PCD grains which can subsequently work as a chip storage place during grinding process. Sometimes the PCD grains will also fall off from the tool surface due to the excessive removal of the entire cobalt bonds around them. The fall of diamond grains will accelerate the material removal process during EDM process as next spark will be exposed to the conductive cobalt material again, but it will also enhance the wear progression during grinding process.

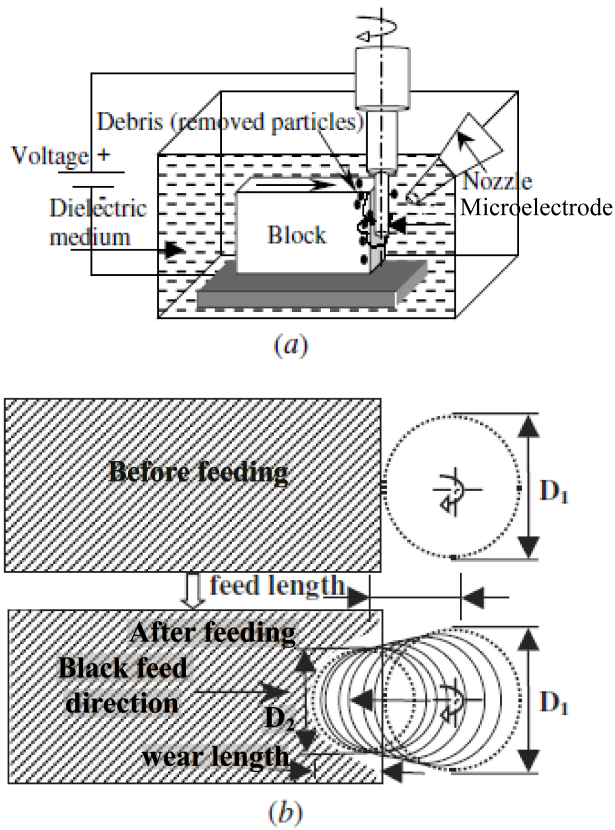

Figure 2. (a) Principle of Block EDM method (b) Schematic representation of feed [25].

In this process, surface roughness can be controlled by varying capacitance and voltage [35]. Compared with the other methods, such as the WEDG and mesh electrode methods, the EDM block electrode method involves lower investment cost and is easier to set up. More importantly, it can also produce electrodes on the machine and this greatly reduces the electrode installation error and cost. However, there are few problems associated with this method which require further research to improve its performance. One critical problem is that machining the electrode to the desired diameter becomes difficult because of the occurrence of wear on the rod as well as on the block. Also, the non-uniformity in the spark gap along the discharge area due to the reduction in the size of the rod diameter causes difficulties to control the diameter to the desired level precisely. Hence, the correlation between the primary input machining parameters and the rod diameter must be established to produce microelectrodes to the desired size [25].

DIFFERENT FABRICATION TECHNIQUES

The necessity of on-machine fabrication of microelectrodes is realized due to the requirement of high machining accuracy. Unlike the conventional EDM machining, it is critical to carry out micromachining in EDM systems with a few machining passes, as high volume of material removal in a single step possibly results in electrode breakage, especially when the required size of the electrode is of micrometer scale. On top of that, the movement of the electrode for micromachining preferably sets in the Z-direction (with the electrode moving towards the block from top to bottom) rather than machining in the X direction in order to reduce the machining contact area. This phenomenon has already been proved to reduce accumulation of large amount of debris in the machining area, and thus helps reducing the chance of early breakage of the electrode. For fabrication of both symmetrical and non-symmetrical section micro-electrodes, researchers have come up with several innovative ideas.

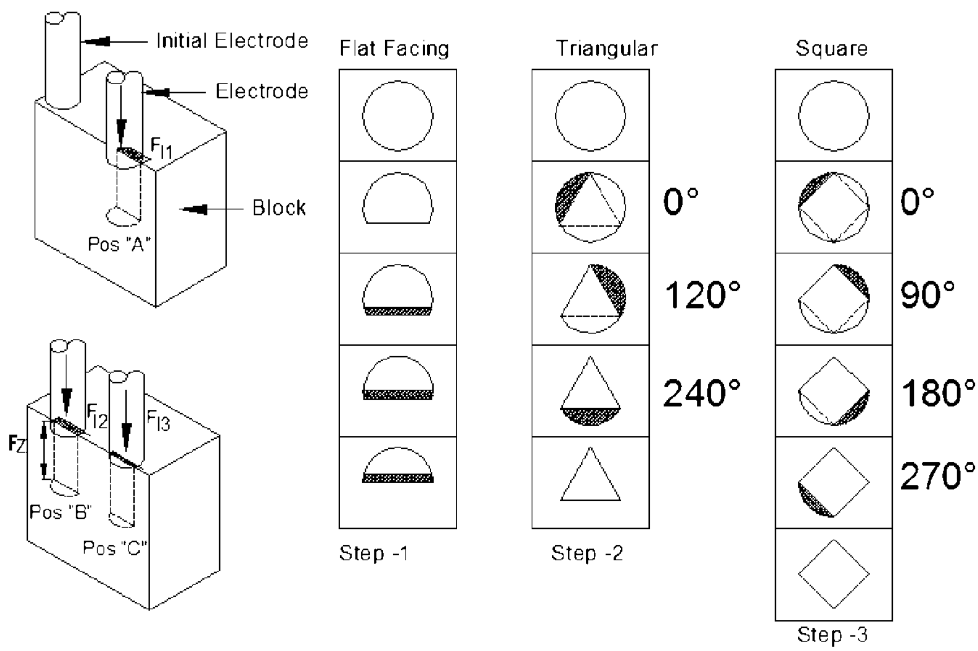

Figure 3. Fabrication methods for Symmetrical Microelectrodes [36].

The first step in micro machining by mechanical material removal process is the fabrication of micro tools. After the micro electrodes are fabricated, those can be used for subsequent micro-EDM, micro cutting or micro-grinding of a workpiece. Figure 3 shows the methodologies of fabrication using block EDM to obtain microelectrodes with different symmetric sections as presented by Ravi et al., 2002. As shown in Figure 3, during the first machining pass, the rod electrode is moved down to a feed length (Fl1) across the locus of the circle up to the desired feed depth in the Z-direction until the position of A. After the completion of the first pass, the electrode is moved further to the respective positions B and C, and the feed length (Fl2, Fl3) of the electrode is set. Then the electrode is fed again downwards direction to the same feed depth (Fz) in the second and third machining passes and so on. Thus, the frontal flat face of the microelectrode is finally produced with desired dimension. Similar procedures of flat facing of the microelectrode is adopted in order to fabricate triangular and rectangular microelectrodes as shown in step 1 with the use of an indexing attachment. The rod electrode is given certain angular rotation after completing one of its faces using the method described in step 1. For example, fabrication of a triangular electrode will require three faces to be machined. The rod electrode is rotated to 0°, 120° and 240° to repeat the same machining procedure, as illustrated in Figure 3. Similarly, the four faces of the rectangular electrode are fabricated using angular rotation of 0°, 90°, 180° and 270°. The tapered and cylindrically stepped microelectrodes are also possible to fabricate by feeding against a tapered and a rectangular block while applying the tool rotation for machining. This method demonstrates the possibility of achieving up to the tip radius of 30 μm. Further attempts to reduce the tip radius less than that result in breakage due to its feeble nature. The machined microelectrodes of tapered, rectangular, triangular and circularly stepped sections are shown in Figures 4(a)–(d), respectively. The accuracy of the rectangular section microelectrode is found to be ±10 μm of 50 μm length. The accuracy of the triangular section microelectrodes is found to be ±5 μm of 120 μm length on each face [36].

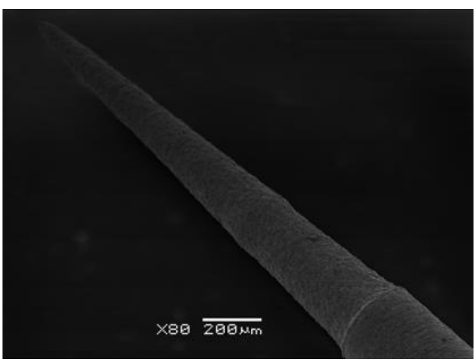

(a)

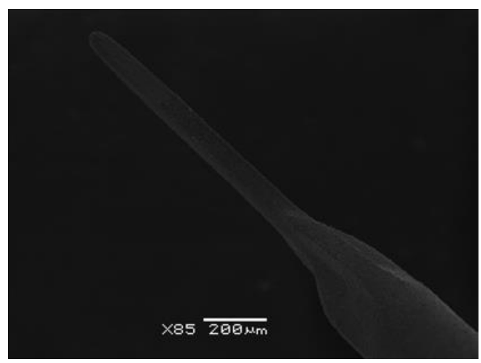

(b)

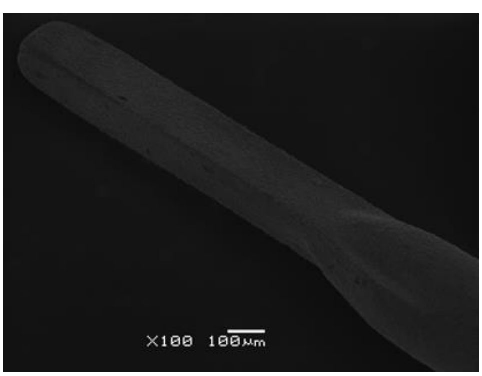

(c)

(d)

Figure 4. Microelectrodes of symmetrical sections: (a) tapered, (b) rectangular, (c) triangular and (d) circularly stepped sections [36].

Researchers also develope another interesting technique to fabricate spherical shaped tool which is also possible to fabricate using Wire Electrodischarge Grinding (WEDG). Due to the diameter precision level of wire which is ± 1 micron, it is not considered feasible to fabricate precision spherical tool which could fulfill the demand for high precision level of micro-grinding. Therefore, a pingauge made of Tungsten carbide, which is of precisely controlled shape and straightness, is chosen as a block electrode for fabricating spherical shape tool.

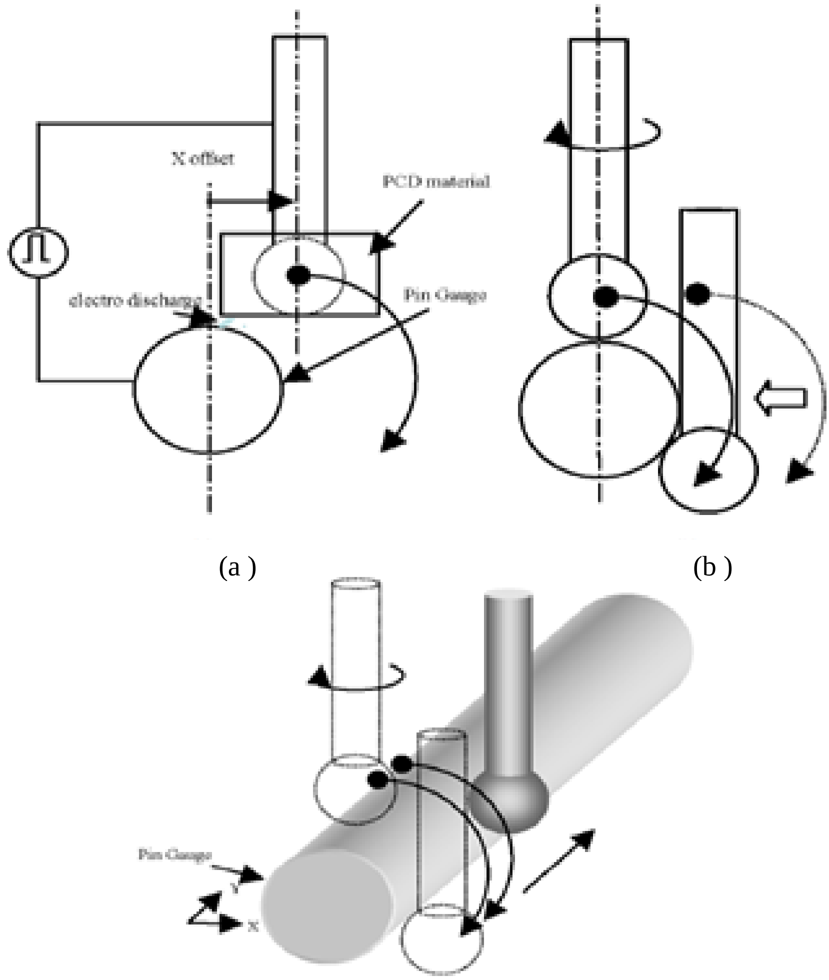

Figure 5. Shaping a spherical PCD tool using Pingauge: (a) Start tool path with X- offset (b) Final tool path and (c) Repetitive shaping to compensate electrode wear [37] .

In order to fabricate spherical tool, the machining path follows a cylindrical shape along the pin gauge with the PCD tool rotating. With time, PCD tool starts to get spherical shape as shown in Figure 5. Figure 5(a) shows the original tool shape and tool path with X- offset which is reduced in the successive steps. The final tool path is defined by the radius of the pin gauge and will result in spherical shape as shown in Figure 5(b). This method is repeated while moving in a positive Y-axis direction, added with the X- movement, compensates for the pin gauge wear. This process is considered completed when there is no discharge detected between the PCD and the gauge.The SEM images of the spherical PCD are shown in Figure

6. The capacitance and voltage used in this fabrication process is 3300 pF an d 110 V. The entire spherical surface is shaped with uniform aspect properties and covered with numerous cutting edges uniformly distributed along the surface. The fabricated spherical shape electrode is of 840 μm diameter and the pin gauge used was of 1mm diameter [37].

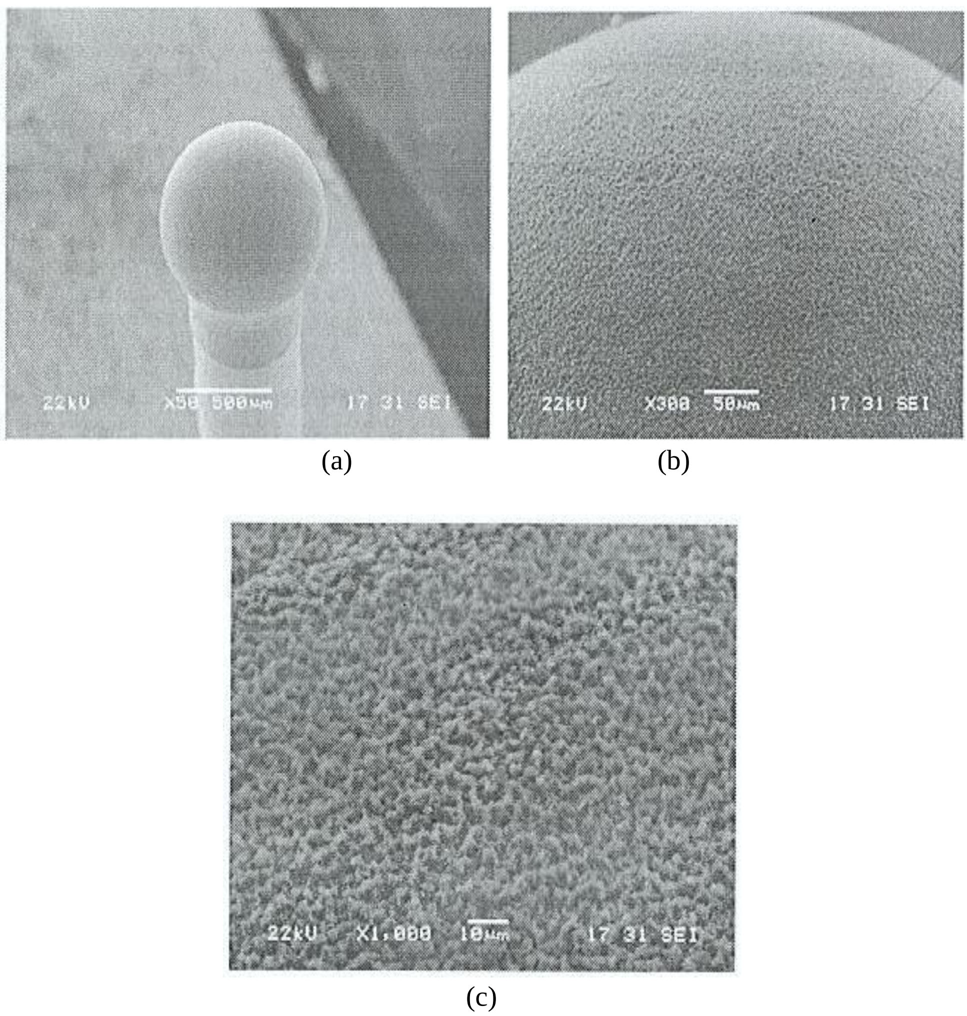

Figure 6. Scanning microscope image of PCD spherical Tool [37].

Although block EDM with the help of indexing proves its merit to fabricate symmetric electrode using the same block as shown by Ravi et al, but fabrication of conical shapes was not possible using that method. To solve this problem, researchers thought of another innovative idea to fabricate conical as well as others symmetrical shapes electrodes using the same set up. For the fabrication of square, circular, D-shape, triangular, conical shape tool of 60º, 90º and 120º, a fixture is designed and manufactured which makes possible the fabrication of all these shapes in single set up. For this purpose, Makino conventional horizontal wire EDM machine is used, with wire as small as 0.00078 inches (0.02 mm) in diameter. Wire EDM conditions are automatically fixed by the wire material and diameter based on work piece material and thickness. In this case, brass wire of 200 μm diameter and workpiece material of Wc (3 mm cut thickness) is used. Angles of these V-shapes are determined to be 60º, 90º, and 120º respectively which facilitate not only the fabrication of three different angle conical shape tool but also the triangular tools with three different angles. Figure 7 illustrates the schematic of this fixture along with the tool for fabricating triangular, conical and square microelectrodes.

The basic of block micro-EDM mechanism will remain same with this method; only change is to use one fixture of desired shape. Figure 7 also shows the methodology of fabricating microelectrodes with different shapes and cross sections. As demonstrated in Figure 7(a), the rod electrode is feed downward from CD edge to the required feed length in Z -direction along the face of triangular slot without tool rotation. Few passes are required to remove the material to have the desired electrode size. From mechanical drawing, the number of passes need to be calculated and dimension of tool should be checked using camera during machining. At first one face of the triangle is prepared, and then next DE edge of triangular slot is used to fabricate another face. Finally, BF edge is used to get the third face of triangular tool. Thus, using this method, fabrication of equilateral triangle and triangle with others angles too are possible which also eliminates the usage of indexing device.

Next for making conical tool, 3 slots of 60º, 90º and 120º are already machined in the tungsten block. For conical tool, the same block is tilted to 90°. Slopes of these triangular slots are used to fabricate different angles conical tools. In Figure 7 (b), PCD rod with rotation is fed along the slop in Z direction. After one pass is finished, tool is moved along Y-axis to have fresh place of cut and then next pass along Z-axis starts. Hence, conical tools of 3 different angles are also possible to fabricate using this methodology. In addition to this, AB, EH, BF, and FG edges of the same block can also be used to fabricate square tool without tool rotation.

Moreover, any of the edges like AB or BF can be used to fabricate circular tool with tool rotation. When tool is given feed along Z-direction without rotation, D-shaped tool is possible to fabricate. Thus, using this simple block, it is possible to fabricate triangular, square, conical, circular and D-shaped tools. Figure 8 shows the fabricated tools using this specifically designed block [28, 35].

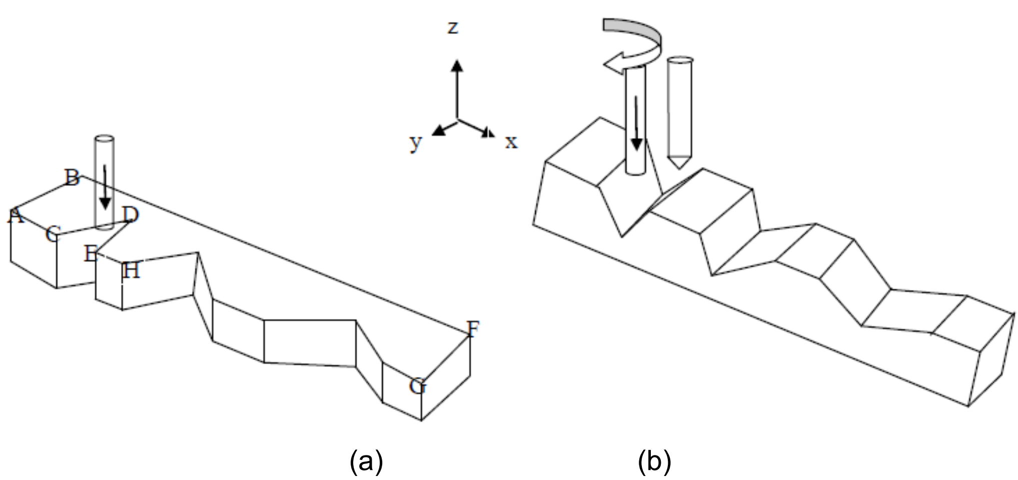

Figure 7. (Continued).

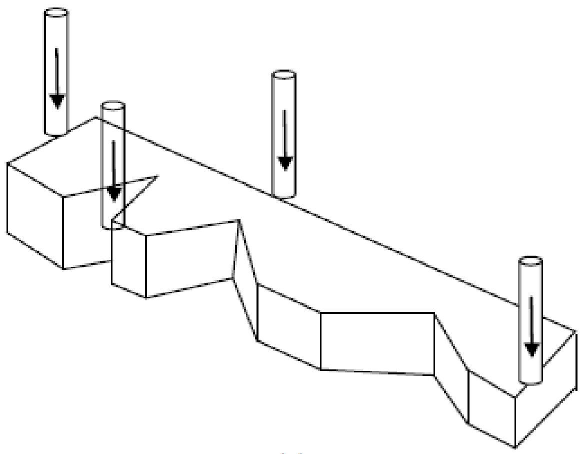

(c)

Figure 7. Schematic diagram (a) Before machining PCD rod along with fixture prepared by wire EDM for triangular microelectrode (b) Same fixture in different orientation for conical micro-electrode preparation (c) Fixture orientation for square and D-shaped tool [35].

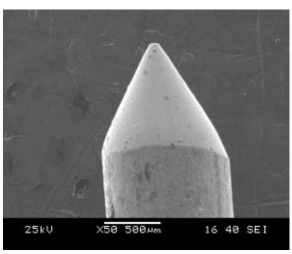

(a)

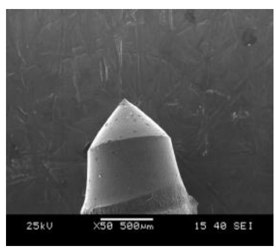

(b)

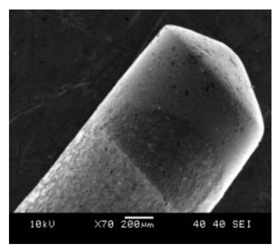

(c)

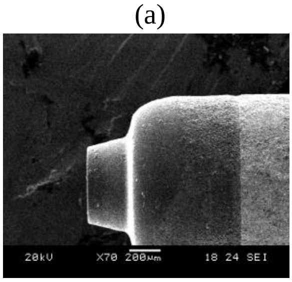

(d)

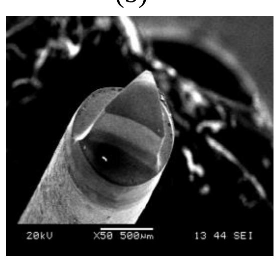

(e)

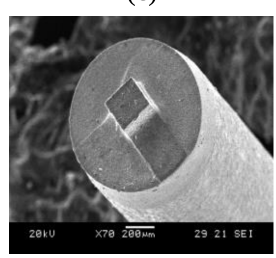

(f)

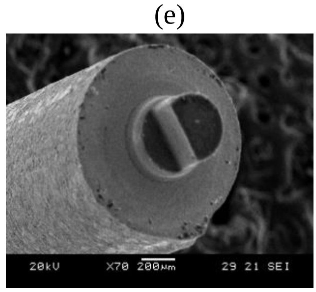

(g)

Figure 8. Conical tool of (a) 60º (b) 90º (c) 120º (d) circular tool (e) triangular tool (f) square tool (g) D-shaped tool [35].

EFFECT OF MACHINING PARAMETERS

Effect of Gap Voltage

Figure 9(a) shows comparison on the effect of gap voltage on machining time during block EDM of PCD and tungsten (W) rod. It has been found that for both the materials, the machining time decreases significantly with the increase of gap voltage. This is due to the reason that with the increase of gap voltage the discharge energy per pulse is increased, which results in larger craters and causes more material removal from work piece. Keeping all other factors constant, an increase in voltage will result in increased energy per spark. It is also observed that, compared to pure tungsten, PCD material needs higher machining time to be fabricated by micro-EDM. This is due to the higher electrical conductivity of tungsten materials which makes it better machinable by micro-EDM. The non-conductive diamond particles of PCD material causes higher machining time during micro-EDM. One important observation at lower gap voltage is that the machining time for W becomes higher than that of PCD material. This is due to the reason that at lower gap voltage the spark gap between the electrodes becomes smaller, which prohibits flushing out of all the debris materials from the machined zone as demonstrated by Jahan et al. (2009) [38]. Therefore, the flushing out of cobalt binder in PCD tool becomes easier than that of tungsten at lower spark gap, which causes sudden increase in machining time for W material.

Effect of Capacitance

The capacitor controls the charging and discharging process as well as the frequency of discharging. Therefore, the performance of the micro-EDM in RC-circuit is more influenced by the capacitance as demonstrated by Jahan et al. (2009) [39]. It has been found in Figure 9(b) that with the increase of capacitance the machining time decreases significantly as the discharge energy increases. As the capacitance value becomes larger, the peak current also increases.

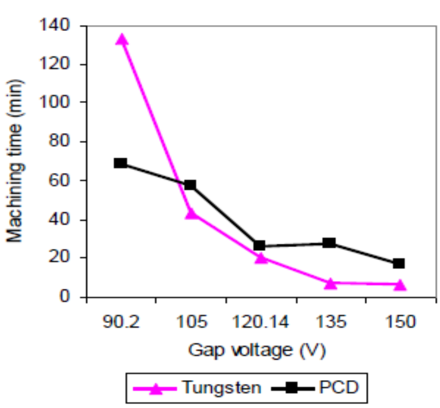

(a)

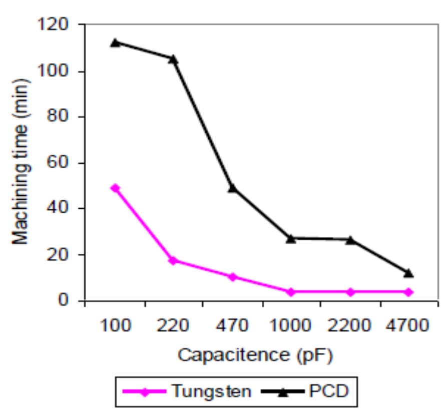

(b)

Figure 9. (Continued).

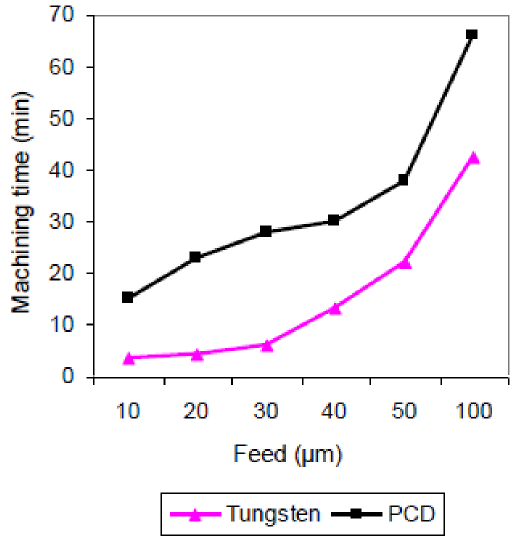

(c)

Figure 9. Effect of operating parameters during fabrication of microelectrodes.

Therefore, the larger capacitance results in deeper craters which increase the material removal. It has been observed that the trend of reduction of machining time with increase of capacitance is more sharp during micro-EDM of PCD compared to W. However, for all the settings of capacitance, the machining time is lower in micro-EDM of W rod. As the melting point of PCD is higher than tungsten, machining time is also higher in case of PCD when removing same amount of materials under same machining condition.

EFFECT OF DEPTH OF FEED IN EACH STEP

Depth of feed during tool electrode fabrication is the offset of the electrode length in X-axis to the sacrificial electrode (see Figure 2). Figure 2(a) shows the schematic representation of the block-µEDM process of tool fabrication. The geometric definition of feed length and wear length during the block-µEDM process are presented in Figure 2(b) as demonstrated by Ravi and Chuan (2002) [25]. Figure 9(c) shows the effect of electrode feed length on the machining time during micro-EDM of PCD and W rod. It is clear that the machining time will be higher for removing materials using a higher feed length, since more material has to be removed. However, if the tool fabrication is carried out in several steps, the overall machining time for fabricating a micro-electrode will be reduced with the increased feed length for a single step. Moreover, if a higher feed length is used during the final stage of fabrication, the fabricated tool may become more tapered. Therefore, the suggestion is that a higher feed length can be applied for rough machining during the first few steps of the fabrication process. However, during the final few steps of the fabrication process, the feed length should be kept low in order to improve surface finish and accuracy [40].

APPLICATIONS OF THE FABRICATED MICROELECTRODES

Several researches have been carried out during past few decades on the feasibility of fabricating micro-features on Tungsten carbide material using EDM. But for non-conductive materials, it is not possible to use micro-EDM, whereas micro-grinding can play important role using the polycrystalline diamond as cutting edge. Conductive binding material in PCD tool facilitates the fabrication of PCD tool using EDM technology and PCD grains assist in microgrinding process followed by fabrication process. It is also known that brittle materials can be machined in the ductile regime when small depth of cuts are used, as depicted by Bifano et al. (1991) and Ngoi and Sreejith (2000) [41, 42]. Nano-scratch tools having diameter that reduces to a sharp point are fabricated by WEDG to investigate the suitability of PCD micro-tools for ductile-mode grinding of brittle, non-conductive materials. Interestingly, similar tool has also been fabricated using block EDM method as shown by Perveen et al. The idea is to maintain single diamond grain on the tip of nano-scratch tools as shown in Figure 10. Subsequently, the tool can be used to do scratch test on ULE® glass (Corning Code 7972) without any rotation. Ductile-mode material removal is clearly observed, as shown in Figure 10(b) The scratch produces ductile chips that are attached to the edge of the groove, and apparently no sub-surface damage is visible on the glass workpiece. This fact recommends that the PCD material could be pretty much suitable for grinding non-conductive brittle materials [43].

The result of scratch test eventually paves the way for additional works to use PCD tools as micro-grinder to machine features on brittle materials. The ∅50 μm cylindrical tool shown in Figure 11(a) is used to grind straight pockets on ULE® glass. The tool traverses along the trajectory with h = 100 nm, l = 500 μm and a feed rate of 1 μm/s. Eventually fifteen passes produce a groove of 1.5 μm deep which results in a surface roughness of just 5.7 nm. A 2D profile scan across the groove shows that the sidewalls are slightly inclined, most likely due to tool wear, and the bottom of the groove is slightly arched, possibly due to elastic rebound of the material under the tool. Although the material removal rate (MRR) is extremely low (about 3×10^{-7} mm^3/min), the sidewalls still reveal some brittle fractures that indicate the feed rate or the cutting depth might still be too large [Figure 11(b)]. Figure 11(c) demonstrates the SEM image of a similar crescent shaped groove ground on ULE® glass.

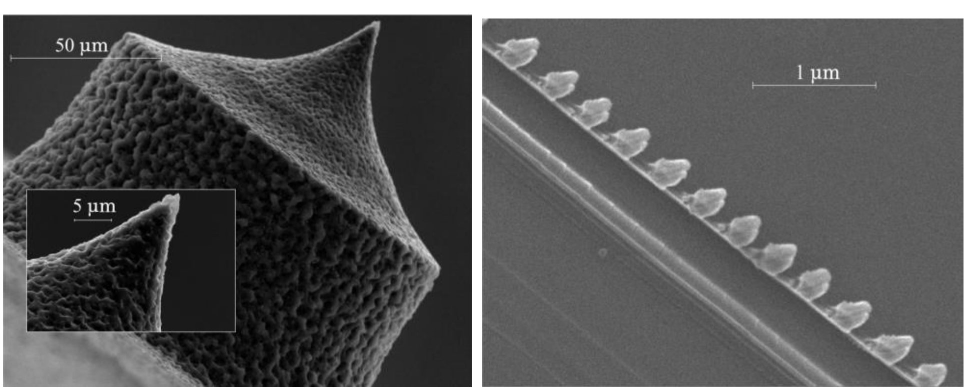

Figure 10. (a) PCD scratch tool produced using WEDG process (b) Scratch in ULE® glass fabricated with this tool [43].

At certain axial depth of cut, the material removal mechanism experiences transition from ductile to brittle fracture as indicated by the fractures on the bottom surface of groove. The profile of groove shown in Figure 11(c) suggests that axial depth of cut varies along the groove and the bottom of surface is not flat unlike the straight groove presented in Figure 11(b). This fact also reveals that higher value of cutting forces and machining compliance may cause this sort of deflection. The most compliant component of the machine loop is the fixture to hold the work piece. Unfortunately, glass workpiece is difficult to clamp due to its brittleness, therefore improved fixture design in future might help to eliminate this issue [15, 43].

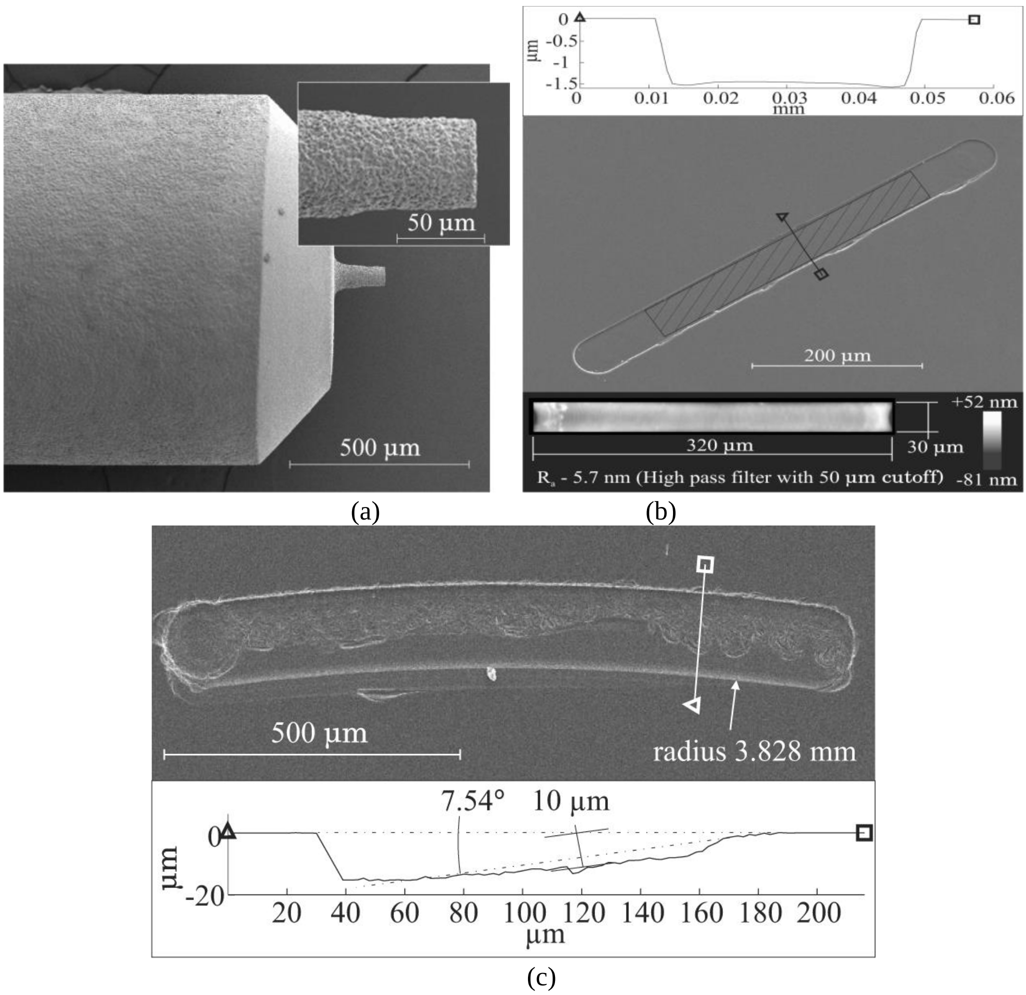

Figure 11. (a) A cylindrical ∅50 µm PCD tool used to cut pockets in ULE® glass (b) Groove ground in ULE® glass using the tool (c) Crescent shaped groove ground into ULE® glass and 2D profile across groove [43].

The method of point processing leads to the formation of small flat plane and micro-concave cylindrical surface with a radius of 4 mm on tungsten carbide material. Figure 12(b) demonstrates the methodology of this microgrinding. Tool path is oriented in the Z-axis direction which is perpendicular to the rotational direction in order to avoid surface aspect of result as shown in Figure 12(c) and (d). Following that, the tool is repeatedly stepped towards Y-axis direction. During rough machining, cutting feed step is maintained 2 μm along X-axis for each increment and for Y-axis feed step is 100 μm. During final machining, feed step is set 2 μm and 1 μm for the X- and Y-axis respectively. The feed rate and rotation used in final step is 1 mm/s and 3000 rpm. As seen from Figure 13(a), the ground surface exhibits mirror finish. The surface generated by the arc envelope grinding is of 5 nm Ra and 28 nm in PV (equivalent to Rz). It is also pretty much clear that an aspect is formed on the machined surface and a visible mark is also created in the direction of tool rotation as shown in Figure 13(c). However, granular unevenness characteristics of tungsten carbide is identified to be rougher.

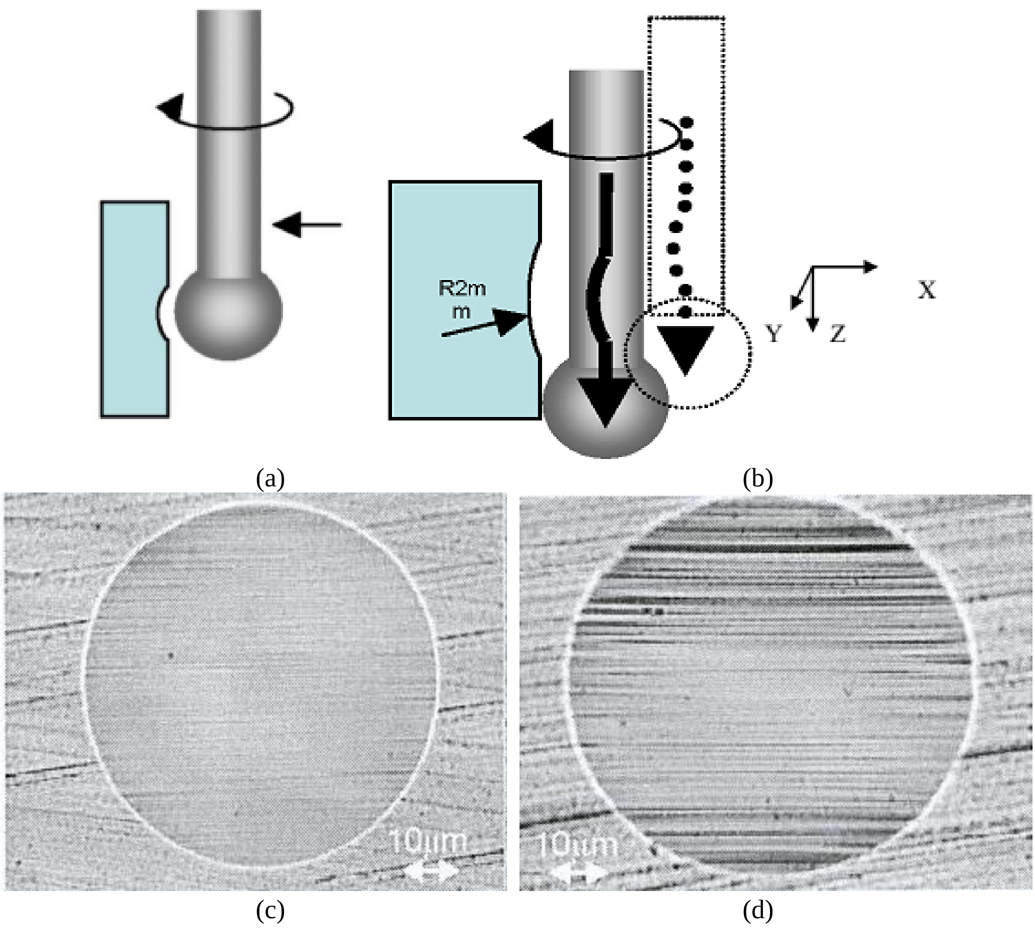

Figure 12. (a) Procedure to point spherical tool (b) Procedure of shaping flat and cylindrical surface using Spherical PCD tool (c) Optical image of pointed shapes on Tungsten carbide formed by PCD spherical tool using 10 pF , 80Volts (d) 3300pf , 110 volts [37].

Apart from cylindrical shape, it is also feasible to fabricate concave and convex shape using this spherical tool. The methodology for forming convex spherical surface which is of 1 mm spherical radius is shown in Figure 14(a). This is generated by moving the spherical PCD tool in a circular path in the YZ- plane with feed direction in X plane.

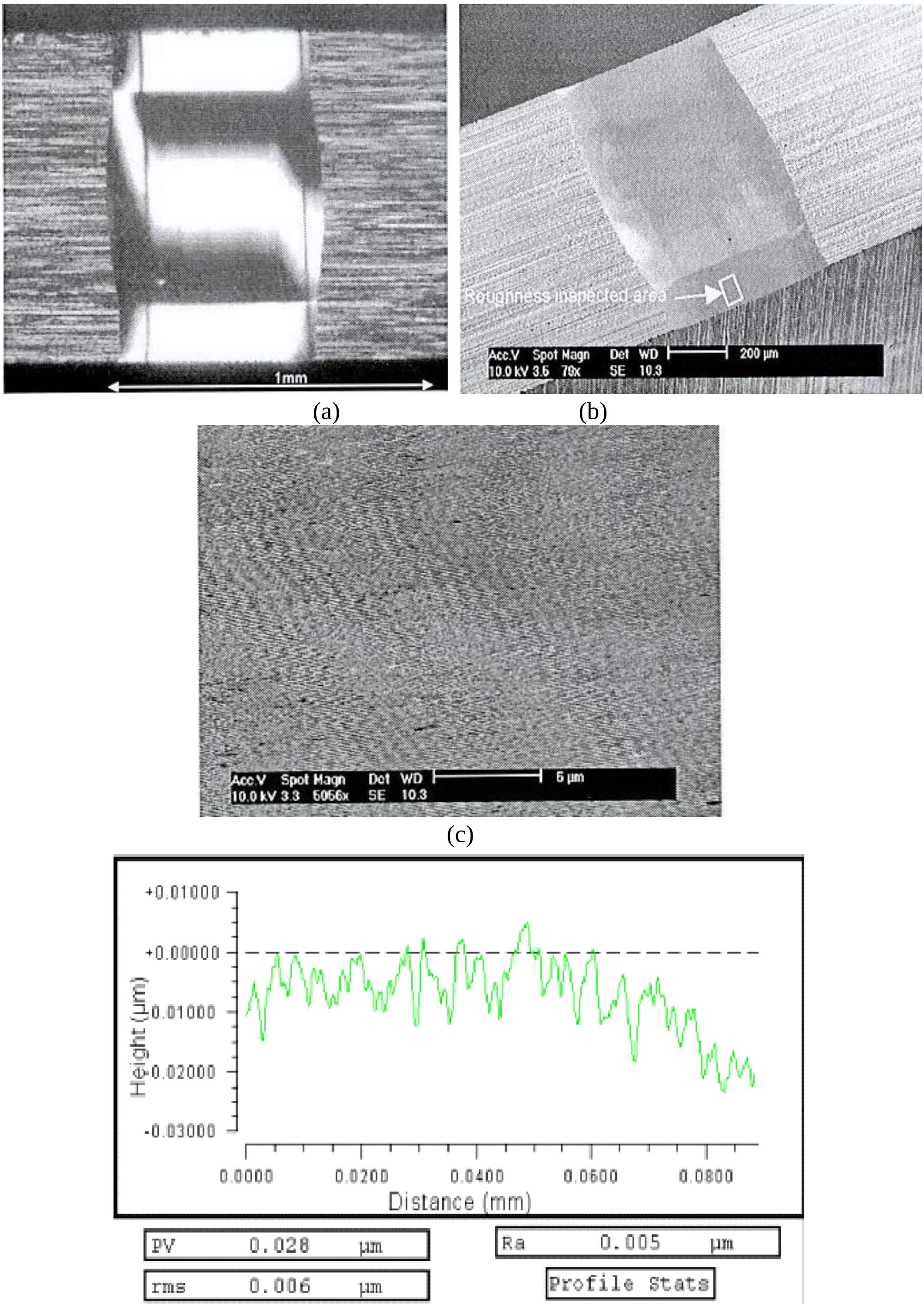

(a) (b) (c) (d)

Figure 13. (a) Optical image of shaped flat and cylindrical surface on Tungsten carbide. (b) SEM image of machines and also surface roughness data [37].

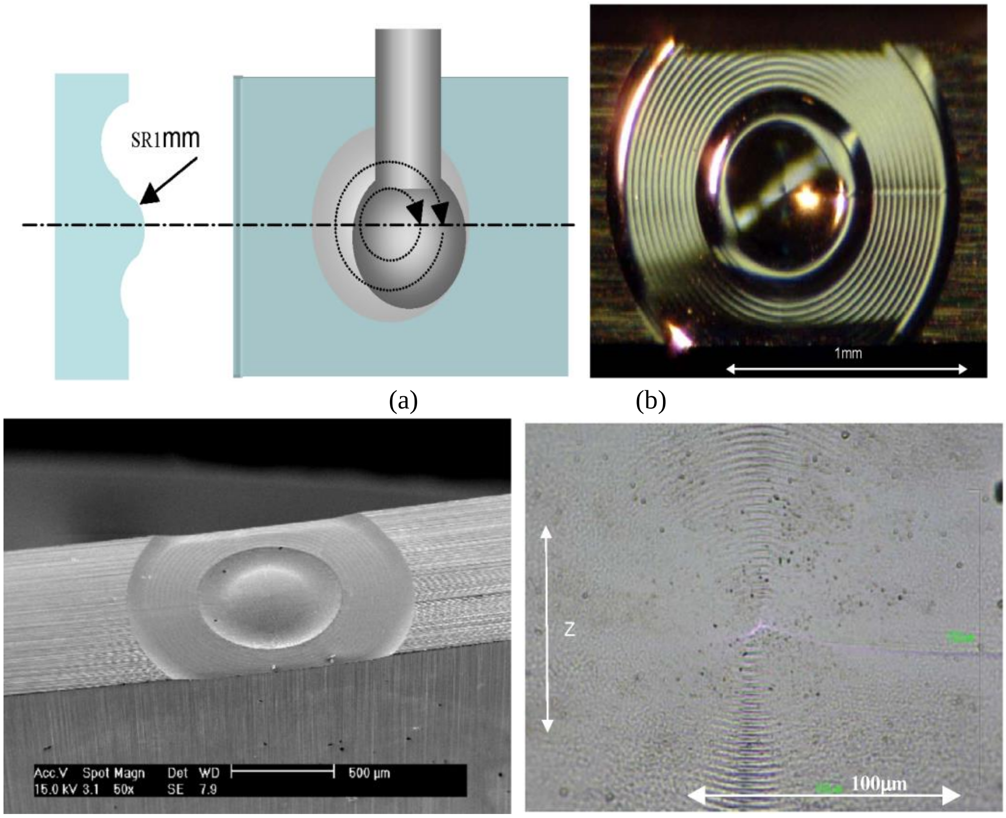

(a) (b)

(c) (d)

Figure 14. (a) Procedure of shaping convex spherical surface (b) Optical image of shaped convex spherical surface (c) SEM image of a shaped convex spherical surface.(d) Optical microscopic image of a shaped convex spherical surface on Tungsten carbide [37].

The final diameter of convex surface achieved using this tool is 0.5 mm and the circumference portion is machined by rough machining only. The roughening process step in radial direction is maintained 20 μm and cutting unit in X-axis is 2 μm per step. The finishing step in radial direction is set to be 2 μm. The feed rate and rotation is set 2 mm/min and 4000 rpm for both rough and finish machining.

Figure 14(b) and (c) demonstrate the optical and SEM image of convex surface while Figure 14(d) presents the optical image of center of convex surface. It is obvious that the surface finish is appeared to be mirror in general. Moreover, after observing the vertical domain from top to bottom, in Figure 15(a),the tool marks of finishing process are visible as a transfer of the radial direction, whereas in horizontal domain no tool marks are visible and grain structure of tungsten carbide is clear enough.

The radial marks are suspected to be generated due to the following reasons. During the processing, the cutting area is small point whereas the workpiece and tool are convex shaped. When the tool rotation is parallel to the tool travel, the resulting surface reveals the tool marks at the point of contact from each path step. Conversely, when tool rotation is perpendicular to the tool travel, the resulting surface does not reveal any tool marks, because of the small points of contact envelope. Optimization of the feed step size and the tool path possibly can reduce this tool marks.

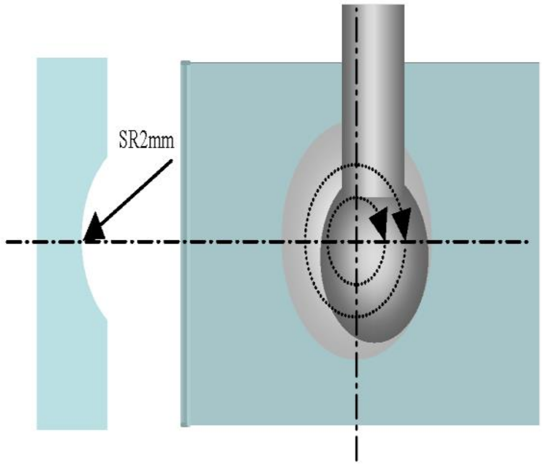

(a)

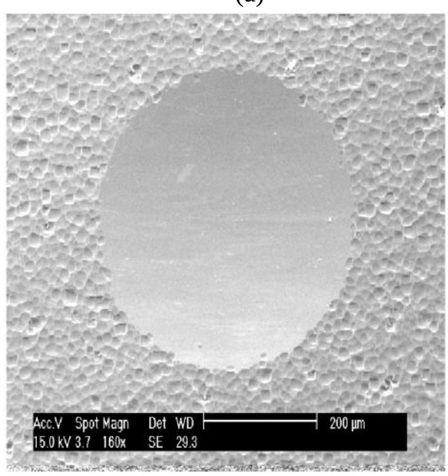

(b)

Figure 15. (a) Procedure of shaping a concave spherical surface (b) SEM image of a concave spherical shaped on silicon [37].

The procedure of generating a concave spherical surface which is of 2 mm spherical radius and diameter of 400 μm is shown in Figure 15(a). Feed rate used is 4 mm/min and PCD tool fabricated using 10 pF, 80 V energy is used for this case.

Figure 15(b) shows the SEM image of concave surface on Silicon wafer. The whole plane is found to be formed with uniform minute tool mark. The process is very similar to convex surface generation but due to concave shape, this surface does not contain any singular domain. The cutting area is around 53 μm at a depth of 1 μm so that the tool marks created by the each step feed are eliminated and consequently results in uniform surface [37].

Several other micro-features are fabricated using microelectrodes generated using Block EDM method without replacing them from machine. Due to the presence of diamond grain cutting edges and electrically conductive cobalt materials, PCD microelectrodes facilitate their applications in both conductive and non-conductive materials. Figure 16 shows some of the features fabricated on glass, Nickel and Tungsten carbide. Triangular, Square and D-shaped tools can be also used to create triangular, square and D-shaped hole on the tungsten material by reverse EDM but that is not the focus of this chapter. In addition to circular tool, D-shaped, triangular and square tools also are used to microground pockets on both glass and Tungsten carbide using tool rotation. On top of that, letter N and M are fabricated on the BK7 glass as well.

These shapes are created on the glass surfaces to investigate whether different microstructures which are really useful in Micro-fluidic channel can be fabricated on the glass or not. Therefore, different complex shapes and structures may possibly be fabricated on the brittle materials using these kinds of tools with similar techniques in future [28, 44].

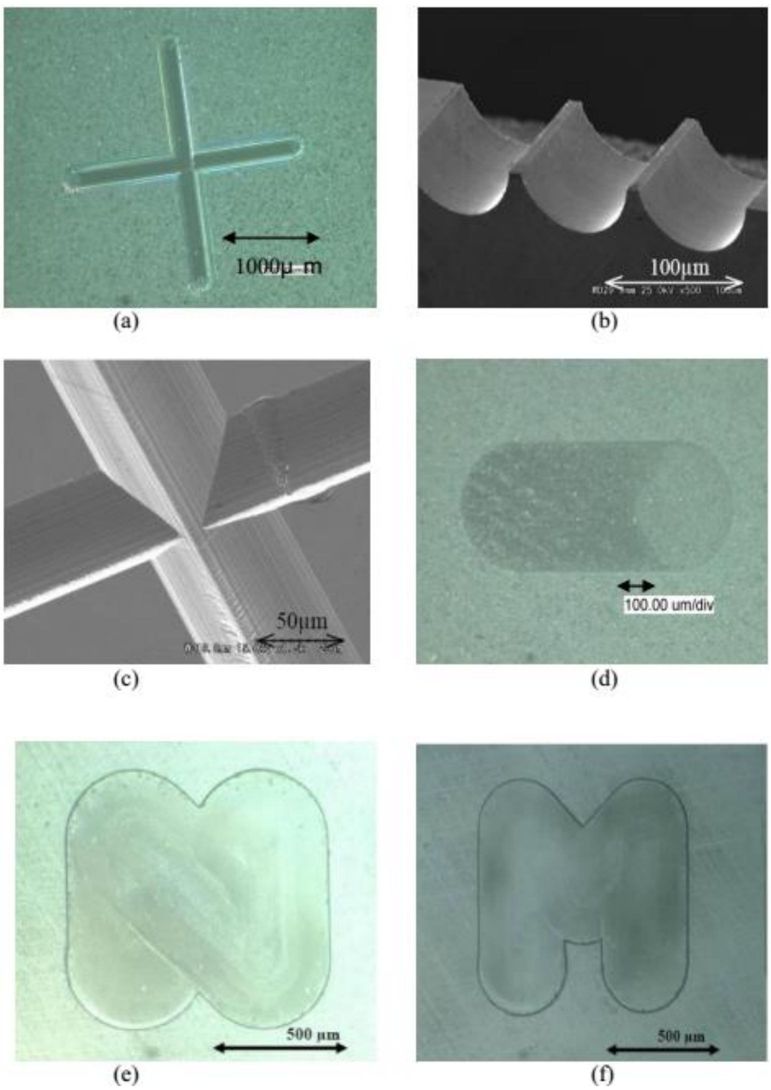

Figure 16. (a) V groove by conical tool 120º (b) Profile on tungsten Carbide by circular tool (c) V groove on Ni Surface (d) Pocket on BK7 Glass(d) Shape N on Bk7 glass (e) Shape M on Bk7 glass [28, 44].

MICROGRINDING MECHANISM

In order to shed some light on the microgrinding mechanism, Wada et al. investigates the material removal procedure for conical tool made of PCD material. Figure 17 shows a conceptual diagram of the V groove machining method. V groove machining is primarily done by cutting the workpiece to the depth of D with the tool revolving at the rotational speed R and mechanically removing the work area by moving the tool around at the feed rate of F. By adjusting the vertex angle of the conical tip, V-grooves of any angle can be machined. When performing ultra-accurate cutting of brittle materials, such as silicon, a common problem comes from the damage caused by ductile/brittle transition. As a solution of this problem, controlling the cutting depth with the cutting edge enables specular finishing in the ductile cutting mode. In this method, it is considered that the process progresses through the microscopic grinding caused by the surface roughness of diamond particles. The conical shaped tool is a composition of numerous diamond cutting edges, which performs numerous microscopic cuttings on the work surface due to the rotational motion of particles and feed movement of the tool itself. It is also considered that, if the stress of the work surface during cutting exceeds a certain limit, the brittle fracture mode predominates, resulting in defects. The volume V of work piece removed by each particle during one revolution of the tool is independent of the cutting depth of the tool but is given by the following equation using the tool feed rate F and rotational speed R. It is considered that, if V exceeds a certain value, the cutting mode changes from the ductile cutting mode to the brittle cutting mode, which would also cause defects on the work surface.

$$V = k*F/R \text{ (k is a constant)} \tag{1}$$

To verify the above equation, a V groove machining experiment with different feed rates and rotational speeds of the tool are performed and occurrence of defects after machining is checked. As workpiece sample, single-crystal silicon wafers are used (Sumitomo Metal Industries, Ltd.).

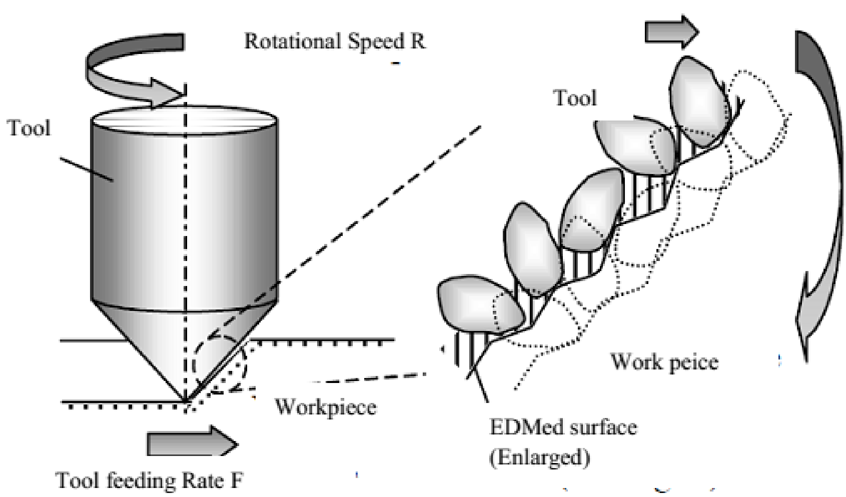

Figure 17. Conceptual diagram of V groove machining mechanism [44].

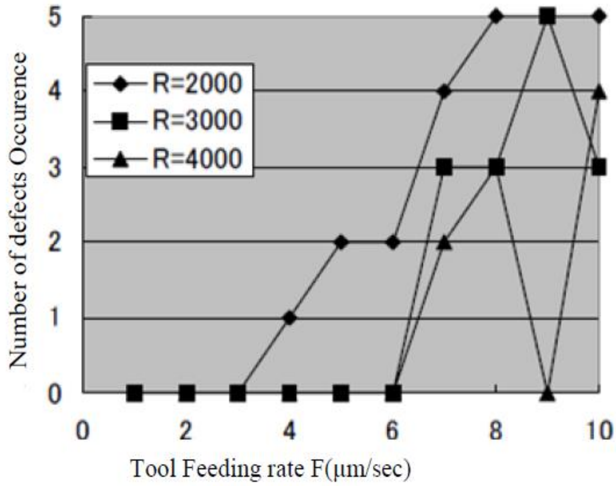

Figure 18. Tool feeding rate and number of defects occurrence [44].

The sample is machined in stationary oil in the orientated flat and horizontal directions. V-groove machining is performed five times with cutting depth D=5 μm for a cutting length of 100 μm and the number of defects are observed after machining. Figure 18 describes the relationship between the tool feed rate F and the number of defect occurrences for different rotational speeds R. It is comprehended that the greater the tool feed rate F or the smaller the rotational speed R, the higher the defects may occur: this also shows good agreement with the characteristics of the above equation [44].

MICROELECTRODE WEAR

Although, block EDM research related to microelectrode focuses primarily on tool fabrication process, very few researchers investigate on tool wear due to micro-grinding process. Figure 19 gives a relative scenario of shaped PCD tool surfaces after grinding micro-slots on the glass material. It is found that except circular one; D shaped, triangular and square tools have the tendency of wearing more as seen from SEM image of tools in Figure 19. This is basically due to the sharp edge of the tool which experiences more wear and becomes round. When circular tool experiences wear or re-sharpening, it becomes smaller in diameter but still remains round. Hence, a worn-out circular tool does not affect the machining performance significantly. On the other hand, when the edges of square or triangular tool experience wear, wear is usually non-uniform as all the four or three edges cannot wear out at the same rate. For the shaped tool it is also found that edge rounding or pull out of grain is the main wear mechanism. At the same time machining condition varies from sharp edge to round edge. In contrast to conventional sharp edge cutting model, chip shearing in micromachining occurs along the rounded tool edge. Therefore, this large edge radius affects the magnitude of ploughing and shearing forces. Higher plastic deformation results from larger cutting edge radius. As a result, surface roughness as well as cutting force kept changing with this wear of square and triangular tool [35].

In order to find the wear on the bottom of the PCD tool, Morgan et al. has conducted some observation with circular PCD tool. A measurement on the bottom of the pocket is made with the Scanning Whitelight Interferometer (SWLI) as shown in Figure 20. The wear of the PCD tool due to machining of ULE glass is monitored with 3D SWLI measurements of the circular surface on the bottom of the tool. The bottom surface is found to be very smooth with an average roughness (Ra) of 0.3 nm, and the flatness of the pocket is within 1.5 μm over the 500 μm length. The non-flatness is most likely due to the compliance of the nanopositioning stage.

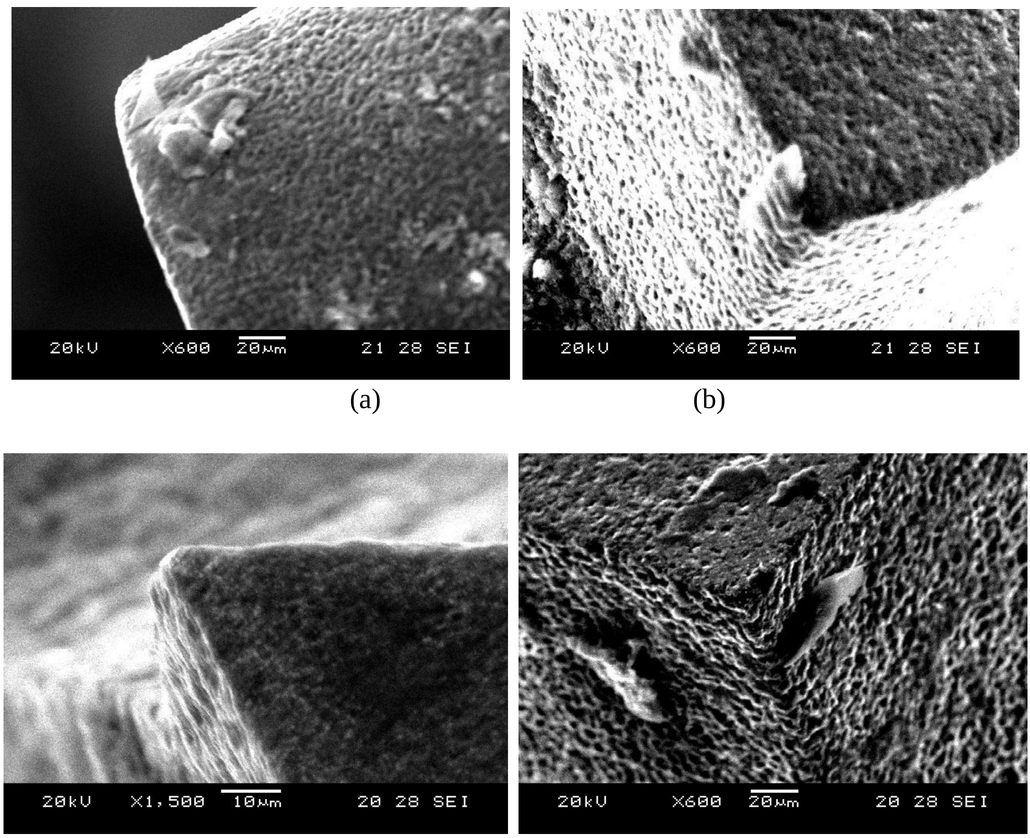

Figure 19. SEM image of Tool after machining (a) Circular (b) D-shape (c) Triangular (d) Square tool [35].

Figure 20(a) shows the form of the tool's circular surface after each of the ten pockets machined on ULE glass and Figure 20(b) shows contour plot of machined surface on ULE glass with flatness profile along the length of the pocket. The blue and dark red regions indicate the valleys and the peaks, respectively. Each contour plot is rotated to a similar orientation so that the repeatability of the pattern is discernible. Very little change in the form is observed between pockets 1 and 7; in fact, the forms after pockets 1 and 6 are nearly identical. A significant change in the form starts to appear between pocket 7 and 8 and remains same for rest of the pocket. This sudden change in form is also accompanied by a jump in the peak-to-valley height, which increases from around 1.6 μm to about 2.4 μm. This suggests that glass swarf adhered to the tool, thereby increasing the height of the peaks [15].

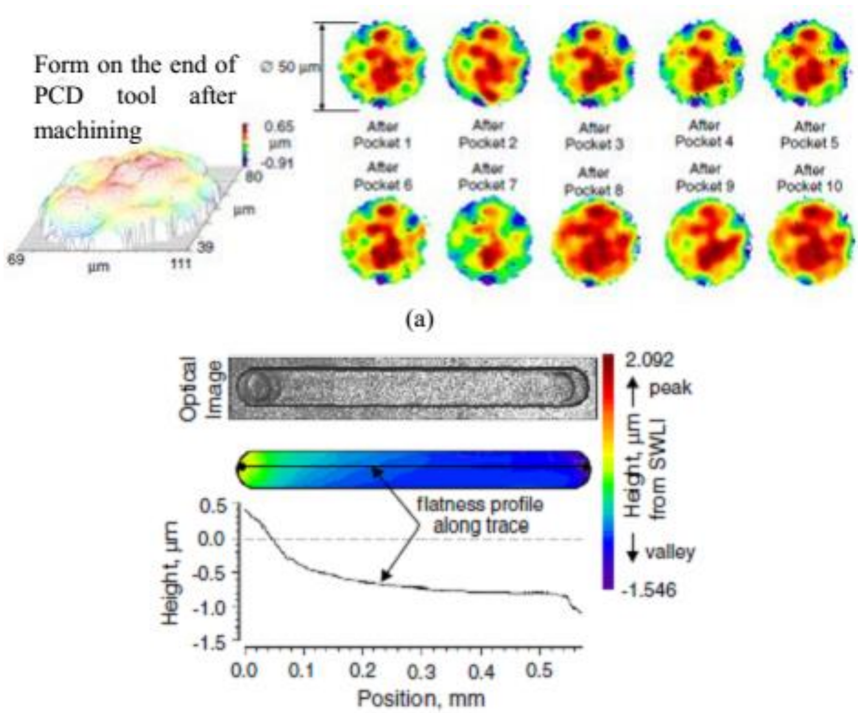

(b)

Figure 20. Form of circular end of PCD tool after cutting ten successive pockets in ULE glass; typical peak to valley height is about 2 μm.(b) Form and flatness of pocket machined in ULE glass using PCD tool[15].

REFERENCES

[1] Yin, S., et al., Micro V-Groove Grinding Technique of Large Germanium Immersion Grating Element for Mid-Infrared Spectrograph(<Special Issue>Advanced Manufacturing Technology). JSME international journal. *Series C, Mechanical systems, machine elements and manufacturing*, 2004. 47(1): p. 59-65.

[2] Khan Malek, C., et al., Deep microstructuring in glass for microfluidic applications. *Microsystem Technologies*, 2007. 13(5-6): p. 447-453.

[3] Nakasuji, T., et al., Diamond Turning of Brittle Materials for Optical Components. *CIRP Annals - Manufacturing Technology*, 1990. 39(1): p. 89-92.

[4] Fang, F.Z. and L.J. Chen, Ultra-Precision Cutting for ZKN7 Glass. *CIRP Annals - Manufacturing Technology*, 2000. 49(1): p. 17-20.

[5] Takahashi, T. and P.D. Funkenbusch, Micromechanics of diamond composite tools during grinding of glass. *Materials Science and Engineering: A*, 2000. 285(1–2): p. 69-79.

[6] Gao, G.F., et al., Research on the surface characteristics in ultrasonic grinding nano-zirconia ceramics. *Journal of Materials Processing Technology*, 2009. 209(1): p. 32-37.

[7] Sun, X., et al., An investigation into parallel and cross grinding of BK7 glass. *Precision Engineering*, 2006. 30(2): p. 145-153.

[8] Luo, S.Y., Y.Y. Tsai, and C.H. Chen, Studies on cut-off grinding of BK7 optical glass using thin diamond wheels. *Journal of Materials Processing Technology*, 2006. 173(3): p. 321-329.

[9] Sinhoff, V. and W. König, Generative Precision Grinding of Optical Glass. *CIRP Annals - Manufacturing Technology*, 1998. 47(1): p. 253-258.

[10] Suratwala, T., et al., Sub-surface mechanical damage distributions during grinding of fused silica. *Journal of non-crystalline solids,* 2006. 352(52): p. 5601-5617.

[11] Agarwal, S. and P.V. Rao, Experimental investigation of surface/subsurface damage formation and material removal mechanisms in SiC grinding. *International Journal of Machine Tools and Manufacture*, 2008. 48(6): p. 698-710.

[12] Matsumura, T., et al., A Study on Cutting Force in the Milling Process of Glass. *Journal of Manufacturing Processes,* 2005. 7(2): p. 102-108.

[13] Matsumura, T. and T. Ono, Cutting process of glass with inclined ball end mill. *Journal of Materials Processing Technology*, 2008. 200(1–3): p. 356-363.

[14] Cai, M.B., X.P. Li, and M. Rahman, Study of the mechanism of nanoscale ductile mode cutting of silicon using molecular dynamics simulation. *International Journal of Machine Tools and Manufacture,* 2007. 47(1): p. 75-80.

[15] Morgan, C.J., R.R. Vallance, and E.R. Marsh, Micro machining glass with polycrystalline diamond tools shaped by micro electro discharge machining. *Journal of Micromechanics and Microengineering*, 2004. 14(12): p. 1687.

[16] Kozak, J., K. Rajurkar, and S. Wang, Material removal in WEDM of PCD blanks. Journal *of Manufacturing Science and Engineering*, 1994. 116(3): p. 363-369.

[17] Liu, Y., Y. Guo, and J. Liu, Electric discharge milling of polycrystalline diamond. Proceedings of the Institution of Mechanical Engineers, *Part B: Journal of Engineering Manufacture*, 1997. 211(8): p. 643-647.

[18] Nakazawa, H., *Principles of precision engineering*. 1994: Oxford University Press, USA.

[19] Mamalis, A., et al., Two-stage electro-discharge machining fabricating superhard cutting tools. *Journal of materials processing technology*, 2004. 146(3): p. 318-325.

[20] Egashira, K., Cutting of Hard and Brittle Materials with a Microtool. *Journal-Japan Society for Precision Engineering*, 2001. 67(1): p. 157-161.

[21] Friedrich, C., P. Coane, and M. Vasile, Micromilling development and applications for microfabrication. *Microelectronic engineering*, 1997. 35(1): p. 367-372.

[22] Yu, Z.Y., T. Masuzawa, and M. Fujino, Micro-EDM for Three-Dimensional Cavities - Development of Uniform Wear Method. *CIRP Annals - Manufacturing Technology,* 1998. 47(1): p. 169-172.

[23] Pham, D.T., et al., Micro-EDM—recent developments and research issues. *Journal of Materials Processing Technology*, 2004. 149(1–3): p. 50-57.

[24] Ho, K.H. and S.T. Newman, State of the art electrical discharge machining (EDM). International *Journal of Machine Tools and Manufacture*, 2003. 43(13): p. 1287-1300.

[25] Ravi, N. and S.X. Chuan, The effects of electro-discharge machining block electrode method for microelectrode machining. *Journal of micromechanics and microengineering*, 2002. 12(5): p. 532.

[26] Jung-Chou, H., et al., Using a helical micro-tool in micro-EDM combined with ultrasonic vibration for micro-hole machining. *Journal of Micromechanics and Microengineering*, 2006. 16(12): p. 2705.

[27] Philbin, P. and S. Gordon, Characterisation of the wear behaviour of polycrystalline diamond (PCD) tools when machining wood-based composites. *Journal of Materials Processing Technology*, 2005. 162: p. 665-672.

[28] Perveen, A., Y. Wong, and M. Rahman. Fabrication of PCD Micro Tools Using Block EDM Method and Their Application to Different Microstructures in Brittle and Hard Materials. in ASME , International Manufacturing Science and Engineering Conference. 2010. *American Society of Mechanical Engineers.*

[29] Perveen, A., et al., A study on microgrinding of brittle and difficult-to-cut glasses using on-machine fabricated poly crystalline diamond (PCD) tool. *Journal of Materials Processing Technology*, 2012. 212(3): p. 580-593.

[30] Masuzawa, T., et al., Wire Electro-Discharge Grinding for Micro-Machining. *CIRP Annals - Manufacturing Technology*, 1985. 34(1): p. 431-434.

[31] Allen, D.M., Micro-electrodischarge machining. *Proc. 1997 IEE Colloquium on Recent Advances in Micromachining Techniques* 1997: p. 7/1–7/2.

[32] Liu W, R.M., Wong Y S Micro machining of silicon by electrical discharge machining SME Technical Paper MR01-237 2001: p. 1-7.

[33] Takahata, K., N. Shibaike, and H. Guckel. A novel micro electro-discharge machining method using electrodes fabricated by the LIGA process. in Micro Electro Mechanical Systems, 1999. MEMS'99. *Twelfth IEEE International Conference on. 1999. IEE*E.

[34] Jahan, M.P., et al., On-machine fabrication of high-aspect-ratio micro-electrodes and application in vibration-assisted micro-electrodischarge drilling of tungsten carbide. *Proceedings of The Institution of Mechanical Engineers Part B-journal of Engineering Manufacture*, 2010. 224(5): p. 795-814.

[35] Perveen, A., W. San, and M. Rahman, Fabrication of different geometry cutting tools and their effect on the vertical micro-grinding of BK7 glass. *The International Journal of Advanced Manufacturing Technology*, 2012. 61(1-4): p. 101-115.

[36] Ravi, N. and H. Huang, Fabrication of symmetrical section microfeatures using the electro-discharge machining block electrode method. *Journal of Micromechanics and Microengineering*, 2002. 12(6): p. 905.

[37] Masaki, T., et al., Study on shaping spherical Poly Crystalline Diamond tool by Micro-electro-Discharge Machining and micro-grinding with the tool. *International Journal of Surface Science and Engineering*, 2007. 1(4): p. 344-359.

[38] Jahan, M., Y. Wong, and M. Rahman, A study on the fine-finish die-sinking micro-EDM of tungsten carbide using different electrode materials. *Journal of materials processing technology*, 2009. 209(8): p. 3956-3967.

[39] Jahan, M., Y. Wong, and M. Rahman, A study on the quality micro-hole machining of tungsten carbide by micro-EDM process using transistor and RC-type pulse generator. *Journal of materials processing technology*, 2009. 209(4): p. 1706-1716.

[40] Perveen, A.,Jahan ,M., Rahman, M., Wong, Y., A study on microgrinding of brittle and difficult-to-cut glasses using on-machine fabricated poly crystalline diamond (PCD) tool. *Journal of Materials Processing Technology*,2012.212(3):p.580-593.
[41] Bifano, T.G., T. Dow, and R. Scattergood, Ductile-regime grinding: a new technology for machining brittle materials. *Journal of Manufacturing Science and Engineering*, 1991. 113(2): p. 184-189.
[42] Ngoi, B. and P. Sreejith, Ductile regime finish machining-A review. *The International Journal of Advanced Manufacturing Technology*, 2000. 16(8): p. 547-550.
[43] Morgan, C.J., R.R. Vallance, and E.R. Marsh, Micro-machining and micro-grinding with tools fabricated by micro electro-discharge machining. *International Journal of Nanomanufacturing*, 2006. 1(2): p. 242-258.
[44] Wada, T., T. Masaki, and D.W. Davis. Development of micro grinding process using micro EDM trued diamond tools. in ASPE Proceeding, *Annual Meeting*. 2002.

In: Electrical Discharge Machining (EDM)
Editor: M. P. Jahan
ISBN: 978-1-63483-591-6

Chapter 11

ELECTRICAL DISCHARGE MACHINING CHARACTERISTICS AND OPTIMIZATION OF NEWER MATERIALS

S. Gopalakannan*

Department of Mechanical Engineering,
Adhiparasakthi Engineering College, Melmaruvathur, Tamilnadu, India

ABSTRACT

Metal Matrix Composites (MMCs) and Metal Matrix Nano Composites (MMNCs) are the recent advanced materials having the properties of lightweight, high specific strength and high wear resistance. MMCs are composed of metallic base material called matrix, which is reinforced with a hard ceramic reinforcement. Due to possession of higher hardness and reinforcement strength, composite materials are difficult to be machined by traditional techniques.

Hence, Electrical Discharge Machining (EDM) process becomes viable method to machine these kinds of composite materials. Since the EDM process does not involve mechanical energy, the material removal rate is not influenced by the material properties like hardness, strength, toughness etc. To exploit the potential industrial applications and investigate proper manufacturing processes, machinability of electrical discharge machining of MMC needs to be studied for reliable and economical production. The correlation between the major machining parameters, electrical current and on-time, and crater size on machining Al/SiC was established and it was concluded that the crater size of Al/SiC was larger than steel, and for effective EDM large electrical current and short on time were recommended.

Keywords: EDM, metal matrix composites, metal matrix nano composites

* Corresponding Author: S Gopalakannan, E-mail: gopalakannan75@gmail.com

INTRODUCTION

In the area of engineering materials, the focus is on developing new materials and processing technologies to make products that are energy efficient and cost effective. Metal matrix composite is one of the recent materials gaining wide applications in the automotive and aerospace industries.

However the full potential of these materials hindered with the difficulties experienced in machining of metal matrix composites (MMC). Machinability of MMCs has received considerable attention because of the high tool wear due to the presence of the hard reinforcement particles [1]. This hard reinforcement particle causes premature failure to the cutting tool, leading to higher machining cost. The efficient and economic machining of MMCs is required for the desired dimensions and surface quality. Kannan et al. investigated the effect of reinforcement size and volume fraction of aluminium MMC with Al_2O_3 and reported that the tool wear increases with increase in particle size and volume fraction, with the former showing dominant effect on tool wear. They also studied the tribological aspects of machining Al 7075 reinforced with 10 wt% Al_2O_3 and concluded that a better surface finish is obtained by the application of cutting fluid [2]. Sahin et al., conducted experiments on tool wear and surface roughness in turning of Al 2024 reinforced with 10 wt% Al_2O_3 and opined that 10% of Al_2O_3 offers a better surface finish; it increases with increase in weight percentage of the particle [3]. The investigation on the mechanical properties and machinability of SiC reinforced aluminium MMC was carried out by Tamer Ozben et al., and reported that 10% of SiC offers better tensile strength. Machinability of the aforesaid material yielded higher tool wear as the SiC% is increased [4]. Further, surface was affected by feed rate and cutting speed. End milling of plain aluminium and Al/SiC was carried out with high speed steel cutter and concluded that the surface roughness is lesser in pure aluminium than Al/SiC, where as plain aluminium offers lesser tool wear than Al/SiC MMC [5]. From the earlier investigations carried out by different researchers that the aluminium reinforced with 10 wt% of hard ceramic particles gives better mechanical properties, whereas increase in particle addition deteriorates the elongation and tensile strength. These MMCs are fabricated by stir casting method and the samples prepared are used for characterization and EDM studies.

Based on the literatures from the previous research, it is observed that aluminium MMCs are difficult to be machined by these traditional machining techniques. Nontraditional machining techniques such as water jet machining, laser machining and wire EDM can be applied but these processes are mainly limited to linear cutting [6]. Laser cutting and abrasive water jet machining had been used for machining aluminium and MMCs and found suitable for rough cutting applications [7].

Since the cost for using laser machining is generally prohibitive and EDM wire-cut process is not appropriate for a metal matrix composite workpiece due to excessive breakage of the electrode wire, sinking EDM becomes an optimal choice for the machining of aluminium MMCs composite owing to its easy control in operation and precise criterion of high complex-shape components [6].

MACHINING OF NEWER MATERIALS

EDM of Die Steels

In EDM process the performance is determined by material removal rate (MRR), electrode wear (EW), surface roughness (SR), surface quality (SQ) and dimensional accuracy (DA). Ho and Newman (2003) reported that research areas in EDM could be classified into three major categories: (i) machining performance measures, (ii) the effect of process parameters and (iii) design and manufacture of electrode. They also concluded that machining performance depends on the wear and surface quality. A series of investigations have been conducted by Soni and Chakraverthi [8]. They studied the surface quality, material removal rate, electrode wear rate, and dimensional accuracy of die steels and alloy steels in EDM. It is reported that the migration of appreciable amount of material takes place between electrode and workpiece during machining of die steel using rotating copper-tungsten electrode and the migrated element was observed in the re-solidified layer of the workpiece. Experiments which were carried out on AISI P20 tool steel as work material and copper as electrode show that the roughness of finished surface increases with an increase in the discharge voltage, pulse current, and pulse duration [9]. Marafona and Araujo investigated the influence of the hardness of the alloy steel on material removal rate and surface roughness of the work material [10].

Payal et al., investigated EN-31 tool steel with copper, brass and graphite as tool electrodes and reported that the debris removed from the workpiece as ligaments and sheets and in some cases it is removed as chunks. All the three specimens machined by different electrodes showed different pattern of heat affected zones, in which graphite has a deeper heat affected zone than that of brass and copper [11]. Gopalakannan and Senthilvelan investigated on the effect of electrode materials on EDM of 316L and 17-4PH stainless steel and concluded that copper electrode offers higher MRR and lower surface roughness than copper tungsten and graphite electrode [12].

Zarepour et al., conducted experiments on EDM of DIN 1.2714 hot work tool steel and reported that pulse on time and pulse current were found to have significant effect on electrode wear [13]. The effect of machining parameters on the surface roughness was experimentally investigated and found that surface roughness had an increasing trend with an increase in the discharge duration [14].

A study of electrode wear on machining of 2080 die steel with central hole on the cylindrical copper electrode revealed that the inner and outer edge radii were found to be increasing with pulse time, discharge current and dielectric fluid pressure [15]. Kang and Kim studied the EDM characteristics of nickel based heat resistant alloys and reported that MRR and EWR behaved non-linearly with respect to the pulse duration [16]. Chattopadhyay et al., investigated the machining characteristics of EN-8 steel with copper electrode in rotary EDM and found that electrode rotation significantly improved the surface quality [17]. The investigation of super alloy was carried out by Hewidy et al., and observed that MRR was more influenced by peak current, duty factor and electrode rotation whereas surface roughness was strongly influenced only by peak current and duty factor [18].

EDM of Metal Matrix Composites

To exploit the potential industrial applications and investigate proper manufacturing processes, machinability of electrical discharge machining of MMC needs to be studied for reliable and economical production [19]. Hocheng et al., presented the correlation between the major machining parameters, electrical current and on-time, and crater size on machining Al/SiC and concluded that the crater size of Al/SiC was larger than steel, and for effective EDM large electrical current and short on time were recommended [20]. A study on the feasibility of using EDM process for machining cast Al/SiC MMC were carried out and found that the SiC particles shield and protect the aluminium matrix from being vaporized, thus reduced the MRR. The un-melted SiC particles dropout from the MMC together with surrounding molten aluminium droplets, and the power levels such as voltage and current dominate all other factors and greatly affect the MRR and surface finish [21].

Ramulu and Taya investigated machinability of 15 vol.% and 25 vol.% SiC whisker/2124 aluminum matrix (SiC_w/ Al) composites and observed that machining time was higher for 25 vol.% SiC_w/Al than that of 15% SiC_w/Al composite [22]. Muller and Monaghan studied the electro-erosion characteristic of SiC/Al and found that the Al matrix surrounding the reinforcing particles was melted. The SiC particles were then dislodged from the matrix and flushed away by the dielectric fluid [7].

Karthikeyan et al., worked on mathematical modeling for EDM of Al/SiC particulate composites. They investigated the effects of the percent volume of SiC, current and pulse duration on the MRR, TWR, and SR [23]. The analysis of the experimental observations showed that the above-mentioned performance measures were greatly influenced by the percent volume of SiC present in material, current, and pulse duration. Mohan et al., evaluated the machining feasibility of Al-20% SiC and Al-25% SiC composites and concluded that the MRR was found high with positive polarity and increased with increase in current. The increase of either the pulse duration or volume percentage of SiC results in decrease in MRR and it increases with increase in rotational speed [24]. Nevertheless the TWR decreased when volume percentage of silicon carbide particle was less where as it increased with increase in current. The study also reported that the surface roughness value decreased with decrease in pulse current and increased while the volume percentage of SiC was added more.

Narendar Singh et al., worked on Al/10%SiC_p as-cast metal matrix composites to investigate the effect of current, pulse on-time and flushing pressure on metal removal rate, tool wear rate, taper, radial overcut, and surface roughness of machined material and reported that the MRR and EWR was found to be higher for larger current and pulse on-time settings at the expense of taper, radial overcut, and surface finish [25]. Mohan et al., investigated the machining characteristics of SiC/6025 Al composite using rotary electro-discharge machining with a tube electrode [26]. The conclusions drawn are; (i) MRR and SR improve with the decrease in hole diameter but electrode wear increases. (ii) The increase in volume percentage of SiC has resulted in decrease in material removal rate, surface roughness, and increase in electrode wear. (iii) The increase in rotational speed of the tube electrode has produced higher material removal rate, electrode wear, and better surface quality.

Sushant Dhar et al., worked on mathematical modeling of cast Al-4Cu-6Si alloy-10 wt% SiC_p composites. The objective of the work was to evaluate the effect of current, pulse on-time and air gap voltage on material removal rate, tool wear rate, and radial overcut [27]. The mathematical model developed can be used to predict the optimal conditions suitable for machining of the work samples. Linear programming was used to find the optimum conditions for maximum MRR with reduced TWR and radial overcut. All the three performance measures increased significantly in a nonlinear trend with increase in current. The material removal rate and radial over cut were found to increase with increase in pulse duration. The effect of gap voltage was found to have little, but it had considerable effect on the three responses.

Akshay Dvivedi et al., investigated the machinability of Al 6063 SiC_p metal matrix composite and obtained optimal setting of process parameters and concluded that the increase in electrical parameters beyond optimum setting resulted not only in a decrease in MRR but also increased TWR with dimensional inaccuracy. Also, it was found that high value of pulse current, pulse-on time, and pulse offsetting resulted in maximum MRR within selected range of process parameters [28].

Wang and Yan studied the machining characteristics of Al_2O_3/6061Al composite using rotary electro-discharge machining with a tube electrode. They reported that the machining process of the Al_2O_3/6061 Al composite by EDM-drilling was feasible in comparison to other machining processes. The observed value of MRR and tool wear rate with rotating hollow tube electrode was found higher than that of solid electrode. The overall advantage still makes this revised technology an acceptable tool. The peak current and volume fraction significantly affect the MRR, TWR and SR. In contrast, the rotating speed and flushing pressure of the electrode have minor effects on the same performance measures [29].

Yan and Wang worked on optimization of the blind-hole drilling of Al_2O_3/6061Al composite using rotary electro-discharging machining by adopting Taguchi methodology for experimental design. The blind-hole drilling with a rotational eccentric through-hole electrode results in higher MRR and electrode wear [30]. Even though the tool wear rate is high, the overall performance of this new EDM blind-hole drilling is widely accepted [31]. The electrical parameters much significantly influence the machining process than the non-electrical parameters. The polarity of the electrode largely affects either the MRR or the SR, whereas the peak current mainly influences the electrode wear.

EDM of Ceramic Composites

The effect of the machining parameters on material removal rate, relative wear ratio, and surface roughness in EDM of tungsten carbide have been studied by Lee and Li [32]. They reported that the copper electrode exhibits the best performance with regard to surface finish and copper tungsten yields a low electrode wear. They also investigated the surface integrity of tungsten carbide and reported that the depth of the damaged layer, width and number of micro cracks increased with increase in pulse current and pulse duration. The effect of machining parameters on material removal rate, electrode wear rate, surface quality and diametric over-cut on tool steels were investigated in detail and concluded that copper and graphite electrode yielded in the best machining rate. Mohd Abbas et al., presented the current research trends on machining and modeling techniques in predicting EDM performances [33].

Luis et al., reported that the material removal rate and electrode wear in die sinking EDM of silicon carbide and conductive ceramics using copper electrode by applying design of experiments [34]. While studying the machining characteristics of tungsten carbide-cobalt (WC-Co) composite and ceramics by EDM process, it is observed that increasing the pulse on time enhances the machining instability which has significant effect on the surface finish of the workpiece [35]. The EDM of carbon-carbon composites were investigated by applying Taguchi method, and concluded that lowest values of input parameters reduced the electrode wear drastically, whereas the MRR had increased substantially [36].

Electrode Material and Die-Electric Fluid

Electrode wear takes place during EDM operation when the electrode gets eroded due to the sparking action. The rate of electrode wear is considerably lesser than that of work material. The high electrode wear rate is one of the major problems in EDM. High electrode wear results in result in inaccurate dimension. Due to these reasons, suitable combination of work material and electrode materials has been studied by previous researchers. Therefore selection of suitable electrode material, shape and size are found to be a paramount factor. Brass, copper, copper-tungsten and graphite are the widely used electrode materials. In order to find a suitable electrode material, Singh et al., investigated the EDM of EN-31 tool steel with various electrode materials like, copper, copper-tungsten, brass and aluminium, and concluded that copper is found to a better electrode material and offers better surface finish, high MRR, low diameteral overcut and less electrode wear. The copper electrode offers less electrode wear while comparing to brass on machining of aluminium and mild steel [37].

Wear of copper electrode was studied by applying Taguchi's standard orthogonal array in die-sinking EDM of tool steel used in moulds and dies [17]. Muttamara et al., investigated the effect of electrode polarities in copper, graphite and copper-infiltrated graphite electrodes while generating the conductive layer formation in EDM of alumina [38]. Jahan et al., experimented micro-EDM of tungsten carbide using different electrode materials of tungsten, copper tungsten and silver tungsten and reported that silver tungsten electrodes are capable of producing smooth and shiny surfaces with lesser degree of surface defects [39].

Her and Weng compared copper and tungsten carbide electrodes on machining of copper and concluded that copper electrode provides better surface roughness and low electrode wear than tungsten carbide [40]. Che Haron et al., investigated the copper and graphite electrode performance in EDM of XW42 tool steel and observed that copper electrode offers higher MRR and lower EWR than graphite. The limitation of using graphite as electrode material is that it forms carbon from graphite, and generate a conductive layer, which affects the output characteristics [41, 42].

Lee et al., studied the relationship between electrode size and surface cracking and concluded that smaller diameter electrodes cause no crack zone, which permits wider choice of machining parameters to be adopted [43]. Sohani et al., reported that the circular electrode yields better MRR and EWR than triangular, rectangular and square shaped electrode. Hence, based on the past literatures, copper electrode of diameter 10 mm has been selected for the present work [44]. The use of kerosene as a dielectric fluid is very common in the published research. Distilled water, water solutions of sugar, glycol, glycerin and polyethylene glycol are also used as dielectric fluids. The use of kerosene gives a better MRR with higher current compared with other dielectrics. EWR increases with increasing current for kerosene while it decreases with other dielectrics. In a study, where the use of kerosene and distilled water dielectrics are compared, it is stated that the carbide formed on the work piece with the use of kerosene has a higher melting temperature than the oxide layer formed with the use of distilled water, and the carbide layer needs higher pulse energy for melting and evaporation [45]. With kerosene dielectric, the resolidified layer is thicker and the occurrence of micro cracks is reduced with the use of distilled water. Copper tools give much lower surface roughness values compared with other tool materials for kerosene [46]. Hence all the experiments were conducted with kerosene as a dielectric fluid.

Modeling and Optimization of EDM Parameters

The machining parameters are usually selected based on either the experience or proposed guidelines of the manufacturers. This selection procedure does not lead to the optimal and economically effective use of the machines and the quality of the surface generated. Sometimes, scientific methods based on Taguchi orthogonal array are used. Taguchi method can analyze and provide optimum parameter for a given set of independent parameters and a response variable [47]. Puertas and Luis investigated the EDM process by applying full factorial design of experiments combined with regression to obtain the optimum manufacturing conditions [48]. Optimization of magnetic force assisted EDM by using Taguchi method. The experimental results show that the magnetic force assisted EDM has a higher MRR, a lower EWR and a smaller SR as compared with a standard EDM [49]. Lajis et al., investigated the EDM of tungsten carbide by applying Taguchi method in order to determine the main effects, significant factors and optimum machining conditions [50]. If there are multiple response variables for the same set of independent variables, the methodology provides a different set of optimum operating conditions for each response variable. For example, in EDM optimum condition for maximizing MRR need not be the same for, minimizing EWR and SR. To obtain a solution that gives the best possible MRR at the lowest possible SR are necessary in some instances. In such circumstances, the Taguchi method may not provide appropriate solution [51].

In a complex and a multivariate system such as EDM machining, the relationships between various factors are unclear. Such systems often are called grey that give poor, incomplete, and uncertain information [52]. Theories of grey relational analysis have attracted considerable interests among the researchers. The optimization of micro EDM and micro WEDM processes based on Taguchi method with fuzzy logic and grey relational analysis were carried out and concluded that the machining performance can be improved efficiently through this approach [53]. Optimization of turning operations were investigated by adopting Taguchi based grey relational analysis in order to obtain a optimal set of parameters like cutting force, speed, feed, depth of cut towards their output characteristics of surface roughness [54]. The multi response optimization of various machining processes like drilling, sand casting, welding were successfully carried out by applying Taguchi based grey relational analysis, and the results reveal that the best combination of process parameters can obtained by this method [55].

Modeling and multi objective optimization of EDM process were carried out by using non-dominating sorting genetic algorithm, and the tested results showed that the developed model could be applied for predicting the response parameters [56]. Haddad et al., investigated the cylindrical wire electrical discharge turning using Taguchi method to determine the influence process parameters. Further, response surface methodology was used to model the influence of parameters on the machining performance [57]. Puri and Bhattacharya carried out experiments on WEDM through response surface methodology and established a mathematical model correlating the input parameters with the response [58]. George et al., conducted experiments on the basis of response surface method and developed empirical models correlating process variables and their interactions. The developed models reveal that pulse current is the most significant parameter on the response function followed by gap voltage and pulse on time [59].

In recent years, the application of both Taguchi method and response surface method have adopted for evaluation of machining performance. The experiments were planned based on Taguchi method and second order models were developed using response surface method [60]. Aman Aggarwal et al., carried out a comparative analysis of CNC turned parts using both Taguchi method and response surface method. They used four parameters at three levels and conducted 27 experiments for Taguchi method and 30 experiments for face centered central composite design of response surface method [61]. The results revealed that (i) Significance of interactions and square terms of parameters is more clearly predicted in RSM than Taguchi method. (ii) RSM technique can model the response in terms of significant parameters, their interactions and square terms, which is not provided by Taguchi method. (iii) 3D surfaces generated by RSM can help in visualizing the effect of parameters on response in the entire range specified whereas Taguchi method gives the average values of response at given level of parameters. Thus RSM can better predict the effect of parameters on response and is a better tool for optimization. Hence the face centered central composite design of RSM is used for the plan of experiments.

Desirability Function

A single response optimization algorithm provides a single optimal solution. However most of the multi response problems, in principle, give rise to a set of optimal solution instead of a single optimal solution. A single optimal solution will not serve the purpose, as these objectives are conflicting in nature; also, the choice of output depends on the user and the environment of the problem. For two or more output responses, the input parameters have been optimized simultaneously using composite desirability optimization technique. In multi response optimization, a measure of how the solution has satisfied the combined goals for all responses must be assured [62].

Derringer and Suich describe a multiple response method called desirability. It is an attractive method for industry for the optimization of multiple quality characteristic problems [63]. The method makes use of an objective function D(X), called the desirability function (utility transfer function) and transform an estimated response into a scale-free value (di) called desirability. The desirable ranges are from 0 to 4 (least to most desirable, respectively). One represents the ideal case; zero indicates one or more responses outside their acceptable limits. Composite desirability is the weighted geometric mean of the individual desirability's for the responses. The factor settings with maximum total desirability are considered to be optimal parameter conditions. The simultaneous objective function is a geometric mean of all transformed responses. The optimization is accomplished by (i) obtaining the individual desirability (d) for each response, (ii) combining the individual desirability's to obtain the combined or composite desirability (D) and (iii) maximizing the composite desirability and identifying the optimal input variable settings.

EDM Studies of Aluminium Nanocomposites

In the present study the experiments were designed on the basis of the central composite design (CCD) technique. The factorial portion of CCD is a full factorial design with all combination of the factors at two levels (high, +1, and low, -1) and composed of eight star points, and six central points (coded level 0), which is the midpoint between the high and low levels, corresponds to an α value of 1. The "face-centered CCD" involves 30 experimental observations at four independent input variables [64].

The experiments were performed on a die-sinking EDM of type Grace D-6030S, carried out for 20 minutes to acquire a more accurate result. The work materials of size 20mm diameter and 30mm thick and electrolytic copper electrode of 10mm diameter was used. The circular electrode is preferred over the other shapes of electrodes, provides higher MRR and lower EWR [65]. Commercial grade kerosene was employed as the dielectric fluid and impulse jet flushing system was used to flush away the eroded materials from the sparking zone. The material removal rate and electrode wear values have been calculated by weight difference of the workpiece and electrode material before and after the machining using a digital weighing scale of 0.001 gram precision. The average surface roughness value R_a (μm) was chosen to assess the surface finish quality. The surface roughness measurements for the machined surface were performed with a Kosaka Surfcoder SE 1200.

The machining performance criteria selected for this study were based on performance characteristics such as material removal rate (MRR), electrode wear ratio (EWR) and surface roughness (SR).

$$MRR=(w_{jb}-w_{ja})/t \qquad (1)$$

where w_{jb} and w_{ja} are weights of the work piece before and after machining, and the machining time. Electrode wear (EW) is expressed as the ratio of difference of weight of the tool electrode before and after machining to the machining time.

$$EW=(w_{eb}-w_{ea})/t \qquad (2)$$

where w_{eb} and w_{ea} are weights of the tool electrode before and after machining, and the machining time.

RESULTS AND DISCUSSION

The selected process parameters were varied up to three levels and face centered central composite design was adopted to design the experiments. Response Surface Methodology was used to develop the second order regression equation relating response characteristics and process variables.

Table 1. Machining parameters with their levels

Parameters	Labels	Levels		
		-1	0	+1
Voltage(V) volt	A	40	50	60
Pulse current(I_p) Amps	B	6	10	14
Pulse on time(T_{on}) µs	C	4	6	8
Pulse off time(T_{off})µs	D	5	7	9

Table 2. Design layout and experimental results

Exp. No	Voltage	Current	T_{on}	T_{off}	MRR (g/min)	EWR (g/min)	SR (µm)
1	40	6	4	9	0.016	0.001	3.012
2	60	6	8	9	0.092	0.004	5.326
3	50	10	4	7	0.115	0.006	6.325
4	50	10	6	7	0.285	0.009	9.425
5	50	6	6	7	0.128	0.005	4.321
6	60	14	4	5	0.256	0.007	7.802
7	40	14	8	9	0.613	0.015	11.438
8	40	6	8	9	0.087	0.003	3.986
9	50	10	6	9	0.274	0.008	7.247
10	40	6	4	5	0.071	0.003	4.025
11	60	10	6	7	0.403	0.011	16.852
12	60	6	8	9	0.591	0.013	18.982
13	50	10	6	7	0.284	0.007	6.245
14	50	10	8	7	0.427	0.010	3.124
15	40	14	4	9	0.101	0.002	4.038
16	50	10	6	7	0.281	0.006	6.546
17	50	10	6	7	0.286	0.008	9.891
18	60	6	4	9	0.0197	0.001	3.281
19	60	14	8	5	0.626	0.016	19.235
20	60	6	4	5	0.071	0.002	3.854
21	40	14	8	5	0.65	0.018	21.085
22	60	14	4	9	0.077	0.003	4.826
23	50	14	6	7	0.518	0.012	14.892
24	50	10	6	7	0.28	0.007	8.643
25	60	6	8	5	0.139	0.004	6.128
26	50	10	6	7	0.288	0.009	10.819
27	40	14	4	5	0.299	0.008	9.218
28	40	6	8	5	0.146	0.005	6.918
29	50	10	6	5	0.474	0.012	16.21
30	40	10	6	7	0.367	0.009	10.025

The Table 1 shows both coded and actual values of the four machining parameters and their possible ranges. The experimental matrix that was adopted in this study in the coded form is shown in Table 2. Altogether 30 experiments were conducted for nano composites using response surface methodology.

Mathematical Model for MRR, EWR and SR

The fit summary recommended that the quadratic model is statistically significant for analysis of MRR and SR and linear model for EWR. The results quadratic and linear models are given in ANOVA Table 3. The model F value implies that the model is significant. The values of "Probability greater than F" in Table 3 for the term of models are less than 0.05 (i.e., α=0.05, or 95% confidence) indicates that the obtained models are considered to be statistically significant, which is desirable as it demonstrates that the terms in the model have a significant on the responses [66].

Table 3. The ANOVA table for the fitted models

a) For MRR

Sourse	SS	df	MS	F-value	Prob>F	
Model	1.03	14	0.073	30.83	< 0.0001	Significant
Residual	0.36	15	2.38E-003			
Lack of Fit	*0. 36*	*10*	3.53E-003	9345.72	*0.32485*	Not significant
Pure Error	*4.60E-005*	*5*	9.200*E-006*			
Cor Total	1.06	29				
Std. Dev.	0.049			R-Squared	0.9664	
Mean	0.280			Adj R-Squared	0.9351	
C.V. %	17.15			Pred R-Squared	0.8601	
Predicted residual error of sum of squares (PRESS) =0.15				AdeqPrecision	20.320	

b) For EWR

Sourse	SS	df	MS	F-value	Prob>F	
Model	5.533E-004	14	3.973E-005	19.68	< 0.0001	Significant
Residu al	3.0134E-005	15	2.009E-006			
Lack of Fit	*2.274E-005*	*10*	*2.279E-006*	1.55	0.3272	Not significant
Pure Error	*7.333E-005*	5	1.467E-006			
Cor Total	5.835E-004	29				
Std. Dev.	1.417E-003			R-Squared	0.9484	
Mean	7.467E-003			Adj R-Squared	0.9002	
C.V.	%18.98			Pred R-Squared	0.8309	
Predicted residual error of sum of squares (PRESS)	9.8640E-005			Adeq Precision	17.560	

c) For SR

Sourse	SS	df	MS	F-value	Prob>F	
Model	684.47	14	48.89	48.89	< 0.0006	Significant
Residual	119.22	15	7.95			
Lack of Fit	102.18	*10*	10.22	3.00	0.1186	Not significant
Pure Error	17.04	*5*	3.41			
Cor Total	803.69	29				
Std. Dev.	2.82			R-Squared	0.9517	
Mean	8.79			Adj R-Squared	0.8132	
C.V.	%32.07			Pred R-Squared	0.7658	
Predicted residual error of sum of squares (PRESS)	69.03			Adeq Precision	9.808	

When the multiple regression co efficient R^2 approaches unity, the better the response model fits the actual data. It exists the less the difference between the predicted and actual data.

Further the value of adequate precision (AP) in this model, which compares the range of the predicted value at the design point to the average prediction error, is well above 4. The value of the ratio is greater than 4, which presents the adequate model discrimination. These models obtained present higher values of the determination coefficients (R^2) and adequate precision (AP) at the same time. The values were obtained as follows: R^2 = 0.9664and AP= 20.320 for MRR; R^2 = 0.9484 and AP= 17.560 for EWR; R^2 = 0.9517 and AP= 9.808 for SR. Consequently, these obtained mathematical models of MRR, EWR and SR can be regard as significant effect for fitting and predicting the experimental results and the meantime the test of Lack-of-fit also displays to be insignificant. The backward elimination process eliminates the insignificant terms to adjust the fitted quadratic models. These insignificant model terms can be removed and the test of lack of fit displays to be insignificant as it is desired. Through the backward elimination process, the final quadratic models of response equations are presented in Eq.4-Eq.6 given below.

This model can be used to navigate the design space as the adequate precision ratio indicates an adequate signal. The final response equations for MRR, EWR and SR are:

Material removal rate:

$$MRR = +0.32+0.16*B+0.13*C-0.048*D+0.092*B*C-0.078*C^2 \tag{3}$$

Electrode wear rate:

$$EWR = +8.583E-003+3.667E-003*B+3.056E-003*C-1.389E-003*D+2.062E-003*B*C-6.875E-004*B*D-1.861E-003*C^2 \tag{4}$$

Surface roughness:

$$SR = +9.46+3.93*B+2.77*C-1.80*D+2.29*B*C+3.80*A^2-4.91*C^2 \tag{5}$$

The Effect of Process Parameters on Material Removal Rate

Figure 1 shows the estimated response surface for MRR in relation to the design parameters of voltage, pulse current, pulse on time and pulse off time. The higher discharge energy normally requires higher pulse current and higher voltage that erodes the material. This higher discharge energy erodes the surrounding aluminium which melts loosens the bonded B_4C particles.

These particles were easily expelled from the machined cavity [65]. However the cavity depth increases, the debris and unbonded B_4C normally became harder to expel from the machining zone, requires larger duration of pulse off time shown in Figure 1. Shorter pulse off time reduces the debris removal time, hence the debris disturbs the electrical discharge and causes short-circuit, results in low MRR. Therefore the optimal values of process parameters are necessary to achieve maximum MRR.

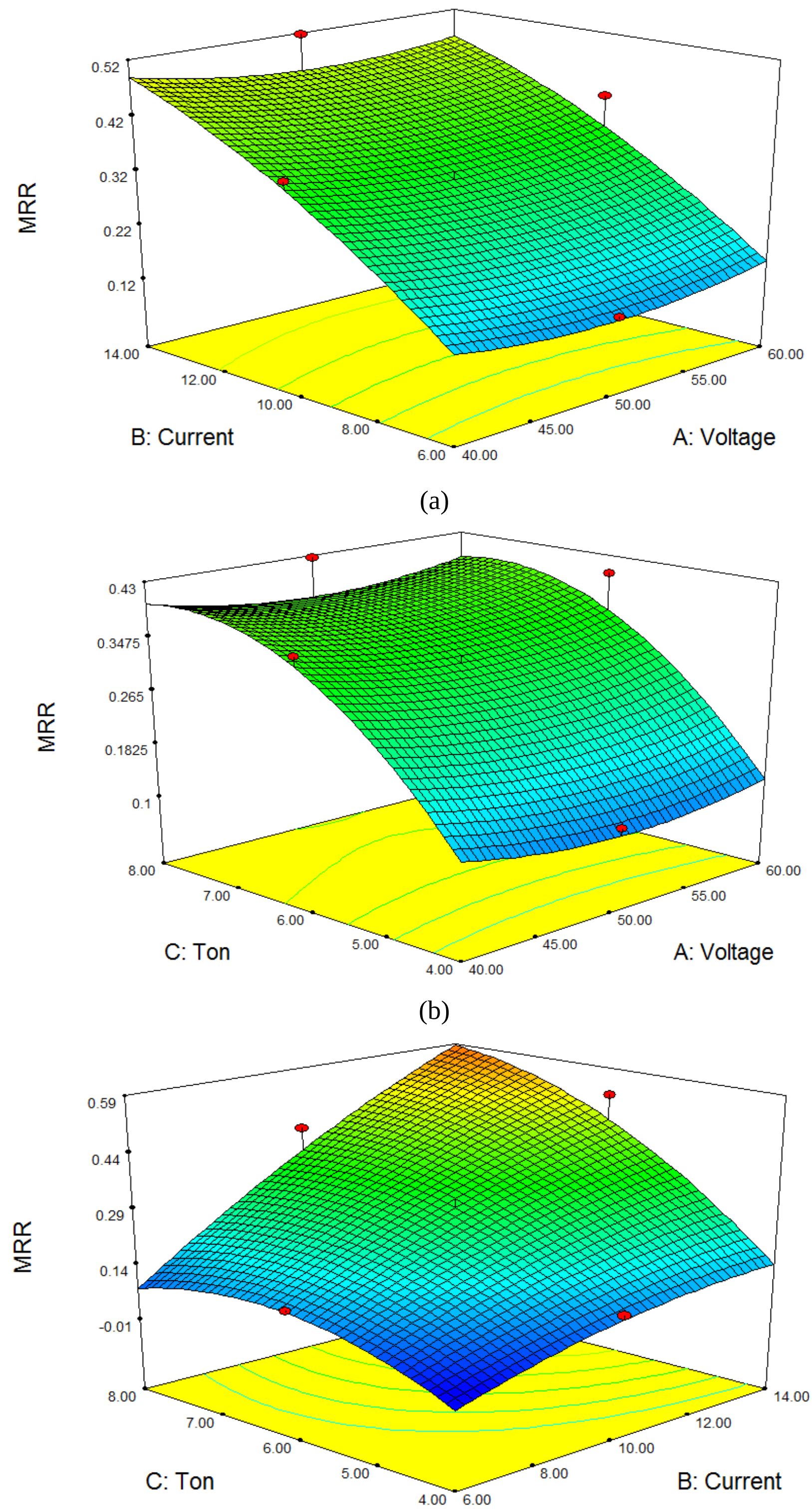

(a)

(b)

(c)

Figure 1. (a), (b) and (c) shows the response graph of MRR of Al 7075+1.5 wt% B_4C.

The Effect of Process Parameters on Electrode Wear Rate

During erosion of the electrode, the cracked carbon from the dielectric fluid may be deposited on the surface of tool electrode, which protects them from further erosion. Generally longer pulse duration, lower pulse current and shorter pulse off time tends to increase the possibility of carbon deposition on the electrode surface, which helps to minimize the electrode wear. The electrode wear is low at smaller current and hence shorter pulse off time is sufficient for the dielectric to restore its dielectric properties with minimum thermal loss [67]. As the eroded cavity was shallower, the debris can be easily flushed away from the machined zone and the same is reflected in the Figure 2. The estimated response surface for EWR in relation to the design parameters of pulse current, pulse on time and pulse off time is shown in Figure 2. As can be seen from the Figure 2(a), the EWR increases considerably with increase in pulse current and pulse on time. The EWR is more at higher value of Ton and T off, whereas the EWR increases with respect to pulse current.

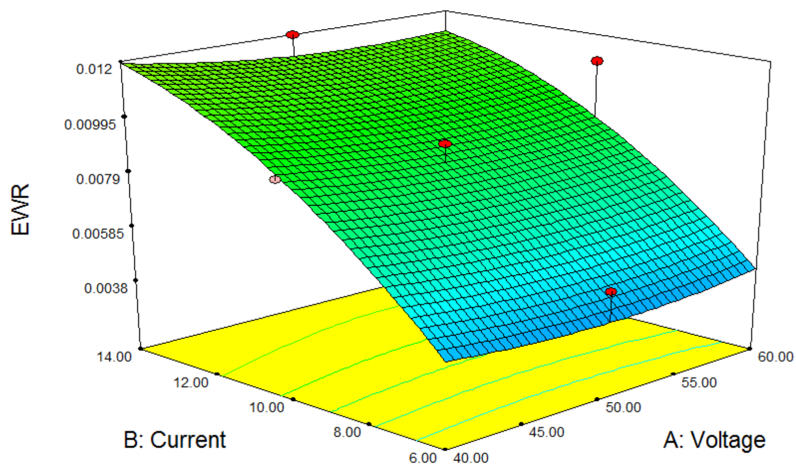

(a)

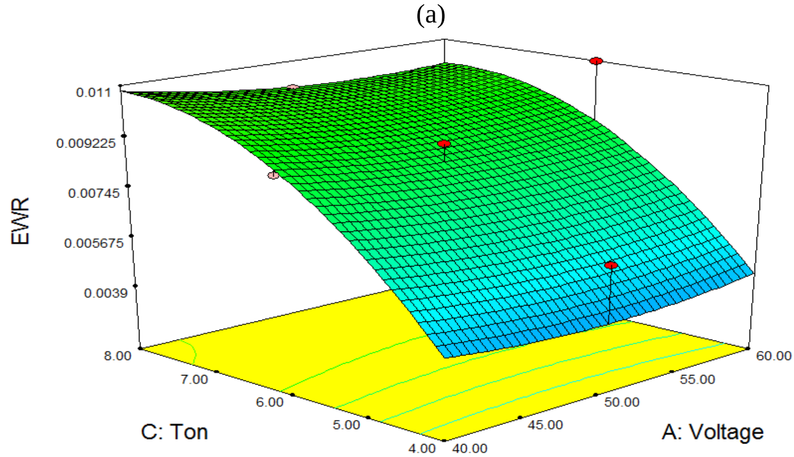

(b)

Figure 2. (Continued).

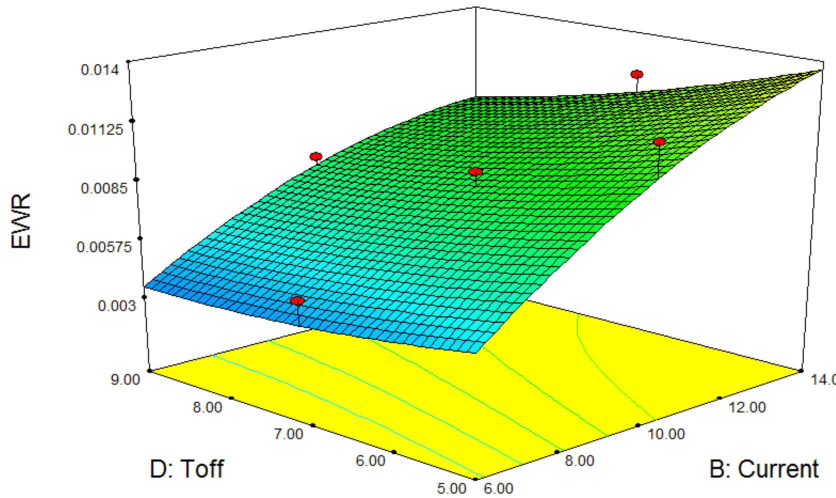

(c)

Figure 2. (a), (b) and (c) shows the response graph of EWR of Al 7075+1.5 wt% B_4C.

The Effect of Process Parameters on Surface Roughness

The effect of the various process parameters on the surface roughness investigated though the response surface methodology. Figure 3 shows the response graphs of the most influencing parameters pulse current, pulse on time and pulse off time. When any one of this parameter is increased, it enhances the surface roughness value. The variation of the surface roughness with pulse current is similar for different pulse on time. The higher the input power associated with increase in pulse current causes more frequent cracking of dielectrics leading to more frequent melt and expulsion [68]. This in turn gives higher density debris, which contains hard B_4C particles accumulated on the machining zone results in poor surface finish. The estimated response surface for SR in relation to the design parameters of pulse current and voltage is shown in Figure 3(a), pulse current and pulse on time in Figure 3(b), pulse off time and pulse current in Figure 3(c). Thus longer pulse off time enable the dielectric to flush away the debris and yields better surface finish.

Multi Response Optimization

Selection of the optimal machining parameter combination for achieving improved process performance, e.g., material removal rate, electrode wear rate and surface roughness, is a challenging task in EDM operation due to the presence of a large number of process variables and complicated stochastic process mechanism. Derringer and Suich describes a multiple response method called desirability. This method makes use of an objective function D (X), called the desirability function (Utility transfer function) and transform an estimated response into a scale-free value (di) called desirability [64]. The desirable range is from 0 to 1 (least to most desirable, respectively). A value of 1 represents the ideal case; 0 indicates that one or more responses are outside their acceptable limits.

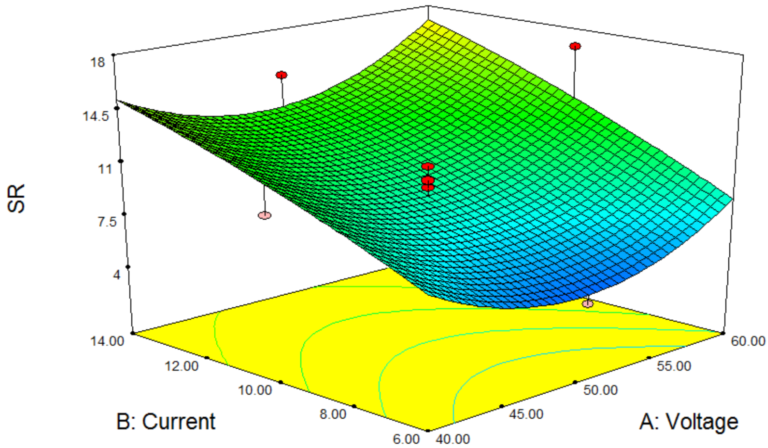

(a)

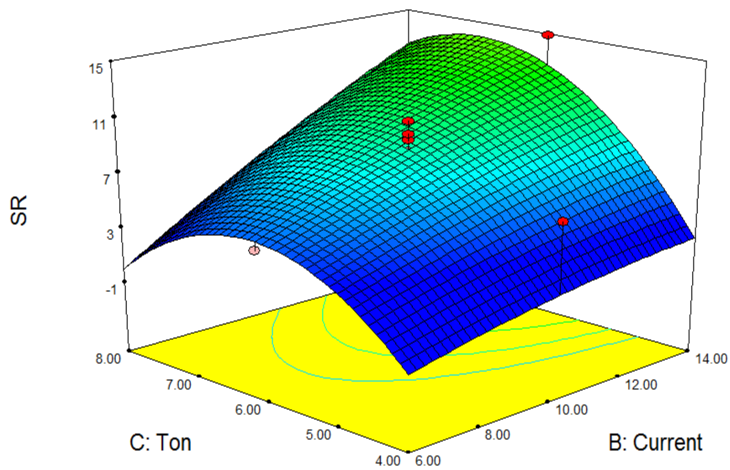

(b)

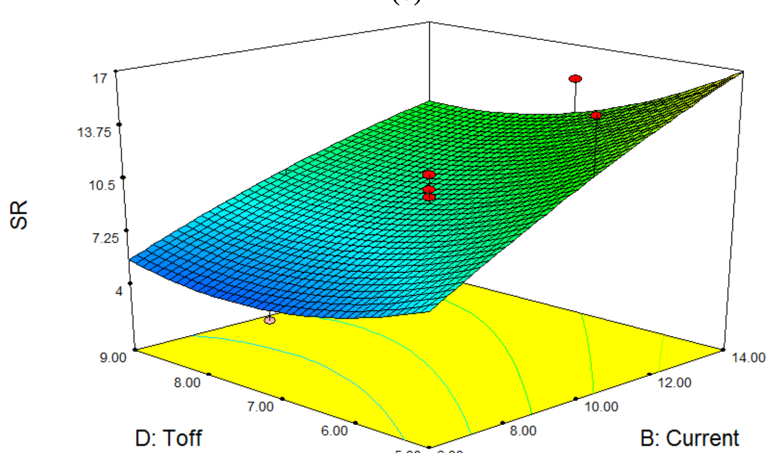

(c)

Figure 3. (a), (b) and (c) shows the response graph of SR of Al 7075+1.5 wt% B_4C.

Table 4. Range of input parameters and responses for desirability

Process Parameter	Goal	Lower Limit	Upper Limit	Lower Weight	Upper Weight	Importance
Voltage	In range	40	60	1	1	3
Current	In range	6	14	1	1	3
Pulse on time	In range	4	8	1	1	3
Pulse off time	In range	5	9	1	1	3
MRR	Maximize	0.016	0.65	1	1	3
EWR	Minimize	0.001	0.018	1	1	3
SR	Minimize	3.012	21.085	1	1	3

The factor settings with maximum total desirability are considered to be the optimal parameter conditions. The simultaneous objective function is a geometric mean of all transformed responses. This combination has been evaluated with the help of Design Expert Software. Three responses i.e., MRR, EWR, and SR, have been optimized simultaneously using developed models, based on composite desirability optimization technique. The optimality solution is to evaluate the input process parameters in experiment range for maximizing MRR and minimizing both EWR and SR. The range and goals of input parameters and the output characteristics are given in Table 4. The goal of optimization is to find a set of conditions that will meet all the goals. It is not necessary that the desirability value is 1.0 as the value is completely dependent on how closely the lower and upper limits are set relative to the actual optimum.

Table 5. Input parameters and optimum values of Al+1.5wt% B_4C MMNC

Parameter	Goal	Optimum value
Voltage [V]	In range	46.13
Pulse Current [A]	In range	9.06
Pulse on time [µs]	In range	8.00
Pulse off time [µs]	In range	8.75

Table 6. Predicted and observed values of responses of Al+1.5wt% B_4C MMNC

Response	Goal	Predicted	Observed	Error [%]
MRR [g/min]	Maximize	0.3178	0.3263	2.7
EWR [g/min]	Minimize	0.0085	0.009	5.88
SR [µm]	Minimize	4.199	4.029	-4.12

A set of 22 optimal solutions is derived for the specific design space constraints for MRR, EWR and SR. The set of conditions possessing highest desirability value is selected as optimum condition for the desired responses [62-66]. The optimal set of conditions with higher desirability function is given in Table 5. The confirmation experiments were performed to verify the optimal input parameter settings for MRR, EWR and SR, and compared with optimal response value. Table 6 shows the percentage of error for experimental validation of the developed models for the responses with optimal parametric setting during EDM. From the analysis of Table 6, it can be observed that the error calculated is small. Obviously, the result confirms excellent reproducibility of the experiment conclusions.

The ramp function graph and bar graph Figure 4 and Figure 5 show the desirability for output responses. The dot on each ramp reflects the factor setting or response prediction for that response characteristic. The height of the dot shows how much desirable it is. A linear ramp function is created between low value and the goal or the high value and the goal as the weight for each parameter was set equal to one. Bar graph shows the overall desirability function of the responses. Desirability varies from 0 to 1 depending upon the closeness of the response towards target. The bar graph describes how well each variable satisfies the criterion, value close to one are considered good.

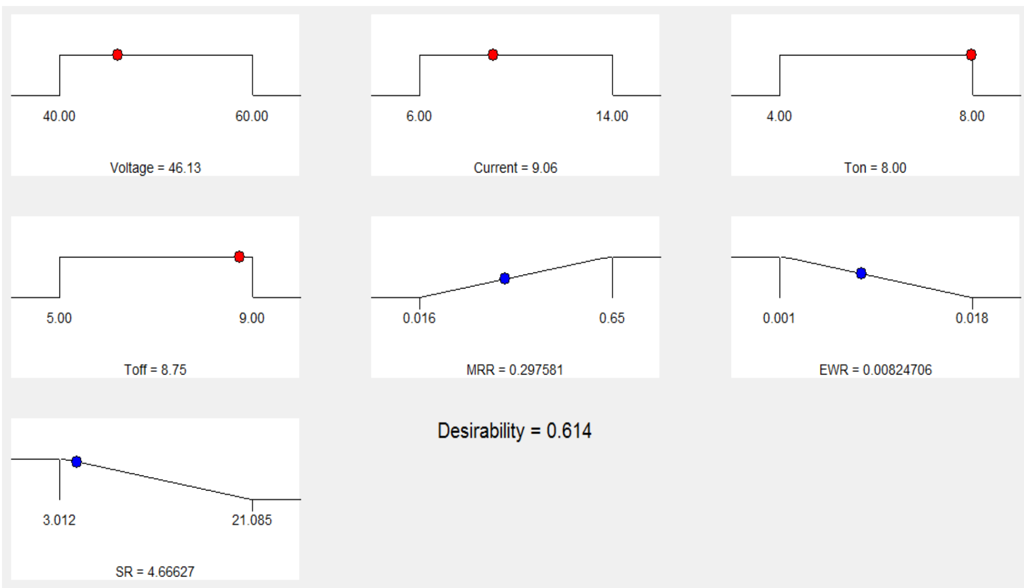

Figure 4. Ramp function graph of Desirability for Al+1.5wt% B_4C MMNC.

Desirability 3D-plots were drawn by keeping the input parameters in range and output response MRR at maximum, EWR at minimum and SR at minimum. Figure 6 shows a plot of desirability function distribution of desired responses of Al+1.5wt% B_4C MMNC according to current and voltage. It can be interpreted that overall desirability value is less in the region of high pulse current and voltage. The near optimal region was located at the left top region of the plot, which had overall desirability value greater than 0.614 that gradually reduced while moving right and backwards. Hence the interpreted desirability of 0.614 which indicates the closeness of the response target.

In order to observe the better resolution of the finished surface, the sample of the confirmation experiments were investigated for SEM and AFM analysis shown in Figure 7 and Figure 8 respectively. It is evident that the effect of pulse current and pulse on time has a direct relationship with the length of micro cracks. At low values of pulse current and pulse on time reduces the length and number of micro cracks. From the SEM micrograph it was clear that there are very few EDM damaged layer and less micro cracks on the machined surface [69, 70].

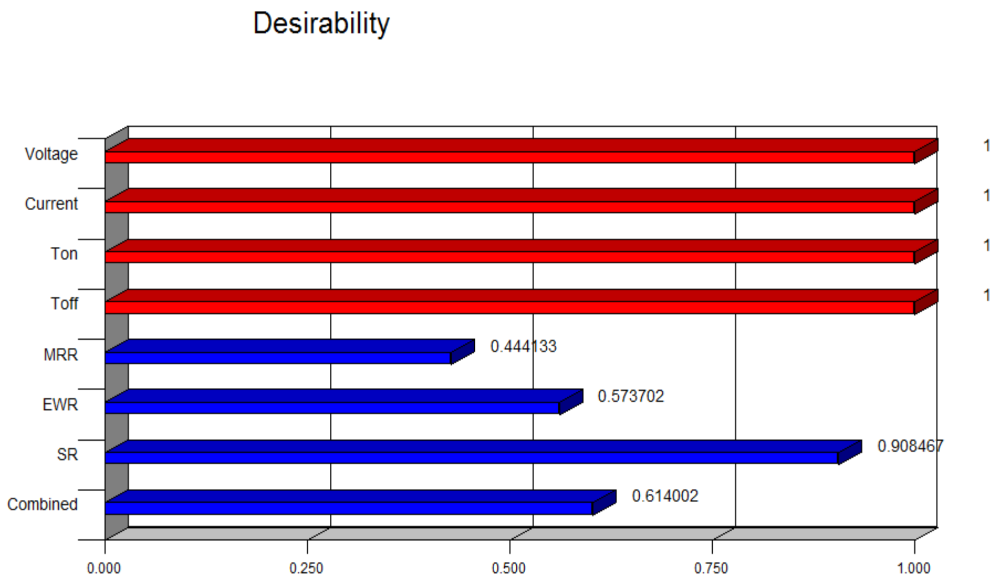

Figure 5. Bar graph of Desirability of Al+1.5wt% B_4C MMNC.

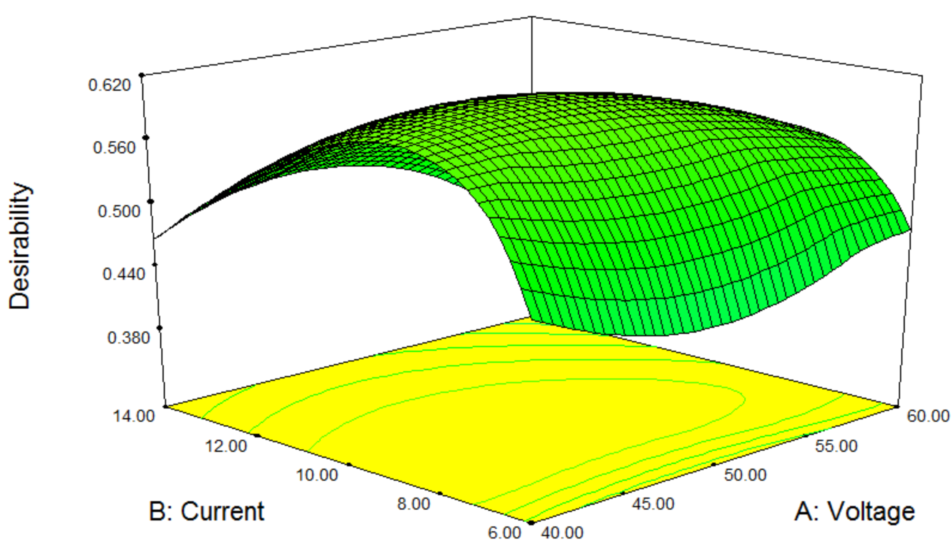

Figure 6. 3D response graph of Desirability of Al+1.5wt% B_4C MMNC.

The workpiece surface texture at low pulse current and pulse off time, the craters are shallow and pockmarks is also low whereas at higher pulse current and pulse duration the craters are deeper. The Figure 8 shows 3D surface texture showing lower crater height of the machined surfaces results in lower surface roughness value, which is, reflected in the surface texture AFM image [71].

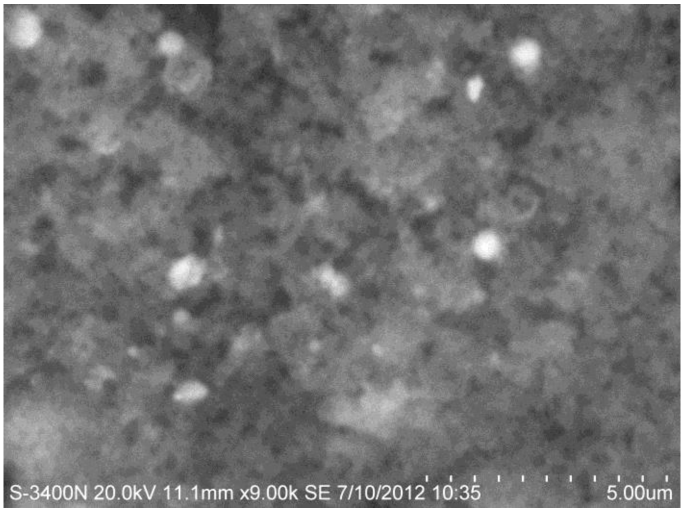

Figure 7. SEM image of the EDMed surface of Al+1.5wt% B_4C MMNC.

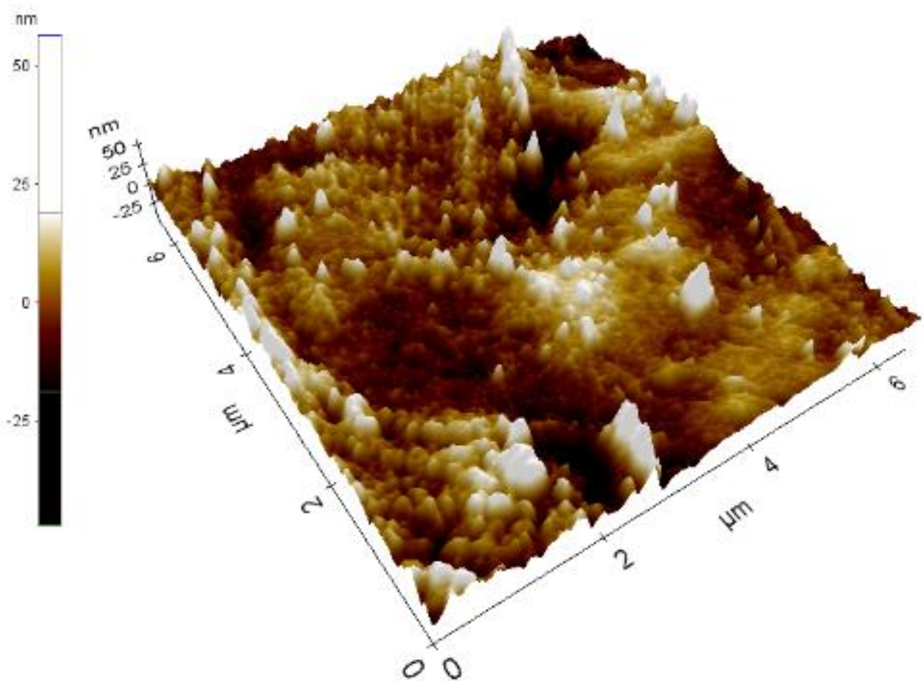

Figure 8. AFM image of the EDMed surface of Al+1.5wt% B_4C MMNC.

CONCLUSION

In this study, the MRR, EWR and SR in EDM process of Al+1.5wt% B_4C MMNC using copper electrode were modeled, analyzed and optimized through RSM. Summarizing the main features, the following conclusions could be drawn:

1. The predicted values concur well with the experimental values reasonably and also R^2 of MRR, EWR and SR of the MMCs.
2. Mathematical models were developed in the form of multiple regression equations calculating with dependent parameters with independent parameters and compared with the experimental results.
3. Pulse current was found to be the most significant factor that affects all the three output parameters viz., MRR, EWR and SR of the three MMCs.
4. The important factors that affect the MRR are pulse current, pulse on time and pulse off time whereas voltage remains less significant. The pulse current and pulse on time have statistical significance on both EWR and SR.
5. The effect of pulse on time is insignificant on EWR but strongly influences SR. Hence to achieve better surface finish low value of pulse on time is recommended.
6. The optimum parameter of combination for Al+1.5wt% B_4C obtained using desirability function approach are Voltage 46.00 V, Pulse current 9.00 A, Pulse on time 8.00μs and pulse off time 5.00μs for maximizing MRR, minimizing EWR and SR. The results of confirmation experiment agree well with the predicted optimal settings.

The research findings along with developed mathematical models and multi response optimization will provide effective guidelines and the results would be a good technical database for the aerospace, automobile and military applications in fabrication and machining aspects.

REFERENCES

[1] Hung, N.P., Boey, F.Y.C., Khor, K.A., Oh, C.A., Lee, H.F., (1995). Machinability of cast and powder formed aluminium alloys reinforced with SiC particles. *Journal of Material Processing Technology* 48, 291-297.

[2] Kannan, S., Kishawy, H.A., Deiab, I.M., Surappa, M.K., (2006). On the Role of Reinforcements on Tool Performance during Cutting Metal Matrix Composites. *Journal of Manufacturing Processes* 8(2), 67-75.

[3] Sahin, Y., Kok, M., Celik, M. (2002). Tool Wear and Surface Roughness of Al_2O_3 particle reinfprced aluminium alloy composites. *Journal of Material Processing Technology* 128, 280-291.

[4] Ozben, T., Kilickap, E., Cakir, O., (2008). Investigation of mechanical and machinability properties of SiC particle reinforced Al-MMC. *Journal of Material Processing Technology* 198, 220-225.

[5] Sornakumar, T., Kathiresan, M., (2010). Machining studies of die cast aluminium alloy-silicon carbide Composites. *Journal of Minerals Metallurgy and Materials* 17, 648-653.

[6] Muller, F., Monaghan, J., (2000). Non–conventional machining of particle reinforced metal matrix composites. *International Journal of Machine Tools and Manufacture* 40, 1351-1366.

[7] John Rozario Jegaraj, J., Ramesh Babu, N., (2007). A soft computing approach for controlling the quality of cut with abrasive water jet cutting system experiencing orifice and focusing tube wear. *Journal of Material Processing Technology* 198, 220-225.

[8] Soni, J.S., Chakraverti, G., (1995). Effect of electrode material properties on surface roughness and dimensional accuracy in electric-discharge machining of high carbon high chromium die steel. *Journal of Industrial Engineering* 76, 46-51.

[9] Kiyak, M., Cakir, O., (2007). Examination of machining parameters on surface roughness in EDM of tool steel. *Journal of Material Processing Technology* 191, 141-144.

[10] Marafona, J.D., Araujo, A., (2009). Influence of workpiece hardness on EDM performance. *International Journal of Machine Tools and Manufacture* 49, 744-748.

[11] Payal, H.S., Choudhry, R., Singh, S., (2008). Analysis of electro discharge machined surfaces of EN-31 tool steel. *Journal of Scientific and Industrial Research* 67, 1072-1077.

[12] Gopalakannan, S., Senthilvelan, T., (2012). Effect of electrode materials on electric discharge machining of 316L and 17-PH stainless steels. *Journal of Minerals and Materials Characterization and Engineering* 11, 685-690.

[13] Zarepour, H., Tehrani. A.F., Karimi, D., Amini, S., (2007). Statistical Analysis of Electrode Wear in EDM of Tool Steel DIN 1.2714 used in forging dies. *Journal of Material Processing Technology* 187-188, 711-714.

[14] Keskin, Y., Halkaci, H.S., Kizil, M., (2006). An experimental study for determination of the effects of machining parameters on surface roughness in electrical discharge machining (EDM). *International Journal of Advanced Manufacturing Technology* 18, 1118-1121.

[15] Cogun, C., Akaslan, S., (2002). The effect of machining parameters on tool electrode edge wear and machining performance in electrical discharge machining (EDM). *Korean Society of Mechanical Engineering International Journal* (16)1, 46-50.

[16] Kang, S.H., Kim, D.E., (2003). Investigation of EDM characteristics of nickel-based heat resistant alloy. *Korean Society of Mechanical Engineering International Journal* 17(10), 1475-1484.

[17] Chattopadhyay, K.D., Verma, S., Satsangi, P.S., Sharma, P.C., (2009). Development of empirical model for different process parameters during rotary electrical discharge machining of copper- steel (EN-8) system. *Journal of Material Processing Technology* 209, 1454-1465.

[18] Hewidy, M.S., El-Taweel, T.A., El-Safty, M.F., (2005). Modelling and machining parameters of wire electrical discharge machining of Inconel 600 using RSM. *Journal of Material Processing Technology* 169, 328-336.

[19] Lau, W.S., Yue, T.M., Lee, T.C., Lee, W.B., (1995). Un-conventional machining of composite materials. *Journal of Material Processing Technology* 48, 199-205.

[20] Hocheng, H., Lei, W.T., Hsu, H.S., (1997). Preliminary study of material removal in electrical discharge machining of SiC/Al. *Journal of Material Processing Technology* 63, 813-818.

[21] Hung, N.P., Yang, L.J., Leong, K.W., (1994). Electric discharge machining of cast metal matrix composites. *Journal of Material Processing Technology* 44, 229-236.

[22] Ramulu, M., Taya, M., (1995). EDM machining of SiC_w/Al composite. *Journal of Material Science* 24, 1103-1108.

[23] Karthikeyan, R., Lakshmi Narayanan, P.R., Nagarazan, R.S., (1999). Mathematical modelling of electric discharge machining of aluminium-silicon carbide particulate composites. *Journal of Material Processing Technology* 87, 59-63.

[24] Mohan, B., Rajadurai, A., Satyanarayana, K.G., (2004). Electric discharge machining of Al-SiC metal matrix composites using rotary tube electrode. *Journal of Material Processing Technology* 153-154, 978-985.

[25] Narendar Singh, P., Raghukandan, K., Rathinasabapathi, M., Pai, B.C., (2004). Electric discharge machining of Al-10%SiCp as-cast metal matrix composites. *Journal of Material Processing Technology* 156-157, 1653-1657.

[26] Mohan, B., Rajadurai, A., Satyanarayana, K.G., (2002). Effect of SiC and rotation on electric discharge machining of Al-SiC composite. *Journal of Material Processing Technology* 124, 297-304.

[27] Dhar, S., Purohit, R., Saini, N., Sharma, A., Hemath Kumar, G., (2007). Mathematical modelling of electric discharge machining of cast Al-4Cu-6Si alloy-10wt% SiC_p composites. *Journal of Material Processing Technology* 194, 24-29.

[28] Akshay, D., Pradeep, K., Inderdeep, S., (2008). Experimental investigation and optimization in EDM of Al 6063 SiC metal matrix composite. *International Journal of Machining Machinability of Materials* 5(3/4), 293-308.

[29] Wang, C.C., Yan, B.H., (2000). Blind-hole drilling of Al_2O_3 Al composite using rotary electro-discharge machining. *Journal of Material Processing Technology* 102, 90-102.

[30] Yan, B.H., Wang, C.C., (1999). The machining characteristics of Al_2O_3/6061Al composite using rotary electro-discharge machining with a tube electrode. *Journal of Material Processing Technology* 952, 222-231.

[31] Yan, B.H., Wang, C.C., Chow, H.M., Lin, Y.C., (2000). Feasibility study of rotary electro-discharge machining with ball burnishing for Al_2O_3 /6061 Al composite. *International Journal of Machine Tools and Manufacture* 40, 1403-1421.

[32] Lee, S.H., Li, X.P., (2001). Study of the effect of machining parameters on machining characteristics in electric discharge machining of tungsten carbide. *Journal of Material Processing Technology* 115, 344-358.

[33] Mohd Abbas, N., Solomon, D.G., Faud Bahari, M., (2006). A review on current research trends in electric discharge machining. *International Journal of Machine Tools and Manufacture* 47, 1214-1228.

[34] Luis, C.J., Puertas, I., (2007). Methodology for developing technological tables used in EDM processes of conductive ceramics. *Journal of Material Processing Technology* 189, 301-309.

[35] Luis, C.J., Puertas, I., Alvarez, L., (2004). Analysis of the influence of EDM parameters on surface quality, MRR and EW of WC-Co. *Journal of Material Processing Technology* 153-154, 1026-1032.

[36] George, P.M., Ragunath, B.K., Manocha, L.M., Ashish, M.W., (2004). EDM machining of carbon-carbon composite-a Taguchi approach. *Journal of Material Processing Technology* 147, 66-71.

[37] Singh, S., Maheshwari, S., Pandey, P.C., (2004). Some investigations into the electric discharge machining of hardened tool steel using different electrode materials. *Journal of Material Processing Technology* 149, 272-277.

[38] Muttamara, A., Fukuzawa, Y., Mohri, N., Tani, T., (2009). Effect of electrode material on electric discharge machining of alumina. *Journal of Material Processing Technology* 115, 344-358.

[39] Jahan, M.P., Wong, Y.S., Rahman, M., (2009 a). A study on the fine-finish die-sinking micro-EDM of tungsten carbide using different electrode materials. *Journal of Material Processing Technology* 209, 3956-3967.

[40] Her, M.G., Weng, F.T., (2001). Micro-hole machining of copper using electro discharge machining process with a tungsten carbide electrode compared with a copper electrode. *International Journal of Advanced Manufacturing Technology* 17, 715-719.

[41] Che Haron, C.H., Md. Deros, B., Ginting, A., Faiziah, M., (2001). Investigation of the influence of machining parameters when machining tool steel using EDM. *Journal of Material Processing Technology* 116, 84-87.

[42] Che Haron, C.H., Ghani, J.A., Burhanuddin, Y., Seong, Y.K., Swee, C.Y., (2008). Copper and graphite electrodes performance in electrical discharge machining of XW42 tool steel. *Journal of Material Processing Technology* 201, 570-573.

[43] Lee, H.T., Rehbach, W.P., Tai, T.Y., Hsu, F.C., (2004). Relationship between electrode size and surface cracking in the EDM machining process. *Journal of Material Science* 39, 6981-6986.

[44] Sohani, M.S., Gaitonde, V.N., Siddeswarappa, B., Deshpande, A.S., (2009). Investigations into the effect of tool shapes with size factor consideration in sink electrical discharge machining (EDM) process. *International Journal of Advanced Manufacturing Technology* 47, 395-402.

[45] Chen, S.L., Yan, B.H, Huang, F.Y., (1999). Influence of kerosene and distilled water as dielectrics on the electric discharge machining characteristics of Ti-6Al-4V. *Journal of Material Processing Technology* 87, 107-111.

[46] Ozgedik, A., Cogun, C., (2006). An experimental investigation tool wear in electric discharge machining. *International Journal of Advanced Manufacturing Technology* 27, 488-500.

[47] Gopalakannan, S., Senthilvelan, T., Kalaichelvan, K., (2012). Electric discharge machining of hybrid metal matrix composites by applying Taguchi method. *International Journal of Manufacturing Technology and Management* 26(1-4), 114-136.

[48] Puertas, I., Luis, C.J., Villa, G., (2005). Material removal rate and electrode wear study on the EDM of silicon carbide. *Journal of Material Processing Technology* 164-165, 889-896.

[49] Lin, Y.C., Chen, Y.F., Wang, D.A., Lee, H.S., (2009). Optimization of machining parameters in magnetic force assisted EDM based on Taguchi method. *Journal of Material Processing Technology* 209, 3374-3383.

[50] Lajis, M.A., Mohd Radzi, H.C.D., Norul Amin, A.K.M., (2009). The Implementation of Taguchi Method on EDM Process of Tungsten Carbide. *European Journal of Scientific Research* 26(4), 611-619.

[51] Yang, S.H., Srinivas, J., Mohan, S., Lee, D.M., Balaji, S., (2009). Optimization of electric discharge machining using simulated annealing. *Journal of Material Processing Technology* 209, 3374-3383.

[52] Jong, H.J., Won, T.K., (2010). Optimization of EDM process for multiple performance characteristics using Taguchi method and Grey relational analysis. *Journal of Mechanical Science and Technology* 24(5), 1083-1090.

[53] Somashekhar, K.P., Ramachandran, N., Mathew, J., (2010). Optimization of material removal rate in micro electric discharge machining process using artificial neural network and genetic algorithms. *Materials and Manufacturing Processes* 25 (6), 467-475.

[54] Ranganathan, S., Senthilvelan, T., (2011). Multi-response optimisation of machining parameters in hot turning using grey analysis. *International Journal of Advanced Manufacturing Technology* 56, 455-462.

[55] Noorul Haq, A., Marimuthu, P., Jeyapaul, R., (2008). Multi response optimization of machining parameters of drilling Al/SiC metal matrix composite using grey relational analysis in the Taguchi method. *International Journal of Advanced Manufacturing Technology* 37, 250-255.

[56] Mandal, D., Pal, S.K., Saha, P., (2007). Modeling of electrical discharge machining process using back propagation neural network and multi-objective optimization using non-dominated sorting genetic algorithm-II. *Journal of Material Processing Technology* 186, 154-162.

[57] Haddad, M.J., Tajik, M., Fadaei Tehrani, A., Mohammadi, A., Hadi, M., (2009). An experimental investigation of cylindrical wire electrical discharge turning process using Taguchi approach. *International Journal of Material Forming* 2, 167-179.

[58] Puri, A.B., Bhattacharya, B., (2005). Modeling and analysis of white layer depth in a wire cut EDM process through response surface methodology. *International Journal of Advanced Manufacturing Technology* 25, 301-307.

[59] George, P.M., Ragunath, B.K., Manocha, L.M., Warrier, A.M., (2004). Modeling of machinability parameters of carbon-carbon composite-a response surface approach. *Journal of Material Processing Technology* 153-154, 920-924.

[60] Kilickap, E., (2010). Modeling and optimization of burr height in drilling of Al-7075 using Taguchi method and Response surface methodology. *International Journal of Advanced Manufacturing Technology* 49, 911-923.

[61] Agarwal, A., Singh, H., Kumar, P., Singh, M., (2008). Optimisation of power consumption for CNC turned parts using response surface methodology and Taguchi's technique-A comparative study. *Journal of Material Processing Technology* 200, 373-384.

[62] Ramakrishnan, R., Karunamoorthy, L., (2008). Modeling and multi-response optimization of Inconel 718 on machining of CNC WEDM process. *Journal of Material Processing Technology* 207, 343-349.

[63] Natarajan, U., Periyanan, P.R., Yang, S.H., (2011). Multiple-response optimization for micro-end milling process using response surface method. *International Journal of Advanced Manufacturing Technology* 44, 100-113.

[64] Gopalakannan, S., Senthilvelan, T., (2014). Optimization of Machining Parameters for EDM Operations based on Central Composite Design and Desirability Approach. *Journal of Mechanical Science and Technology* 28(3), 1045-1053.

[65] Gopalakannan, S., Senthilvelan, T., (2013). A parametric study of electric discharge machining process parameters on machining of cast Al/B_4C metal matrix nanocomposites. *Journal of Engineering Manufacture* 227(7), 993-1004.

[66] Taweel, T.L., Gouda, S.A., (2010). Performance analysis of wire electrochemical turning process-RSM approach. *International Journal of Advanced Manufacturing Technology* 53, 181-180.
[67] Chiang, K.T., (2008). Modeling and analysis of the effects of machining parameters on the performance characteristics in EDM process of Al2O3+TiC mixed ceramic. *International Journal of Advanced Manufacturing Technology* 37, 523-533.
[68] Garg, R.K., Singh, K.K., Sachdeva, A., Sharma, V.S., Ojha, K., Singh, S., (2010). Review of research work in sinking EDM and WEDM on metal matrix composite materials. *International Journal of Advanced Manufacturing Technology* 50(5-8), 799-809.
[69] Jahan, M.P., Rahman, M., Wong, Y.S., (2010). Study on the nano-powder-mixed sinking and milling micro-EDM of WC-Co. *International Journal of Advanced Manufacturing Technology* 27, 488-500.
[70] Ho, K.H., Newman, S.T., (2003). State of the art electrical discharge machining (EDM). *International Journal of Machine Tools and Manufacture* 43, 1287-1300.
[71] Jahan, M.P., Anwar M.M., Wong, Y.S., Rahman, M., (2009 b). Nano finishing of hard materials using micro-electrodischarge machining. *Journal of Engineering Manufacture* 223, 1127-1142.

In: Electrical Discharge Machining (EDM)
Editor: M. P. Jahan
ISBN: 978-1-63483-591-6

Chapter 12

ELECTRO-DISCHARGE MACHINING FOR NON-METAL BASED FABRICATION PROCESS

Tanveer Saleh*
Department of Mechatronics Engineering,
International Islamic University Malaysia, Malaysia

ABSTRACT

Machining is a regulated material removal process from a piece of raw material which can be divided into mainly two major groups "Conventional Machining Processes" and "Non-Conventional Machining Processes." Turning, boring, milling, shaping, broaching, slotting, grinding etc., fall under the category of conventional machining processes. Similarly there are several examples of non-conventional machining such as Abrasive Jet Machining (AJM), Electro-chemical Machining (ECM) and Ultrasonic Machining (USM) etc. Electro-Discharge Machining/ Wire Electro-Discharge Machining are other nonconventional machining technology which is extensively used for metal based fabrication process. Electro-discharge machining (EDM) makes use of electrical energy to transform into thermal energy. This process enables machining of any material, which is electrically conductive, irrespective of its brittleness, hardness or strength. The basic principle of this machining type is when the material of the workpiece is removed through high frequency sparks between the tool and the workpiece immersed into the dielectric fluid like oil, de-ionized water etc. Wire electro-discharges machining (WEDM) is a variant of EDM based method for non-contact machining using wire as the machining tool. When very low energy (in µ-joule range) is used for creating these sparks, the process is called as µ-WEDM. Silicon (Si) is an important engineering material that is used mostly in Electronics and MEMS (Micro Electro-Mechanical System) based applications. As mentioned above EDM/WEDM technology is mainly used for metal based fabrication process however, in recent times researchers are using this method for non-metal based machining processes like Vertically Aligned Carbon Nanotube, Carbon Nanotube Composite, Conductive Polymer, Ceramics and Semiconductor materials. This chapter will discuss about the application of

* Corresponding Author address; Email:tanveers@iium.edu.my

EDM/WEDM technology for nonmetal based machining both in macro and micro domain.

Keywords: EDM, WEDM, ceramic, semiconductor, glass, composite, CNT

1. INTRODUCTION

Machining processes can be divided into mainly two groups "Conventional Machining Processes" and "Non-Conventional Machining Processes." Turning, boring, milling, shaping, broaching, slotting, grinding etc fall under the category of conventional machining processes. Similarly there are several examples of non-conventional machining such as Abrasive Jet Machining (AJM), Electro-discharge Machining (EDM), Electro-chemical Machining (ECM) and Ultrasonic Machining (USM) etc. In conventional machining usually harder material is used as tool for changing the shape of a workpiece by cutting operation. Machining hard metals and alloys using conventional methods involves longer time and higher energy, and therefore, an increase in costs. Conventional machining may also higher tool wear and deteriorated quality in the product owing to induced residual stresses during manufacturing. Conventional machining can be defined as a process of using mechanical (motion) energy. On the other hand, most non-conventional machining has no direct contact between the tool and workpiece. It has several other features and the three main forms of energy that are used in these processes are thermal energy, chemical energy and electrical energy. If one asks why we need the non-conventional machine? The simple answer is, in several industries, hard and brittle materials like tungsten carbide (used for making cutting tools), high speed steels (used for making gear cutters, drills, milling cutters), stainless steels, ceramics etc. are often used. If such materials are machined with the help of conventional machining processes, either the tool undergoes extreme wear (in case of hard materials) or the workpiece material is damaged (in case of brittle materials). This is because, in conventional machining, there is a direct contact between the tool and the workpiece. Large cutting forces are involved, and material, are removed in the form of chips. A huge amount of heat is produced in the workpiece. This induces residual stresses, which degrades the life and quality of the workpiece material. To overcome all these drawbacks, non-conventional machining processes are used to machine hard and brittle materials. As well as to machine soft materials, in order to get better dimensional accuracy. The best way to give a clear vision of these two machining groups (conventional and non-conventional) is to introduce a comparison between them. In conventional processes generally macroscopic chip formation by shear deformation. While material removal may occur with chip formation or even no chip formation may take place in non-conventional processes. Back to conventional processes, there is a physical tool present such as a cutting tool in a Reamer Machine. While there may not be a physical tool present in non-conventional processes such as in laser jet machining. Again in conventional machining the tool should be harder than the workpiece under the machining conditions. While as mentioned in the above, there may not be a physical tool present in non-conventional machining. There are number of cases where conventional machining involves lower accuracy and surface finish than the non-conventional machining. Tool life in the conventional might be less than the non-conventional (e.g ECM) due to high surface contact and wear. In the conventional, there are always noisy operations that cause sound pollutions.

On the other hand there is no sound pollution in the non-conventional machining processes. Conventional machining (unlike the non-conventional machining) requires lower capital cost and simple set-up of equipment. Skilled or un-skilled operator can run the conventional machining, while only skilled operator can run the non-conventional that generally operates using automated processes.

Electrical discharge machining (EDM) is an important non-conventional manufacturing method that was developed in 1940s. It has been accepted worldwide as a standard process in manufacturing of forming tools to produce plastics mouldings, castings, press tools, forgings, etc. The origin of electrical discharge machining goes back to 1770. An English scientist Joseph Priestly discovered the erosive effect of electrical discharges. Later in 1943, Russian scientists B.R. and N.I. Lazarenko at Moscow University had the idea of exploiting the destructive effect of an electrical discharge. They also were behind developing a controlled process for machining materials that are conductors of electricity. The Russian scientists perfected the electrical discharge process. The process consisted of a succession of discharges that took place between two conductors separated from each other by a film of non-conducting liquid, called a dielectric. However, it was only in the 1980s, with the advent of Computer Numerical Control (CNC) in the EDM that brought about tremendous advancement in improving the efficiency of the machining operation. This process enables machining of any material, which is electrically conductive, irrespective of its hardness, shape or strength. The EDMing process is very complex and stochastic in nature. More than one discipline is involved in this single machining process, such as electrodynamics, electromagnetic, thermodynamic, and hydrodynamic. Difficulty arises in developing a comprehensive process model for EDM because of its multidisciplinary nature. In the EDM process, material is removed by action of electrical discharge between the tool and the workpiece.

The basic principle of the machining is a process when the material of the workpiece is removed through high frequency sparks between the tool (electrode) and the workpiece immersed into the dielectric fluid like oil, de-ionized water etc. But talking about very low energy (in μ-joule range) to create these sparks lead to call of the process as μ-EDM. This μ-EDM is a promising machining technology to produce features in micron domain for different engineering applications.

The main difference between conventional EDM and μ-EDM lies in the level of discharge energy and size of the tool used during the operation. In μ-EDM very low discharge energy with high frequency is used (~μ-Joule). Further, typical tool and feature size in μ-EDM are in order of less than or equal to 100 μm. Wire electrical discharges machining (WEDM) is the variant of EDM based method for non-contact machining. WEDM is a type of EDM operation where the cutting tool is a rotating wire spool and the electric discharge energy is applied between the wire and the workpiece. The WEDM process can also be carried out in micron domain with wire size below 100 μm of diameter.

EDM and WEDM are widely used for electrically conductive materials because of its physical nature of operation. However, recently scientists are using this method for non-metal based machining processes like Vertically Aligned Carbon Nanotube, Carbon Nanotube Composite, Conductive Polymer, Ceramics and Semiconductor materials. In the subsequent sections EDM/WEDM application on non-metallic material will be discussed in detail.

2. ELECTRO-DISCHARGE MACHINING OF SEMI-CONDUCTOR MATERIALS

Semiconductor materials like Silicon (Si), Germanium (Ge) are the most common materials after metal that have been used as workpiece for machining by EDM or WEDM process. Silicon (Si) is one of the most common semiconductor materials which are used in the field of MEMS based fabrication and in electronics. Therefore, this is the most common semiconductor material tested for EDM/ WEDM operation.

Masaki et al., [1] are among the first few researchers who tried Micro-EDM for Si. The range of discharge energy used was in a range of 0.1 μJ. In this study author conducted a comparison of micro-hole boring by EDM for Si and steel. It was observed, that for steel initially machining was smooth without occurring much short circuit. However, after certain machining depth EDM was slow with high short circuit occurrence. The reason behind this could be as insufficient removal of machined chips and occurrence of a secondary electro-discharge. In the case of Si, feeding speed was found to be uniform throughout the machining and overall higher compared to steel. Authors also found that electrode wear is considerably small for Si than steel. Finally author concluded that micro-EDM of Si is more efficient than steel because silicon is mechanically fragile and micro cracks formed due to thermal shocks and melting during EDM machining improves the efficiency.

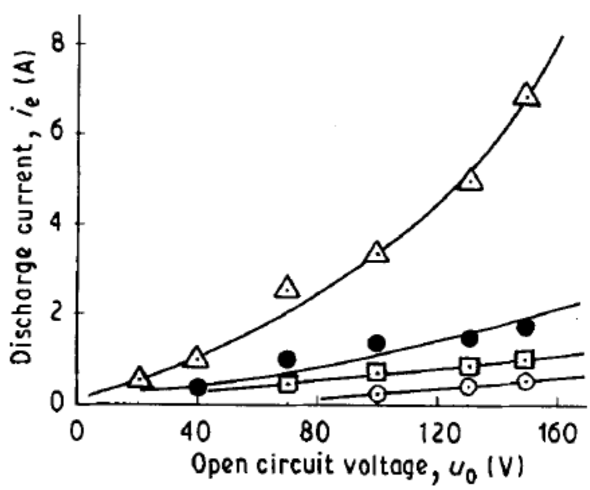

Figure 1. Pulse current/voltage characteristics of the wire EDM conducting system. Cutting width, CW= 10 mm. 1 (●) 2 (⊙) 3 (⚠) 4 (⊡) [2].

In 1992 Luo et al., [2] introduced slicing of highly doped n-type single-crystal (resistivity 7-15 Ω–cm) Si ingots by Wire EDM technique. Researchers used pulse type EDM generator with pulse parameters as follows, such as pulse duration (1-256 μs), pulse interval (2-512 μs), peak current (0.1-20A), open circuit voltage (10-180 V) and discharge current rise time (0-40 μs). Luo et al. studied the effect of metallic coating (Nickel plated) and polarity of the electrical contact on the slicing efficiency. Four types of combination were examined as stated below,

1. Normal polarity connection (electrode wire (-) pole, silicon ingot (+) pole) with the ingot chemically nickel plated;
2. Normal polarity connection without the ingot chemically nickel plated;
3. Reversed polarity connection (electrode wire (+) pole; silicon ingot (-) pole) with the ingot chemically nickel plated and
4. Reversed polarity connection without the ingot chemically nickel plated.

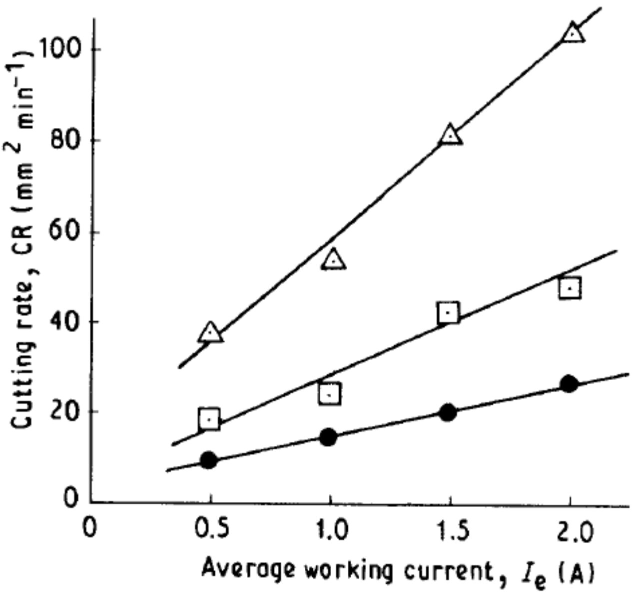

Figure 2. Comparative CR experiments with the dielectrics. CW = 40 mm, t_o = 220 μs, t_i = 70 μs, 1 (●) 3% emulsion . (⊡) 7% emulsion (△) kerosene [2].

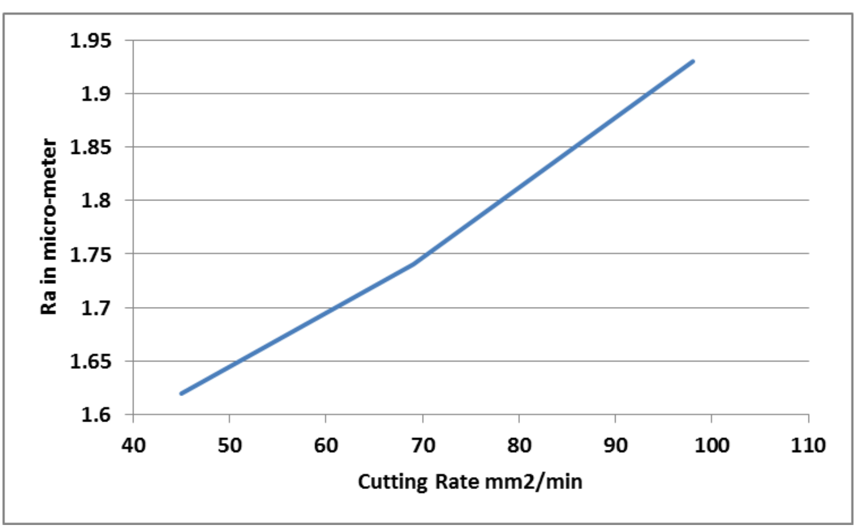

Figure 3. Relationship between Ra and Cutting Rate [2].

Figure 1 shows the relationship between Open Circuit Voltage (v_o) and Discharge Current (i_e) for all four combinations. Figure 2 describes the cutting rate for all four combinations. It is obvious from Figure 1 that number three combination i.e., “reversed polarity connection (electrode wire (+) pole; silicon ingot (-) pole) with the ingot chemically nickel plated” provides highest discharge current and machining efficiency. Discharge current is higher for third combination because of forward biasing of the workpiece. Figure 2 shows effect of dielectric on the cutting speed. Kerosene was found to be best for higher cutting rate. Finally surface roughness was examined by varying the cutting rate, which is illustrated in Figure 3. Higher cutting rate produces bad surface quality because of higher discharge energy.

Staufert et al., [3] investigated the characteristics of a Si micro-spring fabricated by WEDM machining. Figure 4 shows the SEM image of the fabricated spring after some post processing. Finally author concluded that, the whole fabrication process including WEDM, was able to develop a spring that is of purely single crystalline structure. The linearity and lifecycle of the spring is extremely good and can operate for three-million cycles without any problem at all.

Study conducted by Reynaertset al., 1997 [4] showed some important theoretical aspects of electro discharge machining of Si. Compared to the more traditional silicon micromachining technologies, the EDM has several substantial advantages: EDM requires a low installation cost, it requires little job overhead, it is also very flexible, and it can easily machine complex shapes. Erosion index is a parameter that is used to indicate whether the material can easily be machined by EDM. This index is governed by the following equation

$$C_m = \lambda c T_m^2 \tag{1}$$

where, λ is heat conductivity, c is specific heat, T_m is melting point. If the index is high material have more resistance to be eroded by electrical discharge thus can be used as EDM tool. Table 1 shows erosion index for several materials.

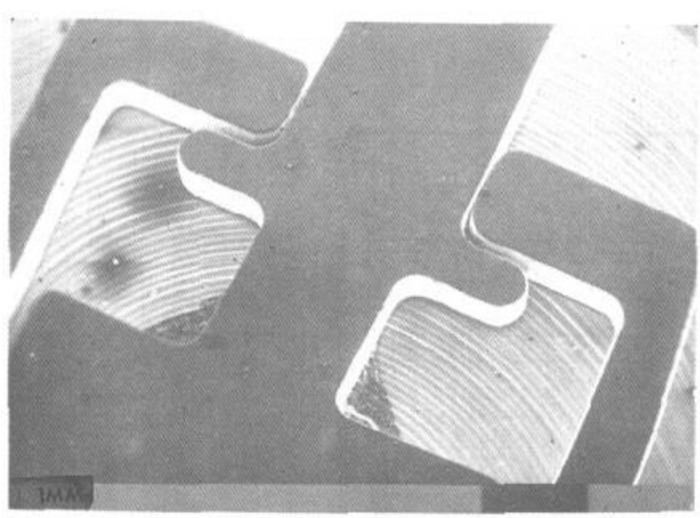

Figure 4. μ-Spring fabricated by WEDM process [3].

Table 1. Erosion index of few common materials [4]

Material	C_m
Copper	2.79
Tungsten	2.99
Steel	0.23
Silicon	0.0075

Interestingly Si has significantly low erosion index, which indicates it is feasible to machine Si by EDM. Further, the authors believe that the EDM can offer a much better dimensional control than laser cutting, especially for machining features like blind holes. However, the main challenge is the surface resistance of Si. Reynaerts et al., suggested following two alternatives to overcome this challenge.

- Adjusting the polarity of the workpiece to make it forwardly biased i.e., for p type Si workpiece should be + ve and vice versa.
- Application of temporary conductive coating to overcome surface potential barrier.

Authors also discussed how EDM can influence several characteristics of Si such as Surface roughness (which can be controlled by controlling the current), residual thermal stress and micro cracks (which can be eliminated by etching of 10- 35 μm depth), contamination of dielectric material (so far none has reported this). In their second paper Reynaerts et al., 1997 [5] reported several application of EDM based micro fabrication of Si such as construction of 45^o micro-mirrors in Si etched V-groove arrays. Another example of the applications is an acceleration sensor (accelerometer); the suspension system of the mass was machined with the μ-EDM.

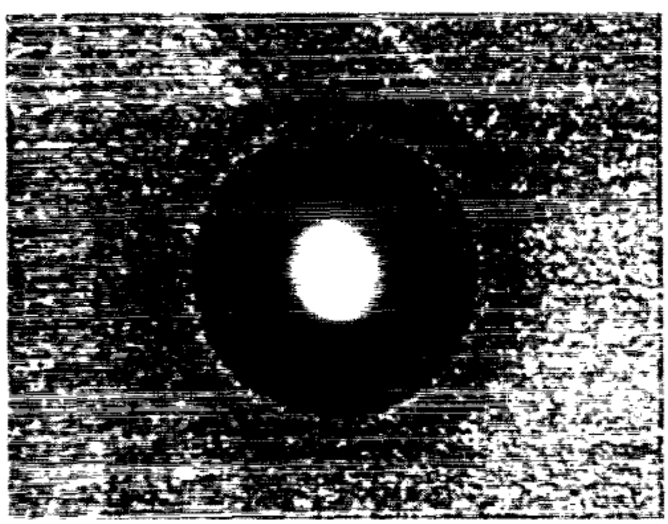

Figure 5. Conical hole machined by EDM on a Si workpiece [6].

The last application in this work was a Si micro-spring used to perform one-dimensional measurements. These applications show how the μ-EDM of the Si is a manufacturing technique which offers a large design freedom with high accuracy. It is very suitable for machining complex 3D mechanical structures that would be difficult to machine otherwise. The average surface roughness achieved by EDM was 0.35 μm Ra.

Study on machining of 3-D micro structures on Si by EDM further continued by Dominiek et al., [6] in 1998. In this study they wanted to investigate the effect of crystallographic orientation of Si on EDM process and found that the influence is insignificant. Figure 5 shows a conical through hole with a cone angle of 60^{o} machined on Si surface by EDM. Top diameter of the hole was 521 μm and bottom diameter of the plane was 129 μm.

Figure 6. Si micro gear produced by EDM [6].

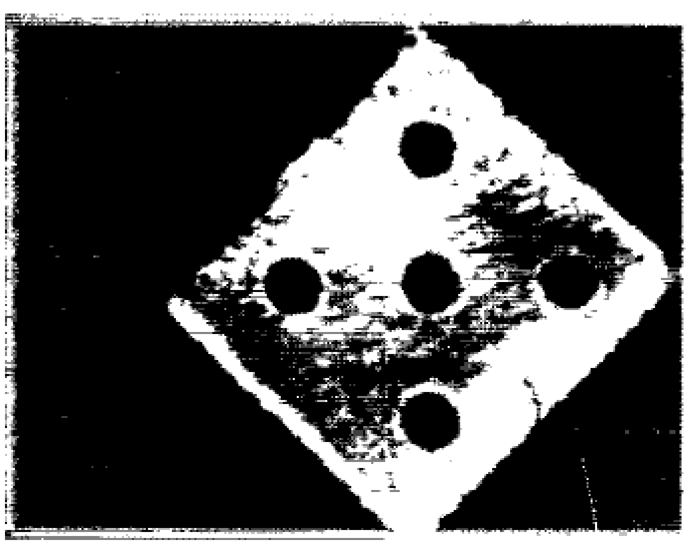

Figure 7. <50 μm diameter micro hole produced by EDM on a Si workpiece [6].

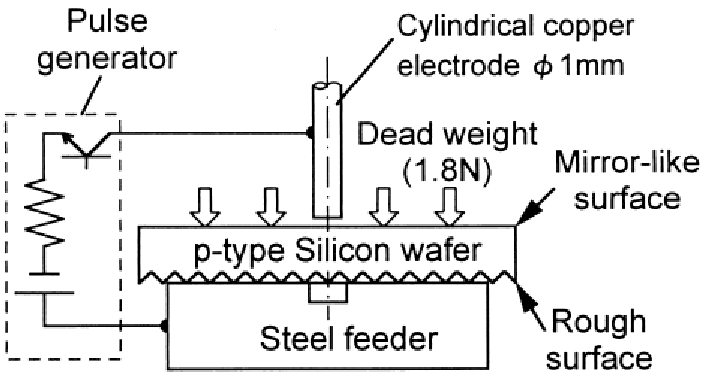

Figure 8. Experimental setup [7].

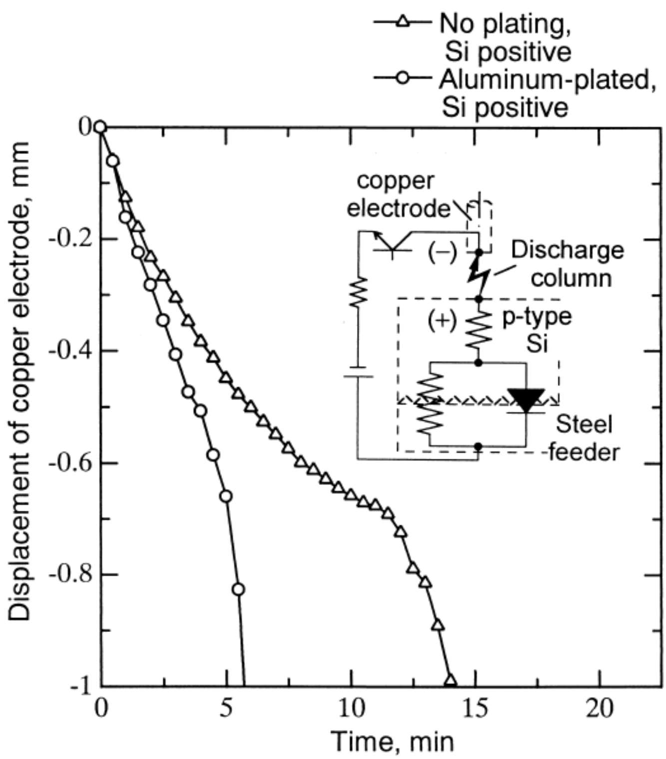

Figure 9. Piercing rate of p-type Si for two different cases Al plated and not plated [7].

Authors [6] also studied the process to produce micro mirror with 14 nm of Ra and micro gears. Figure 6 shows the example of Si micro gear assembly produced by EDM. Figure 7 shows micro holes (diameter < 50 μm) produced by EDM on Si. However, measurement of circularity and inclination of these holes were not investigated in this study.

Kunieda et al., [7] improved the EDM efficiency of Si by applying conductive paint hence reducing the contact resistance. Figure 8 shows the experimental setup for the study. The rough surface was plated with conductive coating. Authors also alter the polarity to carry on comparative study. Figure 9 and Figure 10 show the results of piercing speed for different condition. It is obvious from these to figures that best machining rate is achieved when sample is coated to maintain an ohmic contact and is forward biased (i. e p-type Si is +ve charged and n-type Si is –ve charged). This is because in these cases discharge current was found to reach to its maximum level as compared to other condition hence the machining rate.

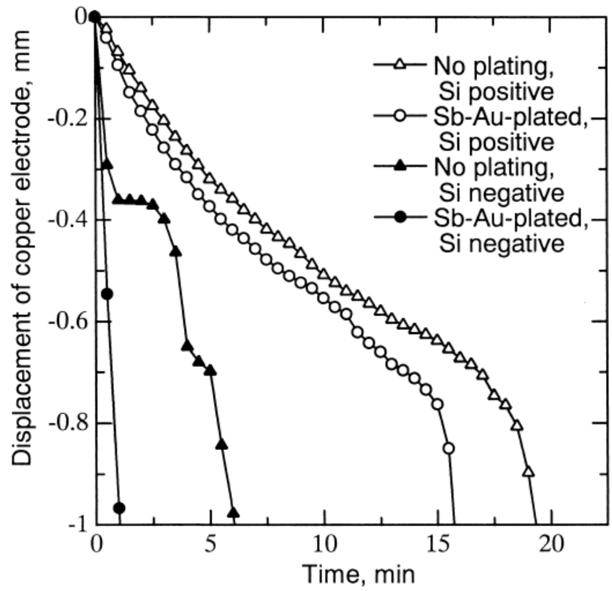

Figure 10. Piercing rate of n-type Si for four different cases by varying plating condition and polarity [7].

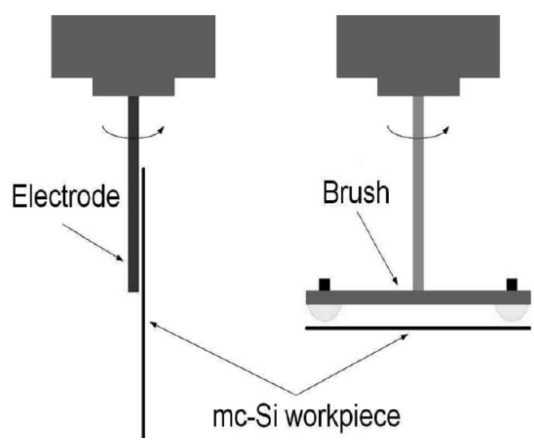

Figure 11. mc-Si texturing process by EDM [9].

Song et al., in 2000 [8] studied performance of micro-EDM on highly doped P-type silicon. It was observed material removal mechanism is different for silicon than conventional metal micro-EDM; besides melting and evaporation there is a significant contribution from thermal spallation, which is a kind of direct mechanical material damage without melting.

The paper also presented that micro crack generation is not only a function of sparking energy but also it has high dependence on the silicon crystal lattice. In order to get micro crack free silicon surfaces author suggested maintaining the sparking energy to low levels, which are much lower than the voltage levels used in metal micro-EDM. Finally authors suggested reducing thermal spallation to its minimum, to obtain smooth and crack free machined surfaces.

Qian et al., (2002) [9] used EDM technology to texture monocrystalline Silicon (mc-Si) substrate for solar cell application. Figure 11 shows the arrangement of their texturing setup using EDM. Vertical mounting of the workpiece was not proven to be feasible for EDM-texturing process because of alignment and clamping difficulties. The surface roughness of original mc-Si was Ra =1.1 µm, and Rt = 11.4 µm which was changed to Ra =3 µm, and Rt = 30 µm after EDM texturing process. Figure 12 shows the effect of texturing on the optical reflectivity of the substrate. It was observed that texturing effect reduces the optical reflectivity. However, low reflectivity does not necessarily indicate better efficiency for solar cell application. It was found that (Figure 13), substrate textured by EDM contains a lot of re-deposited amorphous silicon balls, that have a bad effect on the emitter doping, so they needs to be removed by subsequent etching process. Finally Figure 14 shows comparison of solar cell efficiency between textured wafer and un-textured wafer.

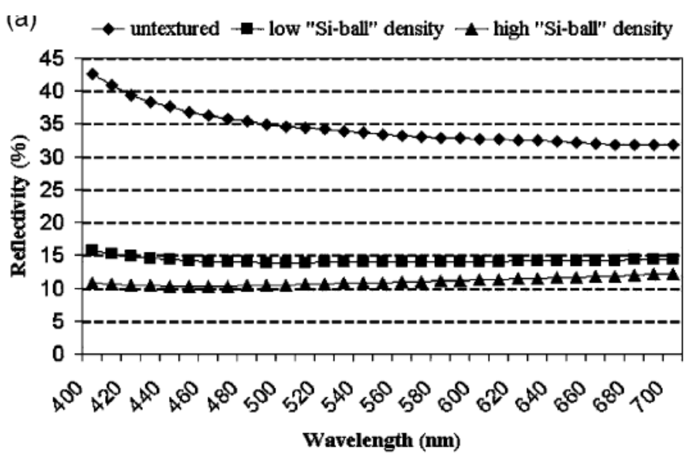

Figure 12. Reflection from original and textured substrate [9].

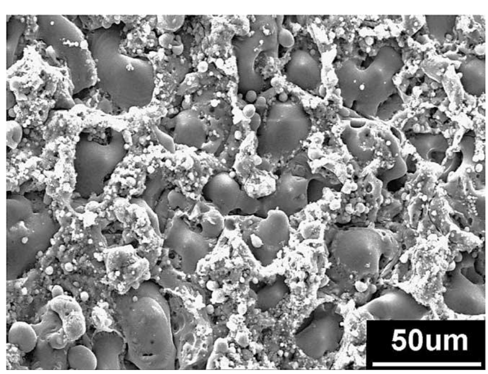

Figure 13. Amorphous Si balls after EDM texturing [9].

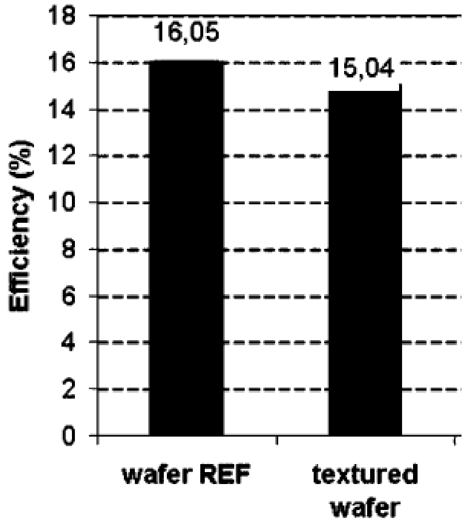

Figure 14. Solar cell efficiency of un-textured wafer and textured wafer [9].

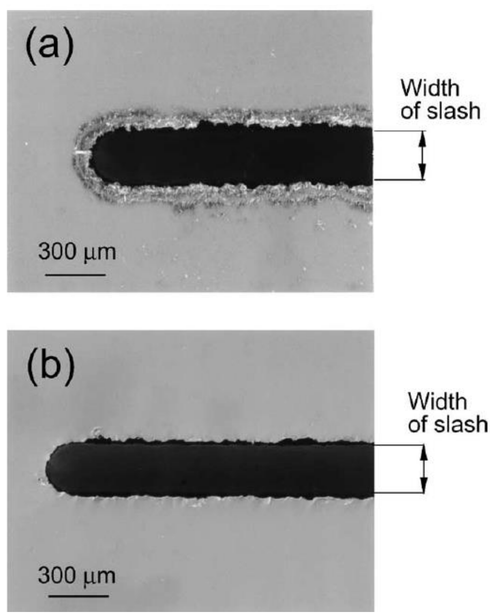

Figure 15. Nomarski microscope picture of surfaces cut in (a) water and (b) oil are shown [10].

Takino et al., in 2004 and 2005[10] studied the effect of cutting by WEDM on the shape accuracy of polished single-crystal silicon. The polished Si cut in water and in oil have degradation in some ways, such as rough regions, cracks, or chips. For cutting in water, polished Si workpieces have chips and cracks near cut sections, and are extremely rough. The rough regions are seemed to be Si dioxide and result from the WEDM oxidization of the surfaces. Moreover, the polished Si far from the cut sections is somehow roughened. While cutting in oil, polished Si are smooth near the cut section and almost flat, although they have chips and cracks. So, experimentally and according to this investigation, WEDM in oil is better than that in water for cutting polished single-crystal silicon to obtain high-quality surfaces, although the improvement was not significant. Figure 15 shows the WEDM cut Si in water and oil.

The same research group discussed a method for cutting smoothly polished single-crystal silicon surfaces by WEDMing to obtain a high-quality surface [11]. Products cannot be cut out from blanks by the finish-cutting operation alone. Therefore, the rough cutting operation is necessary as the first process in actual mirror production. And the finished cutting operation should be adopted as a subsequent process. Finished cutting in oil was used for removing the regions with defects, such as cracks or roughness that is generated during rough cutting as shown in Figure 16.

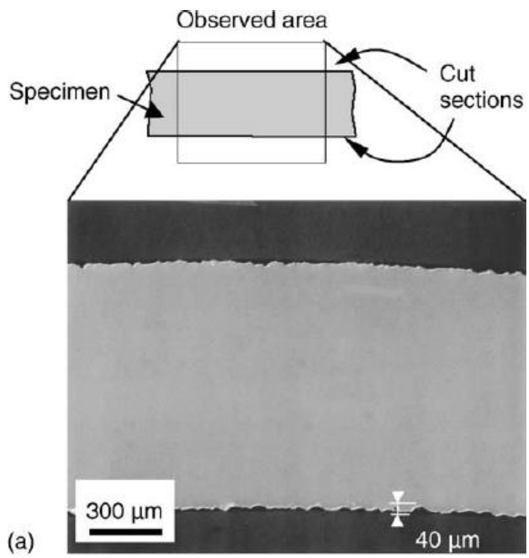

Figure 16. WEDMed polished Si sample after finish cutting [11].

Further, researchers also made an attempt to avoid the roughness induced by rough cutting in water by preventing surfaces from coming into contact with water during the cutting process. For this purpose, a mask was applied to the polished surfaces before cutting.

Okomoto et al., [12] developed a multi wire WEDM system to perform slicing of Si ingot. It was observed by the researchers that nozzle flushing of dielectric fluid impedes the consistency of the pitch distance between the cut slots. On the other hand if the workpiece is immerged in the dielectric fluid the pitch distance between the slots remains consistent as explained in Figure 17. It shows the difference of kerf shapes for two supply methods of working fluid. When the working fluid was supplied by nozzle, the pitch of kerf was greatly varies due to the surface tension of working fluid generated between wire electrodes. On the other hand, constant kerf pitch is attainable by immersion method. It was observed by the researchers that machining time is shorter with increasing wire speed as shown in Figure 18. However, as the removal rate increases the surface roughness deteriorates with the increase of specific resistance of dielectric fluid (Figure 19).

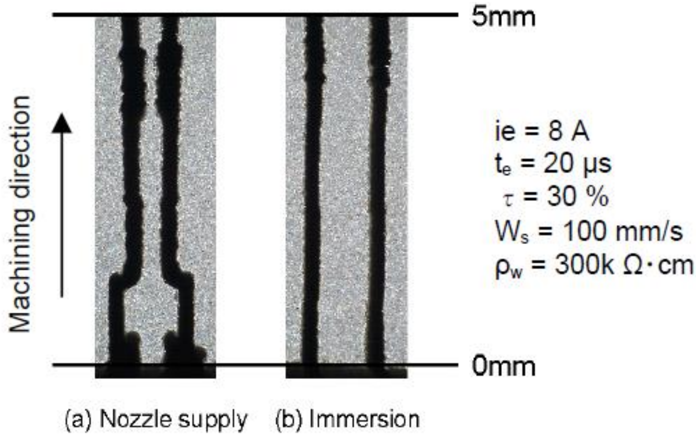

Figure 17. Difference of kerf shape by different dielectric supply method [12].

Rakwal et al., [13] carried out an interesting study on the fabrication of high aspect ratio silicon microelectrode arrays by micro-wire electrical discharge machining (μ-WEDM). An arrays 144 micro electrodes were fabricated with a uniform cross section of 250μm by 250μm. The length of the electrode was 5 mm. The machining time required for fabricating this array of electrode was 8h. Fabrication process was conducted in two steps i.e rough cut (150V and 9.9 nF) and finish cut (150V and 3.3nF). Figure 20 shows the SEM image of the machined electrodes. Authors reported that minimum dimension electrode that can be machined by WEDM alone is 120 μm by 120μm. Further a two-step chemical etching process to remove the recast layer and to reduce the cross sections of the electrodes (Figure 21).

M. P. Jahan et al., [14] experimentally investigated μ-EDM of Si wafer with various features (holes, slots) and machining conditions. Effect of gap voltage was studied for material removal rate (MRR), spark gap, tapper ratio, electrode wear ratio and circularity. Figure 22 summarizes the result.

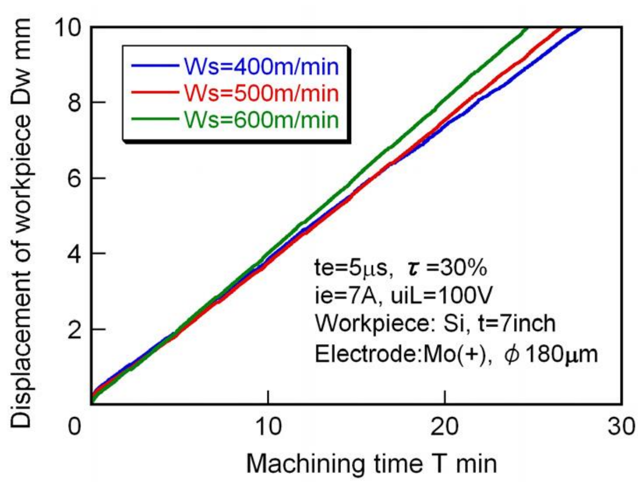

Figure 18. Machining time for various wire speed [12].

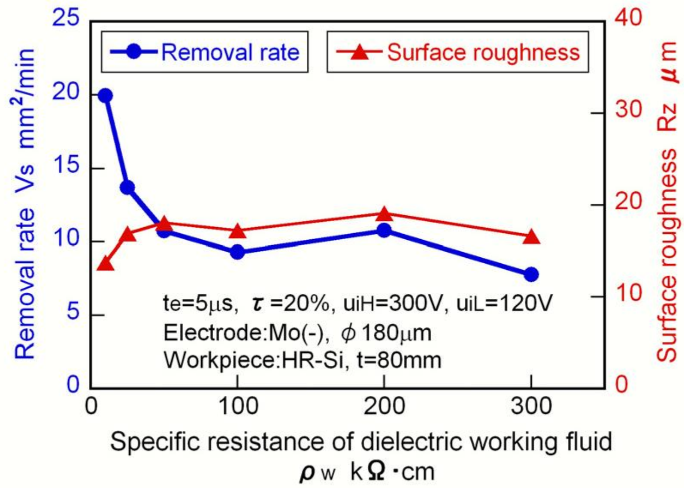

Figure 19. Study of surface roughness and removal rate [12].

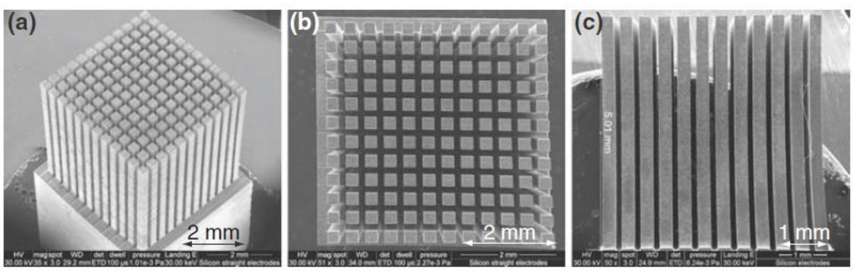

Figure 20. Array of Si electrode machined by WEDM process. Dimension 250μm by 250μm with a height of 5mm [13].

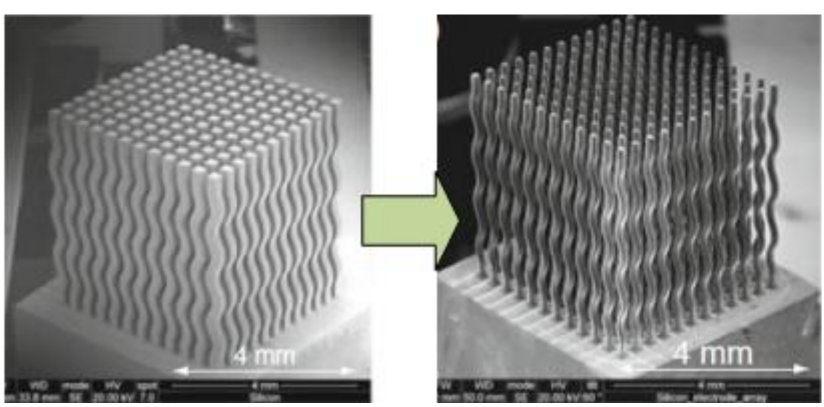

Figure 21. Thinning of electrode dimension by chemical etching process after machined by WEDM process [13].

It was observed that MRR increases with gap voltage and MRR is higher for positive voltage due to the forward biasing of p-type Si workpiece. Spark gap also increases with higher gap voltage due to higher sparking current. Other parameters also shows increasing trend with high open circuit voltage. All these parameters are the performance characteristics for micro-EDM process. Except for MRR all parameters are preferred to be low for micro-EDM operation. It is obvious from the study that high voltage causes high discharge energy is not good for micro EDM process, that is why researchers prefer high frequency RC circuit with low discharge energy for micro EDM operation.

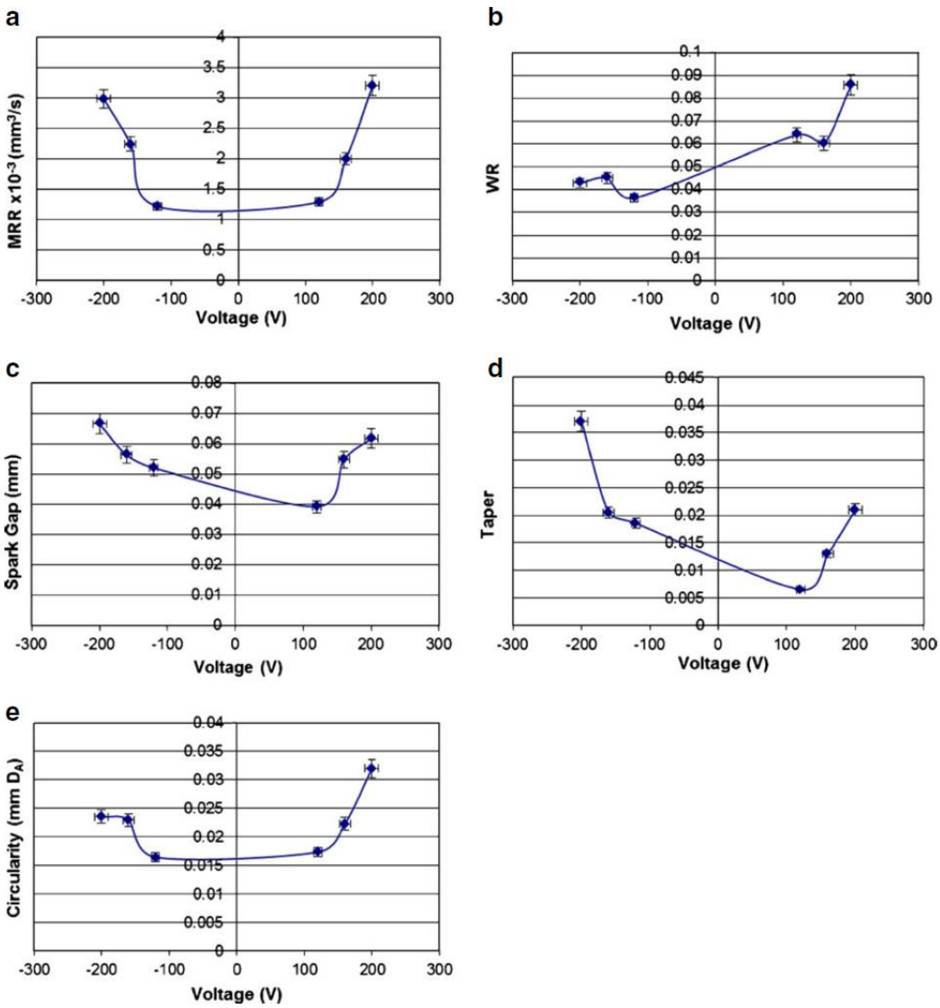

Figure 22. Effect of voltage on a MRR, b WR, c spark gap, d taper, and e circularity of the micro-holes machined by μ-EDM on Si workpiece [14].

Huai Yu et al., [15] proposed an interesting method of implementation of auxiliary circuit to improve on the EDM efficiency. Figure 23 describes the principle of conventional and proposed EDM power circuit. The characteristics of both the circuits are explained in Figure 24. It can be seen from the Figure 24 that there is a significant delay T_d which may hinder the efficiency of the overall EDM process. One solution to overcome this problem is to increase the open circuit voltage V_m considerably high so that breakdown occurs more rapidly.

However, this will eventually increase the discharge current which will result bad surface and larger kerf width.

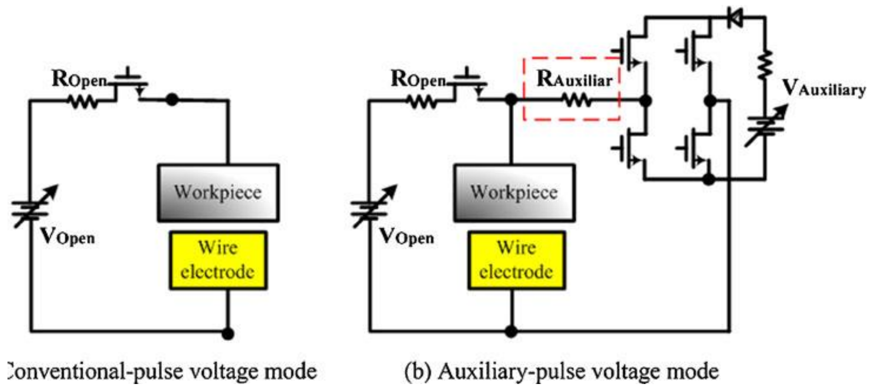

Figure 23. Circuits of conventional and auxiliary-pulse voltage [15].

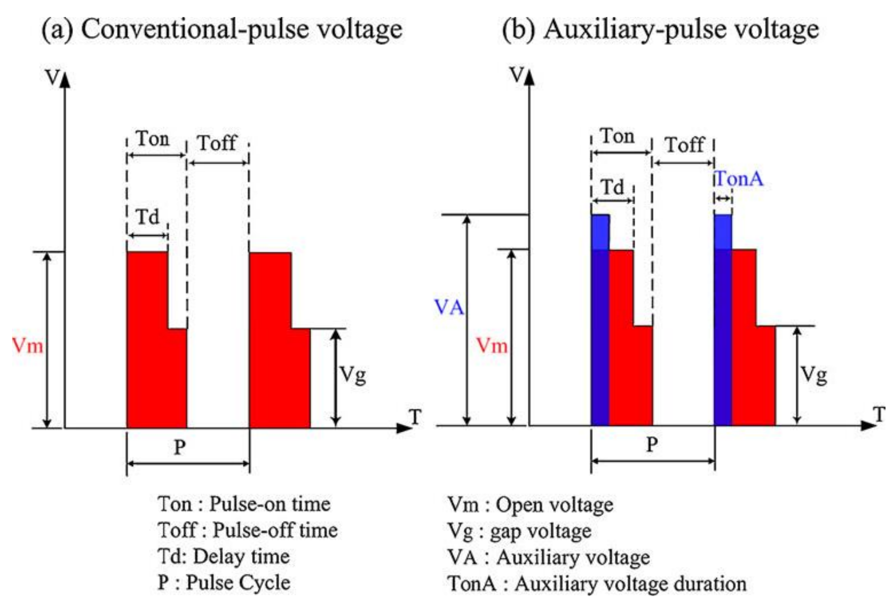

Figure 24. Characteristic diagram of conventional- and auxiliary pulse voltage supply [15].

In order to address this issue Huai Yu et al., proposed the new circuit design as shown in Figure 23 (b). In this case the auxiliary voltage is applied for a short period of time with high resistance $R_{axiliary}$ in series so that this extra high voltage V_A is used only to breakdown the insulation. This characteristic is explained in Figure 24 (b). Figure 25 shows a comparative study of machining time for both conventional pulse circuit and auxiliary pulse circuit. Clearly auxiliary pulse voltage obtained higher machining speed by applying an auxiliary voltage in microseconds. As a result of this, machining of polysilicon by WEDM can proceed at a faster speed and better surface quality can be achieved (Figure 25).

Recently Gregory Allen Crawford from MIT [16] used Design of Experiments to characterize EDM process of highly doped Si wafer. He investigated surface roughness (Ra) and material removal rate (MRR) for both EDM and WEDM. The investigation was carried out statistically and optimized parameters were used for micro machining of Si wafer. Figure 26 shows cantilever beam machined on Si wafer by WEDM process.

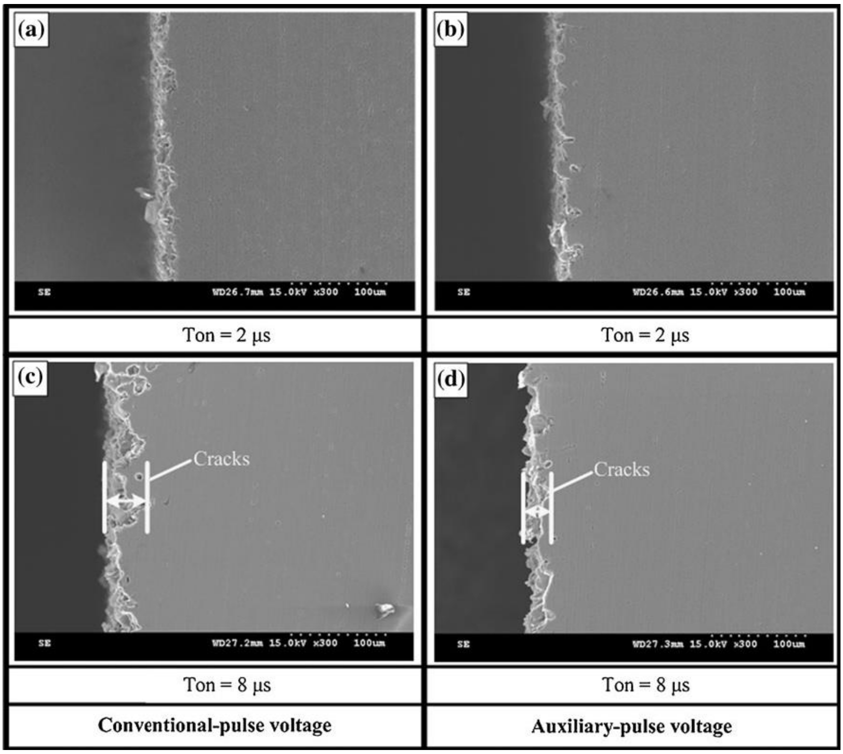

Figure 25. SEM cross-sectional micrographs of workpiece machined by conventional- and auxiliary-pulse voltage [15].

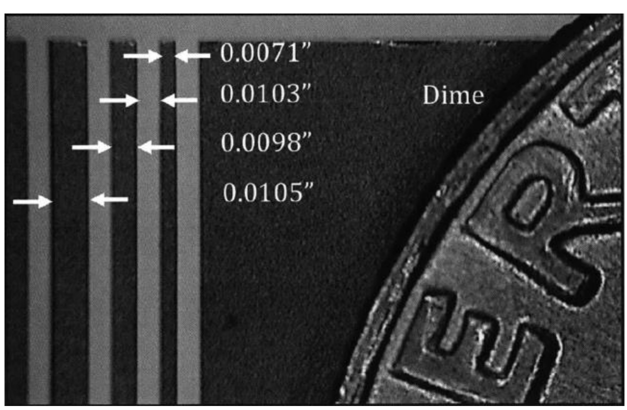

Figure 26. Cantilever beam on Si [16].

Liu Zhidong et al., [17] proposed an interesting servo control method in order to machine Si by WEDM method. In conventional metal WEDM/EDM short circuit voltage and discharge voltage is significantly lower than open circuit voltage and can be used as a feedback signal for the machine feed control (Figure 27). However, in case of Si machining there is not much difference in terms of value for open circuit, discharge and short circuit voltage (Figure 27), therefore voltage alone may not be useful as a feedback parameter for Si machining by WEDM.

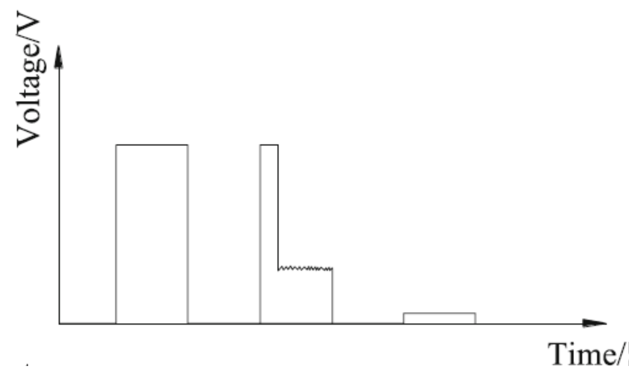

(a)

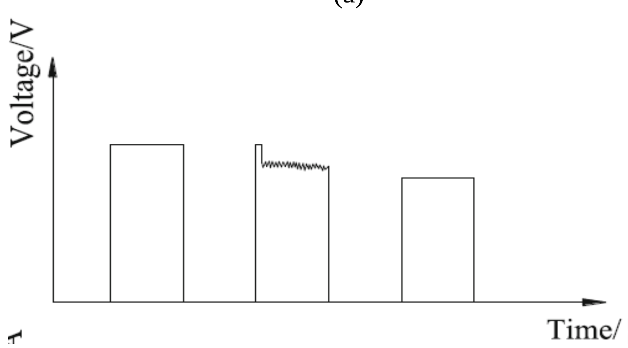

(b)

Figure 27. Voltage characteristics in EDM. (a) Metal (b) Si [17].

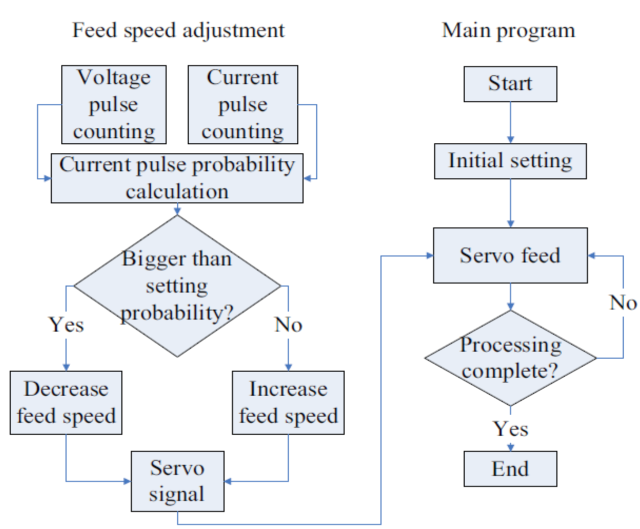

Figure 28. Feed control algorithm proposed by Liu Zhidong et al., [17].

Liu Zhidong et al., [17] proposed to monitor the current pulse as a feedback parameter in this case. The algorithm is explained in Figure 28. The current sensor detects the real-time current; also voltage is monitored. A microprocessor carries out the processing to calculate current pulse production probability as the feedback parameter. The feed speed is controlled in real time, which ensures that the average current pulse probability is same as the set value. Figure 29 shows a Si gear machined by WEDM that uses the feed control algorithm explained above.

Saleh et al., [18] studied to develop and characterize the process of improved µ-WEDM and µ-EDM of Si by temporarily coat Si with a high conductive metal (gold in this study). Micro-WEDM process stability was found to be improved (~ 100 x for different machining condition) if coated Si wafer is used as compared to uncoated Si workpiece. Material removal rate (MRR) was also found to be increased by a good margin (~ 30% average) for coated Si wafer. Machined slots were found to be more uniform though kerf width was slightly larger for coated Si wafer. In case of µ-EDM operation, gold coated Si also enhanced the machining as compared to uncoated Si.

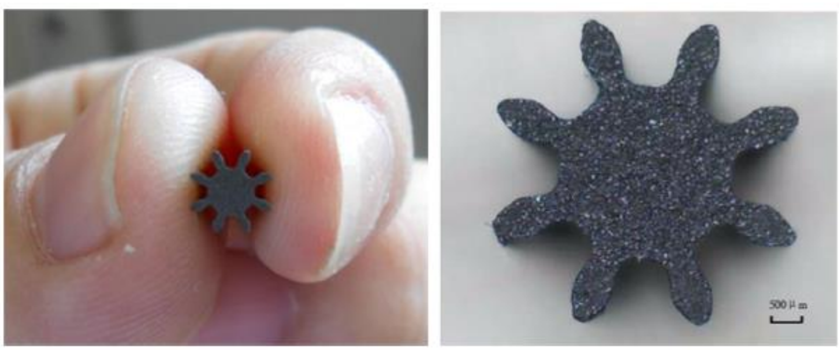

Figure 29. Cutting sample of tiny, complex, and non-linear workpiece [17].

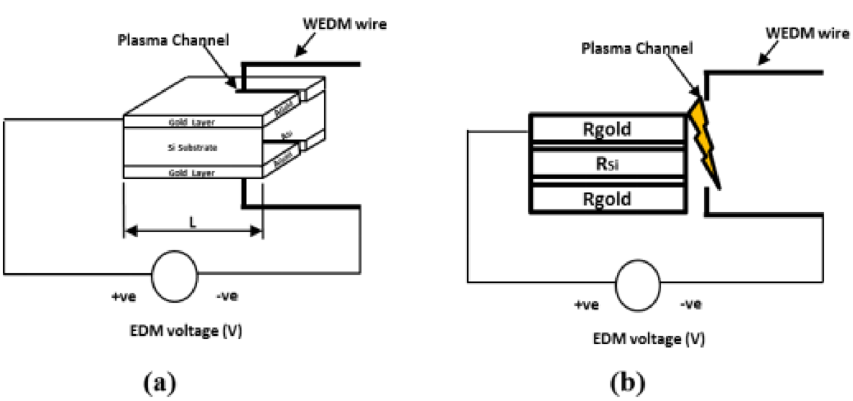

Figure 30. (a) Simplified Model of the WEDM Zone (b) Analogous Electric Circuit [18].

In this case MRR was increased by up to 7 x times for coated samples. Overall this new method of µ-WEDM and µ-EDM technique of polished Si wafer has been found to be more efficient and useful. Removal of the conductive coating without damaging the substrate is a challenge for this process which was carried out successfully by selective etching method. In order to explain the concept, authors proposed a simple model of the actual WEDM zone as shown in the Figure 30 (a). The analogous electrical circuit model is shown in Figure 30 (b). The equivalent resistance of the modified workpiece can be determined from the following formulation which describes that equivalent resistance becomes closer to coating material specific resistance as the resistance increases. Authors also describe the process model and analogous circuit for μ-EDM as shown in Figure 31. In this case coating configuration reduces the contact resistance between the Si workpiece and metallic work table ($R_{Au/metal}$) and enhances the EDM process.

$$\rho_{eq} = \lim_{K_2 \to 0} \frac{(2K_2 + 1)}{2K_2 + K_1} K_1 \rho_{Si} = \rho_{Si} \tag{5}$$

$$\rho_{eq} = \lim_{K_2 \to \infty} \frac{(2K_2 + 1)}{2K_2 + K_1} K_1 \rho_{Si} = K_1 \rho_{Si} = \rho_{gold} \tag{6}$$

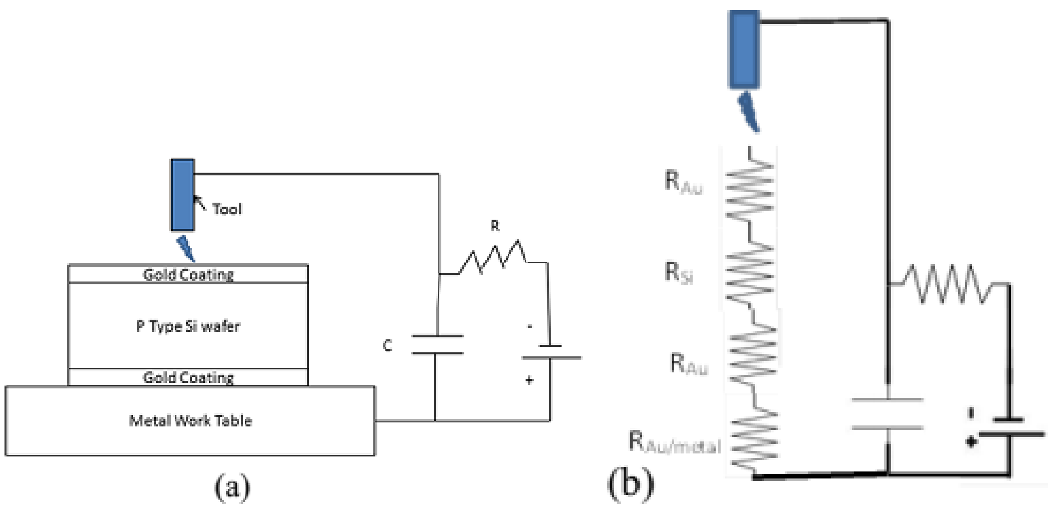

Figure 31. (a) μ-EDM operation for gold coated Si (b) Equivalent electrical model [18].

For gold coated Si MRR (by WEDM) was increased as compared to uncoated Si. At 105V and 0.1nF it was increased by ~20% and at 105V and 10 nF it was increased by ~123% as compared to uncoated Si. Figure 32 also displays the evidence of enhanced material removal rate for Si coated by gold. It can be observed in Figure 32 that MRR increases with discharge energy for coated Si. However, in the case of WEDMing of uncoated Si machining was not possible at low discharge energy (minimum discharge energy required for machining was ~550 nJ for uncoated Si).

Similar phenomenon was observed during μ-EDM operation of gold coated Si. Table 2 shows the comaprative data of machining time for gold coated and uncoated Si (by μ-EDM). It is very clear that machining rate or MRR for gold coated silicon samples is much higher than uncoated silicon sample, especially in high discharge energy process (85 V and 10 nF).

This enhancement of MRR of coated Si is due to the low contact resistance as mentioned earlier.

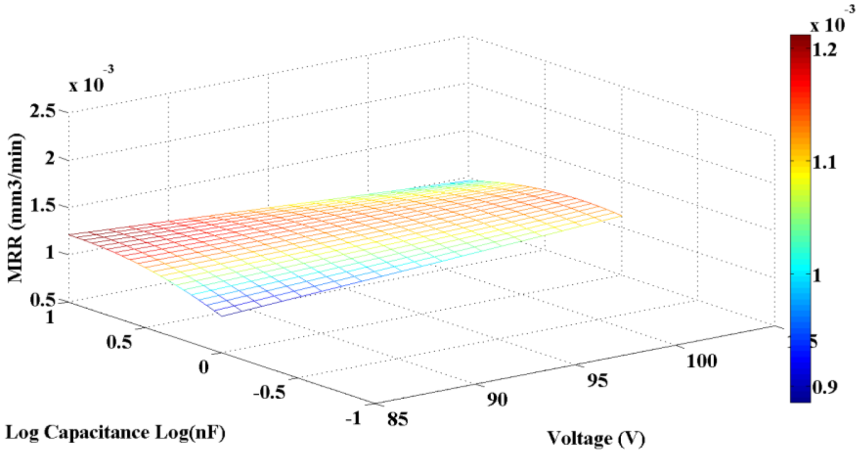

(a)

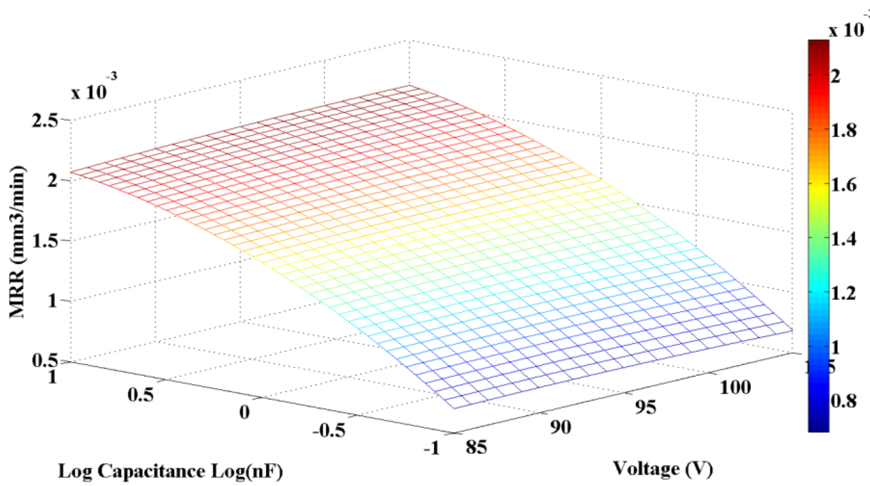

(b)

Figure 32. Study of Material Removal Rate (MRR) with working Voltage and applied Capacitance. (a) uncoated Si (b) gold coated Si b [18].

Table 2. Difference in μ-EDM Machining time [18]

Sample Type	Voltage Value (V)	Capacitance Value (nF)	Machining Time (min.)
Si	85	10	88.2166
Gold coated Si	85	10	9.0333
Si	95	1	39.0333
Gold coated Si	95	1	14.9333
Si	105	0.1	43.2833
Gold coated Si	105	0.1	21.7833

Finally researchers completely removed the gold coating from the sample without damaging the Si substrate. Figure 33 shows the sample (with EDX result) with gold coating and sample after removing the gold coating.

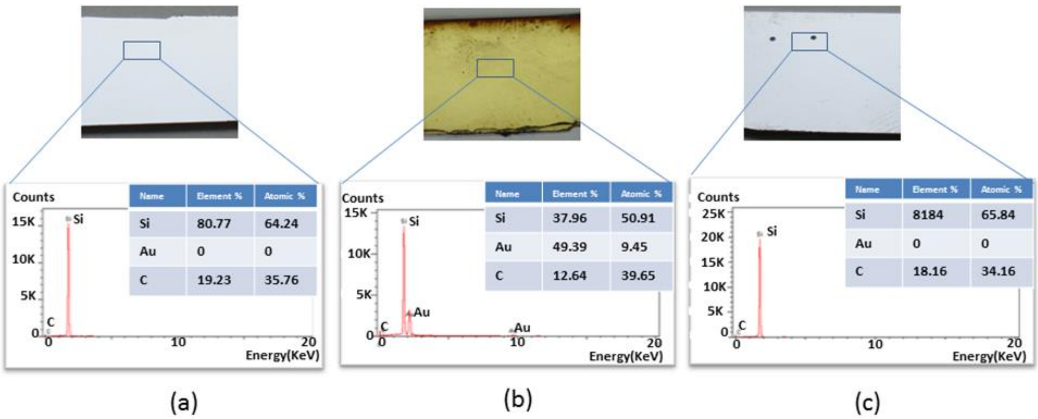

Figure 33. Electron Dispersive X-ray (EDX) analysis of samples (a) Original Si (b) Gold coated Si substrate (c) Si substrate after removal of gold [18].

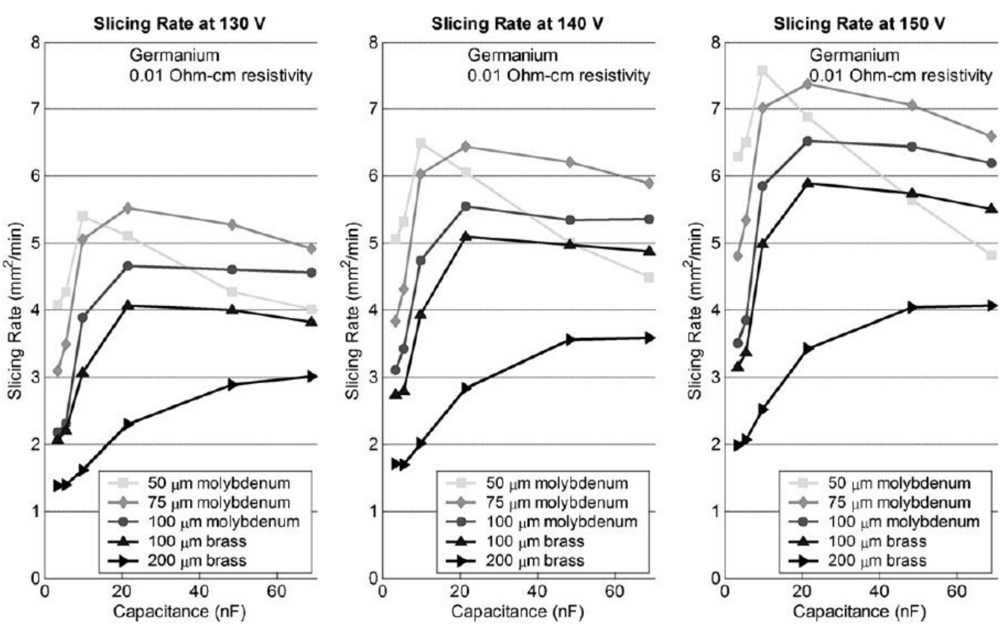

Figure 34. Slicing rate for molybdenum wire with diameter 50, 75 and 100µm and brass wire with diameter 100 and 200µm [19].

Bamberg et al., [19] experimentally investigated WEDM machining of doped semi-conductor material germanium. A series of experiments were carried out by the researchers to investigate the relationship between slicing rate and different types and size of electrode wires. Figure 34 shows dependence of slicing rate on discharge energy, types and size of the electrode wire. It can be observed from the figure that molybdenum wire provides higher slicing rate as compared to brass wire. Further, in the case of brass wire larger diameter reduces the machining rate but for molybdenum wire relationship between size of the wire and slicing rate is not conclusive. Figure 35 shows the study of surface roughness. For all the condition the range of average surface roughness achieved was 3μm-4μm. Moreover, types and size of electrode wire does not have much impact on the obtained surface quality.

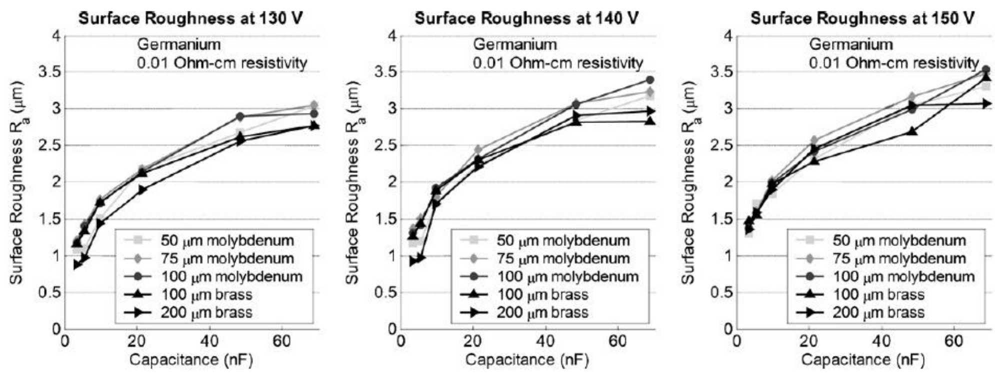

Figure 35. Surface roughness for molybdenum wire with diameter 50, 75 and 100μm and brass wire with diameter 100 and 200μm [19].

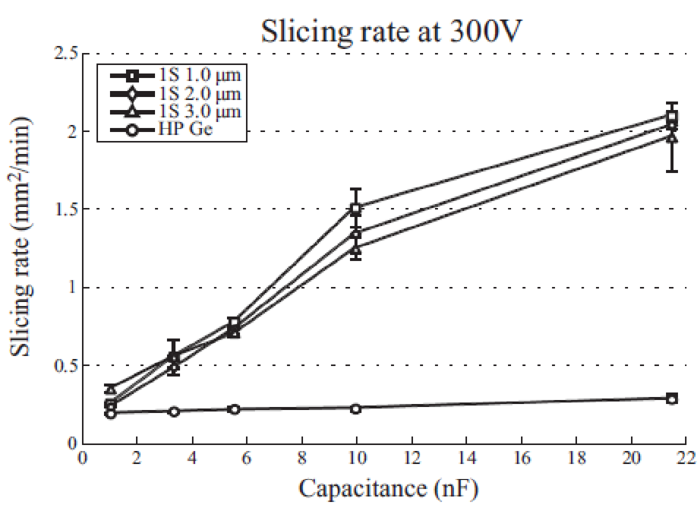

Figure 36. Slicing rate of Al coated (1.0, 2.0, and 3.0 m at 1 side) versus HP Ge [20].

Lee et al., [20] recently investigated WEDM machining of pure germanium by conductive metal coating. Figure 36 shows the comparative study of slicing rate for coated and uncoated HP Ge (high purity germanium). It can be observed very clearly that coating enhances the slicing rate significantly (up to 7 x). However, amount of thickness does not affect much on the slicing rate. Figure 37 shows study of slicing rate with different coating side. It is obvious from the figure that double side coated sample yields highest slicing rate as compared to uncoated and 1 side coated sample. The maximum slicing rate achieved for double side coated sample was 27 x faster compared to uncoated HP Ge. It was also observed that Kerf width is smaller under same machining condition for double sided coated sample than single sided coated sample. Authors also studied effect of Ni and Al as the coating material. Al was proven to be a better option to increase the slicing rate as it has lower barrier height on n-type Ge as compared to Ni.

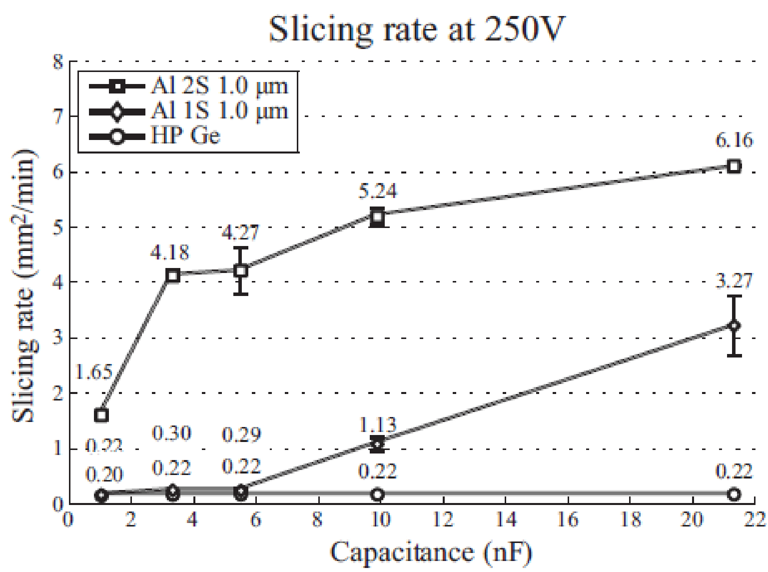

Figure 37. Average slicing rate with standard deviation of Al coated (1.0 μm thickness at 1 and 2 sides) versus HP Ge [20].

3. Electro-Discharge Machining of Vertically Aligned Carbon Nano Tube Array (CNT Forest)

Carbon nanotubes (CNTs) have highly attractive mechanical, electrical, optical, and thermal properties [21]. The formation of patterned CNT forests has widely been conducted through selective growth of the forests by chemical vapor deposition (CVD) on pre-patterned catalyst on the substrate. However, this technique is limited to producing two-dimensional patterns with uniform height. Micropatterning of three-dimensional, free-form structures with high aspect ratios in pure CNT forests was recently demonstrated by UBC (University of British Columbia) research group in Canada using a process based on micro-electro-discharge machining (μEDM) [21-25]. This research group has conducted a series of study on this area which will be discussed here.

In their first study Takahata group experimented the feasibility of μ-EDMing operation of CNT forest. Unlike conventional μ-EDM Khalid et al., **[21]** used air as the dielectric medium for the study. Liquid dielectric medium was not used because it damages the integrity of original CNT forest due to capillary action. It was found that too low voltage (~ 10 V) could not produce enough spark and visible marks were observed due to mechanical touching. Further too high voltage (~ 80 V) usually damages resultant structure due to excessive spark gap. Optimal voltage level was found to be in a range of ~ 30 V. Figure 38 explains the phenomena. Further it was observed that usual spark gap resulted in this operation is 10 μm, which is quite high. This limits the resolution of the resultant structure. Average discharge current was observed to be 20 mA with 20 nS pulse duration. In their study Khalid et. al successfully machined a thin wall of 5 μm with 20 times aspect ratio as shown in Figure 39.

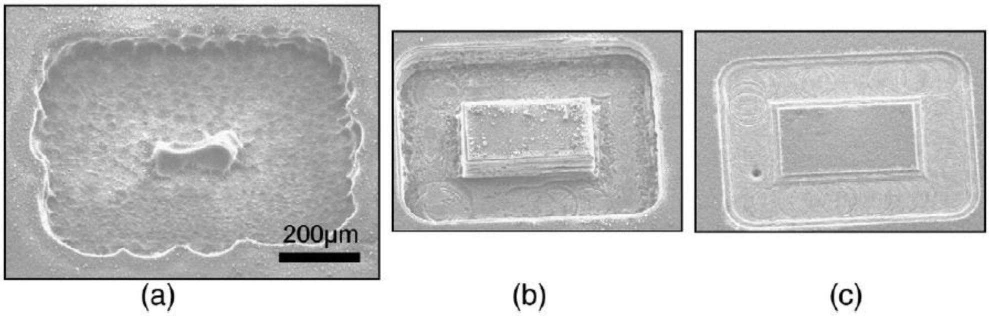

Figure 38. SEM images with the same magnification showing μEDM results for the same pattern created with (a) 80 V, (b) 30 V, and (c) 10 V [21].

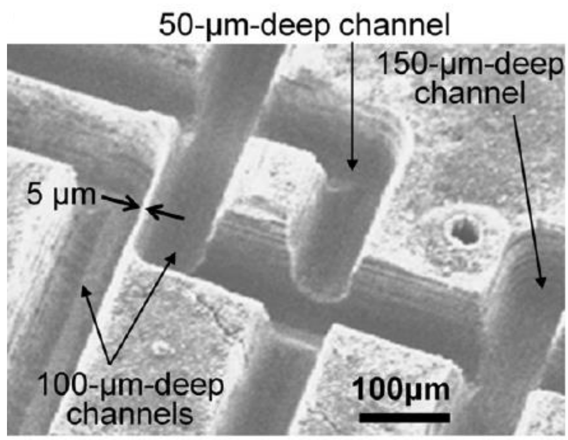

Figure 39. Multi-level microchannel structures patterned in a CNT forest [21].

Masoud et al., tried [22] to investigate the physical mechanism of the μ-EDM process of CNT forest. They suggested that EDM process of is unlike the electro thermal erosion process metal EDM. Rather it is more like an oxidation process similar to oxygen plasma etching and oxygen is very much needed in the process. Figure 40 and Figure 41 show the effect of oxygen on the resultant structure of the CNT forest and on the machining rate respectively. It can be observed from the figures that no oxygen environment is not suitable for the operation as it results bad quality structure (Figure 40) with unstable machining (Figure 41). However, 21% and 50% oxygen condition stabilize the machining condition with no short circuit detection but the structure produced by 50% oxygen condition is somewhat rougher. Therefore authors concluded that air is the most suitable medium for μ-EDM operation of CNT forest.

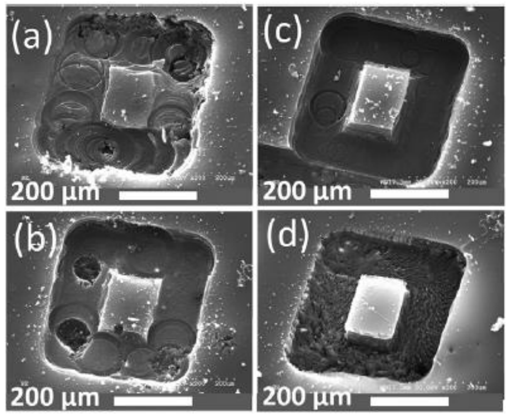

Figure 40. SEM images of lEDMed CNT forests in N2 gas mixed with (a) 0% O2 (oxygen free), (b) 10% O2, (c) 21% O2, (d) 50% O2 [22].

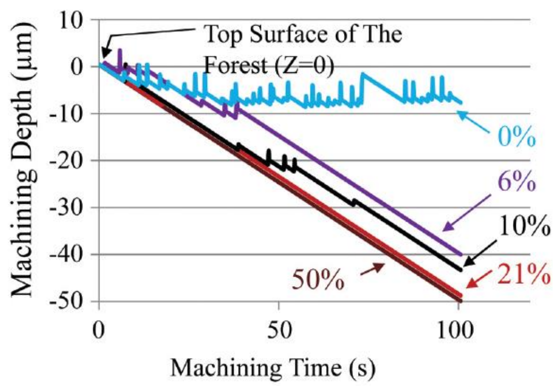

Figure 41. Progressions of electrode feeding in µEDM of a CNT forest with different O2 concentrations in N2 at 30 V and 10 pF [22].

The machining tolerance, or the discharge gap clearance between a forest and the µEDM electrode, was reported to be 10 µm or more as mentioned earlier. This is significantly larger than typical values (of one to a few µm) involved in standard µEDM with dielectric liquid. Toward achieving higher precision and nano-scale removal in dry µEDM of CNT forests Saleh et al., [23, 24] proposed a new concept of reverse µEDM of the CNT forest where the CNT forest was set to be negative. The hypothesis behind this idea was as follows, in typical EDM (including µEDM), the workpiece and the electrode are generally arranged to be the anode and the cathode, respectively to reduce the tool wear. However, CNT is known to be an efficient field emitter because of its nano scale tip radii. Therefore if CNT forest is set to be –ve polarity then it would be possible to initiate the discharge at low voltage subsequently can reduce the spark gap. It was found by the authors that for lower voltages the reverse-polarity µEDM exhibited advantageous effects towards miniaturization in the CNT removal process with higher precision. The previous studies reported that the lowest value of the optimal voltage with the normal polarity was around 30V , and that further lowering of the voltage led to mechanical grinding of the CNTs [21]. However, Figure 42 shows SEM image of the samples machined at 20 V using both normal and reverse polarity, reverse-polarity machining produced smoother surfaces compared to normal-polarity processing. One possible cause of this result may be the difference in the discharge current between the two cases – the reverse-polarity process produces higher current than the normal-polarity for the same voltage. This may allow the former to remove CNTs effectively, whereas the latter suffers from insufficient removal because of smaller discharge currents, possibly causing mechanical abrasion of the forest. The above effect was further verified with deeper patterning with both polarities at 10 V (with 10 pF) in this case. The results in Figures 4(c) and 4(d) indicate that the reverse-polarity process produced sharper, smoother, and cleaner microstructures compared to the normal-polarity case. Moreover, the patterns created with the reverse polarity exhibited a narrower width in the machined grooves compared to those with the normal polarity even though identical electrode and machining conditions were used.

From the dimensions shown in Figure 4, as well as the diameter (93 μm) of the electrode used, the discharge gap clearance is calculated to be 7.5 μm for the normal polarity, whereas for the reverse polarity it is 2.5 μm, which is 3× smaller (and shows a ~4× improvement over the previous result reported in [21]). This means that the reverse μEDM enables much tighter tolerances and higher precision in CNT forest patterning. Figure 43 shows some patterns machined using reverse μEDM of CNT forest.

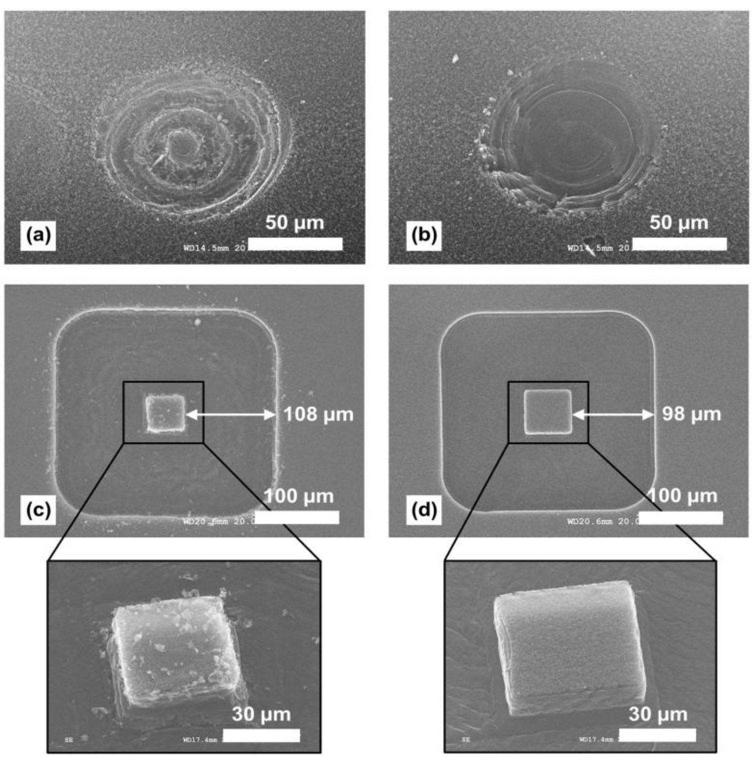

Figure 42. The upper two SEM images show shallow cavities machined in a CNT forest using 20 V and 10 pF with (a) normal polarity and (b) reverse polarity. The lower two SEM images show micropatterns machined in a CNT forest using 10 V and 10 pF with (c) normal polarity and (d) reverse polarity, for a depth of 40 μm with 1-μm-step electrode feeding in the Z direction. The images in (c) and (d) also show close-up views of the microstructures created in the cavities [23].

Saleh et al., [25] further studied μEDMing operation of CNT forest to achieve even tighter tolerance. In this research they used Sulphur Hexafluoride (SF6)+ O2 instead of N2+O2 as the dielectric medium which has 3 x higher dielectric strength. In this case the tool needs to approach much closer to the CNT forest to attain the discharge hence smaller spark gap. From their findings, Saleh et. al concluded that reverse μEDM in the new gas system was effective in lowering the machining voltage, leading to finer and cleaner CNT removal compared to the normal-polarity condition. Moreover, with a discharge voltage of 25 V and an O2 concentration of 20%, the use of SF6 was revealed to give better results compared to N2, the conventional ambient medium; the discharge gap could be reduced to 4.2 μm. At a lower voltage level (10 V), an N2 ambient with 20% O2 produced an even smaller discharge gap, although the occurrence of short circuits slowed the removal process somewhat. Further, SF6-O2 gas system at 25 V was demonstrated to enable not only more stable and faster processing but also relatively higher machining quality compared to the optimal N2-O2 ambient case at 10V.

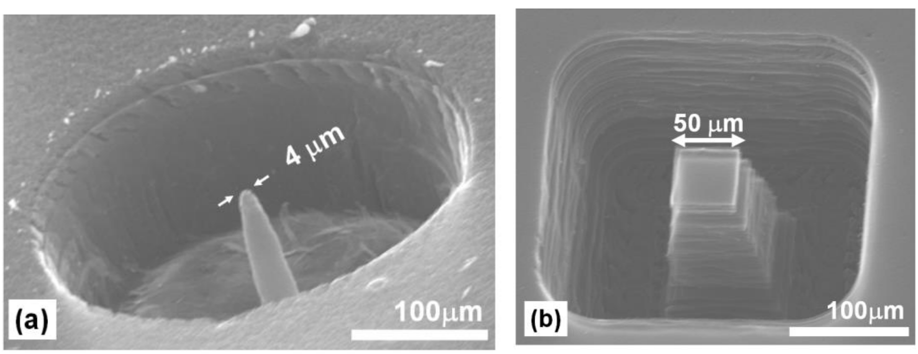

Figure 43. SEM images of high-aspect-ratio microstructures patterned using reverse μEDM at 10V by scanning a cylindrical electrode along a circular or square orbit: (a) A needle-like microstructure with an aspect ratio of ~25; (b) a deep pyramid structure [24].

4. Electro-Discharge Machining of Conductive Polymer and Ceramics

Polypyrrole and other conducting polymers are of interest in actuators, sensors, energy storage devices and organic electronics. The patterning of these polymers can be challenging, particularly polypyrrole due to its insolubility. Muntakim et al., [26] proposed for the first time micro patterning of polypyrrole conductive polymer for using it as an actuator for catheter application. In the first step author studied the through hole making process on polypyrrole by μEDM. It was observed that both wet EDM and dry EDM can be used. However, in case of wet EDM minimum voltage requirement was observed to be 60 V as shown in Figure 44. In case of scanning EDM it was observed that dry EDM produces micro cracks on the resultant EDMed trench (Figure 45) whereas in case of wet EDM structures are free from any kind of mechanical distortion (Figure 46). This is due to lack of flushing hence causing trapped debris to form electrical paths for short circuiting or arcing between the tool and workpiece that led to thermal damage including micro-cracks.

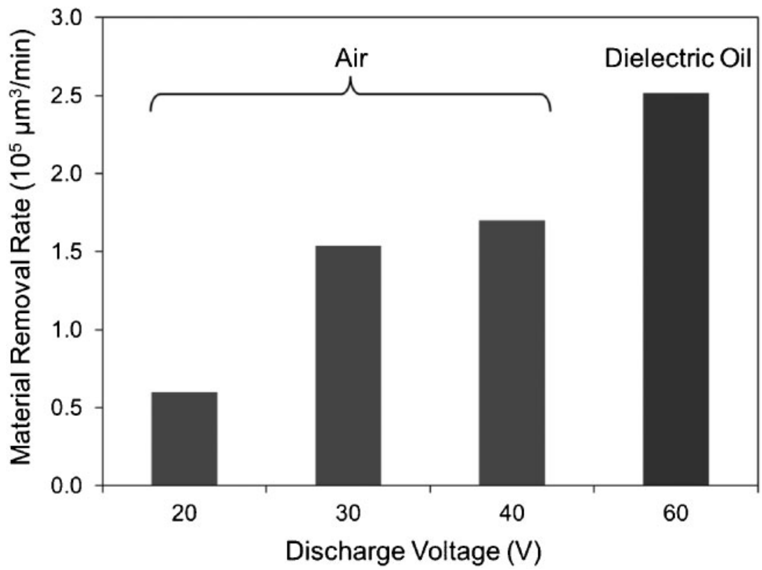

Figure 44. Material removal rates measured in through-hole μEDM of polypyrrole in air and dielectric oil with different discharge voltages [26].

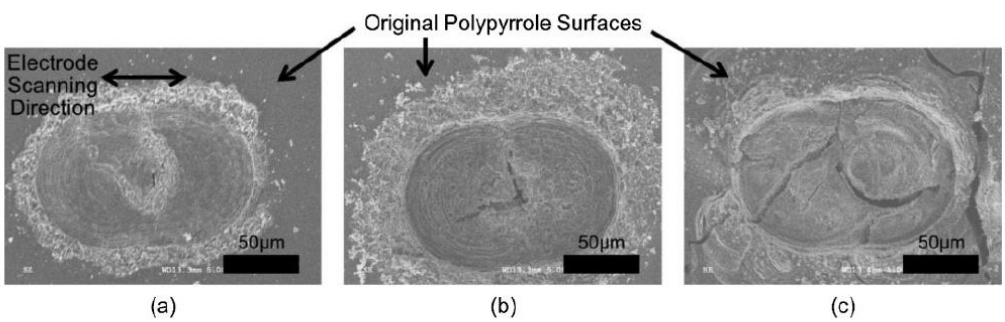

Figure 45. SEM images of dry mEDM results from dead-ended slot patterning implemented with discharge voltages of a) 20 V, b) 30 V, and c)40 V on polypyrrole in air [26].

Hanaoka et al., [27] studied to machine insulating ceramics by EDM using assistive electrode method (AEM). In his studied he tested Si3N4, Si3N4/CNT composite and Si3N4/GNP (Graphene nano pellet) composite. A schematic of the assisting electrode method is shown in Figure 47. The surface of the insulating workpiece is coated by a conductive material. (1) At the first stage of EDM, discharge occurs between the tool electrode and the covered layer, similar to EDM of conductors. (2) Discharge occurs between the electrode and the conductive material. At this time electrically conductive carbonized layer is formed on the insulating surface. (3) The carbide products come in contact with the insulating material itself. (4) The carbide products generated from the dissociation of the working oil during the electrical discharge ande maintain the electrical conductivity at the discharged area, even after the assisting electrode material is completely removed. Figure 48 shows the Material Removal Rate (MRR) for different samples. It is clear that for material with higher conductivity MRR is higher. Moreover, higher conductive material may not also require AEM method for machining.

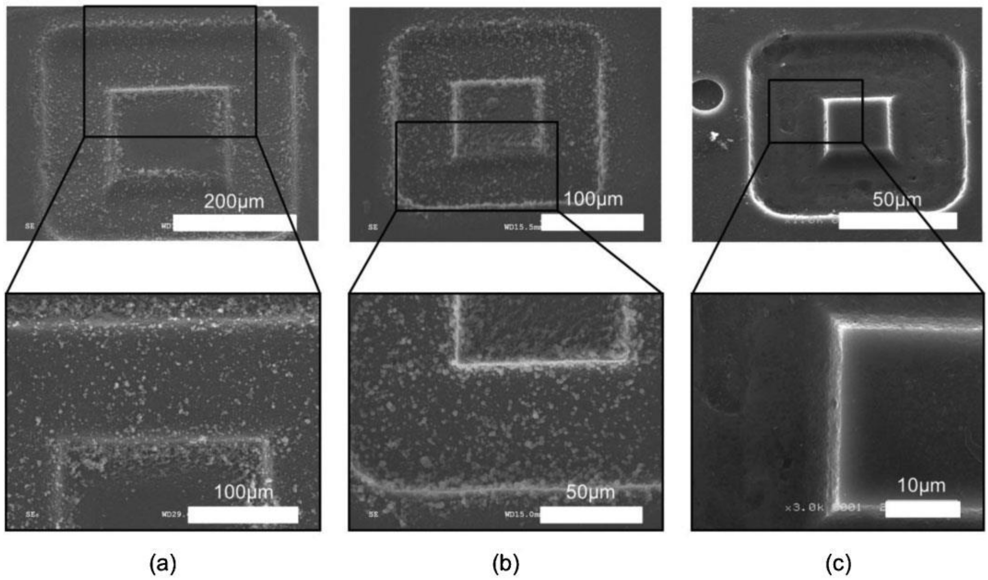

Figure 46. SEM images of differently sized square patterns created in polypyrrole samples through wet μEDM in the oil using the electrodes with diameters of a) 100 μm, b) 50μm, and c) 20μm [26].

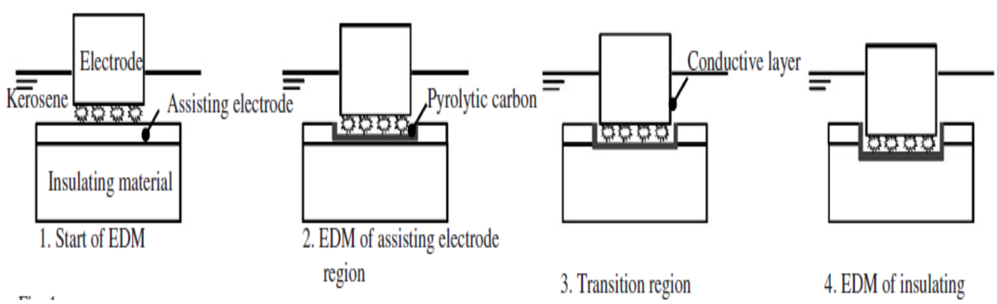

Figure 47. Assistive electrode mechanism (AEM) for EDMing of insulating material [27].

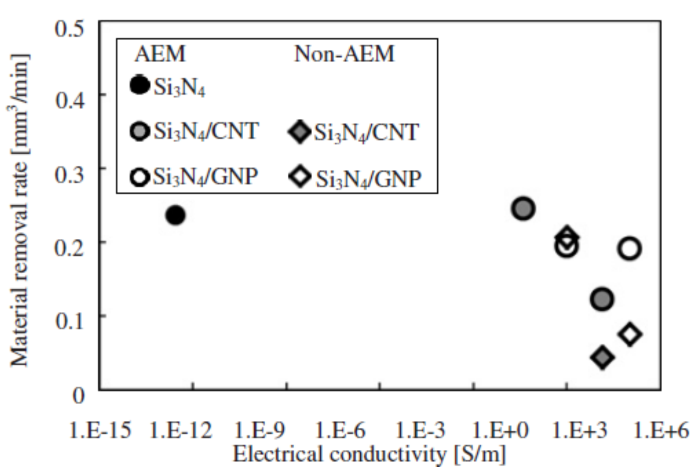

Figure 48. Material removal rate as a function of the electrical conductivity [27].

Wang et al., [28] investigated blind hole machining for Al2O3/6061Al metal matrix composite (MMC). They tried three ‘electrode feeding’ method in this study and compared the result of material removal rate (MRR), tool wear and surface roughness. Three electrode feeding methods are namely stationary electrode, rotational electrode and through hole electrode with flushing. Figure 49 summarizes the result of their experimental study.

Figure 49 clearly explains that flushing electrode method gives higher MRR with linear profile machining rate. This is due to efficient removal of accumulated debris from the blind hole. However, this method introduces higher tool wear which might affect the accuracy if not properly compensated. Further, average surface roughness was found to be almost independent of electrode feeding mechanism.

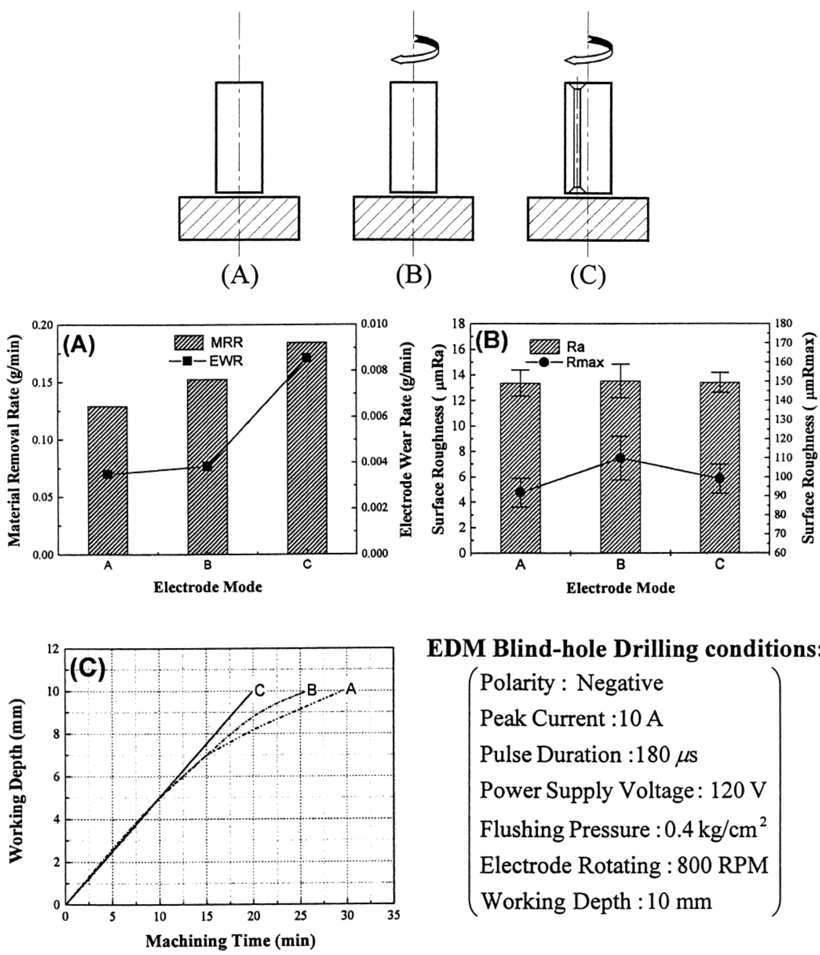

Figure 49. Machining characteristics of the Al2O3/6061Al sample versus the electrode mode of EDMBhD. (A and B modes: electrode using side flushing; C mode: electrode using electrode injection flushing.) (A) MRR and EWR; (B) surface roughness; (C) cutting feed-rate [28].

Esteban et al., [29] developed ceramic/semiconductor/metal nano composite by sintering method and later machined it by Wire Electro Discharge Machining (WEDM). Three types of samples were prepared as described in table 3. The electrical resistivity of the samples were

14.0·10-4 Ω·cm, for ZT, and 7.2·10-4 Ω·cm, for ZTN (Table 1). At first ZT was not machinable by EDM, however by adding small amount of metal the resistivity of the composite drastically reduced and became machinable by EDM without compromising the mechanical properties. The authors concluded that metal nano particle plays an important role in reducing the resistivity of the composite hence can be machined to achieve desirable features by EDM.

Tak et al., [30] experimentally investigated EDM machining of Al2O3/CNTs composite material. CNTs was used to increase the conductivity of the composite as shown in Figure 50. The taper angle was evaluated as this one of the key parameters to be characterized in EDM. It was observed that higher concentration of CNT improves the conductivity however, it is not always helpful for machining as it causes violent sparks resulting inadequate dimensional accuracy as shown in Figure 51.

Table 3. Properties of developed composite by sintering method

Symbol	Material	Measured density (g/cm^3)	Relative density (%)	Vickers hardness (GPa)	Toughness ($MPa{\cdot}m^{1/2}$)	Flexural strength (MPa)	Electrical resistivity ($(\Omega{\cdot}cm){\cdot}10^{-4}$)
Z	3Y-TZP	5.99±0.2	99.0±0.2	11.0±0.2	4.9±0.2	752±16	---
ZT	3Y-TZP/TiC (28 vol% TiC)	5.65±0.2	98.5±0.2	13.8±0.3	4.5±0.2	727±15	14.0±1.0
ZTN	3Y-TZP/TiC/Ni (20 vol% TiC, 8 vol% Ni)	6.00±0.2	99.1±0.2	11.5±0.2	6.0±0.2	804±21	7.2±1.0

Asfana et al., [31] carried out experimental investigation on µEDM machining of zirconia (ZrO2) by assistive electrode method (AEM) as explained earlier. They tried four configurations as shown in Figure 52.

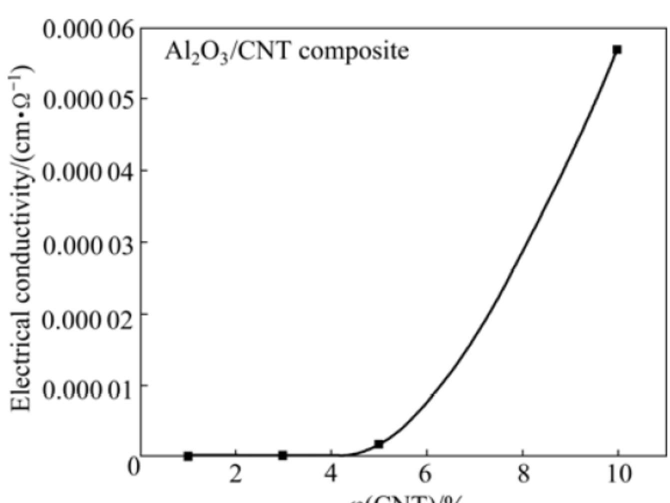

Figure 50. Electrical conductivity Al2O3/CNT composites for various CNT concentration [30].

They found that stable machining was achievable when Copper (Cu) tape was used as the assistive electrode. Authors also studied the effect of polarity and flushing method on the machining of ZrO2. It was found that normal polarity machining i.e., workpiece +ve and electrode –ve reveals better result as shown in Figure 53. Further submerged EDM operation was proven to be better because in this case debris and carbon elements maintained a continuous conductive layer on the machined zone for further machining to take place.

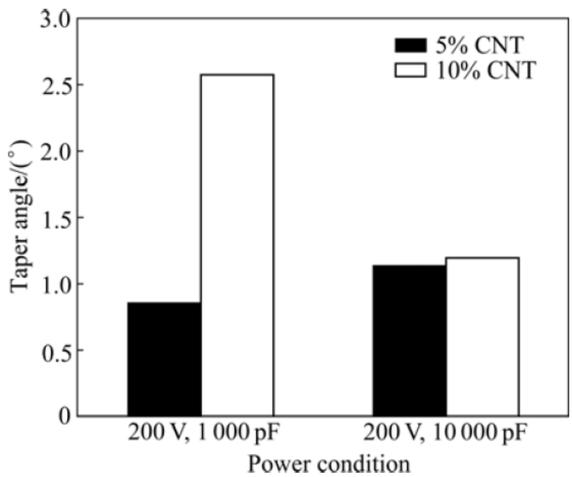

Figure 51. Comparison of taper angles under power conditions and different CNT concentration [30].

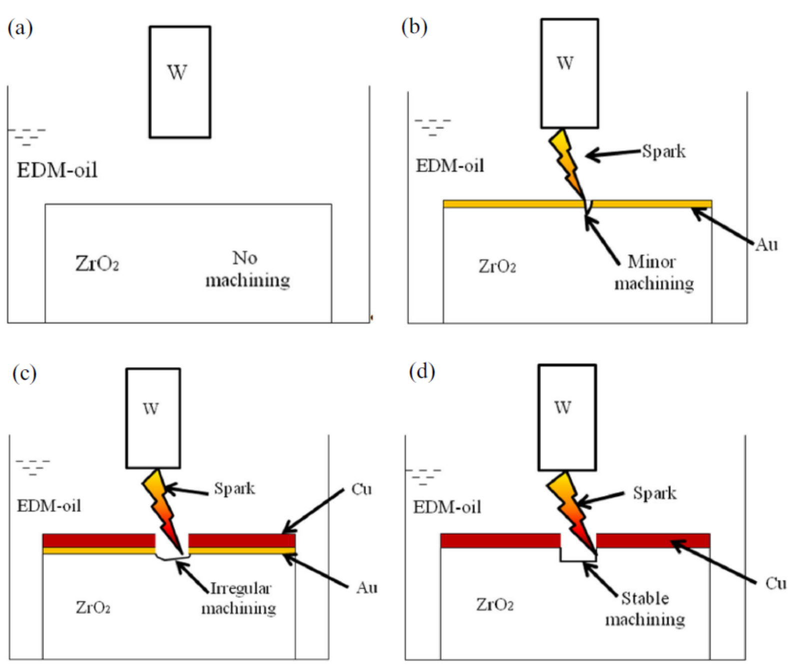

Figure 52. Machining setup with a ZrO2 without AE, b ZrO2 with Au coating, c ZrO2 with adhesive Cu and Au coating, and d ZrO2 with adhesive Cu coating [31].

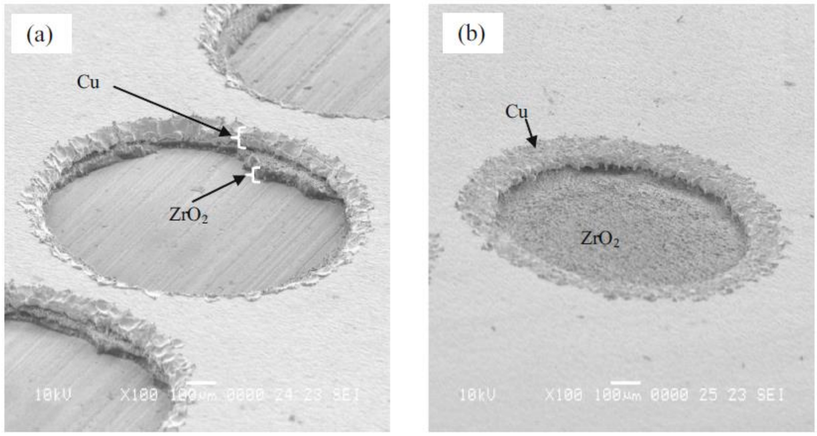

Figure 53. SEM images for machined area of ZrO2 due to micro-EDM with same machining condition a workpiece positive polarity and b negative polarity of workpiece [31].

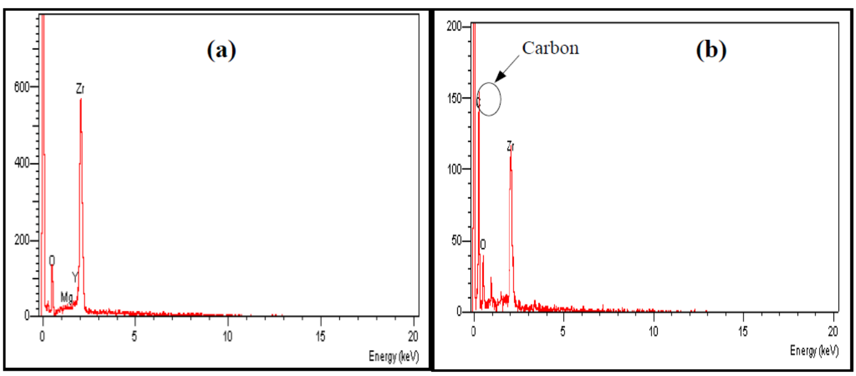

Figure 54. (a) EDX analysis of pure ZrO2 no C is present. (b) EDX analysis of EDMed ZrO2 sample. It shows presence of pyrolytic C [32].

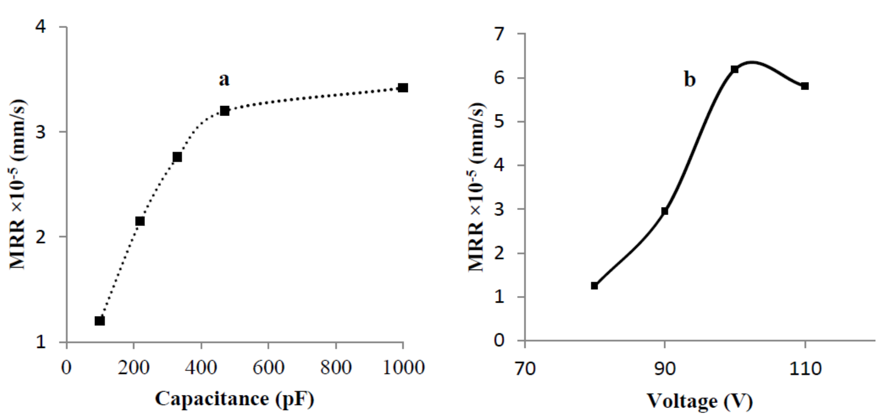

Figure 55. MRR of ZrO2 EDM (a) variation due to discharge capacitance (b) variation due to applied voltage [32].

Sabur et al., [32,33] investigated μEDM milling of ZrO2 using assistive electrode method. Adhesive copper foil was used in this purpose as described in [31]. It was observed that after milling operation machined ZrO2 surface contains high percentage of C, which indicates formation pyrolytic carbon during the EDM operation. Figure 54 shows the result of EDX analysis of the pure ZrO2 and EDM milled ZrO2.

Figure 55 shows effect discharge voltage and capacitance on the Material Removal Rate (MRR) of ZrO2 by μEDM. It is understood from the figure that MRR for ZrO2 is similar to that of metal EDM. As the discharge energy increases by increases voltage or capacitor MRR also increase. Authors also reported the average surface roughness (Ra) achieved by EDM operation of ZrO2 was 0.295 μm.

Schubert et al., [34] also studied μEDM milling of ZrO2 by using assistive electrode method. Further they compared it with metal μEDM milling. In this research authors used two level of discharge energies namely CF100 (smallest value) to CF104, representing discharge currents of i=3A to i=8.5A and discharge durations of te=100ns and te =180ns, respectively.

Figure 56 shows comparison of surface roughness between 1.5920 steel and ZrO2 sample for EDM operation at different energy level. It can be seen that rougher surface is produced on ZrO2 sample for both in lower and higher discharge energy. Another interesting observation made by the researchers is that during EDMing of ZrO2 the discharge pulse generated is significantly higher than EDMing of steel. This concept is described in Figure 57. It is a well-known phenomenon that high frequency shorter pulse is desired for micro-edm operation to avoid any kind of arcing.

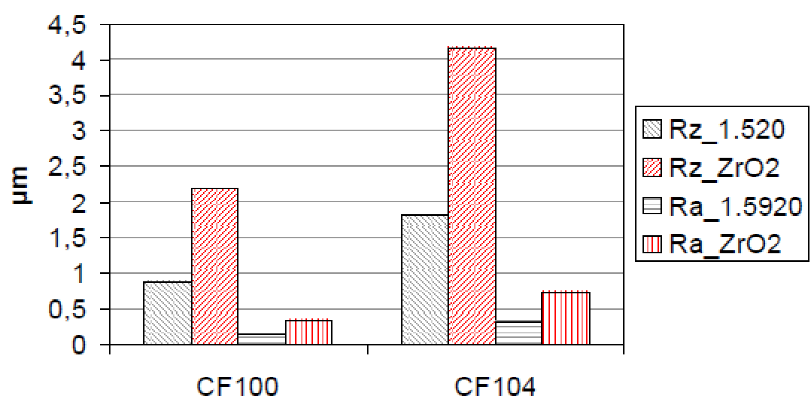

Figure 56. EDMed surface roughness at different discharge energy for steel and ZrO2 [34].

Zhang et al., [35] also conducted experimental study on EDM machining of hot pressed aluminium oxide based ceramics. They concluded that conductive ceramics will yield better machinability by EDM as compared to metal. This is because of their very low thermal conductivity. Their experimental result also revealed that material removal rate, the surface roughness, and the diameter of discharge point all increase with increasing pulse-on time and discharge current.

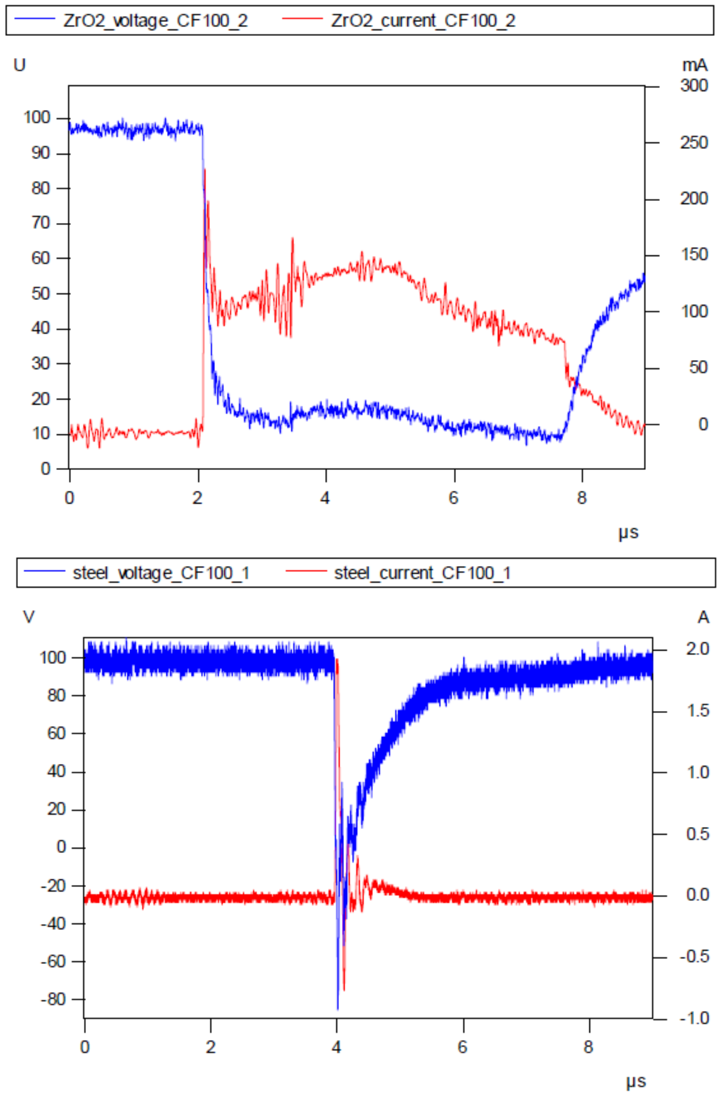

Figure 57. Single discharge for EDM (a) ZrO2 (b) Steel [34].

5. Electrochemical-Discharge Machining (ECDM) of Glass

Wuthrich et al., [36] discussed the phenomenon of electrochemical discharge machining of non-conductive material such as glass. At first the sample is submerged an appropriate electrolyte solution. After that a constant DC voltage or a pulsed voltage is applied between the anode and cathode as shown in the Figure 58. As the voltage goes up electrochemical discharges happen after reaching a critical value which depends on the geometry and concentration of the used electrolyte. A typical threshold voltage level is 30 V. At this huge generation of gas bubble forms a gas film and isolates the tool electrode from the electrolyte. The electrical field in this film becomes high enough to allow electrical discharges between the electrode and the electrolyte. The heat generated by these discharges and probably some chemical etching contribute to the eroding of the, to be machined substrate if it is positioned in the near vicinity of the electrode.

In their earlier study Wuthrich et al., [37] machined borosilicate glass using ECDM method. Figure 59 shows the SEM image of the micro channel machined by ECDM method on the glass sample. In this study researchers varied several parameters such as working distance between the tool and workpiece, applied voltage and glass composition.

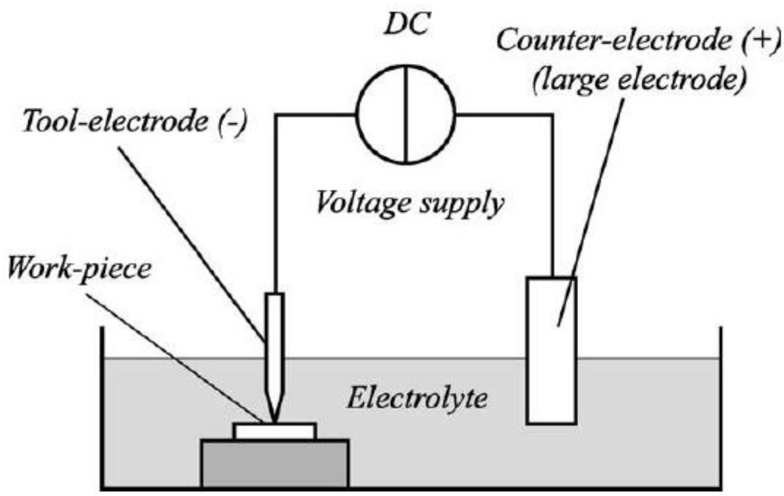

Figure 58. Principle of Electrochemical Discharge machining [36].

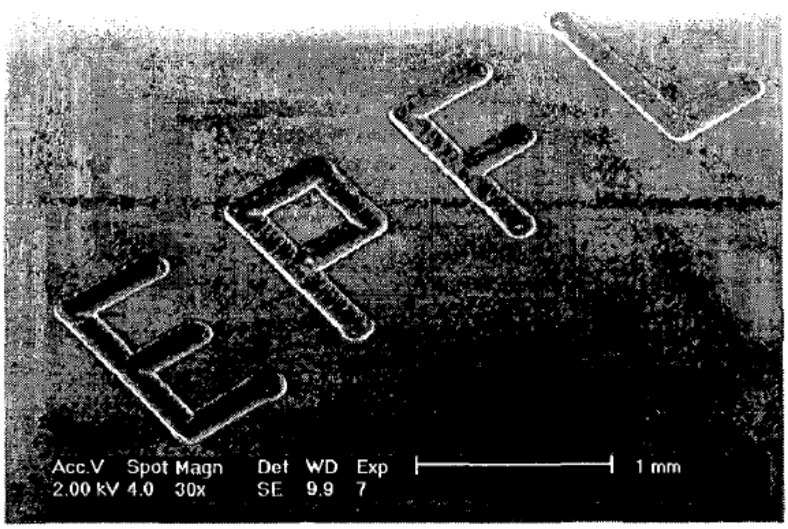

Figure 59. Micro Channel machined by ECDM method on glass [37].

Yan et al., [39] proposed another machining technique for glass micro machining. In this case the authors fabricated micro tool using μEDM method and then carried out micro machining of glass by ultrasonic vibration machining (MUSM) using the fabricated tool. The process is explained in Figure 61. Micro hole tapper-ness is a very important parameters to be considered in any micro machining. This was studied by the researchers under various parameter variations such as slurry concentration and grain size, USM vibration amplitude, rotational speed of the tool and federate. In all cases it was observed that tapper-ness increases with the increase of all the parameters such as rotational speed of the tool, federate etc.

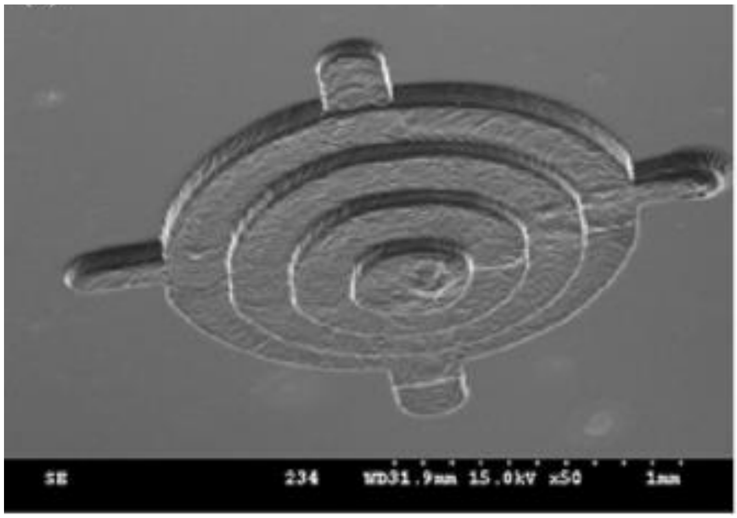

Figure 60. 3-D micro structure machined by ECDM method on pyrex glass [38].

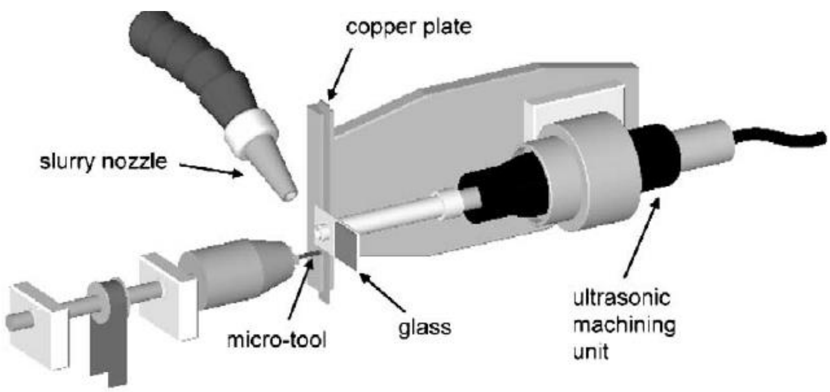

Figure 61. The detail diagrams of experimental apparatus at MUSM process [39].

CONCLUSION

Electro-discharge machining is a well-established non-conventional machining process mostly used for metal based fabrication. This machining method is used both in micro and macro domain. This chapter describes that EDM can be useful for non-metallic manufacturing process. Semiconductor material like Si also can be machined by EDM process. However, some measures need to be taken to enhance the machining such as forward biasing of Si by applying appropriate polarity and applying temporary conductive coating. Carbon Nanotube forest samples (CNT forest) can also be patterned (top down approach) by

EDM. However, challenge of higher discharge gap can be overcome by using reverse polarity and high dielectric strength medium. Non-conductive material like glass and ceramic can also me machined by EDM by electrochemical discharge machining (ECDM) and assistive electrode method (AEM).

REFERENCES

[1] Masaki, T., K. Kawata, and T. Masuzawa. Micro electro-discharge machining and its applications. in Micro Electro Mechanical Systems, 1990. Proceedings, An Investigation of Micro Structures, Sensors, Actuators, Machines and Robots. *IEEE. 1990. IEEE*.

[2] Luo, Y., C. Chen, and Z. Tong, Investigation of silicon wafering by wire EDM. *Journal of materials science*, 1992. 27(21): p. 5805-5810.

[3] Staufert, G., A. Dommann, and D. Lauger, Behaviour of a silicon spring fabricated by wire electro-discharge machining. *Journal of Micromechanics and Microengineering*, 1993. 3(4): p. 232.

[4] Reynaerts, D., P.-H.s. Heeren, and H. Van Brussel, Microstructuring of silicon by electro-discharge machining (EDM)—part I: theory. *Sensors and Actuators A: Physical*, 1997. 60(1): p. 212-218.

[5] Reynaerts, D., et al., Microstructing of silicon by electro-discharge machining (EDM)—part II: applications. *Sensors and Actuators A: Physical*, 1997. 61(1): p. 379-386.

[6] Reynaerts, D., W. Meeusen, and H. Van Brussel, Machining of three-dimensional microstructures in silicon by electro-discharge machining. *Sensors and Actuators A: Physical*, 1998. 67(1): p. 159-165.

[7] Kunieda, M. and S. Ojima, Improvement of EDM efficiency of silicon single crystal through ohmic contact. *Precision engineering*, 2000. 24(3): p. 185-190.

[8] Song, X., et al., Experimental study of micro-EDM machining performances on silicon wafer. in Proceedings of SPIE's 2000 *Symposium on Micromachining and Microfabrication*, Santa Clara, USA. 2000.

[9] Qian, J., et al., EDM texturing of multicrystalline silicon wafer and EFG ribbon for solar cell application. *International Journal of Machine Tools and Manufacture*, 2002. 42(15): p. 1657-1664.

[10] Takino, H., et al., Cutting of polished single-crystal silicon by wire electrical discharge machining. *Precision engineering*, 2004. 28(3): p. 314-319.

[11] Takino, H., et al., High-quality cutting of polished single-crystal silicon by wire electrical discharge machining. *Precision Engineering*, 2005. 29(4): p. 423-430.

[12] Okamoto, Y., et al., Development of multi-wire EDM slicing method for silicon ingot. in *Proceedings of ASPE Annual Meeting and the 12th* ICPE. 2008.

[13] Rakwal, D., et al., Fabrication of compliant high aspect ratio silicon microelectrode arrays using micro-wire electrical discharge machining. *Microsystem technologies*, 2009. 15(5): p. 789-797.

[14] Jahan, M.P., et al., An experimental investigation into the micro-electrodischarge machining behavior of p-type silicon. *The International Journal of Advanced Manufacturing Technology*, 2011. 57(5-8): p. 617-637.

[15] Yu, P.-H., et al., Improvement of wire electrical discharge machining efficiency in machining polycrystalline silicon with auxiliary-pulse voltage supply. *The International Journal of Advanced Manufacturing Technology*, 2011. 57(9-12): p. 991-1001.

[16] Crawford, G.A., Process characterization of electrical discharge machining of highly doped silicon. 2012, DTIC Document.

[17] Zhidong, L., et al., Automatic control of WEDM servo for silicon processing using current pulse probability detection. *The International Journal of Advanced Manufacturing Technology*, 2014. 76(1-4): p. 367-374.

[18] Saleh, T., A.N. Rasheed, and A.G. Muthalif, Experimental study on improving μ-WEDM and μ-EDM of doped silicon by temporary metallic coating. *The International Journal of Advanced Manufacturing Technology*, 2015: p. 1-13.

[19] Bamberg, E. and D. Rakwal, Experimental investigation of wire electrical discharge machining of gallium-doped germanium. *Journal of materials processing technology*, 2008. 197(1): p. 419-427.

[20] Lee, S., M.A. Scarpulla, and E. Bamberg, Effect of metal coating on machinability of high purity germanium using wire electrical discharge machining. *Journal of Materials Processing Technology*, 2013. 213(6): p. 811-817.

[21] Khalid, W., et al., High-aspect-ratio, free-form patterning of carbon nanotube forests using micro-electro-discharge machining. *Diamond and Related Materials*, 2010. 19(11): p. 1405-1410.

[22] Dahmardeh, M., A. Nojeh, and K. Takahata, Possible mechanism in dry micro-electro-discharge machining of carbon-nanotube forests: A study of the effect of oxygen. *Journal of Applied Physics*, 2011. 109(9): p. 093308.

[23] Saleh, T., et al., Field-emission-assisted approach to dry micro-electro-discharge machining of carbon-nanotube forests. *Journal of Applied Physics*, 2011. 110(10): p. 103305.

[24] Saleh, T., et al., High-precision dry micro-electro-discharge machining of carbon-nanotube forests with ultralow discharge energy. in Micro Electro Mechanical Systems (MEMS), 2012 *IEEE 25th International Conference on. 2012. IEEE.*

[25] Saleh, T., et al., Dry micro-electro-discharge machining of carbon-nanotube forests using sulphur-hexafluoride. *Carbon*, 2013. 52: p. 288-295.

[26] Anwar, M.M., et al., Micropatterning polypyrrole conducting polymer by pulsed electrical discharge. *Macromolecular Materials and Engineering*, 2014. 299(2): p. 198-207.

[27] Hanaoka, D., et al., Electrical discharge machining of ceramic/carbon nanostructure composites. *Procedia CIRP*, 2013. 6: p. 95-100.

[28] Wang, C.C. and B.H. Yan, Blind-hole drilling of Al 2 O 3/6061Al composite using rotary electro-discharge machining. *Journal of materials processing technology*, 2000. 102(1): p. 90-102.

[29] Lopez-Esteban, S., et al., Electrical discharge machining of ceramic/semiconductor/metal nanocomposites. *Scripta Materialia*, 2010. 63(2): p. 219-222.

[30] Hyun-Seok, T., et al., Characteristic evaluation of Al 2 O 3/CNTs hybrid materials for micro-electrical discharge machining. *Transactions of Nonferrous Metals Society of China*, 2011. 21: p. s28-s32.

[31] Banu, A., M.Y. Ali, and M.A. Rahman, Micro-electro discharge machining of non-conductive zirconia ceramic: investigation of MRR and recast layer hardness. *The International Journal of Advanced Manufacturing Technology*, 2014. 75(1-4): p. 257-267.

[32] Sabur, A., et al., MICRO-EDM FOR MICRO-CHANNEL FABRICATION ON NONCONDUCTIVE ZrO 2 CERAMIC. *International Journal of Automotive and Mechanical Engineering* (IJAME), 2014. 10: p. 1841-1851.

[33] Sabur, A., et al., Investigation of Material Removal Characteristics in EDM of Nonconductive ZrO 2 Ceramic. *Procedia Engineering*, 2013. 56: p. 696-701.

[34] Schubert, A., et al., Micro-EDM milling of electrically nonconducting zirconia ceramics. *Procedia CIRP*, 2013. 6: p. 297-302.

[35] Zhang, J., T. Lee, and W. Lau, Study on the electro-discharge machining of a hot pressed aluminum oxide based ceramic. *Journal of materials processing technology*, 1997. 63(1): p. 908-912.

[36] Wüthrich, R. and V. Fascio, Machining of non-conducting materials using electrochemical discharge phenomenon—an overview. *International Journal of Machine Tools and Manufacture*, 2005. 45(9): p. 1095-1108.

[37] Fascio, V., et al., 3D microstructuring of glass using electrochemical discharge machining (ECDM). in Micromechatronics and Human Science, 1999. MHS'99. *Proceedings of 1999 International Symposium on. 1999. IEEE*.

[38] Zheng, Z.-P., et al., 3D microstructuring of Pyrex glass using the electrochemical discharge machining process. *Journal of micromechanics and microengineering*, 2007. 17(5): p. 960.

[39] Yan, B., et al., Study of precision micro-holes in borosilicate glass using micro EDM combined with micro ultrasonic vibration machining. *International Journal of Machine Tools and Manufacture*, 2002. 42(10): p. 1105-1112.

In: Electrical Discharge Machining (EDM)
Editor: M. P. Jahan
ISBN: 978-1-63483-591-6

Chapter 13

MICRO ELECTRICAL DISCHARGE MACHINING OF REACTION-BONDED SILICON CARBIDE

***Pay Jun Liew*[*1] *and Jiwang Yan*[2]**
[1]Manufacturing Process Department,
Faculty of Manufacturing Engineering,
Universiti Teknikal Malaysia Melaka, Hang Tuah Jaya, Melaka, Malaysia
[2]Department of Mechanical Engineering,
Faculty of Science and Technology,
Keio University, Kohoku-ku, Yokohama, Japan

ABSTRACT

In recent years, reaction-bonded silicon carbide (RB-SiC) has become an important material in manufacturing optical molding dies for aspherical lenses and microlens arrays, due to its superior material properties such as high hardness and strength at elevated temperature, high thermal conductivity, chemical stability, wear resistance and low density. However, due to its high hardness, RB-SiC is typically difficult to machine by mechanical machining methods. As an alternative method, electrical discharge machining (EDM) has emerged as a possibly effective machining tool to fabricate complex micro-structures on hard and difficult-to-cut materials like RB-SiC. However, the high resistivity of RB-SiC is the main limiting factor for the discharge current of micro-EDM, which directly affects the machining efficiency. In this chapter, a novel machining process, namely hybrid micro-EDM of RB-SiC by combining ultrasonic cavitation and carbon nanofibers will be introduced. The effect of carbon nanofiber concentration and ultrasonic vibration on electro discharging behavior, material removal rate, surface topography and stability of machining process will be described. The machining mechanism involving the material migration phenomenon will be clarified. By using the hybrid EDM process, material migration was significantly suppressed and machining efficiency was improved 5-7 times. High aspect ratio micro holes were successfully fabricated on RB-SiC. The content of this chapter is based on a series of previously published journal papers of the present authors [1-3].

* Corresponding Author: Pay Jun Liew, E-mail: payjun@utem.edu.my

Keywords: Reaction-bonded silicon carbide (RB-SiC), micro-EDM, carbon nanofibers, material migration, ultrasonic cavitation, micro fabrication

INTRODUCTION

Reaction-Bonded Silicon Carbide (RB-SiC)

Silicon carbide is one of the most important materials of the group of non-oxide ceramics. It is well suited for wide applications in harsh environments, due to its good thermal conductivity, high radiation resistance and high breakdown voltage [4]. Recently, the use of SiC as molding dies for manufacturing aspherical glass lenses is getting popular [5], owing to its superior characteristics. Among the ceramics materials, RB-SiC is considered as one of the most promising materials of the SiC ceramics family. The fabrication process for RB-SiC is slightly different from the conventional methods for the SiC. From the viewpoints of dense structure, low processing temperature, good shape capability, low cost and high purity, reaction sintering is considered as one of the new processes for SiC [6].

RB-SiC has excellent properties, such as high thermochemical stability, low density, high stiffness, high hardness, high thermal conductivity and low activation. Some typical material properties of the RB-SiC are shown in Table 1. The electrical resistivity of RB-SiC is around 1453 Ωcm, which is very high compared to other conductive materials.

Table 1. Material properties of RB-SiC

Properties	Values
Si/SiC volume ratio (%/%)	12/88
Density ρ (g/cm^3)	3.12
Young modulus E (GPa)	407
Softening temperature (ºC)	1375
Electrical resistivity (Ωcm)	~1453
Vickers hardness (GPa)	25-35
Bending strength R_T (MPa)	780
Thermal expansion coefficient (10^{-6}/K)	3.23
Thermal conductivity (W/m·K)	143
Porosity (%)	<0.1

Figure 1 shows the surface microstructures of the RB-SiC ceramics, which examined using transmission electron microscopy (TEM). In the TEM micrograph, dark grey grains are 6H-SiC and the light grey regions around them are intergrain Si bonds (size less than 1 µm). It is noticed that a few 6H-SiC grains are directly bonded to each other without the presence of Si bonds at the grain boundaries, resulting in a very dense structure.

RB-SiC has a wide variety of industrial applications. Nowadays, RB-SiC has been thought to be a prospective material for the large-scale light-weight mirrors which used in the precision optical system. Besides that, it is also widely used as molding dies for manufacturing ultraprecision glass lenses in optical manufacturing industry. Due to its excellent thermo-mechanical characteristics such as high thermal stability and conductivity, RB-SiC also has been used extensively as heat exchanger parts for hydrogen production systems [7].

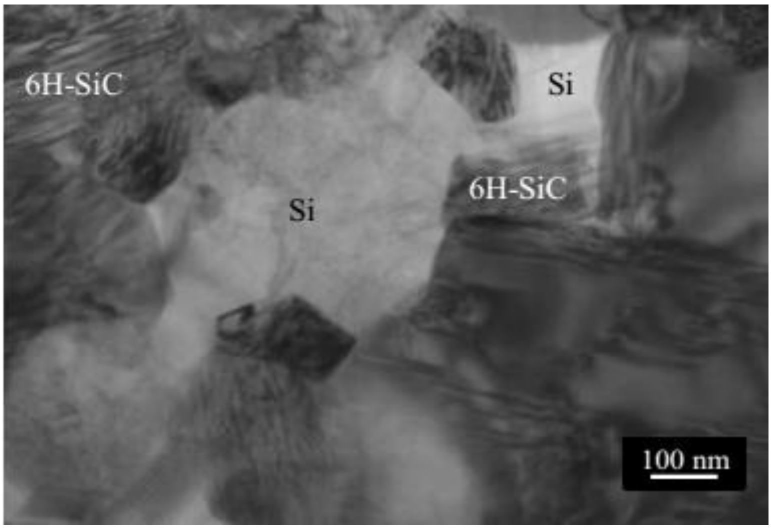

Figure 1. Microstructures of RB-SiC observed by TEM.

Machining Processes for RB-SiC

To obtain a good surface finish and high dimensional accuracy on hard and brittle RB-SiC ceramic material remained a challenging issue. Due to its high hardness (Vickers hardness 25-35 GPa), RB-SiC is extremely difficult to be machined. Many efforts have been made by previous researchers on abrasive machining of RB-SiC. For example, Tam et al. [8] investigated the lapping and polishing of RB-SiC using various kinds of abrasives. The fabrication process of RB-SiC optical components was divided into two stages. At first, for rapid removal of surface error and initial smoothing, a plate fixed with solid pellet-shaped diamond abrasives was used. Subsequently, felt buffs and diamond abrasives were used to perform fine error removal and surface polishing.

Besides lapping and polishing, grinding process also has been widely used to machine hard and brittle material. For instance, Dai et al. [9] used electrolytic in-process dressing (ELID) to grind the high strength RB-SiC. For comparison, cup type and straight type metal bond diamond wheels were used for the grinding test. Generally speaking, even though these abrasive machining processes could produce a very fine surface finish, but the material removal rate is low and the production cycle is long, which normally include many separate operations. Furthermore, it is rather difficult to generate micro-structures such as micro-lens array, micro pyramids on the RB-SiC molding dies with abrasive machining processes.

Single point diamond turning (SPDT) is another important machining method to fabricate micro-structures on hard and brittle material such as single crystal silicon, glass and ceramic. Diamond cutting of RB-SiC was attempted by Yan et al. [10]. Although diamond cutting could produce a high material removal rate, however, severe tool wear still remains to be a problem, which limits its application in industrial.

Recently, electrical discharge machining (EDM) has become popular to machine hard ceramics material. The growing popularity of EDM can be attributed to its advantages, such as low installation cost and its ability to machine complex three-dimensional shapes easily regardless of material hardness [11]. Furthermore, during machining with micro-EDM, there is no direct contact between the electrode and workpiece, thus eliminating mechanical stress, chatter and vibration problems [12]. EDM has been used extensively for machining various ceramic materials. For example, a comparative study of the die-sinking EDM of three different ceramic materials was carried out by Puertas and Luis [13]. Clijsters et al. [14] also manufactured complex parts on SiSiC materials using EDM. However, most ceramics are not sufficiently conductive, which is a major problem when applying EDM to ceramics materials. Konig et al. [15] indicated that 100 Ωcm is the upper limit of electrical resistivity for a ceramic workpiece to be machined by EDM. As pure SiC has a far higher electrical resistivity (~ 10^5 Ωcm), it is impossible to be machined directly by EDM. For RB-SiC, due to the presence of free Si (normally poly-crystalline) and other small-amount additives in the SiC bulk, the electrical conductivity can be improved to some extent [16]. The conductivity of RB-SiC, however, is still very poor if compared to other conductive materials. Hence, the EDM machining efficiency of RB-SiC is extremely low and the EDM process is unstable. For these reasons, this chapter will introduce new technologies for improving the EDM machinability of low conductivity RB-SiC mold material.

METHODS

Carbon Nanofiber Assisted Micro EDM

In order to improve the EDM machinability if low conductivity RB-SiC, carbon nanofibers assisted micro-EDM of RB-SiC was proposed [1]. In this process, carbon nanofibers measuring 150 nm in diameter and 6-8 μm in length were added into the dielectric fluid. Figure 2 shows schematic models for conventional micro-EDM and carbon nanofibers assisted micro-EDM, respectively. Unlike the conventional EDM, carbon nanofibers can arrange themselves in the form of micro chains by interlocking to each other. This is helpful to form bridging networks between electrode and workpiece. The excellent electrical conductivity of carbon nanofiber also reduces the insulating strength of the dielectric fluid and increases the spark gap distance between the electrode and workpiece. As a result, the frequency of electro discharge and the material removal rate in the EDM of RB-SiC might be improved. Furthermore, multiple fine discharges might occur with the addition of carbon nanofibers, leading to a reduction in crater size on the workpiece surface, and in turn, a better surface finish might be obtained.

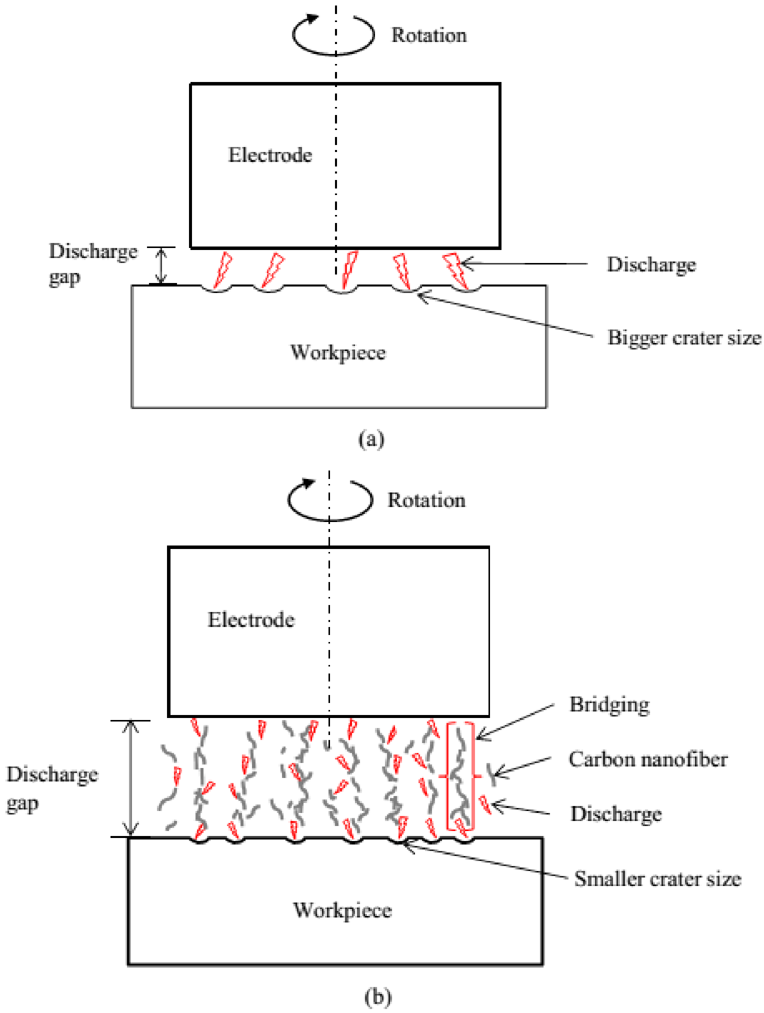

Figure 2. Schematic model for (a) conventional EDM and (b) carbon nanofibers assisted micro-EDM.

Carbon Nanofibers

Carbon nanofibers with the size of 150 nm in diameter and 6-8 μm in length were used as an additive in this study. Figure 3 and Figure 4 show a scanning electron microscope (SEM) and transmission electron microscopy (TEM) micrograph of the carbon nanofibers, respectively. Material properties of the carbon nanofibers are shown in Table 2.

Different fiber concentrations ranging from 0 to 0.28 g/L were used. The dielectric fluid used was hydrocarbon dielectric oil CASTY-LUBE EDS, which has a high flash point. Some of the properties of dielectric fluid are shown in Table 3. In order to prepare the mixed dielectric, the required amounts of carbon nanofibers and dielectric fluid were measured separately before being mixed together and homogenized in a mixer for 20 minutes. This is to ensure that the carbon nanofibers are dispersed uniformly in the dielectric fluid.

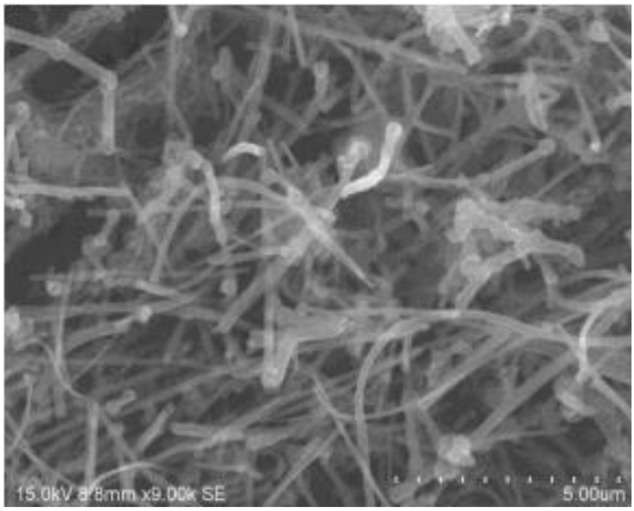

Figure 3. SEM micrograph of carbon nanofibers.

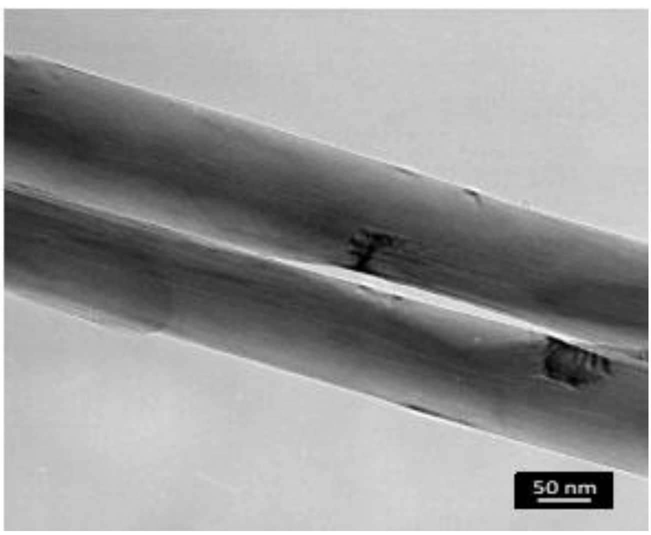

Figure 4. TEM micrograph of carbon nanofibers.

Table 2. Material properties of carbon nanofibers

Properties	Value
Diameter (nm)	150
Length (µm)	6-8
Density (g /cm^3)	2.1
Conductivity (Ωcm)	10^{-4}
Thermal conductivity (W/m.K)	1200

Table 3. Properties of dielectric fluid

Properties	Value
Type	CASTY-LUBE EDS
Density (g /cm^3) (15ºC)	0.767
Ignition point (ºC)	90
Kinetic viscosity (mm^2/s)(40 ºC)	2.24

Machining Equipment and Conditions

The experiments were carried out using a micro EDM machine Panasonic MG-ED82W. This machine has a Resistor–Capacitor (RC) discharge circuit, with a stepping resolution of 0.1 µm. Tungsten rods with 300 µm diameters were used as tool electrodes. The tool electrode tips were dressed by using wire electro discharge grinding (WEDG) before the EDM of RB-SiC, in order to improve their form accuracy. After each EDM cycle, electrode dressing was also performed because the tip electrode, especially the corner, will wear.

Next, for comparison, two types of EDM tests were carried out under different fiber concentrations: (1) depth-controlling method, where die-sinking micro-EDM tests were performed until a depth of 20 µm, and (2) time-controlling method, where each trial run was performed for duration of 5 minutes. Normally, depth-controlling method is used for rough machining (shape generating) and time-controlling method is used for fine machining (surface finishing). Table 4 shows the experimental conditions.

Table 4. Experimental conditions

Rotational speed	3000 rpm
Voltage	110 V
Condenser capacitance	3300 pF
Feed rate	3 µm/s
Dielectric fluid	EDM oil CASTY-LUBE EDS
Additive	Carbon nanofibers (CNFs)
Concentration	0~ 0.28 g/L
Machining time	5 minutes
Cavity depth	20 µm

Machining Conditions for Material Migration Phenomena

For investigating the material migration between electrode and workpiece, each micro-EDM test was performed on the sample for duration of 3 minutes, and average of three repetitions for each parameter setting was taken. First, EDM oil CASTY-LUBE EDS was used as dielectric fluid, and then carbon nanofibers were added into the EDM oil at different concentrations for comparison. The extent of material migrations between the tool electrode and the RB-SiC workpiece was investigated experimentally. Table 5 summarizes the experimental conditions.

Table 5. Experimental conditions

Rotational speed	3000 rpm
Voltage	60~110 V
Condenser capacitance	stray capacitance (~1), 10, 110, 220, 3300 pF
Feed rate	3 μm/s
Dielectric fluid	EDM oil CASTY-LUBE EDS
Additive CNFs size Concentration	Carbon nanofibers (CNFs) Diameter = 0.15 μm Length = 6~8 μm 0.06~0.28 g/L
Machining time	3 minutes

Ultrasonic Cavitation Assisted Micro EDM

In micro-EDM, due to the narrow sparking gap, the removal of debris is remaining a challenging issue, especially in deep hole machining and fine finishing with lower discharge energy. When the debris concentration at the bottom of the gap between the electrode and workpiece reaches a certain critical value, it will not only cause unstable machining, but also worsened the surface finish of the workpiece. In order to improve the machining efficiency of RB-SiC ceramic material and to prevent from tool material deposition on workpiece, a hybrid EDM process by combining ultrasonic cavitation and carbon nanofibers is introduced [3].

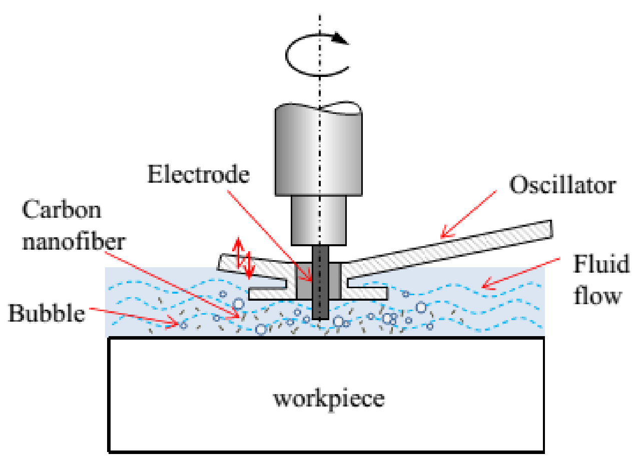

Figure 5. Schematic diagram of cavitation assisted micro-EDM.

The EDM method by combining ultrasonic cavitation and carbon nanofibers is schematically shown in Figure 5. Suitable amount of carbon nanofibers are added and mixed uniformly in the dielectric fluid and then a probe-type oscillator horn (Figure 6) is placed into the dielectric fluid over the workpiece. Then, when ultrasonic vibration is applied to the dielectric fluid, intense ultrasonic waves travel through the liquid, generating small cavities that enlarge and collapse. This phenomenon is called as cavitation [17]. Normally, in micro-EDM, the debris is removed by the gaseous bubbles escaping from the working area through the narrow discharge gap [18-19]. In this chapter, instead of gaseous bubbles, the ultrasonic cavitation will dominate the removal of discharge-induced debris. Thus, stable machining performance will be obtained. The probe-type vibrator (oscillator horn) used in this chapter enables concentrative vibration of the dielectric fluid in the machining region, whereas the unmachined regions are less affected. Therefore, very strong ultrasonic cavitation may be generated at very low energy consumption. From this meaning, the vibration mechanism in this study is distinctly different from those in traditional ultrasonic vibration which is applied to the dielectric tank.

Machining Equipment and Conditions

To excite vibration of dielectric fluid, a probe-type ultrasonic cavitation generator (Figure 6) SC-450 (Taga Electric Co., Ltd., Japan) with a power output of 50W was used in this experiment. It has vibration frequency of 20 kHz and maximum amplitude of 14 μm. The electrode was inserted through the hole at the end of the oscillator horn of a cavitation generator during the EDM process.

Figure 6. Photograph of the probe-type oscillator horn used in the experiment.

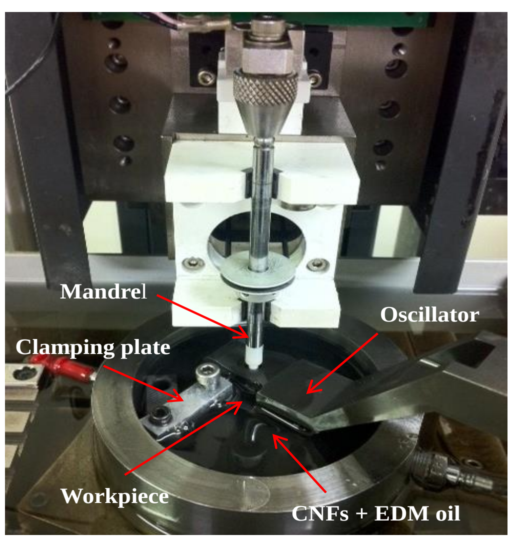

Figure 7. Experimental setup for ultrasonic cavitation assisted micro-EDM with addition of carbon nanofibers.

Table 6. Experimental conditions

Rotational speed	3000 rpm
Voltage	80 V, 100 V
Condenser capacitance	stray capacitance (~ 1 pF), 3300 pF
Feed rate	3 μm/s
Vibration frequency	20±1.5 kHz
Vibration amplitude	0~14 μm
Working distance	1~4 mm
Dielectric fluid	EDM oil CASTY-LUBE EDS
Additive CNFs size Concentration	Carbon nanofibers (CNFs) Diameter = 0.15 μm Length = 6~8 μm 0.06 g/L
Machining time	30~150 s

The ultrasonic vibration was applied to the dielectric fluid by the oscillator horn, to cause the cavitation effect. The oscillator horn was placed approximately 2-3 mm from the workpiece. Ultrasonic vibration was applied to the dielectric fluid directly by the oscillator horn, which causes the cavitation effect. Figure 7 shows a photograph of the experimental setup.

For comparison, two types of micro EDM tests were carried out, namely, (1) ultrasonic cavitation in pure EDM oil, and (2) ultrasonic cavitation in EDM oil mixed with carbon nanofibers. Micro hole machining was performed on the sample for duration of specified time, and average of three tests for each parameter setting was taken. Electrode dressing was performed after each EDM cycle by using wire electro discharge grinding (WEDG) in order to improve the form accuracy. Table 6 shows the experimental conditions.

RESULTS AND DISCUSSION

Carbon Nanofiber Assisted Micro EDM

Electro Discharge Behavior

In order to examine the effect of carbon nanofiber addition on electro discharge behavior, a high speed camera system was used to observe the EDM region. Figure 8 shows high speed camera images of spark generation during micro-EDM under conditions without carbon nanofiber addition and with carbon nanofiber addition (concentration 0.06 g/L), respectively.

It is clear that the spark region in Figure 8 (b) is distinctly bigger than that in (a), indicating that electro discharge has been significantly activated by the addition of carbon nanofiber.

Next, an oscilloscope Texio DCS 9515 was used to observe the discharge voltage waveforms. Figure 9 shows the voltage waveforms for micro-EDM without carbon nanofiber addition and with carbon nanofiber addition (concentration 0.06 g/L), respectively. Under the same period of time (1000 μs), the pulse number of discharge voltage in Figure 9(b) is 37, while that in Figure 9 (a) is only 2. This result demonstrates again that due to the carbon nanofiber addition, the electro discharge characteristics of RB-SiC have been greatly improved in EDM. It should be noted that in Figure 9(b), a multiple discharging effect (several discharging paths are generated within one single input pulse) was observed within a single input pulse, indicating that the discharging energy has been dispersed by the fiber addition.

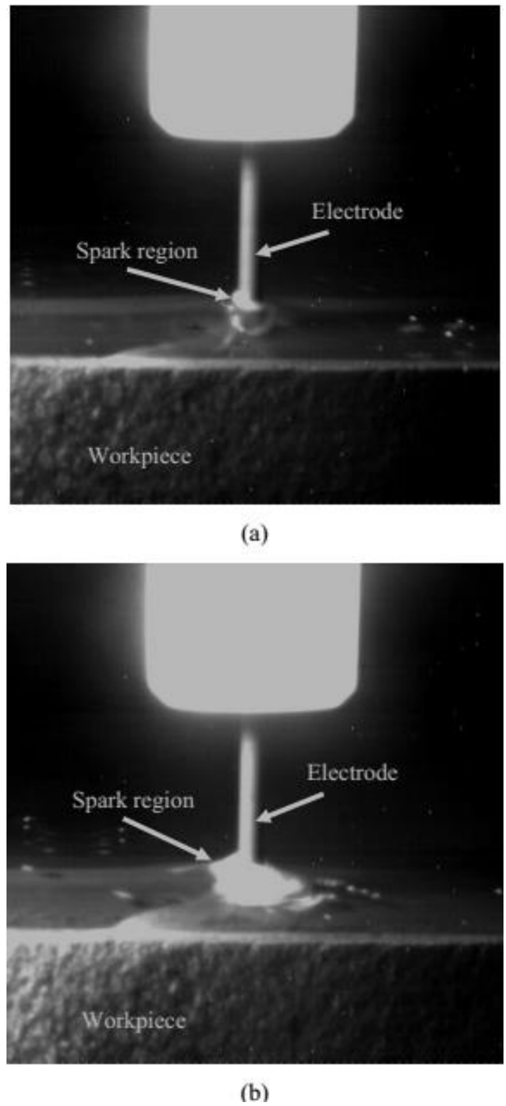

Figure 8. High speed camera observation of spark generation during micro-EDM: (a) without and (b) with carbon nanofiber addition.

Material Removal Rate

Material removal rate (MRR) is defined as the volume of material removed from workpiece over a period of time. The laser probe profilometer NH-3SP was used to scan across the machined area, as shown in Figure 10, and the volume of material removed was obtained by analyzing the three-dimensional surface topography.

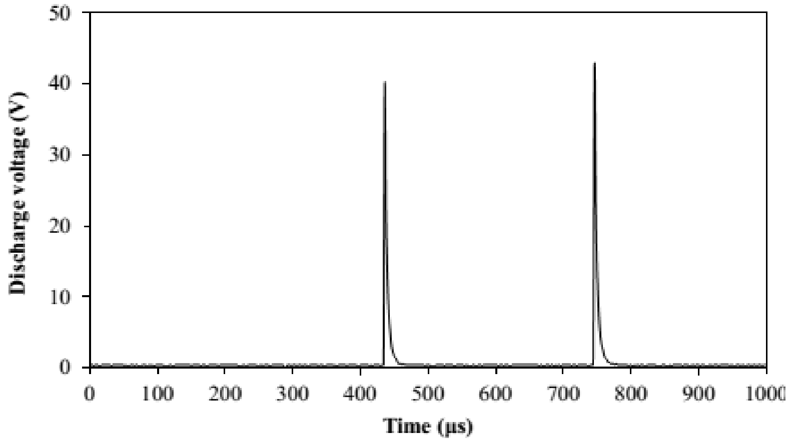

(a)

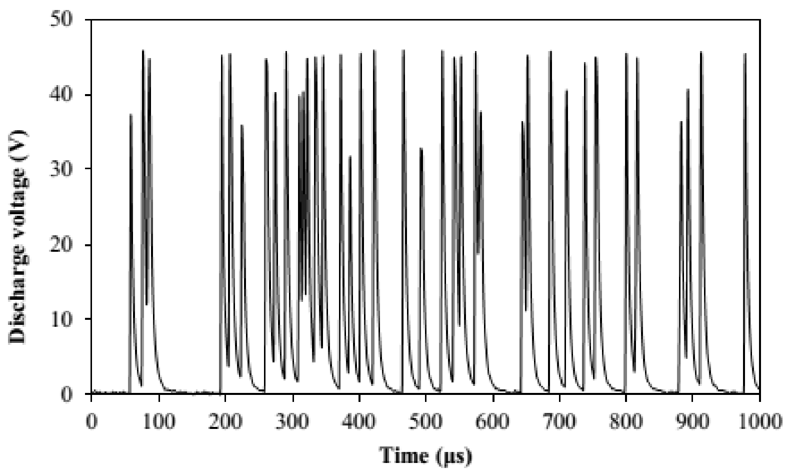

(b)

Figure 9. Discharge voltage waveform during micro-EDM: (a) without and (b) with carbon nanofiber addition.

Figure 11 shows the effect of concentration of carbon nanofiber on the MRR of RB-SiC. Without the carbon nanofibers in the dielectric fluid, the MRR is extremely low. However, the MRR increases rapidly with the increase of the concentration of carbon nanofibers, and the maximum MRR is found at the concentration of 0.17 g/L for both time-controlling and depth-controlling conditions. This result is demonstrates again that the frequency of discharge was increased and the EDM machinability has been improved by adding carbon nanofibers into the dielectric fluid.

It should be pointed out that there is an optimum range for carbon nanofiber concentration. In Figure 11, the MRR tends to reduce (for the depth controlling machining) or keep almost constant (for the time-controlling machining) for fiber concentrations higher than 0.17 g/L. This trend is consistent with that reported by Jahan et al. [20]. At an excessively high concentration of powders (in this case, carbon nanofibers) additive, the deposited powders cannot be removed easily from the machining gap and caused the secondary sparking. This secondary sparking makes the machining unstable and increases the machining time, leading to the reduction of MRR.

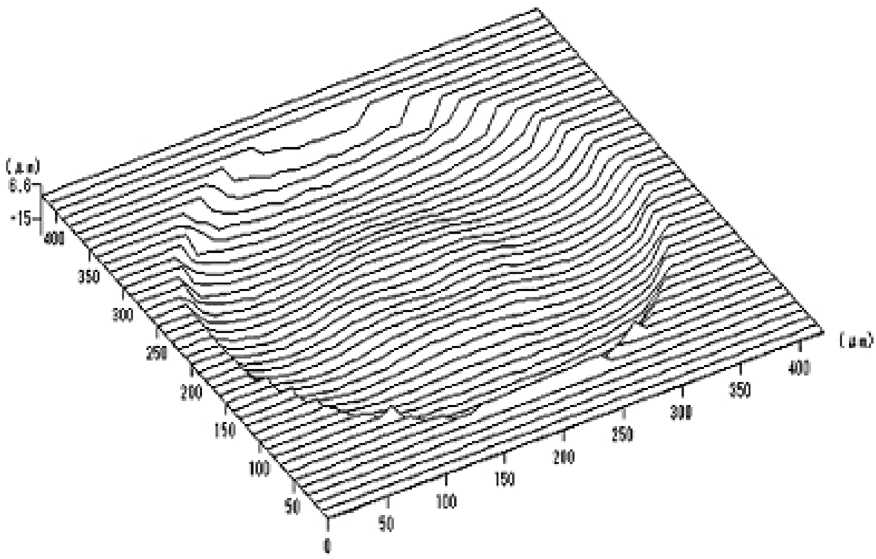

Figure 10. Three-dimensional topography of a machined cavity for the measurement of volume of material removed from workpiece.

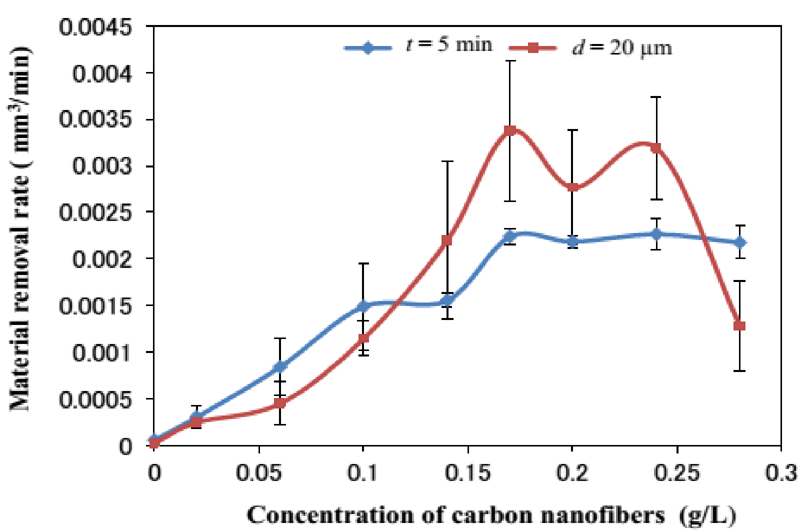

Figure 11. Effect of carbon nanofibers concentration on material removal rate.

Surface Topography

Figure 12 shows SEM micrographs of the machined micro cavities obtained with and without carbon nanofiber addition, respectively, under the time-controlling conditions. The left micrographs are low-magnification views and the right ones are high-magnification views of the center regions of the left ones. It is clear that the machined surface with carbon nanofibers additive (Figure 12(b)) is smoother than the one obtained with pure dielectric fluid (Figure 12(a)). Without the carbon nanofibers additive, the materials of RB-SiC were removed as large flakes, leading to very large craters (10 micron level); while with carbon nanofiber addition, the surface craters are extremely small (micron level). For comparison, SEM micrographs of the machined micro cavities under the depth-controlling conditions are shown in Figure 13. Similarly, the machined surface with fiber additive is apparently smoother (Figure 13 (b)) than the one obtained with pure dielectric fluid (Figure 13(a)).

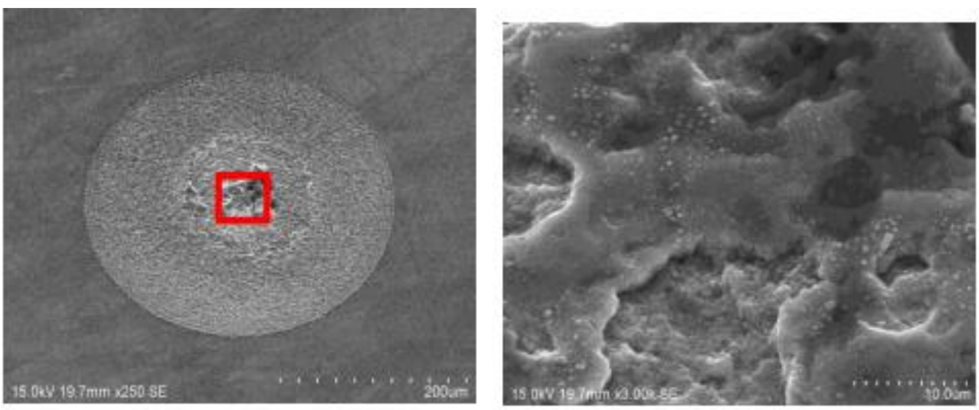

(a)

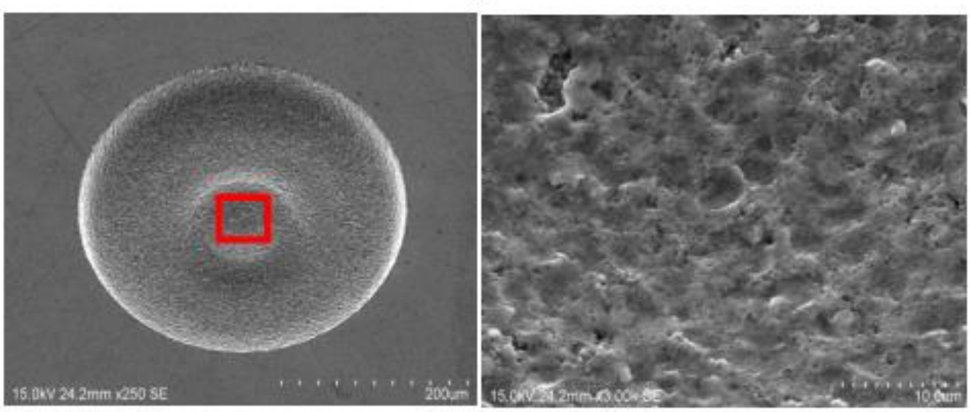

(b)

Figure 12. Comparison of machined surface after machining time of 5 min: (a) without and (b) with 0.06 g/L carbon nanofibers.

As mentioned in [1], the sparking gap has been increased with carbon nanofiber additive in the dielectric fluid; consequently the debris causing secondary discharge can be flushed out from the gap more easily. The adhesion of resolidified debris on the machined surface was reduced, which results a better surface topography. Furthermore, the discharge distribution became more uniform, hence uniformly small craters were produced on the machined surface [21]. If no carbon nanofibers were used, however, the discharging process is unstable, and material is removed through spalling, in which surface layers of the workpiece material are fractured as large flakes by thermal shocks. This is distinctly different from normal spark erosion which involves melting, dissociation and evaporation of material [22]. This result strongly demonstrates that adding carbon nanofibers in the dielectric fluid is helpful for improving the surface finish of RB-SiC.

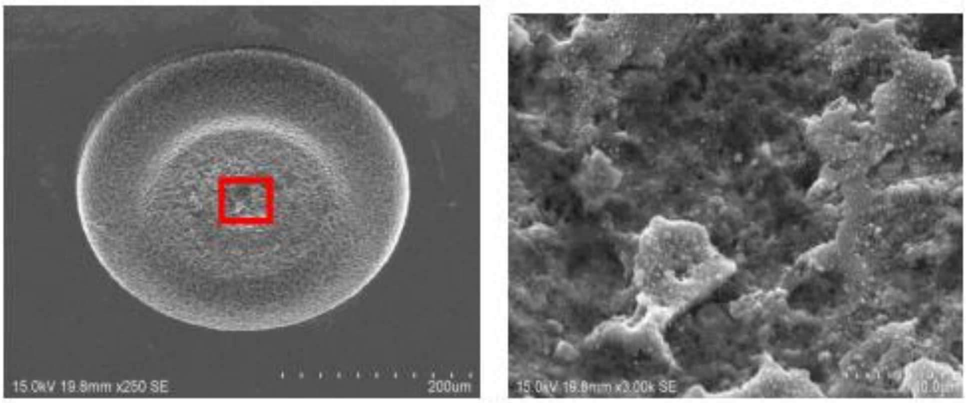

(a)

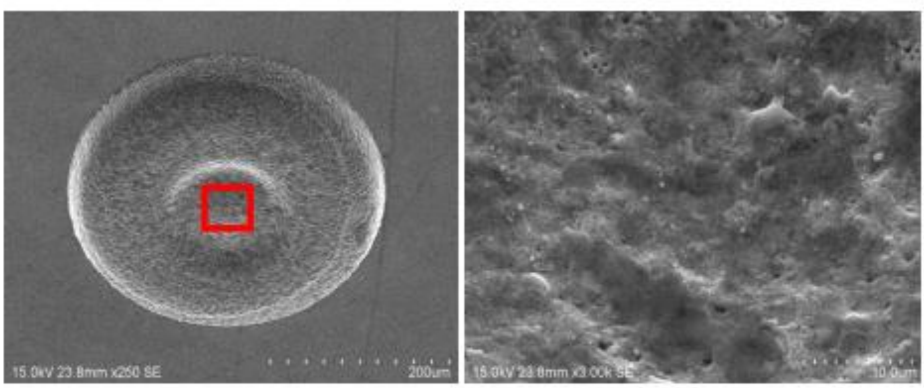

(b)

Figure 13. Comparison of machined surface at machining depth of 20 μm: (a) without and (b) with 0.06 g/L carbon nanofibers.

In addition, it can be seen from Figure 12 and Figure 13 that cone-shape protrusions were formed in the center of the micro cavities. This is presumably because of the debris were not drawn out from the center region and second electric discharges occurred. However, the cone-shape protrusions were smaller by using carbon nanofibers mixed dielectric fluid compared to the one obtained with pure dielectric fluid. The sparking gap in the carbon nanofibers mixed dielectric fluid is bigger, so the stagnation of debris in the center of the micro cavity is reduced.

Material Migration Phenomena in Micro EDM

Material Deposition Phenomena

In the experiments, we found that the finished surface of RB-SiC is covered by small particles after EDM under a few conditions. For instance, Figure 14 (c) and Figure 14 (e) show SEM micrographs of micro cavities obtained under fine machining conditions (voltage 80 V, stray capacitance ~ 1 pF) with/without adding carbon nanofibers in dielectric oil, respectively. In the figures, (d) and (f) are high-magnification views of the micro cavities in (c) and (e), respectively. It is clear that for both machining conditions, lots of small white particles (size ~ 1 μm) were formed on the machined surface, which are uniform in size and distribution. Since these white particles did not appear before the EDM tests, as depicted in Figure 14(a) and Figure 14(b), it is obvious that the particles were generated during EDM due to material migration and deposition on the machined surface. According to present authors [2], the material deposition rate is closely related to workpiece surface roughness, voltage and capacitance of the electrical discharge circuit. Carbon nanofiber addition also can significantly reduce the deposition of tool material on the workpiece surface.

Cross-Sectional TEM Observation

To examine the microstructures of the deposited material, the machined surface was cross-sectioned by mechanical polishing and FIB, and observed by SEM and TEM, respectively. Figure 15 shows SEM micrograph of machined surface after polishing of the cross-section. It is seen that white tungsten particles with an average size around 1 μm were deposited inside the craters on the machined surface. A few tungsten particles might have been removed partially from the surface during polishing, leaving residual white layers.

Figure 16 is a cross-sectional TEM micrograph of a micro cavity machined at 70 V and stray capacitance (~ 1 pF). It shows that tungsten particles (black region A) were firmly deposited in the crater of the workpiece which is composed of 6H-SiC and Si grains. On the surface region where obvious W particles were not deposited, a dark layer of material (region B) with a thickness of approximately 40-50 nm is formed, the compositions and microstructure of which looks different from the bulk material.

To confirm the microstructure of the deposited particle and dark layer, electron diffraction analysis was done using the TEM, as shown in Figure 17. In Figure 17 (a), only fuzzy rings are shown, indicating that the deposited tungsten in Zone A has an amorphous structure. In contrast, in Figure 17 (b), a series of concentric rings resulting from many diffraction spots also can be seen, demonstrating that the deposited dark layer on the machined surface is poly-crystalline.

Similar amorphous/poly-crystalline layers on bulk materials were also observed in mechanical machining processes. For example, in the diamond turning of RB-SiC [10], amorphization of silicon matrix and dislodgement of SiC grains were confirmed. In diamond cutting of single crystalline silicon [23], an amorphous layer with a thickness ranging from the nanometer level to the submicron level was formed on the workpiece surface. In single point diamond turning of single-crystal SiC (6H) [24], original single-crystal SiC material was transformed into an amorphous material, on the surface and within the chip.

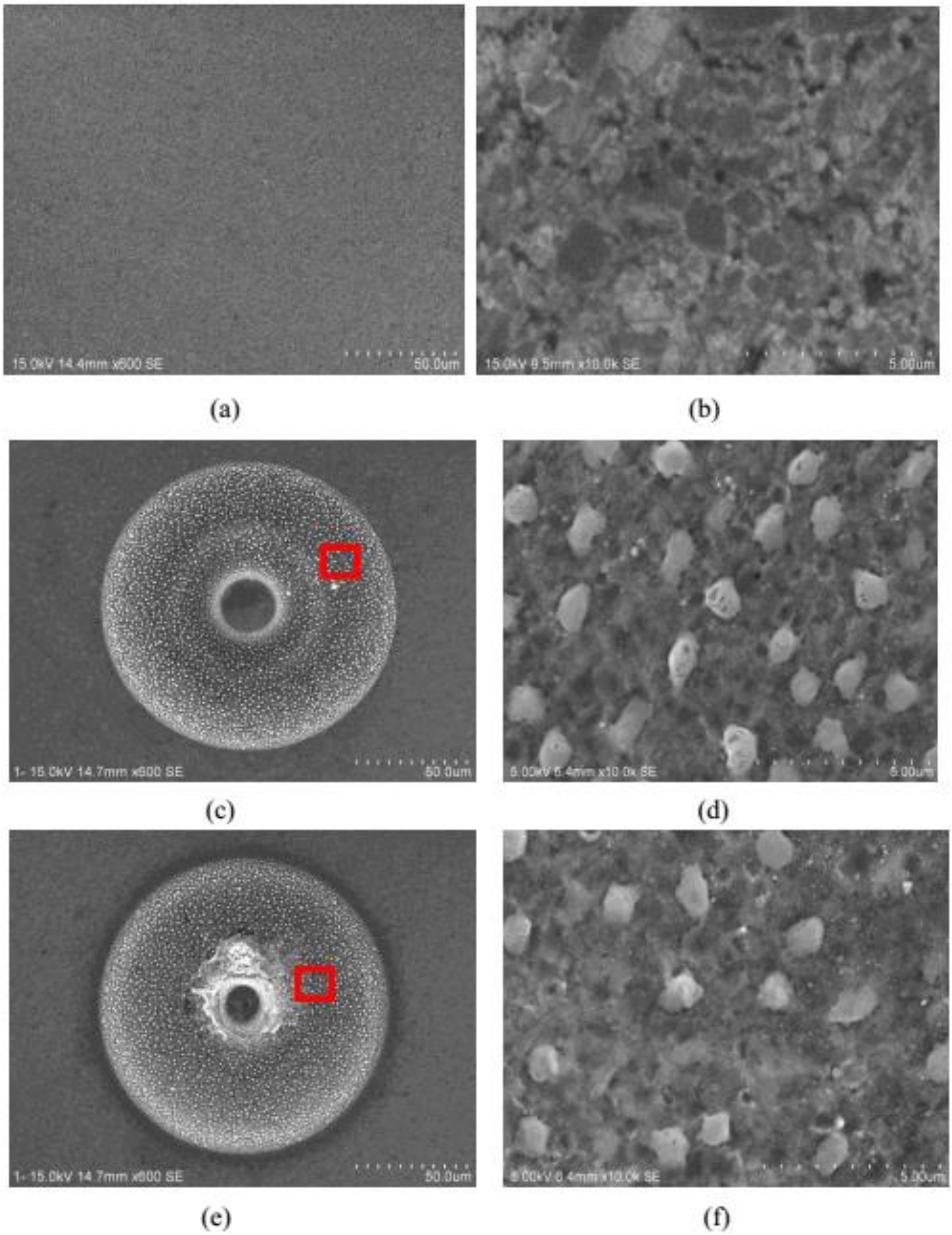

Figure 14. SEM micrographs of (a) unmachined surface, (b) unmachined surface at high magnification, (c) micro cavity machined without carbon nanofibers, (d) tungsten deposition in a rectangle (c), (e) micro cavity machined with 0.06 g/L carbon nanofibers, (f) tungsten deposition in a rectangle (e).

Subsurface deformation of various types of single crystal SiC was also confirmed in molecular dynamics simulation of nanometer level cutting [25], and the subsurface crystal lattice deformed layer depths were quantified by subtracting the uncut chip thickness. However, it should be noted that the amorphous/poly-crystalline layer was deposited on the workpiece from the tool electrode and not phase-transformed from the bulk material by mechanical stresses. From this meaning, it is clear that the formation mechanism of the subsurface layer in this work is distinctly different from those in mechanical machining processes such as diamond turning.

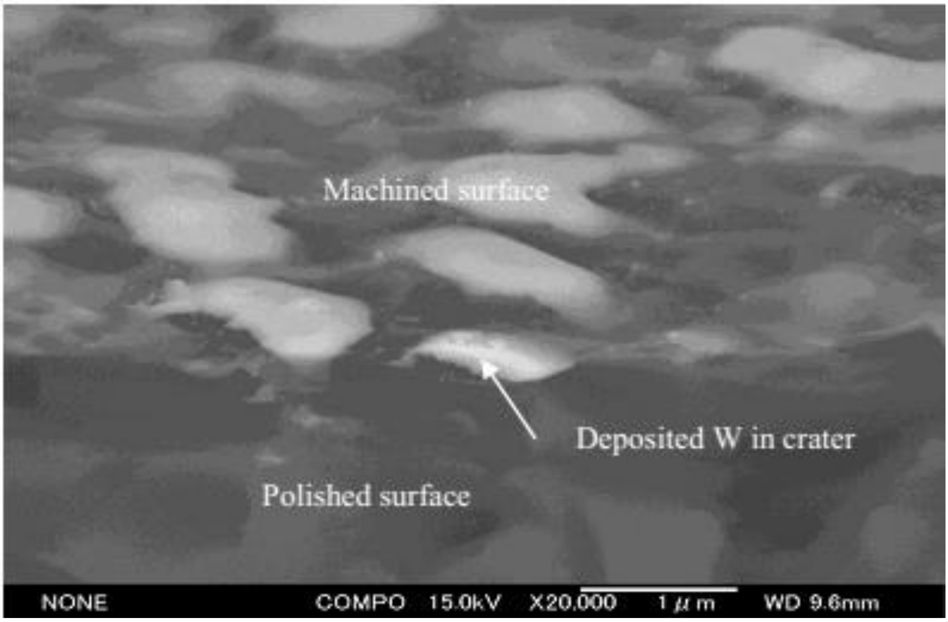

Figure 15. SEM micrographs of machined surface after surface polishing.

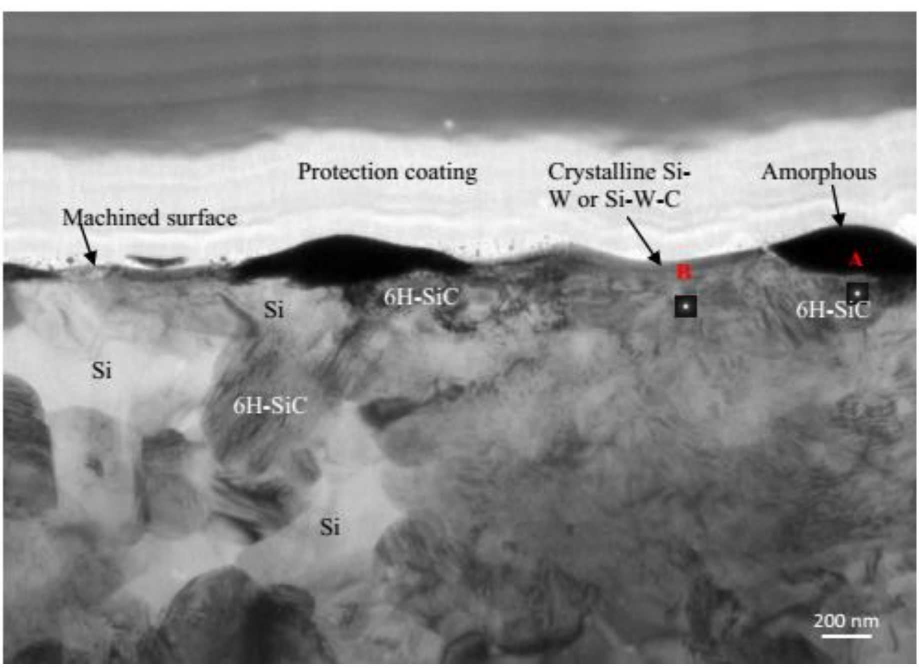

Figure 16. Cross-sectional TEM micrograph of micro cavity machined at 70V and stray capacitance.

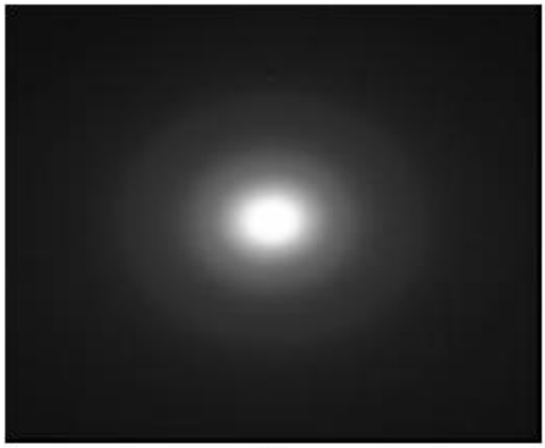

(a)

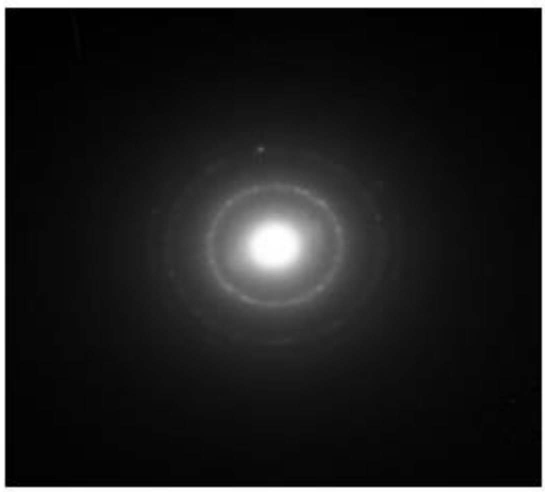

(b)

Figure 17. Electron diffraction pattern at: (a) zone A, indicating an amorphous structure and (b) zone B, showing a crystalline structure.

To further confirm the elemental composition of the deposited material in zone A and zone B, EDX analysis was done on the cross-section of the sample, as depicted in Figure 18. Figure 18(a) clearly shows that the deposited material in zone A is tungsten (W). However, in Figure 18(b), besides tungsten (W), carbon (C) and silicon (Si) were also found, indicating that the interdiffusion of W, Si and C might have occurred. The cross-sectional sample of the tungsten electrode tip after the EDM process was also examined using TEM.

In Figure 19, micro craters were found on the tungsten electrode tip, verifying that some of the tungsten grains were melted and removed during the EDM process. The EDX analysis results in Figure 20 (a) indicated that carbon (C) exists on the tungsten electrode tip, whereas no C element was detected inside the tool material (Figure 20(b)). The C element on the electrode surface might have been migrated from either the workpiece material or the CNFs.

Another explanation is that the C element might be generated during the decomposition of dielectric oil at high temperature in EDM.

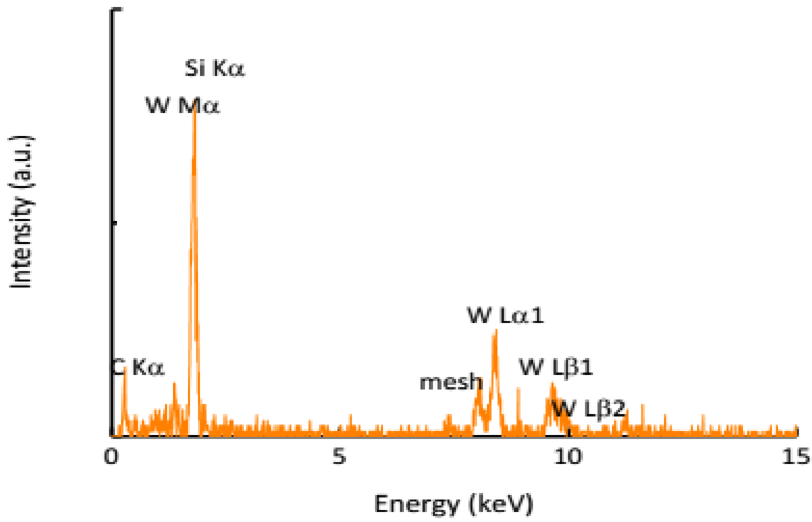

(a)

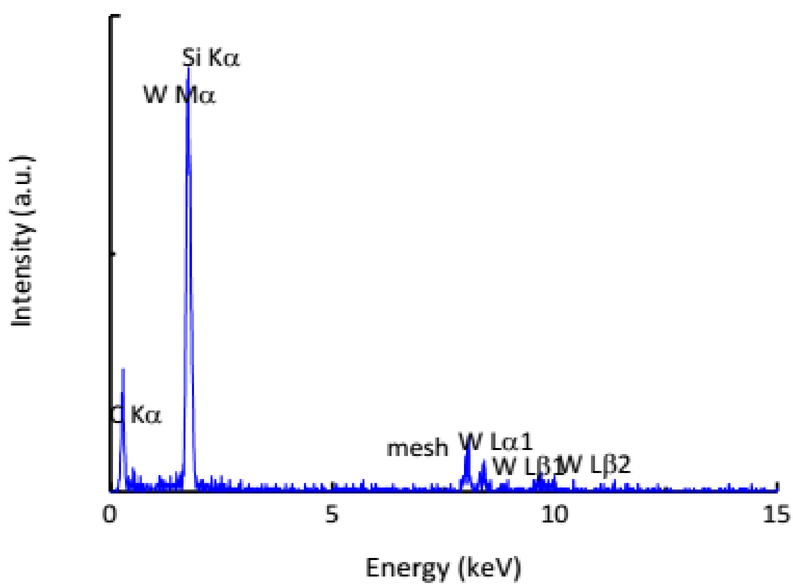

(b)

Figure 18. EDX spectrum analysis at: (a) zone A and (b) zone B in Figure 16.

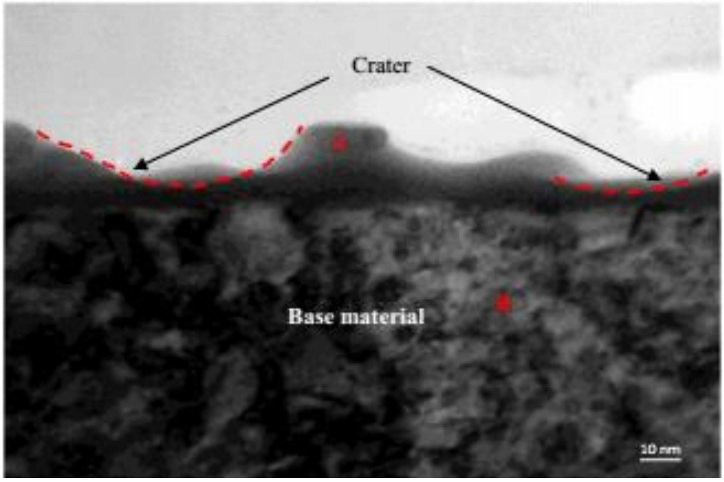

Figure 19. Cross-sectional TEM micrograph of tungsten electrode tip after EDM process.

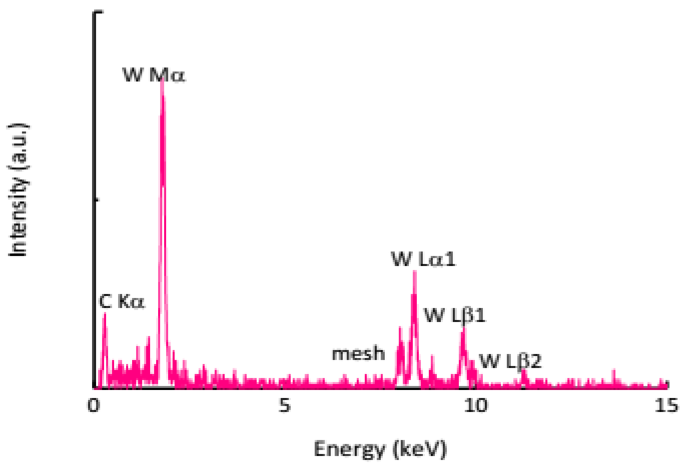

(a)

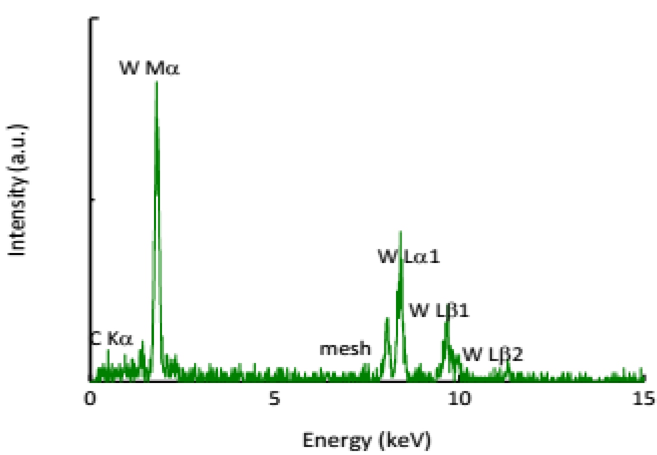

(b)

Figure 20. EDX spectrum analysis at: (a) zone A and (b) zone B in Figure 19.

Material Migration Mechanism

Figure 21 shows a schematic model for material migration. During the EDM process, the Si matrix, in conjunction with sintering agents, possesses a higher electrical conductivity than the 6H-SiC grains, so it is preferentially removed by melting and vaporisation [15], leaving craters on the surface (Figure 21(a)). At the same time, heat concentration on the electrode causes the electrode surface melted. The melted electrode material maybe migrated towards the workpiece under an electric field, then resolidified and deposited onto the workpiece. The melted tungsten deposited inside the craters more easily than on the flat regions, forming small particles, as depicted in Figure 21(b). Similarly, Murray et al. [26] reported that nanometer-sized tungsten crystals from electrode were mixed in with the discharge melt pool, as solid particles and their crystalline structure is maintained. In the flat region, however, a thin interdiffusion layer is generated where the melted tungsten reacted with silicon and carbon from the workpiece material.

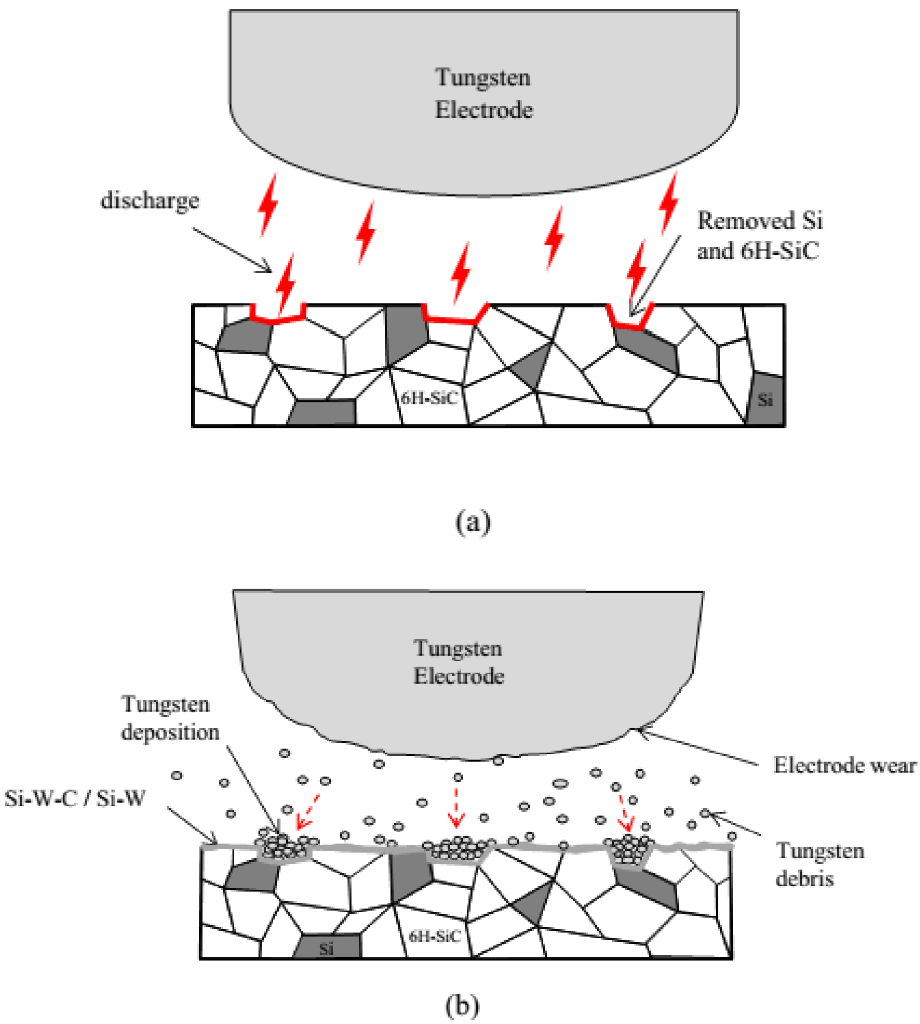

Figure 21. Schematic models for (a) material removal of Si and 6H-SiC during micro-EDM and (b) deposition of electrode material on workpiece surface.

According to Mohri et al. [27], the deposition of electrode material changed the characteristics of the workpiece surface. The workpiece surface has fewer cracks, higher corrosion resistance and wear resistance after EDM. On the other hand, tool material deposition causes surface contamination and surface roughening of the workpiece. Therefore, generally speaking, material migration should be promoted in rough machining and suppressed in fine machining.

Ultrasonic Cavitation Assisted Micro EDM

Hybrid Effect of Ultrasonic Cavitation and Carbon Nanofiber Addition

Figure 22 shows changes in machined hole depth under conditions (1) ultrasonic cavitation in pure EDM oil, and (2) ultrasonic cavitation in carbon nanofibers mixed EDM oil, respectively. The vibration amplitude in this case is 10 μm. Compared to using ultrasonic cavitation in pure EDM oil, when using ultrasonic cavitation in carbon nanofibers mixed EDM oil the material removal rate and the depth of micro hole is increased by 5-7 times. Due to the vibration-induced cavitation bubbles and strong stirring effect, the carbon nanofibers are distributed uniformly in the machining region without aggregation. As a result, the carbon nanofibers can fully play their role in EDM, leading to increases in discharge gap, discharge frequency and material removal rate. From this meaning, there is a kind of synergistic effect between ultrasonic cavitation and carbon nanofiber addition for improving machining performance in the micro EDM of RB-SiC.

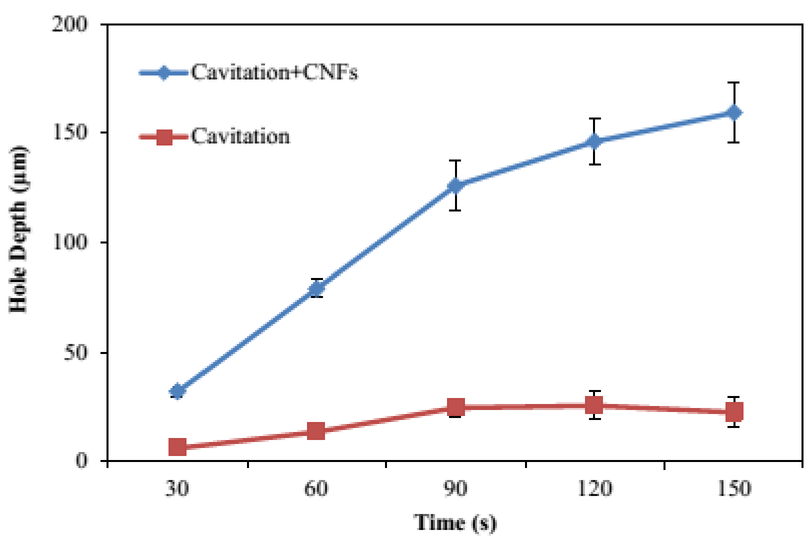

Figure 22. Change in depth of micro hole with time when ultrasonic cavitation is used in dielectric oil with/without CNF addition.

Stability of Machining Process

As the EDM machine employs an automatic feed control system, if short circuit occurs because of tool-workpiece contact or adhesion of debris, then the tool electrode is moved in the reverse direction of the feed to maintain the tool-workpiece gap. This back-feeding action indicates the EDM process is unstable and results in the increase of machining time [28]. In this chapter, in order to investigate the machining stability, we captured and tracked the electrode movement.

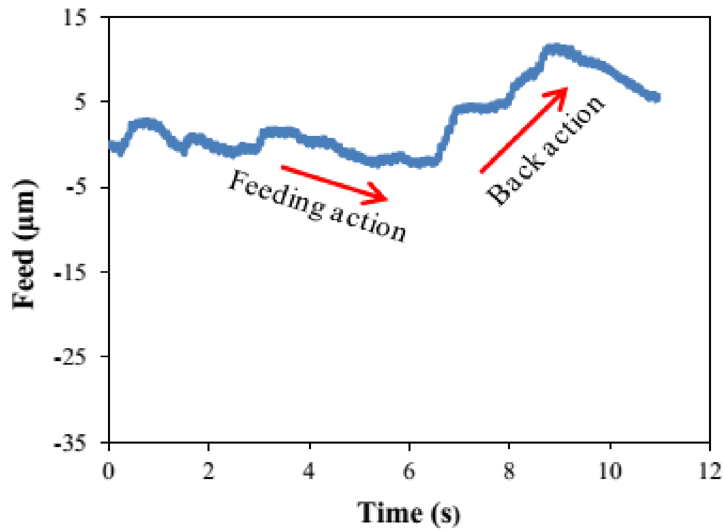

(a)

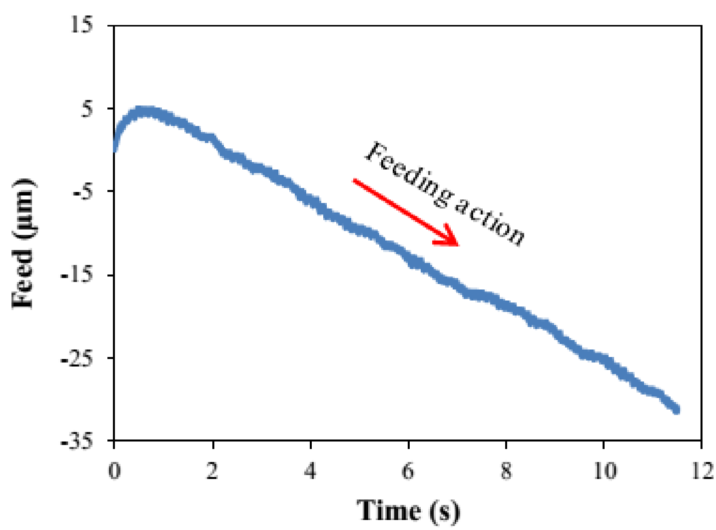

(b)

Figure 23. Measurement results of electrode movement with ultrasonic cavitation in (a) pure EDM oil and (b) carbon nanofibers mixed EDM oil.

Figure 23 shows the measurement results of electrode movement when ultrasonic cavitation was used in pure EDM oil and carbon nanofibers mixed EDM oil. Frequent back-feeding actions occurred in Figure 23(a), indicating the occurrence of abnormal discharge and unstable machining situation. In Figure 23(b), however, continuous feeding action of electrode toward the workpiece is observed without reverse action. This result demonstrates again that the hybrid process of ultrasonic cavitation and addition of carbon nanofibers in dielectric fluid improves the process stability and material removal rate. Besides that, this hybrid process is effective to improve the surface topography and hole geometry [3].

Effect of Ultrasonic Vibration on Tool Material Deposition

Figure 24 presents SEM micrographs of surface machined at low energy for fine machining (70 V, stray capacitance,) with carbon nanofibers addition in dielectric fluid (concentration 0.06 g/L) with/without ultrasonic vibration. Without ultrasonic cavitation, many tungsten particles are deposited on the workpiece surface (Figure 24a).

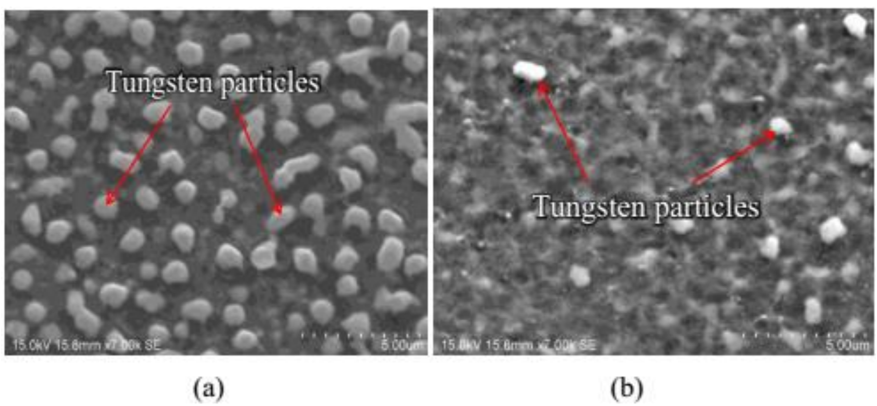

Figure 24. SEM micrograph of surface machined with carbon nanofibers addition and (a) without ultrasonic cavitation and (b) with ultrasonic cavitation.

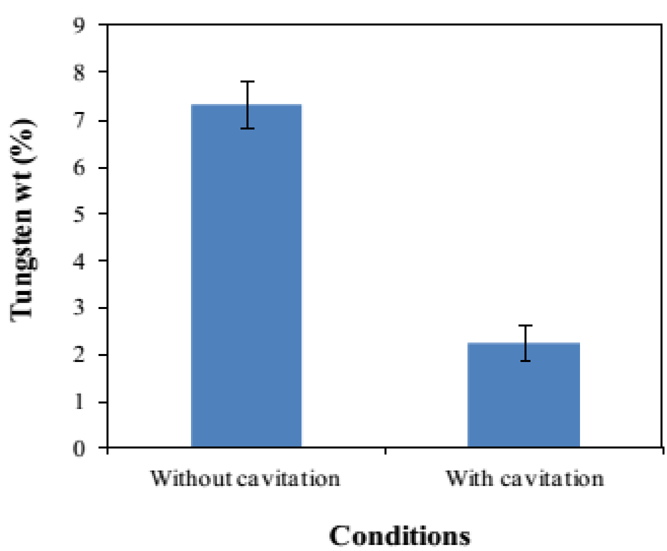

Figure 25. Weight percentage of deposited electrode material with/without cavitation.

In contrast, with ultrasonic cavitation the tungsten particle deposition is reduced significantly (Figure 24b). Figure 25 shows tungsten weight percentage analysed by EDX for both conditions. The weight percentage of deposited tungsten decreases by a factor of 3 by using ultrasonic cavitation. With ultrasonic cavitation, the cavitation bubbles oscillate rapidly at the working area, preventing the tungsten debris deposition.

Process Mechanism

To reveal the hybrid micro EDM process mechanism, we observed the machining tests with/without ultrasonic cavitation using a high speed camera.

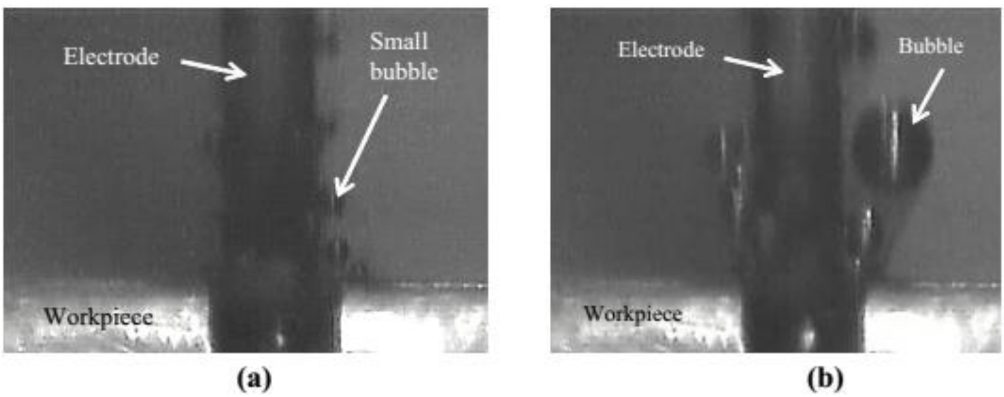

Figure 26. High speed camera observation of micro EDM without ultrasonic cavitation: (a) early stage and (b) later stage.

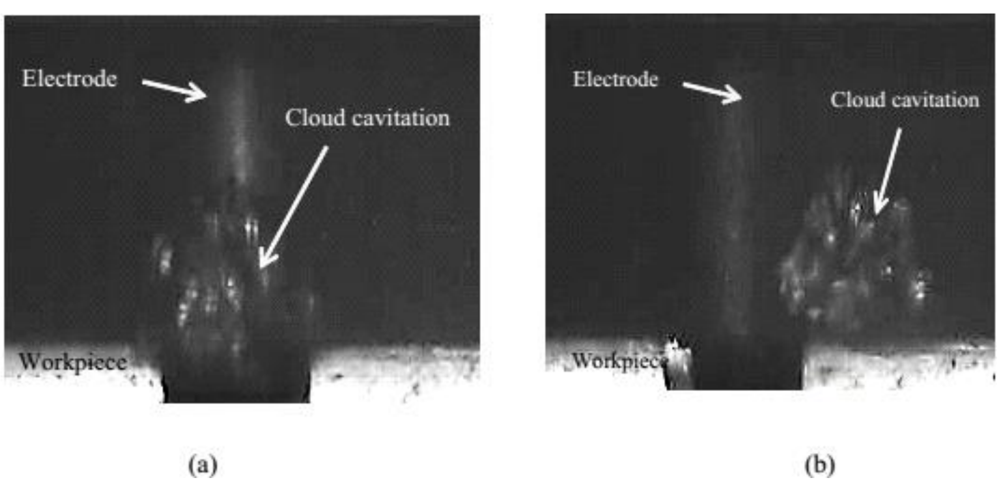

Figure 27. High speed camera observation of micro EDM with ultrasonic cavitation, showing (a) cloud cavitation formation and (b) oscillation of cloud cavitation.

As shown in Figure 26 without ultrasonic cavitation, lots of small bubbles are created first (Figure 26a), and then these small bubbles continue to grow in size until they finally collapse (Figure 26b). In contrast, with ultrasonic cavitation, the cavitation bubbles tend to accumulate, forming cloud cavitation (Figure 27a). These clouds cavitation oscillate around the working area rapidly, helping to remove debris from the sparking gap (Figure 27b). In deeper region, as shown in Figure 28, cavitation bubbles are also observed. Due to the buoyancy force, these cavitation bubbles rise towards the surface region, which is helpful to carry out the debris from the machining gap.

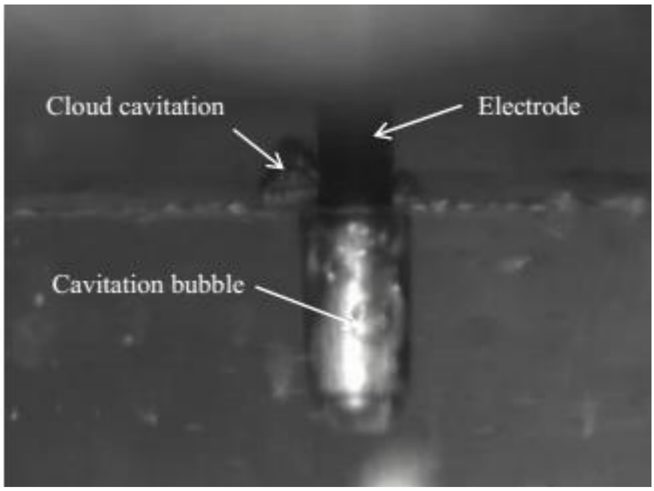

Figure 28. High speed camera observation of deep region when using ultrasonic cavitation.

Cavitation phenomenon is strongly related to acoustic pressure P_{ac}, as determined in equation (1) (Ghiculescu et al., 2009):

$$P_{ac} = 2\pi f_{us} A \rho c \tag{1}$$

where f_{us} is oscillations frequency (Hz), ρ dielectric fluid density (kg/m^3), c sound velocity in dielectric (m/s) and A vibration amplitude (m). According to Ghiculescu et al. [29], to produce cavitation, P_{ac} must be greater than a cavitation threshold. The cavitation threshold mainly depends on the ambient pressure (1 bar) [30]. In this study, f_{us} = 20 kHz, A =10 µm, ρ =767 kg/m^3 and c =1320 m/s. Under these conditions, the acoustic pressure P_{ac} is 1.27 MPa. From this result, we can see that the acoustic pressure is far greater than the ambient pressure. In other words, the acoustic pressure is sufficiently high to cause cavitation bubbles in this study.

Normally, in a cavitation process, bubbles grow and collapse. However, in the present study, we found that cloud cavitation oscillating around the machining area instead of collapse. According to Suslick [17], cavity growth depends on the intensity of sound. In the case of low intensity ultrasound (20 kHz), the cavity size will not grow and collapse as the one induced by high intensity ultrasound. Instead, these cavities will simply oscillate, often nonlinearly, for many cycles of expansion and compression. A cloud cavitation will be formed when these stable cavities gathered at equilibrium position, i.e., the pressure nodes level [31]. In a cloud cavitation, the nonlinear bubble dynamics produces nonlinear interactive effects which cause cascading of fluctuation energy [32-33]. Due to the fluctuating energy in the dielectric fluid, the debris might be flushed out from the gap.

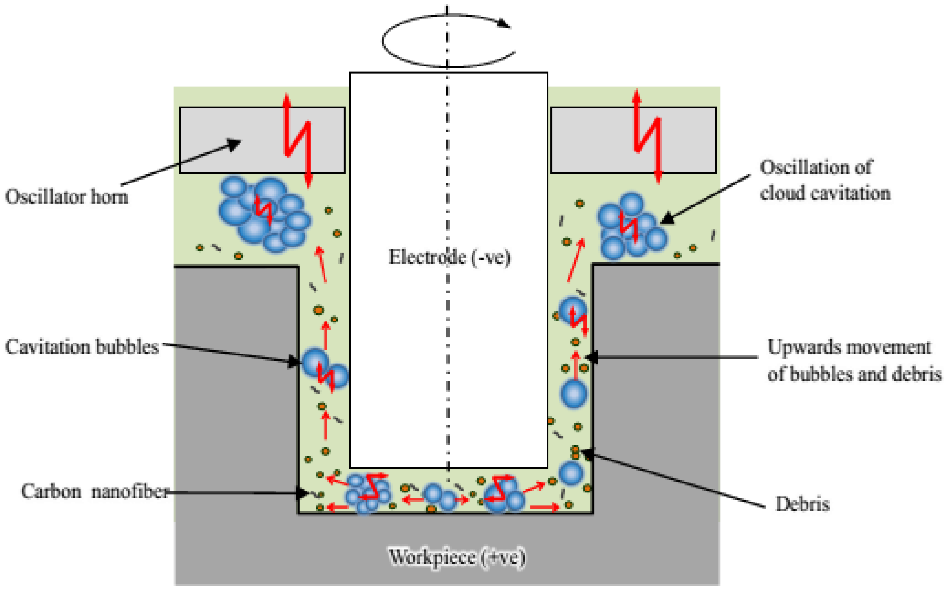

Figure 29. Schematic model for debris removal through the cavitation assisted micro EDM of a deep micro hole.

The schematic model for debris removal through the cavitation assisted micro EDM of a deep micro hole is shown in Figure 29. By using ultrasonic vibration, two effects might be expected. One is the vibration-induced stirring effect which is helpful to uniformly distribute the carbon nanofibers in the dielectric fluid. The other is the vibration-induced cloud cavitation bubbles which help to flush out the debris. Due to these two effects, short circuit and unstable machining can be prevented, leading to significant improvement in EDM performance. From this meaning, the proposed hybrid micro EDM method in this study provides possibility for high-efficiency precision manufacturing of micro structures on ultra-hard RB-SiC ceramic materials.

Application: Fabrication of High Aspect Ratio Micro Hole

Next, we attempted to fabricate high aspect ratio micro holes using the hybrid effects of ultrasonic cavitation and carbon nanofiber addition in dielectric fluid. Tungsten rods with diameters of 50 µm and 23 µm were used as tool electrodes. SEM micrographs of the machined micro holes are shown in Figure 30. An aspect ratio of 11.5 was achieved within 10 minutes by using the 50 µm diameter tool, and an aspect ratio of 21.7 was obtained with the 23 µm electrode in 4 minutes.

In order to examine the inner surface quality of the high aspect ratio micro hole, the sample in Figure 30(a) was cross-sectioned by a diamond cutter and polished using diamond slurry and observed by SEM. Figure 31 shows an SEM micrograph of the hole cross section.

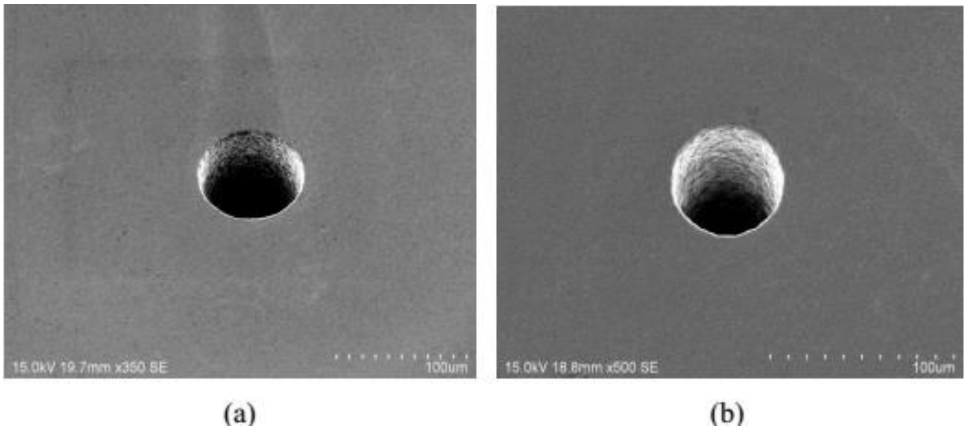

Figure 30. Micro holes obtained with (a) 50 µm and (b) 23 µm diameter tool electrodes.

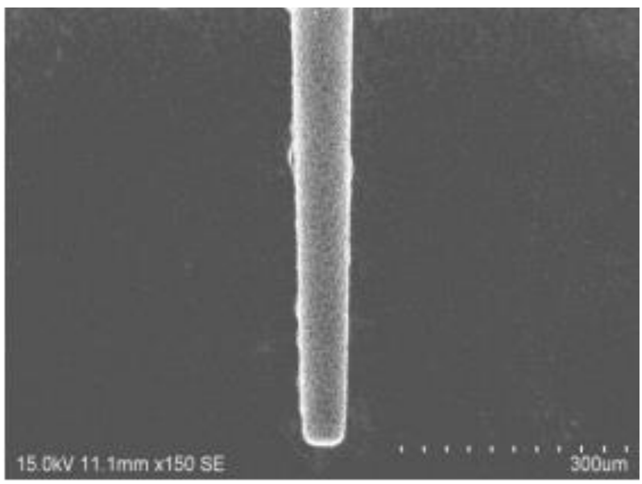

Figure 31. SEM micrograph of a cross-sectioned high aspect ratio micro hole.

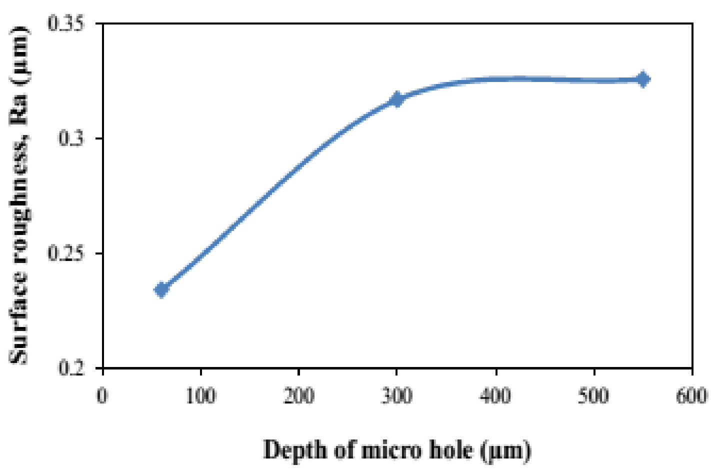

Figure 32. Surface roughness at different depth of micro hole.

The bottom of the micro hole is flat without cone shape protrusion. The surface roughness of hole side walls were then measured using the laser probe profilometer at three locations of different hole depth. As shown in Figure 32, the surface roughness ranges from 0.24 to 0.32 μmRa and does not show obvious change with the depth of micro hole. This result indicates that the ultrasonic cavitation is effective even at the deep region of the micro hole.

CONCLUSION

In this chapter, a novel machining process, namely hybrid micro-EDM process by combining ultrasonic cavitation and carbon nanofibers was introduced. The effects of carbon nanofibers addition and ultrasonic cavitation on the EDM performance of RB-SiC were investigated systematically.

The main conclusions from this chapter can be summarized as follows:

1. Adding carbon nanofibers into the dielectric fluid can significantly improve the electro discharge frequency, and in turn, improve the material removal rate. Without carbon nanofiber addition, the RB-SiC material was removed by spalling of large flakes, causing large surface craters. With fiber addition, however, the crater size could be significantly reduced.
2. Ultrasonic vibration induces two major effects. One is stirring effect, which is helpful to uniformly distribute the carbon nanofibers in the dielectric fluid. The other is the cloud cavitation bubbles which help to flush out the debris. The effect of ultrasonic vibration is significant only when carbon nanofibers are mixed in the dielectric fluid.
3. Combining ultrasonic cavitation and carbon nanofibers addition can improve the material removal rate, machining stability, and reduce the deposition of tool material on the workpiece surface. Micro holes having ten micron level diameters and high aspect ratios (>20) were successfully fabricated on reaction-bonded silicon carbide in a few minutes.

The proposed hybrid micro-EDM process is an effective approach to fabricate high aspect ratio micro holes and microstructures on RB-SiC and other hard-brittle materials.

REFERENCES

[1] Liew, P.J., Yan, J., Kuriyagawa, T., (2013a). Carbon nanofibre assisted micro electro discharge machining of reaction-bonded silicon carbide. *Journal of Materials Processing Technology* 213(7), 1076-1087.

[2] Liew, P.J., Yan, J., Kuriyagawa, T., (2013b). Experimental investigation on material migration phenomena in micro-EDM of reaction-bonded silicon carbide. *Applied Surface Science* 276, 731-743.

[3] Liew, P.J., Yan, J., Kuriyagawa, T., (2014). Fabrication of deep micro-holes in reaction-bonded SiC by ultrasonic cavitation assisted micro-EDM. *International Journal of Machine Tools & Manufacture* 76, 13-20.

[4] Choyke, W.J., Matsunami, H., Pensl, C., (2004). *Silicon carbide-recent major advances*, Germany.

[5] Hall, C., Tricard, M., Murakoshi, H., Yamamoto, Y., Kuriyama, K., Yoko, H., (2005). New mold manufacturing techniques. *Proceedings of SPIE* 5868, 58680V.

[6] Suyama, S., Kameda, T., Itoh, Y., (2003). Development of high-strength reaction-sintered silicon carbide. *Diamond and Related Materials* 12, 1201-1204.

[7] Suyama, S., Itoh, Y., (2006). Development of applications for high-strength reaction-sintered silicon carbide. *Toshiba Review* 61(6), 72-75.

[8] Tam, H.Y., Cheng, H.B., Wang, Y.W., (2007). Removal rate and surface roughness in the lapping and polishing of RB-SiC optical components. *Journal of Materials Processing Technology* 192-193, 276-280.

[9] Dai, Y., Ohmori, H., Lin, W., Eto, H., Ebizuka, N., Tsuno, K., (2005). ELID grinding properties of high-strength reaction-sintered SiC. *Key Engineering Materials* 291-292, 121-126.

[10] Yan, J., Zhang, Z., Kuriyagawa, T., (2009a). Mechanism for material removal in diamond turning of reaction-bonded silicon carbide. *International Journal of Machine Tools and Manufacture* 49(5), 366-374.

[11] Reynaerts, D., Meeusen, W., Brussel, H.V., (1998). Machining of three-dimensional microstructures in silicon by electro-discharge machining. *Sensors and Actuators A* 67, 159-165.

[12] Ho, K.H., Newman, S.T., (2003). State of the art electrical discharge machining (EDM). *International Journal of Machine Tools and Manufacture* 43, 1287-1300.

[13] Puertas, I., Luis, C.J., (2004). A study on the electrical discharge machining of conductive ceramics. *Journal of Materials Processing Technology* 153-154, 1033-1038.

[14] Clijsters, S., Liu, K., Reynaerts, D., Lauwers, B., (2010). EDM technology and strategy development for the manufacturing of complex parts in SiSiC. *Journal of Materials Processing Technology* 210, 631-641.

[15] Konig, W., Dauw, D.F., Levy, G., Panten, U. (1988). EDM-future steps towards the machining of ceramics. *Annals of the CIRP* 37(2), 623-631.

[16] Wilhelm, M., Kornfeld, M., Wruss, W., (1999). Development of SiC-Si composites with fine-grained SiC microstructures, *Journal of the European Ceramic Society* 19, 2155-2163.

[17] Suslick, K.S., (1989). The chemical effects of ultrasound. *Scientific American* 260, 80-86.

[18] Yu, Z.Y., Zhang, Y., Li, J., Luan, J., Zhao, F., Guo, D., (2009). High aspect ratio micro-hole drilling aided with ultrasonic vibration and planetary movement of electrode by micro-EDM. *CIRP Annals - Manufacturing Technology* 58, 213-216.

[19] Wang, J., Han, F., Cheng, G., Zhao, F., (2012). Debris and bubble movements during electrical discharge machining. *International Journal of Machine Tools and Manufacture* 58, 11-18.

[20] Jahan, M.P., Rahman, M., Wong, Y.S., (2010a). Modelling and experimental investigation on the effect of nanopowder-mixed dielectric in micro-electrodischarge

machining of tungsten carbide. *Proceedings of the Institution of Mechanical Engineers, Part B: Journal of Engineering Manufacture* 224(11), 1725-1739.

[21] Jahan, M.P., Rahman, M., Wong, Y.S., (2010b). Study on the nano-powder-mixed sinking and milling micro-EDM of WC-Co. *The International Journal of Advanced Manufacturing Technology* 53, 167-180.

[22] Trueman, C.S., Huddleston, J., (2000). Material removal by spalling during EDM of ceramics. *Journal of the European Ceramic Society* 20, 1629-1635.

[23] Yan, J., Asami, T., Harada, H., Kuriyagawa, T., (2009b). Fundamental investigation of subsurface damage in single crystalline silicon caused by diamond machining. *Precision Engineering* 33(4), 378-386.

[24] Patten, J., Gao, W., Yasuto, K., (2005). Ductile regime nanomachining of single-crystal silicon carbide. *ASME Journal of Manufacturing Science and Engineering* 127, 522-532.

[25] Luo, X., Goel, S., Reuben, R.L., (2012). A quantitative assessment of nanometric machinability of major polytypes of single crystal silicon carbide. *Journal of the European Ceramic Society* 32, 3423-3434.

[26] Murray, J.W., Fay, M.W., Kunieda, M., Clare, A.T., (2013). TEM study on the electrical discharge machined surface of single-crystal silicon. *Journal of Materials Processing Technology* 213, 801-809.

[27] Mohri, N., Saito, N., Tsunekawa, Y., (1993). Metal surface modification by electrical discharge machining with composite electrode. *Annals of the CIRP* 42(1), 219-222.

[28] Endo, T., Tsujimoto, T., Mitsui, K., (2008). Study of vibration-assisted micro-EDM-The effect of vibration on machining time and stability of discharge. *Precision Engineering* 32, 269-277.

[29] Ghiculescu, D., Marinescu, N.I., Jitianu, G., Seritan, G., (2009). On precision improvement by ultrasonics-aided electrodischarge machining. *Estonian Journal of Engineering* 15(1), 24-33.

[30] Barger, J.E., (1964). Thresholds of acoustic cavitation in water. *Technical Memorandum* 57, 1-174.

[31] [31] Laborde, J.L., Bouyer, C., Caltagirone, J.P., Gerard, A., (1998). *Acoustic bubble cavitation at low frequencies, Ultrasonics* 36, 589-594.

[32] Kumar, S., Brennen, C.E., (1991). Nonlinear effects in the dynamics of clouds of bubbles. *Journal of the Acoustical Society of America* 89, 707-714.

[33] Brennen, C.E., (1995). *Cavitation and Bubble Dynamics*, Oxford University Press, Inc, New York.

In: Electrical Discharge Machining (EDM)
Editor: M. P. Jahan
ISBN: 978-1-63483-591-6

Chapter 14

ELECTRICAL DISCHARGE MACHINING OF SHAPE MEMORY ALLOYS

M. P. Jahan **[*]** ***and Pegah Kakavand***
Department of Architectural and Manufacturing Sciences, Western Kentucky University, Bowling Green, KY, US

ABSTRACT

In recent years, shape memory alloys (SMAs) are widely used in various important applications for automotive, biomedical and aerospace industries. SMAs are generally known as difficult-to-cut materials for their unique properties such as super-elasticity, shape recovery capability, stress hysteresis, and overall mechanical strength. Electrical Discharge Machining (EDM) is one of the non-traditional technologies that are used for machining difficult-to-cut materials. This chapter will provide an overview of the existing research works on the EDM of SMAs. The chapter begins with a brief history, properties, applications, and challenges in machining of SMAs. The EDM and wire-EDM of SMAs are presented in three broad categories: parametric study, surface characteristics, and modeling and optimization. In addition, the research on the EDM based advanced processes, such as micro-EDM and hybrid machining of SMAs are also presented. Finally, suggestions have been provided on the future research scopes in the area of EDM of SMAs.

Keywords: EDM, shape memory alloys, SMAs, micro-EDM, wire-EDM, Ni-Ti alloy

INTRODUCTION AND HISTORY OF SMAS

Nickel-Titanium (Ni-Ti) alloy, most commonly known as ‘Nitinol’ is the most widely used SMAs. The term ‘Nitinol’ tells about the history of the discovery of Ni-Ti SMA. The term ‘Nitinol’ represents **Ni**ckel-**Ti**tanium-**N**aval **O**rdnance **L**aboratory. Buehler and his co-workers at the U.S. Naval Ordnance Laboratory discovered the shape memory effect in an

[*] Corresponding author: M.P. Jahan, E-mail: muhammad.jahan@wku.edu.

equiatomic alloy of nickel and titanium in early 1960s [1], which provided a breakthrough in the research of SMAs.

Although, the Ni-Ti alloy and its shape memory properties are reported in 1960s, the first observation of pseudoelastic behaviour of materials were reported by Ölander [2] in 1932 in an Au-Cd alloy. The reversible martensitic phase transformation of a Cu-Zn alloy with the change of temperature was also reported by Greninger & Mooradian in 1938 [3]. However, the basic phenomenon of the shape memory effect was reported as late as 1951 by Chang and Read [4]. At present there are many shape memory alloys reported in the literature such as: InTl, CuZn, and CuAlNi, that exhibit similar reversible martensitic phase transformation and shape memory effect [5]. In addition, it is one of the main areas of research in current days to discover new materials with shape recovery and reversible martensitic phase transformation. Although, there are many materials and alloys that exhibit the properties of shape memory alloy, Ni-Ti mostly represent the group SMAs. Therefore, this paper will focus on electrical discharge machining of mostly Ni-Ti alloy. However, the EDM of other SMAs has also been presented in this paper.

PROPERTIES AND APPLICATIONS OF SMAs

Characteristics and Properties of SMA

Nickel – Titanium (NiTi) alloys are the most important class of shape memory alloys and inter-metal binary combinations [6]. NiTi alloys are very popular in industries due to properties such as shape memory effect (SME), superelasticity, adaptive responses, memorized capability, high damping characteristics, stress hysteresis and magnetic resonance imaging (MRI) compatibility [6,7].

Nickel – Titanium is one of the shape memory alloys or smart metal with the capability of changing the shape by changing heat and the temperature. When SMA deforms through heating, it can regain its original shape. Deformation temperature is the phase transformation temperature of austenite to martensite and vice versa. NiTi shape memory alloys have two totally different phases (temperature-dependent crystal structures): martensite (lower temperature) and austenite (higher temperature or parent phase). The fundamental reason of NiTi's super elasticity and memorability is a revocable martensite transformation in the solid phase [8] (see Figure 1).

Table 1. The mechanical properties of NiTi [8]

Properties	Austenite	Martensite
Young's modulus (GPa)	30-83	20-45
Ultimate tensile strength (MPa)	800-1900	800-1900
Elongation at failure (%)	20-25	20-25
Recoverable strain (%)	8-10	8-10
Poisson ratio	0.33	0.33

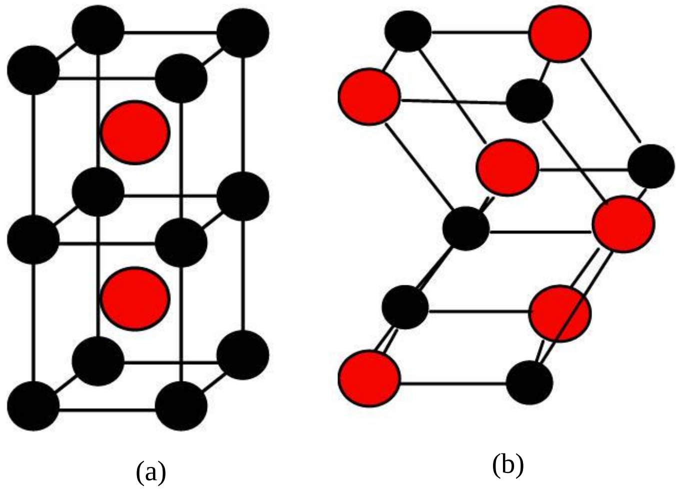

Figure 1. (a) Austenite and (b) Martensite structure [8].

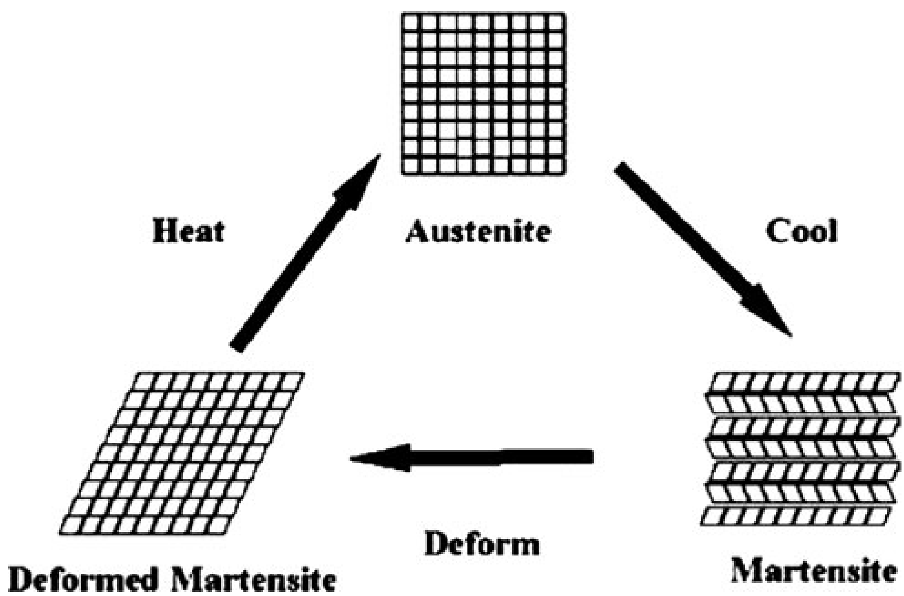

Figure 2. The shape-memory effect of NiTi SMA [9].

Properties such as Young's modulus, electrical resistance and damping behavior are remarkably different for the two phase transformations of NiTi, as can be seen from Table 1 [8]. NiTi-SMA gets their unique physical properties from the rare behavior of Nitinol in phase transformation, which is contingent on the temperature of austenite and martensite in atomic scale. Nitinol remains in the austenite phase in relatively higher temperatures and in martensite phase in relatively lower temperatures. This distinct behavior in transformation between the two phases means that a product made of NiTi-SMA transforms to its martensitic phase when cooled below the transformation temperature, which allows for easy deformation of the product (see Figure 2).

There are two common shape memory effects: the one-way and two-way shape memory effects. As the names suggest, the difference between the two is that, the one-way has only one original form, while the two-way effect allows the sample to remember two different original forms [9].

For the one-way shape memory effect, or, simply, shape memory effect, shape recovery is achieved only during heating. A complex arrangement is produced through several variants of martensite by the stress-free cooling of austenite. While average macroscopic transformation strain would equal zero, the boundaries between the martensite variants and twinning interfaces will be very mobile. Detwinning is achieved at stress level much lower than the plastic yield level of martensite, and yet large inelastic strain can be observed. These strains are recovered by the reverse transformation that is induced by heating, and since the stress has now reoriented the martensite variants, reversion to austenite creates another large transformation strain (Figure 3) [9]. This strain will have the same amplitude but in opposite direction to the inelastic strain. This will return the SMA to its original shape of the austenitic phase. It is worthy to note that further cooling will result in multiple self-accommodated martensite with no significant shape change.

With this shape memory method, the sample is cooled below the M_f (Martensite finish) temperature to form properly first, and then heated above the A_f (Austenite finish) temperature until it gets its austenitic shape. The method is then repeated 20 to 30 times for the procedure to be completed. The sample will finally obtain its planned shape below M_f temperature and any other shape above the A_f temperature (Figure 4) [8].

In the two-way shape memory effect, the sample is deformed above the M_s (Martensite start) temperature in order to create martensite reference variables that are obtained by stress, and then cooled up to below the M_f temperature. Once the sample is heated up above the A_f temperature, the sample will retake its original austenitic shapes [10,11].

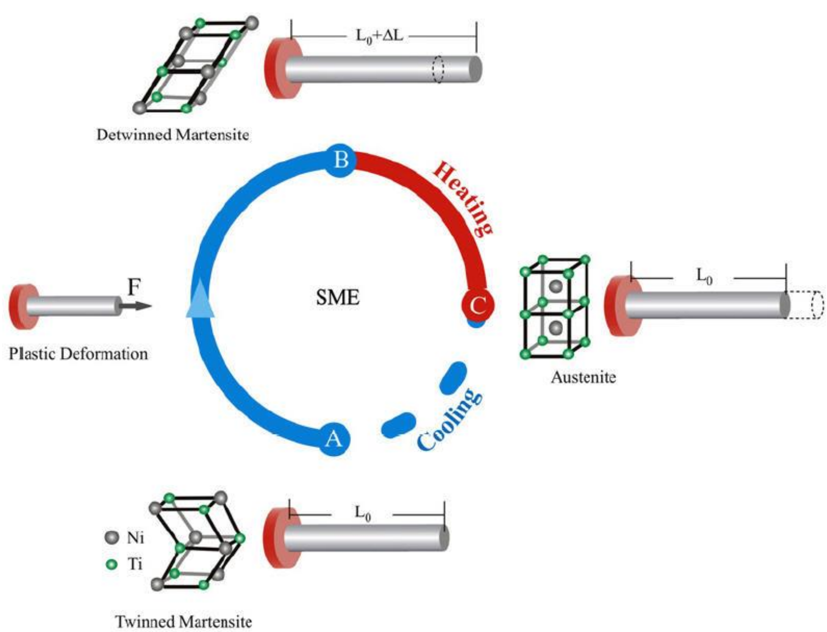

Figure 3. Shape memory effect phenomenon in shape memory alloys [8].

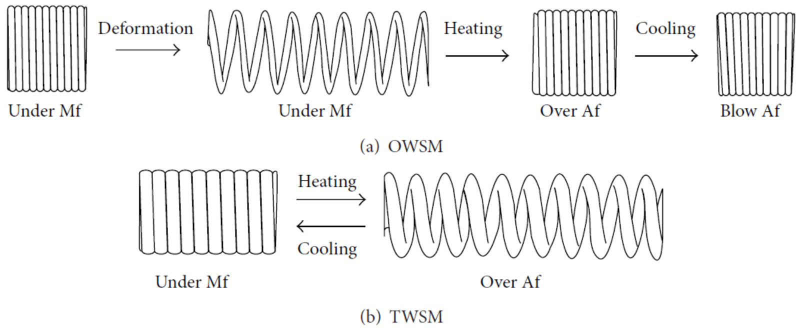

Figure 4. Two instructions of two-way memory training [10].

One of the important characteristics of SMAs is the strain increasing nearly 8% heating above austenite finish temperature [8]. SMAs produce high actuation strains (~6-10%), stresses (~100-400 MPa) and work output (~10 MJ/m3) as a result of reversible martensitic phase transformations [12].

Applications of SMA

The unique properties of NiTi SMAs have resulted in many applications in the medical, aerospace, robotics, military, automotive, and biomedical industries.

One of the important application of NiTi shape memory alloy is the use as smart components for actuators and sensors [8]. In recent years, NiTi alloys are replacing conventional sensors and actuators because of their unique property along with lightweight, reliability and costs. In addition, NiTi alloys are also used in the manufacturing of smart composites for vibration and shape control [8]. Nitinol is used in extremely resilient glass frames and in mechanical watch [13]. It is sometimes used as a temperature control system because of its shape changing capability that can activate a switch or variable resistor [13]. In recent years, nitinol is also used in cell-phone technology as retractable antenna due to its flexibility and mechanical memory nature [13]. Some other important applications of NiTi shape memory alloys as smart materials are couplings, toys, cryogenically activated die, and bubble memory sockets [14]. Another important application of NiTi shape memory materials is use as thin film in Micro-Electro-Mechanical Systems (MEMS). The examples of MEMS devices where thin film of NiTi is used are NiTi-Silicon bi-layer micro-grippers [15] and micro-valves for fluid control [16].

NiTi shape memory alloy is widely used in biomedical implants ranging from orthopedic to orthodontic applications due to its biocompatibility. Some of the common examples of biomedical applications of this material are spinal vertebral spacer, spinal rod, knee implant accessories, orthodontic arch wires, active catheters, medical staples, plates for fractured bone, nail for marrow cavity, vascular stent and so on [17].

Another important area of applications of NiTi SMAs is in heat engines for automotive and aerospace industries because of its stability at higher temperature. The first large-scale commercial application of NiTi was in couplers in the Grumman F-14 fighter jet in 1971 [18].

In addition, nitinol wire is used in heat engines to produce mechanical energy from hot and cold heat sources [19].

EDM OF SMAS

In recent years, Nickel-Titanium (Ni-Ti) alloy, most commonly known as 'Nitinol', has become an important candidate to be machined using the electrical discharge machining (EDM) process. The EDM process is becoming increasing popular for machining various SMAs because of their poor machinability in conventional mechanical machining processes. The low thermal conductivity and elastic modulus of NiTi alloy have made the conventional machining processes difficult to apply for machining this material economically because of significant tool wear and poor quality surface finish [20]. In addition, the strain hardening behavior, high toughness and viscosity, and the unique superelastic behavior have made the conventional machining of NiTi SMAs complicated [21]. Some of the problems associated with the conventional machining of SMAs are higher tool wear, excessive machining time, less dimensional accuracy due to severe strain hardening and pseudoelasticity [22]. In order to overcome these difficulties associated with conventional machining processes there have been many research works on the electrical discharge machining of NiTi SMA at different scales using different varieties of EDM process, such as die-sinking EDM, wire-EDM, micro-EDM and EDM-based hybrid techniques. The application of EDM in SMAs arises from the difficulty of machining complex shapes features in shape memory alloy with higher accuracy using the conventional machining processes. The EDM is capable of machining SMAs to produce complex shaped features, parts and components with comparatively higher accuracy [23,24]. In recent years, investigations have been carried out on different aspects of the EDM of shape memory alloys, such as selection of dielectric and tool materials, parametric optimization, modeling and simulation, surface modification after the EDM and so on. The following section will provide a detail overview of the research works reported in the literature on various aspects of EDM of SMAs.

Effect of EDM Parameters on Machining Performance of SMAs

In order to understand the machinability of SMAs using the EDM process, it is important to understand the effect of different operating parameters on the machining performance parameters. In EDM, selection of major operating parameters depends on the type of pulse generators [25]. For an RC type pulse generator the major operating parameters are gap voltage, capacitance, and resitance [25]. On the other hand, for transistor type pulse generator the major parameters are gap voltage, peak current, pulse duration, pulse interval, and duty ratio [25]. In addition, there are gap control parameters that influences the machining stability during the EDM process, which influences the machining performance indirectly [26]. Some of the gap control parameters that influecnes the EDM process are 'short' detection parameter, 'open' parameter, EDM gap control speed, gap feed rate, gap threshold voltage and gap control factor [26,27]. The machining performance of the EDM process is evaluated by material removal rate (MRR), tool wear ratio (TWR) or electrode wear ratio (EWR), and surface roughness (SR) or average surface roughness (R_a).

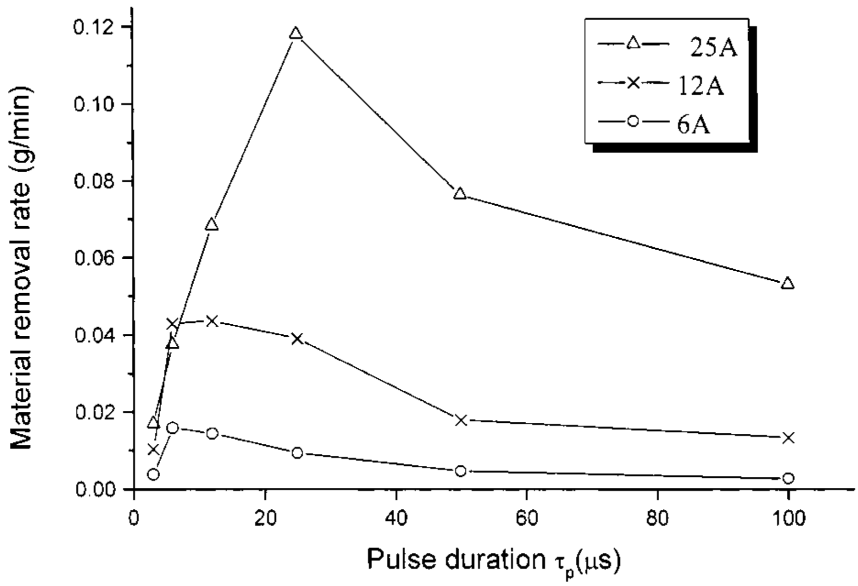

(a)

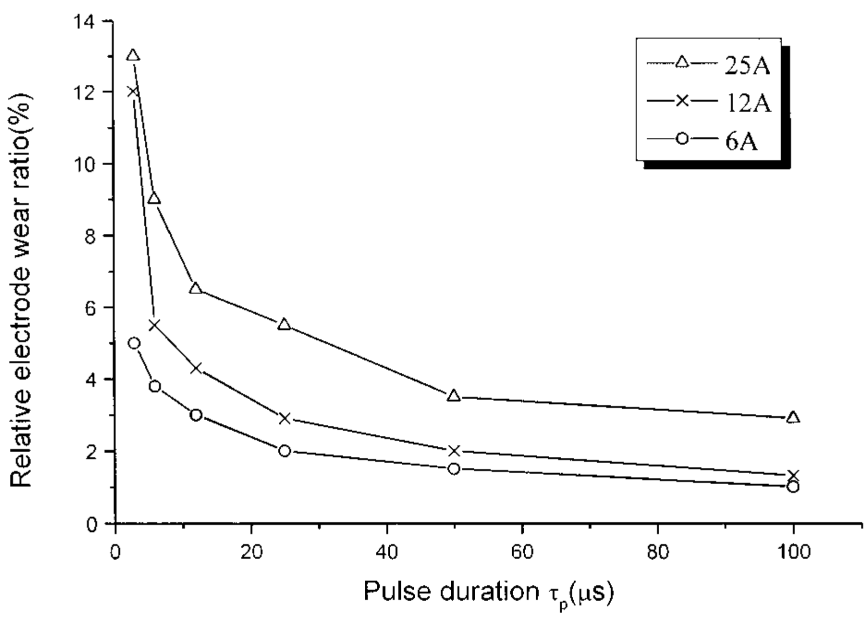

(b)

Figure 5. The effect of pulse duration and pulse current on the (a) MRR and (b) EWR during the EDM of NiTi SMA [28].

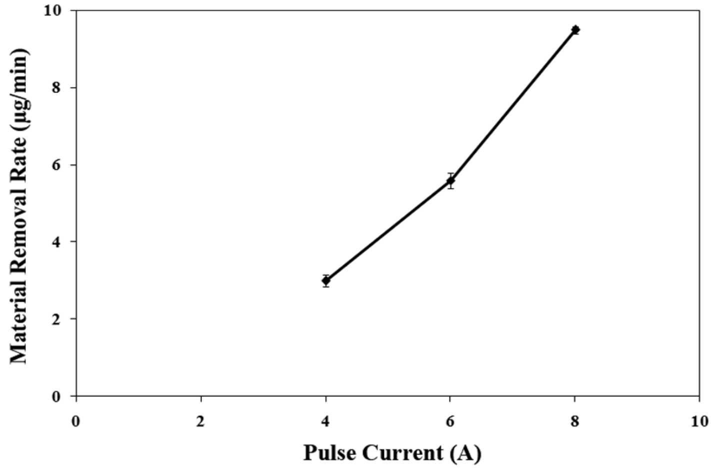

(a)

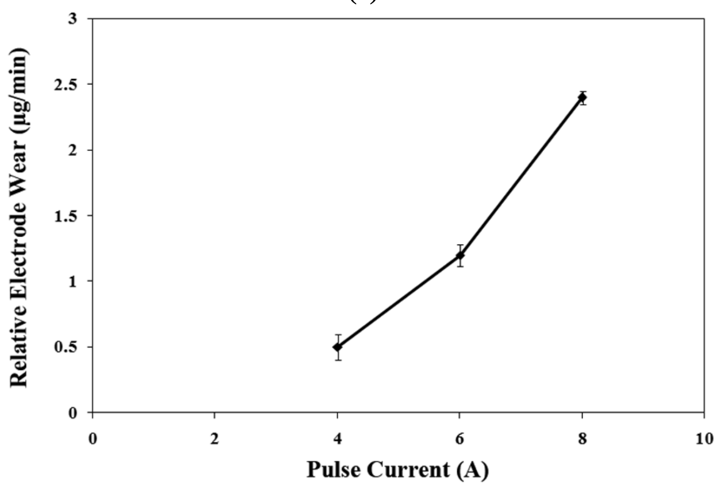

(b)

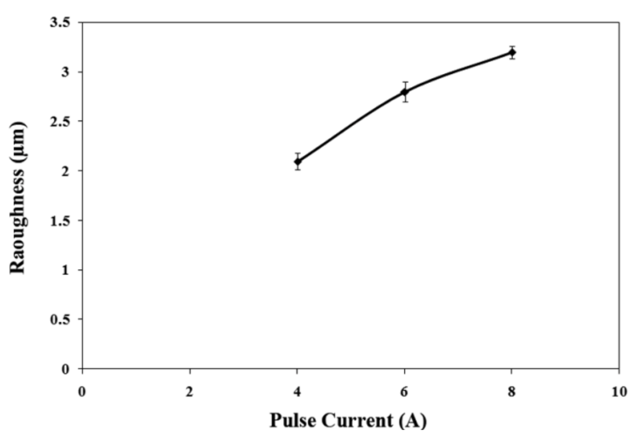

(c)

Figure 6. The effect of pulse current on (a) MRR, (b) relative EWR and (c) SR during EDM of NiTi SMA [29].

There have been several studies on the machinability of SMAs with EDM process. Lin et al. [28] investigated the electro-discharge machining characteristics of NiTi shape memory alloy by varying different operating parameters and ovserving their effect on EDM performance parameters. It was found that the pulse current and the pulse duration have significant influence on the MRR and surface finish during the EDM of NiTi SMA. A longer pulse duration and lower peak current could provide improved machining performance during EDM of SMAs. In their study, they investigated the effect of pulse duration on the MRR and EWR at different settings of peak current. It was also found that the both MRR and EWR increased with the increase of peak current. Figure 5 shows the effect of pulse duration and peak current on the MRR and EWR during the EDM of NiTi SMA [28]. It was found that with the increase of pulse duration the MRR increased up to a certain limit then started to decrease with further increase of pulse duration. The higher pulse current was found to produce higher MRR. In case of electrode wear ratio (EWR), it was found that the EWR decreased significantly at the increase of pulse duration for certain values, then remained unchanged at very higher settings of pulse duration. Lin et al. [28] varied different composition of SMAs ($Ti_{49}Ni_{51}$, $Ti_{50}Ni_{50}$ and $Ti_{50}Ni_{40}Cu_{10}$) during the EDM process and found similar machining behavior against different operating parameters.

Alidoosti et al. [29] also investigated the machining characterisitics of NiTi SMA based on full factorial design. They varied the pulse current and pulse interval and used two different electrode materials (W-Cu and Cu) to investigate the effect of operating parameters on EDM performance during machining of NiTi SMA. It was reported that there was no significant difference in the machining performance of W-Cu and Cu electrode for EDM of NiTi alloy [29]. However, the EDM performance depends greatly on the pulse duration and pulse interval parameters. They found that with the increase of pulse current, the MRR, EWR and SR increases due to the increase of discharge energy, as shown in figure 6 [29]. On the other hand, with the increase of pulse duration, the MRR increases first up to certain limit then decreases again at higher settings of pulse duration. The relative EWR was found to reduce with the increase of pulse duration, whereas the SR was found to increase with the increase of pulse duration. Figure 7 represents the effect of pulse current and pulse duration on the MRR, relative EWR and SR during EDM of NiTi SMA [29].

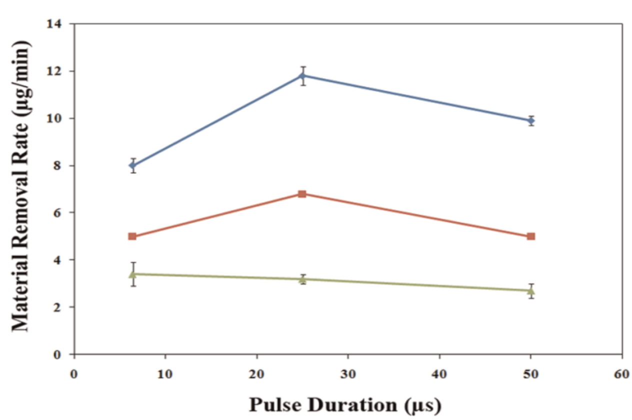

(a)

Figure 7. (Continued).

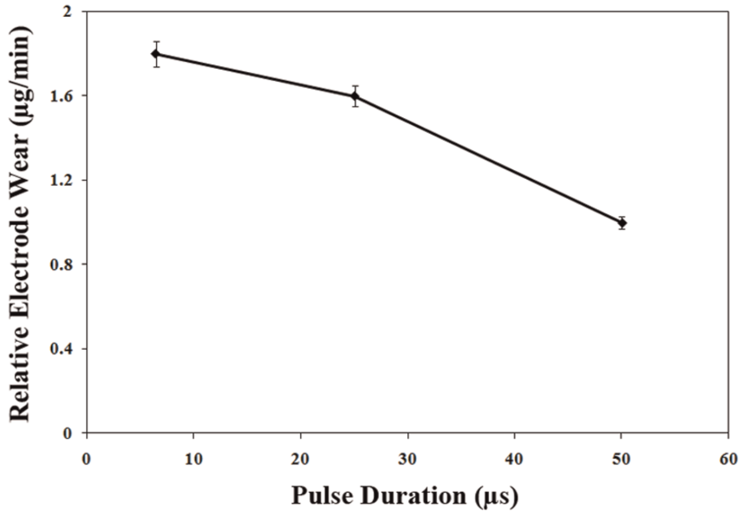

(b)

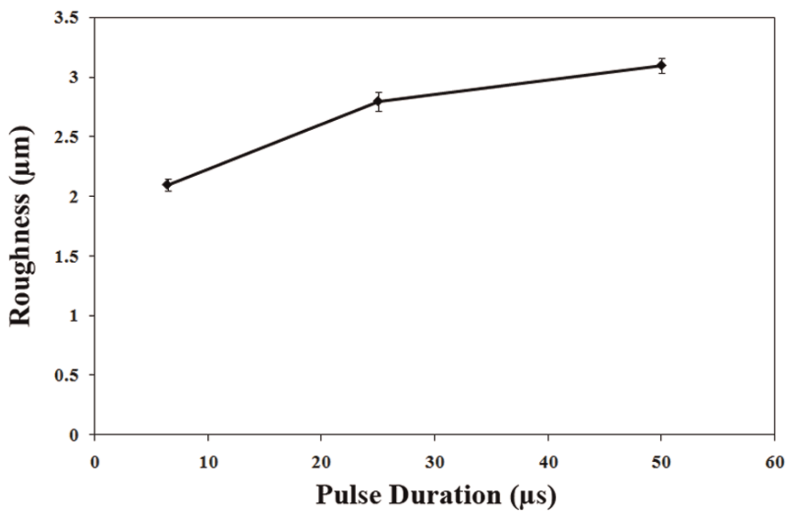

(c)

Figure 7. The effect of pulse duration on (a) MRR, (b) relative EWR and (c) SR during EDM of NiTi SMA [29].

Chen et al. [30] investigated the EDM machinability of two NiTi based SMAs, i.e., Ti50Ni49.5Cr0.5 and Ti35.5Ni49.5Zr15. It was reported that the MRR of NiTiX alloys exhibited reverse relationship to the products of respective alloy's melting point and thermal conductivity [30]. It was also reported that the surface roughness after the EDM process has a co-relationship with the product of pulse duration and pulse interval. Figure 8 shows the relationship of surface roughness with the product of pulse duration and pulse interval parameters [30]. It was found that the surface roughness increases steadily with the increase of product of pulse duration and pulse interval.

Huang et al. [31] investigated the EDM machinability of $Ni_{50.6}Ti_{49.4}$ alloy and compared the machining of NiTi SMA for wire-EDM and laser machining processes. It was found that laser machining using a ultrasot pulse laser can provide lower surface roughness and heat affected zone in the NiTi SMA after machining compared to those generated during the wire EDM [31]. They also investigated the effect of major operating parameters on the machining performance for both wire-EDM and laser machining of NiTi SMA. Figure 9 shows the effect of current on the cutting width, surface roughness and material removal rate during the WEDM of NiTi SMA [32].

Daneshmand et al. [32] compared the EDM machinability of NiTi60 SMA for without and with tool rotation. They investigated the effect of pulse current, gap voltage, pulse duration and pulse interval on the MRR, SR and tool wear rate for traditional and rotational EDM of NiTi60 SMA. The experimental results were then analyzed using Taguchi's design of experiments. It was found that irrespective of tool rotational speed the operating parameters have similar effect on the machining performance, although the tool rotational speed of 200 RPM led to less material removal rate and better surface roughness and tool wear [32]. Figure 10 shows the effect of voltage on the MRR, tool wear rate and SR for both traditional and rotation EDM of NiTi60 SMA. It was found that for both traditional and rotational EDM, the MRR, tool wear rate and SR increased with the increase of voltage. It was also found that for all settings of voltage, the rotation EDM provided lower MRR, tool wear rate and surface roughness than traditional EDM.

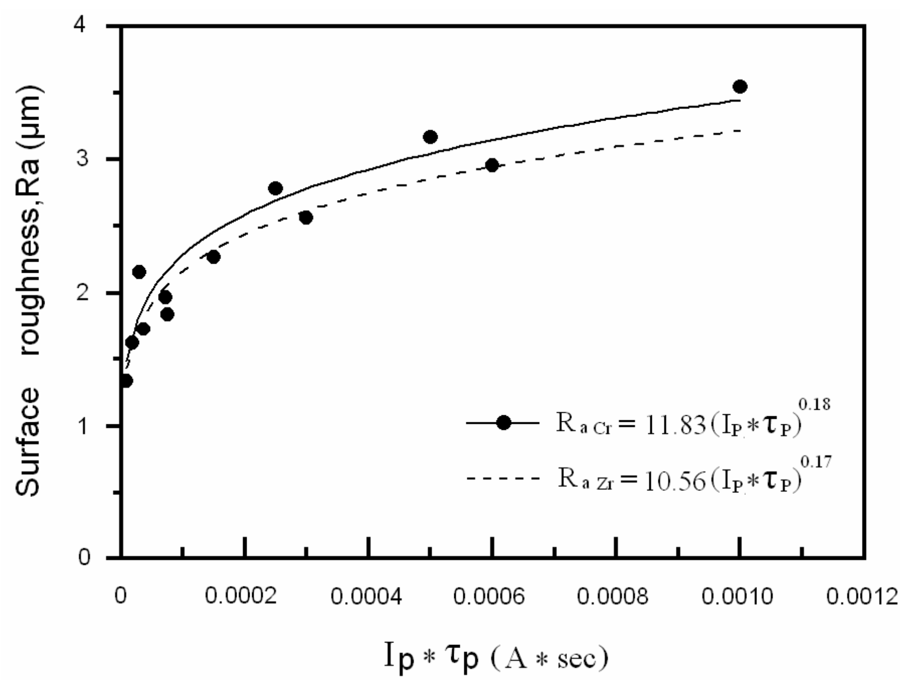

Figure 8. The relationship between surface roughness and product of pulse duration and pulse interval during EDM of Ti50Ni49.5Cr0.5 and Ti35.5Ni49.5Zr15 SMAs [30].

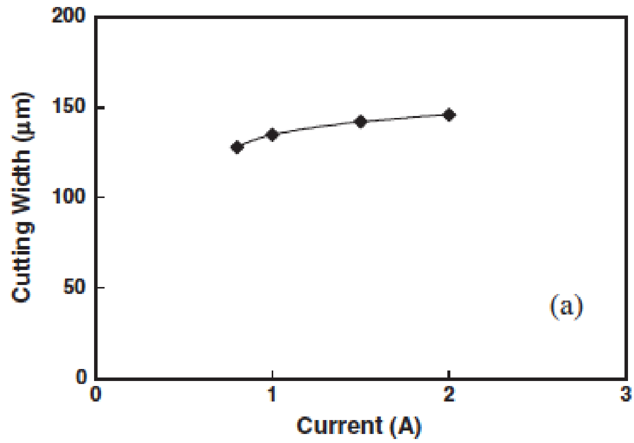

(a)

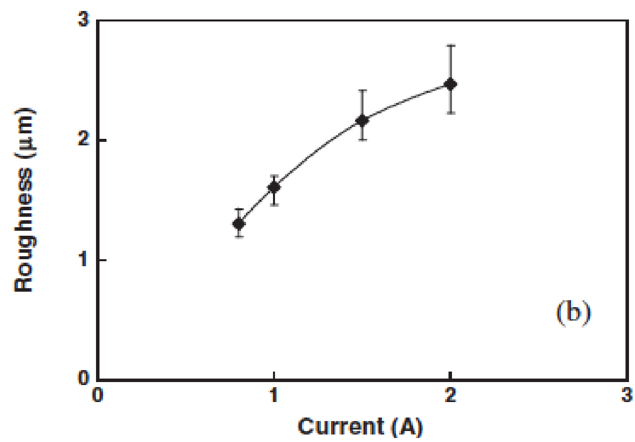

(b)

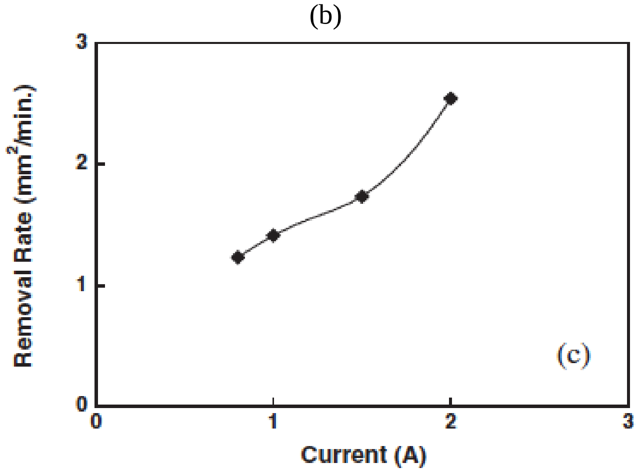

(c)

Figure 9. The effect of current on the (a) cutting width, (b) surface roughness and (c) material removal rate during wire EDM of $Ni_{50.6}Ti_{49.4}$ shape memory alloy [31].

Besides EDM of NiTi SMAs, there have been research on the EDM of other shape memory alloys. Chen et al. [33] investigated the EDM characteristics of a NiAlFe ternary shape memory alloy and compared the EDM performance of that against NiTiZr alloy. It was reported that an improved machining performance could be obtained during EDM of NiAlFe SMA by setting the machining parameters at lower pulse energy settings [33]. The pulse current, pulse duration and gap voltage should be set at lower values in order to generate lower pulse energy during EDM of NiAlFe SMA. It was also found that NiAlFe produces comparatively lower MRR that than of NiTiZr at the same parameter settings during EDM. Figure 11 shows the comparison of MRR for $Ni_{60}Al_{24.5}Fe_{15.5}$ and $Ti_{35.5}Ni_{49.5}Zr_{15}$ alloys after machined by the EDM process [33].

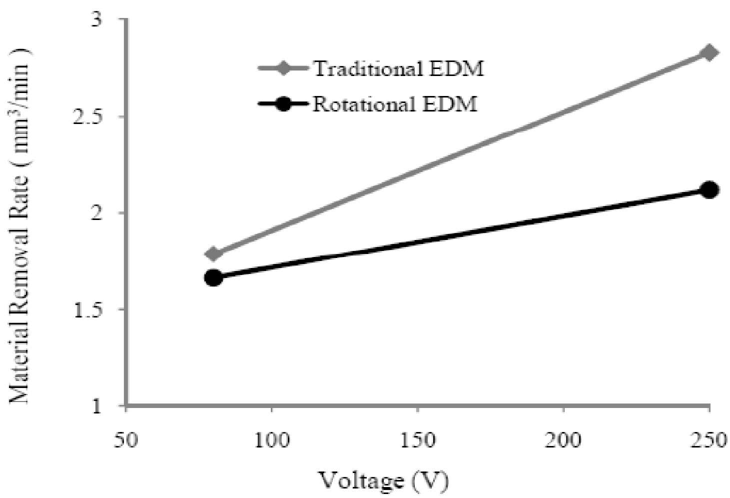

(a)

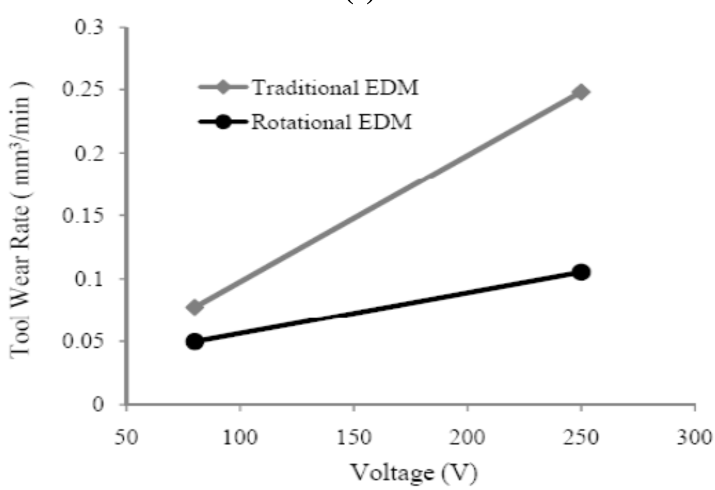

(b)

Figure 10. (Continued).

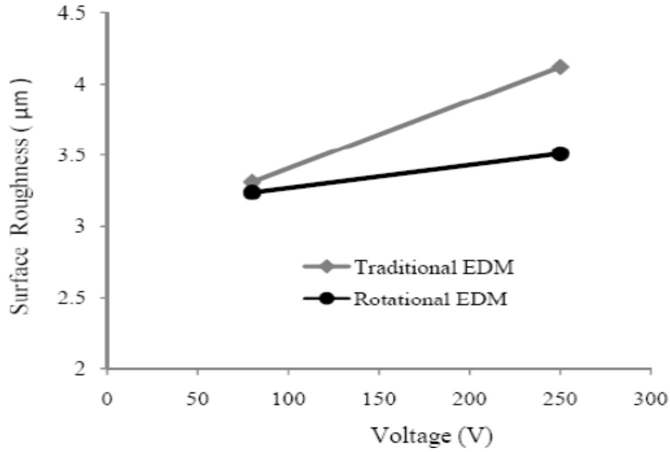

(c)

Figure 10. The effect of voltage on (a) MRR, (b) tool wear rate, and (c) surface roughness for traditional and rotation EDM of NiTi60 SMA [32].

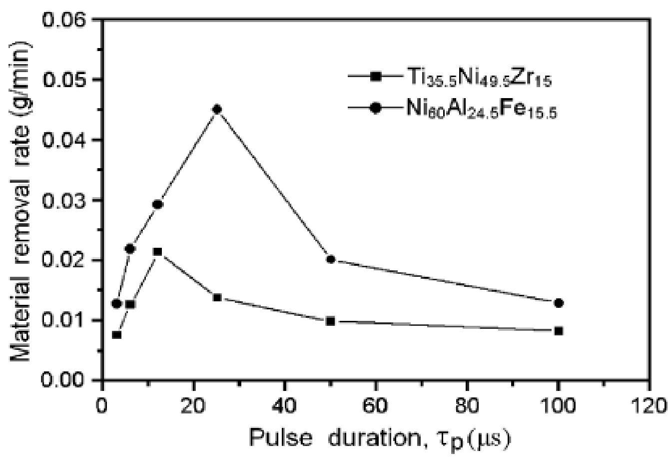

Figure 11. Comparison of MRR for $Ni_{60}Al_{24.5}Fe_{15.5}$ and $Ti_{35.5}Ni_{49.5}Zr_{15}$ alloys after EDM using different pulse duration and a constant pulse current of 10 A [33].

Design of Experiments, Optimization and Modeling during EDM of SMAs

After investingating the effect of different operating parameters on the machining performance characteristics during the EDM process, it is necessary to identify the optimum or best parameters settings for machining any particular materials. The identification of optimum parameters can be statistical as well as by the best judgement of experimental results. In this section, the statistical analyses during EDM of SMAs are presented. There have been several statistical tools reported in literature for identification of optimum parameters during EDM, such as design of experiments (DOE), one-factor-at-a-time (OFAT), analysis of variance (ANOVA), response surface methodology (RSM) and so on.

There have been several research on the optimization of EDM parameters during machining of shape memory alloys by different statistical techniques. Daneshmand et al. [34] investigated the effect of EDM parameters on the surface roughness and material removal rate during EDM of NiTi60 SMA. In order to analyze the results, the authors used the design of experiments (DOE), the Taguchi's method, LI8 orthogonal array and the Minitab@16.1.1 software. In order to optimize the ouput parameters, which were MRR, TWR and SR, the orthogonal array of LI8 (2^1 X 3^3) were used. There were 18 experiments and 4 factors used in the study to optimize the operating parameters. Figure 12 presents the effect of all the operating parameters on the performance characteristics during EDM of NiTi60 SMA [34]. The curves were generated from the statistical analysis experimental results. It was found from the statistical analyses that the maximum MRR could be achieved at a parameters setting of 250 V, current of 20 A, pulse duration of 100 µs and pulse interval of 30 µs. The relative elctrode wear was found to be lowest at 80 V, 20 A, 100 µs, and 70 µs parameters combination. The average surface roughness was found to be minimum at 80 V, 10 A, 35 µs and 200 µs combination of input parameters.

In another similar study, Sabouni and Daneshmand [35] investigated the effect of EDM process parameters during the machining of NiTi SMA using graphite electrode. The operating parameters varied were voltage, discharge current, pulse-on-time, and pulse-off-time. The Taguchi's method, LI8 orthogonal array and the 'Minitab R.16.1.1' software were employed for the design of experiment. Figure 13 shows the effect of different input parameters on the MRR, tool wear rate, relative electrode wear ratio and surface roughness during EDM of NiTi SMA using graphite tool. The maximum rate of MRR during EDM of NiTi SMA was achieved with a discharge current of 15 A, voltage of 80 V, pulse-on-time of 35 µs and pulse-off-time of 70 µs. On the other hand, the minimum rate of graphite tool wear was achieved with a discharge current of 10 A, voltage of 250 V, pulse-on-time of 50 µs and pulse-off-time of 30µs. The minimum value of surface roughness in the EDM of NiTi SMA was achieved with a discharge current of 10 A, voltage of 80 V, pulse-on-time of 35 µs and pulse-off-time of 70 µs.

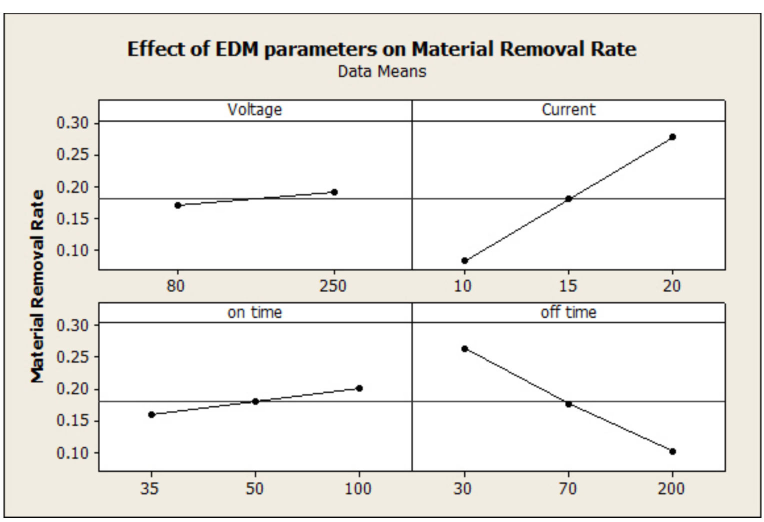

(a)

Figure 12. (Continued).

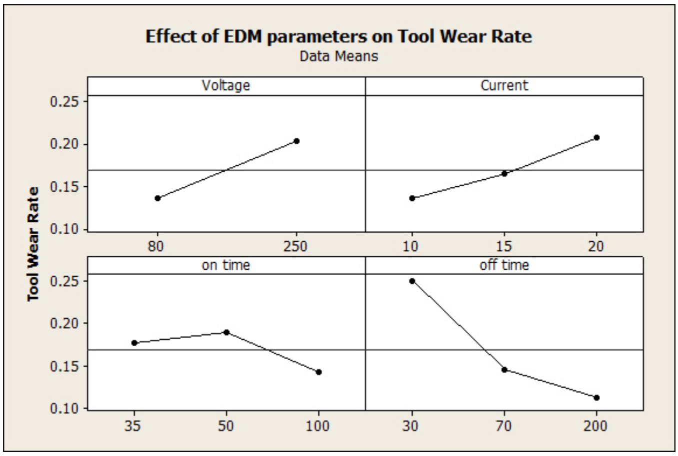

(b)

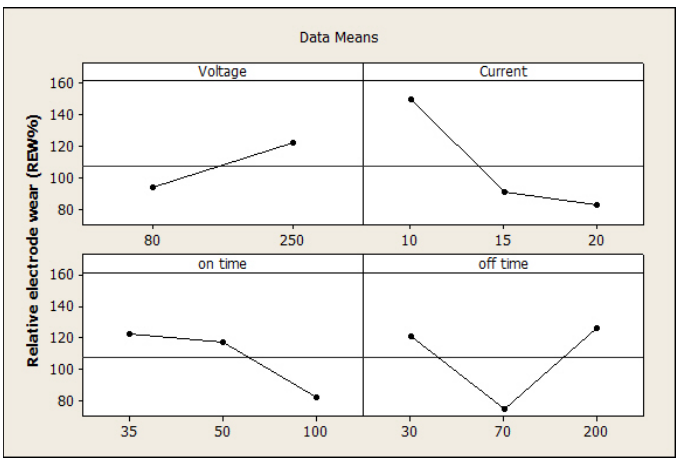

(c)

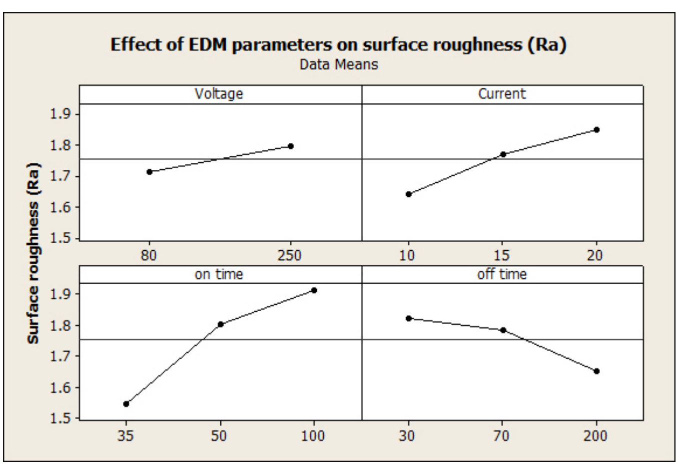

(d)

Figure 12. Effect of EDM parameters on the (a) MRR, (b) tool wear rate, (c) relative electrode wear and (d) surface roughness for EDM of NiTi60 SMA [34].

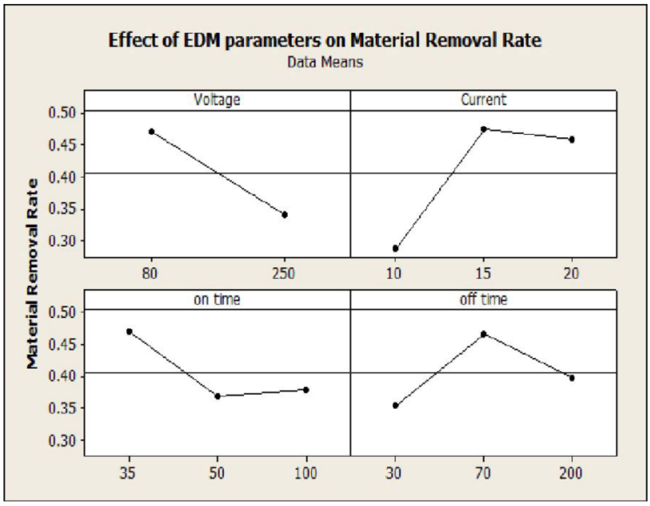

(a)

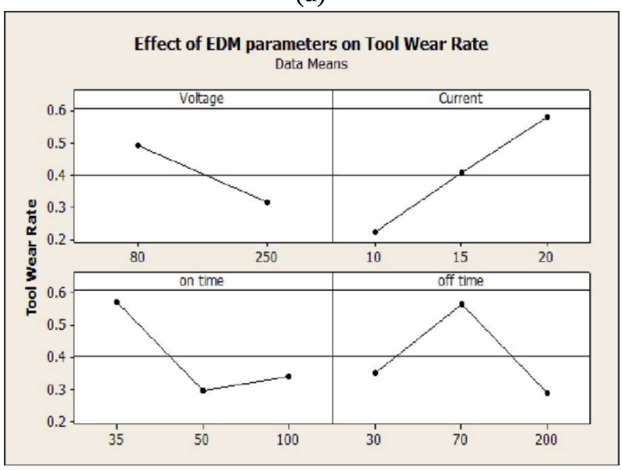

(b)

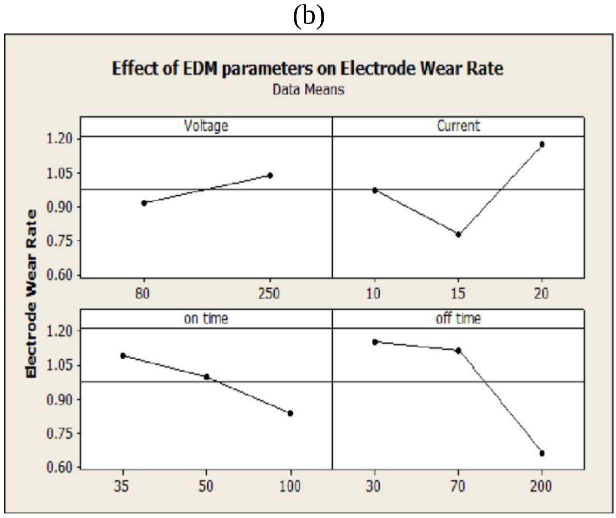

(c)

Figure 13. (Continued).

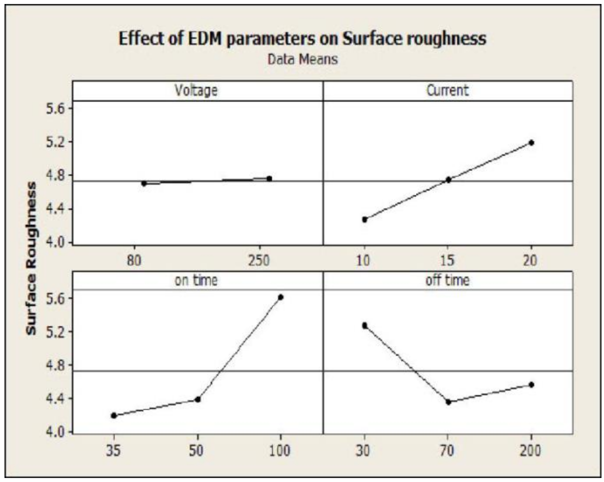

(d)

Figure 13. Effect of EDM parameters on the (a) MRR, (b) tool wear rate, (c) relative electrode wear and (d) surface roughness for EDM of NiTi SMA using graphite tool [35].

Surface Quality, Integrity and Modification of SMAs after EDM

Besides the surface roughness, there are other indicators that present the overall surface quality or integrity. The machined workpiece surface integrity includes the microstructures, surface topography, micro-cracks, composition and hardness, under a wide range of machining conditions [36]. Moreover, the machined surface suffers from surface modification during the EDM because of the electrothermal nature of the material removal. The surface integrity and the composition changes have direct influence on the mechanical properties and future usefulness of the machined part [36].

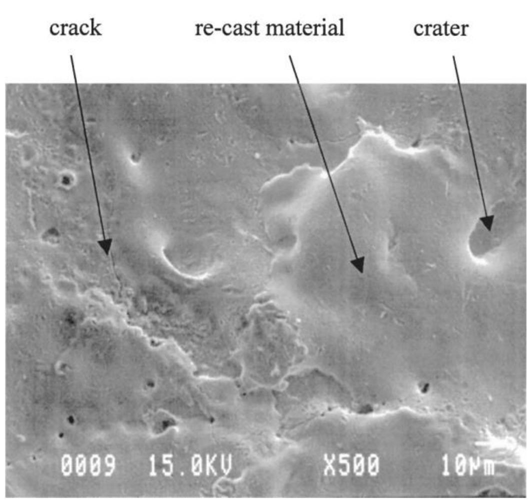

(a)

Figure 14. (Continued).

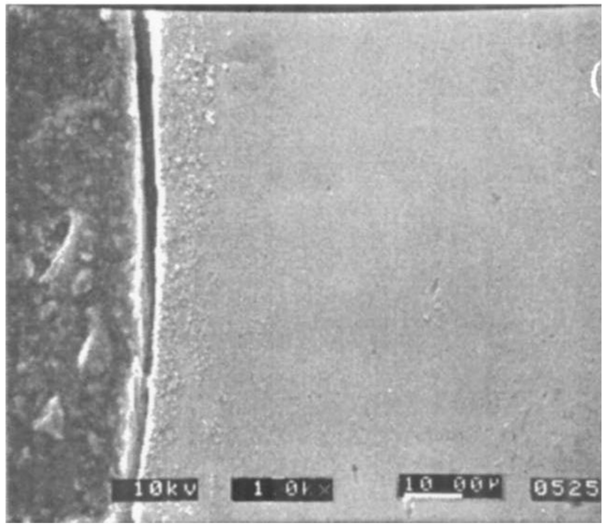

(b)

Figure 14. SEM image of (a) machined surface topography of NiTi SMA, and (b) formation of recast layer at peak current of 25 A and pulse duration of 50 μs [28].

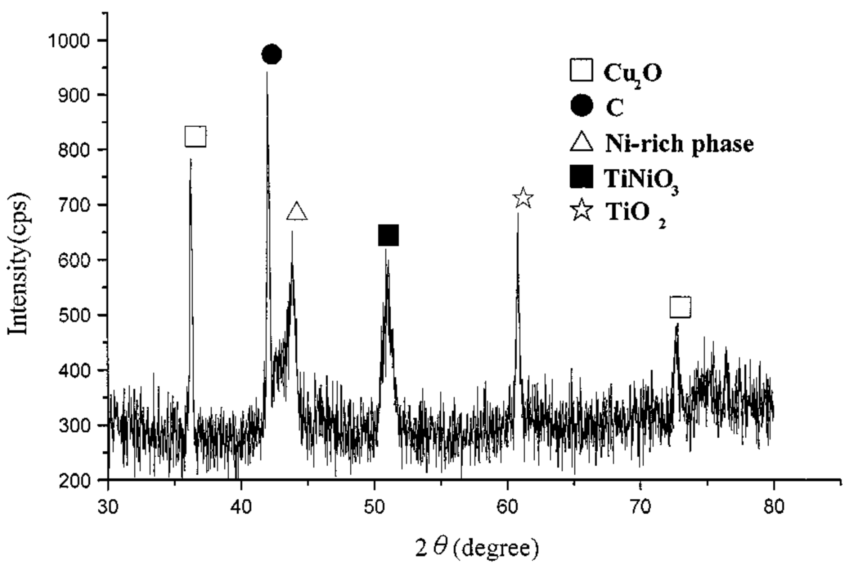

Figure 15. The XRD pattern analysis of the NiTi SMA after EDM [28].

Lin et al. [28] investigated the microstructure and composition of NiTi surface after EDM. It was reported that the EDM surfaces are full of craters due to electrical discharges in addition to the recast layer owing to the melting and evaporation. The EDMed surface also consisted of lots of small micro-cracks. Figure 14(a) shows SEM images of the topography of the NiTi SMA surface after EDM showing cracks, recast layers and craters [28]. Figure 14(b) shows the cross-sectional image of the machined surface clearly indicating the recast layer on the NiTi SMA surface after EDM.

In addition, they reported the formation of titanium oxides on the surface of NiTi after the EDM process. After analyzing the surface using X-Ray Diffraction (XRD) analysis, it was found that the EDMed surface of NiTi SMA was composed of TiO_2, $TiNiO_3$, Cu_2O, C and Ni-rich phase. Figure 15 shows the XRD analysis showing all the compounds formed on the NiTi machined surface after EDM [28].

Alidoosti et al. [29] also investigated the microstructure and composition of NiTi surface after EDM in a similar study. They have also reported the similar findings reported by Lin et al. [28]. However, they performed the EDX analysis from various spots of the machined surface after EDM as shown in figure 16 [29]. As can be seen from the tables in the figure 16, the amount of carbon increased significantly at the machined surface as denoted by point ‘A’. The amount of carbon is comparatively lower at the recast layer (denoted by point ‘B’) and there is no carbon inside the base material (denoted by point ‘C’). The findings clearly indicate the influx of carbon after the EDM process, which migrates from the decomposition of hydrocarbon dielectric oil used in EDM [25].

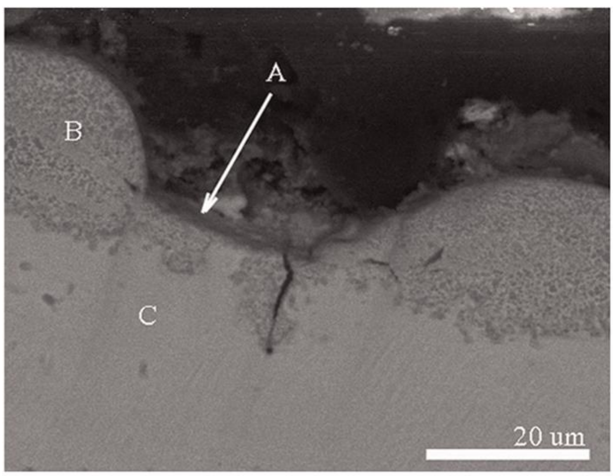

(a)

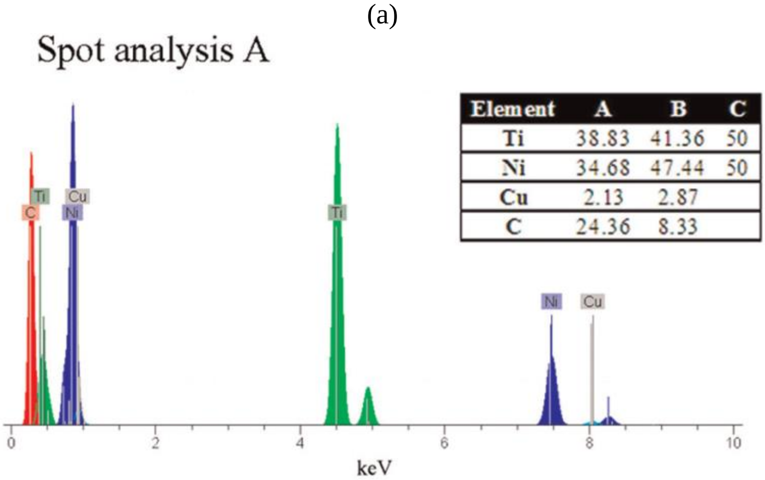

(b)

Figure 16. (a) Backscattered electron images of the cross-section of NiTi SMA surface after EDM, and (b) EDX spectrum analysis from various spots on the machined surface [29].

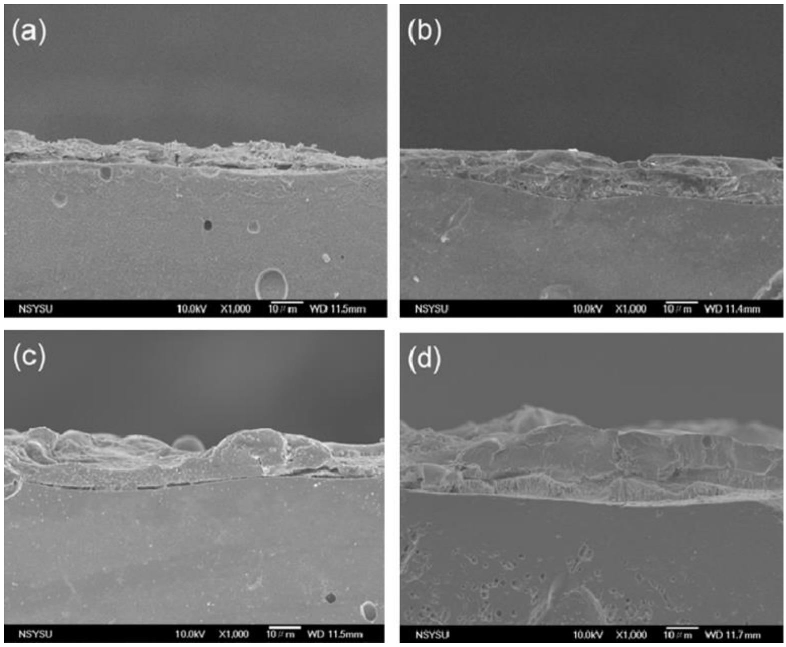

Figure 17. Variation of recast layer thickness of $Ti_{35.5}Ni_{48.5}Zr_{16}$ surface after EDM using 7 A current at different settings of pulse duration; (a) 3 μs, (b) 12 μs, (c) 25 μs and (d) 50 μs [37].

Hsieh et al. [37] investigated the surface characteristics and shape recovery ability of $Ti_{35.5}Ni_{48.5}Zr_{16}$ and $Ni_{60}Al_{24.5}$ $Fe_{15.5}$ ternary shape memory alloys after the EDM process. They found the similarity in the surface characteristics between the two SMAs and reported that the machined surface is composed of craters, recast layer of molten metals and micro-cracks. They also calculated the thickness of recast layers and found that the thickness increased with the increase of pulse duration for both the materials. In addition, the discharge crater sizes also increased with the increase of pulse duration, and hence pulse discharge energy [37]. Figure 17 shows the variation of recast layer thickness of the $Ti_{35.5}Ni_{48.5}Zr_{16}$ surface after EDM at different settings of pulse duration [37].

Liu et al. [38] investigated the differences in surface characteristics for one single main cut and multiple trim finish cut during the wire-EDM of NiTi SMA. It was found that there is significant difference in the surface characteristics generated from a single main cut and multiple finish cut. The single main cut was found to generate higher thickness of recast layer (2 – 8 μm) with various surface defects and micro cracks. On the other hand, the finish cut was found to reduce the recast layer thickness significantly (0 – 2 μm) in addition to reducing the surface defect [38].

Figure 18 shows the surface topography of NiTi SMA for different cutting regime using different levels of discharge energy [38]. The cut denoted by 'MC' represents the main cut using the higher discharge energy level. The TC1, TC2 and TC4 represent finish trim cuts with comparatively lower discharge energy, while TC4 used the lowest level of discharge energy. It can be seen from figures that the amount of surface defects decreases with the decrease of discharge energy. There are more micro cracks, voids and debris on the surface machined by main cut. Figure 19 shows the comparison of recast layer thickness for main cut and finish trim cuts [38]. The figure 19(a) clearly shows the non-uniform white layer with micro cracks and micro voids on the cross-section of the surface machined by main cut. However, the thickness of white or recast layer reduced significantly in trim cuts. The lowest thickness of white layer was observed for TC4 where the discharge energy used was lowest. In addition, no significant micro cracks were oversved on the recast layer formed by the finish trim cut.

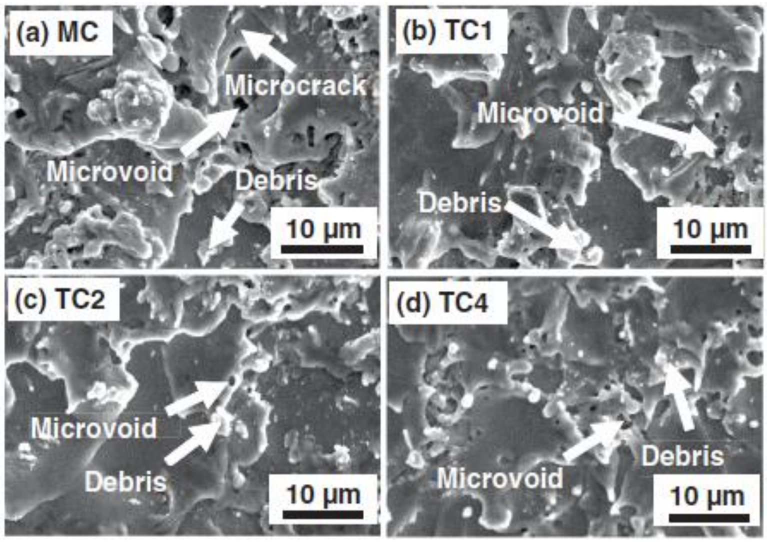

Figure 18. Comparison of surface topography of the NiTi SMA after machined by WEDM using different level of discharge energy; (a) MC (highest discharge energy), (b) TC1, (c) TC2 and (d) TC4 (lowest discharge energy) [38].

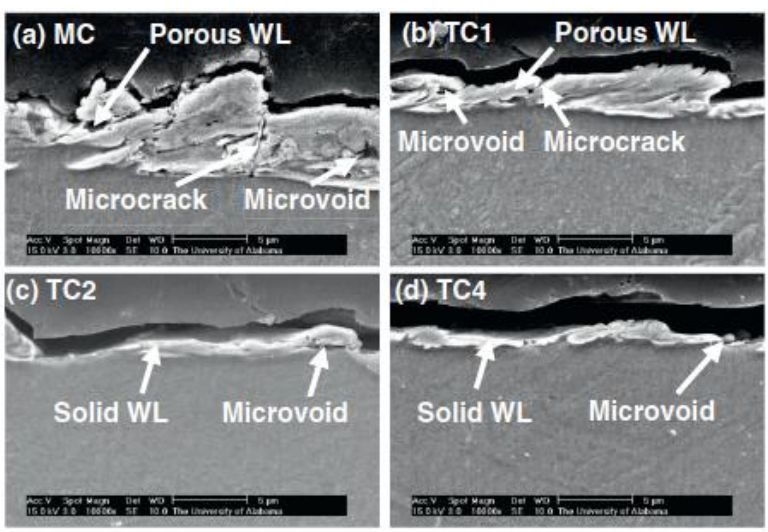

Figure 19. Comparison of recast layer thickness and surface defect of the NiTi SMA surface after machined by WEDM using different level of discharge energy; (a) MC (highest discharge energy), (b) TC1, (c) TC2 and (d) TC4 (lowest discharge energy) [38].

Mechanical Properties Changes of SMAs after EDM

The mechanical properties of any material greatly depends on the surface and sub-surface integrity and the quality after machining. As EDM is an electro-thermal process of removing materials, the machined surface suffers from subsequent heating and cooling processes. As a results, it is important to know the effect of EDM parameters on the machined surface and hence the possible mechanical properties changes of the materials. The mechanical properties that could possibly alter because of the EDM process are hardness at surface and sub-surface, residual stress, bending strength, fatigue strength etc [36].

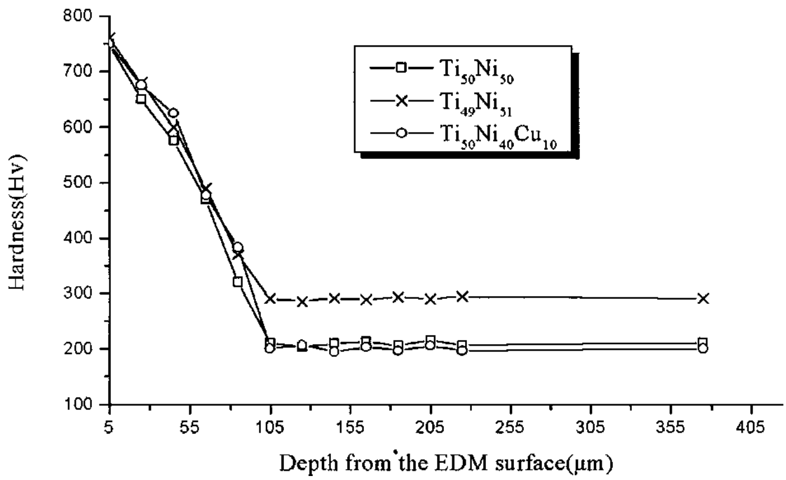

(a)

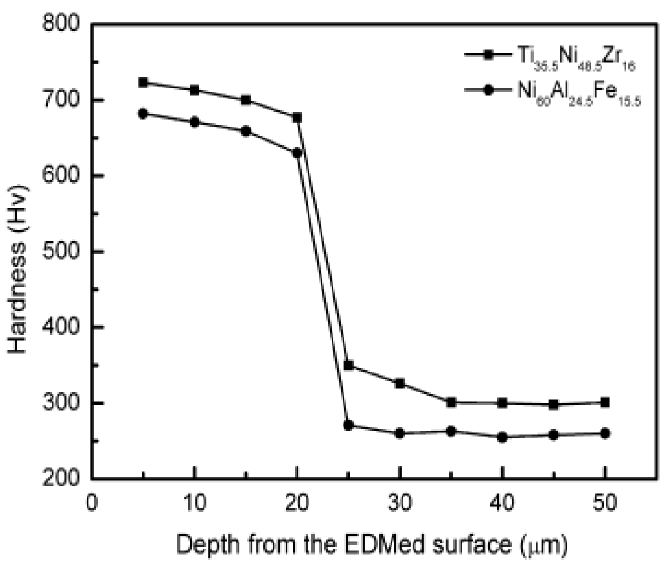

(b)

Figure 20. Variation of hardness of SMA from the machined surface to inside of the material after EDM; (a) NiTi SMA [28], and (b) $Ti_{35.5}Ni_{48.5}Zr_{16}$ and $Ni_{60}Al_{24.5}$ $Fe_{15.5}$ [37].

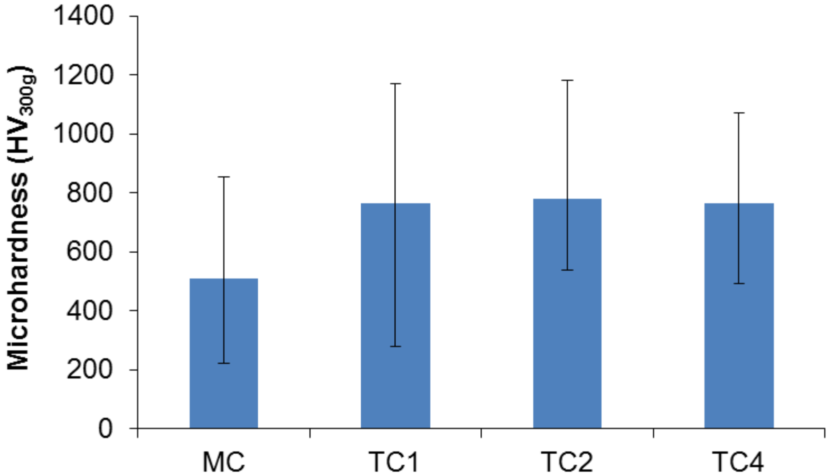

(a)

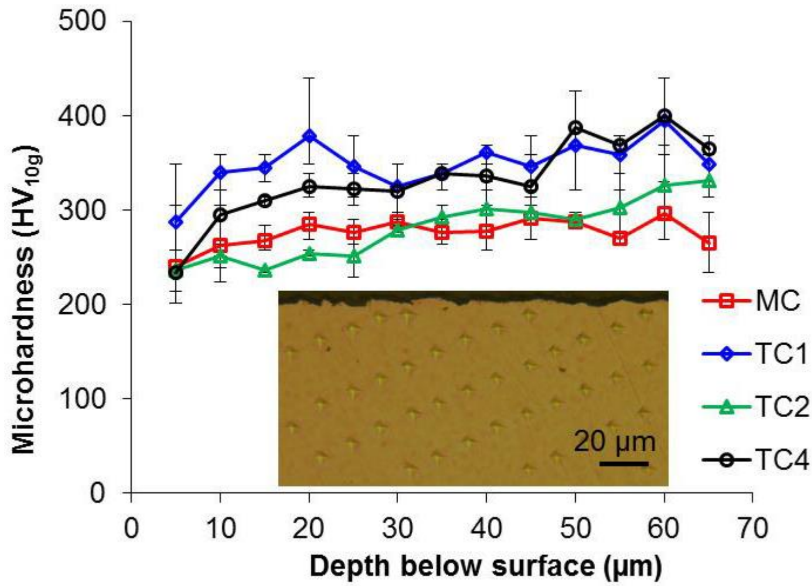

(b)

Figure 21. (a) Comparison of surface microhardness for main cut and finish trim cuts (MC: highest discharge energy and TC4: lowest discharge energy), and (b) variation of microhardness after WEDM of NiTi SMA at different depths below machined surface [38].

Lin et al. [28] investigated the changes in surface hardness of NiTi SMA after the EDM process. It was reported that the hardness of the machined surface increased due to the EDM process. However, the hardness was found to decrease at higher depths from the machined surface, and became unchanged after about 100 micron from the EDM surface [28]. Figure 20(a) shows the change in hardness of the NiTi SMA at various depth from the machined surface to inside of the material [28]. They also performed the bending strain test to investigate the shape recovery of NiTi SMA after EDM. It was reported that the NiTi SMA showed nearly perfect shape recovery in a normal bending strain and a slightly reduced shape recovery at higher bending strain [28].

Hsieh et al. [37] investigated the surface hardness of two different shape memory alloys: $Ti_{35.5}Ni_{48.5}Zr_{16}$ and $Ni_{60}Al_{24.5}$ $Fe_{15.5}$ after EDM and reported the similar findings to that of Lin et al. [28]. However, in their study they reported a critical depth of recast layer after which there is sudden decrease of hardness of materials for EDM. The hardness was found to reduce slowly with the increase of depth from the machined surface, with maximum hardness at the EDM surface. Figure 20(b) shows the variation of hardness of the two SMAs as a function of depth from the machined surface [37].

Liu et al. [38] performed a comparative experimental investigation to identify the differences in the microhardness of the EDMed surface of NiTi SMA for rough cut and finish cut using different levels of discharge energy in wire-EDM. The microhardness for various cuts was measured at the top of machined surface and compared as shown in figure 21(a). It was found that average microhardness is lower for rough cut and higher for finish cut. The findings indicate that the machined surface microhardness increases with the reduction of discharge energy [38]. However, the micro hardness of the recast layer could be different than that of the surface microhardness as shown in previous figures [28, 37]. Liu et al. [38] also investigated the microhardness at different depths of the machined surface for all four different cuts. They reported slight increment in the microhardness at higher depths from the machined surface for both main cut and trim cuts, as can be seen from figure 21(b). However, the differences in microhardness was not as significant as reported by Lin et al. [28] and Hsieh et al. [37].

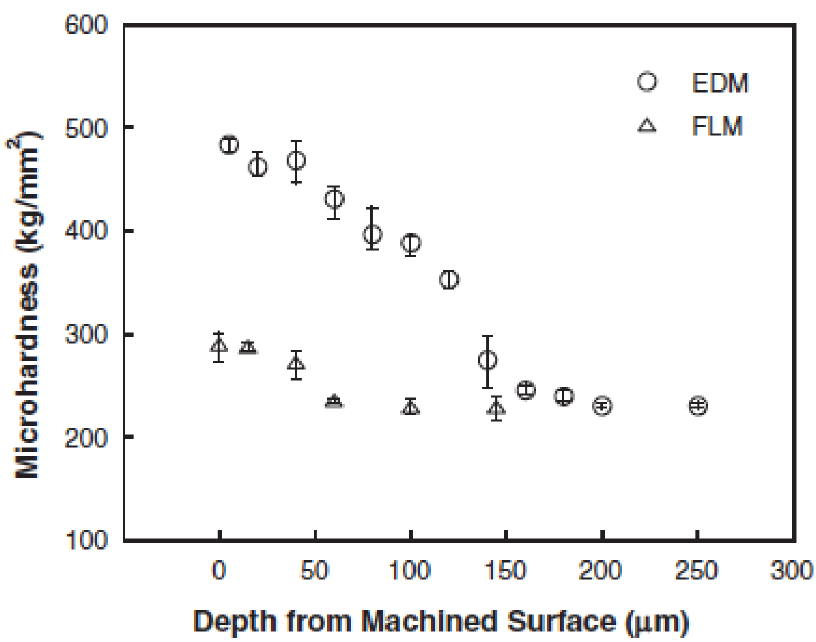

Figure 22. Comparison of microhardness for EDM and FLM processes [31].

Huang et al. [31] compared the thickness of recast layer and microhardness of the NiTi surface after machined by EDM and femtosecond laser machining (FLM). It was reported that the FLM produced comparatively lower thickness of recast layer than the EDMed surface. However, the EDM surface was found to produce lower recast layer thickness than the machined surface by Nd:YAG laser [31]. The average depth of hardened layer produced during the FLM, EDM and Nd:YAG laser machining was found to be 50 μm, 105 μm and 180 μm respectively [31]. Similar to the recast layer thickness, the microhardness was also found to be lower on the surface machined by FLM process compared to that of EDM [31]. However, for both EDM and FLM processes, the microhardness decreases with the increase of depths from the machined surface to the inside of the materials [31]. Figure 22 shows the comparison of microhardness of NiTi SMA machined by EDM and FLM processes [31]. The figure 22 shows the variation of microhardness at different depths under the machined surface for both EDM and FLM processes. The figure clearly shows the reduction of microhardness with the increase of depth from machined surface. In addition, for all the depths, the microhardness is lower for the surface machined by FLM process.

Micro-EDM of SMAs

With the increased demand for miniaturized product, micro-EDM has become an alternative option for machining difficult-to-cut materials. Although, there have been significant amount of research works on various types of EDM of SMAs, very few research studies have been conducted on the micro-EDM of SMAs. Rasheed et al. [39] investigated the effect of operating parameters on the material removal rate, tool wear and surface finish during the micro-EDM of NiTi SMA. The authors used DOE and ANOVA for analyzing the effect of various parameters on the machining performance. The effect of operating parameters during the micro-EDM was reported to be almost similar to the effects in conventional EDM of NiTi SMA. It was reported that the MRR and surface roughness were greatly influenced by discharge voltage, capacitance and selection of electrode materials [39]. The tool wear ratio and surface roughness were found to be lower at lower discharge energy during the micro-EDM of NiTi SMA. In this study, tungsten electrode was recommended for better MRR and brass electrode was recommended for better surface finish [39]. Figures 23 and 24 shows the SEM images of the micro-holes machined in NiTi SMA using tungsten and brass electrodes respectively [39].

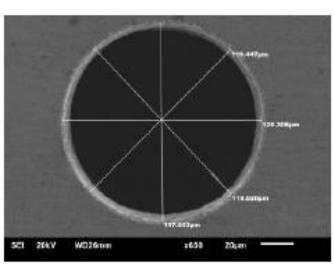

(a)

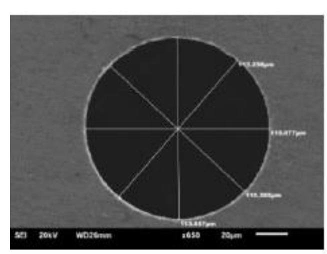

(b)

Figure 23. SEM images of (a) entrance and (b) exit side of the micro-hole machined in NiTi SMA using brass electrode [39].

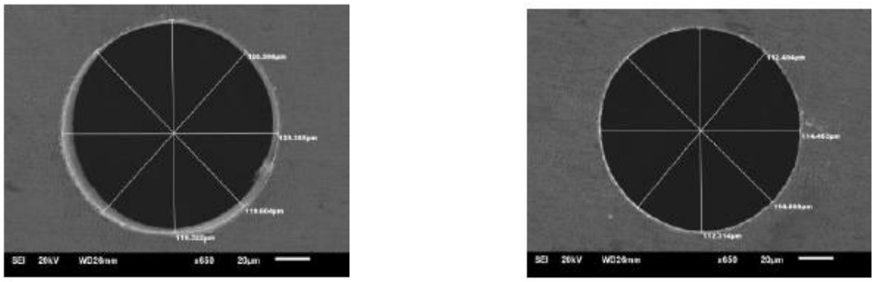

(a) (b)

Figure 24. SEM images of (a) entrance and (b) exit side of the micro-hole machined in NiTi SMA using tungsten electrode [39].

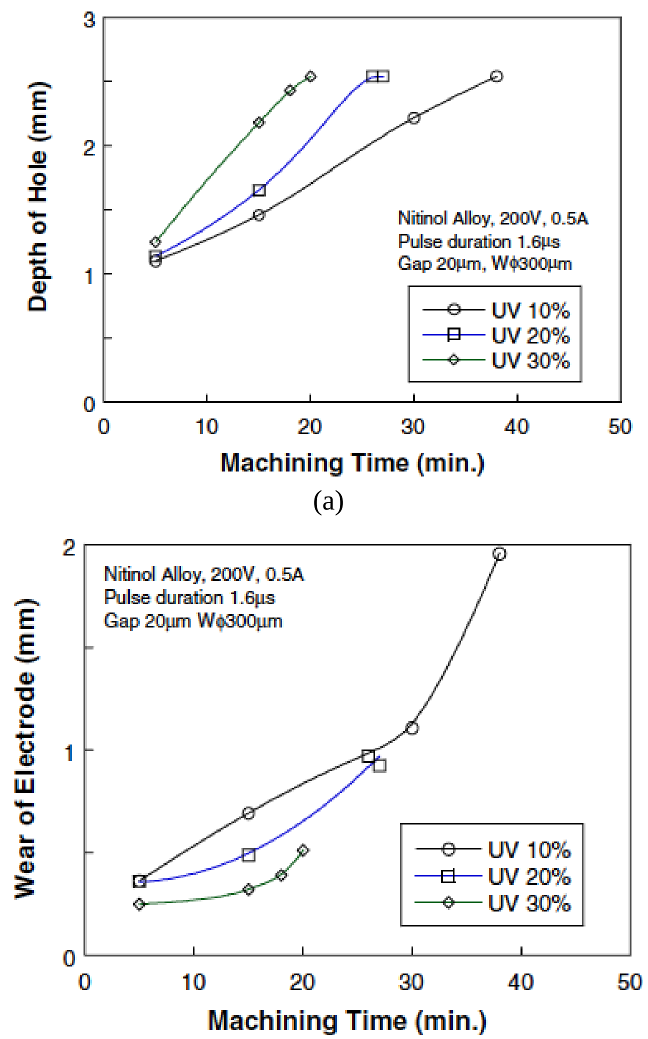

(a)

(b)

Figure 25. The effect of intensity of ultrasonic vibration on (a) depth of hole and (b) electrode wear during micro-EDM of NiTi SMA [41].

EDM-Based Hybrid Machining of SMAs

The hybrid manufacturing processes can be defined as: “Hybrid manufacturing processes are based on the simultaneous and controlled interaction of process mechanisms and/or energy sources/tools having a significant effect on the process performance” [40]. In recent years, EDM-based hybrid machining processes are getting popular as those processes can overcome the difficulties associated with the EDM process. Huang et al. [41] investigated the effectiveness of ultrasonic vibration in enhancing the flushing condition and overall EDM performance during the micro-EDM of NiTi SMA. It was reported that the introduction of ultrasonic vibration increased the machining efficiency by 60 times, without increasing the electrode wear significantly [41]. The main reason for the improvement in machining performance was reported to be the improvement in flushing conditions. Figure 25 shows the effect of ultrasonic vibration on the depth of micro-holes and electrode wear during micro-EDM of NiTi SMA [41].

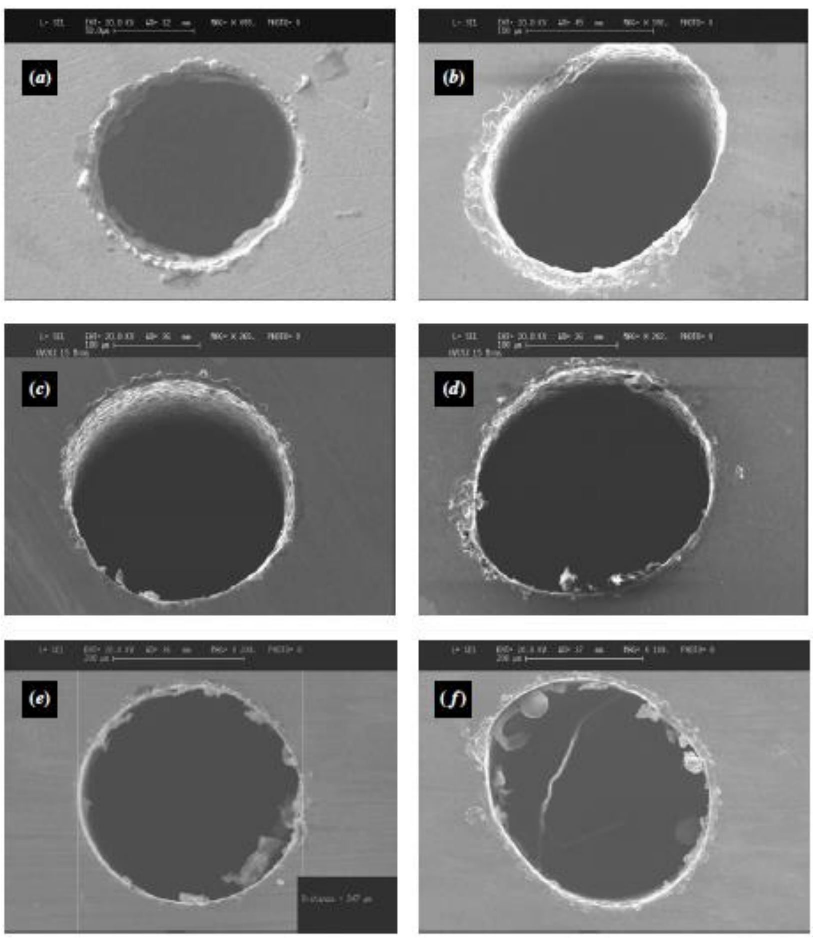

Figure 26. Entrance side of the micro-holes in NiTi SMA machined using (a) and (b) 100 μm, (c) and (d) 200 μm, (e) and (f) 300 μm. (Machining conditions: UV 10%, Gap 20 μm, Voltage 200 V, Current 0.5A, Pulse duration 1.6 μs).

Although, the application of vibration during the EDM was found to improve the depth of the micro-holes and electrode wear, too much vibration intensity can affect the dimensional accuracy of the micro-holes adversely [42]. Although the changes in dimensional accuracy was not reported by Huang et al. [41], the SEM images of the micro-holes presented in the paper showed distortion in the circularity after applying vibration assistance in EDM. Figure 26 shows the entrance side of the micro-holes machined in NiTi SMA by vibration assisted micro-EDM using different electrode diameters [41]. It can be seen from the SEM images that almost all the holes sufferred from the distortion of circularity after applying vibration assistance in EDM.

CONCLUSION

This chapter presented a comprehensive review of the research works conducted on the EDM of shape memory alloys. The chapter started with a brief introduction of the structure, properties and applications of shape memory alloys. The reasons for the difficulty in machining of SMAs using conventional machining processes are discussed. The EDM of various SMAs are discussed in detail by grouping them under six major headings: effect of EDM parameters, modeling and statistical analysis, surface quality and integrity, mechanical properties changes after EDM, micro-EDM of SMAs, and EDM-based hybrid machining of SMAs.

The shape memory alloys are found to be difficult-to-cut using conventional machining processes because of their strain hardening and pseudoelasticity. On the other hand, EDM is found to be capable of machining these materials successfully with higher accuracy. Although there have been numerous research on the EDM of NiTi SMA, many research questions are still unsolved. A major portion of the research works are on the basic parametric study focusing on the effect of operating parameters on the machining performance during EDM of SMAs. There have been several research focusing on the surface quality, integrity and changes in the hardness of the machined surface after EDM. The surface generated in the SMAs after EDM is very important to consider, as one of the major applications of SMAs is in biomedical industries. In order to qualify to be used as a biomedical implant, the parts or components machined by EDM should have a biocompatible surface. As nickel (Ni) of NiTi SMA is known to be responsible for allergic issues in human body, it is important to investigate the composition of machined surface generated by the EDM and to identify the amount of free nickel on the surface. Therefore, future research should focus more on the biocompatibility study of SMAs after machined by the EDM process.

Another area of future research topic in the field of EDM of SMAs will be micro scale EDM and hybrid machining of SMAs. Although a significant amount of research have been carried out on EDM and WEDM of SMAs, very few research have been conducted on the micro-EDM and EDM-based hybrid machining of SMAs. Micro-EDM has important industrial applications in the fabrication of automotive nozzles, spinnerets, micro-moulds and dies, fiber-optics and MEMS, aerospace, medical and biomedical applications, micro-electronics and micro-tools. Therefore, more research is needed on the applicability of NiTi alloys for micro scale parts and components for above mentioned applications. Micro-EDM can surely be applied to fabricate parts and components in SMAs for those applications. In addition, hybrid machining processes, i.e., integrating more than one processes in a single setup, can necessarily solve the difficulties faced during machining of SMAs using EDM. The hybrid micromachining technologies have the potential to combine the strength and to complement the weakness of different processes. Some of the future directions for research in the field of EDM of SMAs include investigating the ways of improving dimensional accuracy, investigating the effect of uniuqe properties of SMAs on EDM performance, improving the process capability of EDM for machining SMAs, advanced on-line monitoring of the process, developing knowledge based system and development of hybrid machining processes for machining SMAs.

ACKNOWLEDGMENT

The authors would also like to acknowledge the partial supports from WKU internal grant RCAP-1 Award #14-8054 and external grant KY-NSF EPSCoR subaward #3048111570-15-094.

REFERENCES

[1] Buehler, W. J., Gilfrich, J. W. & Wiley, R. C. (1963). Effects of low-temperature phase changes on the mechanical properties of alloys near composition TiNi. *Journal of Applied Physics*, *34*, p 475.

[2] Ölander, A. (1932). An Electrochemical Investigation of Solid Cadmium-Gold Alloys. *Journal of the American Chemical Society*, *54*(10). 3819–3833.

[3] Greninger, A. B. & Mooradian V. G. (1938). Strain transformation in metastable beta copper-zinc and beta copper-tin alloys. *Trans. AIME*, *128*, 337-368.

[4] Chang, L. C. & Read, T. A. (1951). Plastic Deformation and Diffusionless Phase Changes in Metals-The Gold-Cadmium Beta Phase, *AIME Transactions*, *189*, 47–52.

[5] Gen, Satoh, 2013. Modification and Integration of Shape Memory Alloys through Thermal Treatments and Dissimilar Metal Joining, *PhD thesis*, *Columbia University*, USA

[6] Machado, L. G. & Savi, M. A. (2003). Medical applications of shape memory alloys. *Brazilian Journal of Medical and Biological Research*, *36*(6). 683-691.

[7] Key to Metals A. G. (2009). Applications of Shape Memory Alloys in the medical field. Retrieved from Total material: http://www.keytometals.com/page.aspx?-ID=CheckArticle&site=ktn &NM=212.

[8] Falvo, A. (2008). Thermomechanical characterization of Nickel-Titanium Shape Memory Alloys, PhD thesis, Department of Mechanical Engineering, University of Calabria, Italy.

[9] Li, Q., Zeng, Y. & Tang, X. (2010). The applications and research progresses of nickel–titanium shape memory alloy in reconstructive surgery. *Australasian Physical & Engineering Sciences in Medicine*, *33*(2). 129-136.

[10] Elahinia, M. H., Hashemi, M., Tabesh, M. & Bhaduri, B. S. (2012). Manufacturing and processing of NiTi implants: A review. *Journal of Progress in Materials Science, 57*, 911–946.

[11] LotfiNeyestanak, A. A. & Daneshmand, S. (2013). The Effect of Operational Cutting Parameters on Nitinol-60 in Wire Electrodischarge Machining. *Advances in Materials Science and Engineering*., http://dx.doi.org/10.1155/2013/457186.

[12] Kaynak, Y., Karaca, H. E. & Jawahir, I. S. (2011). Cryogenic machining of NiTi shape memory alloy. In *6th International Conference and Exhibition on Design and Production of Machines and Dies/Molds*. 23-26 June 2011 ATILIM University, Ankara, Turkey.

[13] Chu, Y. Y. & Zhao, L. C., eds. (2002). *Shape Memory Materials and Its Applications*, Trans Tech Publications Ltd., ISBN 0-87849-896-6.

[14] Miller, R. K. & Walker, T. (1989). *Survey on shape memory alloys*, p. 17.

[15] Huang, W. (2002). Fabrication of NiTi shape-memory alloy microdevices using laser, *Proceedings of SPIE* 4915(65). 234–240.

[16] Kohl M. (2000). Thin film shape memory microvalves with adjustable operation temperature. *Sensors and Actuators A: Physical 83*(1-3). 214–219.

[17] Bahraminasab, M. & Bin Sahari, B. (2013). NiTi Shape Memory Alloys, Promising Materials in Orthopedic Applications, *Shape Memory Alloys - Processing, Characterization and Applications*, Dr. Francisco Manuel Braz Fernandes (Ed.). ISBN: 978-953-51-1084-2, InTech.

[18] Melton K. N. (1998). General Applications of SMA's and Smart Materials, *Shape Memory Materials*, K. Otsuka, and C.M. Wayman, eds., Cambridge University Press, Cambridge, p. 220.

[19] Nitinol Heat Engine Kit (2007). Retrieved from http://www.imagesco.com/nitinol/heat-engine.html, *Images Scientific Instruments*.

[20] Lin, H. C., Lin, K. M., & Chen, Y. C. (2000). Study on the machining characteristics of TiNi shape memory alloys, *Journal of Materials Processing Technology*, 105/3:327-332.

[21] Yan, Z., Cui, L. S. & Zheng, Y. J. (2007). Microstructure and Martensitic Transformation Behaviors of Explosively Welded NiTi/NiTi Laminates. *Chinese Journal of Aeronautics*, *20*(2). 168–171.

[22] Jaware, V. B. & Takale (2015). Review on EDM and Wire-EDM machining of TiNi Shape Memory Alloys. *International Journal of Engineering Technology*, *Management and Applied Sciences*, *3*(1). 99-108.

[23] Manjaiah, M., Narendranath, S. & Basavarajappa, S. (2014). Review on non-conventional machining of shape memory alloys. *Transactions of Nonferrous Metals Society of China*, *24*, 12-21.

[24] Hsieh, S. F., Chen, S. L., Lin, H. C., Lin, M. H. & Chiou, S. Y. (2009). The machining characteristics and shape recovery ability of Ti – Ni – X (X - Zr - Cr) ternary shape memory alloys using the wire electro-discharge machining. *International Journal of Machine Tools and Manufacture, 49*, 509–514.

[25] Jahan, M. P., Wong, Y. S. & Rahman, M. (2009). A study on the quality micro-hole machining of Tungsten Carbide by micro-EDM process using Transistor and RC-type pulse Generator. *Journal of Materials Processing Technology*, *209*(4). 1706-1716.

[26] Jahan, M. P., Wong, Y. S. & Rahman, M. (2009). Effect of nonelectrical and gap control parameters in the micro-EDM of WC-Co. *Journal of Machining & Forming Technologies*, 1/2, 51-78.

[27] Jahan, M. P., Kakavand, P., Kwang, E. L. M., Rahman, M. & Wong, Y. S. (2015). An Experimental Investigation into the Micro-Electro-Discharge Machining Behaviour of Aluminium Alloy (AA 2024). *International Journal of Advanced Manufacturing Technology*, *78*, 1127-1139.

[28] Jahan, M. P., Wong, Y. S. & Rahman, M. (2009). A study on the fine-finish die-sinking micro-EDM of Tungsten Carbide using different electrode materials. *Journal of Materials Processin Technology*, *209*(8). 3956-3967.

[29] Lin, H. C., Lin, K. M. & Cheng, I. S. (2001). The electro-discharge machining characteristics of TiNi shape memory alloys. *Journal of materials science*, *36*(2). 399-404.

[30] Alidoosti, A., Ghafari-Nazari, A., Moztarzadeh, F., Jalali, N., Moztarzadeh, N. & Mozafari, M. (2013). Electrical discharge machining characteristics of nickel-titanium shape memory alloy based on full factorial design. *Journal of Intelligent Material Systems and Structures*, *24*(13). 1546-1556.

[31] Chen, S. L., Hsieh, S. F., Lin, H. C., Lin, M. H. & Huang, J. S. (2007). Electrical discharge machining of TiNiCr and TiNiZr ternary shape memory alloys. *Materials Science and Engineering A*, 445–446, 486–492.

[32] Huang, H., Zheng, H. Y. & Liu, Y. (2005). Experimental investigations of the machinability of $Ni_{50.6}Ti_{49.4}$ alloy. *Smart Mater. Struct.*, *14*, S297–S301.

[33] Daneshmand. S., Farahmand. E. K., Lotfi. N. A. A. & Mortazavi. G. M. (2013). Experimental investigations into Electro Discharge Machining of NiTi Shape Memory Alloys using rotational tool. *International Journal of Electrochemical science*, *8*, 7484–7497.

[34] Chen, S. L., Hsieh, S. F., Lin, H. C., Lin, M. H. & Huang, J. S. (2008). Electrical discharge machining of a NiAlFe ternary shape memory alloy. *Journal of Alloys and Compounds*, *464*, 446–451.

[35] Daneshmand, S., Kahrizi, E. F., Ghahi, M. M. (2012). Investigation of EDM Parameters on Surface Roughness and Material Removal Rate of NiTi60 Shape Memory Alloys. *Australian Journal of Basic and Applied Sciences*, *6*(12). 218-225.

[36] Sabouni, H. R. & Daneshmand, S. (2012). Investigation of the parameters of EDM process performed on smart NiTi alloy using graphite tools. *Life Science Journal*, *9*(4). 504-510.

[37] Jahan, M. P., Rahman, M. & Wong, Y. S. (2011). A review on the conventional and micro electrodischarge machining of tungsten carbide. *International Journal of Machine Tools and Manufacture*, *51*(12). 837-858.

[38] Hsieh, S. F., Hsue, A.W. J., Chen, S. L., Lin, M. H., Ou, K. L. & Mao, P. L. (2013). EDM surface characteristics and shape recovery ability of $Ti_{35.5}Ni_{48.5}Zr_{16}$ and $Ni_{60}Al_{24.5}$ $Fe_{15.5}$ ternary shape memory alloys. *Journal of Alloys and Compounds*, *571*, 63–68.

[39] Liu, J. F., Li, L. & Guo, Y. B. (2014). Surface integrity evolution from main cut to finish trim cut in W-EDM of shape memory alloy. *Procedia CIRP*, *13*, 137-142.

[40] Rasheed, M. S., Al-Ahmari, A. M., El-Tamimi, A. M. & Abidi, M. H. (2012). Analysis of Influence of micro-EDM Parameters on MRR, TWR and Ra in Machining Ni-Ti

Shape Memory Alloy. *International Journal of Recent Technology and Engineering*, *1*(4). 32-37.

[41] Lauwers, B. (2012). Surface Integrity in Hybrid Machining Processes, keynote paper, *1st CIRP Conference on Surface Integrity*, Bremen 30/01/2012-01/02/2012.

[42] Huang, H., Zhang, H., Zhou, L. & Zheng, H. Y. (2003). Ultrasonic vibration assisted electro-discharge machining of microholes in Nitinol. *J. Micromech. Microeng.*, *13*, 693–700.

[43] Jahan, M. P., Wong, Y. S. & Rahman, M. (2012). Evaluation of the effectiveness of low frequency workpiece vibration in deep-hole micro-EDM drilling of tungsten carbide. *Journal of Manufacturing Processes 14*(3). 343–359.

INDEX

F

G

H

I

L

M

N

O

P

R

S

T

U

V

W